THESE DE DOCTORAT

NNT : 2024UPASM023

Étude de l'influence du noyau sur la motilité cellulaire

Study of the influence of the cell nucleus on cell motility

Thèse de doctorat de l'Université Paris-Saclay et du Politecnico di Torino

École doctorale n° 574 : mathématiques Hadamard (EDMH).
Spécialité de doctorat : Mathématiques Appliquées.
Graduate School : Mathématiques.
Référent : Université d'Évry Val d'Essonne.

Thèse préparée dans les unités de recherche **Laboratoire de Mathématiques et Modélisation d'Évry (Université Paris-Saclay, CNRS, Univ Evry)** et **Dipartimento di Scienze Matematiche "Giuseppe Luigi Lagrange" (Politecnico di Torino)**, sous la direction de **Nicolas MEUNIER**, Professeur des Universités à l'Université d'Évry Val d'Essonne, la co-direction de **Luigi PREZIOSI**, Professore Ordinario au Politecnico di Torino

Thèse soutenue à Paris-Saclay, le 20 septembre 2024, par

Claire ALAMICHEL

Composition du jury

Membres du jury avec voix délibérative

Vincent CALVEZ Directeur de recherche, CNRS, Université de Bretagne Occidentale	Président
Astrid DECOENE Professeure, Université de Bordeaux	Rapporteure & Examinatrice
Pierre GABRIEL Professeur, Université de Tours	Rapporteur & Examinateur
Rachele ALLENA Professeure, Université Côte d'Azur	Examinatrice
Muriel BOULAKIA Professeure, Université de Versailles Saint-Quentin	Examinatrice
Chiara GIVERSO Associate Professor, Politecnico di Torino	Examinatrice

This work is supported by a public grant overseen by the French National research Agency (ANR) as part of the « Investissements d'Avenir » program, through the "ADI 2020" project funded by the IDEX Paris-Saclay, ANR-11-IDEX-0003-02.

This work is supported by the Italian Ministry of Education, Universities and Research through the MIUR grant "Dipartimenti di Eccellenza 2018-2022" (Project no. E11G18000350001).

université PARIS-SACLAY | ÉCOLE DOCTORALE de mathématiques Hadamard (EDMH)

Titre : Étude de l'influence du noyau sur la motilité cellulaire
Mots clés : modèle à frontière libre, simulations numériques, modélisation, bifurcation, onde progressive, motilité cellulaire

Résumé : La motilité cellulaire est un phénomène impliqué dans de nombreux processus biologiques comme la propagation des cancers, la réponse immunitaire, la cicatrisation ou le développement embryonnaire. Ce phénomène est assuré par la capacité d'une cellule à se déformer d'une configuration symétrique, non polarisée, à une configuration asymétrique, polarisée, et à maintenir cette configuration asymétrique. Dans cette thèse, nous nous intéressons plus particulièrement au rôle du noyau dans ce phénomène. Pour cela, un modèle à frontière libre en dimension 2 est introduit. La cellule est modélisée par un fluide incompressible comportant une structure rigide modélisant le noyau. Des marqueurs de polarité sont présents dans le fluide et ceux-ci transduisent de manière active les forces appliquées par et sur le cytosquelette. Le modèle proposé permet également de modéliser l'effet de l'undercooling et de l'environnement extérieur sur la motilité cellulaire. Les différentes composantes du modèle sont étudiées de manière séparée dans la thèse.

Nous étudions l'influence du noyau sur la motilité cellulaire. Pour cela nous considérons différents modèles dont un modèle déformable, un rigide et deux modèles jouets. Nous montrons que ces modèles admettent des états stationnaires. Via l'analyse linéaire de la stabilité, nous montrons qu'il existe un seuil à partir duquel l'état stationnaire radialement symétrique est instable. Pour chacun de ces modèles un schéma numérique aux éléments finis est développé. Les résultats numériques obtenus permettent de mettre en avant le lien entre la position du noyau dans la cellule et la polarisation de la cellule. Ils sont qualitativement en accord avec les observations biologiques. L'analyse des trajectoires est également réalisée. Un modèle analogue en dimension 1 qui est une équation non-locale et non-linéaire de Fokker-Planck est introduit. Nous montrons que celui-ci est bien posé. L'existence d'états stationnaires et d'ondes progressives est également étudiée. Un second modèle en dimension 1 basé sur une seconde modélisation est étudié.

L'effet de l'undercooling sur la motilité cellulaire est étudié. En montrant l'existence d'ondes progressives et d'états stationnaires, nous illustrons que celui-ci a un effet stabilisant. L'existence d'ondes progressives est prouvée via un théorème de bifurcation. Nous montrons également à l'aide de l'analyse linéaire de la stabilité qu'il existe un seuil à partir duquel l'état stationnaire est instable.

L'influence de la présence de signaux extérieurs attractifs sur la motilité cellulaire est aussi investiguée. Nous montrons l'existence d'un état stationnaire et l'existence d'une gamme de paramètres pour laquelle celui-ci est stable et une autre pour laquelle il est instable. Numériquement, nous illustrons qu'il existe une compétition entre forces induites par les marqueurs de polarité et celles induites par le signal extérieur.

Cette thèse comporte également un travail effectué durant l'école d'été CEMRACS 2022. Un modèle d'un des mécanismes ayant lieu à la membrane, l'endocytose, y est présenté. Après avoir étudié le modèle, un schéma aux volumes finis est présenté. Celui-ci permet d'obtenir des résultats en accord avec les résultats biologiques.

université PARIS-SACLAY | ÉCOLE DOCTORALE de mathématiques Hadamard (EDMH)

Title: Study of the influence of the cell nucleus on cell motility
Keywords: free boundary model, numerical simulations, modelling, bifurcation, travelling wave, cell motility

Abstract: Cell motility is a phenomenon involved in many biological processes such as cancer propagation, immune response, wound healing and embryonic development. This phenomenon is ensured by a cell's ability to deform from a symmetrical, non-polarised configuration to an asymmetrical, polarised configuration, and to maintain this asymmetrical configuration. In this thesis, we focus on the role of the nucleus in this phenomenon. To this end, a free boundary model in dimension 2 is introduced. The cell is modelled by an incompressible fluid with a rigid structure modelling the nucleus. Polarity markers are present in the fluid and these actively transduce the forces applied by and on the cytoskeleton. The proposed model also models the effect of undercooling and the external environment on cell motility. The different components of the model are studied separately in the thesis.

We are studying the influence of the nucleus on cell motility. We consider various models, including a deformable model, a rigid model and two toy models. We prove that these models admit stationary states. Using linear stability analysis, we demonstrate that there exists a threshold above which the radially symmetric stationary state is unstable. For each of these models, a finite element numerical scheme is developed. The numerical results obtained highlight the link between the position of the nucleus in the cell and the polarisation of the cell. They are in qualitative agreement with biological observations. Trajectory analysis is also carried out. An analogous model in dimension 1, which is a non-local and non-linear Fokker-Planck equation, is introduced. We show that it is well posed. The existence of stationary states and travelling waves is also studied. A second model in dimension 1 based on a second modelling is studied.

The effect of undercooling on cell motility is studied. By proving the existence of travelling waves and stationary states, we illustrate that undercooling has a stabilising effect. The existence of travelling waves is proved using a bifurcation theorem. We also demonstrate, using linear stability analysis, that there exists a threshold above which the stationary state is unstable.

The influence of the presence of attractive external signals on cell motility is also investigated. We prove the existence of a stationary state and the existence of a range of parameters for which it is stable and another for which it is unstable. Numerically, we illustrate that there is competition between the forces induced by the polarity markers and those induced by the external signal.

This thesis also includes a work carried out during the CEMRACS 2022 summer school. A model of one of the mechanisms taking place at the membrane—endocytosis—is presented. After studying the model, a finite volume scheme is presented. This provides results that are consistent with biological results.

Acknowledgements

My first thanks go to my thesis supervisors, Nicolas Meunier and Luigi Preziosi. Thank you for entrusting me with such an interesting research topic and for giving me the opportunity to have an international experience, spanning two countries. It was very enriching, and I learned a lot during these four years with you. A very special thanks for all the time spent resolving the administrative issues caused by the international cotutelle. Merci Nicolas d'avoir toujours été disponible pour moi, répondre à mes questions et de m'avoir transmis tant de savoirs mathématiques. Merci de m'avoir soutenue pour aller au bout de cette thèse. Merci pour votre bienveillance qui m'a aidée à apprendre à avoir confiance en moi et oser demander de l'aide. Ce n'est sûrement pas encore parfait, mais je crois que ces années m'ont bien fait progresser sur ce point. Merci aussi pour votre attention toujours présente et de vous être toujours inquiété si j'allais bien. Grazie mille Luigi, for your warm welcome in Turin. Thank you for the meetings where you introduced me to many different things, which allowed me to enrich my mathematical culture. Thank you for your support, good humor, and encouragement.

Je remercie également Astrid Decoene et Pierre Gabriel d'avoir accepté de rapporter ma thèse et de faire partie du jury. Je tiens aussi à remercier Rachele Allena, Muriel Boulakia, Vincent Calvez et Chiara Giverso d'avoir accepté de faire partie du jury de ma thèse. Merci pour l'intérêt que vous avez porté à mes travaux.

Je tiens également à remercier Christèle Etchegaray, Raphaël Voituriez, Thomas Lepoutre et Aline Lefebvre-Lepot pour le temps qu'ils m'ont accordé au cours de ma thèse.

En finissant cette thèse, j'ai une pensée pour les enseignants que j'ai croisé au cours de ma scolarité. Je tiens tout particulièrement à remercier Étienne Fouvry pour le rôle qu'il a eu durant mes études. Merci de m'avoir encouragée à continuer dans la voie que j'ai choisie et de m'avoir fait découvrir le monde de la recherche. Les séances de travail avec vous lors des TER de L3 et M1 toujours ponctuées d'humour étaient une vraie échappatoire durant ces années qui n'ont pas été si faciles pour moi.

J'ai eu la chance d'être accueillie dans deux laboratoires ayant des atmosphères très agréables. Je remercie tous mes collègues du LaMME. Merci aux doctorants avec qui j'ai pu passer de beaux moments et qui m'ont suivi dans l'organisation et l'animation de notre petit séminaire, merci Vincent d'avoir insufflé cette idée. Un merci tout spécial à Arnaud et Liudmila avec lesquels je partageais mon bureau. Merci à vous deux pour votre écoute, votre attention envers moi sans faille et surtout merci de m'avoir tant de fois remonté le moral. Merci également Perrine pour ton soutien et nos discussions qui étaient de vraies petites bulles notamment durant la période de rédaction. Merci Margot pour toutes nos discussions le soir avant de quitter le labo. Merci Carène pour ton soutien et ton écoute quand j'en avais besoin. Merci Cyril et Jamel, assurer vos TD était très plaisant. Merci Julia pour ton aide dans la préparation de mes TD de méthodologie. Merci Maouloud et Maurice de m'avoir aidée avec tous les aspects informatiques. Merci Valérie d'avoir toujours répondu avec une efficacité incroyable à mes demandes de mission et autres demandes administratives. Merci Diego de m'avoir incitée à présenter mes travaux et de m'en avoir donné l'opportunité de le faire.

I also thank all my colleagues at DISMA. Thank you Chiara for welcoming me. I hope one day to have the time to finish the simulations in the channel. Thank you to the PhD students for your generous welcome and patience with my slightly erratic English and non-existent Italian when I first arrived. Thank you for including me in your adventures, introducing me to your culture, and especially your good cheeses. Thank you Matteo for our long, always enriching discussions, your presence especially when I was unsure of having a roof over my head and I had COVID, and for all the moments we shared. Thank you Juan for your infectious joy, your listening, and your more than warm welcome when I needed to come back to Turin for administrative tasks. Thank you Patri for more than helping me open up and integrate, for your support during difficult times and for all the ice creams shared. Thank you Francesca for your listening and incredible kindness. Thank you Giovanni for the moments shared, for your listening and presence when things were a bit rough. Thank you Vincenzo

for your spontaneity and all the shared laughter. Thank you Martina for the conversations between our two offices, which, among other things, helped me put my anxieties a little bit away. Thank you Sara for being such a considerate office mate. Thank you Giada for always making sure I was well. Thank you Leonardo for the long discussions about life and the random french words. Thank you Giulia for your welcome and enthusiasm that always swept me along with you. Thank you Marco for teaching me how to make pasta and for the French-Italian conversations. Thank you Elisa for your listening and presence. Merci Astrid pour ton écoute, ton soutien et ton attention, merci également pour tous les moments partagés ensuite en France. Thank you all for making my stays in Turin full of joy, laughter, and discoveries. Thank you also for the little trips organized in Europe afterward, which were lovely escapes in my daily routine. Grazie per tutto!

J'ai eu l'opportunité de participer au CEMRACS à l'été 2022. Merci aux organisateurs. Un merci un peu plus particulier à Hélène de me proposer l'opportunité de continuer dans la recherche avec un post-doc enthousiasmant. Merci Nathan, travailler avec toi durant ces cinq semaines était très agréable, merci d'avoir su composer avec mes petites angoisses et mon souci du détail. Merci Romain, Erwan et Juan pour votre encadrement plein de bonne humeur. Merci aussi à Saoussen. Merci Léo pour nos débriefs du soir, ton écoute, ta présence et ton amitié durant ces six semaines ainsi que tout au long de ma thèse.

Je tiens aussi à remercier mes amis. Merci d'avoir accepté mes silences et d'avoir toujours répondu présent quand j'en avais besoin. Merci Hadrien pour ton amitié, les balades ponctuées de rires ainsi que ta présence tout au long de mes études. Merci Amandine, Anaïs, Clémence et Julie pour votre présence depuis de nombreuses années, votre amitié m'est précieuse. Merci Pierrick pour ton écoute, les balades et de m'avoir permis de retrouver un peu de France à Turin. Merci Marion pour nos longs échanges par messages et ton écoute. Merci Léa pour nos discussions et ton soutien. Merci Léna pour tes encouragements et le partage de tes aventures. Merci Charlotte pour nos échanges toujours enrichissants. Merci Adrien, Maud et Damien pour les moments au viet ou ailleurs, votre écoute et soutien. Merci Francesca pour les petites aventures artistiques et aux JO. Un merci à tous ceux que j'ai croisé durant ces années aux scouts. Le scoutisme m'a permis d'avoir un espace où m'évader le temps de week-ends, soirées ou semaines de camp. Un merci plus spécial aux SP, Cyril, Eugénie, Cécile et Sylvain. Un merci tout particulier à mes anciens cochefs. Je garde un super souvenir de mon dernier camp en tant que cheftaine, merci Nico, Justine, Nathalie, Emmanuelle et Armand d'avoir permis qu'il soit beau. Merci Céline, Hélène, Louise, Rémi et Siméon pour nos retrouvailles toujours joyeuses. Merci pour ces moments hors du temps, dans la nature, au coin du feu ou les uns chez les autres. Merci à la MAO d'avoir rendu beaucoup de samedis après-midi insouciants et hors de tous les problèmes du monde. Un merci particulier à Rémy, Xavier, Antoine et Astrid. Un grand merci, François, d'avoir rendu mes trajets quotidiens vers Évry plus courts et ponctués d'anecdotes insolites.

Enfin, un grand merci à ma famille. Merci Maman et Papa de m'avoir soutenue tout au long de ma thèse et depuis toujours, merci de faire de la maison un refuge dont la porte est toujours ouverte et d'avoir supporté le bruit de la machine à coudre (ainsi que le bazar associé) lorsque j'avais besoin de me vider l'esprit en restant à l'intérieur. Merci Maman de m'avoir montré qu'on peut faire des maths en étant une fille. Merci Papa pour les relectures de mon anglais, peut-être qu'à force as-tu la sensation d'être devenu incollable sur la motilité cellulaire. Un grand merci à mes frère et sœurs, Louise, Émile et Bénédicte. En vrac, merci pour les jeux de société, les rires, les visionnages de Drag Race, les instants de cuisine toujours dans des proportions raisonnées et tout ce que j'omets dans cette courte liste. Merci Mamie et Grand-Père, passer mes vacances chez vous a toujours été source de repos et de partage. J'ai une pensée pour mes deux grands-pères qui ont ouvert la voie des sciences et de la recherche dans ma famille. Une pensée pour ma Mamie Sylvette, tes cours d'anglais du mercredi m'ont été bien utile et je sais (enfin) me débrouiller en anglais. Merci Anita pour notre correspondance et ta présence. Merci Marie-Françoise d'avoir pris le temps de relire toute mon introduction et d'en avoir grandement amélioré l'anglais. Merci à toute ma famille, mes oncles et tantes, mes cousins et cousines, merci pour tous les moments partagés ensemble.

Contents

Synthèse en français

Cette thèse porte sur l'étude mathématique de l'influence du noyau sur la motilité cellulaire et consiste au développement d'un modèle mathématique de la motilité cellulaire prenant en compte le noyau et à l'étude de ce dernier de manière théorique ainsi qu'à l'aide de simulations numériques. Nous présentons en premier le contexte biologique : la motilité cellulaire. Nous présentons ensuite le modèle. Enfin nous présentons les résultats obtenus.

Contexte biologique

La cellule est un système complexe qui contient de nombreuses molécules interagissant entre elles et menant à différents phénomènes remarquables tels que le mouvement des cellules. Dans cette thèse, nous nous intéressons à la modélisation de la motilité cellulaire. Celle-ci est impliquée dans différents processus biologiques importants comme le développement embryonnaire, la cicatrisation, la réponse immunitaire ou la propagation des cancers.

La motilité cellulaire est un processus complexe qui repose sur la capacité d'une cellule à se polariser. Cela signifie que la cellule est capable de briser sa symétrie interne et d'avoir un avant et un arrière définis (Danuser et al., 2013; Reig et al., 2014). Une fois que la cellule est polarisée, la migration cellulaire peut avoir lieu et est décrite par un cycle de quatre étapes (Abercrombie, 1980) (voir fig. 1).

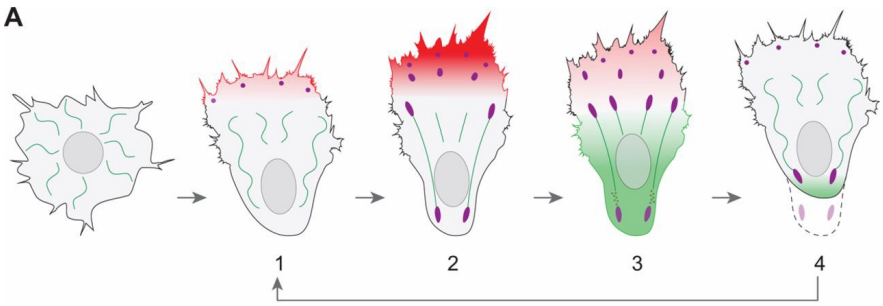

Figure 1: **Représentation schématique du cycle de quatre étapes de la migration cellulaire.** *Les événements dépendant de la polymérisation de l'actine sont représenté en rouge et ceux dépendant de la myosine en vert. Les adhésions au substrat sont représentées en violet. Image tirée de Reig et al. (2014).*

Nous pouvons noter qu'une fois que la cellule est polarisée, le noyau est situé à l'arrière de la cellule et qu'il y a une accumulation à l'avant ou à l'arrière de marqueurs de polarité. Ces marqueurs peuvent, par exemple, être de la myosine ou ses activateurs, des régulateurs de la polymérisation de l'actine ou des molécules impliquées dans la régulation de la dynamique des microtubules (Maiuri et al., 2015). La forme de la cellule est également un marqueur de polarisation de celle-ci. La polarisation et la migration cellulaire peuvent avoir lieu de manière spontanée ou en réponse à un stimuli extérieur.

Les forces permettant la motilité cellulaire sont générées par le cytosquelette, un réseau de protéines présent dans le cytoplasme. Les deux principales sont la force induite par la pro-

trusion de la cellule liée au phénomène de treadmilling de l'actine et la force induite par la contraction des fibres d'acto-myosine (voir fig. 1). Le treadmilling de l'actine crée des protrusions à l'avant ainsi que l'attachement de la cellule au substrat. La contraction des fibres d'acto-myosine, fibres composées d'actine et de myosine, permet la contraction du cytosquelette ce qui induit la rétractation de l'arrière de la cellule ainsi que le détachement de la cellule du substrat à cet endroit.

Le noyau est le plus grand organite de la cellule. Il est entouré de membrane plasmique. Bien que plus rigide que le reste de la cellule, le noyau est capable de se déformer. Le noyau est relié au cytosquelette via le complexe LINC, un complexe formé de protéines. Cela permet la transmission de forces entre le noyau et la cellule (Thiam, 2014). Sa position dans la cellule est également un marqueur de polarité et influence la polarisation de la cellule.

À la suite de la course mondiale des cellules,Maiuri et al. (2015) ont mis en évidence l'existence d'un couplage universel entre la vitesse et la persistance des cellules (dit loi de l'UCSP). La persistance est la capacité d'une cellule à conserver sa direction de mouvement. Celle-ci est dite conservée tant qu'elle ne dévie pas de plus de 90° de la direction initiale. Le temps de persistance est le temps pendant lequel la cellule maintient sa direction initiale de mouvement et la vitesse de persistance est la vitesse moyenne durant ce temps. La loi de l'UCSP donne que le temps de persistance est proportionnel à une exponentielle de la vitesse de persistance.

Il a également été mis en évidence que les cellules peuvent avoir trois types de trajectoires. Premièrement, elles peuvent être browniennes et sont caractérisées par l'absence d'état polarisé et un temps de persistance faible. Deuxièmement, elles peuvent être persistantes et sont caractérisées par un long temps de persistance et une longue durée de vie d'un état polarisé. Troisièmement, elles peuvent être intermittentes, dans ce cas les trajectoires alternent entre des phases browniennes et des phases persistantes (Maiuri et al., 2015).

Présentation du modèle

Afin de modéliser le phénomène de motilité cellulaire en prenant en compte le noyau de la cellule, nous proposons dans cette thèse un modèle à frontière libre de type interface mince. Le modèle est dans un cadre deux-dimensionnel. Ce modèle reprend les idées du modèle de Lavi et al. (2020) et peut être vu comme un enrichissementde ce modèle qui est un modèle ne prenant pas en compte le noyau de la cellule. Le domaine de la cellule, dépendant du temps, est noté $\Omega(t) \subset \mathbb{R}^2$ où $t \geq 0$ désigne le temps. Nous notons A_Ω l'aire de la cellule. Le domaine du noyau est noté $N(t)$ et nous supposons que pour tout $t \geq 0$ nous avons $N(t) \subset \Omega(t)$. Le

modèle est donné par :

$$
\begin{cases}
\mathbf{u} + \nabla P = 0 & \text{dans } \Omega(t) \setminus N(t), \quad (1a)\\
\operatorname{div}(\mathbf{u}) = 0 & \text{dans } \Omega(t) \setminus N(t), \quad (1b)\\
V_n = \mathbf{u} \cdot \mathbf{n} & \text{sur } \partial\Omega(t), \quad (1c)\\
P = \gamma\kappa + \chi_c f_{\text{act}}(c) + \chi_s g(\nabla s \cdot \mathbf{n}) - f_{\text{NB}} - f_{\text{obs}} + \chi_u f_{\text{und}}(V_n) & \text{sur } \partial\Omega(t), \quad (1d)\\
\mathbf{u}_{\text{nucl}}(t) = \dfrac{1}{\xi_{\text{nucl}}|N|}\left(\displaystyle\int_{\partial N(t)} P(t,\mathbf{x})\mathbf{n}\,\mathrm{d}\sigma + \mathbf{f}_{\text{BN}}\right) & \quad (1e)\\
\mathbf{u} \cdot \mathbf{n} = \mathbf{u}_{\text{nucl}} \cdot \mathbf{n} & \text{sur } \partial N(t), \quad (1f)\\
\partial_t c = \operatorname{div}\left(\nabla c - (1-a)\,\mathbf{u}c - \alpha \dot{W}_t^Q c\right) & \text{dans } \Omega(t) \setminus N(t), \quad (1g)\\
\left(\nabla c + a\mathbf{u}c - \alpha \dot{W}_t^Q c\right) \cdot \mathbf{n} = 0 & \text{sur } \partial(\Omega(t) \setminus N(t)), \quad (1h)\\
c(0,\mathbf{x}) = c^{\text{in}}(\mathbf{x}) & \text{dans } \Omega(0) \setminus N(0), \quad (1i)
\end{cases}
$$

où

- κ est la courbure (positive pour un cercle) de la frontière libre $\partial\Omega$ et $\gamma \geq 0$ est la tension de surface,
- V_n est la vitesse normale de la frontière libre $\partial\Omega$ et $\mathbf{n}$ le vecteur normal sortant à $\Omega \setminus N$,
- $\chi_c > 0$, f_{act} est la force active de traction et dépend de la concentration de marqueurs, cette force modélise l'effet du cytosquelette sur la cellule,
- $\chi_s > 0$, g est la force qui dépend du signal extérieur s,
- f_{obs} est la force de contact induite par les obstacles sur le bord de la cellule,
- $\chi_u > 0$, f_{und} est la force qui dépend de la vitesse normale du bord de la cellule qui peut être vue comme un effet d'undercooling et qui traduit la force induite par la friction du bord de la cellule,
- $\xi_{\text{nucl}} > 0$,
- f_{NB} est la force induite par le noyau sur le bord extérieur de la cellule et $\mathbf{f}_{\text{BN}}$ celle induite par le bord extérieur de la cellule sur le noyau,
- $a \in [0,1]$,
- $\alpha \geq 0$ et $\dot{W}_t^Q$ le bruit coloré associé à un processus Q-Wiener,
- c^{in}, $\Omega(0)$, $N(0)$ désignent les conditions initiales,
- σ est une mesure sur le bord.

Le cytoplasme de la cellule est modélisé par un fluide qui occupe le domaine $\Omega(t) \setminus N(t)$ et qui contient des marqueurs de polarité d'arrière ayant pour concentration c. Le fluide satisfait la loi de Darcy (eq. (1a)) et est incompressible (eq. (1b)). Nous supposons que la membrane, modélisée par l'interface entre le fluide et l'extérieur de la cellule $\partial\Omega$ se déplace à la vitesse du fluide (eq. (1c)). Les marqueurs diffusent dans le fluide et sont transportés à la vitesse du fluide (eq. (1g)). Le terme a représente la proportion de marqueurs attachés et qui ne sont pas transportés par le fluide. Un bruit coloré en espace $\dot{W}_t^Q$ est ajouté au champ d'advection des

marqueurs. Celui-ci modélise les réorganisations internes du cytosquelette. Nous supposons également que la quantité totale de marqueurs M est conservée au cours du temps, ce qui est assuré par les conditions de bord (eq. (1h)).

Comme première approche, dans cette thèse, nous supposons que le noyau est rigide et de forme circulaire. Nous avons alors pour tout $t \geq 0$, $N(t) = b(\mathbf{x}_{\text{nucl}}(t), R_{\text{nucl}})$. Nous supposons que le noyau est relié au bord de la cellule par des liens. Ainsi, le noyau induit une force sur le bord de la cellule que nous notons $\mathbf{f}_{\text{BN}}$. Le noyau induit une force réciproque sur le bord de la cellule et celle-ci est notée f_{NB} (voir fig. 2 pour une représentation graphique). L'expression de ces forces est alors donnée par :

$$\mathbf{f}_{\text{BN}}(t) = \delta \int_{\partial\Omega(t)} \frac{\mathbf{v}_{\text{BN}} \cdot \mathbf{n}}{\left(\|\mathbf{v}_{\text{BN}}\| - R_{\text{nucl}}\right)^{\beta}} \mathbf{n} \, \mathrm{d}\sigma,$$

et pour tout $\mathbf{x}_B \in \partial\Omega(t)$

$$f_{\text{NB}}(t, \mathbf{x}) = -\delta \frac{\mathbf{v}_{\text{BN}} \cdot \mathbf{n}}{\left(\|\mathbf{v}_{\text{BN}}\| - R_{\text{nucl}}\right)^{\beta}},$$

où $\mathbf{v}_{\text{BN}} = \mathbf{x}_{\text{nucl}} - \mathbf{x}_B$ et $\delta > 0$, $\beta > 1$.

Nous supposons qu'au bord du noyau il y a continuité des vitesses normales (eq. (1f)). La vitesse du noyau (eq. (1e)) est obtenue à l'aide du bilan des forces et en supposant que le noyau a un mouvement rigide (Lefebvre, 2007). Les forces s'exerçant sur le noyau sont la force de friction sur le substrat, la force induite par le fluide sur le noyau et la force induite par le bord de la cellule sur le noyau.

Enfin, nous supposons que les marqueurs induisent une force au bord de la cellule. Cela modélise l'action du cytosquelette sur la cellule. Nous faisons l'hypothèse de marqueurs d'arrière, cela signifie qu'une haute concentration en marqueurs définit l'arrière de la cellule. Cette force a pour expression $-\chi_c f_{\text{act}}(c)$ avec $\chi_c > 0$ et f_{act} une fonction positive. Nous supposons également la présence dans l'environnement de la cellule d'obstacles et de signaux extérieurs. Ces signaux et obstacles induisent des forces sur la cellule. La force induite par les signaux extérieurs est donnée par $-\chi_s g(\nabla s \cdot \mathbf{n})$ et la force induite par le contact avec les obstacles est donnée par f_{obs}. Nous supposons aussi que la membrane subit une force de friction différente du reste du cytoplasme. Cela mène à un effet d'undercooling. Cette force est notée $-\chi_u f_{\text{und}}(V_n)$ où V_n est la vitesse normale du bord de la cellule. Ainsi en écrivant le bilan des forces qui s'exercent au bord de la cellule, nous obtenons la condition de bord sur la pression (eq. (1d)), c'est l'équation de Young-Laplace perturbée.

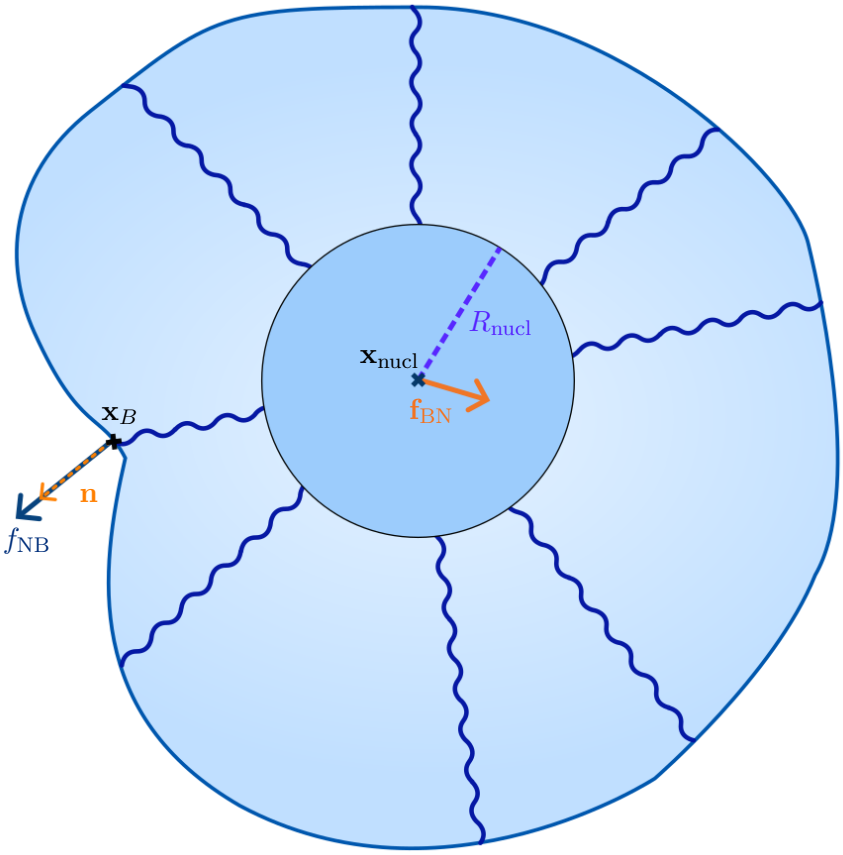

Figure 2: **Hypothèses faites pour la modélisation du noyau.** *Le domaine du fluide $\Omega(t)\backslash N(t)$ est représenté en bleu pâle et le domaine du noyau $N(t)$ est représenté en bleu un peu plus foncé. Quelques liens entre le noyau et le bord de la cellule sont représentés par les lignes ondulées bleues foncées. La force induite par le noyau sur le bord de la cellule f_{NB} est représentée pour un point $\mathbf{x}_B$ du bord. La force induite par le bord de la cellule sur le noyau $\mathbf{f}_{\text{BN}}$ est représentée en orange.*

Résultats de la thèse

Dans cette thèse les différentes composantes du modèle sont étudiées séparément.

Impact du noyau sur la motilité cellulaire

Un modèle en dimension 1 : Dans le chapitre 2 un modèle en dimension 1 analogue au modèle général est étudié. Dans ce cas, la cellule est représentée par un segment de longueur fixe $[-1, 1]$. Nous supposons ici que les marqueurs de polarité peuvent s'attacher et se détacher au bord de la cellule et nous notons μ_+ la quantité de marqueurs attachés en 1 et μ_- celle en

-1. Dans le référentiel de la cellule, le modèle est donné par:

$$\begin{cases} \partial_t c\,(t,x) = \partial^2_{xx} c\,(t,x) + a u\,(t)\ \partial_x c\,(t,x)\,, & x \in\,]-1,1[\,, \quad \text{(2a)} \\ \partial_x c\,(t,\pm 1) + a u\,(t)\ c\,(t,\pm 1) = \mp \dfrac{\mathrm{d}}{\mathrm{d}t}\mu_\pm\,(t)\,, & \text{(2b)} \\ \dfrac{\mathrm{d}}{\mathrm{d}t}\mu_\pm\,(t) = k_{\mathrm{on}}\, c\,(t,\pm 1) - k_{\mathrm{off}}\, \mu_\pm\,(t)\,, & \text{(2c)} \\ u\,(t) = \dfrac{\chi_c}{2}\left(\mu_-\,(t) - \mu_+\,(t)\right) - \dfrac{1}{2}\, g\left(X_N\,(t)\right), & \text{(2d)} \\ \dfrac{\mathrm{d}}{\mathrm{d}t} X_N\,(t) = \left(\dfrac{1}{\xi_{\mathrm{nucl}}} - 1\right) u\,(t) + \dfrac{1}{\xi_{\mathrm{nucl}}}\, g\left(X_N\,(t)\right), & \text{(2e)} \end{cases}$$

que nous complétons par la condition initiale suivante :

$$\begin{cases} c\,(0,x) = c^0\,(x)\,, & x \in [-1,1]\,, \quad \text{(3a)} \\ \mu_\pm\,(0) = \mu^0_\pm, & \text{(3b)} \\ X_N\,(0) = X^0_N, & \text{(3c)} \end{cases}$$

où $\mu^0_\pm \geq 0$ et $X^0_N \in [-1,1]$. À l'aide de l'étude d'un problème découplé et d'un argument de point fixe, nous montrons que, sous certaines conditions sur la condition initiale (3), le modèle (2) est bien posé.

Proposition. *Supposons que c^0 est tel que $\int_{-1}^{1} c^0\,(x) \log c^0\,(x)\ \mathrm{d}x < +\infty$. Supposons aussi que $\mu^0_+, \mu^0_- \in [0,M]$ sont tels que $\int_{-1}^{1} c^0\,(x)\ \mathrm{d}x + \mu^0_+ + \mu^0_- = M$. Supposons de plus que $X^0_N \in [-1,1]$. Alors il existe une unique solution (c, μ_+, μ_-, X_N) au problème (2) pour tout temps.*

Nous montrons ensuite que le modèle admet un état stationnaire non-polarisé et symétrique ainsi que des ondes progressives. Enfin, un schéma numérique aux volumes finis est décrit afin de pouvoir réaliser des simulations numériques du modèle. Ce schéma permet bien de retrouver les états stationnaires et ondes progressives du modèle. Des simulations numériques sont présentées et permettent de faire de premières conclusions sur le rôle du noyau dans la motilité cellulaire et le fait que le modèle donne des résultats en accord avec les observations biologiques. Celles-ci permettent d'illustrer que le phénomène de polarisation est nécessaire à la migration cellulaire et que la position du noyau à l'arrière de la cellule permet une polarisation rapide de la cellule.

Étude de deux modèles rigides jouets : Dans les chapitres 4 et 5 deux modèles jouets sont présentés. Ces deux modèles sont des modèles pour lesquels la cellule est supposée rigide. Pour le premier, appelé modèle de la couronne, la position du noyau dans la cellule est fixe. Dans ce cas le modèle est donné par:

$$\begin{cases} \partial_t c = \mathrm{div}\left(\nabla c - (1-a)\,\mathbf{u} c - \alpha \dot{W}^Q_t c\right) & \text{dans } \Omega\,(t) \setminus N\,(t)\,, \\ \left(\nabla c + a \mathbf{u} c - \alpha \dot{W}^Q_t c\right) \cdot \mathbf{n} = 0 & \text{sur } \partial\left(\Omega\,(t) \setminus N\,(t)\right), \\ \mathbf{u}\,(t) = \dfrac{-\chi_c}{A_\Omega} \displaystyle\int_{\partial\Omega(t)} f_{\mathrm{act}}\,(c)\,\mathbf{n}\,\mathrm{d}\sigma, \end{cases}$$

avec $\Omega(t) = B(\mathbf{x}_{\text{cell}}(t), R_0)$ et $\Omega(t) = B(\mathbf{x}_{\text{nucl}}(t), R_{\text{nucl}})$. Nous avons:

$$\frac{\mathrm{d}}{\mathrm{d}t}\mathbf{x}_{\text{cell}}(t) = \mathbf{u}(t)$$

et

$$\frac{\mathrm{d}}{\mathrm{d}t}\mathbf{x}_{\text{nucl}}(t) = \mathbf{u}(t).$$

La vitesse de déplacement de la cellule $\mathbf{u}$ est obtenue à l'aide du bilan des forces sur la cellule. Lorsque le bruit est négligé ($\alpha = 0$), le modèle admet un unique état stationnaire défini par :

$$\begin{cases} c^0(\mathbf{x}) = \dfrac{M}{|\Omega^0 \setminus N^0|}, & \mathbf{x} \in \Omega^0 \setminus N^0, \\ \mathbf{u}^0(\mathbf{x}) = 0, & \mathbf{x} \in \Omega^0 \setminus N^0, \\ \Omega^0 = B(0, R_0) \text{ et } N^0 = B(0, R_{\text{nucl}}). \end{cases}$$

Pour le second, appelé modèle avec une particule, la dynamique du noyau est négligée, nous supposons que le noyau n'induit pas de force sur le bord de la cellule et que le bord de la cellule n'en induit pas sur le noyau. Dans ce cas, le modèle est donné par :

$$\begin{cases} \mathbf{u} + \nabla P = 0 & \text{dans } \Omega(t) \setminus N(t), \\ \operatorname{div}(\mathbf{u}) = 0 & \text{dans } \Omega(t) \setminus N(t), \\ \mathbf{u} \cdot \mathbf{n} = \mathbf{u}_{\text{cm}} \cdot \mathbf{n} & \text{sur } \partial\Omega(t), \\ \mathbf{u} \cdot \mathbf{n} = \mathbf{u}_{\text{nucl}} \cdot \mathbf{n} & \text{sur } \partial N(t), \\ \mathbf{u}_{\text{nucl}}(t) = \dfrac{1}{\xi_{\text{nucl}}|N|} \displaystyle\int_{\partial N(t)} P(t,\mathbf{x})\mathbf{n}\,\mathrm{d}\sigma, & \\ \mathbf{u}_{\text{cm}}(t) = \dfrac{-\chi_c}{A_\Omega} \displaystyle\int_{\partial\Omega(t)} f_{\text{act}}(c)\,\mathbf{n}\,\mathrm{d}\sigma + \dfrac{|N|}{A_\Omega}(1-\xi_{\text{nucl}})\,\mathbf{u}_{\text{nucl}}(t), & \\ \partial_t c = \operatorname{div}\left(\nabla c - (1-a)\,\mathbf{u}c - \alpha \dot{W}_t^Q c\right) & \text{dans } \Omega(t) \setminus N(t), \\ \left(\nabla c + a\mathbf{u}c - \alpha \dot{W}_t^Q c\right) \cdot \mathbf{n} = 0 & \text{sur } \partial(\Omega(t) \setminus N(t)), \\ \Omega(t) = B(0, R_0) + \displaystyle\int_0^t \mathbf{u}_{\text{cm}}(s)\,\mathrm{d}s, & \\ N(t) = B(0, R_{\text{nucl}}) + \displaystyle\int_0^t \mathbf{u}_{\text{nucl}}(s)\,\mathrm{d}s. & \end{cases}$$

Nous pouvons noter qu'en général, puisque $\mathbf{u}_{\text{cm}} \neq \mathbf{u}_{\text{nucl}}$, le domaine fluide n'est pas un domaine rigide mais un domaine déformable. La vitesse $\mathbf{u}_{\text{cm}}$ est obtenue à l'aide du bilan des forces sur la cellule. Lorsque le bruit est négligé, ce modèle admet un unique état stationnaire radialement symétrique défini par :

$$\begin{cases} \mathbf{u}^0(\mathbf{x}) = 0, & \mathbf{x} \in \Omega^0 \setminus N^0, \\ P^0(\mathbf{x}) = 0, & \mathbf{x} \in \Omega^0 \setminus N^0, \\ \mathbf{u}^0_{\text{nucl}} = 0, & \\ \mathbf{u}^0_{\text{cm}} = 0, & \\ c^0(\mathbf{x}) = \dfrac{M}{|\Omega^0 \setminus N^0|}, & \mathbf{x} \in \Omega^0 \setminus N^0, \\ \Omega^0 = B(0, R_0) \text{ et } N^0 = B(0, R_{\text{nucl}}). \end{cases}$$

Pour ces deux modèles, nous définissons $\chi_c^* = \dfrac{1}{ac^0 f'_{\text{act}}(c^0)}$ et montrons le résultat suivant sous l'hypothèse $\xi_{\text{nucl}} = 1$ dans le cas du modèle avec une particule ou en toute généralité dans le cas de la couronne :

Théorème. *Si $\chi_c < \chi_c^*$, alors l'état stationnaire est linéairement stable. À l'opposé, si $\chi_c > \chi_c^*$, alors l'état stationnaire est linéairement instable.*

Nous proposons ensuite un schéma numérique aux éléments finis pour ces deux modèles. Ces schémas numériques s'appuient, lorsque c'est nécessaire, sur une méthode de décomposition du problème sur la vitesse et la pression afin de séparer les conditions de bord, une gestion du potentiel contact entre le noyau et le bord de la cellule à l'aide d'un algorithme d'Uzawa et d'une discrétisation en élements finis du bruit (Boulakia et al., 2015). Après avoir vérifié que les schémas numériques donnent des résultats en accord avec les observations théoriques, nous simulons des trajectoires. Nous obtenons des observations similaires à celles obtenues au chapitre 3 lorsque nous ne considèrons pas de noyau et que la cellule est supposée rigide. Les travaux du chapitre 3 sont effectués en collaboration avec Christèle Etchegaray et Nicolas Meunier. Les trajectoires satisfont la loi de l'UCSP et des gammes de paramètres sont trouvées de manière à retrouver les trois types de trajectoires.

Étude d'un modèle rigide : Dans le chapitre 6, un modèle rigide prenant en compte la dynamique du noyau est étudié. Le modèle est donné par :

$$
\begin{cases}
\mathbf{u} + \nabla P = 0 & \text{dans } \Omega(t) \setminus N(t), \quad (4a)\\
\operatorname{div}(\mathbf{u}) = 0 & \text{dans } \Omega(t) \setminus N(t), \quad (4b)\\
\mathbf{u}_{\text{nucl}}(t) = \dfrac{1}{\xi_{\text{nucl}} |N|} \left(\displaystyle\int_{\partial N(t)} P(t,\mathbf{x}) \mathbf{n} \, \mathrm{d}\sigma + \mathbf{f}_{\text{BN}} \right), & (4c)\\
\mathbf{u}_{\text{cm}}(t) = \dfrac{-\chi_c}{A_\Omega} \displaystyle\int_{\partial\Omega(t)} f_{\text{act}}(c) \, \mathbf{n} \, \mathrm{d}\sigma + \dfrac{|N|}{A_\Omega} (1 - \xi_{\text{nucl}}) \, \mathbf{u}_{\text{nucl}}(t), & (4d)\\
\mathbf{u} \cdot \mathbf{n} = \mathbf{u}_{\text{cm}} \cdot \mathbf{n} & \text{sur } \partial\Omega(t), \quad (4e)\\
\mathbf{u} \cdot \mathbf{n} = \mathbf{u}_{\text{nucl}} \cdot \mathbf{n} & \text{sur } \partial N(t), \quad (4f)\\
\partial_t c = \operatorname{div}\left(\nabla c - (1-a) \, \mathbf{u} c - \alpha \dot{W}_t^Q c \right) & \text{dans } \Omega(t) \setminus N(t), \quad (4g)\\
\left(\nabla c + a \mathbf{u} c - \alpha \dot{W}_t^Q c \right) \cdot \mathbf{n} = 0 & \text{sur } \partial(\Omega(t) \setminus N(t)), \quad (4h)\\
\Omega(t) = B(0, R_0) + \displaystyle\int_0^t \mathbf{u}_{\text{cm}}(s) \, \mathrm{d}s, & (4i)\\
N(t) = B(0, R_{\text{nucl}}) + \displaystyle\int_0^t \mathbf{u}_{\text{nucl}}(s) \, \mathrm{d}s. & (4j)
\end{cases}
$$

Lorsque le bruit est négligé, ce modèle admet un unique état stationnaire donné par :

$$\begin{cases} \mathbf{u}^0(\mathbf{x}) = 0, & \mathbf{x} \in \Omega^0 \setminus N^0, \quad (5a) \\ P^0(\mathbf{x}) = 0, & \mathbf{x} \in \Omega^0 \setminus N^0, \quad (5b) \\ \mathbf{u}^0_{\mathrm{nucl}} = 0, & (5c) \\ \mathbf{u}^0_{\mathrm{cm}} = 0, & (5d) \\ c^0(\mathbf{x}) = \dfrac{M}{|\Omega^0 \setminus N^0|}, & \mathbf{x} \in \Omega^0 \setminus N^0, \quad (5e) \\ \Omega^0 = B(0, R_0) \text{ et } N^0 = B(0, R_{\mathrm{nucl}}). & (5f) \end{cases}$$

Nous posons $\chi_c^* = \dfrac{1}{ac^0 f'_{\mathrm{act}}(c^0)}$. Le théorème suivant est également démontré :

Théorème. *Lorsque $\xi_{\mathrm{nucl}} = 1$, si $\chi_c < \chi_c^*$, alors l'état stationnaire (5) est linéairement stable. À l'opposé, si $\chi_c > \chi_c^*$, alors l'état stationnaire (5) est linéairement instable.*

Ce théorème est démontré en trois étapes. Premièrement, nous linéarisons le problème (4) autour de l'état stationnaire (5). Nous en déduisons un problème aux valeurs propres. Deuxièmement, nous étudions le signe des parties réelles des valeurs propres. L'état stationnaire est stable si toutes les valeurs propres sont de partie réelle négative et instable sinon. Pour cela, à l'aide de l'analyse de Fourier, nous décomposons le problème aux valeurs propres en des problèmes plus simples. Enfin, nous dérivons des problèmes plus simples, une condition explicite sur les valeurs propres. Nous montrons alors que lorsque $\chi_c > \chi_c^*$ il existe une valeur propre dont la partie réelle est positive et que lorsque $\chi_c < \chi_c^*$ toutes les valeurs propres ont une partie réelle négative. Ce raisonnement est inspiré de ceux menés par Alazard et al. (2022); Lavi et al. (2020).

Enfin, un schéma numérique aux volumes finis est écrit. Ce schéma s'appuie sur les mêmes éléments que ceux développés pour les modèles de la couronne et avec une particule. Les simulations numériques effectuées sont comparées avec celles obtenues aux chapitres 4 et 5. Celles-ci mettent en avant que la dynamique du noyau promeut le caractère intermittent des trajectoires. Ce modèle permet également de mettre en avant le lien entre le positionnement du noyau à l'intérieur de la cellule et la polarisation de la cellule.

Les simulations numériques permettent également de valider une autre approche, plus heuristique, pour modéliser les forces qui s'appliquent entre le noyau et le bord de la cellule.

Étude du modèle déformable : Le chapitre 7 est dédié à l'étude du modèle déformable avec la dynamique du noyau. Le modèle étudié est donné par :

$$\begin{cases} \mathbf{u} + \nabla P = 0 & \text{dans } \Omega(t) \setminus N(t), & \text{(6a)} \\ \operatorname{div}(\mathbf{u}) = 0 & \text{dans } \Omega(t) \setminus N(t), & \text{(6b)} \\ V_n = \mathbf{u} \cdot \mathbf{n} & \text{sur } \partial\Omega(t), & \text{(6c)} \\ P = \gamma\kappa + \chi_c f_{\text{act}}(c) - f_{\text{NB}} & \text{sur } \partial\Omega(t), & \text{(6d)} \\ \mathbf{u}_{\text{nucl}}(t) = \dfrac{1}{\xi_{\text{nucl}} |N|} \left(\displaystyle\int_{\partial N(t)} P(t,\mathbf{x}) \mathbf{n} \, \mathrm{d}\sigma + \mathbf{f}_{\text{BN}} \right) & & \text{(6e)} \\ \mathbf{u} \cdot \mathbf{n} = \mathbf{u}_{\text{nucl}} \cdot \mathbf{n} & \text{sur } \partial N(t), & \text{(6f)} \\ \partial_t c = \operatorname{div}(\nabla c - (1-a)\mathbf{u}c) & \text{dans } \Omega(t) \setminus N(t), & \text{(6g)} \\ (\nabla c + a\mathbf{u}c) \cdot \mathbf{n} = 0 & \text{sur } \partial(\Omega(t) \setminus N(t)), & \text{(6h)} \\ c(0,\mathbf{x}) = c^{\text{in}}(\mathbf{x}) & \text{dans } \Omega(0) \setminus N(0). & \text{(6i)} \end{cases}$$

Nous montrons l'existence d'un unique état stationnaire radialement symétrique défini par :

$$\begin{cases} \mathbf{u}^0(\mathbf{x}) = 0, & \mathbf{x} \in \Omega^0 \setminus N^0 & \text{(7a)} \\ P^0(\mathbf{x}) = \dfrac{\gamma}{R_0} + \chi_c f_{\text{act}}(c^0) - \dfrac{\delta R_0}{(R_0 - R_{\text{nucl}})^\beta}, & \mathbf{x} \in \Omega^0 \setminus N^0 & \text{(7b)} \\ \mathbf{u}^0_{\text{nucl}} = 0, & & \text{(7c)} \\ c^0(\mathbf{x}) = \dfrac{M}{|\Omega^0 \setminus N^0|}, & \mathbf{x} \in \Omega^0 \setminus N^0 & \text{(7d)} \\ \Omega^0 = B(0,R_0) \text{ et } N^0 = B(0,R_{\text{nucl}}), & & \text{(7e)} \end{cases}$$

où $R_0 = \sqrt{\frac{A_\Omega}{\pi}}$. Nous posons $\chi_c^* = \dfrac{1}{ac^0 f'_{\text{act}}(c^0)}$ et montrons le résultat suivant :

Théorème. *Lorsque $\xi_{\text{nucl}} = 1$, si $\chi_c < \chi_c^*$, alors l'état stationnaire (7) est linéairement stable. À l'opposé, si $\chi_c > \chi_c^*$, alors l'état stationnaire (7) est linéairement instable.*

Pour démontrer ce résultat, premièrement, nous linéarisons le problème (6) autour de l'état stationnaire (7) et en déduisons un problème aux valeurs propres. Ensuite, à l'aide de l'analyse de Fourier, nous décomposons le problème aux valeurs propres en des problèmes plus simples indexés par $m \in \mathbb{N}$. Nous montrons que pour les cas $m = 0$ et $m \geq 2$ alors toutes les valeurs propres sont de partie réelle négative. L'étude du cas $m = 1$ montre que lorsque $\chi_c > \chi_c^*$ il existe une valeur propre dont la partie réelle est positive et que lorsque $\chi_c < \chi_c^*$ toutes les valeurs propres ont une partie réelle négative. Ce raisonnement est inspiré de ceux menés par Alazard et al. (2022); Lavi et al. (2020).

Nous proposons un schéma numérique pour simuler ce modèle. Ce schéma numérique est un schéma semi-implicite en temps et avec une discrétisation aux éléments finis en espace. Ce schéma s'appuie sur une discrétisation implicite de la courbure qui est liée à la minimisation du périmètre de la cellule (Lavi et al., 2023). Pour éviter les potentiels contacts entre le bord de la cellule et le noyau, deux méthodes sont proposées. L'une repose sur la projection des vitesses dans un espace de vitesses admissibles, ce qui est réalisé via un algorithme d'Uzawa (Lefebvre, 2007). L'autre repose sur l'ajout d'une force répulsive de contact entre le bord de la cellule et le noyau. Les simulations numériques effectuées via ce schéma permettent de

mettre en avant que le modèle permet de reproduire de manière qualitative le phénomène de polarisation et de migration cellulaire. En effet, comme illustré par la figure 3, nous observons que pour certains paramètres, après une perturbation de l'état stationnaire, la cellule se polarise puis migre à une vitesse constante.

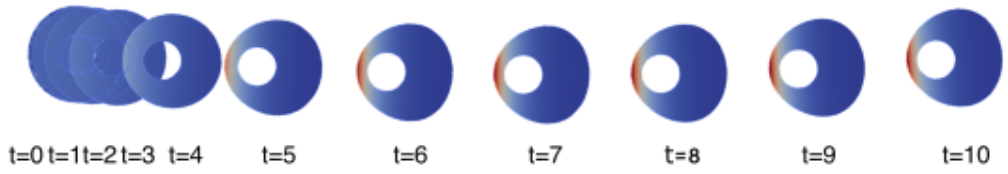

Figure 3: **Illustration du phénomène de polarisation suivi de la migration cellulaire.** *La cellule est représentée aux temps $t \in \{0, 1, 2, \ldots, 9, 10\}$. Nous observons que jusqu'au temps $t = 6$, la cellule se polarise : le noyau de la cellule est placé à l'arrière de la cellule et la concentration en marqueurs augmente dans cette zone (les zones rouges représentent les zones où la concentration en marqueurs est haute). Ensuite, lorsque $t \geq 6$, il semble qu'une onde progressive est atteinte. En effet, nous observons que la forme de la cellule est conservée au cours du temps, que la cellule semble se déplacer à une vitesse constante et que dans le référentiel de la cellule, la concentration de marqueurs et la position du noyau sont fixes. Voir fig. 7.9 pour plus de détails.*

Un modèle heuristique en dimension 1 : Le chapitre 8 est consacré à l'étude d'un modèle heuristique en dimension 1 de la motilité cellulaire avec prise en compte du noyau. Ces travaux sont effectués en collaboration avec Thomas Lepoutre et Nicolas Meunier. La modélisation choisie pour ce modèle diffère du cadre présenté précédemment. Nous supposons que les marqueurs peuvent s'attacher et se détacher de la membrane de la cellule et que le taux d'attachement dépend de la position du noyau tandis que le taux de détachement est constant. Le modèle, dans le référentiel de la cellule est donné par :

$$\begin{cases} \partial_t c\,(t,x) = \partial^2_{xx} c\,(t,x) + \partial_x \left[\eta\, \delta\mu\,(t)\, c\,(t,x)\right], & x \in]-1,1[, \quad \text{(8a)} \\ \partial_x c\,(t,\pm 1) + \eta\, \delta\mu\,(t)\, c\,(t,\pm 1) = \mp \dfrac{\mathrm{d}}{\mathrm{d}t}\mu_\pm\,(t), & \text{(8b)} \\ \dfrac{\mathrm{d}}{\mathrm{d}t}\mu_\pm\,(t) = \alpha_\pm\,(X_N\,(t))\, c\,(t,\pm 1) - \beta \mu_\pm\,(t), & \text{(8c)} \\ X_N\,(t) = X_N^0 e^{-k_1 t} - k_2 \displaystyle\int_0^t \delta\mu\,(s)\, e^{k_1(s-t)}\, \mathrm{d}s, & \text{(8d)} \\ c\,(0,x) = c^0\,(x),\ \mu_\pm\,(0) = \mu_\pm^0,\ X_N\,(0) = X_N^0, & x \in]-1,1[, \quad \text{(8e)} \end{cases}$$

avec c^0, $\mu_\pm^0$ et X_N^0, la condition initiale, donnés. Le modèle considéré est une équation nonlocale, non-linéaire de Fokker-Planck. À l'aide de l'étude d'un problème découplé et d'un argument de point fixe, nous montrons que, sous certaines conditions sur la condition initiale, le modèle (8) est bien posé.

Proposition. *Supposons que c^0 est tel que $\int_{-1}^1 c^0\,(x) \log c^0\,(x)\ \mathrm{d}x < +\infty$. Supposons également que $\mu_+^0, \mu_-^0 \in [0, M]$ sont tels que $\int_{-1}^1 c^0\,(x)\ \mathrm{d}x + \mu_+^0 + \mu_-^0 = M$. Supposons de plus que $X_N^0 \in [-1, 1]$. Alors il existe une unique solution (c, μ_+, μ_-, X_N) au modèle (8) définie pour tout temps.*

Nous montrons que le modèle (8) admet un état stationnaire non-polarisé. Nous montrons également que sous certaines conditions, le modèle admet des ondes progressives. Enfin, à l'aide d'un schéma numérique aux volumes finis, nous présentons des simulations numériques qui illustrent que cette heuristique permet de retrouver, pour certains paramètres, le comportement intermittent des trajectoires. Nous observons que la polarisation de la cellule s'accompagne du positionnement du noyau à l'arrière de la cellule. La dynamique d'attachement modifiée par la présence du noyau semble permettre la dépolarisation de la cellule et l'observation de comportements intermittents.

Étude de l'effet de l'undercooling sur la motilité cellulaire

Dans le chapitre 9, l'effet de l'undercooling sur le motilité cellulaire est étudié. Le modèle étudié ne prend plus en compte le noyau et sa dynamique. Il est donné par l'expression suivante :

$$\begin{cases} \mathbf{u} + \nabla P = 0 & \text{dans } \Omega(t), & \text{(9a)} \\ \operatorname{div}(\mathbf{u}) = 0 & \text{dans } \Omega(t), & \text{(9b)} \\ V_n = \mathbf{u} \cdot \mathbf{n} & \text{sur } \partial\Omega(t), & \text{(9c)} \\ P = \gamma\kappa + \chi_c f_{\text{act}}(c) + \chi_u f_{\text{und}}(V_n) & \text{sur } \partial\Omega(t), & \text{(9d)} \\ \partial_t c = \operatorname{div}(\nabla c - (1-a)\,\mathbf{u}c) & \text{dans } \Omega(t), & \text{(9e)} \\ (\nabla c + a\mathbf{u}c) \cdot \mathbf{n} = 0 & \text{sur } \partial\Omega(t), & \text{(9f)} \\ c(0,\mathbf{x}) = c^{\text{in}}(\mathbf{x}) & \text{dans } \Omega(0). & \text{(9g)} \end{cases}$$

Ce modèle peut être vu comme un enrichissement du modèle de Lavi et al. (2020) qui est retrouvé lorsque $\chi_u = 0$. Nous montrons que ce modèle (9) admet un unique état stationnaire donné par :

$$\begin{cases} c^0(\mathbf{x}) = \dfrac{M}{|\Omega|} & \mathbf{x} \in \Omega^0, & \text{(10a)} \\ P^0(\mathbf{x}) = \dfrac{\gamma}{R_0} + \chi_c f_{\text{act}}\left(c^0(\mathbf{x})\right) & \mathbf{x} \in \Omega^0, & \text{(10b)} \\ \mathbf{u}^0(\mathbf{x}) = 0 & \mathbf{x} \in \Omega^0, & \text{(10c)} \\ \Omega^0 = B(0, R_0), & & \text{(10d)} \end{cases}$$

où $R_0 = \sqrt{\dfrac{A_\Omega}{\pi}}$. Nous posons $\chi_c^* = \dfrac{R_0 + \chi_u f'_{\text{und}}(0)}{R_0 a c^0 f'_{\text{act}}(c^0)}$ et montrons le résultat suivant qui permet de dire que l'undercooling a un effet stabilisant. En effet, le seuil χ_c^* est plus grand lorsque l'undercooling est pris en compte que lorsqu'il est absent.

Théorème. *Si* $\dfrac{\chi_c}{\chi_c^*} < 1$ *alors l'état stationnaire* (10) *est linéairement stable. À l'opposé, si* $\dfrac{\chi_c}{\chi_c^*} > 1$, *alors l'état stationnaire* (10) *est linéairement instable.*

Pour montrer ce théorème, en s'inspirant de Alazard et al. (2022); Lavi et al. (2020), dans un premier temps nous linéarisons le modèle (9) autour de l'état stationnaire (10). Nous déduisons du problème linéarisé un problème aux valeurs propres. Pour étudier le signe de la partie réelle des valeurs propres, nous décomposons le problème aux valeurs propres en des problèmes plus simples à l'aide de l'analyse de Fourier. Nous montrons que lorsque $\dfrac{\chi_c}{\chi_c^*} < 1$ alors toutes les valeurs propres ont une partie réelle négative. Nous déduisons une condition explicite sur les valeurs propres et montrons que lorsque $\dfrac{\chi_c}{\chi_c^*} > 1$, il existe une valeur propre de partie réelle positive.

Ensuite, nous étudions l'existence d'ondes progressives. Nous caractérisons les ondes progressives du modèle (9) et montrons que si une onde progressive existe alors elle est de la forme donnée par le résultat suivant :

Proposition. *Soit $V > 0$ donné. L'onde progressive associée à la vitesse V est donnée pour tout $(x, y) \in \tilde{\Omega}$ par :*

$$\begin{aligned} P(x,y) &= p_1 - Vx && \text{avec } p_1 \in \mathbb{R}, \\ c(x,y) &= \frac{M}{\int_{\tilde{\Omega}} e^{-aVx'} \,\mathrm{d}x' \,\mathrm{d}y'} e^{-aVx}, \end{aligned}$$

avec $\partial\tilde{\Omega}$ caractérisé par l'équation sur la courbure suivante :

$$\gamma\kappa(x,y) = p_1 - Vx - \chi_c f_{\mathrm{act}}\left(\frac{Me^{-aVx}}{\int_{\tilde{\Omega}} e^{-aVx'} \,\mathrm{d}x' \,\mathrm{d}y'}\right) - \chi_u f_{\mathrm{und}}(Vn_x),$$

où $(x, y) \in \partial\tilde{\Omega}$.

Soit X et Y les espaces fonctionnels suivants :

$$\begin{aligned} X &= \left\{\rho \in \mathcal{C}^{2,\alpha}_{\mathrm{per}}(-\pi,\pi) : \rho(\theta) = \rho(-\theta), \forall\theta \in (-\pi,\pi)\right\}, \\ Y &= \left\{\rho \in \mathcal{C}^{0,\alpha}_{\mathrm{per}}(-\pi,\pi) : \rho(\theta) = \rho(-\theta), \forall\theta \in (-\pi,\pi)\right\}. \end{aligned}$$

En montrant que la fonctionnelle $\mathcal{F} : \mathbb{R}\times X\times\mathbb{R}\times\mathbb{R} \to Y\times\mathbb{R}\times\mathbb{R}$ définie pour tout $(\chi_c, \rho, V, p_1) \in \mathbb{R}\times X\times\mathbb{R}\times\mathbb{R}$ par :

$$\begin{aligned} \mathcal{F}(\chi_c,\rho,V,p_1) = \Big(&\gamma\kappa(\theta) + \chi_c f_{\mathrm{act}}\left(c_1(V,\rho)\, e^{-aV(R_0+\rho(\theta))\cos\theta}\right) + \chi_u f_{\mathrm{und}}(Vn_1(\theta)) \\ &+ V(R_0+\rho(\theta))\cos\theta - p_1 - \frac{\gamma}{R_0}; \\ &\int_{-\pi}^{\pi} (R_0+\rho(\theta))^2 - R_0^2 \,\mathrm{d}\theta; \int_{-\pi}^{\pi} \rho(\theta)\cos\theta \,\mathrm{d}\theta\Big). \end{aligned}$$

satisfait le théorème de bifurcation de Crandall and Rabinowitz (1971), nous montrons l'existence d'ondes progressives pour le modèle (9) :

Théorème. *Pour tout $a \in (0, 1]$, $\gamma > 0$, $R_0 > 0$ et $\chi_u > 0$ il existe une famille d'ondes progressives au problème (9) $\left(\tilde{\Omega}_\chi, V_\chi\right)$ paramétrée par $\chi \in (\chi_c^*, +\infty)$ telle que $\left|\tilde{\Omega}_\chi\right| = \pi R_0^2$.*

Étude de l'impact d'un signal extérieur sur la motilité cellulaire

Le chapitre 10 est consacré à l'étude de l'impact d'un signal extérieur sur la motilité cellulaire. Le modèle étudié est le suivant :

$$\begin{cases} \mathbf{u} + \nabla P = 0 & \text{dans } \Omega(t), & \text{(11a)} \\ \operatorname{div}(\mathbf{u}) = 0 & \text{dans } \Omega(t), & \text{(11b)} \\ P = \gamma\kappa + \chi_c f_{\mathrm{act}}(c) + \chi_s g(\nabla s\cdot\mathbf{n}) & \text{sur } \partial\Omega(t), & \text{(11c)} \\ V_n = \mathbf{u}\cdot\mathbf{n} & \text{sur } \partial\Omega(t), & \text{(11d)} \\ \partial_t c = \operatorname{div}(\nabla c - (1-a)\,\mathbf{u}c) & \text{dans } \Omega(t), & \text{(11e)} \\ (\nabla c + a\mathbf{u}c)\cdot\mathbf{n} = 0 & \text{sur } \partial\Omega(t), & \text{(11f)} \\ c(0,\mathbf{x}) = c^{\mathrm{in}}(\mathbf{x}) & \text{dans } \Omega(0). & \text{(11g)} \end{cases}$$

Sous l'hypothèse que le signal extérieur est radialement symétrique c'est à dire qu'il existe $\psi_s : \mathbb{R}^+ \longrightarrow \mathbb{R}$ telle que pour tout $\mathbf{x} \in \mathbb{R}^2$, le signal extérieur s'écrit $s(\mathbf{x}) = \psi_s(\|\mathbf{x}\|)$, nous montrons l'existence d'un unique état stationnaire radialement symétrique donné par :

$$\begin{cases} \mathbf{u}^0 = 0 & \text{dans } \Omega^0, \quad (12a) \\ P^0 = \dfrac{\gamma}{R_0} + \chi_c f_{\text{act}}\left(c^0\right) + \chi_s g\left(s'\left(R_0\right)\right) & \text{dans } \Omega^0, \quad (12b) \\ c^0 = \dfrac{M}{\pi R_0^2} & \text{dans } \Omega^0, \quad (12c) \\ \Omega^0 = B\left(0, R_0\right), & (12d) \end{cases}$$

où $R_0 = \sqrt{\frac{A_\Omega}{\pi}}$. La stabilité de l'état stationnaire est étudiée dans le cas où le signal est, en plus, monotone, c'est à dire qu'il existe $\eta \in \mathbb{R}$ et $\psi_s : \mathbb{R}^+ \longrightarrow \mathbb{R}^+$ fonction monotone telle que pour tout $\mathbf{x} \in \mathbb{R}^2$, le signal extérieur s'écrit $s(\mathbf{x}) = \eta\psi_s(\|\mathbf{x}\|)$. Nous avons alors le résultat suivant :

Théorème. *Soit* $K_s = \chi_s g'\left(s'\left(R_0\right)\right) s''\left(R_0\right)$ *et* $\chi_c^* = \dfrac{1}{ac^0 f'_{\text{act}}\left(c^0\right)}$. *Si* $K_s > 0$, *alors nous avons :*

1. *Si* $0 < \dfrac{\chi_c}{\chi_c^*} \leq 1$ *alors l'état stationnaire* (12) *est linéairement stable.*
2. *Si* $\dfrac{\chi_c}{\chi_c^*} > 1 + \frac{3}{8} K_s R_0$ *alors l'état stationnaire est linéairement instable.*

La démonstration de ce théorème s'inspire de Alazard et al. (2022). Dans un premier temps nous linéarisons le modèle (11) autour de l'état stationnaire (12). Nous déduisons du problème linéarisé un problème aux valeurs propres. Pour étudier le signe de la partie réelle des valeurs propres, nous décomposons le problème aux valeurs propres en des problèmes plus simples à l'aide de l'analyse de Fourier. Nous montrons que lorsque $0 < \dfrac{\chi_c}{\chi_c^*} \leq 1$ alors $\lambda = 0$ est une valeur propre de multiplicité 2 et toutes les autres valeurs propres sont de partie réelle négative. Nous montrons que lorsque $\dfrac{\chi_c}{\chi_c^*} > 1 + \frac{3}{8} K_s R_0$, il existe une valeur propre de partie réelle positive. Nous étudions également le problème rigide associé.

Nous proposons un schéma numérique aux élements finis pour le problème rigide. Les simulations numériques effectuées permettent d'illustrer qu'il existe un équilibre entre la force induite par les marqueurs sur le bord de la cellule et celle induite par le signal extérieur. Enfin, l'étude de l'impact de la présence d'obstacles dans l'environnement de la cellule y est brièvement abordée sous le point de vue numérique. Cette étude sera approfondie dans de futurs travaux.

Modélisation de la compartimentation au sein de la voie de signalisation intracellulaire

Enfin, le chapitre 11 présente un travail effectué durant l'école d'été CEMRACS 2022 en collaboration avec Juan Calvo, Erwan Hingant, Saoussen Latrach, Nathan Quiblier et Romain Yvinec. Ce travail est soumis et accepté. Nous présentons une nouvelle approche de modélisation des voies de signalisation activées par les récepteurs, qui prend en compte la compartimentation des récepteurs et de leurs effecteurs, à la fois à la surface cellulaire et dans des vésicules intracellulaires dynamiques appelées endosomes. Le premier élément constitutif du modèle concerne la dynamique des compartiments. Il prend en compte la création

d'endosomes *de novo*, c'est-à-dire l'endocytose, puis le recyclage des endosomes à la surface cellulaire ou leur dégradation, ainsi que la fusion des endosomes via une dynamique de coagulation. Le deuxième élément constitutif concerne les réactions biochimiques à la surface des cellules et dans chaque compartiment intracellulaire. Les deux parties du modèles sont couplées par le transfert de molécules qui se produit à chaque événement modifiant les compartiments.

Le modèle est formulé comme une équation aux dérivées partielles avec terme intégrale, avec des opérateurs de transport, de coagulation et des termes sources, couplée à une équation intégro-différentielle. Dans ce travail, nous prouvons des conditions suffisantes pour obtenir une ergodicité exponentielle pour la distribution en taille des compartiments intracellulaires. Nous concevons en outre un schéma de volumes finis pour simuler notre modèle. Enfin, nous montrons deux cas d'application qui montrent un accord qualitatif avec des données publiées récemment, prouvant que notre modèle peut aider à capturer la complexité spatio-temporelle de l'activation des voies de signalisation.

Références

Abercrombie, M. (1980). The Croonian Lecture, 1978 - The crawling movement of metazoan cells. Proceedings of the Royal Society of London. Series B. Biological Sciences, 207(1167):129–147. 1

Alazard, T., Magliocca, M., and Meunier, N. (2022). Traveling wave solution for a coupled incompressible Darcy's free boundary problem with surface tension. arXiv:2205.04365 [math]. 9, 10, 12, 14

Boulakia, M., Genadot, A., and Thieullen, M. (2015). Simulation of SPDEs for Excitable Media Using Finite Elements. Journal of Scientific Computing, 65(1):171–195. 8

Crandall, M. G. and Rabinowitz, P. H. (1971). Bifurcation from simple eigenvalues. Journal of Functional Analysis, 8(2):321–340. 13

Danuser, G., Allard, J., and Mogilner, A. (2013). Mathematical Modeling of Eukaryotic Cell Migration: Insights Beyond Experiments. Annual Review of Cell and Developmental Biology, 29(1):501–528. 1

Lavi, I., Meunier, N., and Pantz, O. (2023). Implicit like time discretization for the one-phase Hele-Shaw problem with surface tension. arXiv:2305.06180 [cs, math]. 10

Lavi, I., Meunier, N., Voituriez, R., and Casademunt, J. (2020). Motility and morphodynamics of confined cells. Physical Review E, 101(2):022404. Publisher: American Physical Society. 2, 9, 10, 12

Lefebvre, A. (2007). Modélisation numérique d'écoulements fluide/particules. phdthesis, Université Paris Sud. 4, 10

Maiuri, P., Rupprecht, J.-F., Wieser, S., Ruprecht, V., Bénichou, O., Carpi, N., Coppey, M., De Beco, S., Gov, N., Heisenberg, C.-P., Lage Crespo, C., Lautenschlaeger, F., Le Berre, M., Lennon-Dumenil, A.-M., Raab, M., Thiam, H.-R., Piel, M., Sixt, M., and Voituriez, R. (2015).

Actin Flows Mediate a Universal Coupling between Cell Speed and Cell Persistence. Cell, 161(2):374–386. 1, 2

Reig, G., Pulgar, E., and Concha, M. L. (2014). Cell migration: from tissue culture to embryos. Development, 141(10):1999–2013. 1

Thiam, H.-R. (2014). Cell migration under confinement: how can a cell squeeze through narrow gaps? 2

1 - Biological context and modelling

1.1 . Biological context

1.1.1 . Cell organisation

The cell is regarded as the fundamental unit of life, as all living organisms are made up of cells. Although cells can greatly vary in size, shape and function, they all behave according to the same principles. There are two main types of cells: eukaryotic cells which have nuclei, and prokaryotic cells which lack nuclei. In this thesis, we focus on eukaryotic cells, which are animals, plants, and fungi cells. We briefly present here the structure of a cell (see fig. 1.1 for a schematic view).

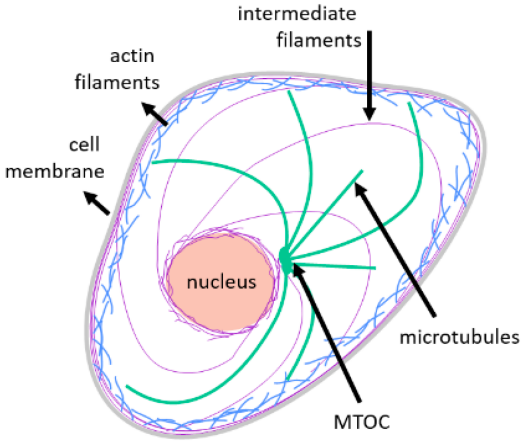

Figure 1.1: **Schematic representation of a cell.** *Taken from Kubiak et al. (2020).*

The cell is enclosed by the plasma membrane. It protects and separates the contents of the cell from the external environment. It also enables communication with the external environment. It is made up of a lipid bilayer formed from phospholipid molecules and containing proteins. The plasma membrane contributes to the mechanical properties of cell movement via membrane tension. Membrane tension induces an opposite force to membrane extension. It results from the inextensible nature of the bilayer, which creates in-plane tension, and from the energy derived from adhesion between the cytoskeleton and the membrane. As the cell is deformed, membrane tension changes rapidly, causing the cell surface tension to vary. Membrane tension also regulates polarisation between the front and rear of the cell (Thiam, 2014). However, the length of the membrane can vary, particularly as a result of endocytosis, exocytosis or invagination (Kosmalska et al., 2015).

The cytoplasm and the nucleus are within the plasma membrane. The cytoplasm is made up of several organelles and the cytosol. The organelles are cell structures separated from the cytosol and enclosed by the plasma membrane. They carry out many essential functions for the cell. Mitochondria — which are involved in cellular respiration — are one example. The cytosol is an aqueous gel containing numerous molecules and proteins, including the

cytoskeleton—a network of protein filaments. Three types of filament can be distinguished: actin filaments, intermediate filaments and microtubules. The cytoskeleton plays a very important role in the cell's shape and ability to move (Alberts et al., 2002).

Actin filaments are the thinnest. They are composed of actin. Actin is present in two forms in the cell: globular actin in monomeric form and filamentous actin in polymeric form. When the concentration of monomeric actin exceeds a critical threshold, actin polymerises at the filament end present in that zone. Conversely, if one end of an actin filament is located where the concentration of globular actin is below the critical threshold, the filament depolymerises. Actin filaments are polarised, with a plus end and a minus end. Each end has a different critical threshold, which allows actin filaments to grow asymmetrically (Asnacios and Hamant, 2012). Thus an actin monomer moves in the actin filament from the plus end to the minus end — a process known as treadmilling (see fig. 1.2). This also results in a retrograde flow of actin monomers from the boundary of the cell towards the interior. The more actin polymerises, the greater this retrograde flow.

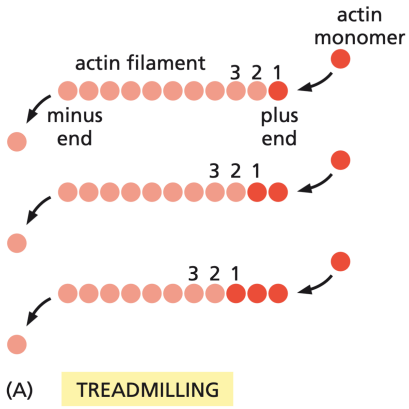

Figure 1.2: **Schematic representation of actin treadmilling.** *Taken from Alberts et al. (2002).*

Actin filaments can assemble with different molecules. For example, by associating with the Arp 2/3 molecule, actin filaments can form a network and bind to the plasma membrane to form the cell cortex. Also, by associating with myosin, they create stress fibres that allow the cell to contract when moving.

Microtubules are the thickest and most rigid filaments. They are composed of tubulin and are also polarised filaments. One of their ends is always connected to the centrosome (or MTOC) located near the nucleus. They are particularly essential in the process of cell division and the internal organisation of the cell.

Intermediate filaments have a thickness between that of actin filaments and microtubules. They constitute a family of non-polarised filaments and are composed of a wide variety of proteins. Intermediate filaments differ according to cell types. They form a network surrounding the nucleus and are connected to the cell plasma membrane. Specifically, they create a mesh around the nucleus called the nuclear lamina which increases the rigidity of the nuclear envelope (Lammerding, 2011). These filaments are not polarised and rarely depolymerise. Their stability allows them to support the structure of the cell (Ndiaye et al., 2022; Cooper, 2000).

The nucleus is the largest organelle in the cell. Like all organelles, it is membrane enclosed.

It is composed of a nuclear envelope and contains the organism's genetic information encoded in DNA molecules. The interior of the nucleus is made up of the nucleoplasm which, like the cytoplasm, is made up of an aqueous gel containing proteins (in particular DNA), including actin filaments. It is able to deform as the shape of the cell varies. When the cell is compressed, the nucleus shrinks, whereas when the cell contracts, the nucleus becomes rounder. The nucleus is linked to the cytoskeleton by LINC, a protein complex. This contributes to the transmission of forces from the nucleus to the cell and from the cell to the nucleus (Thiam, 2014; Lammerding, 2011).

1.1.2 . Cell motility

Cell motility is an important mechanism in several biological phenomena such as embryogenesis, wound healing, the immune response and the spread of cancer. It is the ability of a cell to move by deforming its shape. This movement can be spontaneous or induced in response to an external cause. To initiate movement, the cell needs to polarise. Polarisation breaks the symmetry of the non-motile cell resulting in cells with defined front and rear (Danuser et al., 2013; Reig et al., 2014). Once the cell is polarised, cell migration consists of a four-step cycle (Danuser et al., 2013; Abercrombie, 1980).

Polarisation. The phenomenon of polarisation enables a cell to switch from a symmetrical non-polarised state to an asymmetrical polarised one. This phenomenon triggers cell motility. It can occur spontaneously through the self-reorganisation of the cytoskeleton or in response to external factors that induce cytoskeletal reorganisation. Polarisation involves three phases (Yam et al., 2007). A schematic view of it is represented in fig. 1.3. Phase I is the slow rear retraction. Self-organisation of the actin cytoskeleton causes fluctuations in the contractility of actin-myosin filaments. Due to the increased contractility of the actin-myosin filaments at the prospective rear part of the cell, the actin retrograde flow increases and polarises near the nucleus in the direction of the potential motion. This causes the rear part to retract slightly and become thinner whereas there are no significant changes in what results as the front part. Phase II is the fast rear retraction. In the rear part, the contractility of the actin-myosin filaments and the actin retrograde flux increase. The actin filaments depolymerised. All this induces a loss of adhesion with the substrate and the retraction of the rear part. At this phase, the shape of the cell is no longer symmetric and the nucleus starts to be located at the rear part while there are still no significant changes in the front part. Phase III is the maturation. During this phase, all the rear collapse and the cell starts to move slowly. At the front part, the actin retrograde flux decreases, and the polymerisation of actin filaments increases. This initiate protrusion. The front part creates new adhesive bonds with the substrate. At the end of this phase, the cell is polarised and motion can be observed. It is important to notice that polarisation starts with the definition of the rear part (Cramer, 2010) and that the nucleus positioning at the cell's rear is independent of the cell's elongation and depends on the myosin (Gomes et al., 2005; Cramer, 2010).

Cell migration. Once the cell is polarised, cell migration can occur. This process is described by a four-step cycle (Abercrombie, 1980), as depicted schematically in fig. 1.4.

During the first step, actin polymerisation increases at the cell leading edge. This induces the protrusion of the lamellipodium, which is a thick and very thin layer of actin filaments as-

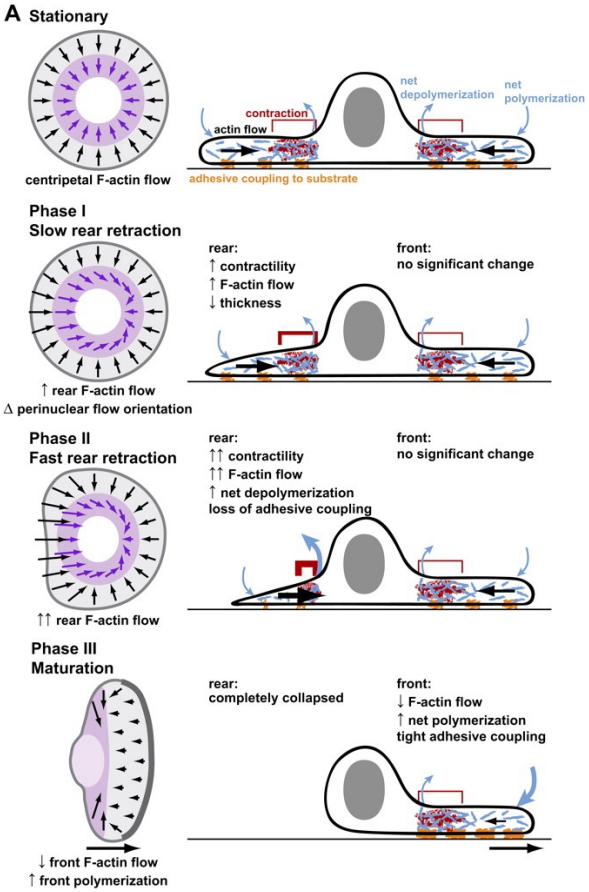

Figure 1.3: **Schematic representation of polarisation and of each phase involved in the transition from symmetrical to asymmetrical cell organisation.** *Taken from Yam et al. (2007).*

sembled in a mesh connected to the cytoplasmic membrane, and filopodia, which form when actin filaments bundle together in parallel arrays. This allows the creation of new adhesions with the substrate that are initially unstable. These adhesions mature during the second step, becoming stable focal contacts. At these points, the cell adheres strongly to the substrate. These focal contacts associate with stress fibres that are aligned in the direction of the cell's movement. The other end of the stress fibres is connected to the cytoskeleton in the region around the nucleus. Some may be linked to adhesion sites at the rear of the cell. During the third step, the stress fibres contract, pushing the nucleus and the surrounding cytoskeleton forward. This leads to the release of the old adhesions at the rear of the cell, allowing the rear of the cell to retract in the fourth step.

1.1.3 . Trajectories and UCSP law

Trajectories. Cell may have different motion behaviour. The trajectories can be very different. Cell trajectories can be classified into three groups (Maiuri et al., 2015).

First, cells may have a ballistic behavior even in the absence of external causes (Petrie et al., 2009; Bosgraaf and Van Haastert, 2009). In this case, the trajectory is said to be *persistent*. Cells

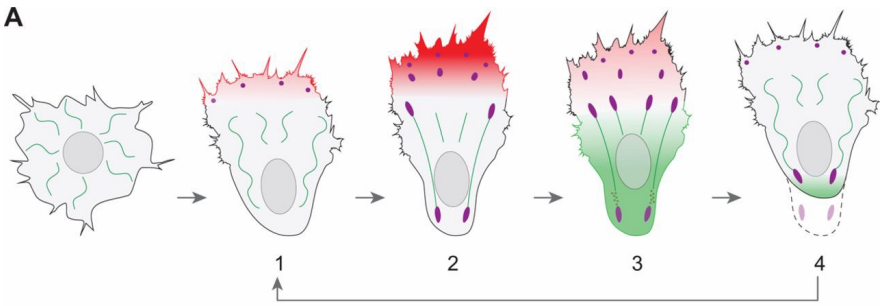

Figure 1.4: **Schematic representation of the four-step cycle of the cell migration.** *Actin polymerisation-dependent events are represented in red, myosin-dependent events in green and substrate adhesions in purple. Taken from Reig et al. (2014).*

with this type of trajectory are characterised by their ability to maintain their direction of motion. This property is called directional persistence or, when there is no ambiguity, simply persistence (Maiuri et al., 2015; Loosley et al., 2015). Persistence can be quantified in several different way, the first one is directionality or tortuosity which is defined as the ratio between displacement made by the cell and the total migration path length (Loosley et al., 2015; Petrie et al., 2009; Gorelik and Gautreau, 2014). Directionality quantifies the straightness of the trajectory and thus, persistence corresponds to directionality close to 1. The main defect of this quantity is that it is dependent on the sampling interval so this can lead to persistent trajectories with a directionality close to 0 (Loosley et al., 2015). Persistence can also be described through the properties of persistence time and persistence length. Persistence time is the time during which the cell maintains its original direction of motion. To quantify it, we consider the persistence time as the time required for the cell to change its original direction by at least $\frac{\pi}{2}$ (Maiuri et al., 2015). Other definitions of persistence time can be found in the literature (see for example (Gorelik and Gautreau, 2014; Selmeczi et al., 2008)). Persistence length is the length of the path covered during the persistence time. Associated with these two quantities we can define the mean instantaneous speed as the persistence length over the persistence time. We can then split a trajectory into sub-trajectories depending on its persistence times. A persistent trajectory is then a trajectory that can be partitioned into sub-trajectories with directionality close to 1 on them and a long persistence time. Moreover, when the cell exhibits ballistic behaviour, the cell is polarised. This means that persistent trajectories are characterised by long-lived polarisation time (Maiuri et al., 2015).

Secondly, cells may have a diffusive behaviour. In this case, the trajectory of the cell is said to be *brownian*. Brownian trajectories are characterised by the absence of a stable polarised state (Maiuri et al., 2015). This type of trajectory has a small persistence time and its directionality is close to 0.

Finally, cells may switch from a ballistic phase to a diffusive one (Bénichou et al., 2011). These trajectories are called *intermittent* because the cells switch between polarised and non-polarised phases.

UCSP law. Using the data of the first World Cell Race (Maiuri et al., 2012), a coupling between cell speed and cell persistence (UCSP law) was proved in Maiuri et al. (2015). The UCSP law was

first formulated at the scale of a population of cells. In this case, the cell persistence τ is the average of the persistence times of all the cells of the population and the cell speed ν is the average of all the mean instantaneous speed of the cell population. Then we have:

$$\tau \propto e^{\lambda\nu} \tag{UCSP}$$

with $\lambda > 0$.

It was also showed that the UCSP law is still valid a the cell scale. This means that there exists $\lambda > 0$ such that on each persistent sub-trajectory of a trajectory we have $\tau \propto e^{\lambda\nu}$ where τ is the persistence time of the sub-trajectory and ν the mean instantaneous speed (Maiuri et al., 2015). The fastest cells have a more directional movement whereas the slowest cells have a more diffusive movement. An illustration of the UCSP law is represented in fig. 1.5.

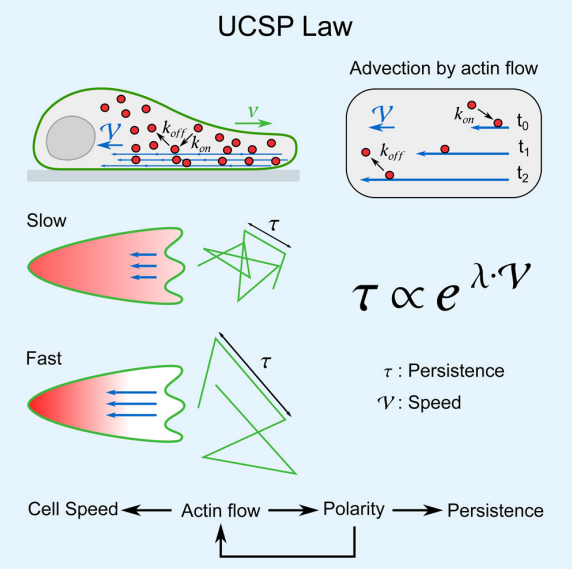

Figure 1.5: **Schematic summary of the UCSP law.** *Taken from Maiuri et al. (2015).*

1.2 . Existing models

Following the description of cell migration by Abercrombie (1980), various models have emerged to propose models of this phenomenon. Some models have focused on one of the steps of cell migration. These models provided a better understanding of the different processes involved in cell motility, for example the model of Mogilner and Oster (1996) has provided a better understanding of the mechanisms involved in actin polymerisation at the cell membrane (see Danuser et al. (2013) for others examples).

Other models have sought to model the cell by integrating all the mechanisms of cell motility into a single model. Several approaches have been proposed. These range from continuous to stochastic approaches. Among the stochastic approaches, we can mention the POTS model (Scianna and Preziosi, 2012), which allows the nucleus to be modelled. Continuous approaches are very varied. There is a wide variety of continuous approaches. In particular, the cell can be seen as a viscous fluid (Blanch-Mercader and Casademunt, 2013; Recho and Truskinovsky,

2013; Lavi et al., 2020). This view has led to the development of new theories in physics, such as the theory of active gels (Prost et al., 2015). Other continuous approaches have also been proposed such as viscoelastic material (Gracheva and Othmer, 2004), polarised gel (Kruse et al., 2005) or phase-field models (Berlyand et al., 2016).

The model studied in this thesis belongs to the models where the cell is seen as a viscous fluid. It is a free boundary model where the cell is represented by an incompressible fluid with surface tension. Similar models without the incompressibility assumption also exist for the study of tumour growth (Friedman and Reitich, 2000).

1.3 . Modelling

In this section we introduce the model studied in the rest of the thesis. First, we give its formulation. Then, in the following subsections, we detail the modelling steps that led to the formulation of the model. The model presented is a free boundary model modelling the cell motility of a cell on a heterogeneous substrate taking into account its nucleus and in the presence of external signals and obstacles.

1.3.1 . Model formulation

Let $\Omega(t) \subset \mathbb{R}^2$ be a connected open set, where $t \geq 0$ denotes time. Let $N(t)$ be a connected open set such that for all $t \geq 0$, $N(t) \subset \Omega(t)$. $\Omega(t)$ models the domain of the cell at time $t \geq 0$ and $N(t)$ the domain of the nucleus. The cytoplasm is therefore represented at time $t \geq 0$ by the domain $\Omega(t) \setminus N(t)$. We assume that this domain $\Omega(t) \setminus N(t)$ is filled with an incompressible fluid having velocity $\mathbf{u}$ and pressure P. Inside this fluid, there are polarity markers of concentration c. We assume that there are no markers outside the cell or in the nucleus and that the fluid cannot enter the nucleus. (See fig. 1.6 for the notations.)

As a first approximation, we assume the nucleus to be rigid. The cell can deform and we assume that the boundary $\partial\Omega$ is free. The model we propose is therefore a free-boundary model with a rigid particle inside. We study a system of equations on a time-dependent domain and whose evolution depends on the evolution of the system.

We assume that an external signal, $s(t, \mathbf{x})$ with $t \geq 0$ and $\mathbf{x} \in \mathbb{R}^2$, is present in the environment of the cell and that this signal induces a force on the cell boundary. We also assume that obstacles may be present in the environment of the cell and that these obstacles induce a contact force f_{obs} with the cell boundary.

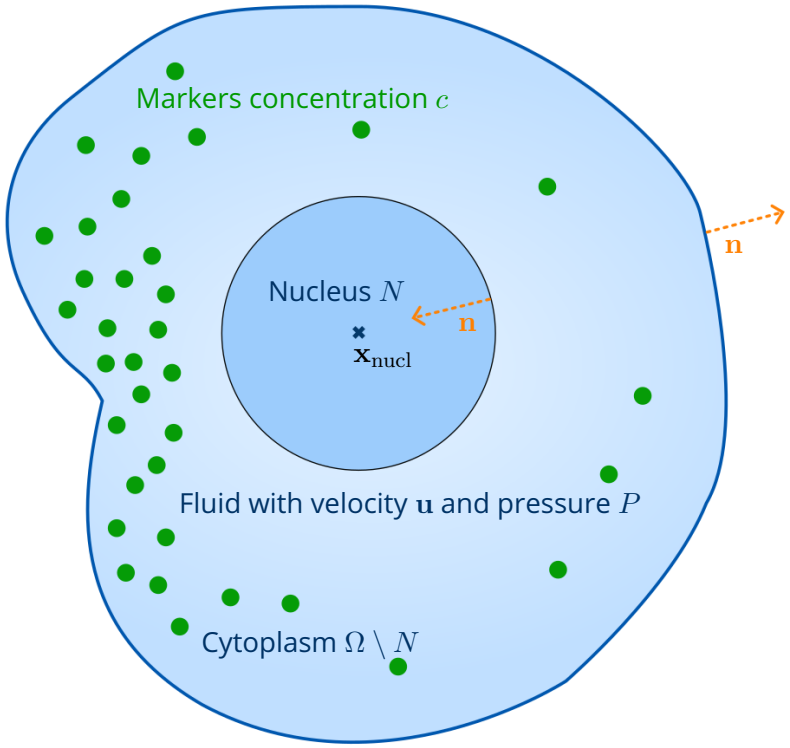

Figure 1.6: **Notations of the model.** *In very light blue is the fluid domain $\Omega(t) \setminus N(t)$ and in slighty darker is the nucleus domain $N(t)$. In green is the markers concentration c. In orange the outward normal vector to $\Omega(t) \setminus N(t)$ is represented on both domain boundaries.*

The model is given by the following system:

$$
\begin{cases}
\mathbf{u} + \xi_{\mathrm{M}} \nabla P = 0 & \text{in } \Omega(t) \setminus N(t), \quad (1.1a) \\
\operatorname{div}(\mathbf{u}) = 0 & \text{in } \Omega(t) \setminus N(t), \quad (1.1b) \\
V_n = \mathbf{u} \cdot \mathbf{n} & \text{on } \partial\Omega(t), \quad (1.1c) \\
P = \gamma\kappa + \chi_c f_{\text{act}}(c) + \chi_s g(\nabla s \cdot \mathbf{n}) - f_{\text{NB}} - f_{\text{obs}} + \chi_u f_{\text{und}}(V_n) & \text{on } \partial\Omega(t), \quad (1.1d) \\
\mathbf{u}_{\text{nucl}}(t) = \dfrac{1}{\xi_{\text{nucl}}(t)\,|N|} \left(\displaystyle\int_{\partial N(t)} P(t,\mathbf{x}) \mathbf{n} \, \mathrm{d}\sigma + \mathbf{f}_{\text{BN}} \right) & \quad (1.1e) \\
\mathbf{u} \cdot \mathbf{n} = \mathbf{u}_{\text{nucl}} \cdot \mathbf{n} & \text{on } \partial N(t), \quad (1.1f) \\
\partial_t c = \operatorname{div}\left(\nabla c - (1-a)\,\mathbf{u} c - \alpha \dot{W}_t^Q c \right) & \text{in } \Omega(t) \setminus N(t), \quad (1.1g) \\
\left(\nabla c + a\mathbf{u} c - \alpha \dot{W}_t^Q c \right) \cdot \mathbf{n} = 0 & \text{on } \partial(\Omega(t) \setminus N(t)), \quad (1.1h) \\
c(0,\mathbf{x}) = c^{\text{in}}(\mathbf{x}) & \text{in } \Omega(0) \setminus N(0), \quad (1.1i)
\end{cases}
$$

where

- ξ_{M} is a function depending on time and space such that for all $t \geq 0$ and $\mathbf{x} \in \mathbb{R}^2$ we have $\xi_M(t,\mathbf{x}) > 0$,

- κ is the curvature (positive for a circle) of the evolving free-boundary $\partial\Omega$ and $\gamma \geq 0$ is the surface tension,
- V_n is the normal velocity of the free-boundary $\partial\Omega$ and $\mathbf{n}$ the outward normal vector to $\Omega \setminus N$,
- $\chi_c > 0$, f_{act} is an active traction force depending on the markers concentration,
- $\chi_s > 0$, g is a force depending on the external signal s,
- $\chi_u > 0$, f_{und} is a force depending on the normal velocity of the boundary, which can be seen as undercooling,
- ξ_{nucl} is a function depending on time such that for all $t \geq 0$ we have $\xi_{\text{nucl}}(t) \neq 0$,
- f_{NB} is the force induced by the nucleus on the cell boundary and $\mathbf{f}_{\text{BN}}$ the force induced by the cell boundary on the nucleus,
- $a \in [0, 1]$,
- $\alpha \geq 0$ and $\dot{W}_t^Q$ the coloured noise associated with a Q-Wiener process,
- c^{in}, $\Omega(0)$, $N(0)$ are the initial conditions,
- σ denotes a measure on the boundary.

1.3.2 . Force balance on the fluid

In this subsection we detail the modelling developed to obtain the fluid dynamics within the fluid domain (eqs. (1.1a) and (1.1b)). To obtain this, we use several approximations for a fluid confined between two plates. Then, we present the kinematic conditions at the boundaries (eqs. (1.1c) and (1.1f)).

1.3.2.1 . Confined fluid approach

We consider the 3-dimensional framework. We assume that the cell is confined between two plates separated by a gap of size $h(\mathbf{x})$ with $\mathbf{x} \in \mathbb{R}^2$ (Lavi et al., 2020). We denote by $\Omega_h(t)$ the 3-dimensional fluid domain at time $t \geq 0$ and we have:

$$\Omega_h(t) = \left\{(x, y, z) \in \mathbb{R}^3 \text{ s.t. } (x, y) \in \Omega(t) \text{ and } z \in [0, h(x, y)]\right\}.$$

At time $t \geq 0$, the nucleus is then modelled by the domain $N_h(t)$ given by:

$$N_h(t) = \left\{(x, y, z) \in \mathbb{R}^3 \text{ s.t. } (x, y) \in N(t) \text{ and } z \in [0, h(x, y)]\right\}.$$

Finally, at time $t \geq 0$, the 3-dimensional fluid domain is defined by $\Omega_f(t)$ given by:

$$\Omega_f(t) = \Omega_h(t) \setminus N_h(t) = \left\{(x, y, z) \in \mathbb{R}^3 \text{ s.t. } (x, y) \in \Omega(t) \setminus N(t) \text{ and } z \in [0, h(x, y)]\right\}.$$

We denote by $\underline{u} = (u_1, u_2, u_3)$ the 3-dimensional fluid flow. We assume that the fluid is viscous with a viscosity of μ and that it is incompressible. We denote ρ the density of the fluid and we assume it to be constant. The shear tensor is given by:

$$\mathbf{\Sigma} = \mu(\nabla\underline{u} + (\nabla\underline{u})^{\intercal}) - P\,Id,$$

where P is the pressure. Moreover, we assume that we can write:

$$\underline{u}(t,x,y,z) = \underline{u}^0(t,x,y,z) + \bar{h}\underline{u}^1(t,x,y,z) + \mathcal{O}\left(\bar{h}^2\right), \tag{1.2a}$$

$$P(t,x,y,z) = P^0(t,x,y) + \bar{h}P^1(t,x,y,z) + \mathcal{O}\left(\bar{h}^2\right), \tag{1.2b}$$

where $\bar{h}$ is the typical size gap. Thus, the first two components of the Navier-Stokes momentum equations are given by:

$$\begin{cases} \partial_t(\rho u_1) + \rho(\underline{u} \otimes \nabla u_1) = \mu\Delta u_1 - \partial_x P & \text{in } \Omega_f(t), \\ \partial_t(\rho u_2) + \rho(\underline{u} \otimes \nabla u_2) = \mu\Delta u_2 - \partial_y P & \text{in } \Omega_f(t). \end{cases} \tag{1.3}$$

The thin-film lubrication approximation allows us to neglect inertia. Thus, eq. (1.3) reduces to:

$$\begin{cases} 0 = \mu\Delta u_1 - \partial_x P & \text{in } \Omega_f(t), \\ 0 = \mu\Delta u_2 - \partial_y P & \text{in } \Omega_f(t). \end{cases} \tag{1.4}$$

The Hele-Shaw approximation allows us to neglect the in-plane viscosity terms. Thus, eq. (1.4) reduces to:

$$\begin{cases} 0 = \mu\partial_{zz}^2 u_1 - \partial_x P & \text{in } \Omega_f(t), \\ 0 = \mu\partial_{zz}^2 u_2 - \partial_y P & \text{in } \Omega_f(t). \end{cases}$$

Using assumption (1.2) we deduce that:

$$\begin{cases} 0 = \mu\partial_{zz}^2 u_1^0(x,y,z) - \partial_x P^0(x,y) & \text{in } \Omega_f(t), \\ 0 = \mu\partial_{zz}^2 u_2^0(x,y,z) - \partial_y P^0(x,y) & \text{in } \Omega_f(t). \end{cases} \tag{1.5}$$

Integrating eq. (1.5) and imposing no-slip condition on $z = 0$ and $z = h(x,y)$ we get:

$$\begin{cases} u_1^0(x,y,z) = -\dfrac{z(h(x,y)-z)}{2\mu}\partial_x P^0(x,y) & \text{in } \Omega_f(t), \\ u_2^0(x,y,z) = -\dfrac{z(h(x,y)-z)}{2\mu}\partial_y P^0(x,y) & \text{in } \Omega_f(t). \end{cases} \tag{1.6}$$

In the sequel we omit the exponent $\cdot^0$.

Let $\mathbf{u}$ be the gap-average planar flow. For all $t \geq 0$ and $(x,y) \in \Omega(t) \setminus N(t)$, we have:

$$\begin{aligned} \mathbf{u}(x,y) &= \frac{1}{h(x,y)} \int_0^{h(x,y)} (u_1(x,y,z), u_2(x,y,z))\, \mathrm{d}z \\ &= -\frac{1}{h(x,y)} \int_0^{h(x,y)} \frac{z(h(x,y)-z)}{2\mu} \nabla P(x,y)\, \mathrm{d}z \\ &= -\frac{h(x,y)^2}{12\mu} \nabla P(x,y). \end{aligned}$$

Setting $\xi_{\mathrm{M}}(\mathbf{x}) = \dfrac{h(x,y)^2}{12\mu}$, we recover eq. (1.1a). In this case ξ_{M}, represents the mobility (Chaplain et al., 2019; Lavi et al., 2020). These approximations allow us to place the problem in the 2-dimensional framework.

Moreover, using the no-slip conditions on $z = 0$ and $z = h(x,y)$, we have for all $t \geq 0$ and $(x,y) \in \Omega(t) \setminus N(t)$:

$$\begin{aligned} \operatorname{div}(\mathbf{u}(x,y)) &= \partial_x \int_0^{h(x,y)} u_1(x,y,z)\, \mathrm{d}z + \partial_y \int_0^{h(x,y)} u_2(x,y,z)\, \mathrm{d}z \\ &= \int_0^{h(x,y)} \partial_x u_1(x,y,z)\, \mathrm{d}z + \int_0^{h(x,y)} \partial_y u_2(x,y,z)\, \mathrm{d}z \\ &= \int_0^{h(x,y)} \operatorname{div}(\underline{u}(x,y,z))\, \mathrm{d}z = 0 \end{aligned}$$

We recover eq. (1.1b).

Remark 1.3.1. *The equation obtained can also be justified in the two-dimensional framework. We assume that the cell is on a rigid substrate and is in frictional contact with it (Giverso and Preziosi, 2018; Callan-Jones et al., 2008). We assume that at time $t \geq 0$ the cytoplasm is modelled by the domain $\Omega(t) \setminus N(t)$ and that this domain is filled by an incompressible viscous fluid with density ρ, viscosity μ, velocity $\mathbf{u}$ and pressure P. Thus, neglecting inertia (Danuser et al., 2013), the balance of forces on the fluid is written as follows:*

$$\operatorname{div}(\boldsymbol{\Sigma}) + \rho\, \mathbf{f}_{\text{fric}} = 0 \quad \text{in } \Omega(t) \setminus N(t),$$

with $\boldsymbol{\Sigma} = \mu(\nabla \mathbf{u} + (\nabla \mathbf{u})^{\intercal}) - P\, Id$ the shear tensor and $\mathbf{f}_{\text{fric}}(t, \mathbf{x}) = -k(\mathbf{x})\, \mathbf{u}(t, \mathbf{x})$ the friction force at time $t \geq 0$ and at position $\mathbf{x} \in \Omega(t) \setminus N(t)$ where, for all $\mathbf{x} \in \mathbb{R}^2$, $k(\mathbf{x})$ is the friction coefficient. By neglecting the viscous terms and setting $\xi_{\text{M}}(\mathbf{x}) = \dfrac{1}{\rho\, k(\mathbf{x})}$, we find the desired dynamics.

1.3.2.2 . Kinematic condition

We assume that the normal velocity of the sharp-interface, V_n, is equal to the normal velocity of the fluid on $\partial\Omega(t)$:

$$V_n = \mathbf{u} \cdot \mathbf{n} \quad \text{on } \partial\Omega(t). \tag{1.7}$$

Recall that we assume that the nucleus has a rigid motion and that we denote $\mathbf{u}_{\text{nucl}}$ its velocity. We then have continuity of velocities on the boundary of the nucleus:

$$\mathbf{u} \cdot \mathbf{n} = \mathbf{u}_{\text{nucl}} \cdot \mathbf{n} \quad \text{on } \partial N(t). \tag{1.8}$$

We recover eqs. (1.1c) and (1.1f).

1.3.3 . Nucleus dynamic

In this subsection we detail the modelling developed to obtain the nucleus dynamics (given by eq. (1.1e)). It is known that the nucleus is stiffer than the cytoplasm (Liu et al., 2014). As a first assumption, we model the nucleus by a rigid particle and we assume that its motion is rigid. This means that it does not deform. If it is moving, it can be translating or rotating. Hence, to model the nucleus and its dynamics, we use the theory of fluid-structure interactions.

We assume that the nucleus is a ball and that we have $N(t) = B(\mathbf{x}_{\text{nucl}}(t), R_{\text{nucl}})$ where $\mathbf{x}_{\text{nucl}}(t) = (x_{\text{nucl}}(t), y_{\text{nucl}}(t))$ is the nucleus centre at time $t \geq 0$, it is also its centre of mass. The assumption of rigid movement implies that for all $t > 0$ there exists, $\mathbf{V}_{\text{nucl}}(t) \in \mathbb{R}^2$ and $\omega_{\text{nucl}}(t) \in \mathbb{R}$ such that for all $\mathbf{x} \in N(t)$:

$$\mathbf{u}_{\text{nucl}}(t, \mathbf{x}) = \mathbf{V}_{\text{nucl}}(t) + \omega_{\text{nucl}}(t)\, (\mathbf{x} - \mathbf{x}_{\text{nucl}}(t))^{\perp}.$$

We also assume that the friction of the nucleus on the substrate is higher. There exists $k_{\text{nucl}} \geq 1$ such that for all $t > 0$ the friction coefficient of the nucleus rubbing on the substrate is given by:

$$\xi_{\text{nucl}}(t) = \frac{k_{\text{nucl}}}{|N|} \int_{N(t)} \frac{1}{\xi_{\text{M}}(\mathbf{x})}\, \mathrm{d}\mathbf{x},$$

where $|N|$ denotes the nucleus area. We omit to note the time dependence since the nucleus area is constant over time. We can note that for all $t > 0$, we have $\xi_{\text{nucl}}(t) > 0$. The friction of the nucleus on the substrate, at time $t > 0$ and at the point $\mathbf{x} \in N(t)$, is given by $-\xi_{\text{nucl}}(t)\, \mathbf{u}_{\text{nucl}}(t, \mathbf{x})$.

The cell boundary induces a force on the nucleus which we note as $\mathbf{f}_{\mathrm{BN}}$. We have:

$$\mathbf{f}_{\mathrm{BN}} = \int_{\partial N(t)} f_{\mathrm{BN}}\left(\mathbf{x}\right)\,\mathrm{d}\sigma,$$

where for all $\mathbf{x} \in \partial N\left(t\right)$ $f_{\mathrm{BN}}\left(\mathbf{x}\right)$ denotes the force induced by the cell boundary at the point $\mathbf{x}$. We assume that f_{BN} is colinear to $\mathbf{n}$.

The fluid induces a force on the nucleus. Let $\mathrm{d}\sigma$ be an infinitesimal part of $\partial N\left(t\right)$. On this infinitesimal part, the force induces by the fluid on the nucleus is given by $P\mathbf{n}\,\mathrm{d}\sigma$ (Lefebvre, 2007).

Thus the force balance on the nucleus leads to:

$$\begin{cases} -\xi_{\mathrm{nucl}}\left(t\right)\displaystyle\int_{N(t)} \mathbf{u}_{\mathrm{nucl}}\left(t,\mathbf{x}\right)\,\mathrm{d}\mathbf{x} + \int_{\partial N(t)} P\left(t,\mathbf{x}\right)\mathbf{n}\,\mathrm{d}\sigma + \mathbf{f}_{\mathrm{BN}} = 0, & \text{(1.9a)} \\ -\xi_{\mathrm{nucl}}\left(t\right)\displaystyle\int_{N(t)} \left(\mathbf{x}-\mathbf{x}_{\mathrm{nucl}}\left(t\right)\right)^{\perp}\cdot\mathbf{u}_{\mathrm{nucl}}\left(t,\mathbf{x}\right)\,\mathrm{d}\mathbf{x} \\ \qquad + \displaystyle\int_{\partial N(t)} P\left(t,\mathbf{x}\right)\left(\mathbf{x}-\mathbf{x}_{\mathrm{nucl}}\left(t\right)\right)^{\perp}\cdot\mathbf{n}\,\mathrm{d}\sigma & \text{(1.9b)} \\ \qquad + \displaystyle\int_{\partial N(t)} \left(\mathbf{x}-\mathbf{x}_{\mathrm{nucl}}\right)^{\perp}\cdot f_{\mathrm{BN}}\left(\mathbf{x}\right)\,\mathrm{d}\mathbf{x} = 0, \end{cases}$$

We observe that we have:

$$\int_{N(t)} \left(\mathbf{x}-\mathbf{x}_{\mathrm{nucl}}\left(t\right)\right)^{\perp}\,\mathrm{d}\mathbf{x} = \int_0^{2\pi}\int_0^{R_{\mathrm{nucl}}} \begin{pmatrix} r\cos\left(\theta+\frac{\pi}{2}\right) \\ r\sin\left(\theta+\frac{\pi}{2}\right)\end{pmatrix} r\,\mathrm{d}r\,\mathrm{d}\theta = 0.$$

Thus, we deduce from eq. (1.9a) the following expression for $\mathbf{V}_{\mathrm{nucl}}$:

$$\mathbf{V}_{\mathrm{nucl}}(t) = \frac{1}{\xi_{\mathrm{nucl}}\left(t\right)|N|}\left(\int_{\partial N(t)} P(t,x)\mathbf{n}\,\mathrm{d}\sigma + \mathbf{f}_{\mathrm{BN}}\right).$$

We can also note that for all $\mathbf{x} \in \partial N\left(t\right)$ we have:

$$\left(\mathbf{x}-\mathbf{x}_{\mathrm{nucl}}\left(t\right)\right)^{\perp} \perp \mathbf{n}\left(\mathbf{x}\right),$$

where $\mathbf{n}\left(\mathbf{x}\right)$ is the normal vector to $N\left(t\right)$ at point $\mathbf{x}$. Thus, since f_{BN} is colinear to $\mathbf{n}$ and:

$$\int_{N(t)} \left(\mathbf{x}-\mathbf{x}_{\mathrm{nucl}}\left(t\right)\right)^{\perp}\cdot\mathbf{u}_{\mathrm{nucl}}\left(t,\mathbf{x}\right)\,\mathrm{d}\mathbf{x} = \omega_{\mathrm{nucl}}\left(t\right)2\pi\frac{R_{\mathrm{nucl}}^3}{3},$$

necessarily, we deduce from eq. (1.9b) that:

$$\omega_{\mathrm{nucl}}\left(t\right) = 0.$$

Then the nucleus velocity is given by:

$$\mathbf{u}_{\mathrm{nucl}}\left(t\right) = \mathbf{V}_{\mathrm{nucl}}\left(t\right) = \frac{1}{\xi_{\mathrm{nucl}}\left(t\right)|N|}\left(\int_{\partial N(t)} P(t,\mathbf{x})\mathbf{n}\,\mathrm{d}\sigma + \mathbf{f}_{\mathrm{BN}}\right). \tag{1.10}$$

The choice of the expression for f_{BN} is detailled in section 1.3.9.

The eq. (1.10) corresponds eq. (1.1e).

1.3.4 . Conservation of the domain area

In this subsection, we show that formally, the cell area is constant over time. Let $A_\Omega(t)$ be the surface area of the cell domain at time $t \geq 0$. We extend the definition of $\mathbf{u}$ to the whole cell by posing:

$$\mathbf{u} = \mathbf{u}_{\text{nucl}} \quad \text{on } N(t).$$

Thus, we have:

$$\operatorname{div}(\mathbf{u}) = 0 \quad \text{on } \Omega(t). \tag{1.11}$$

From the incompressibility constraint (1.11) and the kinematic condition (1.7), we have, for all $t \geq 0$:

$$\begin{aligned}\frac{\mathrm{d}}{\mathrm{d}t} A_\Omega(t) = \frac{\mathrm{d}}{\mathrm{d}t} |\Omega(t)| = \frac{\mathrm{d}}{\mathrm{d}t} \int_{\Omega(t)} 1 \,\mathrm{d}\mathbf{x} = \int_{\partial\Omega(t)} V_n \,\mathrm{d}\sigma \\ = \int_{\partial\Omega(t)} \mathbf{u}\cdot\mathbf{n} \,\mathrm{d}\sigma = \int_{\Omega(t)} \operatorname{div}(\mathbf{u}) \,\mathrm{d}\mathbf{x} = 0.\end{aligned}$$

Thus, formally, the surface area of the cell domain is constant in time and we denote it by A_Ω. For all $t \geq 0$, we have:

$$A_\Omega = |\Omega(t)|.$$

Since the nucleus is assumed to be rigid, we also have that its area is conserved over time and we denote it $|N|$. From this we deduce that the area of the fluid domain $\Omega(t) \setminus N(t)$ is also constant over time and we denote it A.

1.3.5 . Force balance on the cell boundary

In this subsection, we detail the force balance at the boundary of the cell $\partial\Omega$. The boundary of the cell is subjected to various forces. We begin by describing these forces, then we write the force balance.

1.3.5.1 . Force induced by the markers

The markers induce an active force F_c on the boundary of the cell (Lavi et al., 2020). We assume that the markers are rear markers. This means that the rear part of the cell is defined by the part where the presence of markers is highest and the front part of the cell by the part where the presence of markers is lowest (Maiuri et al., 2015). We can therefore say that either the force induced by the markers inhibits an outward pushing force (e.g. the force induced by actin polymerisation) or induces an inward pulling force (e.g. the force induced by actomyosin contraction). Thus, we have for $t \geq 0$ and $\mathbf{x} \in \partial\Omega(t)$:

$$F_c(t,\mathbf{x}) = -\chi_c f_{\text{act}}(c(t,\mathbf{x})),$$

with $\chi_c > 0$ and the following assumptions on f_{act}:

$$f_{\text{act}} \in C^1(\mathbb{R}^+), \tag{1.12a}$$
$$f_{\text{act}} \text{ is an increasing function}, \tag{1.12b}$$
$$f_{\text{act}}(0) = 0, \tag{1.12c}$$
$$\lim_{x\to+\infty} f_{\text{act}}(x) = L_c < +\infty. \tag{1.12d}$$

For example we can choose the following saturation function for f_{act}:

$$f_{\text{act}}(x) = \frac{x(1+c_s)^2}{c_s(x+c_s)},$$

with $c_s > 0$ a saturation parameter. This function follows the four conditions of (1.12) with $L_c = \frac{(1+c_s)^2}{c_s}$.

1.3.5.2 . Force induced by the friction of the boundary

The cell membrane modelled by the outer boundary of the domain $\partial\Omega$ rubs against the substrate. This induces a frictional force F_u whose intensity depends on the normal velocity of the boundary. We have for $t \geq 0$ and $\mathbf{x} \in \partial\Omega(t)$:

$$F_u(t, \mathbf{x}) = -\chi_u f_{\text{und}}(V_n(t, \mathbf{x})),$$

with $\chi_u > 0$ and the following assumptions on f_{und}:

$$f_{\text{und}} \in C^1(\mathbb{R}^+), \tag{1.13a}$$
$$f_{\text{und}} \text{ is an odd function and increasing function,} \tag{1.13b}$$
$$f'_{\text{und}}(0) > 0. \tag{1.13c}$$

We recall that V_n denotes the normal velocity of the boundary. Note that this force can be seen as undercooling.

1.3.5.3 . Force induced by the external signals

The environment of the cell may contain external signals (e.g. the presence of pathogens for a neutrophil). These signals can either be attractive or repulsive. Receptors on the boundary of the cell perceive these signals and the perception of these signals induces a force on the boundary of the cell. We assume that these signals are given and independent of the cell. We consider that we can treat these signals as if there were only one. We can then have a signal with attractive and repulsive zones. We denote $s(t, \mathbf{x})$ the external signal at time $t \geq 0$ and position $\mathbf{x} \in \mathbb{R}^2$. Let $O \subset \mathbb{R}^2$ be an open set. The signal is said to be attractive on O if s has a local minimum on O and is said to be repulsive on O if s has a local maximum on O.

We assume that the action of the signal on the cell depends on variations in the signal. This means that the force F_s induced by the signal on the boundary of the cell depends on the gradient of the external signal. For $t \geq 0$ and $\mathbf{x} \in \Omega(t)$, we have:

$$F_s(t, \mathbf{x}) = -\chi_s g(\nabla s(t, \mathbf{x}) \cdot \mathbf{n}),$$

with g such that:

$$g \in C^1(\mathbb{R}), \tag{1.14a}$$
$$g \text{ is an odd function and a increasing function,} \tag{1.14b}$$
$$\lim_{x \to +\infty} g(x) = L_s < +\infty. \tag{1.14c}$$

For example we can choose the following expression for g:

$$g(x) = \tanh(\varsigma_s x),$$

where $\varsigma_s > 0$ is a saturation parameter. This function follows the three conditions of (1.14) with $L_s = 1$.

1.3.5.4 . Force induced by the obstacles

The cell environment contains obstacles. These can have variable geometries and model the extra-cellular matrix. In particular, they can have the geometry of channels. The cell and

these obstacles cannot overlap. The position and geometry of the obstacles are assumed to be fixed and given. We note $\Lambda \subset \mathbb{R}^2$ the obstacles domain.

One way of ensuring that the cell and the obstacles do not overlap is to add a non-overlap constraint to the cell velocity (Lefebvre, 2007; Cucchi et al., 2020). The interaction between the cell and the obstacles can also be modelled by a contact force, and this is the choice made here.

We denote $f_{\text{obs}}(t, \mathbf{x})$ the force induced by the obstacles on the boundary of the cell at the point $\mathbf{x} \in \partial\Omega(t)$ at time $t \geq 0$. We assume that if at time $t \geq 0$ the distance between the cell and the obstacles is greater than the threshold $r_0 > 0$ then the cell does not perceive the obstacles and for all $\mathbf{x} \in \partial\Omega(t)$ we have $f_{\text{obs}}(t, \mathbf{x}) = 0$. Otherwise, if at time $t \geq 0$ the distance between the obstacles and the cell is smaller than the threshold r_0 then the obstacle induces a non-zero force at the point $\mathbf{x} \in \partial\Omega(t)$ given by:

$$f_{\text{obs}}(t, \mathbf{x}) = \lambda \int_{\partial\Lambda} \mathbb{1}_{d(\mathbf{x},\tilde{\mathbf{x}})<r_0} \left(e^{-\frac{d(\mathbf{x},\tilde{\mathbf{x}})}{r_1}} - e^{-\frac{r_0}{r_1}} \right) \mathbf{n}_\Lambda \, \mathrm{d}\sigma(\tilde{\mathbf{x}}) \cdot \mathbf{n},$$

where $\lambda > 0$, $r_0 > 0$, $r_1 > 0$, $\mathbf{n}_\Lambda$ is the outward normal vector to Λ, $\mathbf{n}$ is the outward normal vector to Ω at the point $\mathbf{x}$, and for all $\mathbf{x}, \tilde{\mathbf{x}} \in \mathbb{R}^2$, $d(\mathbf{x}, \tilde{\mathbf{x}})$ denotes the euclidean distance between $\mathbf{x}$ and $\tilde{\mathbf{x}}$.

1.3.5.5 . Force induced by the nucleus

The nucleus which is inside the cell induces a force on the cell boundary. We denote it f_{NB}. This force can be seen as the opposite force to $\mathbf{f}_{\text{BN}}$ and satisfies

$$\int_{\partial\Omega(t)} f_{\text{NB}} \mathbf{n} \, \mathrm{d}\sigma + \mathbf{f}_{\text{BN}} = 0. \tag{1.15}$$

We refer to section section 1.3.9 for the choice of expression for f_{NB}.

1.3.5.6 . Force balance

The Young-Laplace equation on $\partial\Omega(t)$ is perturbed as follow:

$$P - \chi_c f_{\text{act}}(c) - \chi_s g(\nabla s \cdot \mathbf{n}) - \chi_u f_{\text{und}}(V_n) + f_{\text{NB}} + f_{\text{obs}} = \gamma\kappa, \tag{1.16}$$

where γ denotes the surface tension and κ the curvature.

We can note that $\chi_c f_{\text{act}}$, $\chi_s g$, $\chi_u f_{\text{und}}$, f_{NB} and f_{obs} are forces per unit of length. The eq. (1.16) corresponds to eq. (1.1d).

1.3.6 . Markers dynamic

In this subsection we detail the modelling developed to obtain the markers concentration dynamics within the fluid domain (eqs. (1.1g) to (1.1i) with $\alpha = 0$, see section 1.3.7 for the case $\alpha > 0$). As a reminder that we assume the presence of c concentration markers inside the fluid. c denotes here the gap integrated concentration. These markers can either be free inside the fluid or attached to the plates or the substrate (see section 1.3.2.1). We can consequently define two populations: the population of attached markers with concentration c_{p} and the population of unattached markers with concentration c_{f} (Lavi, 2019). We assume that both populations are diffusing in the domain. The population of attached markers diffuses within the domain with diffusion coefficient D_{p} while the population of unattached markers has diffusion coefficient D_{f}. The population of attached markers is not convected while the

population of unattached markers is convected at fluid velocity $\mathbf{u}$. The markers have constant attachment and detachment rates with the plates. We note k_{on} the rate of attachment and k_{off} the rate of detachment. The dynamics of the two populations are given by:

$$\begin{cases} \partial_t c_{\mathrm{p}} - \operatorname{div}\left(D_{\mathrm{p}} \nabla c_{\mathrm{p}}\right) = k_{\mathrm{on}} c_{\mathrm{f}} - k_{\mathrm{off}} c_{\mathrm{p}} & \text{in } \Omega\left(t\right) \setminus N\left(t\right), \\ \partial_t c_{\mathrm{f}} - \operatorname{div}\left(D_{\mathrm{f}} \nabla c_{\mathrm{f}} - \mathbf{u}\, c_{\mathrm{f}}\right) = k_{\mathrm{off}} c_{\mathrm{p}} - k_{\mathrm{on}} c_{\mathrm{f}} & \text{in } \Omega\left(t\right) \setminus N\left(t\right). \end{cases}$$

Let $a = \frac{k_{\mathrm{on}}}{k_{\mathrm{on}} + k_{\mathrm{off}}}$ be the steady fraction of attached markers that are not convected by the fluid flow. Assuming rapid rates of attachment and detachment, at the steady balance, we obtain $c_{\mathrm{p}} = ac$ and $c_{\mathrm{f}} = (1-a)\, c$. Let $D = aD_{\mathrm{p}} + (1-a)\, D_{\mathrm{f}}$. Hence we have:

$$\partial_t c = \operatorname{div}\left(D \nabla c - (1-a)\, \mathbf{u}\, c\right) \quad \text{in } \Omega\left(t\right) \setminus N\left(t\right). \tag{1.17}$$

We impose non flux condition on the boundaries:

$$D \nabla c + a \mathbf{u}\, c \quad \text{on } \partial\left(\Omega\left(t\right) \setminus N\left(t\right)\right). \tag{1.18}$$

The problem (1.17)-(1.18) is complemented with an initial condition given by:

$$c(0, \mathbf{x}) = c^{\mathrm{in}}(\mathbf{x}) \quad \text{in } \Omega\left(0\right) \setminus N\left(0\right), \tag{1.19}$$

with c^{in} given.

Let $M\left(t\right)$ be the total quantity of markers at time $t \geq 0$:

$$M\left(t\right) = \int_{\Omega(t) \setminus N(t)} c\left(t, \mathbf{x}\right)\, \mathrm{d}\mathbf{x}.$$

Using the boundary condition eq. (1.18) and the kinematic conditions eqs. (1.7) and (1.8), we have for all $t \geq 0$:

$$\begin{aligned} \frac{\mathrm{d}}{\mathrm{d}t} M\left(t\right) &= \int_{\Omega(t) \setminus N(t)} \partial_t c \, \mathrm{d}\mathbf{x} + \int_{\partial(\Omega(t) \setminus N(t))} c V_n \, \mathrm{d}\sigma \\ &= \int_{\Omega(t) \setminus N(t)} \operatorname{div}\left(D \nabla c - (1-a)\, \mathbf{u} c\right)\, \mathrm{d}\mathbf{x} + \int_{\partial(\Omega(t) \setminus N(t))} c \mathbf{u} \cdot \mathbf{n} \, \mathrm{d}\sigma \\ &= \int_{\partial(\Omega(t) \setminus N(t))} \left(D \nabla c - (1-a)\, \mathbf{u} c\right) \cdot \mathbf{n} \, \mathrm{d}\sigma + \int_{\partial(\Omega(t) \setminus N(t))} c \mathbf{u} \cdot \mathbf{n} \, \mathrm{d}\sigma \\ &= \int_{\partial(\Omega(t) \setminus N(t))} \left(D \nabla c + a \mathbf{u} c\right) \cdot \mathbf{n} \, \mathrm{d}\sigma = 0. \end{aligned}$$

Thus, formally, the total quantity of markers is constant in time and we denote it by M. For all $t \geq 0$, we have:

$$M = \int_{\Omega(t) \setminus N(t)} c\left(t, \mathbf{x}\right)\, \mathrm{d}\mathbf{x}.$$

The three eqs. (1.17) to (1.19) corresponds to eqs. (1.1g) to (1.1i) in the case $\alpha = 0$ and if we either take $D = 1$, or we scale the equations by writing lengths in units of $R_0 = \sqrt{\frac{A + \pi R_{\mathrm{nucl}}^2}{\pi}}$, time in units of $\frac{R_0^2}{D}$ and markers concentration in units of the mean planar concentration $c_m = \frac{M}{A}$.

1.3.7 . Adding a noise to the deterministic model

Combining the results of the previous subsections, we obtain a deterministic model. Cell motility is not fully deterministic and noise is playing a role in it. We distinguish two sources of noise: extrinsic and intrinsic noise. The stochastic fluctuations in the system under consideration are considered as the intrinsic noise whereas the extrinsic noise is related to the stochastic processes outside the system under consideration (Tsimring, 2014). To model these noise sources and their effects on cell dynamics, we choose to add a space coloured noise to the advection field of the marker transport-diffusion equation. This choice is motivated by the probabilistic nature of biochemical reactions of the markers.

To add noise to our model, we use a method similar to the one used in chapter 7 of Etchegaray's thesis. (Etchegaray, 2016). We will use a Q-Wiener process. A Q-Wiener process and therefore the noise associated with this process are defined on a probability space associated with a bounded open space independent of time. As we intend to add noise in the advection field to the marker transport-diffusion equation, we would like to define noise associated with the current geometry of the cell which depends of the time. This does not seem trivial. To circumvent this difficulty as the area of the cell is constant over time and the perimeter of the cell finite, there exists a bounded open $O \subset \mathbb{R}^2$ such that for all $t \geq 0$ we have $\Omega(t) \setminus N(t) - \mathbf{x}_{\mathrm{cm}}(t) \subset O$ with $\mathbf{x}_{\mathrm{cm}}(t)$ the cell centre of mass at time t (see section 1.3.8 for details on the definition and the dynamic of the cell centre of mass). We can then define a two-dimensional Q-Wiener process on this open O and define the coloured noise associated with this process.

Let us recall the definition of Q-Wiener process, we use the one of Peszat and Zabczyk (2007).

Definition 1.3.2 (Q-Wiener process)**.** *Let Q be a non-negative symmetric trace-class operator on $L^2(O)$. There exists a probability space $(O, \mathcal{F}, \mathbb{P})$ on which we can define a stochastic process $\left(W_t^Q, t \in \mathbb{R}_+\right)$ on $L^2(O)$ such that:*

- *For each $t \in \mathbb{R}_+$, W_t^Q is a $L^2(O)$-valued random variable,*
- *We have $W_0^Q = 0_{L^2(O)}$ $\mathbb{P}$-almost surely,*
- *$\left(W_t^Q, t \in \mathbb{R}_+\right)$ is a Lévy process: it has independent and stationary increments:*
  - *independent increments: for any sequence $t_1 < \cdots < t_n$, the random variables $W_{t_2}^Q - W_{t_1}^Q, \ldots, W_{t_n}^Q - W_{t_{n-1}}^Q$ are independent,*
  - *stationary increments: for two times $s < t$, the random variable $W_t^Q - W_s^Q$ has same law as W_{t-s}^Q,*
- *$\left(W_t^Q, t \in \mathbb{R}_+\right)$ is a Gaussian process: for any $t \in \mathbb{R}_+$ and any $\phi \in L^2(O)$, $\left(W_t^Q, \phi\right)$ is a real centred Gaussian random variable with variance $t(Q\phi, \phi)$,*
- *$\left(W_t^Q, t \in \mathbb{R}_+\right)$ is a $L^2(O)$-valued pathwise continuous process $\mathbb{P}$-almost surely.*

The stochastic process $\left(W_t^Q, t \in \mathbb{R}_+\right)$ is a Q-Wiener process.

We also recall the definition of non-negative symmetric linear operator on $L^2(O)$ admitting a kernel (Boulakia et al., 2015).

Definition 1.3.3. *A non-negative symmetric linear operator $Q : L^2(O) \longrightarrow L^2(O)$ is a linear operator defined on $L^2(O)$ such that for all $\phi_1, \phi_2 \in L^2(O)$,*

$$(Q\phi_1, \phi_2) = (Q\phi_2, \phi_1), \qquad (Q\phi_1, \phi_1) \geq 0.$$

Let q be a non-negative definite symmetric real valued integrable function on $O \times O$. We say that Q has the kernel q if,

$$\forall \phi \in L^2(O), \forall \mathbf{x} \in O, \quad Q\phi(\mathbf{x}) = \int_O \phi(\mathbf{y})\, q(\mathbf{x}, \mathbf{y})\, \mathrm{d}\mathbf{y}.$$

Remark 1.3.4. *Let $Q : L^2(O) \longrightarrow L^2(O)$ be a non-negative symmetric operator with kernel q. Then Q is a trace class operator, with trace given by:*

$$\mathrm{Tr}(Q) = \int_O q(\mathbf{x}, \mathbf{x})\, \mathrm{d}\mathbf{x}.$$

Let Q be the non-negative symmetric linear operator with kernel q given by

$$q(\mathbf{x}, \mathbf{y}) = \frac{1}{4\zeta^2} e^{-\frac{\pi}{4\zeta^2}|\mathbf{x}-\mathbf{y}|^2},$$

where $\mathbf{x}, \mathbf{y} \in O$ and $\zeta > 0$ is a parameter that controls the spatial correlation. This choice is the same as the one done in Boulakia et al. (2015) or Etchegaray (2016). Let W_t^Q be a bidimensional Q-Wiener process associated to the operator Q. Let $\dot{W}_t^Q$ be the coloured noise associate to this Q-Wiener process. $\dot{W}_t^Q$ can be interpret as the limit of $\frac{W_{t+\varepsilon}^Q - W_t^Q}{\varepsilon}$ when ε tends to 0 (Kloeden and Platen, 1992).

Then we modify the deterministic markers dynamics eqs. (1.17) to (1.19) as follows:

$$\begin{cases} \partial_t c = \mathrm{div}\left(\nabla c - (1-a)\,\mathbf{u}c - \alpha \dot{W}_t^Q c\right) & \text{in } \Omega(t) \setminus N(t), \quad \text{(1.20a)} \\ \left(\nabla c + a\mathbf{u}c - \alpha \dot{W}_t^Q c\right) \cdot \mathbf{n} = 0 & \text{on } \partial(\Omega(t) \setminus N(t)), \quad \text{(1.20b)} \\ c(0, \mathbf{x}) = c^{\mathrm{in}}(\mathbf{x}) & \text{in } \Omega(0) \setminus N(t), \quad \text{(1.20c)} \end{cases}$$

with $\alpha > 0$ and $\dot{W}_t^Q$ evaluated at the point $\mathbf{x} - \mathbf{x}_{\mathrm{cm}}(t)$ with $\mathbf{x} \in \Omega(t) \setminus N(t)$. Noise is added so that the total quantity of markers remains constant over time. In fact, we have:

$$\begin{aligned} \frac{\mathrm{d}}{\mathrm{d}t} \int_{\Omega(t)\setminus N(t)} c\, \mathrm{d}\mathbf{x} &= \int_{\Omega(t)\setminus N(t)} \partial_t c\, \mathrm{d}\mathbf{x} + \int_{\partial(\Omega(t)\setminus N(t))} c V_n\, \mathrm{d}\sigma \\ &= \int_{\Omega(t)\setminus N(t)} \mathrm{div}\left(\nabla c - (1-a)\,\mathbf{u}c - \alpha \dot{W}_t^Q c\right) \mathrm{d}\mathbf{x} + \int_{\partial(\Omega(t)\setminus N(t))} c\,\mathbf{u}\cdot\mathbf{n}\, \mathrm{d}\sigma \\ &= \int_{\partial(\Omega(t)\setminus N(t))} \left(\nabla c - (1-a)\,\mathbf{u}c - \alpha \dot{W}_t^Q c\right)\cdot\mathbf{n}\, \mathrm{d}\sigma + \int_{\partial(\Omega(t)\setminus N(t))} c\,\mathbf{u}\cdot\mathbf{n}\, \mathrm{d}\sigma \\ &= \int_{\partial(\Omega(t)\setminus N(t))} \left(\nabla c + a\mathbf{u}c - \alpha \dot{W}_t^Q c\right)\cdot\mathbf{n}\, \mathrm{d}\sigma = 0. \end{aligned}$$

In this way, a space-correlated noise is added to the deterministic model. We choose to do it instead of a white noise in order to avoid non trivial effects that can appear when we discretize our model (Walsh, 2005; Hairer et al., 2012).

1.3.8 . External force balance

In this section, by deriving the dynamic laws governing the first momentum of $\Omega(t)$, we obtain an insight into the behaviour of the model in the case where the substrate is homogeneous, i.e. ξ_M is independent of time and space. We assume that for all $t \geq 0$ and $\mathbf{x} \in \Omega(t)$, $\xi_M(t, \mathbf{x}) = 1$. We deduce from this computation the velocity of the cell's centre of mass and the external force balance.

Let $\mathcal{M}_1$ be the first momentum of $\Omega(t)$. For all $t \geq 0$, we have:

$$\mathcal{M}_1(t) = \int_{\Omega(t)} \mathbf{x} \, \mathrm{d}\mathbf{x}.$$

Using the incompresisbility constraint (1.1b), the darcy law (1.1a), the boundary condition (1.1d) and the nucleus velocity expression (1.1e), we have that for all $t \geq 0$:

$$\begin{aligned}
\frac{\mathrm{d}}{\mathrm{d}t}\int_{\Omega(t)} x \, \mathrm{d}x \, \mathrm{d}y &= \int_{\partial\Omega(t)} x V_n \, \mathrm{d}\sigma = \int_{\partial\Omega(t)} x\mathbf{u}\cdot\mathbf{n} \, \mathrm{d}\sigma \\
&= \int_{\Omega(t)\setminus N(t)} \operatorname{div}(x\mathbf{u}) \, \mathrm{d}x \, \mathrm{d}y + \int_{N(t)} \operatorname{div}(x\mathbf{u}_{\mathrm{nucl}}) \, \mathrm{d}x \, \mathrm{d}y \\
&= \int_{\Omega(t)\setminus N(t)} \nabla x \cdot \mathbf{u} \, \mathrm{d}x \, \mathrm{d}y + \mathbf{u}_{\mathrm{nucl}} \cdot \int_{N(t)} \nabla x \, \mathrm{d}x \, \mathrm{d}y \\
&= -\int_{\Omega(t)\setminus N(t)} \operatorname{div}(P\nabla x) \, \mathrm{d}x \, \mathrm{d}y + |N| \, \mathbf{u}_{\mathrm{nucl},x} \\
&= -\int_{\partial\Omega(t)} P\nabla x \cdot \mathbf{n} \, \mathrm{d}\sigma - \int_{\partial N(t)} P\nabla x \cdot \mathbf{n} \, \mathrm{d}\sigma + |N| \, \mathbf{u}_{\mathrm{nucl},x} \\
&= -\int_{\partial\Omega(t)} \left(\gamma\kappa + \chi_c f_{\mathrm{act}}(c) + \chi_s g(\nabla s \cdot \mathbf{n}) - f_{\mathrm{NB}} - f_{\mathrm{obs}} + \chi_u f_{\mathrm{und}}(V_n)\right) \mathbf{n}_x \, \mathrm{d}\sigma \\
&\quad - \int_{\partial N(t)} P\mathbf{n}_x \, \mathrm{d}\sigma + |N| \, \mathbf{u}_{\mathrm{nucl},x} \\
&= -\int_{\partial\Omega(t)} \left(\gamma\kappa + \chi_c f_{\mathrm{act}}(c) + \chi_s g(\nabla s \cdot \mathbf{n}) - f_{\mathrm{NB}} - f_{\mathrm{obs}} + \chi_u f_{\mathrm{und}}(V_n)\right) \mathbf{n}_x \, \mathrm{d}\sigma \\
&\quad - \xi_{\mathrm{nucl}} |N| \, \mathbf{u}_{\mathrm{nucl},x} + \mathbf{f}_{\mathrm{BN},x} + |N| \, \mathbf{u}_{\mathrm{nucl},x}.
\end{aligned}$$

Anagously, for all $t \geq 0$, we have:

$$\begin{aligned}
\frac{\mathrm{d}}{\mathrm{d}t}\int_{\Omega(t)} y \, \mathrm{d}x \, \mathrm{d}y = -\int_{\partial\Omega(t)} &\left(\gamma\kappa + \chi_c f_{\mathrm{act}}(c) + \chi_s g(\nabla s \cdot \mathbf{n}) - f_{\mathrm{NB}} - f_{\mathrm{obs}} + \chi_u f_{\mathrm{und}}(V_n)\right) \mathbf{n}_y \, \mathrm{d}\sigma \\
&- \xi_{\mathrm{nucl}} |N| \, \mathbf{u}_{\mathrm{nucl},y} + \mathbf{f}_{\mathrm{BN},y} + |N| \, \mathbf{u}_{\mathrm{nucl},y}.
\end{aligned}$$

Using the fact that $\int_{\partial\Omega(t)} \kappa\mathbf{n} \, \mathrm{d}\sigma = 0$ and eq. (1.15), it follows that for all $t \geq 0$:

$$\begin{aligned}
\frac{\mathrm{d}}{\mathrm{d}t}\mathcal{M}_1(t) = -\int_{\partial\Omega(t)} &\left(\chi_c f_{\mathrm{act}}(c) + \chi_s g(\nabla s \cdot \mathbf{n}) - f_{\mathrm{obs}} + \chi_u f_{\mathrm{und}}(V_n)\right) \mathbf{n} \, \mathrm{d}\sigma \\
&+ (1 - \xi_{\mathrm{nucl}}) |N| \, \mathbf{u}_{\mathrm{nucl}}.
\end{aligned}$$

Let $\mathbf{x}_{\mathrm{cm}}(t)$ be the centre of mass of $\Omega(t)$ at time $t \geq 0$. We have:

$$\mathbf{x}_{\mathrm{cm}}(t) = \frac{1}{A_\Omega}\int_{\Omega(t)} (x, y) \, \mathrm{d}x \, \mathrm{d}y = \frac{1}{A_\Omega}\mathcal{M}_1(t).$$

We also define the velocity of the centre of mass $\mathbf{u}_{\mathrm{cm}}$. For all $t \geq 0$, we have:

$$\mathbf{u}_{\mathrm{cm}}(t) = \frac{\mathrm{d}}{\mathrm{d}t}\mathbf{x}_{\mathrm{cm}}(t).$$

Thus we have:

$$\mathbf{u}_{\mathrm{cm}}(t) = \frac{1}{A_\Omega}\frac{\mathrm{d}}{\mathrm{d}t}\mathcal{M}_1(t).$$

It follows that for all $t \geq 0$:

$$\mathbf{u}_{\mathrm{cm}}(t) = -\frac{1}{A_\Omega}\int_{\partial\Omega(t)} \left(\chi_c f_{\mathrm{act}}(c) + \chi_s g\left(\nabla s \cdot \mathbf{n}\right) - f_{\mathrm{obs}} + \chi_u f_{\mathrm{und}}(V_n)\right)\mathbf{n}\,\mathrm{d}\sigma + \frac{|N|}{A_\Omega}\left(1-\xi_{\mathrm{nucl}}\right)\mathbf{u}_{\mathrm{nucl}}. \quad (1.21)$$

We recognise that eq. (1.21) is the balance of external forces on the cell.

1.3.9 . Modelling of the forces between the cell boundary and the nucleus

In this section, we detail the modelling choices made in sections 1.3.3 and 1.3.5.5 concerning the forces acting between the nucleus and the boundary of the cell and give an expression of these forces.

First approach. We recall that the nucleus and the boundary of the cell interact with each other via the cytoskeleton and in particular via the intermediate filaments. We propose here a simplified approach to these interactions by assuming that the nucleus is connected to the boundary of the cell via links and that each point $\mathbf{x}_B$ on the boundary of the cell is connected by a link to a single point $\mathbf{x}_N$ on the boundary of the nucleus where $\mathbf{x}_N$ is the point of intersection between the segment $[\mathbf{x}_N, \mathbf{x}_B]$ and the boundary of the nucleus ∂N. We assume that each link induces a force at $\mathbf{x}_N$ and at $\mathbf{x}_B$. We then note g_B and g_N the forces induced by the link at the point $\mathbf{x}_B$ and $\mathbf{x}_N$, respectively. By the action-reaction principle, we have $g_B + g_N = 0$.

Naturally, we are tempted to assume that the forces g_B and g_N are directed along the vector $\mathbf{x}_B\mathbf{x}_N$. This choice seems in accordance with physics. Nevertheless, we choose the forces g_B and g_N as directed along the vector normal to $\partial\Omega$ in $\mathbf{x}_B$ (see fig. 1.7). This choice, although less intuitive, allows us to retain the formalism of Hele-Shaw cells with a Darcy fluid. The tangential velocity at the outer boundary of the cell remain zero. If we take the first choice, which seems more in accordance with physics, we have to consider a Stokes fluid.

Finally, we assume that the smaller the distance between $\mathbf{x}_B$ and $\mathbf{x}_N$, the greater the intensity of the forces g_N and g_B.

Let $\mathbf{x}_B \in \partial\Omega$ be a point of the cell boundary. We set $\mathbf{v}_{\mathrm{BN}} = \mathbf{x}_{\mathrm{nucl}} - \mathbf{x}_B$ which is colinear vector with the vector $\mathbf{x}_B\mathbf{x}_N$. We can note that $\mathbf{v}_{\mathrm{BN}} \cdot \mathbf{n} < 0$. Since the nucleus is a ball of radius R_{nucl}, the distance between $\mathbf{x}_B$ and $\mathbf{x}_N$ is then given by $\|\mathbf{v}_{\mathrm{BN}}\| - R_{\mathrm{nucl}}$. A way of ensuring these two assumptions is to set:

$$g_B = -\delta\frac{\mathbf{v}_{\mathrm{BN}} \cdot \mathbf{n}}{\left(\|\mathbf{v}_{\mathrm{BN}}\| - R_{\mathrm{nucl}}\right)^\beta}\mathbf{n}$$

and

$$g_N = \delta\frac{\mathbf{v}_{\mathrm{BN}} \cdot \mathbf{n}}{\left(\|\mathbf{v}_{\mathrm{BN}}\| - R_{\mathrm{nucl}}\right)^\beta}\mathbf{n},$$

with $\beta > 1$ and $\delta > 0$ and $\mathbf{n}$ the outward normal vector to Ω at $\mathbf{x}_B$.

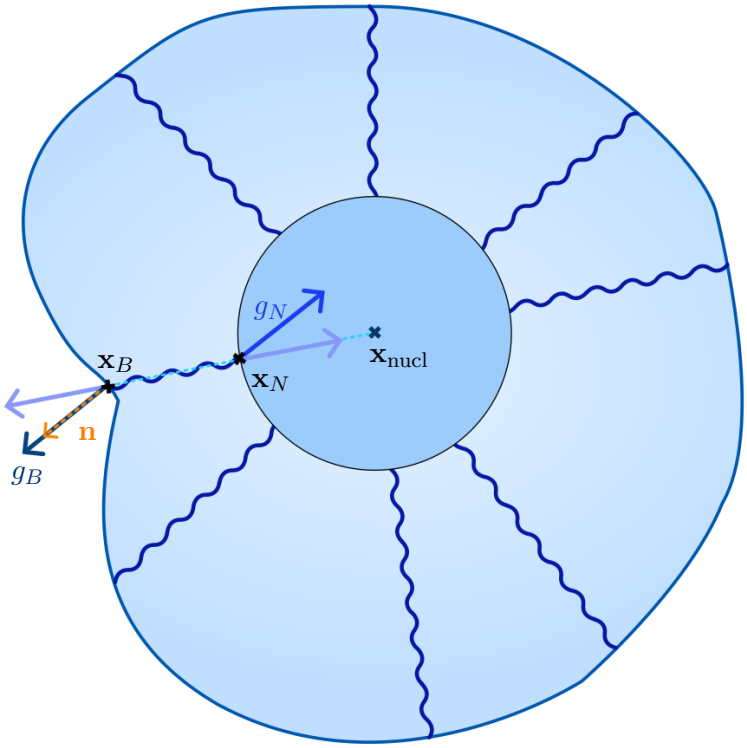

Figure 1.7: **Illustration of the modelling for the forces between the nucleus and the boundary of the cell.** *The links between the nucleus and the cell boundary are represented by the dark blue wavy lines. An example of the forces induced by a link is shown. The dark blue arrows represent these forces. The lilac arrows represent the forces with the more in accordance with physics hypothesis, when the forces induced by the link are directed along the axis of the link.*

Next we establish the link between $\mathbf{f}_{\text{BN}}$, f_{NB} and the forces g_B and g_N. $\mathbf{f}_{\text{BN}}$ represent the force induced by the cell boundary on the nucleus. Consequently, we sum up all the forces induced by the links on the nucleus and we have for all $t \geq 0$:

$$\mathbf{f}_{\text{BN}}(t) = \delta \int_{\partial\Omega(t)} \frac{\mathbf{v}_{\text{BN}} \cdot \mathbf{n}}{\left(\|\mathbf{v}_{\text{BN}}\| - R_{\text{nucl}}\right)^{\beta}} \mathbf{n} \, \mathrm{d}\sigma. \tag{1.22}$$

f_{NB} corresponds to the normal coordinate of the force induced by a link at the point $\mathbf{x}_B$ and we then have for all $t \geq 0$ and $\mathbf{x} \in \partial\Omega(t)$:

$$f_{\text{NB}}(t, \mathbf{x}) = -\delta \frac{\mathbf{v}_{\text{BN}} \cdot \mathbf{n}}{\left(\|\mathbf{v}_{\text{BN}}\| - R_{\text{nucl}}\right)^{\beta}}. \tag{1.23}$$

Heuristic approach. We suggest another more heuristic approach to model the $\mathbf{f}_{\text{BN}}$ and f_{NB} forces. In this approach, the nucleus is connected to the cell's centre of mass by a spring (see fig. 1.8).

In this case, the elastic potential energy is given by:

$$J = \frac{k}{2} \left(\frac{1}{|\Omega|} \int_{\partial\Omega} \mathbf{x} \, \mathrm{d}\mathbf{x} - \frac{1}{|N|} \int_{\partial N} \mathbf{x} \, \mathrm{d}\mathbf{x} \right)^2,$$

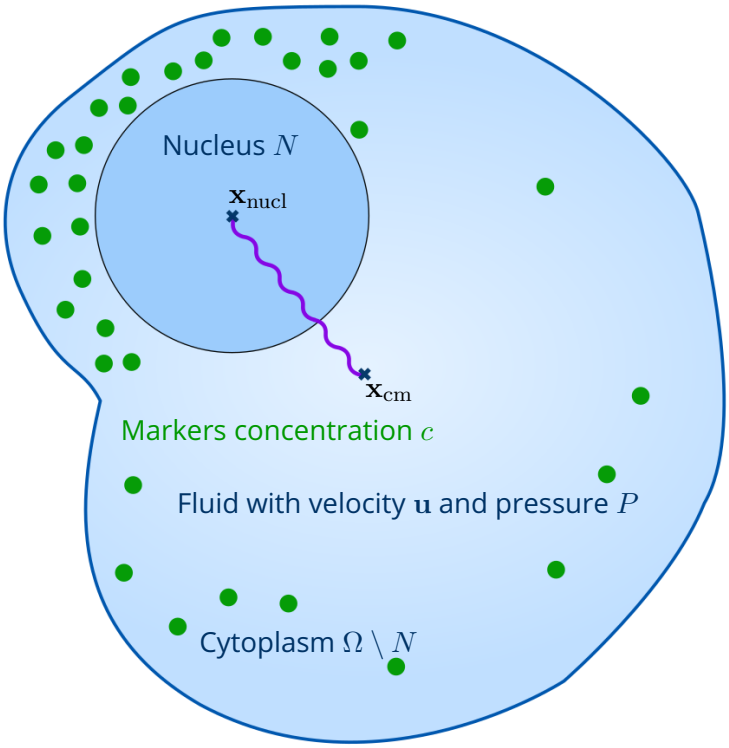

Figure 1.8: **Illustration of the model using the heuristic approach.** *The nucleus is connected to the cell's centre of mass by a spring.*

with $k > 0$ the spring constant and $\frac{1}{|\Omega|}\int_{\partial\Omega} \mathbf{x}\,\mathrm{d}\mathbf{x} - \frac{1}{|N|}\int_{\partial N} \mathbf{x}\,\mathrm{d}\mathbf{x} = \mathbf{x}_{\text{cm}} - \mathbf{x}_{\text{nucl}}$ the relative position of the nucleus centre. We derive the energy with respect to the velocity of deformation of the domain and for all velocity v admitting V as trace on $\partial\Omega$ and ∂N, we have:

$$\frac{\partial J}{\partial v}(v) = k\left(\mathbf{x}_{\text{cm}} - \mathbf{x}_{\text{nucl}}\right) \cdot \left(\frac{1}{|\Omega|}\int_{\partial\Omega} \mathbf{x}V \cdot \mathbf{n}\,\mathrm{d}\sigma + \frac{1}{|N|}\int_{\partial N} \mathbf{x}V \cdot \mathbf{n}\,\mathrm{d}\sigma\right),$$

with $\mathbf{n}$ the outward normal vector to $\Omega \setminus N$.

We deduce that the force induced on the nucleus g_N at the point $\mathbf{x}_N \in \partial N$ is given by:

$$g_N(\mathbf{x}_N) = \frac{-k\left(\mathbf{x}_{\text{cm}} - \mathbf{x}_{\text{nucl}}\right) \cdot \mathbf{x}_N}{|N|}\mathbf{n},$$

where $\mathbf{n}$ is the outward normal vector to $\Omega \setminus N$ at the point $\mathbf{x}_N$. Similarly, the force induced on the boundary g_B at the point $\mathbf{x}_B \in \partial\Omega$ is given by:

$$g_B(\mathbf{x}_B) = \frac{-k\left(\mathbf{x}_{\text{cm}} - \mathbf{x}_{\text{nucl}}\right) \cdot \mathbf{x}_B}{|\Omega|}\mathbf{n},$$

Thus, at time $t \geq 0$, the force induced on the whole nucleus $\mathbf{f}_{\text{BN}}(t)$ is given by the sum of all the forces induced at the points of the nucleus and we have:

$$\mathbf{f}_{\text{BN}}(t) = \int_{\partial N(t)} \frac{-k\left(\mathbf{x}_{\text{cm}}(t) - \mathbf{x}_{\text{nucl}}(t)\right) \cdot \mathbf{x}_N}{|N|}\mathbf{n}\,\mathrm{d}\sigma = -k\left(\mathbf{x}_{\text{nucl}}(t) - \mathbf{x}_{\text{cm}}(t)\right). \tag{1.24}$$

This force corresponds to the restoring force of a spring.

Moreover, at times $t \geq 0$, f_{NB} corresponds to the normal coordinate of the force induced by a link at the point $\mathbf{x}_B$ and we then have for all $\mathbf{x} \in \partial\Omega(t)$:

$$f_{\mathrm{NB}}(t, \mathbf{x}) = \frac{-k\left(\mathbf{x}_{\mathrm{cm}}(t) - \mathbf{x}_{\mathrm{nucl}}(t)\right) \cdot \mathbf{x}}{|\Omega|}. \tag{1.25}$$

The forces $\mathbf{f}_{\mathrm{BN}}$ and f_{NB} defined by eqs. (1.24) and (1.25) satisfy eq. (1.15).

1.4 . Outline of the thesis

In chapters 2 and 4 to 7, the impact of the nucleus on cell motility is studied. In chapter 2, a one-dimensional model analogous to the general model is studied. Numerical simulations provide initial conclusions about the role of the nucleus in cell motility and illustrate that the model produces results consistent with biological observations.

In chapters 4 and 5, two toy models are presented. For these two models, the stationary states and their stability are studied. These two models produce observations similar to those obtained in chapter 3 when the nucleus is not considered and the cell is assumed to be rigid. The trajectories satisfy the UCSP law, and parameter ranges are found to reproduce the three types of trajectories.

In chapter 6, a rigid model that takes the nucleus dynamics into account is studied. Numerical simulations, compared with those obtained in chapters 4 and 5, highlight that the dynamics of the nucleus promote the intermittent nature of the trajectories. This model also highlights the positioning of the nucleus within the cell and its link to polarisation.

Chapter 7 is dedicated to the study of the deformable model with nucleus dynamics. The stationary states and their stability are studied. A finite element numerical scheme is proposed. Numerical simulations obtained via this scheme highlight that the model qualitatively reproduces the phenomena of polarisation and cell migration. This illustrates the role of the nucleus in cell motility.

Chapter 8 is devoted to the study of a heuristic one-dimensional model of cell motility that takes the nucleus into account. Using a finite volume numerical scheme, numerical simulations illustrate that this heuristic can reproduce, for certain parameters, the intermittent behaviour of the trajectories.

In chapter 9, the effect of undercooling on cell motility is studied. The stationary state is studied. Using a bifurcation argument, the existence of traveling waves is demonstrated. These results also illustrate the stabilizing effect of undercooling.

Chapter 10 is dedicated to studying the impact of an external signal on cell motility. Using numerical results, it is illustrated that there is a trade-off between the force induced by the markers on the cell boundary and the force induced by the external signal.

Finally, chapter 11 presents work carried out during CEMRACS 2022. A model of one of the mechanisms occurring at the membrane—endocytosis—is presented. After studying the model, a finite volume scheme is presented. This scheme yields results consistent with biological observations.

Note that some of the elements previously presented in the model are not studied in this thesis. Indeed, throughout this thesis, we assume that the substrate is homogeneous and therefore that for all $\mathbf{x} \in \mathbb{R}^2$ we have $\xi_M(\mathbf{x}) = 1$. This will be the subject of future work.

Additionally, the study of the presence of obstacles in the cell's environment is briefly covered in chapter 10. This study will be further explored in future work.

Bibliography

Abercrombie, M. (1980). The Croonian Lecture, 1978 - The crawling movement of metazoan cells. Proceedings of the Royal Society of London. Series B. Biological Sciences, 207(1167):129–147. 19, 22

Alberts, B., Johnson, A., Lewis, J., Raff, M., Roberts, K., and Walter, P. (2002). Molecular Biology of the Cell. Garland Science, 4th edition. 18

Asnacios, A. and Hamant, O. (2012). The mechanics behind cell polarity. Trends in Cell Biology, 22(11):584–591. 18

Berlyand, L., Potomkin, M., and Rybalko, V. (2016). Phase-field model of cell motility: Traveling waves and sharp interface limit. Comptes Rendus. Mathématique, 354(10):986–992. 23

Blanch-Mercader, C. and Casademunt, J. (2013). Spontaneous Motility of Actin Lamellar Fragments. Physical Review Letters, 110(7):078102. Publisher: American Physical Society. 22

Bosgraaf, L. and Van Haastert, P. J. M. (2009). Navigation of Chemotactic Cells by Parallel Signaling to Pseudopod Persistence and Orientation. PLoS ONE, 4(8):e6842. 20

Boulakia, M., Genadot, A., and Thieullen, M. (2015). Simulation of SPDEs for Excitable Media Using Finite Elements. Journal of Scientific Computing, 65(1):171–195. 33, 34

Bénichou, O., Loverdo, C., Moreau, M., and Voituriez, R. (2011). Intermittent search strategies. Reviews of Modern Physics, 83(1):81–129. arXiv:1104.0639 [cond-mat, physics:physics]. 21

Callan-Jones, A. C., Joanny, J.-F., and Prost, J. (2008). Viscous Fingering-like Instability of Cell Fragments. Physical Review Letters, 100(25):258106. arXiv:0804.0707 [cond-mat, q-bio]. 27

Chaplain, M. A. J., Giverso, C., Lorenzi, T., and Preziosi, L. (2019). Derivation and Application of Effective Interface Conditions for Continuum Mechanical Models of Cell Invasion through Thin Membranes. SIAM Journal on Applied Mathematics, 79(5):2011–2031. 26

Cooper, G. M. (2000). The Cell. Sinauer Associates, 2nd edition. 18

Cramer, L. P. (2010). Forming the cell rear first: breaking cell symmetry to trigger directed cell migration. Nature Cell Biology, 12(7):628–632. 19

Cucchi, A., Etchegaray, C., Meunier, N., Navoret, L., and Sabbagh, L. (2020). Cell migration in complex environments: chemotaxis and topographical obstacles. ESAIM: Proceedings and Surveys, 67:191–209. 31

Danuser, G., Allard, J., and Mogilner, A. (2013). Mathematical Modeling of Eukaryotic Cell Migration: Insights Beyond Experiments. Annual Review of Cell and Developmental Biology, 29(1):501–528. 19, 22, 27

Etchegaray, C. (2016). Mathematical and numerical modelling of cell migration. phdthesis, Université Paris Saclay (COmUE). 33, 34

Friedman, A. and Reitich, F. (2000). Symmetry-breaking bifurcation of analytic solutions to free boundary problems: An application to a model of tumor growth. Transactions of the American Mathematical Society, 353(4):1587–1634. 23

Giverso, C. and Preziosi, L. (2018). Mechanical perspective on chemotaxis. Physical Review E, 98(6):062402. 27

Gomes, E. R., Jani, S., and Gundersen, G. G. (2005). Nuclear Movement Regulated by Cdc42, MRCK, Myosin, and Actin Flow Establishes MTOC Polarization in Migrating Cells. Cell, 121:451–463. 19

Gorelik, R. and Gautreau, A. (2014). Quantitative and unbiased analysis of directional persistence in cell migration. Nature Protocols, 9(8):1931–1943. Number: 8 Publisher: Nature Publishing Group. 21

Gracheva, M. E. and Othmer, H. G. (2004). A continuum model of motility in ameboid cells. Bulletin of Mathematical Biology, 66(1):167–193. 23

Hairer, M., Ryser, M. D., and Weber, H. (2012). Triviality of the 2D stochastic Allen-Cahn equation. Electronic Journal of Probability, 17(none). arXiv:1201.3089 [math-ph]. 34

Kloeden, P. E. and Platen, E. (1992). Probability and Statistics. In Kloeden, P. E. and Platen, E., editors, Numerical Solution of Stochastic Differential Equations, Applications of Mathematics, pages 1–50. Springer, Berlin, Heidelberg. 34

Kosmalska, A. J., Casares, L., Elosegui-Artola, A., Thottacherry, J. J., Moreno-Vicente, R., González-Tarragó, V., Del Pozo, M. A., Mayor, S., Arroyo, M., Navajas, D., Trepat, X., Gauthier, N. C., and Roca-Cusachs, P. (2015). Physical principles of membrane remodelling during cell mechanoadaptation. Nature Communications, 6(1):7292. 17

Kruse, K., Joanny, J. F., Jülicher, F., Prost, J., and Sekimoto, K. (2005). Generic theory of active polar gels: a paradigm for cytoskeletal dynamics. The European Physical Journal E, 16(1):5–16. 23

Kubiak, A., Zieliński, T., Pabijan, J., and Lekka, M. (2020). Nanomechanics in Monitoring the Effectiveness of Drugs Targeting the Cancer Cell Cytoskeleton. International Journal of Molecular Sciences, 21(22):8786. Number: 22 Publisher: Multidisciplinary Digital Publishing Institute. 17

Lammerding, J. (2011). Mechanics of the Nucleus. In Prakash, Y. S., editor, Comprehensive Physiology, pages 783–807. Wiley, 1 edition. 18, 19

Lavi, I. (2019). Physical modeling of cell motility and morphodynamics. phdthesis, Sorbonne Université. 31

Lavi, I., Meunier, N., Voituriez, R., and Casademunt, J. (2020). Motility and morphodynamics of confined cells. Physical Review E, 101(2):022404. Publisher: American Physical Society. 23, 25, 26, 29

Lefebvre, A. (2007). Modélisation numérique d'écoulements fluide/particules. phdthesis, Université Paris Sud. 28, 31

Liu, H., Wen, J., Xiao, Y., Liu, J., Hopyan, S., Radisic, M., Simmons, C. A., and Sun, Y. (2014). In Situ Mechanical Characterization of the Cell Nucleus by Atomic Force Microscopy. ACS Nano, 8(4):3821–3828. Publisher: American Chemical Society. 27

Loosley, A. J., O'Brien, X. M., Reichner, J. S., and Tang, J. X. (2015). Describing Directional Cell Migration with a Characteristic Directionality Time. PLOS ONE, 10(5):e0127425. 21

Maiuri, P., Rupprecht, J.-F., Wieser, S., Ruprecht, V., Bénichou, O., Carpi, N., Coppey, M., De Beco, S., Gov, N., Heisenberg, C.-P., Lage Crespo, C., Lautenschlaeger, F., Le Berre, M., Lennon-Dumenil, A.-M., Raab, M., Thiam, H.-R., Piel, M., Sixt, M., and Voituriez, R. (2015). Actin Flows Mediate a Universal Coupling between Cell Speed and Cell Persistence. Cell, 161(2):374–386. 20, 21, 22, 29

Maiuri, P., Terriac, E., Paul-Gilloteaux, P., Vignaud, T., McNally, K., Onuffer, J., Thorn, K., Nguyen, P. A., Georgoulia, N., Soong, D., Jayo, A., Beil, N., Beneke, J., Hong Lim, J. C., Pei-Ying Sim, C., Chu, Y.-S., Jiménez-Dalmaroni, A., Joanny, J.-F., Thiery, J.-P., Erfle, H., Parsons, M., Mitchison, T. J., Lim, W. A., Lennon-Duménil, A.-M., Piel, M., and Théry, M. (2012). The first World Cell Race. Current Biology, 22(17):R673–R675. 21

Mogilner, A. and Oster, G. (1996). Cell motility driven by actin polymerization. Biophysical Journal, 71(6):3030–3045. 22

Ndiaye, A.-B., Koenderink, G. H., and Shemesh, M. (2022). Intermediate Filaments in Cellular Mechanoresponsiveness: Mediating Cytoskeletal Crosstalk From Membrane to Nucleus and Back. Frontiers in Cell and Developmental Biology, 10:882037. 18

Peszat, S. and Zabczyk, J. (2007). Stochastic Partial Differential Equations with Lévy Noise: An Evolution Equation Approach. Encyclopedia of Mathematics and its Applications. Cambridge University Press, Cambridge. 33

Petrie, R. J., Doyle, A. D., and Yamada, K. M. (2009). Random versus directionally persistent cell migration. Nature Reviews Molecular Cell Biology, 10(8):538–549. 20, 21

Prost, J., Jülicher, F., and Joanny, J.-F. (2015). Active gel physics. Nature Physics, 11(2):111–117. 23

Recho, P. and Truskinovsky, L. (2013). Asymmetry between pushing and pulling for crawling cells. Physical Review E, 87(2):022720. Publisher: American Physical Society. 22

Reig, G., Pulgar, E., and Concha, M. L. (2014). Cell migration: from tissue culture to embryos. Development, 141(10):1999–2013. 19, 21

Scianna, M. and Preziosi, L. (2012). Multiscale Developments of the Cellular Potts Model. Multiscale Modeling & Simulation, 10(2):342–382. 22

Selmeczi, D., Li, L., Pedersen, L. I., Nrrelykke, S. F., Hagedorn, P. H., Mosler, S., Larsen, N. B., Cox, E. C., and Flyvbjerg, H. (2008). Cell motility as random motion: A review. The European Physical Journal Special Topics, 157(1):1–15. 21

Thiam, H.-R. (2014). Cell migration under confinement: how can a cell squeeze through narrow gaps? 17, 19

Tsimring, L. S. (2014). Noise in biology. Reports on Progress in Physics, 77(2):026601. 33

Walsh, J. B. (2005). Finite Element Methods for Parabolic Stochastic PDE's. Potential Analysis, 23(1):1–43. 34

Yam, P. T., Wilson, C. A., Ji, L., Hebert, B., Barnhart, E. L., Dye, N. A., Wiseman, P. W., Danuser, G., and Theriot, J. A. (2007). Actin–myosin network reorganization breaks symmetry at the cell rear to spontaneously initiate polarized cell motility. The Journal of Cell Biology, 178(7):1207–1221. 19, 20

2 - Analogous model in dimension 1

In this chapter, in collaboration with Nicolas Meunier, we introduce a one-dimensional model analogous to the general model (1.1) when considering the forces induced by the nucleus on the cell boundary and by the cell boundary on the nucleus, given by (1.22) and (1.23). This model is enriched by a dynamic of attachment and detachment of markers to the cell membrane. Here, we assume that the substrate is homogeneous and that there are neither obstacles nor external signals. We also neglect the effects of undercooling and noise. The one-dimensional model considered is a non-local, non-linear Fokker-Planck equation. After modelling the problem in one dimension, we prove that it is well-posed. We also study the stationary states of the model. Then, we construct a finite volume numerical scheme in order to simulate it. The study of the numerical results indicates that the model produces behaviours consistent with the biological context, highlighting the importance of positioning the nucleus at the rear of the cell for polarisation and the initiation of cell migration.

2.1 . Modelling

In this section, we write an analogous model in dimension 1 to the model (1.1) when the substrate is homogeneous, there is no external obstacles or signal and the effects of undercooling and noise are neglected. We recall that in dimension 2 the model of interest is then given by:

$$\begin{cases} \mathbf{u} + \nabla P = 0 & \text{in } \Omega(t) \setminus N(t), & \text{(2.1a)} \\ \operatorname{div}(\mathbf{u}) = 0 & \text{in } \Omega(t) \setminus N(t), & \text{(2.1b)} \\ P = \chi_c f_{\text{act}}(c(t,\mathbf{x})) - f_{\text{NB}} + \gamma\kappa & \text{on } \partial\Omega(t), & \text{(2.1c)} \\ V_n = \mathbf{u}\cdot\mathbf{n} & \text{on } \partial\Omega(t), & \text{(2.1d)} \\ \mathbf{u}\cdot\mathbf{n} = \mathbf{u}_{\text{nucl}}\cdot\mathbf{n} & \text{on } \partial N(t), & \text{(2.1e)} \\ \mathbf{u}_{\text{nucl}}(t) = \dfrac{1}{\xi_{\text{nucl}}|N|}\left(\displaystyle\int_{\partial N(t)} P(t,\mathbf{x})\mathbf{n}\,\mathrm{d}\sigma + \mathbf{f}_{\text{BN}}\right), & & \text{(2.1f)} \\ \partial_t c = \operatorname{div}(\nabla c - (1-a)\,\mathbf{u}c) & \text{in } \Omega(t) \setminus N(t), & \text{(2.1g)} \\ (\nabla c + a\mathbf{u}c)\cdot\mathbf{n} = 0 & \text{on } \partial(\Omega(t) \setminus N(t)), & \text{(2.1h)} \\ c(0,\mathbf{x}) = c^0(\mathbf{x}) & \text{in } \Omega(0). & \text{(2.1i)} \end{cases}$$

In dimension one, the cell domain is modeled by a segment $[b_-(t), b_+(t)]$. As in the two-dimensional case, we assume the cell to be filled with a fluid. This fluid is assumed to be incompressible. Then the length of the cell domain $b_+(t) - b_-(t)$ is constant in time. Initially, we assume to have $[b_-(0), b_+(0)] = [-1, 1]$. Thus for all $t > 0$, we have $b_+(t) - b_-(t) = 2$. We also assume that the fluid has a velocity u and a pressure P. Inside the fluid, markers of concentration c are present. We denote X_N the nucleus position. Analogous to the model (2.1), for all $t > 0$, we have:

$$\begin{cases} u + \partial_x P = 0 & \text{in }]b_-(t), b_+(t)[, & \text{(2.2a)} \\ \partial_x u = 0 & \text{in }]b_-(t), b_+(t)[, & \text{(2.2b)} \\ P = \chi_c f_{\text{act}}(c) - f_{\text{NB}} & \text{on } \{b_-(t), b_+(t)\}, & \text{(2.2c)} \end{cases}$$

where we recall that $\chi_c f_{\text{act}}$ is the active force of coupling between the markers and the fluid and f_{NB} is the force induce by the nucleus on the cell boundary.

Thus from eq. (2.2b) we have that there exists a function K_1 depending only on the time such that for all $x \in]b_-(t), b_+(t)[$:

$$u(t,x) = K_1(t).$$

Combining it with eq. (2.2a), there exists a function K_2 depending only on the time such that for all $x \in]b_-(t), b_+(t)[$:

$$P(t,x) = -K_1(t)\, x + K_2(t).$$

Using the boundary conditions eq. (2.2c) we deduce that:

$$u(t) = \frac{\chi_c \left(f_{\text{act}}\left(c\left(t, b_-(t)\right)\right) - f_{\text{act}}\left(c\left(t, b_+(t)\right)\right)\right) + f_{\text{NB}}\left(t, b_+(t)\right) - f_{\text{NB}}\left(t, b_-(t)\right)}{2}.$$

In dimension 2, f_{NB}, the force per unit of length exerted by the nucleus on the cell boundary, was defined by eq. (1.23). To find an equivalent in dimension 1, we project it on the x-axis. Thus we have:

$$f_{\text{NB}}\left(t, b_\pm(t)\right) = \mp\delta \frac{X_N(t) - b_\pm(t)}{\left|X_N(t) - b_\pm(t)\right|^\beta + \varepsilon}$$

where $\varepsilon > 0$ small.

In dimension 1, analogously to eqs. (2.1g) and (2.1h), the dynamic on the concentration writes:

$$\begin{cases} \partial_t c = \partial_{xx}^2 c - (1-a)\, u\, \partial_x c & \text{in }]b_-(t), b_+(t)[, \\ \partial_x c + a u\, c = 0 & \text{on } \{b_-(t), b_+(t)\}. \end{cases}$$

To write the dynamic of the nucleus position, we project the two-dimensional expression on the x-axis. Then, for all $t > 0$, we have:

$$\frac{\mathrm{d}}{\mathrm{d}t} X_N(t) = \frac{1}{\xi_{\text{nucl}}} u(t) + \frac{1}{\xi_{\text{nucl}}}\, \delta \left(\frac{X_N(t) - b_+(t)}{\left|X_N(t) - b_+(t)\right|^\beta + \varepsilon} + \frac{X_N(t) - b_-(t)}{\left|X_N(t) - b_-(t)\right|^\beta + \varepsilon} \right).$$

For all $x, x_+, x_- \in \mathbb{R}$, we set:

$$g_N(x, x_+, x_-) = \delta \left(\frac{x - x_+}{|x - x_+|^\beta + \varepsilon} + \frac{x - x_-}{|x - x_-|^\beta + \varepsilon} \right).$$

The model is then given by:

$$\begin{cases} \partial_t c(t,x) = \partial_{xx}^2 c(t,x) - (1-a)\, u(t)\ \partial_x c(t,x) & \text{in }]b_-(t), b_+(t)[, \\ \partial_x c(t,x) + a u(t)\ c(t,x) = 0 & \text{on } \{b_-(t), b_+(t)\}, \\ u(t) = \dfrac{1}{2}\left[\chi_c \left(f_{\text{act}}\left(c\left(t, b_-(t)\right)\right) - f_{\text{act}}\left(c\left(t, b_+(t)\right)\right)\right)\right] & \\ \qquad\qquad - \dfrac{1}{2} g_N\left(X_N(t), b_+(t), b_-(t)\right), & \\ \dfrac{\mathrm{d}}{\mathrm{d}t} X_N(t) = \dfrac{1}{\xi_{\text{nucl}}} u(t) + \dfrac{1}{\xi_{\text{nucl}}}\, g_N\left(X_N(t), b_+(t), b_-(t)\right). & \end{cases}$$

In the frame of reference of the cell, the model writes:

$$\begin{cases} \partial_t c(t,x) = \partial^2_{xx} c(t,x) + a u(t)\ \partial_x c(t,x) & \text{in }]-1,1[\,, \quad (2.3a) \\ \partial_x c(t,x) + a u(t)\ c(t,x) = 0 & \text{on } \{-1,1\}\,, \quad (2.3b) \\ u(t) = \dfrac{\chi_c\left(f_{\text{act}}\left(c(t,-1)\right) - f_{\text{act}}\left(c(t,1)\right)\right)}{2} - \dfrac{1}{2} g_N\left(X_N(t),1,-1\right), & (2.3c) \\ \dfrac{\mathrm{d}}{\mathrm{d}t} X_N(t) = \left(\dfrac{1}{\xi_{\text{nucl}}} - 1\right) u(t) + \dfrac{1}{\xi_{\text{nucl}}}\, g_N\left(X_N(t),1,-1\right). & (2.3d) \end{cases}$$

The model is complemented with an initial condition given by:

$$\begin{cases} c(0,x) = c^0(x) & \text{in } [-1,1]\,, \\ X_N(0) = X_N^0, \end{cases}$$

with $X_N^0 \in [-1,1]$.

In order to avoid blow-up phenomena, as in Etchegaray et al. (2017) or in Calvez et al. (2012), we enrich the model (2.3) with dynamical exchange of markers at the cell boundary. We denote $\mu_\pm(t)$ the quantity of markers at the membrane at location $b_\pm(t)$ and at time t. We assume that the markers can attach and detach from the membrane. Unlike in the case of the model (2.3), where the concentration of markers at the cell boundary exerts a feedback effect on the fluid velocity and therefore on the velocity of the cell, the feedback effects on the fluid comes from the markers attached to the membrane. In the frame of reference of the cell, the exchange dynamic at the membrane is given by:

$$\frac{\mathrm{d}}{\mathrm{d}t}\mu_\pm(t) = k_{\text{on}}\, c(t,\pm 1) - k_{\text{off}}\, \mu_\pm(t)\,,$$

where $k_{\text{on}} > 0$ is the rate of attachment and $k_{\text{off}} > 0$ the rate of detachment.

Setting $f_{\text{act}}(\mu) = \mu$, we have:

$$u(t) = \frac{\chi_c}{2}\left(\mu_-(t) - \mu_+(t)\right) + \frac{\delta}{2}\left(\frac{X_N(t)-1}{|X_N(t)-1|^\beta + \varepsilon} + \frac{X_N(t)+1}{|X_N(t)+1|^\beta + \varepsilon}\right).$$

For all $x \in [-1,1]$, we also set:

$$g(x) = \delta\left(\frac{x-1}{|x-1|^\beta + \varepsilon} + \frac{x+1}{|x+1|^\beta + \varepsilon}\right).$$

The equivalent model in dimension 1 of the model (2.1) in the cell frame of reference with the dynamical exchange at the membrane is given by:

$$\begin{cases} \partial_t c(t,x) = \partial^2_{xx} c(t,x) + a u(t)\ \partial_x c(t,x)\,, & x \in]-1,1[\,, \quad (2.4a) \\ \partial_x c(t,\pm 1) + a u(t)\ c(t,\pm 1) = \mp \dfrac{\mathrm{d}}{\mathrm{d}t}\mu_\pm(t)\,, & (2.4b) \\ \dfrac{\mathrm{d}}{\mathrm{d}t}\mu_\pm(t) = k_{\text{on}}\, c(t,\pm 1) - k_{\text{off}}\, \mu_\pm(t)\,, & (2.4c) \\ u(t) = \dfrac{\chi_c}{2}\left(\mu_-(t) - \mu_+(t)\right) - \dfrac{1}{2} g\left(X_N(t)\right), & (2.4d) \\ \dfrac{\mathrm{d}}{\mathrm{d}t} X_N(t) = \left(\dfrac{1}{\xi_{\text{nucl}}} - 1\right) u(t) + \dfrac{1}{\xi_{\text{nucl}}}\, g\left(X_N(t)\right). & (2.4e) \end{cases}$$

The model is complemented with an initial condition given by:

$$\begin{cases} c\left(0,x\right)=c^{0}\left(x\right), & x\in\left[-1,1\right], \quad (2.5a)\\ \mu_{\pm}\left(0\right)=\mu_{\pm}^{0}, & (2.5b)\\ X_{N}\left(0\right)=X_{N}^{0}, & (2.5c) \end{cases}$$

with $\mu_{\pm}^{0}\geq 0$ and $X_{N}^{0}\in[-1,1]$.

The total quantity of markers M is constant over time and for all $t\geq 0$ we have:

$$M=\int_{-1}^{1}c\left(t,x\right)\,\mathrm{d}x+\mu_{-}\left(t\right)+\mu_{+}\left(t\right).$$

2.2 . Well-posedness of the model

In this section we prove that, under some assumptions on the initial condition (2.5), the model (2.4) is well-posed.

Proposition 2.2.1. *Assume that c^{0} is such that $\int_{-1}^{1}c^{0}\left(x\right)\log c^{0}\left(x\right)\,\mathrm{d}x<+\infty$. Assume moreover that $\mu_{+}^{0},\mu_{-}^{0}\in[0,M]$ are such that $\int_{-1}^{1}c^{0}\left(x\right)\,\mathrm{d}x+\mu_{+}^{0}+\mu_{-}^{0}=M$. Assume also that $X_{N}^{0}\in[-1,1]$. Then there exists a unique solution $(c,\mu_{+},\mu_{-},X_{N})$ to the problem (2.4) for all time.*

To prove proposition 2.2.1, as in Lepoutre and Meunier (2022), we will first study an uncoupled model associate to (2.4) and then use a fixed point argument.

2.2.1 . Useful result

In this subsection, we prove a useful lemma which is inspired from Calvez et al. (2012).

Lemma 2.2.2. *Let $f\in L_{+}^{1}\left(-1,1\right)$. If $\int_{-1}^{1}f\log f<+\infty$ then $f\log f\in L^{1}\left(-1,1\right)$ and for all $\gamma>0$ the following inequality holds:*

$$\int_{-1}^{1}f\left(x\right)\left|\log f\left(x\right)\right|\,\mathrm{d}x\leq\int_{-1}^{1}f\left(x\right)\log f\left(x\right)\,\mathrm{d}x+\gamma+\frac{2}{\gamma e}.$$

Proof. We denote $\bar{f}=f\mathbb{1}_{f\leq 1}$ and $m=\int_{-1}^{1}\bar{f}\left(x\right)\,\mathrm{d}x$. The relative entropy between $\bar{f}$ and $x\mapsto\gamma e^{-\gamma x}$ is given by:

$$\begin{aligned}\int_{-1}^{1}\bar{f}\left(x\right)\left(\log\bar{f}\left(x\right)+\gamma x\right)\,\mathrm{d}x&=\int_{-1}^{1}\frac{\bar{f}\left(x\right)}{\gamma e^{-\gamma x}}\log\left(\frac{\bar{f}\left(x\right)}{\gamma e^{-\gamma x}}\right)\gamma e^{-\gamma x}\,\mathrm{d}x+m\log\gamma\\&\geq\int_{-1}^{1}\frac{\bar{f}\left(x\right)}{\gamma e^{-\gamma x}}\gamma e^{-\gamma x}\,\mathrm{d}x\log\left(\int_{-1}^{1}\frac{\bar{f}\left(x\right)}{\gamma e^{-\gamma x}}\gamma e^{-\gamma x}\,\mathrm{d}x\right)+m\log\gamma\\&\geq m\log\left(\gamma m\right)\\&\geq-\frac{1}{\gamma e}.\end{aligned}$$

We also have:

$$\frac{-\gamma}{2}\leq\int_{-1}^{1}\bar{f}\left(x\right)\gamma x\,\mathrm{d}x\leq\frac{\gamma}{2}.$$

Since:

$$\int_{-1}^{1} f(x) |\log f(x)| \, \mathrm{d}x = \int_{-1}^{1} f(x) \log f(x) \, \mathrm{d}x - 2 \int_{-1}^{1} \bar{f}(x) \log \bar{f}(x) \, \mathrm{d}x,$$

we have:

$$\int_{-1}^{1} f(x) |\log f(x)| \, \mathrm{d}x \leq \int_{-1}^{1} f(x) \log f(x) \, \mathrm{d}x + \gamma + \frac{2}{\gamma e}.$$

□

2.2.2 . An uncoupled PDE

In this subsection, we study the following uncoupled PDE system where, for all $t \geq 0$, μ_+, μ_- and v are given:

$$\begin{cases} \partial_t c(t,x) = \partial_{xx}^2 c(t,x) + v(t) \partial_x c(t,x) & x \in]-1,1[, \quad (2.6a) \\ \partial_x c(t,1) + v(t) c(t,1) = -\left(k_{\mathrm{on}} c(t,1) - k_{\mathrm{off}} \mu_+(t)\right), & (2.6b) \\ \partial_x c(t,-1) + v(t) c(t,-1) = k_{\mathrm{on}} c(t,-1) - k_{\mathrm{off}} \mu_-(t), & (2.6c) \\ c(0,x) = c^0(x) & x \in [-1,1]. \quad (2.6d) \end{cases}$$

We assume c^0, μ_+ and μ_- to be such that:

$$\int_{-1}^{1} c^0(x) \, \mathrm{d}x + \mu_-(0) + \mu_+(0) = M.$$

We want to prove that this problem admits a global solution.

For smooth μ_+, μ_-, α_+, α_-, v and c^0, (2.6) is a parabolic problem and then there exists a local solution c defined over $[0,T]$ with $T > 0$.

Lemma 2.2.3. *Assume $c^0 \geq 0$ and for all $t \geq 0$, $\mu_\pm(t) \geq 0$. Let c be a solution of (2.6) define on $[0,T] \times [-1,1]$. Then c is nonnegative.*

Proof. Let c be a solution of (2.6). We denote $c_- = \min(c, 0)$. We want to prove that $c_- = 0$. Using the Stampacchia argument, we have :

$$\begin{aligned} \frac{1}{2} \frac{\mathrm{d}}{\mathrm{d}t} \|c_-(t)\|_{L^2}^2 &= \int_{-1}^{1} \partial_t c(t,x) \, c_-(t,x) \, \mathrm{d}x \\ &= -\left[k_{\mathrm{on}} c(t,1) - k_{\mathrm{off}} \mu_+(t)\right] c_-(t,1) - \left[k_{\mathrm{on}} c(t,-1) - k_{\mathrm{off}} \mu_-(t)\right] c_-(t,-1) \\ &\quad - \int_{-1}^{1} \left(\partial_x c_-(t,x)\right)^2 + v(t) c(t,x) \partial_x c_-(t,x) \, \mathrm{d}x \\ &= -k_{\mathrm{on}} \left(c_-(t,1)\right)^2 - k_{\mathrm{on}} \left(c_-(t,-1)\right)^2 \\ &\quad + k_{\mathrm{off}} \mu_+(t) c_-(t,1) + k_{\mathrm{off}} \mu_-(t) c_-(t,-1) \\ &\quad - \|\partial_x c_-(t)\|_{L^2}^2 - \int_{-1}^{1} v(t) c_-(t,x) \partial_x c_-(t,x) \, \mathrm{d}x \\ &\leq -\|\partial_x c_-(t)\|_{L^2}^2 - \int_{-1}^{1} v(t) c_-(t,x) \partial_x c_-(t,x) \, \mathrm{d}x \\ &\leq \frac{1}{4} |v(t)|^2 \|c_-(t)\|_{L^2}^2. \end{aligned}$$

We also have $\|c_-(0)\|_{L^2}^2 = 0$. Using Gronwall's lemma, we have that for all $t \in [0,T]$, $\|c_-(t)\|_{L^2}^2 = 0$. Thus for all $t \in [0,T]$ and $x \in [-1,1]$, we have $c(t,x) \geq 0$. □

Lemma 2.2.4. *Assume that $c^0 \in L^1(-1,1)$ is a positive function such that $\int_{-1}^1 c^0(x)\log c^0(x)\,\mathrm{d}x < +\infty$. Assume also that $\mu_\pm \in C^0(\mathbb{R}_+)$ satisfy for all $t>0$, $0<\mu_\pm(0)\,e^{-k_{\mathrm{off}}\,t} \le \mu_\pm(t) \le M$. Assume moreover that $v \in C^0(\mathbb{R}_+)\cap L^\infty(\mathbb{R}_+)$. Then the solution of the uncoupled system (2.6) exists globally in $L^\infty_{loc}(\mathbb{R}_+, L\log L(-1,1)) \cap L^1_{loc}\left(\mathbb{R}_+, W^{1,1}(-1,1)\right)$. In addition, for all $t\ge 0$, we have:*

$$\int_{-1}^1 c(t,x)\,\mathrm{d}x \le \int_{-1}^1 c^0(x)\,\mathrm{d}x + 2k_{\mathrm{off}} M\,t.$$

Proof. First, for all $t\ge 0$, we have:

$$\begin{aligned}
\frac{\mathrm{d}}{\mathrm{d}t}\int_{-1}^1 c(t,x)\,\mathrm{d}x &= \int_{-1}^1 \partial_t c(t,x)\,\mathrm{d}x \\
&= -\left(k_{\mathrm{on}}\,c(t,1) - k_{\mathrm{off}}\,\mu_+(t)\right) - \left(k_{\mathrm{on}}\,c(t,-1) - k_{\mathrm{off}}\,\mu_-(t)\right) \\
&\le k_{\mathrm{off}}\,\left(\mu_+(t)+\mu_-(t)\right) \\
&\le 2k_{\mathrm{off}}\,M.
\end{aligned}$$

Thus, for all $t\ge 0$, we have:

$$\int_{-1}^1 c(t,x)\,\mathrm{d}x \le \int_{-1}^1 c^0(x)\,\mathrm{d}x + 2k_{\mathrm{off}}\,Mt.$$

Using the convexity of the function $x \mapsto (k_{\mathrm{on}}\,x - k_{\mathrm{off}}\,\mu_\pm(t))\log x$, we have that for all $t\ge 0$ and $x\in[-1,1]$:

$$(k_{\mathrm{on}}\,c(t,x) - k_{\mathrm{off}}\,\mu_\pm(t))\log c(t,x) - (k_{\mathrm{on}} - k_{\mathrm{off}}\,\mu_\pm(t))\log\left(\frac{k_{\mathrm{off}}}{k_{\mathrm{on}}}\mu_\pm(t)\right) \ge 0.$$

We also have:

$$\begin{aligned}
&\frac{\mathrm{d}}{\mathrm{d}t}\int_{-1}^1 c(t,x)\log c(t,x) - c(t,x)\,\mathrm{d}x \\
&\quad= \int_{-1}^1 \partial_t c(t,x)\log c(t,x)\,\mathrm{d}x \\
&\quad= -\left(k_{\mathrm{on}}\,c(t,1) - k_{\mathrm{off}}\,\mu_+(t)\right)\log c(t,1) - \left(k_{\mathrm{on}}\,c(t,-1) - k_{\mathrm{off}}\,\mu_-(t)\right)\log c(t,-1) \\
&\qquad - \int_{-1}^1 \left(c(t,x)\,\partial_x \log c(t,x) + v(t)\,c(t,x)\right)\partial_x \log c(t,x)\,\mathrm{d}x \\
&\quad\le -\left(k_{\mathrm{on}} - k_{\mathrm{off}}\,\mu_+(t)\right)\log\left(\frac{k_{\mathrm{off}}}{k_{\mathrm{on}}}\mu_+(t)\right) - \left(k_{\mathrm{on}} - k_{\mathrm{off}}\,\mu_-(t)\right)\log\left(\frac{k_{\mathrm{off}}}{k_{\mathrm{on}}}\mu_-(t)\right) \\
&\qquad - \int_{-1}^1 c(t,x)\left|\partial_x \log c(t,x)\right|^2\,\mathrm{d}x - \int_{-1}^1 c(t,x)\,v(t)\,\partial_x \log c(t,x)\,\mathrm{d}x \\
&\quad\le C_1 + 2k_{\mathrm{on}}t - \frac{1}{2}\int_{-1}^1 c(t,x)\left|\partial_x \log c(t,x)\right|^2\,\mathrm{d}x + \frac{1}{2}\left|v(t)\right|^2\int_{-1}^1 c(t,x)\,\mathrm{d}x \\
&\quad\le C_1 + 2k_{\mathrm{on}}t + \frac{1}{2}\left\|v\right\|_{L^\infty}^2\left(\int_{-1}^1 c^0(x)\,\mathrm{d}x + 2k_{\mathrm{off}}Mt\right),
\end{aligned} \tag{2.7}$$

with $C_1>0$.

Then, integrating the previous inequality, we have:

$$\begin{aligned}\int_{-1}^{1} c\left(t,x\right)\log c\left(t,x\right)\,\mathrm{d}x \leq \int_{-1}^{1} c^{0}\left(x\right)\log c^{0}\left(x\right)\,\mathrm{d}x + C_1 t + k_{\mathrm{on}}t^2 \\ + \frac{1}{2}\left\|v\right\|_{L^\infty}^2\left(t\int_{-1}^{1} c^{0}\left(x\right)\,\mathrm{d}x + k_{\mathrm{off}}Mt^2\right) \\ \leq C_2\left(1+t^2\right),\end{aligned}$$

with $C_2 > 0$.

We can apply the lemma 2.2.2 and we have:

$$\int_{-1}^{1} c\left(t,x\right)\left|\log c\left(t,x\right)\right|\,\mathrm{d}x \leq C_3\left(1+t^2\right),$$

with $C_3 > 0$.

Then, integrating (2.7), we also have:

$$\begin{aligned}\int_0^t\int_{-1}^{1} c\left(s,x\right)\left|\partial_x \log c\left(s,x\right)\right|^2\,\mathrm{d}x\,\mathrm{d}s &\leq C_4\left(1+t^2\right) - \int_{-1}^{1} c\left(t,x\right)\log c\left(t,x\right)\,\mathrm{d}x \\ &\leq C_4\left(1+t^2\right) + \int_{-1}^{1} c\left(t,x\right)\left|\log c\left(t,x\right)\right|\,\mathrm{d}x \\ &\leq C_5\left(1+t^2\right),\end{aligned}$$

with $C_4 > 0$ and $C_5 > 0$.

Thus, finally, we have:

$$\begin{aligned}\int_0^t\int_{-1}^{1}\left|\partial_x c\left(s,x\right)\right|\,\mathrm{d}x\,\mathrm{d}s &= \int_0^t\int_{-1}^{1} c\left(s,x\right)\left|\partial_x \log c\left(s,x\right)\right|\,\mathrm{d}x\,\mathrm{d}s \\ &\leq \left(\int_0^t\int_{-1}^{1} c\left(s,x\right)\,\mathrm{d}x\,\mathrm{d}s\right)^{\frac{1}{2}} \\ &\quad\times\left(\int_0^t\int_{-1}^{1} c\left(s,x\right)\left|\partial_x \log c\left(s,x\right)\right|^2\,\mathrm{d}x\,\mathrm{d}s\right)^{\frac{1}{2}} \\ &\leq C_6\left(1+t^2\right),\end{aligned}$$

with $C_6 > 0$ and this leads to the global existence of c. □

2.2.3 . Fixed point mapping

2.2.3.1 . Useful results

Let c_1 and c_2 be two solutions of (2.6) with two different inputs given by $\left(\mu_{\pm}^1, X_N^1, v^1\right)$ and $\left(\mu_{\pm}^2, X_N^2, v^2\right)$. As in Lepoutre and Meunier (2022) to compare these two solutions, we introduce the Gajewski metric:

$$d_G\left(c_1,c_2\right) = \int_{-1}^{1} h\left(c_1\right) + h\left(c_2\right) - 2h\left(\frac{c_1+c_2}{2}\right)\,\mathrm{d}x,$$

where h is the following function:

$$h\left(a\right) = a\log a - a + 1.$$

We define the function Δ_h by:

$$\Delta_h(c_1, c_2) = h(c_1) + h(c_2) - 2h\left(\frac{c_1 + c_2}{2}\right).$$

We recall the following lemma from Lepoutre and Meunier (2022).

Lemma 2.2.5. *For all $a, b > 0$ and c_1, c_2 positive functions, the following inequalities hold*

$$0 \leq \frac{1}{4}\frac{(b-a)^2}{a+b} \leq \frac{1}{4}\frac{(b-a)^2}{\max(a,b)} \leq \Delta_h(a,b) \leq \frac{1}{4}\frac{(b-a)^2}{\min(a,b)}$$

and

$$d_G(c_1, c_2) \geq \frac{1}{4}\frac{\left(\int_{-1}^1 c_1 \,\mathrm{d}x - \int_{-1}^1 c_2 \,\mathrm{d}x\right)^2}{\int_{-1}^1 c_1 \,\mathrm{d}x + \int_{-1}^1 c_2 \,\mathrm{d}x}.$$

We introduce the following notations $c_m = \frac{c_1 + c_2}{2}$, $q_1 = \frac{c_1}{c_m}$ and $q_2 = \frac{c_2}{c_m}$.

Lemma 2.2.6. *For all $t > 0$ the following inequality hold:*

$$\begin{aligned}
\frac{\mathrm{d}}{\mathrm{d}t} d_G(c_1, c_2)(t) \leq\ & k_{\mathrm{off}}\left(\Delta_h\left(\mu_+^1(t), \mu_+^2(t)\right) + \Delta_h\left(\mu_-^1(t), \mu_-^2(t)\right)\right) \\
& - k_{\mathrm{on}}\left(\Delta_h\left(c_1(t,1), c_2(t,1)\right) + \Delta_h\left(c_1(t,-1), c_2(t,-1)\right)\right) \\
& - \frac{3}{4}\int_{-1}^1 c_1(t,x)\left|\partial_x \log q_1(t,x)\right|^2 + c_2(t,x)\left|\partial_x \log q_2(t,x)\right|^2 \,\mathrm{d}x \\
& + \frac{1}{2}\left(v^1(t) - v^2(t)\right)^2 \int_{-1}^1 c_m(t,x) \,\mathrm{d}x.
\end{aligned}$$

Proof. We have

$$\begin{aligned}
\frac{\mathrm{d}}{\mathrm{d}t} d_G(c_1, c_2)(t) &= \int_{-1}^1 \partial_t c_1(t,x) \log q_1(t,x) + \partial_t c_2(t,x) \log q_2(t,x) \,\mathrm{d}x \\
&= \sum_{i=1}^2 k_{\mathrm{off}}\left[\mu_+^i(t) \log q_i(t,1) + \mu_-^i \log q_i(t,-1)\right] \\
&\quad - k_{\mathrm{on}}\left[c_1(t,1) \log q_1(t,1) + c_2(t,1) \log q_2(t,1)\right] \\
&\quad - k_{\mathrm{on}}\left[c_1(t,-1) \log q_1(t,-1) + c_2(t,-1) \log q_2(t,-1)\right] \\
&\quad - \sum_{i=1}^2 \int_{-1}^1 c_m(t,x)\left(\partial_x \log c_i(t,x) + v^i(t)\right) \partial_x q_i(t,x) \,\mathrm{d}x.
\end{aligned}$$

We notice that the function $q \mapsto \mu_+ \log q + \mu_- \log(2-q)$ reaches its maximum for the value $q^* = \frac{2\mu_+}{\mu_+ + \mu_-}$. Then we have:

$$\begin{aligned}
&\sum_{i=1}^2 k_{\mathrm{off}}\left[\mu_+^i(t) \log q_i(t,1) + \mu_-^i \log q_i(t,-1)\right] \\
&\qquad\qquad \leq k_{\mathrm{off}}\left(\Delta_h\left(\mu_+^1(t), \mu_+^2(t)\right) + \Delta_h\left(\mu_-^1(t), \mu_-^2(t)\right)\right).
\end{aligned}$$

We remark that:

$$c_1(t,\pm 1) \log q_1(t,\pm 1) + c_2(t,\pm 1) \log q_2(t,\pm 1) = \Delta_h\left(c_1(t,\pm 1), c_2(t,\pm 1)\right).$$

We also have

$$
\begin{aligned}
&-\int_{-1}^{1} c_m(t,x)\left(v^1(t)-v^2(t)\right)\partial_x q_1(t,x)\,\mathrm{d}x \\
&\quad=-\frac{1}{2}\int_{-1}^{1} c_1(t,x)\left(v^1(t)-v^2(t)\right)\partial_x \log q_1(t,x)\,\mathrm{d}x \\
&\qquad+\frac{1}{2}\int_{-1}^{1} c_2(t,x)\left(v^1(t)-v^2(t)\right)\partial_x \log q_2(t,x)\,\mathrm{d}x \\
&\quad\leq \frac{1}{4}\int_{-1}^{1} c_1(t,x)\left(v^1(t)-v^2(t)\right)^2\mathrm{d}x+\frac{1}{4}c_1(t,x)\left(\partial_x \log q_1(t,x)\right)^2\mathrm{d}x \\
&\qquad+\frac{1}{4}\int_{-1}^{1} c_2(t,x)\left(v^1(t)-v^2(t)\right)^2\mathrm{d}x+\frac{1}{4}c_2(t,x)\left(\partial_x \log q_2(t,x)\right)^2\mathrm{d}x \\
&\quad\leq \frac{1}{2}\left(v^1(t)-v^2(t)\right)^2\int_{-1}^{1} c_m(t,x)\,\mathrm{d}x \\
&\qquad+\frac{1}{4}\int_{-1}^{1} c_1(t,x)\left|\partial_x \log q_1(t,x)\right|^2+c_2(t,x)\left|\partial_x \log q_2(t,x)\right|^2\mathrm{d}x
\end{aligned}
$$

and

$$
\frac{c_1+c_2}{q_1(2-q_1)}\left|\partial_x q_1\right|^2=c_1\left|\partial_x \log q_1\right|^2+c_2\left|\partial_x \log q_2\right|^2.
$$

By combining all this, the desired result is obtained. □

2.2.3.2 . The fixed point mapping

For a fixed $T>0$, we define the following space $\mathcal{X}$

$$
\mathcal{X}=\left\{\begin{array}{l}(\mu_+,\mu_-,X_N)\in C(0,T),\forall t\in(0,T)\\ 0<\mu_\pm^0 e^{-k_{\mathrm{off}}t}\leq\mu_\pm(t)\leq M \text{ and } -1\leq X_N(t)\leq 1\end{array}\right\}.
$$

We want to study (2.6) with $v(t)=\dfrac{\chi_c}{2}\left(\mu_-(t)-\mu_+(t)\right)-\dfrac{1}{2}g\left(X_N(t)\right)$. From the previous section, we know that, with this choice of velocity, (2.6) admits a global solution.

We also define:

$$
\nu_\pm(t)=\mu_\pm^0 e^{-k_{\mathrm{off}}t}+\int_0^t k_{\mathrm{on}}e^{k_{\mathrm{off}}(s-t)}c(s,\pm1)\,\mathrm{d}s
$$

and the truncation function χ_μ such that for all $x\in\mathbb{R}$:

$$
\chi_\mu(x)=\left\{\begin{array}{ll}0 & \text{if } x<0,\\ x & \text{if } 0\leq x\leq M,\\ 1 & \text{if } x>M.\end{array}\right.
$$

Then we define:

$$
Y_N(t)=X_N^0+\int_0^t\frac{\chi_c}{2}\left(\frac{1}{\xi_{\mathrm{nucl}}}-1\right)\left(\mu_-(s)-\mu_+(s)\right)+\frac{1+\xi_{\mathrm{nucl}}}{2\xi_{\mathrm{nucl}}}g\left(X_N(s)\right)\mathrm{d}s
$$

and the truncation function χ_{x} such that for all $x\in\mathbb{R}$:

$$
\chi_{\mathsf{x}}(x)=\left\{\begin{array}{ll}-1 & \text{if } x<-1,\\ x & \text{if } -1\leq x\leq 1,\\ 1 & \text{if } x>1.\end{array}\right.
$$

Let F be the mapping defined by:

$$\begin{array}{rccc} F: & \mathcal{X} & \longrightarrow & \mathcal{X} \\ & (\mu_+, \mu_-, X_N) & \longmapsto & \left(\chi_\mu(\nu_+), \chi_\mu(\nu_-), \chi_{\mathsf{x}}(Y_N)\right). \end{array}$$

We denote by F^n the function composed n times with itself, that is $F^n = F \circ F \circ \cdots \circ F$. We assume that the two solutions c_1 and c_2 of eq. (2.6) obtained with different inputs $\left(\mu_\pm^1, X_N^1, v^1\right)$ and $\left(\mu_\pm^2, X_N^2, v^2\right)$ are obtained with the same initial conditions c^0, μ_+^0, μ_-^0 and X_N^0.

Proposition 2.2.7. *For all $\left(\mu_+^1, \mu_-^1, X_N^1\right), \left(\mu_+^2, \mu_-^2, X_N^2\right) \in \mathcal{X}$, there exists $C(T)$ such that:*

$$\left\|F^n\left(\mu_+^1, \mu_-^1, X_N^1\right) - F^n\left(\mu_+^2, \mu_-^2, X_N^2\right)\right\|_{\mathcal{X}} \leq \frac{(C(T)T)^n}{n!} \left\|\left(\mu_+^1, \mu_-^1, X_N^1\right) - \left(\mu_+^2, \mu_-^2, X_N^2\right)\right\|_{\mathcal{X}}.$$

Proof. Let $\left(\mu_+^1, \mu_-^1, X_N^1\right), \left(\mu_+^2, \mu_-^2, X_N^2\right)$ be two elements of $\mathcal{X}$. We have:

$$\begin{aligned} &\left\|F\left(\mu_+^1, \mu_-^1, X_N^1\right) - F\left(\mu_+^2, \mu_-^2, X_N^2\right)\right\|_{\mathcal{X}}^2 \\ &= \int_0^T \left(\chi_\mu\left(\nu_+^1(t)\right) - \chi_\mu\left(\nu_+^2(t)\right)\right)^2 \mathrm{d}t \\ &\quad + \int_0^T \left(\chi_\mu\left(\nu_-^1(t)\right) - \chi_\mu\left(\nu_-^2(t)\right)\right)^2 \mathrm{d}t \\ &\quad + \int_0^T \left(\chi_{\mathsf{x}}\left(Y_N^1(t)\right) - \chi_{\mathsf{x}}\left(Y_N^2(t)\right)\right)^2 \mathrm{d}t \end{aligned}$$

First, since χ_{x} is a 1-lipschitz function, we have, for all $t \in [0,T]$:

$$\left(\chi_{\mathsf{x}}\left(Y_N^1(t)\right) - \chi_{\mathsf{x}}\left(Y_N^2(t)\right)\right)^2 \leq \left(Y_N^1(t) - Y_N^2(t)\right)^2.$$

Using the expression of Y_N and the Cauchy-Schwarz inequality, we have:

$$\begin{aligned} &\left(\chi_{\mathsf{x}}\left(Y_N^1(t)\right) - \chi_{\mathsf{x}}\left(Y_N^2(t)\right)\right)^2 \\ &\leq \frac{\chi^2}{2}\left(\frac{1}{\xi_{\mathrm{nucl}}} - 1\right)^2 t\left(\int_0^t \left(\mu_-^1(s) - \mu_-^2(s)\right)^2 \mathrm{d}s + \int_0^t \left(\mu_+^1(s) - \mu_+^2(s)\right)^2 \mathrm{d}s\right) \\ &\quad + \frac{(1+\xi_{\mathrm{nucl}})^2}{2\xi_{\mathrm{nucl}}^2} t \int_0^t \left(g\left(X_N^1(s)\right) - g\left(X_N^2(s)\right)\right)^2 \mathrm{d}s. \end{aligned}$$

g is a differentiable function and its derivative is continuous, then g is a lipshitz function over $[-1,1]$. There exists $C_1 > 0$ a constant such that:

$$\begin{aligned} &\left(\chi_{\mathsf{x}}\left(Y_N^1(t)\right) - \chi_{\mathsf{x}}\left(Y_N^2(t)\right)\right)^2 \\ &\qquad \leq C_1 t \int_0^t \left(\mu_-^1(s) - \mu_-^2(s)\right)^2 + \left(\mu_+^1(s) - \mu_+^2(s)\right)^2 + \left(X_N^1(s) - X_N^2(s)\right)^2 \mathrm{d}s. \end{aligned}$$

Secondly, since χ_μ is a 1-lipschitz function, we have, for all $t \in [0,T]$:

$$\begin{aligned} &\left(\chi_\mu\left(\nu_+^1(t)\right) - \chi_\mu\left(\nu_+^2(t)\right)\right)^2 + \left(\chi_\mu\left(\nu_-^1(t)\right) - \chi_\mu\left(\nu_-^2(t)\right)\right)^2 \\ &\qquad \leq \left(\nu_+^1(t) - \nu_+^2(t)\right)^2 + \left(\nu_-^1(t) - \nu_-^2(t)\right)^2. \end{aligned}$$

We have:

$$\left(\nu_\pm^1(t) - \nu_\pm^2(t)\right)^2 = \left(\int_0^t k_{\mathrm{on}} e^{k_{\mathrm{off}}(s-t)} \left(c_1(s, \pm 1) - c_2(s, \pm 1)\right) \mathrm{d}s\right)^2.$$

Using Cauchy-Schwarz inequality, we have:

$$\begin{aligned}
&\left(\int_0^t k_{\text{on}} e^{k_{\text{off}}(s-t)} \left(c_1(s,\pm 1) - c_2(s,\pm 1)\right) \mathrm{d}s\right)^2 \\
&\leq \left(\int_0^t k_{\text{on}} e^{k_{\text{off}}(s-t)} \left|c_1(s,\pm 1) - c_2(s,\pm 1)\right| \mathrm{d}s\right)^2 \\
&\leq k_{\text{on}}^2 \left(\int_0^t \frac{\left|c_1(s,\pm 1) - c_2(s,\pm 1)\right|^2}{c_1(s,\pm 1) + c_2(s,\pm 1)} \mathrm{d}s\right) \left(\int_0^t e^{2k_{\text{off}}(s-t)} \left(c_1(s,\pm 1) + c_2(s,\pm 1)\right) \mathrm{d}s\right) \\
&\leq k_{\text{on}}^2 \left(\int_0^t \frac{\left|c_1(s,\pm 1) - c_2(s,\pm 1)\right|^2}{c_1(s,\pm 1) + c_2(s,\pm 1)} \mathrm{d}s\right) \left(\int_0^t c_1(s,\pm 1) + c_2(s,\pm 1) \mathrm{d}s\right).
\end{aligned}$$

Using lemma 2.2.5, we have:

$$\begin{aligned}
&\left(\int_0^t k_{\text{on}} e^{k_{\text{off}}(s-t)} \left(c_1(s,\pm 1) - c_2(s,\pm 1)\right) \mathrm{d}s\right)^2 \\
&\qquad \leq 4k_{\text{on}}^2 \left(\int_0^t \Delta_h\left(c_1(s,\pm 1), c_2(s,\pm 1)\right) \mathrm{d}s\right) \left(\int_0^t c_1(s,\pm 1) + c_2(s,\pm 1) \mathrm{d}s\right).
\end{aligned}$$

Using the boundary condition of (2.4) and the constraint on the total quantity of markers, it follows:

$$\begin{aligned}
&\left(\int_0^t k_{\text{on}} e^{k_{\text{off}}(s-t)} \left(c_1(s,\pm 1) - c_2(s,\pm 1)\right) \mathrm{d}s\right)^2 \\
&\qquad \leq 8k_{\text{on}}k_{\text{off}} M(1+t) \int_0^t \Delta_h\left(c_1(s,\pm 1), c_2(s,\pm 1)\right) \mathrm{d}s.
\end{aligned}$$

Integrating the inequality of lemma 2.2.6, we have:

$$\begin{aligned}
&d_G(c_1,c_2)(t) - d_G(c_1,c_2)(0) \\
&\leq \int_0^t k_{\text{off}} \left(\Delta_h\left(\mu_+^1(s), \mu_+^2(s)\right) + \Delta_h\left(\mu_-^1(s), \mu_-^2(s)\right)\right) \mathrm{d}s \\
&\quad - \int_0^t k_{\text{on}} \left(\Delta_h\left(c_1(s,1), c_2(s,1)\right) + \Delta_h\left(c_1(s,-1), c_2(s,-1)\right)\right) \mathrm{d}s \\
&\quad - \frac{3}{4} \int_0^t \int_{-1}^1 c_1(s,x) \left|\partial_x \log q_1(s,x)\right|^2 + c_2(s,x) \left|\partial_x \log q_2(s,x)\right|^2 \mathrm{d}x \, \mathrm{d}s \\
&\quad + \frac{1}{2} \int_0^t \left(v^1(s) - v^2(s)\right)^2 \int_{-1}^1 c_m(s,x) \mathrm{d}x \, \mathrm{d}s.
\end{aligned}$$

Since the initial conditions are the same, we have $d_G(c_1,c_2)(t) \geq 0$ and $d_G(c_1,c_2)(0) = 0$. It leads to:

$$\begin{aligned}
&k_{\text{on}} \int_0^t \Delta_h\left(c_1(s,1), c_2(s,1)\right) + \Delta_h\left(c_1(s,-1), c_2(s,-1)\right) \mathrm{d}s \\
&\quad \leq k_{\text{off}} \int_0^t \left(\Delta_h\left(\mu_+^1(s), \mu_+^2(s)\right) + \Delta_h\left(\mu_-^1(s), \mu_-^2(s)\right)\right) \mathrm{d}s \\
&\qquad + \frac{1}{2} \int_0^t \left(v^1(s) - v^2(s)\right)^2 \int_{-1}^1 c_m(s,x) \mathrm{d}x \, \mathrm{d}s.
\end{aligned}$$

Using the result of lemma 2.2.5, we have:

$$\Delta_h\left(\mu_\pm^1(s),\mu_\pm^2(s)\right)\leq\frac{e^{k_{\text{off}}s}}{4\mu_\pm^0}\left(\mu_\pm^1(s)-\mu_\pm^2(s)\right)^2.$$

Using the expression of v, we have:

$$\begin{aligned}
&\int_0^t\left(v^1(s)-v^2(s)\right)^2\int_{-1}^1 c_m(s,x)\,\mathrm{d}x\,\mathrm{d}s\\
&\quad\leq M\int_0^t\chi^2\left(\left(\mu_-^1(s)-\mu_-^2(s)\right)^2+\left(\mu_+^1(s)-\mu_+^2(s)\right)^2\right)\\
&\qquad+2\left(g\left(X_N^1(s)\right)-g\left(X_N^2(s)\right)\right)^2\mathrm{d}s\\
&\quad\leq C_2\int_0^t\left(\mu_-^1(s)-\mu_-^2(s)\right)^2+\left(\mu_+^1(s)-\mu_+^2(s)\right)^2+\left(X_N^1(s)-X_N^2(s)\right)^2\mathrm{d}s,
\end{aligned}$$

with $C_2>0$.

Hence:

$$\begin{aligned}
&k_{\text{on}}\int_0^t\Delta_h\left(c_1(s,1),c_2(s,1)\right)+\Delta_h\left(c_1(s,-1),c_2(s,-1)\right)\mathrm{d}s\\
&\quad\leq C_3(t)\int_0^t\left(\mu_-^1(s)-\mu_-^2(s)\right)^2+\left(\mu_+^1(s)-\mu_+^2(s)\right)^2+\left(X_N^1(s)-X_N^2(s)\right)^2\mathrm{d}s,
\end{aligned}$$

with $C_3(t)=\max\left(k_{\text{off}}\frac{e^{k_{\text{off}}t}}{4\mu_+^0},k_{\text{off}}\frac{e^{k_{\text{off}}t}}{4\mu_-^0},C_2\right)$.

We thus have:

$$\begin{aligned}
&\left(\chi_\mu\left(\nu_+^1(t)\right)-\chi_\mu\left(\nu_+^2(t)\right)\right)^2+\left(\chi_\mu\left(\nu_-^1(t)\right)-\chi_\mu\left(\nu_-^2(t)\right)\right)^2\\
&\quad\leq k_{\text{on}}C_3(t)\int_0^t\left(\mu_-^1(s)-\mu_-^2(s)\right)^2+\left(\mu_+^1(s)-\mu_+^2(s)\right)^2+\left(X_N^1(s)-X_N^2(s)\right)^2\mathrm{d}s.
\end{aligned}$$

Finally, we have:

$$\begin{aligned}
&\left\|F\left(\mu_+^1,\mu_-^1,X_N^1\right)-F\left(\mu_+^2,\mu_-^2,X_N^2\right)\right\|_{\mathcal{X}}\\
&\quad\leq K(T)\int_0^T\int_0^t\left(\mu_+^1(s)-\mu_+^2(s)\right)^2+\left(\mu_-^1(s)-\mu_-^2(s)\right)^2+\left(X_N^1(s)-X_N^2(s)\right)^2\mathrm{d}s\,\mathrm{d}t,
\end{aligned}$$

which leads to the result. □

2.3 . Stationary solutions

In this section, we compute the stationary states of the model (2.4). To do this, we set $\partial_t c=0$, $\frac{\mathrm{d}}{\mathrm{d}t}\mu_\pm=0$ and $\frac{\mathrm{d}}{\mathrm{d}t}X_N=0$ and solve the associated spatial ODE. We find that there exists one to three stationary states that are not in motion and up to six that are steadily moving.

Proposition 2.3.1. *The model admits a stationary state which is non-polarised, symmetric and not*

in motion given by:

$$\begin{cases} c^{\infty}(x) = \dfrac{M}{2\left(1+\frac{k_{\text{on}}}{k_{\text{off}}}\right)}, & x \in [-1,1], \quad \text{(2.8a)} \\ \mu_{+}^{\infty} = \mu_{-}^{\infty} = \dfrac{M}{2\left(1+\frac{k_{\text{off}}}{k_{\text{on}}}\right)}, & \text{(2.8b)} \\ X_N^{\infty} = 0. & \text{(2.8c)} \end{cases}$$

If ε is sufficiently small, then the model admits two additional stationary states.

Proof. The stationary problem associated with eq. (2.4) is as follows:

$$\begin{cases} c''(x) = 0 & x \in]-1,1[, \quad \text{(2.9a)} \\ c'(\pm 1) = 0, & \text{(2.9b)} \\ k_{\text{on}} c(\pm 1) - k_{\text{off}} \mu_{\pm} = 0, & \text{(2.9c)} \\ \mu_{-} = \mu_{+}, & \text{(2.9d)} \\ X_N \in [-1,1] \text{ s.t. } g(X_N) = 0, & \text{(2.9e)} \\ M = \displaystyle\int_{-1}^{1} c(x)\,\mathrm{d}x + \mu_{-} + \mu_{-}. & \text{(2.9f)} \end{cases}$$

From eqs. (2.9a) and (2.9b) we deduce that c is constant over $[-1,1]$. We set for all $x \in [1,1]$:

$$c(x) = c_1.$$

It follows from eq. (2.9c) that:

$$\mu_{+} = \mu_{-} = \frac{k_{\text{on}}}{k_{\text{off}}} c_1.$$

Using the total mass constraint (2.9f), we deduce that:

$$c_1 = \frac{M}{2\left(1+\frac{k_{\text{on}}}{k_{\text{off}}}\right)}.$$

Finally, g is an odd function. Then $X_N = 0$ is solution of $g(X_N) = 0$. Moreover, graphically for ε small enough and $\beta > 1$, there exists $x_M \in]-1,0[$ and $x_m \in]0,1[$ with $x_m = -x_M$ such that we have:

x	-1	x_M	0	x_m	1
g	< 0	> 0	0	< 0	> 0

then the equation $g(X_N) = 0$ admits three solutions $x_0 \in]x_m,1[$, $-x_0$ and 0 and there exists three stationary states with a non-polarised distribution of the markers. Otherwise, for ε not small enough, g is an increasing function and the equation $g(X_N) = 0$ admits an unique solution $X_N = 0$. □

Proposition 2.3.2. *The model (2.3) admits up to six stationary solutions that are steadily moving if M is such that $M > \frac{1+\xi_{\text{nucl}}}{a\chi_c}\left(1+\frac{k_{\text{off}}}{k_{\text{on}}}\right)$.*

For the sequel we introduce the following notations. Let $\eta = \frac{a\chi_c}{1+\xi_{\text{nucl}}}$. Let Q be the function defined for all $x \in \mathbb{R}$ by:

$$Q(x) = \begin{cases} \dfrac{k_{\text{off}}\left(1-e^{-2\eta x}\right)+\eta k_{\text{on}}\, x\left(1+e^{-2\eta x}\right)}{\eta k_{\text{on}}\left(1-e^{-2\eta x}\right)} & \text{if } x \neq 0, \\ \dfrac{1}{\eta}\left(\dfrac{k_{\text{off}}}{k_{\text{on}}}+1\right) & \text{if } x = 0. \end{cases} \tag{2.10}$$

Sketch of the proof. A travelling wave of the model (2.3), if it exists, satisfies:

$$\begin{cases} c''(x) + auc'(x) = 0 & x \in]-1,1[, \quad (2.11a) \\ c'(\pm 1) + auc(x) = 0, & (2.11b) \\ k_{\text{on}} c(\pm 1) - k_{\text{off}}\mu_{\pm} = 0, & (2.11c) \\ u = \chi_c \dfrac{1}{1+\xi_{\text{nucl}}}\left(\mu_- - \mu_+\right), & (2.11d) \\ X_N \in [-1,1] \text{ s.t. } g(X_N) = -\chi_c \dfrac{1-\xi_{\text{nucl}}}{1+\xi_{\text{nucl}}}\left(\mu_- - \mu_+\right), & (2.11e) \\ M = \displaystyle\int_{-1}^{1} c(x)\,\mathrm{d}x + \mu_- + \mu_-, & (2.11f) \end{cases}$$

with $u \neq 0$.

We deduce from eqs. (2.11a) and (2.11b) that for all $x \in [-1,1]$, we have:

$$c'(x) + auc(x) = 0.$$

Thus for all $x \in [-1,1]$, we have:

$$c(x) = c(-1)\, e^{-au(x+1)}.$$

We also have:

$$\mu_{\pm} = \frac{k_{\text{on}}}{k_{\text{off}}} c(\pm 1).$$

Thus setting $\delta\mu = \mu_- - \mu_+$, it follows:

$$\delta\mu = \frac{k_{\text{on}}}{k_{\text{off}}}\left(c(-1) - c(1)\right) = \frac{k_{\text{on}}}{k_{\text{off}}} c(-1)\left(1-e^{-2au}\right),$$

which gives:

$$c(-1) = \frac{\delta\mu\, k_{\text{off}}}{k_{\text{on}}\left(1-e^{-2au}\right)}.$$

Using the expression of u given by eq. (2.11d) and the definition of η, we then have for all $x \in [-1,1]$ that:

$$c(x) = \frac{\delta\mu\, k_{\text{off}}}{k_{\text{on}}\left(1-e^{-2\eta\,\delta\mu}\right)} e^{-\eta\,\delta\mu(x+1)}.$$

Thus the constraint on the total quantity of markers eq. (2.11f) rewrites:

$$M = Q(\delta\mu).$$

It leads that a travelling wave solution of eq. (2.3), if it exists, is characterised by:

$$\begin{cases} c(x) = \dfrac{\delta\mu\, k_{\text{off}}}{k_{\text{on}}\left(1 - e^{-2\eta\,\delta\mu}\right)} e^{-\eta\,\delta\mu(x+1)} & x \in [-1,1]\,, \quad \text{(2.12a)} \\ \mu_+ = \dfrac{\delta\mu}{1 - e^{-2\eta\,\delta\mu}}\,, & \text{(2.12b)} \\ \mu_- = \dfrac{\delta\mu e^{-2\eta\,\delta\mu}}{1 - e^{-2\eta\,\delta\mu}}\,, & \text{(2.12c)} \\ M = Q(\delta\mu)\,, & \text{(2.12d)} \\ g(X_N) = -\dfrac{\chi_c(\xi_{\text{nucl}} - 1)}{1 + \xi_{\text{nucl}}}\delta\mu\,, & \text{(2.12e)} \end{cases}$$

with $\delta\mu \neq 0$. Therefore, it is sufficient to determine whether such a $\delta\mu$ exists.

Q is an even function. Studying the sign of the derivative of Q, we have:

x	$-\infty$		0		$+\infty$
Q	$+\infty$	$\searrow$	$\frac{1}{\eta}\left(1 + \frac{k_{\text{off}}}{k_{\text{on}}}\right)$	$\nearrow$	$+\infty$

Thus, if $M > \frac{1}{\eta}\left(1 + \frac{k_{\text{off}}}{k_{\text{on}}}\right)$, there exists exactly two solutions $\delta\mu^s$ and $-\delta\mu^s$ such that $Q(\delta\mu^s) = Q(-\delta\mu^s) = M$ with $\delta\mu^s > 0$.

We recall that g is an odd function and that graphically, we have:

x	-1		x_M		0		x_m		1
g	< 0	$\nearrow$	> 0	$\searrow$	0	$\searrow$	< 0	$\nearrow$	> 0

If $-\dfrac{\chi_c(\xi_{\text{nucl}} - 1)}{1 + \xi_{\text{nucl}}}\delta\mu^s < \min(g(x_m), g(-1))$, then there exists no $X_N \in [-1,1]$ such that $g(X_N) = -\dfrac{\chi_c(\xi_{\text{nucl}} - 1)}{1 + \xi_{\text{nucl}}}\delta\mu^s$ and eq. (2.9) admits no travelling waves solutions. Otherwise, associate to $\delta\mu^s$, there exists up to three solutions to the equation $g(X_N) = -\dfrac{\chi_c(\xi_{\text{nucl}} - 1)}{1 + \xi_{\text{nucl}}}\delta\mu^s$ and then up to three stationary states associated to $-\delta\mu^s$. □

Remark 2.3.3. *We note, in particular, that there exists travelling waves where the markers are polarised towards the rear of the cell with the nucleus at the front of the cell.*

2.4 . Numerical study

2.4.1 . Numerical scheme

In this section, we detail the numerical scheme used to simulate the model (2.4). This numerical scheme is obtained after a semi-implicit discretization in time and a finite volume approximation in space.

Grids definition We want to simulate eq. (2.4) over the time interval $[0,T]$, where $T>0$. Let $\Delta t>0$ be the time step. We discretize $[0,T]$ by the set of points $\{t^n = n\,\Delta t,\ n\in\{0,\dots,N\}\}$, where $N=\lfloor\frac{T}{\Delta t}\rfloor$.

Let $J\in\mathbb{N}$. We discretize the space interval $[-1,1]$ into $J+1$ intervals of the same length Δx. We denote by $\left(x_{j-\frac{1}{2}}\right)_{j\in\{0,\dots,J+1\}}$ a regular mesh of $[-1,1]$ and we set:

$$\begin{aligned}
&x_{-\frac{1}{2}} = -1,\\
&\Delta x = x_{\frac{1}{2}} - x_{-\frac{1}{2}},\\
&x_j = \frac{x_{j-\frac{1}{2}}+x_{j+\frac{1}{2}}}{2} = -1+\left(j+\frac{1}{2}\right)\Delta x \quad j\in\{0,\dots,J\}.
\end{aligned}$$

Finite volume approximation For all $n\in\{0,\dots,N\}$ and $j\in\{0,\dots,J\}$, we denote c_j^n an approximation of the function c at the time t^n and at position x_j. We set:

$$c_j^n = \frac{1}{\Delta x}\int_{\Lambda_j} c\left(t^n,x\right)\,\mathrm{d}x.$$

Similarly, we denote by μ_+^n an approximation of $\mu_+\left(t^n\right)$, μ_-^n an approximation of $\mu_-\left(t^n\right)$, X_N^n an approximation of $X_N\left(t^n\right)$ and u^n an approximation of $u\left(t^n\right)$.

First, we write the semi-implicit Euler scheme in time associate to (2.4).

For all $n\in\{0,\dots,N-1\}$, we have:

$$\begin{cases}
\dfrac{c\left(t^{n+1},x\right)-c\left(t^n,x\right)}{\Delta t} = \partial_x\left[\partial_x c\left(t^{n+1},x\right)+au^n c\left(t^n,x\right)\right] \qquad x\in[-1,1], & \text{(2.13a)}\\
\partial_x c\left(t^{n+1},\pm1\right)+au^n c\left(t^{n+1},\pm1\right) = \mp\dfrac{\mu_\pm^{n+1}-\mu_\pm^n}{\Delta t}, & \text{(2.13b)}\\
\dfrac{\mu_\pm^{n+1}-\mu_\pm^n}{\Delta t} = k_{\mathrm{on}}c\left(t^n,\pm1\right)-k_{\mathrm{off}}\mu_\pm^{n+1}, & \text{(2.13c)}\\
u^n = \dfrac{\chi_c}{2}\left(\mu_-^n-\mu_+^n\right)-\dfrac{1}{2}g\left(X_N^n\right), & \text{(2.13d)}\\
\dfrac{X_N^{n+1}-X_N^n}{\Delta t} = \left(\dfrac{1}{\xi_{\mathrm{nucl}}}-1\right)u^n+\dfrac{1}{\xi_{\mathrm{nucl}}}g\left(X_N^n\right). & \text{(2.13e)}
\end{cases}$$

Then integrating eq. (2.13a) over Λ_j for $j\in\{1,\dots,J-1\}$ and using an upwind approximation for the transport term we get:

$$c_j^{n+1} = c_j^n+\frac{\Delta t}{\Delta x^2}\left[c_{j+1}^{n+1}-2c_j^{n+1}+c_{j-1}^{n+1}\right]+a\frac{\Delta t}{\Delta x}\left[A^{\mathrm{up}}\left(u^n,c_j^n,c_{j+1}^n\right)-A^{\mathrm{up}}\left(u^n,c_{j-1}^n,c_j^n\right)\right],$$

where

$$A^{\mathrm{up}}\left(v,x_+,x_-\right) = \begin{cases} vx_+ & \text{if } v\geq 0,\\ vx_- & \text{if } v<0.\end{cases}$$

For $j=0$ and $j=J$, we also integrate eq. (2.13a) and we use the boundary conditions (2.13b) to obtain:

$$\begin{aligned}
c_0^{n+1} &= c_0^n+\frac{\Delta t}{\Delta x^2}\left[c_1^{n+1}-c_0^{n+1}\right]+a\frac{\Delta t}{\Delta x}A^{\mathrm{up}}\left(u^n,c_0^n,c_1^n\right)-\frac{1}{\Delta x}\left(\mu_-^{n+1}-\mu_-^n\right),\\
c_J^{n+1} &= c_J^n-\frac{\Delta t}{\Delta x^2}\left[c_J^{n+1}-c_{J-1}^{n+1}\right]-a\frac{\Delta t}{\Delta x}A^{\mathrm{up}}\left(u^n,c_{J-1}^n,c_J^n\right)-\frac{1}{\Delta x}\left(\mu_+^{n+1}-\mu_+^n\right).
\end{aligned}$$

Moreover we have:

$$\begin{cases} \mu_-^{n+1} = \dfrac{1}{1+\Delta t\, k_{\text{off}}} \left(\mu_-^n + \Delta t\, k_{\text{on}} c_0^n\right), & \text{(2.14a)} \\ \mu_+^{n+1} = \dfrac{1}{1+\Delta t\, k_{\text{off}}} \left(\mu_+^n + \Delta t\, k_{\text{on}} c_J^n\right), & \text{(2.14b)} \\ u^n = \dfrac{\chi_c}{2}\left(\mu_-^n - \mu_+^n\right) - \dfrac{1}{2} g\left(X_N^n\right), & \text{(2.14c)} \\ X_N^{n+1} = X_N^n + \Delta t \left(\dfrac{1}{\xi_{\text{nucl}}} - 1\right) u^n + \dfrac{\Delta t}{\xi_{\text{nucl}}} g\left(X_N^n\right). & \text{(2.14d)} \end{cases}$$

Towards a matrix formulation We store the approximate value of c in $[-1,1]$ at time t^n in a vector C^n, with $n \in \{0,\dots,N\}$. We have

$$C^n = \begin{bmatrix} c_0^n \\ \vdots \\ c_J^n \end{bmatrix}.$$

We introduce the following notations. Let D be the following diffusion matrix:

$$D = \frac{\Delta t}{\Delta x^2} \begin{bmatrix} -1 & 1 & 0 & \cdots & \cdots & 0 \\ 1 & -2 & 1 & \ddots & & \vdots \\ 0 & \ddots & \ddots & \ddots & \ddots & \vdots \\ \vdots & \ddots & \ddots & \ddots & \ddots & 0 \\ \vdots & & \ddots & \ddots & -2 & 1 \\ 0 & \cdots & \cdots & 0 & 1 & -1 \end{bmatrix}.$$

For all $n \in \{0,\dots,N-1\}$, let A^n be the following transport matrix:

$$A^n = a\frac{\Delta t}{\Delta x} \max\left(u^n, 0\right) \begin{bmatrix} 1 & 0 & \cdots & \cdots & 0 \\ -1 & 1 & 0 & \cdots & 0 \\ 0 & \ddots & \ddots & \ddots & \vdots \\ \vdots & \ddots & \ddots & 1 & 0 \\ 0 & \cdots & 0 & -1 & 0 \end{bmatrix} + a\frac{\Delta t}{\Delta x} \min\left(u^n, 0\right) \begin{bmatrix} 0 & 1 & 0 & \cdots & 0 \\ 0 & -1 & \ddots & \ddots & \vdots \\ \vdots & \ddots & \ddots & \ddots & 0 \\ 0 & \cdots & 0 & -1 & 1 \\ 0 & \cdots & \cdots & 0 & -1 \end{bmatrix}.$$

For all $n \in \{0,\dots,N-1\}$, let B^n be the following vector:

$$B^n = \frac{1}{\Delta x} \begin{bmatrix} \mu_-^{n+1} - \mu_-^n \\ 0 \\ \vdots \\ 0 \\ \mu_+^{n+1} - \mu_+^n \end{bmatrix}.$$

Then, in the matrix formulation, eqs. (2.14a) to (2.14c) rewrites:

$$C^{n+1} = C^n + D \cdot C^{n+1} + A^n \cdot C^n - B^n,$$

which leads to:

$$C^{n+1} = (Id - D)^{-1} \left(C^n + A^n \cdot C^n - B^n \right). \tag{2.15}$$

Numerical scheme The numerical scheme to simulate eq. (2.4) is given by the following algorithm:

Algorithm 2.1 : Numerical scheme to simulate eq. (2.4) using a semi-implicit Euler approximation in time and a finite volume approximation in space.

1. Initialisation.
   - $c_j^0 = \dfrac{1}{\Delta x} \displaystyle\int_{\Lambda_j} c^0(x)\, \mathrm{d}x$,
   - $\mu_\pm^0 = \mu_\pm(0)$,
   - $X_N^0 = X_N(0)$.
2. Time iteration. For $n \in \{0, \dots, N-1\}$, do:
   (a) Computation of u^n using eq. (2.14c):
   $$u^n = \frac{\chi_c}{2} \left(\mu_-^n - \mu_+^n \right) - \frac{1}{2} g\left(X_N^n \right).$$
   (b) Computation of μ_-^{n+1} using eq. (2.14a):
   $$\mu_-^{n+1} = \frac{1}{1 + \Delta t\, k_{\mathrm{off}}} \left(\mu_-^n + \Delta t\, k_{\mathrm{on}} c_0^n \right).$$
   .
   (c) Computation of μ_+^{n+1} using eq. (2.14b):
   $$\mu_+^{n+1} = \frac{1}{1 + \Delta t\, k_{\mathrm{off}}} \left(\mu_+^n + \Delta t\, k_{\mathrm{on}} c_J^n \right).$$
   (d) Computation of X_N^{n+1} using eq. (2.14d):
   $$X_N^{n+1} = X_N^n + \Delta t \left(\frac{1}{\xi_{\mathrm{nucl}}} - 1 \right) u^n + \frac{\Delta t}{\xi_{\mathrm{nucl}}} g\left(X_N^n \right).$$
   (e) Computation of the matrix A^n and the vector B^n in order to compute C^{n+1} using eq. (2.15):
   $$C^{n+1} = (Id - D)^{-1} \left(C^n + A^n \cdot C^n - B^n \right).$$

Remark 2.4.1. *We can remark that this scheme preserves the conservation of the mass. Indeed, for all $n \in \{0, \dots, N\}$, we have*

$$\sum_{j=0}^{J} c_j^n + \mu_-^n + \mu_-^n = \sum_{j=0}^{J} c_j^0 + \mu_-^0 + \mu_-^0.$$

2.4.2 . Numerical results

By implementing the algorithm 2.1 in Python, we can run numerical simulations of the model (2.4). In this section we present the numerical results obtained. First, we illustrate that, using the numerical scheme, we can find stationary states and solutions moving at constant velocity in accordance with proposition 2.3.1 and proposition 2.3.2. Once these verifications have been carried out, we show that the model allows us to highlight the action of the nucleus in cell polarisation and migration.

Numerical verifications. To begin, we verify that the numerical scheme captures the unpolarised stationary state (2.8). To do this, we fix the discretization by fixing the time step Δt and the space step Δx and take the following initial condition:

$$\begin{cases} c_j^0 = \dfrac{M}{2\left(1+\frac{k_{\text{on}}}{k_{\text{off}}}\right)} & j \in \{0,\dots,J\}, \quad \text{(2.16a)} \\ \mu_+^0 = \mu_-^0 = \dfrac{M}{2\left(1+\frac{k_{\text{off}}}{k_{\text{on}}}\right)}, & \text{(2.16b)} \\ X_N^0 = 0, & \text{(2.16c)} \end{cases}$$

which corresponds to the discretization of the stationary state (2.8).

Whatever the value of the other parameters, we observe that (2.16) is a stationary state of the numerical scheme (see fig. 2.1 for an example). We observe that the velocity of the cell remains constant over time and is equal to zero. The position of the nucleus remains stable and stays at the center of the cell. The initial quantity of markers on the membrane is also maintained over time.

We also verify that when ε is sufficiently small the numerical scheme captures the others unpolarised stationary states. After setting the discretization and parameter values, we use a dichotomy algorithm to solve the equation $g(y) = 0$ with $y \in [-1, 0)$. We then set the initial discrete condition with:

$$\begin{cases} c_j^0 = \dfrac{M}{2\left(1+\frac{k_{\text{on}}}{k_{\text{off}}}\right)} & j \in \{0,\dots,J\}, \quad \text{(2.17a)} \\ \mu_+^0 = \mu_-^0 = \dfrac{M}{2\left(1+\frac{k_{\text{off}}}{k_{\text{on}}}\right)}, & \text{(2.17b)} \\ X_N^0 = y. & \text{(2.17c)} \end{cases}$$

We observe that (2.17) is a stationary state of the numerical scheme (see fig. 2.2 for an example). Indeed the velocity of the cell remains constant over time and is equal to zero. The position of the nucleus remains stable and stays at its initial position. The initial quantity of markers on the membrane is also maintained over time. We can note that the scheme also capture the third stationary state where the initial nucleus position is defined by $X_N^0 = -y$.

Next, we check that the numerical scheme accurately captures the steady motion solutions (2.12). To do this, first we set the discretization by fixing Δt and Δx and choose parameters. Then we use a dichotomy algorithm to find ν such that $Q(\nu) = M$ and we find $y \in [-1, 1]$ such that $g(y) = -\frac{\chi_c(\xi_{\text{nucl}}-1)\nu}{1+\xi_{\text{nucl}}}$. We then choose as initial condition for the numerical scheme the

(a) Evolution of the cell velocity.

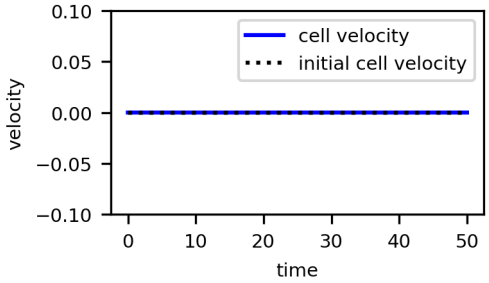

(b) Evolution of the nucleus position in the cell frame of reference.

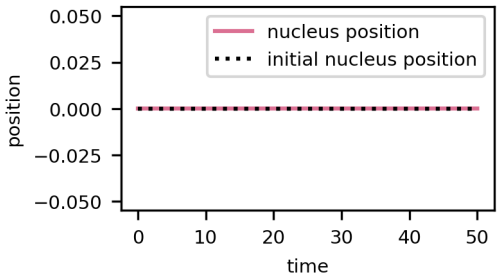

(c) Evolution of the markers quantity at the membrane.

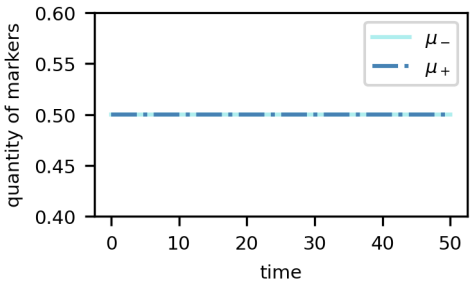

(d) Evolution of the total quantity of markers.

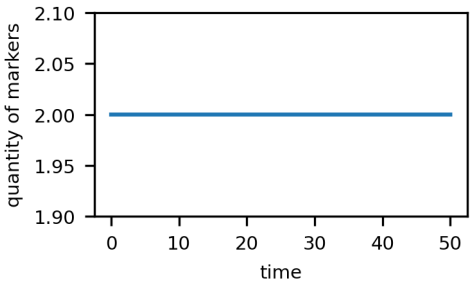

Figure 2.1: **Example of capturing the unpolarised stationary state with the numerical scheme.** *The graph on top left (figure* (a)*) represents the time evolution of the cell velocity. The velocity is constant and equal to zero. The graph on the top right (figure* (b)*) represents the time evolution of the nucleus position in the cell frame of reference. The nucleus remains at the centre of the cell. The graph on the bottom left (figure* (c)*) represents the time evolution of the markers quantity at the membrane. We can see that at both ends of the cell the quantity of markers is constant over time and equal. The cell therefore remains unpolarised. The graph on the bottom right (figure* (d)*) represents the time evolution of the total quantity of markers which remains conserved over time.*
The results presented here are obtained with the parameters $\Delta t = 0.00001$, $\Delta x = 0.004$, *the initial condition given by* (2.16), $M = 2$, $a = 1$, $\chi_c = 2$, $\beta = 2$, $\delta = 1$, $\varepsilon = 0.1$, $k_{\text{on}} = 1$, $k_{\text{off}} = 1$ *and* $\xi_{\text{nucl}} = 1$.

(a) Evolution of the cell velocity.

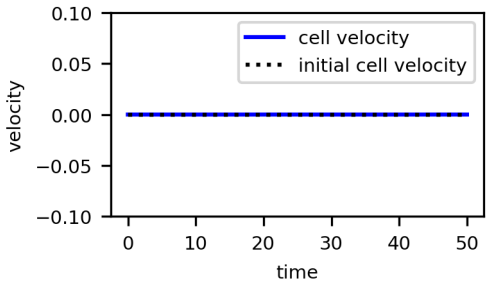

(b) Evolution of the nucleus position in the cell frame of reference.

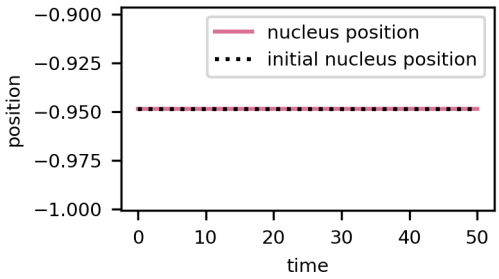

(c) Evolution of the markers quantity at the membrane.

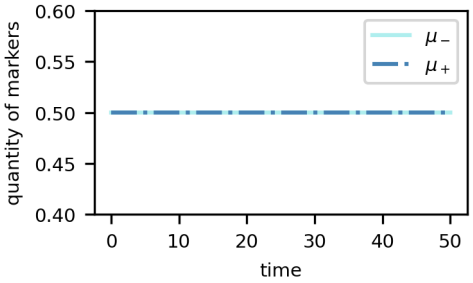

(d) Evolution of the total quantity of markers.

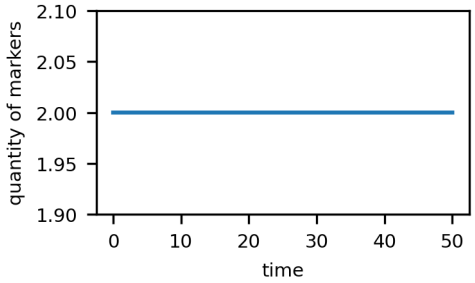

Figure 2.2: **Example of capturing the other stationary state with the numerical scheme.** *The graph on top left (figure* (a)*) represents the time evolution of the cell velocity. The velocity is constant and equal to zero. The graph on the top right (figure* (b)*) represents the time evolution of the nucleus position in the cell frame of reference. The nucleus remains at its initial position. The graph on the bottom left (figure* (c)*) represents the time evolution of the markers quantity at the membrane. We can see that at both ends of the cell the quantity of markers is constant over time and equal. The graph on the bottom right (figure* (d)*) represents the time evolution of the total quantity of markers which remains conserved over time.*
The results presented here are obtained with the parameters $\Delta t = 0.00001$, $\Delta x = 0.004$, *the initial condition given by* (2.17), $M = 2$, $a = 1$, $\chi_c = 2$, $\beta = 2$, $\delta = 1$, $\varepsilon = 0.1$, $k_{\text{on}} = 1$, $k_{\text{off}} = 1$ *and* $\xi_{\text{nucl}} = 1$. *With the parameters chosen, we have that the solutions of the equation* $g(x) = 0$ *are approached by* $x \in \{0, -0.94868, 0.94868\}$, *we choose for the initial condition* $X_N^0 = -0.94868$.

following one:

$$\begin{cases} X_N^0 = y, & \text{(2.18a)} \\ c_j^0 = \dfrac{1}{\Delta x} \displaystyle\int_{\Lambda_j} \dfrac{k_{\text{off}} \nu e^{-\eta\nu(x+1)}}{k_{\text{on}} \left(1 - e^{-2\eta\nu}\right)} \, \mathrm{d}x \qquad j \in \{0, \dots, J\}, & \text{(2.18b)} \\ \mu_+^0 = \dfrac{\nu}{1 - e^{-2\eta\nu}}, & \text{(2.18c)} \\ \mu_-^0 = \dfrac{\nu e^{-2\eta\nu}}{1 - e^{-2\eta\nu}}, & \text{(2.18d)} \end{cases}$$

which corresponds to the discretization of eq. (2.12).

We observe that as soon as there exists ν such that $Q(\nu) = M$ and $y \in [-1, 1]$ such that $g(y) = -\frac{\chi_c(\xi_{\text{nucl}}-1)\nu}{1+\xi_{\text{nucl}}}$, then (2.18) is a steady motion solution of the numerical scheme (see fig. 2.3 for an example). We observe that the cell's velocity remains constant over time and is equal to its initial value. The nucleus position is maintained over time. Additionally, the initial quantity of markers on the membrane is preserved, the cell remains polarised. Moreover the scheme also capture the second steady motion solution associate to $-\nu$. We can also note that the nucleus is place at the rear of the cell.

Thus, the numerical scheme algorithm 2.1 proposed to simulate the model (2.4) produces results consistent with the study of the model.

(a) Evolution of the cell velocity.

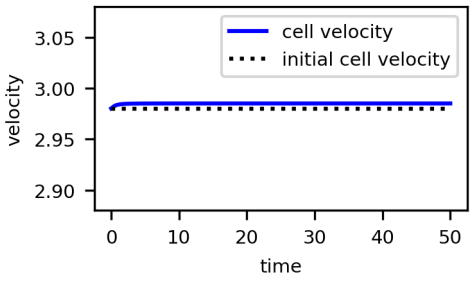

(b) Evolution of the nucleus position in the cell frame of reference.

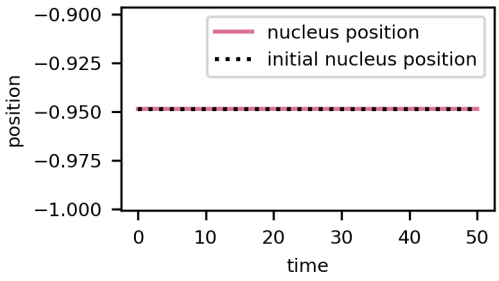

(c) Evolution of the markers quantity at the membrane.

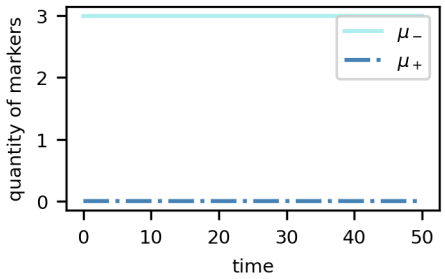

(d) Evolution of the total quantity of markers.

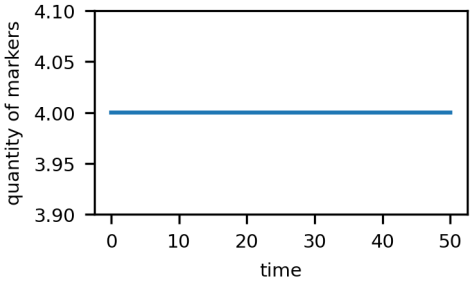

Figure 2.3: **Example of capturing the polarised steady motion solutions with the numerical scheme.** *The graph on top left (figure* (a)*) represents the time evolution of the cell velocity. The velocity is constant and equal to its initial value. The graph on the top right (figure* (b)*) represents the time evolution of the nucleus position in the cell frame of reference. The nucleus remains at its initial position. The graph on the bottom left (figure* (c)*) represents the time evolution of the markers quantity at the membrane. We can see that at both ends of the cell the quantity of markers is constant over time. The cell therefore remains polarised. The graph on the bottom right (figure* (d)*) represents the time evolution of the total quantity of markers which remains conserved over time. The results presented here are obtained with the parameters* $\Delta t = 0.00001$, $\Delta x = 0.004$, *the initial condition given by* (2.18)*,* $M = 4$, $a = 1$, $\chi_c = 2$, $\beta = 2$, $\delta = 1$, $\varepsilon = 0.1$, $k_{\text{on}} = 1$, $k_{\text{off}} = 1$ *and* $\xi_{\text{nucl}} = 1$. *With the parameters chosen, we have that the solutions of the equation* $Q(\nu) = M$ *are approached by* $\nu \in \{-2.9847, 2.9847\}$*, we choose for the initial condition* $\nu = 2.9847$. *With this value of* ν*, the solutions of the equation* $g(y) = -\frac{\chi_c(\xi_{\text{nucl}}-1)\nu}{1+\xi_{\text{nucl}}}$ *are approached by* $y \in \{0, -0.94868\}$*, we choose for the initial condition* $X_N^0 = -0.94868$.

Numerical illustration of the role of the nucleus. We intend now to highlight the impact of the nucleus on the trajectories. First, we illustrate that a perturbation of the symmetric stationary state can lead to cell polarisation and motion. In this case, we illustrate that the polarisation phenomenon seems to be initiated by the displacement of the nucleus out of the centre of the cell, in the area that will become the rear of the cell. Secondly, we illustrate that the position of the nucleus at the rear of the cell is not always necessary for the cell to be in motion. We illustrate this using a numerical result where, although the nucleus is at the centre of the cell, the cell is moving.

We therefore consider a perturbation of the symmetrical stationary state given by:

$$\begin{cases} c_j^0 = \left(\dfrac{M}{2\left(1+\frac{k_{\text{on}}}{k_{\text{off}}}\right)} + X_j \right) \mathbb{1}_{\frac{M}{2\left(1+\frac{k_{\text{on}}}{k_{\text{off}}}\right)}+X_j \geq 0} + \dfrac{M}{2\left(1+\frac{k_{\text{on}}}{k_{\text{off}}}\right)} \mathbb{1}_{\frac{M}{2\left(1+\frac{k_{\text{on}}}{k_{\text{off}}}\right)}+X_j < 0}, & \text{(2.19a)} \\ \mu_\pm^0 = \left(\dfrac{M}{2\left(1+\frac{k_{\text{off}}}{k_{\text{on}}}\right)} + X_\pm \right) \mathbb{1}_{\frac{M}{2\left(1+\frac{k_{\text{off}}}{k_{\text{on}}}\right)}+X_\pm \geq 0} + \dfrac{M}{2\left(1+\frac{k_{\text{off}}}{k_{\text{on}}}\right)} \mathbb{1}_{\frac{M}{2\left(1+\frac{k_{\text{off}}}{k_{\text{on}}}\right)}+X_\pm < 0}, & \text{(2.19b)} \\ X_N^0 = 0, & \text{(2.19c)} \end{cases}$$

with $j \in \{0, \dots, J\}$, X_j a realisation of the random variable $Y \sim \mathcal{N}(0, 0.01)$, and $X_\pm$ a realisation of the random variable $Z \sim \mathcal{N}(0, 0.001)$.

We choose two ranges of parameters. We observe that for the first choice of parameters, illustrated in fig. 2.4, the cell polarises and becomes in motion. First, we observe that the nucleus moves away from the centre rapidly. This leads to the definition of the front and rear of the cell. We observe that the velocity of the cell increases. At the front of the cell the quantity of markers decreases and at the rear of the cell it increases. Once the cell is polarised, it retains its polarisation and moves at a constant velocity. We then observe the migration of the cell. It is interesting to note that we can clearly see the polarisation phases in this numerical simulation.

For the second choice of parameters, shown in fig. 2.5, we can see that the cell is initially unpolarised. After a certain time, the velocity of the cell increases. At the same time, the quantity of markers at the rear of the cell increases and the quantity at the front of the cell decreases. The nucleus remains in the centre of the cell. We can therefore see that the cell may be polarised and moving even if the nucleus remains at the centre of the cell. However, we illustrate in fig. 2.6 that if the nucleus is initially located outside the centre of the cell, then the polarisation of the cell takes place faster and the initial position of the nucleus defines the rear of the cell.

(a) Evolution of the cell velocity.

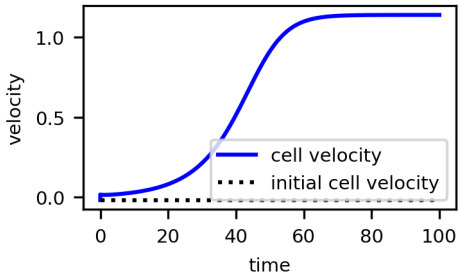

(b) Evolution of the nucleus position in the cell frame of reference.

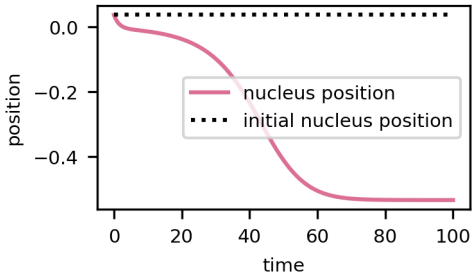

(c) Evolution of the markers quantity at the membrane.

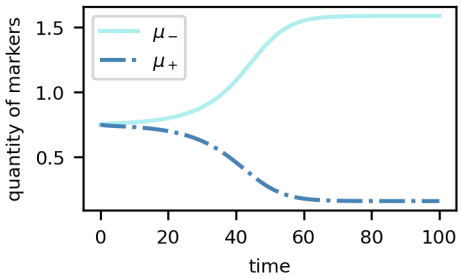

(d) Evolution of the total quantity of markers.

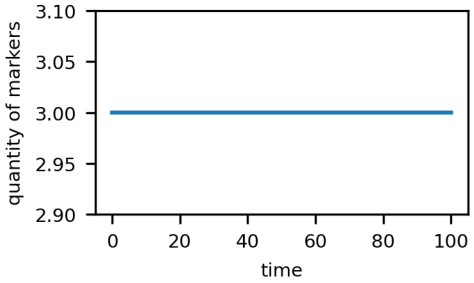

Figure 2.4: **Illustration of cell polarisation leading to migration.** *The graph on top left (figure* (a)*) represents the time evolution of the cell velocity. We observe that the velocity increases and then becomes constant. The graph on the top right (figure* (b)*) represents the time evolution of the nucleus position in the cell frame of reference. The nucleus moves to the rear of the cell to a position, after a certain time the nucleus maintains its position. The graph on the bottom left (figure* (c)*) represents the time evolution of the markers quantity at the membrane. The quantity at the rear of the cell increases and the quantity at the front decreases. The graph on the bottom right (figure* (d)*) represents the time evolution of the total quantity of markers which remains conserved over time. We can split the dynamic into two phases: until* $t = 60$ *the cell polarises and then moves at constant velocity.*
The results presented here are obtained with the parameters $\Delta t = 0.0001$, $\Delta x = 0.004$, *the initial condition given by* (2.19), $M = 3$, $a = 1$, $\chi_c = 2$, $\beta = 3$, $\delta = 0.3$, $\varepsilon = 0.1$, $k_{\text{on}} = 1$, $k_{\text{off}} = 1$ *and* $\xi_{\text{nucl}} = 1.5$.

(a) Evolution of the cell velocity.

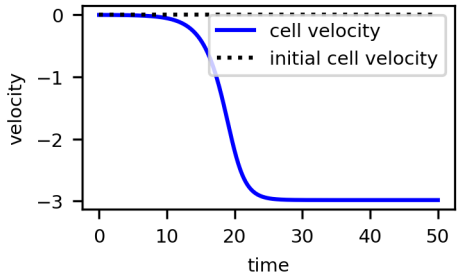

(b) Evolution of the nucleus position in the cell frame of reference.

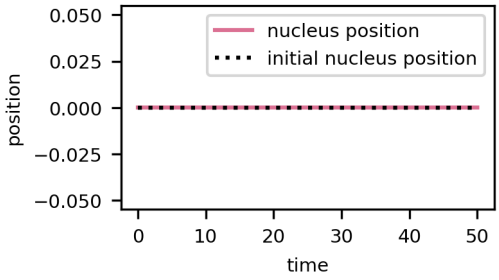

(c) Evolution of the markers quantity at the membrane.

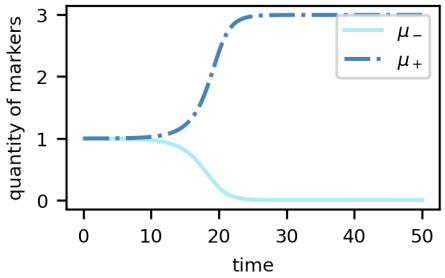

(d) Evolution of the total quantity of markers.

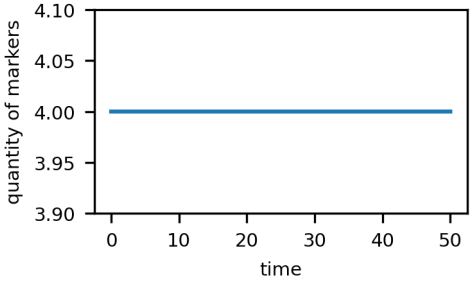

Figure 2.5: **Illustration of cell migration with the nucleus located at the cell centre.** *The graph on top left (figure* (a)*) represents the time evolution of the cell velocity. The velocity increases and then becomes constant. The graph on the top right (figure* (b)*) represents the time evolution of the nucleus position in the cell frame of reference. The nucleus remains at the cell centre. The graph on the bottom left (figure* (c)*) represents the time evolution of the markers quantity at the membrane. The quantity at the rear of the cell increases and the quantity at the front decreases. The graph on the bottom right (figure* (d)*) represents the time evolution of the total quantity of markers which remains conserved over time.*
The results presented here are obtained with the parameters $\Delta t = 0.00001$, $\Delta x = 0.004$, *the initial condition given by* (2.19), $M = 4$, $a = 1$, $\chi_c = 2$, $\beta = 2$, $\delta = 1$, $\varepsilon = 0.1$, $k_{\text{on}} = 1$, $k_{\text{off}} = 1$ *and* $\xi_{\text{nucl}} = 1$.

(a) Evolution of the cell velocity.

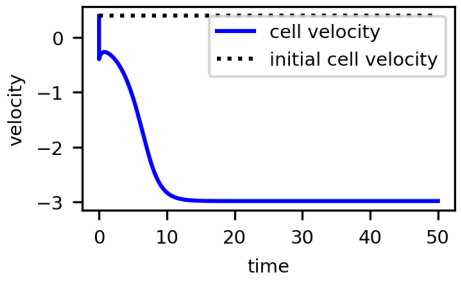

(b) Evolution of the nucleus position in the cell frame of reference.

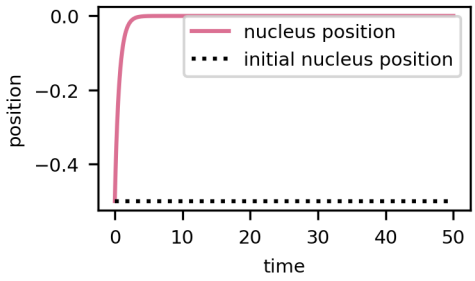

(c) Evolution of the markers quantity at the membrane.

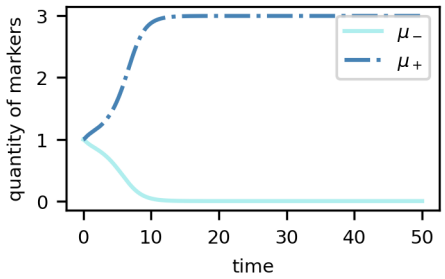

(d) Evolution of the total quantity of markers.

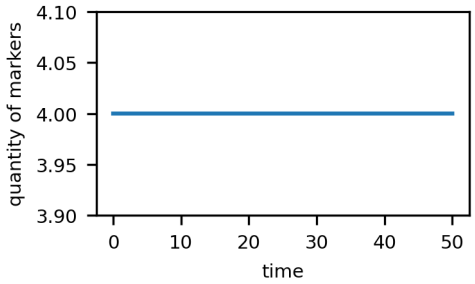

Figure 2.6: **Illustration that the position of the nucleus outside the centre of the cell allows rapid polarisation of the cell.** *The graph on top left (figure* (a)*) represents the time evolution of the cell velocity. The velocity increases rapidly and then becomes constant. The graph on the top right (figure* (b)*) represents the time evolution of the nucleus position in the cell frame of reference. The nucleus returns to the centre of the cell. The graph on the bottom left (figure* (c)*) represents the time evolution of the markers quantity at the membrane. The quantity at the rear of the cell increases and the quantity at the front decreases. We observe that the nucleus initial position defines the rear of the cell. The graph on the bottom right (figure* (d)*) represents the time evolution of the total quantity of markers which remains conserved over time.*
The results presented here are obtained with the parameters $\Delta t = 0.00001$, $\Delta x = 0.004$, *the initial condition given by* $c_j^0 = \frac{M}{2\left(1+\frac{k_{\text{on}}}{k_{\text{off}}}\right)}$ *for* $j \in \{0, \dots, J\}$, $\mu_+^0 = \mu_-^0 = \frac{M}{2\left(1+\frac{k_{\text{off}}}{k_{\text{on}}}\right)}$, *and* $X_N^0 = 0.5$, $M = 4$, $a = 1$, $\chi_c = 2$, $\beta = 2$, $\delta = 1$, $\varepsilon = 0.1$, $k_{\text{on}} = 1$, $k_{\text{off}} = 1$ *and* $\xi_{\text{nucl}} = 1$.

Conclusion. The numerical results highlight that the model illustrates the phenomenon of polarisation is necessary for cell migration. They also show that the position of the nucleus at the rear of the cell enables rapid polarisation. However, the existence of steady motion solutions with the nucleus positioned at the centre of the cell that seems stable suggests that the position of the nucleus outside the centre of the cell does not alone ensure cell polarisation.

Bibliography

Calvez, V., Hawkins, R., Meunier, N., and Voituriez, R. (2012). Analysis of a non local model for spontaneous cell polarisation. SIAM Journal on Applied Mathematics, 72(2):594–622. 47, 48

Etchegaray, C., Meunier, N., and Voituriez, R. (2017). Analysis of a Nonlocal and Nonlinear Fokker–Planck Model for Cell Crawling Migration. SIAM Journal on Applied Mathematics, 77(6):2040–2065. 47

Lepoutre, T. and Meunier, N. (2022). Analysis of a model of cell crawling migration. Communications in Mathematical Sciences, 20(6):1589–1611. 48, 51, 52

3 - Numerical simulations of the cell migration problem on a disk with space-homogeneous advection velocity

In this chapter, in collaboration with Christèle Etchegaray and Nicolas Meunier, we enrich the rigid model analogous to the model developed in Lavi et al. (2020) by adding coloured noise in space to the advection field of the transport-diffusion equation concerning the markers. We develop a finite element numerical scheme to simulate it. After verifying that the numerical scheme gives results in agreement with the theoretical results shown by Lavi et al. (2020) and Meunier and Souplet (2023), we illustrate that numerically the simulated trajectories satisfy the UCSP law and also that we capture the three trajectory regimes. This work will be supplemented in the future by a finite-volume numerical scheme.

3.1 . Modelling

In this section, we derive from the cell motility model introduced in Lavi et al. (2020) a model of cell motility where the cell is rigid. The model introduced in Lavi et al. (2020) corresponds to model (1.1) when the nucleus and its dynamics are not specifically taken into account in the modelling, the substrate is homogeneous and the environment presents neither obstacles nor external signals and the effects of undercooling and noise are neglected. Before deducing a rigid model analogous to the model of Lavi et al. (2020), we recall it.

The cell domain is described by the connected open set $\Omega(t) \subset \mathbb{R}^2$, where $t > 0$ denotes the current time. The cell is filled with an incompressible fluid of velocity $\mathbf{u}$ and pressure P. Inside this fluid, there is the presence of rear markers of density c. The dimensionless model is given by:

$$\begin{cases} \mathbf{u} + \nabla P = 0 & \text{in } \Omega(t), & \text{(3.1a)} \\ \operatorname{div}(\mathbf{u}) = 0 & \text{in } \Omega(t), & \text{(3.1b)} \\ P = \gamma\kappa + \chi_c f_{\text{act}}(c) & \text{on } \partial\Omega(t), & \text{(3.1c)} \\ V_n = \mathbf{u}\cdot\mathbf{n} & \text{on } \partial\Omega(t), & \text{(3.1d)} \\ \partial_t c = \operatorname{div}(\nabla c - (1-a)\,\mathbf{u}c) & \text{in } \Omega(t), & \text{(3.1e)} \\ (\nabla c + a\mathbf{u}c)\cdot\mathbf{n} = 0 & \text{on } \partial\Omega(t), & \text{(3.1f)} \end{cases}$$

where $\chi_c > 0$ and f_{act} satisfies the assumptions (1.12). The problem (3.1) is complemented with an initial condition given by

$$c(0,\mathbf{x}) = c^{\text{in}}(\mathbf{x}) \quad \text{in } \Omega(0), \tag{3.2}$$

where c^{in} is given. The total quantity of markers is constant in time and we denote it by M:

$$M = \int_{\Omega(t)} c(t,\mathbf{x})\,\mathrm{d}\mathbf{x}.$$

The force balance on the system reads:

$$\mathbf{u}_{\text{cm}}(t) = \frac{-\chi_c}{|\Omega(t)|}\int_{\partial\Omega(t)} f_{\text{act}}(c(t,\mathbf{x}))\,\mathbf{n}\,\mathrm{d}\sigma, \tag{3.3}$$

where $\mathbf{u}_{\text{cm}}$ is the velocity of the center of mass.

We now assume the cell to have a circular shape: $\Omega(t)$ is a disk of radius $R > 0$. We assume that the cell moves at the velocity of the centre of mass eq. (3.3) and in this case, the rigid model analogous to the deformable model (3.1) is given by:

$$\begin{cases} \partial_t c = \operatorname{div}(\nabla c - (1-a)\,\mathbf{u}c) & \text{in } \Omega(t), \\ (\nabla c + a\mathbf{u}c)\cdot\mathbf{n} = 0 & \text{on } \partial\Omega(t), \\ \mathbf{u}(t) = \dfrac{-\chi_c}{|\Omega(t)|}\displaystyle\int_{\partial\Omega(t)} f_{\text{act}}(c(t,\mathbf{x}))\,\mathbf{n}\,\mathrm{d}\sigma. \end{cases}$$

Changing of frame of reference to the one of the cell we rewrite the rigid model in the following way:

$$\begin{cases} \partial_t c = \operatorname{div}(\nabla c + a\mathbf{u}c) & \text{in } \Omega_0, \quad (3.4a) \\ (\nabla c + a\mathbf{u}c)\cdot\mathbf{n} = 0 & \text{on } \partial\Omega_0, \quad (3.4b) \\ \mathbf{u}(t) = \dfrac{-\chi_c}{|\Omega_0|}\displaystyle\int_{\partial\Omega(t)} f_{\text{act}}(c(t,\mathbf{x}))\,\mathbf{n}\,\mathrm{d}\sigma, & (3.4c) \end{cases}$$

where $\Omega_0 = \Omega(0) = B(0,R)$.

In addition to this modelling, we take into account stochastic fluctuations in cell motility by proceeding as in section 1.3.7 (see also Boulakia et al. (2015)) and adding a coloured noise to the advection field of the marker transport-diffusion equation. Thus, in the cell frame of reference, we have:

$$\begin{cases} \partial_t c = \operatorname{div}\left(\nabla c + a\mathbf{u}c - \alpha\dot{W}_t^Q c\right) & \text{in } \Omega_0, \quad (3.5a) \\ \left(\nabla c + a\mathbf{u}c - \alpha\dot{W}_t^Q c\right)\cdot\mathbf{n} = 0 & \text{on } \partial\Omega_0, \quad (3.5b) \\ \mathbf{u}(t) = \dfrac{-\chi_c}{|\Omega_0|}\displaystyle\int_{\partial\Omega_0} f_{\text{act}}(c(t,\mathbf{x}))\,\mathbf{n}\,\mathrm{d}\sigma, & (3.5c) \end{cases}$$

with $\alpha > 0$ and $\dot{W}_t^Q$ a Q-Wiener process on Ω_0 (see definition 1.3.2 for a definition) which is a space-correlated noise. This choice is motivated to avoid non trivial effects that can appears when we discretize our model (Walsh, 2005; Hairer et al., 2012).

3.2 . Finite element scheme

In this section, we write a finite element scheme. This scheme will be implement in FreeFem ++ (Hecht, 2012).

3.2.1 . Discretization of the deterministic part

First we discretize in time the deterministic model (3.4). Let Δt be the time step. For $n \in \{0,\dots,N_f\}$ with $N_f \in \mathbb{N}$, we denote $t^n = n\Delta t$, $c^n(\cdot)$ an approximation of the function c at time t^n and $\mathbf{u}^n$ an approximation of the cell velocity at time t^n. We use a semi-implicit Euler scheme in time and we have:

$$\begin{cases} \dfrac{c^{n+1}-c^n}{\Delta t} = \operatorname{div}\left(\nabla c^{n+1} + a\mathbf{u}^n c^{n+1}\right) & \text{in } \Omega_0, \quad (3.6a) \\ \left(\nabla c^{n+1} + a\mathbf{u}^n c^{n+1}\right)\cdot\mathbf{n} = 0 & \text{on } \partial\Omega_0, \quad (3.6b) \\ \mathbf{u}^n = \dfrac{-\chi_c}{|\Omega_0|}\displaystyle\int_{\partial\Omega_0} f_{\text{act}}(c^n(\mathbf{x}))\,\mathbf{n}\,\mathrm{d}\sigma. & (3.6c) \end{cases}$$

To discretize in space our problem, we use a finite element approximation. Let $\mathcal{T}_h$ be a triangulation of Ω_0. We denote by $\mathbb{P}_2$ the set of polynomials of $\mathbb{R}^2$ of degrees less or equal to 2. Let $V_h = \left\{\phi \in H^1(\Omega_0) \,|\, \forall \mathcal{K} \in \mathcal{T}_h, \phi_{|\mathcal{K}} \in \mathbb{P}_2\right\}$ be a finite element set. The finite element discretization of eq. (3.6) is given by:

$$\begin{cases} \displaystyle\int_{\Omega_0} \frac{c^{n+1}-c^n}{\Delta t}\varphi \,\mathrm{d}\mathbf{x} = \int_{\Omega_0} \nabla c^{n+1}\cdot\nabla\varphi + a c^{n+1}\,\mathbf{u}^n\cdot\nabla\varphi \,\mathrm{d}\mathbf{x}, & \forall \varphi \in V_h, \quad (3.7a) \\ \mathbf{u}^{n+1} = \dfrac{-\chi_c}{|\Omega_0|}\displaystyle\int_{\partial\Omega_0} f_{\text{act}}\left(c^{n+1}(\mathbf{x})\right)\mathbf{n}\,\mathrm{d}\sigma. & (3.7b) \end{cases}$$

3.2.2 . Discretization of the noise

We want to run numerical simulations of the model defined by eqs. (3.2) and (3.5) taking into account the noise. To do so, we will enrich our deterministic scheme (3.7) with the discretization of the noise done by Boulakia et al. (2015). We denote by $\dot{W}^{Q,n}$ an approximation of the coloured noise at time t^n, $n \in \{1,\dots,N_f\}$. We set:

$$\dot{W}^{Q,n} = \frac{W^Q_{t^n} - W^Q_{t^{n-1}}}{\Delta t}.$$

From the definition of W^Q_t, we know that $\dot{W}^{Q,n}$ is equal in law to $\dfrac{1}{\sqrt{\Delta t}}W^Q_1$ and that the $\left\{\dot{W}^{Q,n}\right\}_{1\le n\le N_f}$ are independent.

Thus we have that the semi-implicit time discretization and finite element discretization in space of eq. (3.5) reads:

$$\begin{cases} \displaystyle\int_{\Omega_0} \frac{c^{n+1}-c^n}{\Delta t}\varphi \,\mathrm{d}\mathbf{x} = \int_{\Omega_0} \nabla c^{n+1}\cdot\nabla\varphi + a c^{n+1}\left(\mathbf{u}^n + \frac{\alpha}{\sqrt{\Delta t}}W_1^{Q,n}\right)\cdot\nabla\varphi \,\mathrm{d}\mathbf{x}, \quad \forall\varphi\in V_h, \\ \mathbf{u}^{n+1} = \dfrac{-\chi_c}{|\Omega_0|}\displaystyle\int_{\partial\Omega_0} f_{\text{act}}\left(c^{n+1}(\mathbf{x})\right)\mathbf{n}\,\mathrm{d}\sigma, \end{cases}$$

where $\left(W_1^{Q,n}\right)_{1\le n\le N_f}$ is a sequence of independent Q-Wiener processes evaluated at time 1.

From Boulakia et al. (2015), we know that a way to approximate the noise and to compute $W_1^{Q,n} = (\omega_1^n, \omega_2^n)$ relies on the computation of a covariance matrix. Indeed, let $\{P_i, 1\le i\le N_h\}$ be the set of all the nodes of the triangulation $\mathcal{T}_h$, where N_h is the number of nodes of the triangulation, and $\{\psi_i, 1\le i\le N_h\}$ be a basis of the Lagrangian $P1$ finite element. ψ_i is a continuous affine function on Ω_0 such that for all $1\le i,j\le N_h$, we have $\psi_i(P_j) = \delta_{ij}$. For $k\in\{1,2\}$, the $P1$ discretization of ω_k^n is given by

$$\omega_k^n = \sum_{i=1}^{N_h} x_i^n \psi_i.$$

with $\{x_i^n, 1\le i\le N_h\}$ a realisation of a centred Gaussian vector of covariance matrix Σ. We have $\Sigma = (q(P_i,P_j))_{1\le i,j\le N_h}$. Let X be a centred Gaussian vector of covariance matrix Σ. We have

$$X = SY,$$

with Y a Gaussian vector such that for all $1\le i\le N_h$, $Y_i \sim \mathcal{N}(0,1)$ and S such that $\Sigma = SS^T$. Thus to compute $W_1^{Q,n}$, we just have to simulate a realization of a standard Gaussian vector and to compute the Cholesky decomposition S of the covariance matrix Σ.

3.2.3 . Numerical scheme

The numerical scheme to simulate model (3.5) is given by:

Algorithm 3.1 : Numerical scheme to simulate the model eq. (3.5) obtained after time discretization and space discretization with a finite element method.

1. Initialisation: $c^0 = c^{\text{in}}$ the given initial condition and definition of the mesh.
2. Computation of S the Cholesky decomposition of the covariance matrix Σ.
3. Time iteration:
   - Computation of $W_1^{Q,n} = (Sy_1, Sy_2)$ where y_1 and y_2 are two independent realisations of a standard Gaussian vector.
   - Computation of c^{n+1} by solving the weak formulation: searching c^{n+1} such that for all $\varphi \in V_h$ we have:

$$\int_{\Omega_0} \frac{c^{n+1} - c^n}{\Delta t} \varphi \, \mathrm{d}\mathbf{x} = \int_{\Omega_0} \nabla c^{n+1} \cdot \nabla \varphi + a c^{n+1} \left(\mathbf{u}^n + \frac{\alpha}{\sqrt{\Delta t}} W_1^{Q,n} \right) \cdot \nabla \varphi \, \mathrm{d}\mathbf{x}.$$

   - Deduction of $\mathbf{u}^{n+1}$:

$$\mathbf{u}^{n+1} = \frac{-\chi_c}{|\Omega_0|} \int_{\partial\Omega_0} f_{\text{act}} \left(c^{n+1}(\mathbf{x}) \right) \mathbf{n} \, \mathrm{d}\sigma. \tag{3.8}$$

3.3 . Simulation outputs

Simulations provide both the molecular concentration in the domain and the cell velocity over time. In the deterministic case, the time to reach a stationary state is also informative. In the following, we define two polarization indices that are monitored in the general case. Then, we introduce characteristics of single and multiple trajectories in the stochastic case.

3.3.1 . Polarization indices

The indices are based on the molecular concentration at the boundary. More precisely, let $(\theta_k)_{1 \leq k \leq N_y}$ be the angular discretization, with $\theta_k := k\Delta\theta$ and $N_y = \frac{2\pi}{\Delta\theta}$. Let $\mathbf{e}_k$ be the unit vector of direction θ_k. We define:

- the Relative Standard Deviation (RSD) given by the ratio between the standard deviation of $\{\bar{c}^n_{N_r,k}\}_{1 \leq k \leq N_y}$ and its mean, normalized by the boundary's perimeter. More precisely, writing $\bar{C} = \frac{1}{N_y} \sum_{k=1}^{N_y} \bar{c}^n_{N_r,k}$, we have that

$$RSD := \frac{1}{2\pi R \bar{C}} \sqrt{\frac{1}{N_y} \sum_{k=1}^{N_y} |\bar{c}^n_{N_r,k} - \bar{C}|^2}. \tag{3.9}$$

- the normalized Mean Resultant Vector of the sample, given by

$$RV := \frac{1}{\sum_{i=1}^{N_y} \bar{c}^n_{N_r,k}} \sum_{i=1}^{N_y} \bar{c}^n_{N_r,k} \mathbf{e}_k \,,$$

as defined in circular statistics (Jammalamadaka and SenGupta, 2001). Its norm, the Resultant Vector Length (RVL), provides a polarization index.

3.3.2 . Single trajectory

In the case of a stochastic simulation, both the pace and directionality of trajectories are informative. First, descriptive plots can be shown : the velocity norm over time, velocity norm histogram, 2D velocity histogram and cell trajectory. When a bimodal velocity norm distribution is observed, a threshold can be established to separate slow and fast velocities. The 1D velocity histogram and the trajectory can be colored accordingly to emphasize on both regimes. The directionality of trajectories can be further investigated from the following items:

- the scatter plot or histogram of the Δt-turning angles with respect to the corresponding mean velocity norms,
- the Time-Averaged Squared Displacements (or TASD) defined for cell j and for $1 \leq n \leq N_f$ by:

$$TASD_j(n\Delta t) := \frac{1}{N_f - n + 1} \sum_{i=0}^{N_f - n} |\mathbf{z}_j((i+n)\Delta t) - \mathbf{z}_j(i\Delta t)|^2 \,, \tag{3.10}$$

  that is the average of squared displacements over time intervals of $n\Delta t$ (Loosley et al., 2015),
- the data of Persistence Times (T_{pe}) and Persistence Velocities (V_{pe}). It is obtained by splitting the trajectory based on the direction of displacement : a new subtrajectory is defined each time the direction of displacement differs from the initial direction by at least $\pi/2$. Then, each path is associated with its duration and a mean velocity. The whole trajectory can now be shown split by persistent paths, and one can plot T_{pe} values versus V_{pe} values. The UCSP (Maiuri et al., 2015) proposes an exponential relationship between both quantities. Therefore, such a fit is performed.

3.3.3 . Multiple stochastic trajectories

- The MSD (Mean Squared Displacements) is the average of TASD over the cell population : for $1 \leq n \leq N_f$, one has

$$MSD(n\Delta t) := \frac{1}{N_{cell}} \sum_{j=1}^{N_{cell}} TASD_j(n\Delta t) \,. \tag{3.11}$$

- The EASD (Ensemble-Averaged Squared Displacements) is defined from the Squared displacements between each position and the initial position by

$$EASD(n\Delta t) := \frac{1}{N_{cell}} \sum_{j=1}^{N_{cell}} \left(|\mathbf{z}_j(n\Delta t) - \mathbf{z}_j(0)|^2 \right) \,, \tag{3.12}$$

- The Ergodicity is defined as the ratio between TASD of the j-th cell and the EASD.

3.4 . Numerical verifications

When $\alpha = 0$, the model has been studied in various papers. In this section we recall various theoretical results on the model and illustrate that our numerical scheme gives results in agreement with these results. The numerical scheme is implemented using FreeFEM++ (Hecht, 2012).

3.4.1 . Saturation force prevents from blow-up

The study of the linear stability analysis in the rigid case (Lavi et al., 2020) proved that we can observe blow-up in the case of a linear active force f_{act} when $1 - \chi_c a f'_{\text{act}}(\tilde{c})\,\tilde{c} < 0$ with $\tilde{c} = \frac{M}{\pi R^2}$, the rest state. It also showed that choosing a saturation force for f_{act} prevents from the blow-up; in this case we observe convergence to a stable traveling wave. Moreover it proved that while $1 - \chi_c a f'_{\text{act}}(\tilde{c})\,\tilde{c} > 0$ there is no blow up in the case of the linear and saturation force.

Let χ_c^* be the critical value of χ_c, we have:

$$\chi_c^* = \frac{1}{a f'_{\text{act}}(\tilde{c})\,\tilde{c}} \tag{3.13}$$

The criteria $1 - \chi_c a f'_{\text{act}}(\tilde{c})\,\tilde{c} < 0$ is equivalent to $\chi_c > \chi_c^*$.

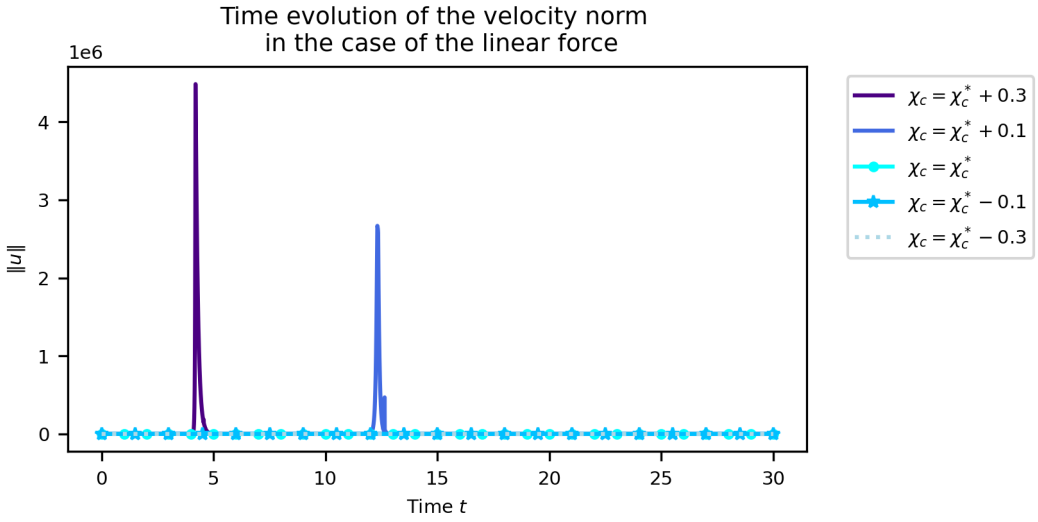

Figure 3.1: **Illustration of the blow-up criteria in the case of the linear force $f_{\text{act}}(c) = c$.** *We observe that when $\chi_c > \chi_c^*$ the velocity norm increases rapidly towards infinity. On the contrary, when $\chi_c \leq \chi_c^*$, the velocity norm is bounded over time. This illustrates that when $\chi_c > \chi_c^*$ with the linear force, blow-up occurs.*
Simulations done with $\Omega_0 = B(0,1)$ with the initial condition $c^{\text{in}}(\mathbf{x}) = K(1 + X(\mathbf{x}))\,\mathbf{1}_{1+X(\mathbf{x})>0}$ where for all $\mathbf{x} \in \Omega_0$, $X(\mathbf{x}) \sim \mathcal{N}(0,1)$ and K such that $\int_{\Omega_0} c^{\text{in}}(\mathbf{x})\,\mathrm{d}\mathbf{x} = M$ and $\mathbf{u}_0 = \frac{-\chi_c}{|\Omega_0|}\int_{\partial\Omega_0} f_{\text{act}}\left(c^{\text{in}}(\mathbf{x})\right)\mathrm{d}\sigma$ and the parameters $M = \pi$, $a = 1$, $\Delta t = 0.005$ and $T_f = 30$.

Numerically, we recover well the blow-up criteria in the linear force case and the fact that saturation force prevents from blow-up. Indeed, once $\chi_c > \chi_c^*$ and the force is linear then the velocity norm tends toward infinity while if $\chi_c \leq \chi_c^*$ the velocity norm remains bounded over time (see fig. 3.1). The saturation force prevents from blow-up. Indeed, in the case of the

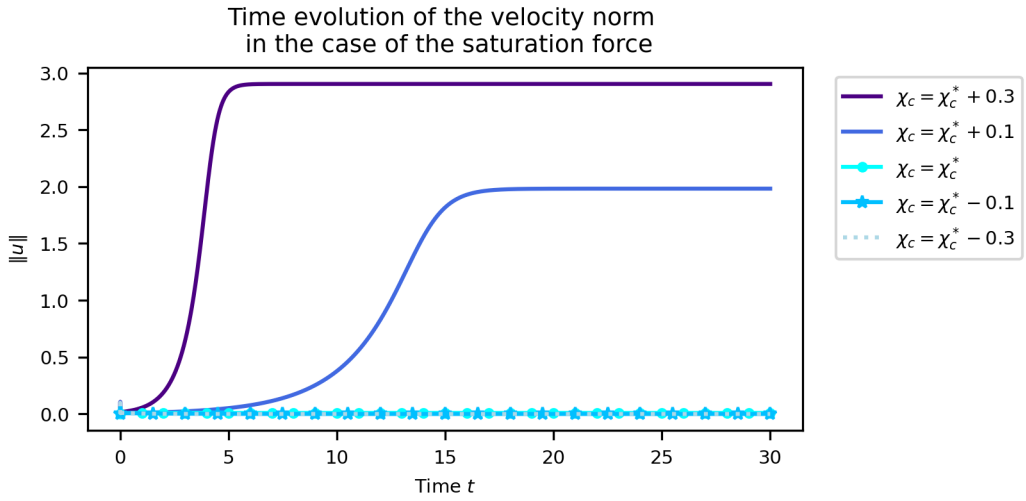

Figure 3.2: **Illustration that the saturation force prevents blow-up.** *Unlike when the active force is the linear force, we can observe that when we choose as active force a saturation force that even when $\chi_c > \chi_c^*$ we have no blow-up and the velocity norm is bounded over time. The saturation force is given by $f_{\text{act}}(c) = \frac{c(1+c_s)^2}{c_s(c+c_s)}$ with $c_s > 0$.*
Simulations done with $\Omega_0 = B(0,1)$ with the initial condition $c^{\text{in}}(\mathbf{x}) = K(1 + X(\mathbf{x}))\mathbf{1}_{1+X(\mathbf{x})>0}$ where for all $\mathbf{x} \in \Omega_0$, $X(\mathbf{x}) \sim \mathcal{N}(0,1)$ and K such that $\int_{\Omega_0} c^{\text{in}}(\mathbf{x})\,\mathrm{d}\mathbf{x} = M$ and $\mathbf{u}_0 = \frac{-\chi_c}{|\Omega_0|}\int_{\partial\Omega_0} f_{\text{act}}\left(c^{\text{in}}(\mathbf{x})\right)\mathrm{d}\sigma$ and the parameters $M = \pi$, $a = 1$, $c_s = 0.5$, $\Delta t = 0.005$ and $T_f = 30$.

saturation force, we observe that the velocity norm remains bounded over time even when $\chi_c > \chi_c^*$ (see fig. 3.2).

3.4.2 . Motility phase diagram

By performing the analysis of the linear stability of the deformable model (3.1), Lavi et al. (2020) showed that in the case of a rigid cell with the saturation force for the active force we can observe three phases of motility: rest, bistable and traveling. The rest phase is characterised by the stability of the rest state and no traveling wave. The traveling phase is characterised by the instability of the rest state and the existence of stable traveling waves. The bistable phase is characterised by the stability of the rest state and the existence of stable traveling waves. Taking $M = \pi$, $R = 1$ and $a = 1$, we have that $\chi_c^* = 1$ and the traveling phase is parameterised by $\chi_c > 1$, the rest phase by $\chi_c < 1 \,\&\, c_s \geq 0.5$ or $\chi_c < \chi^*(c_s) \,\&\, c_s < 0.5$ and the bistable phase is parameterised by $\chi^*(c_s) < \chi_c < 1$ and $c_s < 0.5$, where $\chi^*(c_s)$ is the saddle-node bifurcation point and depends of c_s.

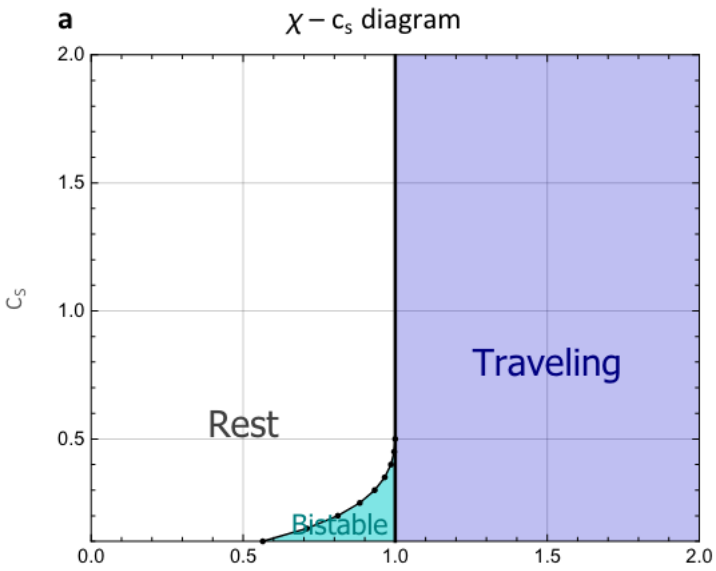

Figure 3.3: **Motility phase diagram.** *The thick black line represents the pitchfork bifurcation taking place at $\chi_c = \chi_c^*$. To the right of this line, shown in blue, the rest state is unstable and there exists a stable travelling wave. To the left of this line, shown in white and cyan, the rest state is stable. The black line with dots represents the saddle-node bifurcation. Above this line, shown in white, there exists no stable travelling wave. Below this line, shown in cyan, there exists a stable travelling wave.*
Taken from Lavi (2019).

We want to ensure that our numerical scheme retains these properties. We show it on some examples.

For the rest of this section K will be a normalization constant ensuring $\int_{\Omega_0} c^{\text{in}}(\mathbf{x})\, \mathrm{d}\mathbf{x} = \pi$ and for all $\mathbf{x} \in \Omega_0$, $X(\mathbf{x}) \sim \mathcal{N}(0,1)$.

Rest phase In this paragraph we want to find parameters χ_c and c_s such that the motility is in the rest phase. We choose $\chi_c = 0.5$ and $c_s = 0.1$. First we want to illustrate the stability of the rest state. The rest state is given by $\tilde{c}(\mathbf{x}) = 1$ and $\tilde{\mathbf{u}} = 0$. We perturbed the rest state by taking as initial condition $c^{\text{in}}(\mathbf{x}) = K(1 + X(\mathbf{x}))\, \mathbf{1}_{1+X(\mathbf{x})>0}$ and $\mathbf{u}_0 = \frac{-\chi_c}{|\Omega_0|} \int_{\partial\Omega_0} f_{\text{act}}\left(c^{\text{in}}(\mathbf{x})\right) \mathrm{d}\sigma$.

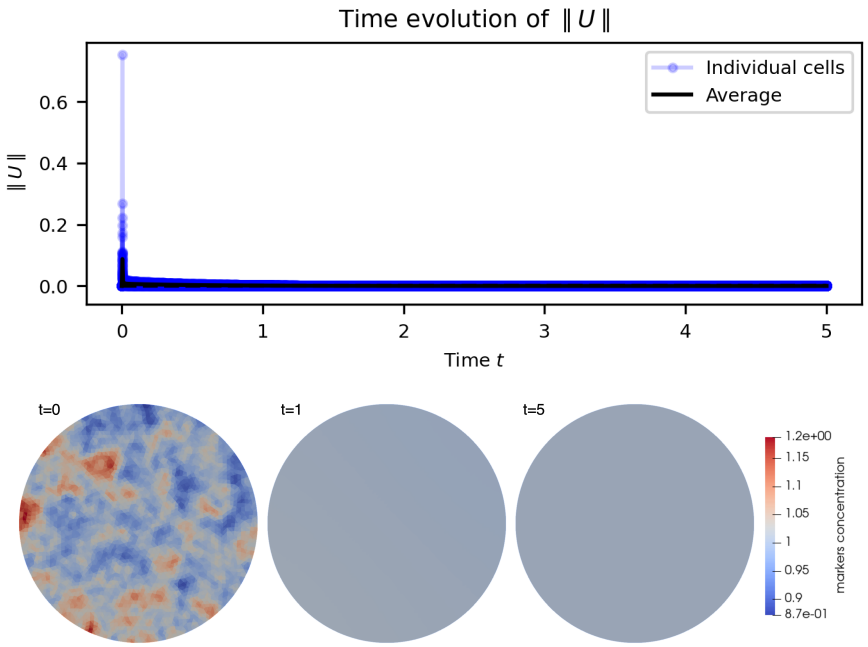

Figure 3.4: **Illustration of the stability of the rest state for $\chi_c = 0.5$ and $c_s = 0.1$.** *On top, evolution of the velocity norm over time for 50 cells. On bottom, evolution over time ($t = 0$, $t = 1$ and $t = 5$) of the markers concentration inside a cell. The red zones correspond to areas of high marker concentration and the blue zones to areas of low marker concentration.*
The initial condition is given by $c^{\text{in}}(\mathbf{x}) = K(1 + X(\mathbf{x}))\mathbf{1}_{1+X(\mathbf{x})>0}$ and $\mathbf{u}_0 = \frac{-\chi_c}{|\Omega_0|}\int_{\partial\Omega_0} f_{\text{act}}\left(c^{\text{in}}(\mathbf{x})\right)\mathbf{n}\,\mathrm{d}\sigma$. The others parameters are $M = \pi$, $R = 1$, $a = 1$, $\Delta t = 0.005$ and $T_f = 5$.

Numerically, the rest state is stable, after a perturbation of it, we can see that the velocity is constant in time and has for value 0 (see fig. 3.4 top) and that the markers concentration is, after a small time, uniformly distributed as in the rest state (see fig. 3.4 bottom).

Secondly we want to illustrate the non-existence of steadily moving solutions. We know that if a steadily moving solution exists then it should be of the form $c(\mathbf{x}) = Ke^{-a\mathbf{u}\cdot\mathbf{x}}$ with $\mathbf{u}$ the velocity. Thus to numerically illustrate the non-existence of traveling wave we choose as initial condition $c^{\text{in}}(\mathbf{x}) = Ke^{-aux}$ where $u \sim \mathcal{U}([-5, 5])$ and $\mathbf{u}_0 = (u, 0)$.

Numerically, we observe that whatever the choice of u, the norm of the cell velocity decrease to 0 (see fig. 3.5 top). It seems that $(c, \mathbf{u})$ converges to the rest state $(\tilde{c}, \tilde{\mathbf{u}})$ (see fig. 3.5 bottom). Without proving that there are no steadily moving solutions with this choice of χ_c and c_s, we can assume that we will not find, numerically, $\mathbf{u}_0$ such that we have a steadily moving solution and that every polarised cell will tends to the rest state, which is unpolarised.

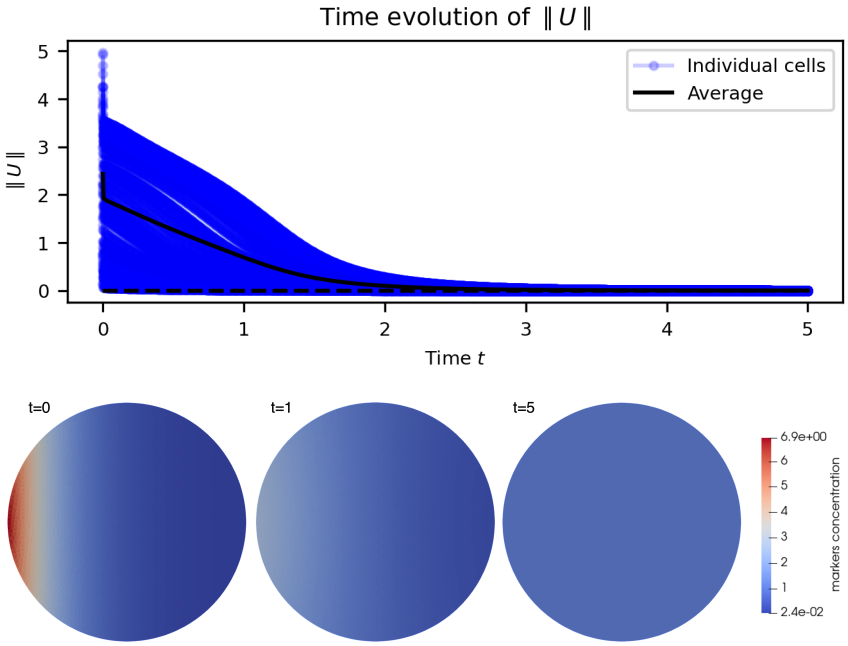

Figure 3.5: **Illustration of the non-existence of steadily moving solutions for $\chi_c = 0.5$ and $c_s = 0.1$.** *On top, evolution of the velocity norm over time for 50 cells. On bottom, example of evolution over time ($t = 0$, $t = 1$ and $t = 5$) of the markers concentration inside a cell. The red zones correspond to areas of high marker concentration and the blue zones to areas of low marker concentration.*
The initial condition is given by $c^{\text{in}}(\mathbf{x}) = Ke^{-aux}$ where $u \sim \mathcal{U}([-5,5])$ and $\mathbf{u}_0 = (u,0)$. The others parameters are $M = \pi$, $R = 1$, $a = 1$, $\Delta t = 0.005$ and $T_f = 5$.

Bistable phase In this paragraph we want to find parameters χ_c and c_s such that the motility is in the bistable phase. We choose $\chi_c = 0.9$ and $c_s = 0.1$. Thus we want to illustrate for these parameters that the rest state is stable and there exists a stable traveling wave. First we illustrate the stability of the rest state. To do it, we use the same procedure as in the case of the rest phase. We perturbed the rest state by taking as initial condition $c^{\text{in}}(\mathbf{x}) = K(1 + X(\mathbf{x}))\,\mathbf{1}_{1+X(\mathbf{x})>0}$ and $\mathbf{u}_0 = \frac{-\chi_c}{|\Omega_0|}\int_{\partial\Omega_0} f_{\text{act}}\left(c^{\text{in}}(\mathbf{x})\right)\mathbf{n}\,\mathrm{d}\sigma$.

Numerically, the rest state is stable, after a perturbation of it, we can see that the velocity is constant in time and has for value 0 (see fig. 3.6 top) and that the markers concentration is, after a small time, uniformly distributed as in the rest state (see fig. 3.6 bottom).

Secondly we want to illustrate the existence of a stable traveling wave. We observe that $c(\mathbf{x}) = Ke^{-aux}$ with $u = 6.51498$ is a steadily moving solution. We perturbed it by taking as initial condition $c^{\text{in}}(\mathbf{x}) = K\left(e^{-aux} + X(\mathbf{x})\right)\mathbf{1}_{e^{-aux}+X(\mathbf{x})>0}$ and $\mathbf{u}_0 = \frac{-\chi_c}{|\Omega_0|}\int_{\partial\Omega_0} f_{\text{act}}\left(c^{\text{in}}(\mathbf{x})\right)\mathbf{n}\,\mathrm{d}\sigma$. Then we study the evolution of the norm velocity and concentration over time. The results are in fig. 3.7.

Numerically, we observe that we found a stable traveling wave. Indeed after a small perturbation the norm of the velocity is constant and we have $\|\mathbf{u}\| = 6.51498$ (see fig. 3.7 top). Moreover we can observe that the markers concentration is steadily in time (see fig. 3.7 bottom). Then we observe that the cell does not change direction over time.

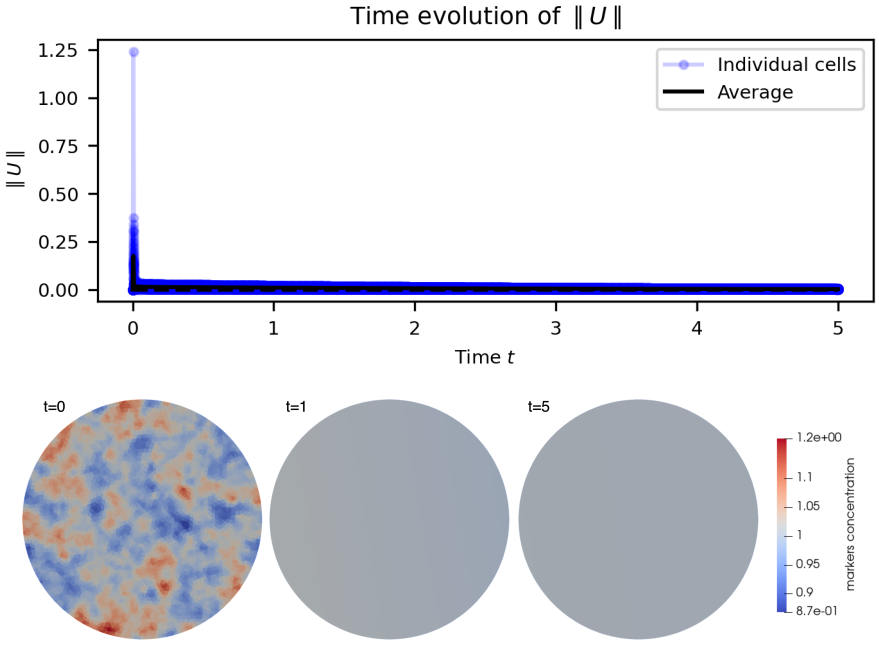

Figure 3.6: **Illustration of the stability of the rest state for $\chi_c = 0.9$ and $c_s = 0.1$.** *On top, evolution of the velocity norm over time for 50 cells. On bottom, evolution over time ($t = 0$, $t = 1$ and $t = 5$) of the markers concentration inside a cell. The red zones correspond to areas of high marker concentration and the blue zones to areas of low marker concentration.*
The initial condition is given by $c^{\text{in}}(\mathbf{x}) = K(1 + X(\mathbf{x}))\mathbf{1}_{1+X(\mathbf{x})>0}$ and $\mathbf{u}_0 = \frac{-\chi_c}{|\Omega_0|}\int_{\partial\Omega_0} f_{\text{act}}\left(c^{\text{in}}(\mathbf{x})\right)\mathbf{n}\,\mathrm{d}\sigma$. The others parameters are $M = \pi$, $R = 1$, $a = 1$, $\Delta t = 0.005$ and $T_f = 5$.

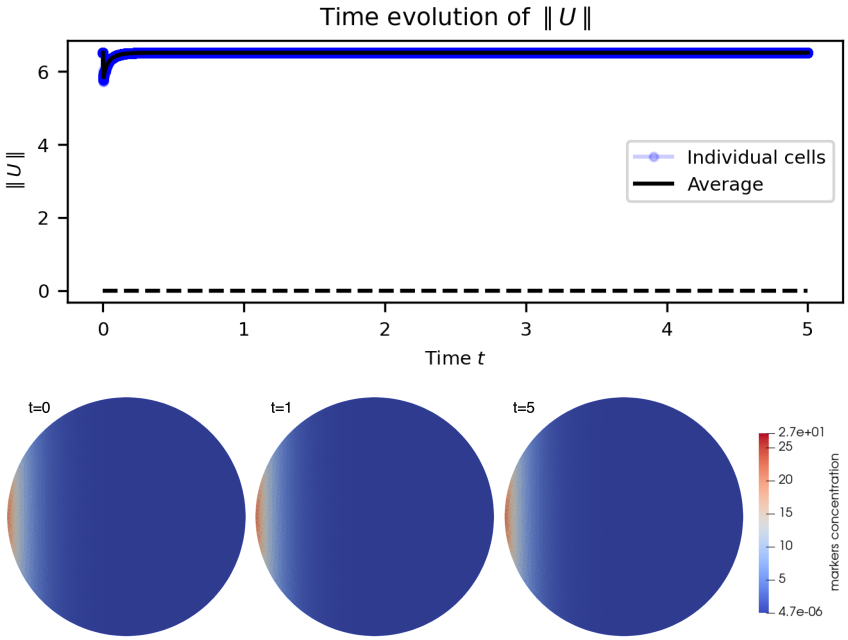

Figure 3.7: **Illustration of the stability of a steadily moving solutions for $\chi_c = 0.9$ and $c_s = 0.1$.** *On top, evolution of the velocity norm over time for 50 cells. On bottom, example of evolution over time ($t = 0$, $t = 1$ and $t = 5$) of the markers concentration inside a cell. The red zones correspond to areas of high marker concentration and the blue zones to areas of low marker concentration.*
The initial condition is given by $c^{\text{in}}(\mathbf{x}) = K\left(e^{-aux} + X(\mathbf{x})\right)\mathbf{1}_{e^{-aux}+X(\mathbf{x})>0}$ with $u = 6.51498$ and $\mathbf{u}_0 = (u, 0)$. The others parameters are $M = \pi$, $R = 1$, $a = 1$, $\Delta t = 0.005$ and $T_f = 5$.

Traveling phase In this paragraph we want to find parameters χ_c and c_s such that the motility is in the traveling phase. We choose $\chi_c = 1.1$ and $c_s = 0.1$. Thus we want to illustrate for these parameters that the rest state is unstable and there exists a stable traveling wave. First we illustrate the instability of the rest state. To do it, we use the same procedure as in the case of the rest phase. We perturbed the rest state by taking as initial condition $c^{\text{in}}(\mathbf{x}) = K(1 + X(\mathbf{x}))\mathbf{1}_{1+X(\mathbf{x})>0}$ and $\mathbf{u}_0 = \frac{-\chi_c}{|\Omega_0|}\int_{\partial\Omega_0} f_{\text{act}}\left(c^{\text{in}}(\mathbf{x})\right)\mathbf{n}\,\mathrm{d}\sigma$.

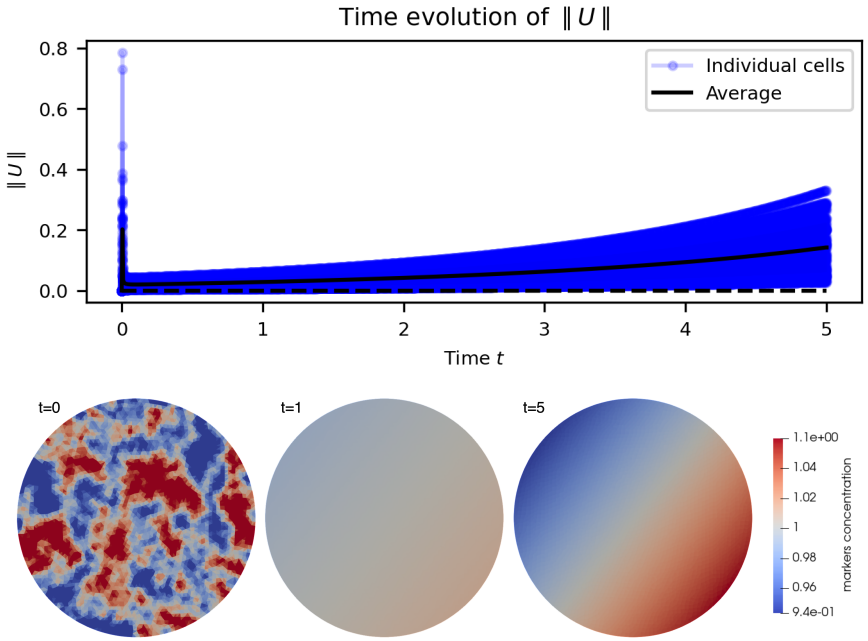

Figure 3.8: **Illustration of the instability of the rest state for $\chi_c = 1.1$ and $c_s = 0.1$.** *On top, evolution of the velocity norm over time for 50 cells. On bottom, evolution over time ($t = 0$, $t = 1$ and $t = 5$) of the markers concentration inside a cell. The red zones correspond to areas of high marker concentration and the blue zones to areas of low marker concentration.*
The initial condition is given by $c^{\text{in}}(\mathbf{x}) = K(1 + X(\mathbf{x}))\mathbf{1}_{1+X(\mathbf{x})>0}$ where for all $\mathbf{x} \in \Omega_0$, $X(\mathbf{x}) \sim \mathcal{N}(0,1)$ and $\mathbf{u}_0 = \frac{-\chi_c}{|\Omega_0|}\int_{\partial\Omega_0} f_{\text{act}}\left(c^{\text{in}}(\mathbf{x})\right)\mathbf{n}\,\mathrm{d}\sigma$. The others parameters are $M = \pi$, $R = 1$, $a = 1$, $\Delta t = 0.005$ and $T_f = 5$.

Numerically, the rest state is unstable. Indeed after a perturbation of it, we can see that the velocity norm increases over time (see fig. 3.8 top) and that the markers concentration is, after a small time, no more uniformly distributed as in the rest state (see fig. 3.8 bottom). We see that after a small perturbation of the rest state, the cell starts to polarize and to move.

Secondly we want to illustrate the existence of a stable traveling wave. We observe that $c(\mathbf{x}) = Ke^{-aux}$ with $u = 7.85613$ is a steadily moving solution. We perturbed it by taking as initial condition $c^{\text{in}}(\mathbf{x}) = K(e^{-aux} + X(\mathbf{x}))\mathbf{1}_{e^{-aux}+X(\mathbf{x})>0}$ and $\mathbf{u}_0 = (u, 0)$.

Numerically, we observe that we found a stable traveling wave. Indeed after a small perturbation the norm of the velocity is constant and we have $\|\mathbf{u}\| = 7.85613$ (see fig. 3.9 top). Moreover we can observe that the markers concentration is steadily in time (see fig. 3.9 bottom). Then we observe that the cell does not change direction over time.

Thus we found three different set of parameters to illustrate the three phases of motility

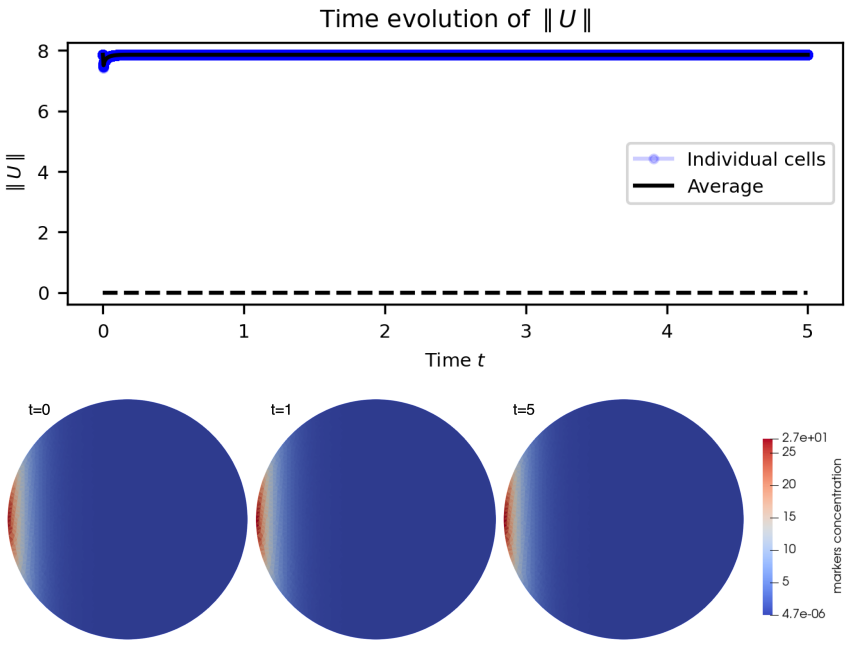

Figure 3.9: **Illustration of the stability of a steadily moving solutions for $\chi_c = 1.1$ and $c_s = 0.1$.** *On top, evolution of the velocity norm over time for 50 cells. On bottom, example of evolution over time ($t = 0$, $t = 1$ and $t = 5$) of the markers concentration inside a cell. The red zones correspond to areas of high marker concentration and the blue zones to areas of low marker concentration.*
The initial condition is given by $c^{\text{in}}(\mathbf{x}) = K\left(e^{-aux} + X(\mathbf{x})\right)\mathbf{1}_{e^{-aux}+X(\mathbf{x})>0}$ with $u = 7.85613$ and $\mathbf{u}_0 = (u, 0)$. The others parameters are $M = \pi$, $R = 1$, $a = 1$, $\Delta t = 0.005$ and $T_f = 5$.

in accordance with the motility phase diagram.

3.4.3 . Long-time behaviour

In Meunier and Souplet (2023), the long-time behaviour of the model is studied for different expressions of f_{act}. Three theorems are proved. First, the following theorem is proved for the case where $a = 1$ and $\chi_c = 1$:

Theorem 3.4.1. *Let $1 \leq m \leq p < \infty$ and assume $f_{\text{act}}(c) = |c|^{m-1}c$ and $c^{\text{in}} \in L^p(\Omega)$.*

(i) Problem (3.4) admits a unique maximal classical solution

$$c \in C^{2,1}(\overline{\Omega}_0 \times (0, T^*)) \cap C([0, T^*); L^p(\Omega_0)).$$

(ii) If $c^{\text{in}} \geq 0$, $c^{\text{in}} \not\equiv 0$, then $c > 0$ in $(\Omega_0 \cup \partial\Omega_0) \times (0, T^*)$.

(iii) If $p > m$ and $T^* < \infty$, then $\lim_{t \to T^*} \|c(t)\|_p = \infty$.

To illustrate theorem 3.4.1, after choosing m, p and c^{in} which satisfy the assumptions of the theorem, we plot the minimum of c over time on $\Omega_0 \cup \partial\Omega_0$ as well as that of the L^P norm of c. As illustrated in fig. 3.10 for $m = 1.1$, $p = 4$ and $c^{\text{in}}(x, y) = Ke^x$ with $K > 0$, we observe that the minimum of c on $\Omega_0 \cup \partial\Omega_0$ is positive for all $t \in [0, T^*)$ and so $c > 0$ in $(\Omega_0 \cup \partial\Omega_0) \times (0, T^*)$. We also observe that $\lim_{t \to T^*} \|c(t)\|_p = \infty$. These observations agree well with theorem 3.4.1 and so the numerical scheme allows us to find the result of the theorem.

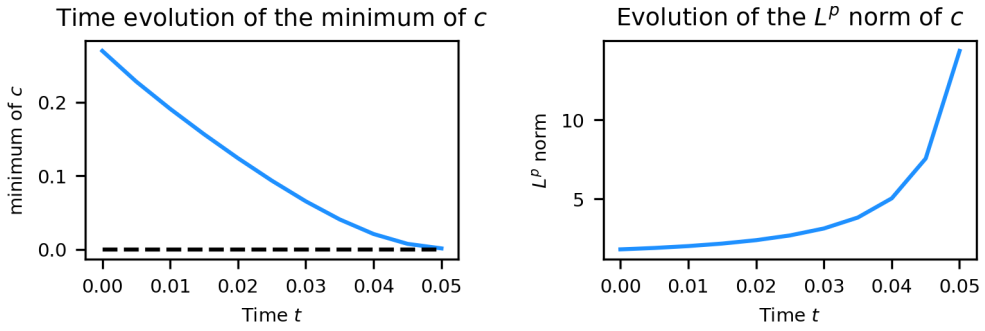

Figure 3.10: **Illustration of the theorem 3.4.1.** *On the left is represented the time evolution on the time interval $[0, T^*)$ of the minimum of c over $\Omega_0 \cup \partial\Omega_0$, we observe that this minimum is always strictly positive then we have $c > 0$ in $(\Omega_0 \cup \partial\Omega_0) \times (0, T^*)$. On the right is represented the time evolution of the L^p norm of c over the time interval $[0, T^*)$. We observe that this norm is increasing and tends to ∞.*
Simulations done with $\Omega_0 = B(0, 1)$ with the initial condition $c^{\text{in}}(x, y) = Ke^x$ where K such that $\int_{\Omega_0} c^{\text{in}}(\mathbf{x})\, \mathrm{d}\mathbf{x} = M$ and the parameters $m = 1.1$, $p = 4$, $M = \pi$, $a = 1$, $\Delta t = 0.005$ and $T_f = 10$.

Secondly, the following theorem is proved for the case where $a = 1$ and $\chi_c = 1$. Let $\bar{c}^{\text{in}} = \frac{1}{|\Omega_0|} \int_\Omega c^{\text{in}}\, \mathrm{d}\mathbf{x}$ denote the average of c^{in}.

Theorem 3.4.2. *Let f satisfy*

$$0 \leq f(s) \leq Cs^m, \quad s \geq 0, \qquad \text{for some } m \in (0, 1) \tag{3.14}$$

with some $C > 0$, and also assume that f is globally Lipschitz continuous. Let $c^{\text{in}} \in L^1(\Omega_0)$, with $c^{\text{in}} \geq 0$.

(i) Problem (3.4) admits a unique global, nonnegative classical solution

$$c \in C^{2,1}(\overline{\Omega}_0 \times (0,\infty)) \cap C([0,\infty); L^1(\Omega_0)). \tag{3.15}$$

Moreover, c is uniformly bounded for $t > 0$ bounded away from 0. Also, if $c^{\text{in}} \not\equiv 0$, then $c > 0$ in $(\Omega_0 \cup \partial\Omega_0) \times (0,\infty)$.

(ii) There exist $\eta_0, \lambda > 0$ such that if $\|c^{\text{in}}\|_1 \leq \eta_0$, then

$$\|c(t) - \bar{c}^{\text{in}}\|_\infty \leq Ce^{-\lambda t}, \quad t \geq 1 \tag{3.16}$$

for some constant $C > 0$.

To illustrate theorem 3.4.2, after choosing m and c^{in} which satisfy the assumptions of the theorem, we plot the minimum and maximum of c over time on $\Omega_0 \cup \partial\Omega_0$. We also show the evolution over time of $\|c(t) - \bar{c}^{\text{in}}\|_\infty$ and illustrate that it decreases exponentially towards 0. As illustrated in fig. 3.11 for $m = 0.3$ and $c^{\text{in}}(x,y) = Ke^x$ with $K > 0$, we observe that the minimum of c on $\Omega_0 \cup \partial\Omega_0$ is globally lower bounded by the minimum of $c^{\text{in}} > 0$. Also, the maximum of c on $\Omega_0 \cup \partial\Omega_0$ is globally upper bounded by the maximum of $c^{\text{in}} > 0$. Thus c is uniformly bounded for $t > 0$, away from 0. We observe that $\|c(t) - \bar{c}^{\text{in}}\|_\infty$ decreases exponentially towards 0. These observations are in good agreement with theorem 3.4.2 and so the numerical scheme allows us to recover the result of the theorem.

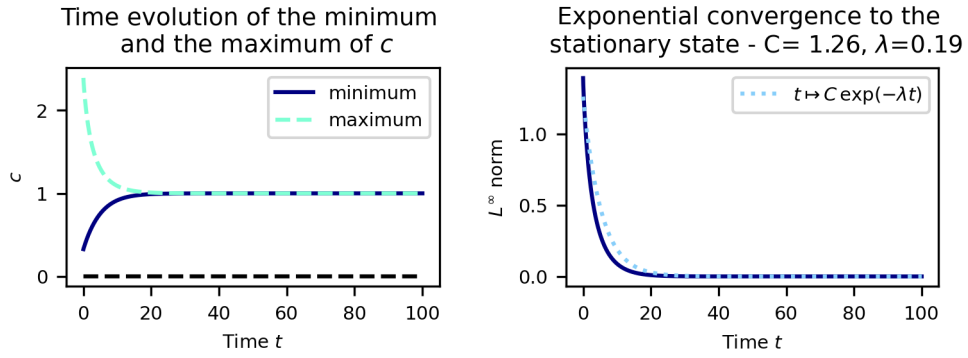

Figure 3.11: **Illustration of the theorem 3.4.2.** *On the left is represented the time evolution of the minimum and the maximum of c over $\Omega_0 \cup \partial\Omega_0$. We observe that c is uniformly bounded for $t > 0$, way from 0. We also observe that $c > 0$ in $(\Omega_0 \cup \partial\Omega_0) \times (0, T_f)$ where T_f is the final time of the numerical simulation. On the right is represented the time evolution of $\|c(t) - \bar{c}^{\text{in}}\|_\infty$. We observe that this norm is exponentially decreasing towards 0. In dash light blue is represented an exponential function such that $\|c(t) - \bar{c}^{\text{in}}\|_\infty \leq Ce^{-\lambda t}$ for $t \in [0, T_f]$.*
Simulations done with $\Omega_0 = B(0,1)$ with the initial condition $c^{\text{in}}(x,y) = Ke^x$ where K such that $\int_{\Omega_0} c^{\text{in}}(\mathbf{x})\, d\mathbf{x} = M$ and the parameters $m = 0.3$, $M = \pi$, $a = 1$, $\Delta t = 0.005$ and $T_f = 100$.

Finally, the following theorem is proved for the case where $a = 1$ and $\chi_c = 1$.

Theorem 3.4.3. *Let $f(c) = c$, $c^{\text{in}} \in L^1(\Omega_0)$, $c^{\text{in}} \geq 0$ and set $M = \|c^{\text{in}}\|_1$.*

(i) If $M \leq 1$, then $T^* = \infty$ and c is uniformly bounded for $t > 0$ bounded away from 0.

(ii) Morever, if $M < 1$, then

$$\lim_{t\to\infty} \|c(t) - \bar{c}^{\text{in}}\|_\infty = 0, \tag{3.17}$$

To illustrate theorem 3.4.3, after choosing M and c^{in} which satisfy the assumptions of the theorem, we plot the minimum and maximum of c over time on $\Omega_0 \cup \partial\Omega_0$. We also show the evolution over time of $\|c(t) - \bar{c}^{\text{in}}\|_\infty$ and illustrate that if $M < 1$ then we have $\lim_{t\to\infty} \|c(t) - \bar{c}^{\text{in}}\|_\infty = 0$ whereas if $M \geq 1$ we do not. As illustrated in figs. 3.12 and 3.13 for $M = 0.9$ and $M = 1$ respectively and $c^{\text{in}}(x, y) = Ke^x$ with $K > 0$, we observe that in both cases the minimum of c on $\Omega_0 \cup \partial\Omega_0$ is globally lower bounded by the minimum of $c^{\text{in}} > 0$. Also, the maximum of c on $\Omega_0 \cup \partial\Omega_0$ is globally upper bounded by the maximum of $c^{\text{in}} > 0$. Thus c is uniformly bounded for $t > 0$, away from 0. We observe that when $M = 0.9$, $\lim_{t\to\infty} \|c(t) - \bar{c}^{\text{in}}\|_\infty = 0$ whereas when $M = 1$ we have $\lim_{t\to\infty} \|c(t) - \bar{c}^{\text{in}}\|_\infty = 0.447288 \neq 0$. These observations are in good agreement with theorem 3.4.3 and so the numerical scheme allows us to recover the result of the theorem.

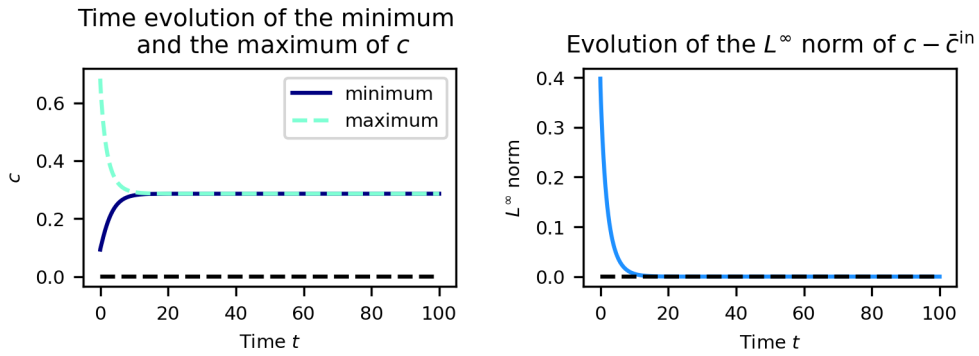

Figure 3.12: **Illustration of the theorem 3.4.3 when $M < 1$.** *On the left is represented the time evolution of the minimum and the maximum of c over $\Omega_0 \cup \partial\Omega_0$. We observe that c is uniformly bounded for $t > 0$, way from 0. We also observe that $c > 0$ in $(\Omega_0 \cup \partial\Omega_0) \times (0, T_f)$ where T_f is the final time of the numerical simulation. On the right is represented the time evolution of $\|c(t) - \bar{c}^{\text{in}}\|_\infty$. We observe that it decreases towards 0.*
Simulations done with $\Omega_0 = B(0, 1)$ with the initial condition $c^{\text{in}}(x, y) = Ke^x$ where K such that $\int_{\Omega_0} c^{\text{in}}(\mathbf{x})\, d\mathbf{x} = M$ and the parameters $M = 0.9$, $a = 1$, $\Delta t = 0.005$ and $T_f = 100$.

These numerical results, in agreement with theoretical results from Lavi et al. (2020); Meunier and Souplet (2023), validate our numerical scheme. We can then study our model numerically by simulating it using algorithm 3.1.

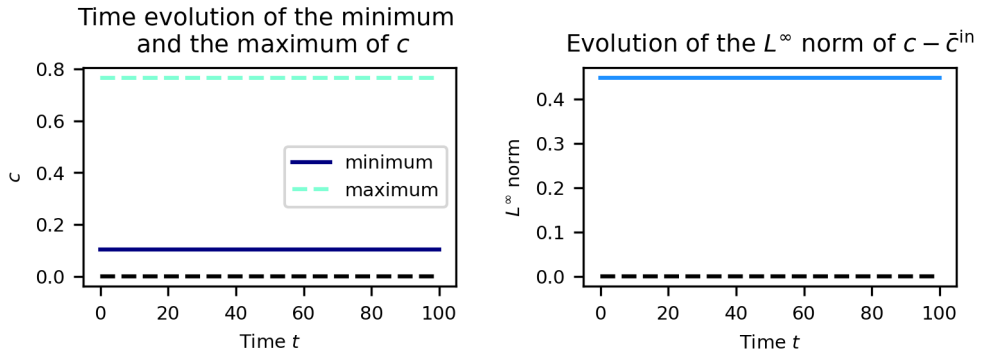

Figure 3.13: **Illustration of the theorem 3.4.3 when $M = 1$.** *On the left is represented the time evolution of the minimum and the maximum of c over $\Omega_0 \cup \partial\Omega_0$. We observe that c is uniformly bounded for $t > 0$, way from 0. We also observe that $c > 0$ in $(\Omega_0 \cup \partial\Omega_0) \times (0, T_f)$ where T_f is the final time of the numerical simulation. On the right is represented the time evolution of $\|c(t) - \bar{c}^{\text{in}}\|_\infty$. We observe that it is constant equals to 0.447288 and thus $\lim_{t\to\infty} \|c(t) - \bar{c}^{\text{in}}\|_\infty \neq 0$.*
Simulations done with $\Omega_0 = B(0,1)$ with the initial condition $c^{\text{in}}(x,y) = Ke^x$ where K such that $\int_{\Omega_0} c^{\text{in}}(\mathbf{x})\, \mathrm{d}\mathbf{x} = M$ and the parameters $M = 1$, $a = 1$, $\Delta t = 0.005$ and $T_f = 100$.

3.5 . Numerical result and capturing the UCSP law

In this section, we investigate whether the model satisfies the UCSP law and whether we can capture the three types of trajectory that cells can have. By choosing a range of suitable parameters, we are able to exhibit a situation where the trajectories are Brownian, a situation where they are persistent and a situation where they are intermittent (see figs. 3.14, 3.18 and 3.22). In all three cases, the trajectories satisfy the UCSP law.

By fixing all the model parameters and varying only χ_c, we observe Brownian trajectories when $\chi_c < \chi_c^*$, intermittent trajectories when $\chi_c = \chi_c^*$ and persistent trajectories when $\chi_c > \chi_c^*$.

In this section, for the numerical results presented, $R = 1$, $M = \pi$ and $a = 1$. As an initial condition c^{in} for the concentration of markers, we choose the function defined for all $\mathbf{x} \in \Omega$ by $c^{\text{in}}(\mathbf{x}) = \dfrac{M}{\pi R^2}$. The noise parameters are set to $\alpha = 0.3$ and $\zeta = 0.2$. Finally, the numerical simulations are performed over the time interval $[0, 15]$ with $\Delta t = 0.005$. Here are the results when $\chi_c = \chi_c^* - 0.3$, $\chi_c = \chi_c^*$ and $\chi_c = \chi_c^* + 0.5$ with χ_c^* defined in eq. (3.13).

Illustration of the case where trajectories are Brownian. In this subsection, we present the results when $\chi_c = \chi_c^* - 0.3$. We then observe that the trajectories are Brownian. This can be seen visually in fig. 3.14 and is confirmed by the study of the EASD and MSD, which are close to 1 (see fig. 3.16). In addition, we can see that the trajectories satisfy the UCSP (see fig. 3.15). We also observe that the cells have a low velocity: the mean norm is close to the intensity α of the noise (see fig. 3.17). These observations are in good agreement with those made about Brownian behaviour in Maiuri et al. (2015).

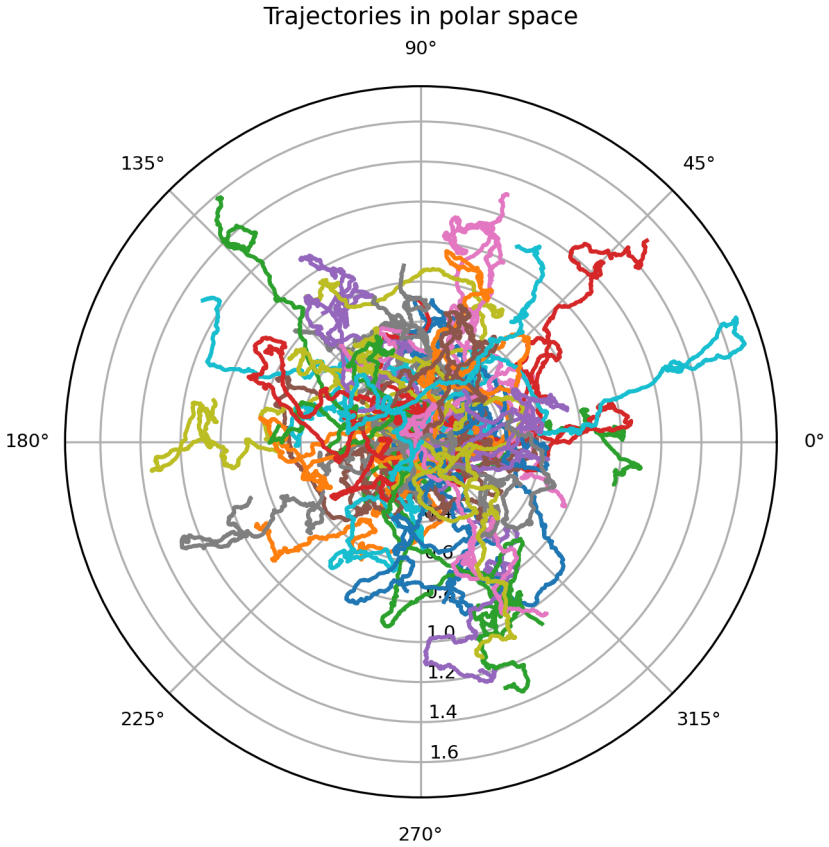

Figure 3.14: **Trajectories in polar coordinates in the case where $\chi_c < \chi_c^*$.** *Each curve represents, in polar coordinates, the trajectory of one cell simulated by algorithm 4.1 on the time interval $[0, 15]$. Visually, the trajectories seem to be Brownian. Fifty cells are represented. The results presented here are obtained with the parameters $\Delta t = 0.005$, $R = 1$, $M = \pi$, $a = 1$, $c^{\text{in}} = \dfrac{M}{\pi R^2}$, $\chi_c = \chi_c^* - 0.3$ with χ_c^* given by (3.13), $f_{\text{act}}(c) = \frac{c(1+c_s)^2}{c_s(c+c_s)}$ with $c_s = 0.5$, $\alpha = 0.3$ and $\zeta = 0.2$.*

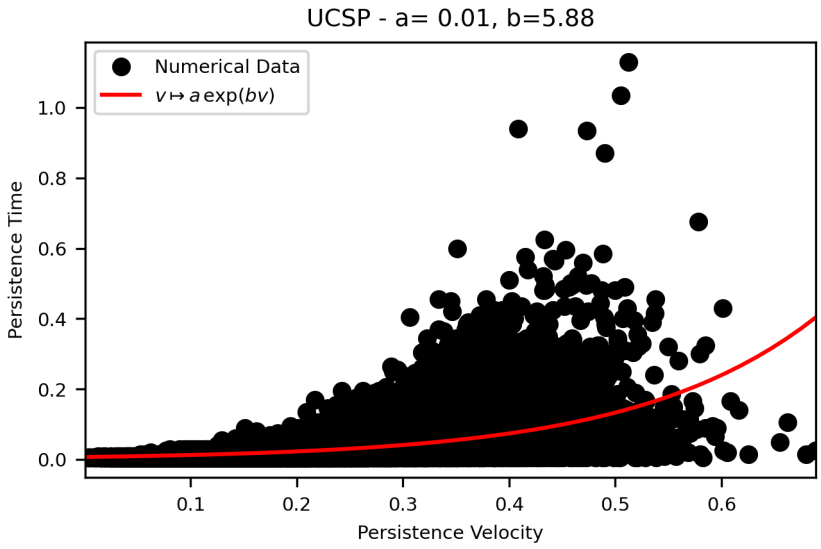

Figure 3.15: **Verification that the trajectories in fig. 3.14 satisfy the UCSP law (case when $\chi_c < \chi_c^*$).** *The persistence time of a locally persistent trajectory portion is plotted as a function of the persistence velocity. Each black dot corresponds to a datum. In red is plotted an interpolation of the points, of form $v \mapsto ae^{bv}$, which corresponds to the UCSP law. We can see that the data corresponds well to the interpolation and that the trajectories satisfy the UCSP law.*
The results presented here are obtained with the parameters $\Delta t = 0.005$, $R = 1$, $M = \pi$, $a = 1$, $c^{\text{in}} = \dfrac{M}{\pi R^2}$, $\chi_c = \chi_c^* - 0.3$ with χ_c^* given by (3.13), $f_{\text{act}}(c) = \frac{c(1+c_s)^2}{c_s(c+c_s)}$ with $c_s = 0.5$, $\alpha = 0.3$ and $\zeta = 0.2$.

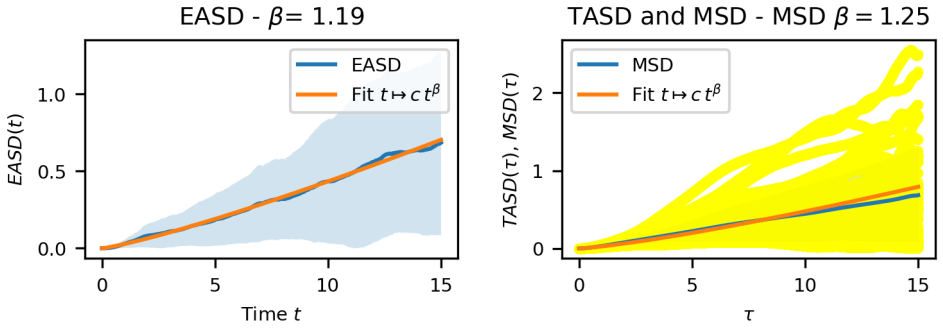

Figure 3.16: **Verification that the trajectories in fig. 3.14 are Brownian (case when $\chi_c < \chi_c^*$).** *On the left is shown in blue the EASD associated with the trajectories in fig. 3.14 and in orange the interpolation of the EASD, in the form $t \mapsto ct^{\beta}$. By the properties of the EASD, as β close to 1, the trajectories in fig. 3.14 are indeed Brownian. This is confirmed by the study of the MSD, which is shown in blue on the right. Also shown on the right are the TASD of each cell in yellow and the interpolation of the MSD in form $t \mapsto ct^{\beta}$ in orange.*
The results presented here are obtained with the parameters $\Delta t = 0.005$, $R = 1$, $M = \pi$, $a = 1$, $c^{\text{in}} = \dfrac{M}{\pi R^2}$, $\chi_c = \chi_c^* - 0.3$ with χ_c^* given by (3.13), $f_{\text{act}}(c) = \frac{c(1+c_s)^2}{c_s(c+c_s)}$ with $c_s = 0.5$, $\alpha = 0.3$ and $\zeta = 0.2$.

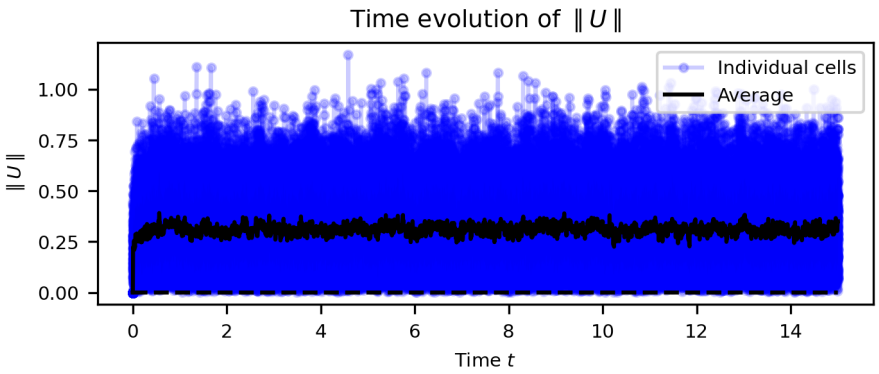

Figure 3.17: **Time evolution of the norm of the velocity of the cells whose trajectories are shown in fig. 3.14 (case when $\chi_c < \chi_c^*$).** *The blue lines show the evolution over time of the norm of the velocity of each cell and the black line shows the evolution of the mean of the norms of the velocities of the cells. We can see that the value of the mean of the norms of the cell velocities corresponds to the choice of α.*
The results presented here are obtained with the parameters $\Delta t = 0.005$, $R = 1$, $M = \pi$, $a = 1$, $c^{\text{in}} = \dfrac{M}{\pi R^2}$, $\chi_c = \chi_c^* - 0.3$ with χ_c^* given by (3.13), $f_{\text{act}}(c) = \frac{c(1+c_s)^2}{c_s(c+c_s)}$ with $c_s = 0.5$, $\alpha = 0.3$ and $\zeta = 0.2$.

Illustration of the case where trajectories are persistent. In this subsection, we present the results when $\chi_c = \chi_c^* + 0.5$. We then observe that the trajectories are persistent. This can be seen visually in fig. 3.18 and is confirmed by the study of the EASD and MSD, which are equal or close to 2 (see fig. 3.20). In addition, we can see that the trajectories satisfy the UCSP (see fig. 3.19). We also observe that the cells have a high velocity (see fig. 3.21). These observations are in good agreement with those made about persistent behaviour in Maiuri et al. (2015).

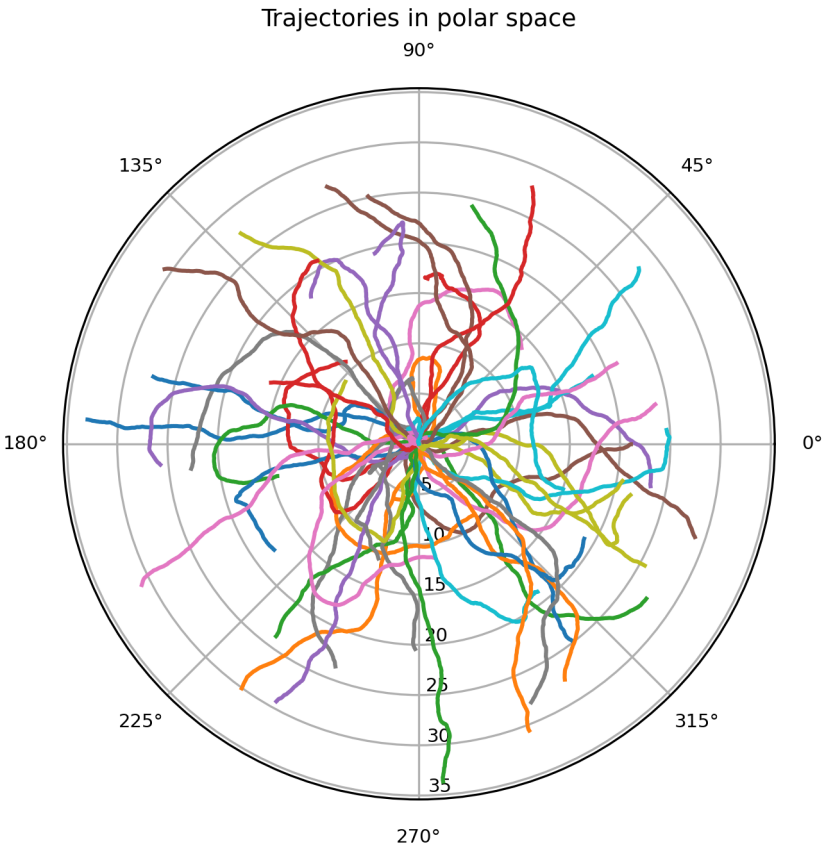

Figure 3.18: **Trajectories in polar coordinates in the case where $\chi_c > \chi_c^*$.** *Each curve represents, in polar coordinates, the trajectory of one cell simulated by algorithm 4.1 on the time interval $[0, 15]$. Visually, the trajectories seem to be persistent. Fifty cells are represented.*
The results presented here are obtained with the parameters $\Delta t = 0.005$, $R = 1$, $M = \pi$, $a = 1$, $c^{\text{in}} = \dfrac{M}{\pi R^2}$, $\chi_c = \chi_c^* + 0.5$ with χ_c^* given by (3.13), $f_{\text{act}}(c) = \frac{c(1+c_s)^2}{c_s(c+c_s)}$ with $c_s = 0.5$, $\alpha = 0.3$ and $\zeta = 0.2$.

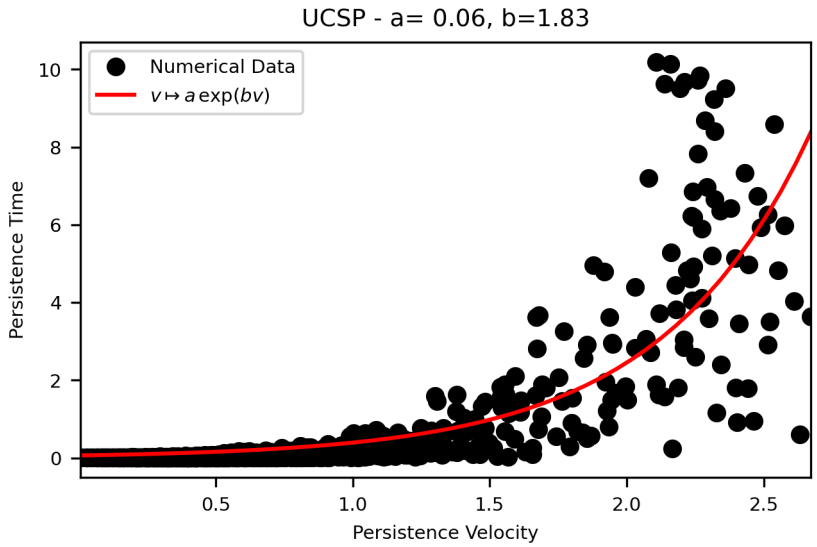

Figure 3.19: **Verification that the trajectories in fig. 3.18 satisfy the UCSP law (case when $\chi_c > \chi_c^*$).** *The persistence time of a locally persistent trajectory portion is plotted as a function of the persistence velocity. Each black dot corresponds to a datum. In red is plotted an interpolation of the points, of form $v \mapsto ae^{bv}$, which corresponds to the UCSP law. We can see that the data corresponds well to the interpolation and that the trajectories satisfy the UCSP law.*
The results presented here are obtained with the parameters $\Delta t = 0.005$, $R = 1$, $M = \pi$, $a = 1$, $c^{\text{in}} = \dfrac{M}{\pi R^2}$, $\chi_c = \chi_c^* + 0.5$ with χ_c^* given by (3.13), $f_{\text{act}}(c) = \frac{c(1+c_s)^2}{c_s(c+c_s)}$ with $c_s = 0.5$, $\alpha = 0.3$ and $\zeta = 0.2$.

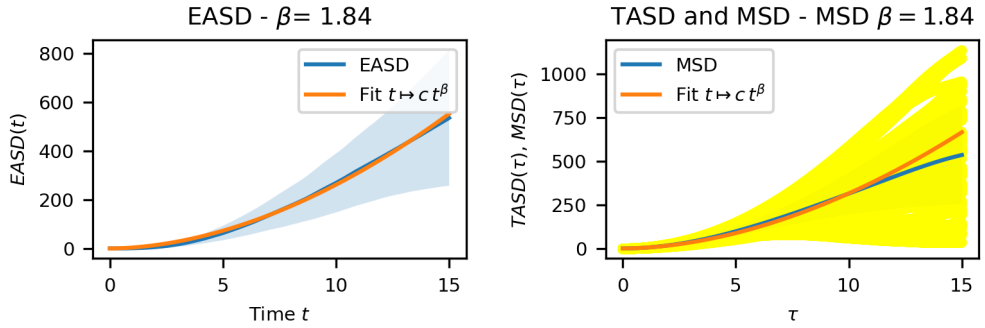

Figure 3.20: **Verification that the trajectories in fig. 3.18 are Brownian (case when $\chi_c > \chi_c^*$).** *On the left is shown in blue the EASD associated with the trajectories in fig. 3.18 and in orange the interpolation of the EASD, in the form $t \mapsto ct^{\beta}$. By the properties of the EASD, as β equals to 2, the trajectories in fig. 3.18 are indeed persistent. This is confirmed by the study of the MSD, which is shown in blue on the right. Also shown on the right are the TASD of each cell in yellow and the interpolation of the MSD in form $t \mapsto ct^{\beta}$ in orange.*
The results presented here are obtained with the parameters $\Delta t = 0.005$, $R = 1$, $M = \pi$, $a = 1$, $c^{\text{in}} = \dfrac{M}{\pi R^2}$, $\chi_c = \chi_c^* + 0.5$ with χ_c^* given by (3.13), $f_{\text{act}}(c) = \frac{c(1+c_s)^2}{c_s(c+c_s)}$ with $c_s = 0.5$, $\alpha = 0.3$ and $\zeta = 0.2$.

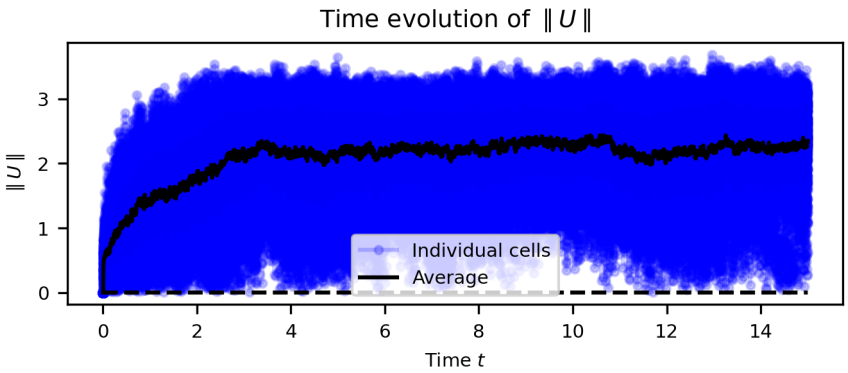

Figure 3.21: **Time evolution of the norm of the velocity of the cells whose trajectories are shown in fig. 3.18 (case when $\chi_c > \chi_c^*$).** *The blue lines show the evolution over time of the norm of the velocity of each cell and the black line shows the evolution of the mean of the norms of the velocities of the cells.*
The results presented here are obtained with the parameters $\Delta t = 0.005$, $R = 1$, $M = \pi$, $a = 1$, $c^{\text{in}} = \dfrac{M}{\pi R^2}$, $\chi_c = \chi_c^* + 0.5$ *with* χ_c^* *given by* (3.13), $f_{\text{act}}(c) = \frac{c(1+c_s)^2}{c_s(c+c_s)}$ *with* $c_s = 0.5$, $\alpha = 0.3$ *and* $\zeta = 0.2$.

Illustration of the case where trajectories are intermittent. In this subsection, we present the results when $\chi_c = \chi_c^*$. We then observe that the trajectories are intermittent. This can be seen visually in fig. 3.22 and is confirmed by the study of the EASD and MSD, which are between 1 and 2 (see fig. 3.24). In addition, we can see that the trajectories satisfy the UCSP (see fig. 3.23). We also observe that the cells have a intermediate velocity: the velocity norm is between the velocities of the case $\chi_c = \chi_c^* - 0.3$ and $\chi_c = \chi_c^* + 0.5$ (see fig. 3.25). These observations are in good agreement with those made about intermittent behaviour in Maiuri et al. (2015).

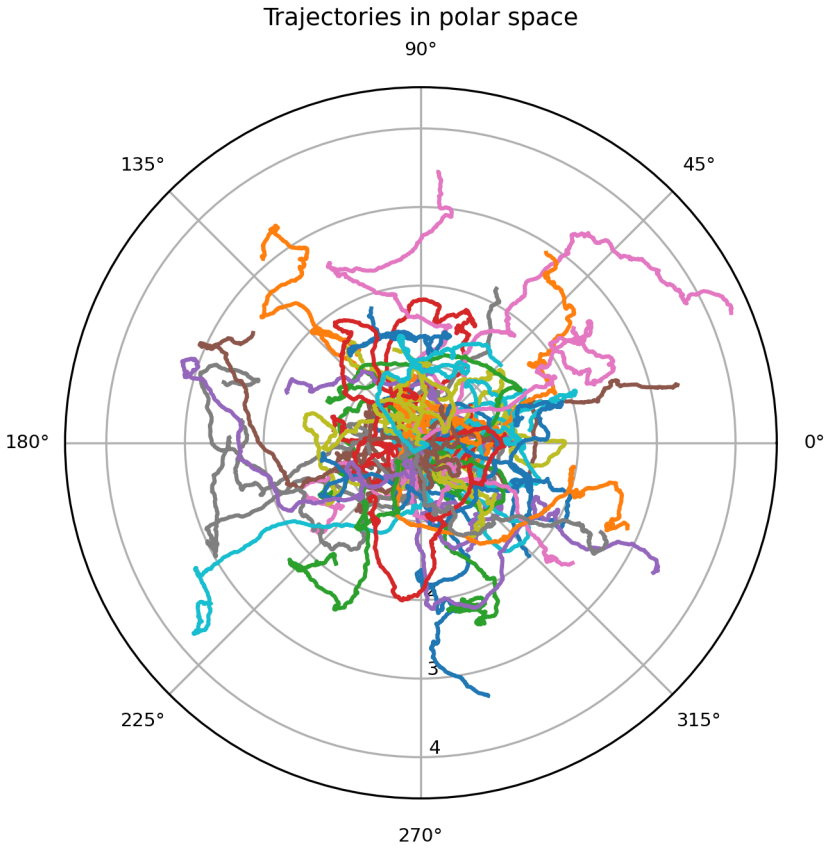

Figure 3.22: **Trajectories in polar coordinates in the case where $\chi_c = \chi_c^*$.** *Each curve represents, in polar coordinates, the trajectory of one cell simulated by algorithm 4.1 on the time interval $[0, 15]$. Visually, the trajectories seem to be intermittent. Fifty cells are represented.*
The results presented here are obtained with the parameters $\Delta t = 0.005$, $R = 1$, $M = \pi$, $a = 1$, $c^{\text{in}} = \dfrac{M}{\pi R^2}$, $\chi_c = \chi_c^*$ with χ_c^* given by (3.13), $f_{\text{act}}(c) = \frac{c(1+c_s)^2}{c_s(c+c_s)}$ with $c_s = 0.5$, $\alpha = 0.3$ and $\zeta = 0.2$.

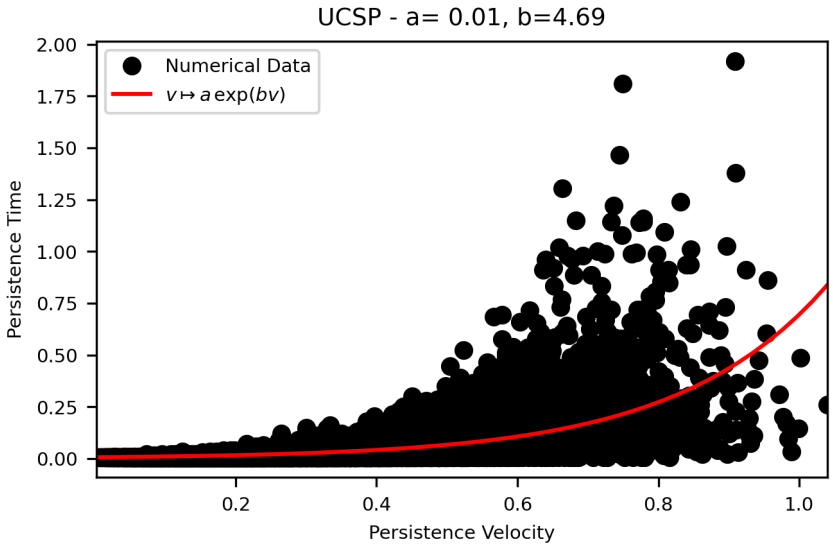

Figure 3.23: **Verification that the trajectories in fig. 3.22 satisfy the UCSP law (case when $\chi_c = \chi_c^*$).** *The persistence time of a locally persistent trajectory portion is plotted as a function of the persistence velocity. Each black dot corresponds to a datum. In red is plotted an interpolation of the points, of form $v \mapsto ae^{bv}$, which corresponds to the UCSP law. We can see that the data corresponds well to the interpolation and that the trajectories satisfy the UCSP law.*
The results presented here are obtained with the parameters $\Delta t = 0.005$, $R = 1$, $M = \pi$, $a = 1$, $c^{\text{in}} = \dfrac{M}{\pi R^2}$, $\chi_c = \chi_c^*$ with χ_c^* given by (3.13), $f_{\text{act}}(c) = \frac{c(1+c_s)^2}{c_s(c+c_s)}$ with $c_s = 0.5$, $\alpha = 0.3$ and $\zeta = 0.2$.

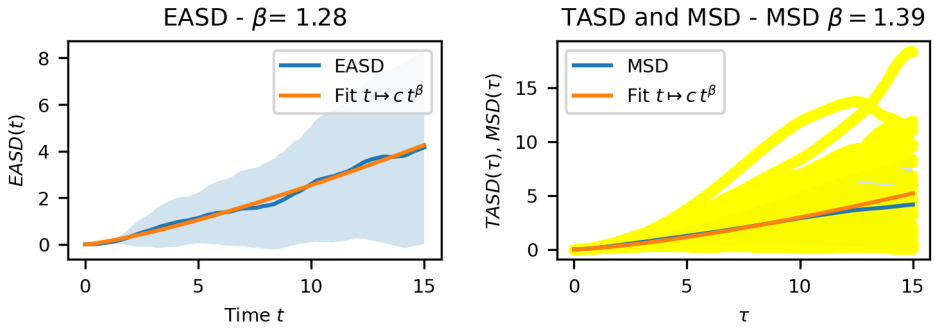

Figure 3.24: **Verification that the trajectories in fig. 3.22 are intermittent (case when $\chi_c = \chi_c^*$).** *On the left is shown in blue the EASD associated with the trajectories in fig. 3.22 and in orange the interpolation of the EASD, in the form $t \mapsto ct^{\beta}$. By the properties of the EASD, as β between 1 and 2, the trajectories in fig. 3.22 are neither Brownian neither persistent. This is confirmed by the study of the MSD, which is shown in blue on the right. Also shown on the right are the TASD of each cell in yellow and the interpolation of the MSD in form $t \mapsto ct^{\beta}$ in orange.*
The results presented here are obtained with the parameters $\Delta t = 0.005$, $R = 1$, $M = \pi$, $a = 1$, $c^{\text{in}} = \dfrac{M}{\pi R^2}$, $\chi_c = \chi_c^*$ with χ_c^* given by (3.13), $f_{\text{act}}(c) = \frac{c(1+c_s)^2}{c_s(c+c_s)}$ with $c_s = 0.5$, $\alpha = 0.3$ and $\zeta = 0.2$.

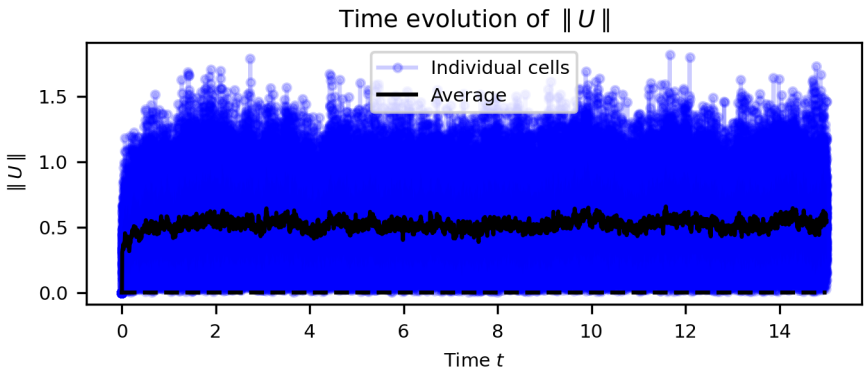

Figure 3.25: **Time evolution of the norm of the velocity of the cells whose trajectories are shown in fig. 3.22 (case when $\chi_c = \chi_c^*$).** *The blue lines show the evolution over time of the norm of the velocity of each cell and the black line shows the evolution of the mean of the norms of the velocities of the cells. We can see that the value of the mean of the norms of the cell velocities corresponds to the choice of α.*
The results presented here are obtained with the parameters $\Delta t = 0.005$, $R = 1$, $M = \pi$, $a = 1$, $c^{\text{in}} = \dfrac{M}{\pi R^2}$, $\chi_c = \chi_c^*$ with χ_c^* given by (3.13), $f_{\text{act}}(c) = \frac{c(1+c_s)^2}{c_s(c+c_s)}$ with $c_s = 0.5$, $\alpha = 0.3$ and $\zeta = 0.2$.

Thus, numerically, we find three ranges of parameters for which the trajectories are either brownian, persistent or intermittent. Moreover, for these three ranges of parameters, the trajectories satisfy the UCSP law.

Bibliography

Boulakia, M., Genadot, A., and Thieullen, M. (2015). Simulation of SPDEs for Excitable Media Using Finite Elements. Journal of Scientific Computing, 65(1):171–195. 74, 75

Hairer, M., Ryser, M. D., and Weber, H. (2012). Triviality of the 2D stochastic Allen-Cahn equation. Electronic Journal of Probability, 17(none). arXiv:1201.3089 [math-ph]. 74

Hecht, F. (2012). New development in freefem++. J. Numer. Math., 20(3-4):251–265. 74, 78

Jammalamadaka, S. R. and SenGupta, A. (2001). Topics in circular statistics, volume 5. World Scientific. 77

Lavi, I. (2019). Physical modeling of cell motility and morphodynamics. phdthesis, Sorbonne Université. 80

Lavi, I., Meunier, N., Voituriez, R., and Casademunt, J. (2020). Motility and morphodynamics of confined cells. Physical Review E, 101(2):022404. Publisher: American Physical Society. 73, 78, 80, 89

Loosley, A. J., O'Brien, X. M., Reichner, J. S., and Tang, J. X. (2015). Describing Directional Cell Migration with a Characteristic Directionality Time. PLOS ONE, 10(5):e0127425. 77

Maiuri, P., Rupprecht, J.-F., Wieser, S., Ruprecht, V., Bénichou, O., Carpi, N., Coppey, M., De Beco, S., Gov, N., Heisenberg, C.-P., Lage Crespo, C., Lautenschlaeger, F., Le Berre, M., Lennon-Dumenil, A.-M., Raab, M., Thiam, H.-R., Piel, M., Sixt, M., and Voituriez, R. (2015). Actin Flows Mediate a Universal Coupling between Cell Speed and Cell Persistence. Cell, 161(2):374–386. 77, 90, 94, 97

Meunier, N. and Souplet, P. (2023). Convergence, concentration and critical mass phenomena in a chemotaxis model with boundary signal production for eukaryotic cell migration. arXiv:2303.08654 [math]. 73, 87, 89

Walsh, J. B. (2005). Finite Element Methods for Parabolic Stochastic PDE's. Potential Analysis, 23(1):1–43. 74

4 - The crown model

In this chapter, we introduce a first toy model which will be useful for highlighting the properties of the nucleus in chapter 6. This model is a simplification of the general model (1.1) obtained when we consider the environment of the cell to be homogeneous, with no obstacles or external signals, when we neglect the friction of the cell boundary and when the links between the nucleus and the membrane are rigid. Informally, this means that δ tends to infinity if we consider $\mathbf{f}_{\mathrm{BN}}$ and f_{NB} defined by eqs. (1.22) and (1.23). We then obtain a model whose fluid domain is rigid and has the shape of a crown. After presenting the modelling leading to this model, we study its stationary states. We then give a numerical scheme for the model, enabling numerical simulations to be performed. Analysis of the numerical results shows that the model captures the three types of trajectories and that these satisfy the UCSP law.

4.1 . Modelling

In this section, we derive from the general model eq. (1.1), the crown model. We keep the same notations as the one from the chapter 1. We assume that the cell's environment is homogeneous, with no obstacles or external signals. We neglect the friction at the boundary of the cell. We assume that $\mathbf{f}_{\mathrm{BN}}$ and f_{NB} are defined by eqs. (1.22) and (1.23). We assume that δ, the parameter of the force between the cell boundary and the nucleus, tends towards infinity. This amounts to assuming that the links connecting the nucleus to the boundary of the cell are rigid and of the same length (see fig. 4.1 for an illustration of the model). Then necessarily, for all $t \geq 0$, $\Omega(t)$ is a ball of radius $R_0 > R_{\mathrm{nucl}}$.

Moreover, the nucleus cannot move in the cell, and the geometry of the cell is fixed. We therefore assume that the cell moves at the velocity of the centre of mass. Thus the model is given by:

$$\begin{cases} \partial_t c = \operatorname{div}\left(\nabla c - (1-a)\,\mathbf{u}c - \alpha \dot{W}_t^Q c\right) & \text{in } \Omega(t) \setminus N(t), \quad (4.1a) \\ \left(\nabla c + a\mathbf{u}c - \alpha \dot{W}_t^Q c\right) \cdot \mathbf{n} = 0 & \text{on } \partial\left(\Omega(t) \setminus N(t)\right), \quad (4.1b) \\ \mathbf{u}(t) = \dfrac{-\chi_c}{A_\Omega} \displaystyle\int_{\partial\Omega(t)} f_{\mathrm{act}}(c)\,\mathbf{n}\,\mathrm{d}\sigma, & (4.1c) \end{cases}$$

with $\Omega(t) = B\left(\mathbf{x}_{\mathrm{cell}}(t), R_0\right)$ and $\Omega(t) = B\left(\mathbf{x}_{\mathrm{nucl}}(t), R_{\mathrm{nucl}}\right)$. We have:

$$\frac{\mathrm{d}}{\mathrm{d}t}\mathbf{x}_{\mathrm{cell}}(t) = \mathbf{u}(t)$$

and

$$\frac{\mathrm{d}}{\mathrm{d}t}\mathbf{x}_{\mathrm{nucl}}(t) = \mathbf{u}(t).$$

Note that the geometry of the cell is fixed over time, and the cell is translated at velocity $\mathbf{u}$. Thus, $\dot{W}_t^Q$ is a coloured noise resulting from a Q-Wiener process defined on $\Omega(0) \setminus N(0)$.

We can note that the total quantity of markers M is conserved over time and we have:

$$M = \int_{\Omega(t)\setminus N(t)} c(t,\mathbf{x})\,\mathrm{d}\mathbf{x}. \quad (4.2)$$

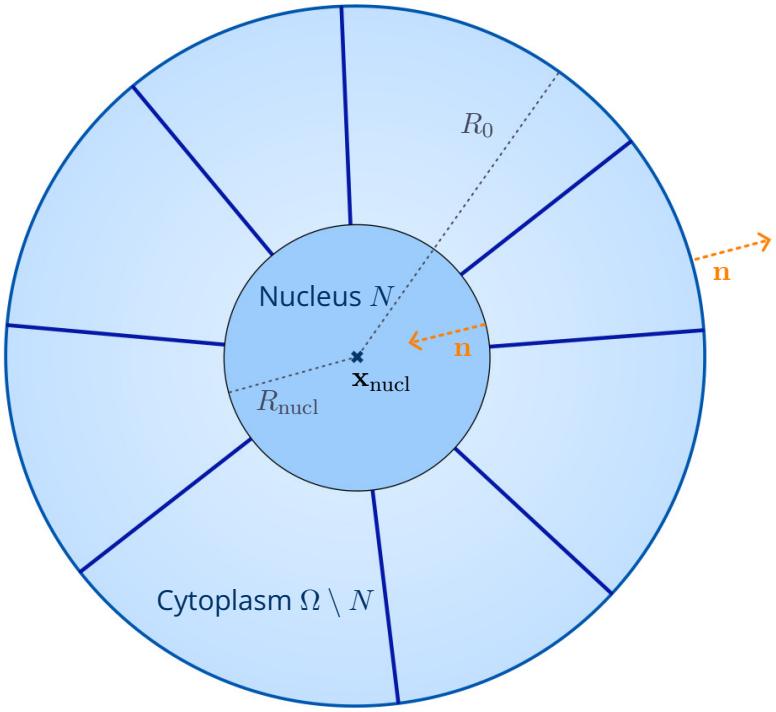

Figure 4.1: **Illustration of the crown model.** *The links between the nucleus and the cell boundary are represented by the dark blue lines. These are rigid and of equal length. So the cell is circular and rigid. The nucleus is at the centre of the cell and, in the cell's frame of reference, is fixed.*

4.2 . Study of the model

In this section, we study the rigid model in the case where noise is neglected. This amounts to take $\alpha = 0$ in the model (4.1). In this case, in the frame of reference of the cell, the rigid model is written:

$$\begin{cases} \partial_t c = \operatorname{div}\left(\nabla c + a\mathbf{u}c\right) & \text{in } \Omega \setminus N, & \text{(4.3a)} \\ \left(\nabla c + a\mathbf{u}c\right) \cdot \mathbf{n} = 0 & \text{on } \partial\left(\Omega \setminus N\right), & \text{(4.3b)} \\ \mathbf{u}\left(t\right) = \dfrac{-\chi_c}{A_\Omega} \displaystyle\int_{\partial\Omega} f_{\text{act}}\left(c\right) \mathbf{n} \, \mathrm{d}\sigma, & & \text{(4.3c)} \end{cases}$$

with $\Omega = B(0, R_0)$ and $N = B\left(0, R_{\text{nucl}}\right)$. First we study the stationary states of the model and their linear stability. Then we show the existence of travelling waves.

4.2.1 . Stationary state

4.2.1.1 . Stationary state and linear stability

Proposition 4.2.1. *The model* (4.3) *admits an unique stationary state given by:*

$$\begin{cases} c^0\left(\mathbf{x}\right) = \dfrac{M}{|\Omega \setminus N|} & \mathbf{x} \in \Omega \setminus N, & \text{(4.4a)} \\ \mathbf{u}^0 = 0. & & \text{(4.4b)} \end{cases}$$

Proof. In the cell frame of reference, the stationary problem associated with the rigid model (4.3) is as follows:

$$\begin{cases} \Delta c = 0 & \text{in } \Omega \setminus N, \\ \nabla c \cdot \mathbf{n} = 0 & \text{on } \partial(\Omega \setminus N), \\ \mathbf{u} = 0. \end{cases}$$

Then we have:

$$\nabla c = 0 \qquad \text{in } \Omega \setminus N.$$

This leads to the conclusion that c is constant over $\Omega \setminus N$ and so, using the constraint on the total quantity of markers eq. (4.2), $\int_{\Omega \setminus N} c(\mathbf{x})\, \mathrm{d}\mathbf{x} = M$, we deduce the result. □

The following theorem gives a criterion for the stability of the stationary state (4.4). We introduce the following notation:

$$\chi_c^* = \frac{1}{a c^0 f'_{\mathrm{act}}(c^0)}. \tag{4.5}$$

Theorem 4.2.2. *If $\chi_c < \chi_c^*$, then the stationary state (4.4) is linearly stable. On the opposite, if $\chi_c > \chi_c^*$, then the stationary state (4.4) is linearly unstable.*

4.2.1.2 . Proof of theorem 4.2.2

The theorem is proved in three steps. The first consists of calculating the linearised problem of problem (4.3) around the stationary state (4.4) and deducing an eigenvalue problem. The stationary state will then be stable if and only if all the eigenvalues of the eigenvalue problem have a negative real part. The second step consists to establish that the eigenvalue problem admits a positive real part eigenvalue, is equivalent to the fact that a simpler problem admits a real part eigenvalue. This step is based on the radially symmetric nature of the problem and Fourier analysis. The third step consists in studying this simpler problem. We can then exhibit a positive real part eigenvalue of it when $\chi_c > \chi_c^*$. Also, using a graphical argument, it consists in illustrating that if $\chi_c < \chi_c^*$ then the eigenvalues of this problem have a negative real part. The arguments used are inspired by those of Lavi et al. (2020); Alazard et al. (2022).

Step 1. The following lemma gives the expression for the linearised problem around the stationaty state (4.4).

Lemma 4.2.3. *The linearised problem associated to eq. (4.3) around the stationary state (4.4) is given by:*

$$\begin{cases} \partial_t \tilde{c} = \Delta \tilde{c} & \text{in } \Omega \setminus N, \quad (4.6a) \\ \left(\nabla \tilde{c} + a \tilde{\mathbf{u}} c^0\right) \cdot \mathbf{n} = 0 & \text{on } \partial(\Omega \setminus N), \quad (4.6b) \\ \tilde{\mathbf{u}}(t) = \dfrac{-\chi_c f'_{\mathrm{act}}\left(c^0\right)}{A_\Omega} \displaystyle\int_{\partial\Omega} \tilde{c}(t, \mathbf{x})\, \mathbf{n}\, \mathrm{d}\sigma. & (4.6c) \end{cases}$$

Proof. We perform a formal expansion of the solution $(c, \mathbf{u})$ of eq. (4.3) around the stationary state $\left(c^0, \mathbf{u}^0\right)$. Let $\varepsilon > 0$ small. For all $t \geq 0$ and $\mathbf{x} \in \Omega \setminus N$, we set:

$$c(t, \mathbf{x}) = c^0 + \varepsilon \tilde{c}(t, \mathbf{x}) + \mathcal{O}\left(\varepsilon^2\right),$$

and

$$\mathbf{u}(t) = \mathbf{u}^0 + \varepsilon\tilde{\mathbf{u}}(t) + \mathcal{O}\left(\varepsilon^2\right).$$

Using the fact that c^0 satisfies eq. (4.4a) and c satisfies (4.3), we deduce that in $\Omega \setminus N$:

$$\partial_t \tilde{c} = \Delta \tilde{c}.$$

We also have on $\partial(\Omega \setminus N)$ that:

$$\begin{aligned}(\nabla c + a\mathbf{u}c)\cdot\mathbf{n} &= \left(\nabla c^0 + \varepsilon\nabla\tilde{c} + a\mathbf{u}^0c^0 + \varepsilon a\mathbf{u}^0\tilde{c} + \varepsilon a\tilde{\mathbf{u}}c^0\right)\cdot\mathbf{n} + \mathcal{O}\left(\varepsilon^2\right)\\ &= \varepsilon\left(\nabla\tilde{c} + a\tilde{\mathbf{u}}c^0\right)\cdot\mathbf{n} + \mathcal{O}\left(\varepsilon^2\right),\end{aligned}$$

which leads to:

$$\left(\nabla\tilde{c} + a\tilde{\mathbf{u}}c^0\right)\cdot\mathbf{n} = 0 \qquad \text{on } \partial(\Omega\setminus N).$$

We also have:

$$\begin{aligned}\mathbf{u}(t) &= \frac{-\chi_c}{A_\Omega}\int_{\partial\Omega} f_{\text{act}}\left(c^0 + \varepsilon\tilde{c} + \mathcal{O}\left(\varepsilon^2\right)\right)\mathbf{n}\,\mathrm{d}\sigma\\ &= \frac{-\chi_c}{A_\Omega}\int_{\partial\Omega}\left(f_{\text{act}}\left(c^0\right) + \varepsilon\tilde{c}f'_{\text{act}}\left(c^0\right) + \mathcal{O}\left(\varepsilon^2\right)\right)\mathbf{n}\,\mathrm{d}\sigma\\ &= \mathbf{u}^0 + \varepsilon\frac{-\chi_c f'_{\text{act}}\left(c^0\right)}{A_\Omega}\int_{\partial\Omega}\tilde{c}\mathbf{n}\,\mathrm{d}\sigma + \mathcal{O}\left(\varepsilon^2\right),\end{aligned}$$

which leads to:

$$\tilde{\mathbf{u}}(t) = \frac{-\chi_c f'_{\text{act}}\left(c^0\right)}{A_\Omega}\int_{\partial\Omega}\tilde{c}\mathbf{n}\,\mathrm{d}\sigma.$$

□

The eigenvalue problem associated with eq. (4.6) is given by:

$$\begin{cases}\lambda\tilde{c} = \Delta\tilde{c} & \text{in } \Omega\setminus N, & \text{(4.7a)}\\ \left(\nabla\tilde{c} + a\tilde{\mathbf{u}}c^0\right)\cdot\mathbf{n} = 0 & \text{on } \partial(\Omega\setminus N), & \text{(4.7b)}\\ \tilde{\mathbf{u}}(t) = \dfrac{-\chi_c f'_{\text{act}}\left(c^0\right)}{A_\Omega}\displaystyle\int_{\partial\Omega}\tilde{c}(t,\mathbf{x})\,\mathbf{n}\,\mathrm{d}\sigma, & & \text{(4.7c)}\end{cases}$$

where $\lambda \in \mathbb{C}$.

Step 2. Using Fourier analysis and the radially symmetric nature of the problem (4.7), we prove the following lemma, which reduces the spectral study of eq. (4.7) to that of a simpler eigenvalue problem.

Lemma 4.2.4. *The problem (4.7) admits an eigenvalue with a positive real part is and only if the following problem admits one.*

$$\begin{cases}\lambda c = \left(\partial^2_{rr} + \dfrac{1}{r}\partial_r - \dfrac{1}{r^2}\right)c & r\in(R_{\text{nucl}}, R_0), & \text{(4.8a)}\\ \partial_r c(R_0) = \dfrac{a\chi_c c^0 f'_{\text{act}}\left(c^0\right)}{R_0}c(R_0), & & \text{(4.8b)}\\ \partial_r c(R_{\text{nucl}}) = \dfrac{a\chi_c c^0 f'_{\text{act}}\left(c^0\right)}{R_0}c(R_0). & & \text{(4.8c)}\end{cases}$$

Proof. Since the problem (4.7) is radially symmetric, we can use the Fourier analysis. Let $\lambda \in \mathbb{C}$ and let $(\tilde{c}, \tilde{\mathbf{u}})$ be an eigenfunction associated with λ. In polar coordinates, for all $r \in (R_{\mathrm{nucl}}, R_0)$ and $\theta \in (-\pi, \pi]$, we set:

$$\tilde{c}(r,\theta) = \sum_{m\in\mathbb{N}} c_{cm}(r)\cos(m\theta) + \sum_{m\in\mathbb{N}} c_{sm}(r)\sin(m\theta).$$

For all $m \in \mathbb{N}$ with $m \neq 1$, we have:

$$\int_{-\pi}^{\pi} \cos(m\theta)\cos(\theta) = \int_{-\pi}^{\pi} \sin(m\theta)\sin(\theta) = 0$$

and

$$\int_{-\pi}^{\pi} \cos(m\theta)\sin(\theta) = \int_{-\pi}^{\pi} \sin(m\theta)\cos(\theta) = 0.$$

We also have:

$$\int_{-\pi}^{\pi} \cos^2(\theta) = \int_{-\pi}^{\pi} \sin^2(\theta) = \pi$$

and

$$\int_{-\pi}^{\pi} \cos(\theta)\sin(\theta) = 0.$$

Thus we have:

$$\int_{\partial\Omega} \tilde{c}\mathbf{n}\,\mathrm{d}\sigma = \pi R_0 \begin{pmatrix} c_{c1}(R_0) \\ c_{s1}(R_0) \end{pmatrix},$$

which leads to:

$$\tilde{\mathbf{u}} = \frac{-\chi_c f'_{\mathrm{act}}(c^0)}{R_0} \begin{pmatrix} c_{c1}(R_0) \\ c_{s1}(R_0) \end{pmatrix}.$$

By linearity of eq. (4.7) and independence of the cosine and sine modes, we deduce that for all $m \neq 1$, c_{cm} and c_{sm} satisfy:

$$\begin{cases} \lambda c_m = \left(\partial^2_{rr} + \dfrac{1}{r}\partial_r - \dfrac{m^2}{r^2}\right) c_m & r \in (R_{\mathrm{nucl}}, R_0), \quad (4.9a) \\ \partial_r c(R_0) = 0, & (4.9b) \\ \partial_r c(R_{\mathrm{nucl}}) = 0. & (4.9c) \end{cases}$$

Similarly when $m = 1$, using the expression of the cell velocity, the functions c_{c1} and c_{s1} satisfy:

$$\begin{cases} \lambda c = \left(\partial^2_{rr} + \dfrac{1}{r}\partial_r - \dfrac{1}{r^2}\right) c & r \in (R_{\mathrm{nucl}}, R_0), \quad (4.10a) \\ \partial_r c(R_0) = \dfrac{a\chi_c c^0 f'_{\mathrm{act}}(c^0)}{R_0} c(R_0), & (4.10b) \\ \partial_r c(R_{\mathrm{nucl}}) = \dfrac{a\chi_c c^0 f'_{\mathrm{act}}(c^0)}{R_0} c(R_0). & (4.10c) \end{cases}$$

From the independence of the cosine and sine modes, we also deduce that studying the spectrum of problem (4.7) is equivalent to study the spectrum of problem (4.9) for all $m \neq 1$ and (4.10).

As for $m \neq 1$ the functions $(r,\theta) \mapsto c_{cm}(r)\cos(m\theta)$ and $(r,\theta) \mapsto c_{sm}(r)\sin(m\theta)$ satisfy:

$$\begin{cases} \lambda c = \Delta c & \text{in } \Omega \setminus N, \\ \nabla c \cdot \mathbf{n} = 0 & \text{on } \partial\Omega \cup \partial N, \end{cases}$$

the eigenvalue problem associated with the heat equation, the problem (4.9) only admits eigenvalues with negative real part. □

Step 3. We study the spectrum of problem (4.8). The solutions of (4.8) are expressed using Bessel functions. We have:

$$c_1(r) = \beta_\lambda J_1\left(-\mathrm{i}\sqrt{\lambda}r\right) + \gamma_\lambda Y_1\left(-\mathrm{i}\sqrt{\lambda}r\right),$$

where J_1 and Y_1 denote respectively the Bessel function of the first kind of order 1 and that of the second kind of order 1, $\lambda \in \mathbb{C}$ is an eigenvalue of the problem and $\beta_\lambda, \gamma_\lambda \in \mathbb{C}$. From eqs. (4.8b) and (4.8c), we deduce that:

$$\begin{aligned}-\mathrm{i}\sqrt{\lambda}\left(\beta_\lambda J_1'\left(-\mathrm{i}\sqrt{\lambda}R_0\right) + \gamma_\lambda Y_1'\left(-\mathrm{i}\sqrt{\lambda}R_0\right)\right)& \\ = \frac{a\chi_c c^0 f'_{\mathrm{act}}\left(c^0\right)}{R_0}\left(\beta_\lambda J_1\left(-\mathrm{i}\sqrt{\lambda}R_0\right) + \gamma_\lambda Y_1\left(-\mathrm{i}\sqrt{\lambda}R_0\right)\right)&\end{aligned}$$

and

$$\begin{aligned}-\mathrm{i}\sqrt{\lambda}\left(\beta_\lambda J_1'\left(-\mathrm{i}\sqrt{\lambda}R_{\mathrm{nucl}}\right) + \gamma_\lambda Y_1'\left(-\mathrm{i}\sqrt{\lambda}R_{\mathrm{nucl}}\right)\right)& \\ = \frac{a\chi_c c^0 f'_{\mathrm{act}}\left(c^0\right)}{R_0}\left(\beta_\lambda J_1\left(-\mathrm{i}\sqrt{\lambda}R_0\right) + \gamma_\lambda Y_1\left(-\mathrm{i}\sqrt{\lambda}R_0\right)\right).&\end{aligned}$$

Thus we have that λ satisfies the following eigenvalue equation:

$$\begin{aligned}G_1(\lambda) = \lambda&\left(J_1'\left(-\mathrm{i}\sqrt{\lambda}R_0\right)Y_1'\left(-\mathrm{i}\sqrt{\lambda}R_{\mathrm{nucl}}\right) - J_1'\left(-\mathrm{i}\sqrt{\lambda}R_{\mathrm{nucl}}\right)Y_1'\left(-\mathrm{i}\sqrt{\lambda}R_0\right)\right)\\ &+ \frac{\mathrm{i}\sqrt{\lambda}a\chi_c c^0 f'_{\mathrm{act}}\left(c^0\right)}{R_0}\Big[J_1\left(-\mathrm{i}\sqrt{\lambda}R_0\right)Y_1'\left(-\mathrm{i}\sqrt{\lambda}R_0\right) - J_1'\left(-\mathrm{i}\sqrt{\lambda}R_0\right)Y_1\left(-\mathrm{i}\sqrt{\lambda}R_0\right)\\ &\quad + J_1'\left(-\mathrm{i}\sqrt{\lambda}R_{\mathrm{nucl}}\right)Y_1\left(-\mathrm{i}\sqrt{\lambda}R_0\right) - J_1\left(-\mathrm{i}\sqrt{\lambda}R_0\right)Y_1'\left(-\mathrm{i}\sqrt{\lambda}R_{\mathrm{nucl}}\right)\Big] = 0.\end{aligned}$$

Using the properties of the Bessel functions, for λ close to zero, we have:

$$\begin{aligned}J_1\left(-\mathrm{i}\sqrt{\lambda}R_0\right) &= \frac{-\mathrm{i}\sqrt{\lambda}R_0}{2} + o(\lambda),\\ J_1'\left(-\mathrm{i}\sqrt{\lambda}R_0\right) &= \frac{1}{2} + \frac{3R_0^2\lambda}{16} + o(\lambda),\\ Y_1\left(-\mathrm{i}\sqrt{\lambda}R_0\right) &= \frac{-2\mathrm{i}}{\pi\sqrt{\lambda}R_0} + \frac{\mathrm{i}(1-2\gamma)\sqrt{\lambda}R_0}{2\pi} + \frac{2}{\pi}J_1\left(-\mathrm{i}\sqrt{\lambda}R_0\right)\log\left(\frac{-\mathrm{i}\sqrt{\lambda}R_0}{2}\right) + o(\lambda),\\ Y_1'\left(-\mathrm{i}\sqrt{\lambda}R_0\right) &= \frac{-2}{\lambda R_0^2\pi} + \frac{1+2\gamma}{2\pi} - \frac{R_0^2\lambda(11-12\gamma)}{32\pi} + \frac{2}{\pi}J_1'\left(-\mathrm{i}\sqrt{\lambda}R_0\right)\log\left(\frac{-\mathrm{i}\sqrt{\lambda}R_0}{2}\right) + o(\lambda),\end{aligned}$$

where γ denotes the Euler's constant. Thus for λ close to zero, we have:

$$\begin{aligned}G_1(\lambda) &= \left(1 - a\chi_c c^0 f'_{\mathrm{act}}\left(c^0\right)\right)\left(\frac{1}{R_0^2\pi} - \frac{1}{R_{\mathrm{nucl}}^2\pi}\right)\\ &\quad + \frac{3\left(R_{\mathrm{nucl}}^4 - R_0^4\right)}{8\pi R_0^2 R_{\mathrm{nucl}}^2}\lambda - a\chi_c c^0 f'_{\mathrm{act}}\left(c^0\right)\frac{3\left(R_0^2 - R_{\mathrm{nucl}}^2\right)}{8\pi R_0^2}\lambda\\ &\quad + \frac{a\chi_c c^0 f'_{\mathrm{act}}\left(c^0\right) - 1}{2\pi}\ln\left(\frac{R_0}{R_{\mathrm{nucl}}}\right)\lambda + o(\lambda),\\ &= g(\lambda) + o(\lambda).\end{aligned}$$

The function g admits $\lambda_1 \in \mathbb{R}$ as root with λ_1 defined by:

$$\lambda_1 = -\frac{\left(1 - a\chi_c c^0 f'_{\text{act}}\left(c^0\right)\right)\left(\frac{1}{R_0^2\pi} - \frac{1}{R_{\text{nucl}}^2\pi}\right)}{\frac{3\left(R_{\text{nucl}}^4 - R_0^4\right)}{8\pi R_0^2 R_{\text{nucl}}^2} - a\chi_c c^0 f'_{\text{act}}\left(c^0\right)\frac{3\left(R_0^2 - R_{\text{nucl}}^2\right)}{8\pi R_0^2} + \frac{a\chi_c c^0 f'_{\text{act}}(c^0) - 1}{2\pi}\ln\left(\frac{R_0}{R_{\text{nucl}}}\right)}.$$

We have:

$$\left(1 - a\chi_c c^0 f'_{\text{act}}\left(c^0\right)\right)\left(\frac{1}{R_0^2\pi} - \frac{1}{R_{\text{nucl}}^2\pi}\right) > 0 \iff a\chi_c c^0 f'_{\text{act}}\left(c^0\right) > 1.$$

We also have:

$$\begin{aligned}
&\frac{3\left(R_{\text{nucl}}^4 - R_0^4\right)}{8\pi R_0^2 R_{\text{nucl}}^2} - a\chi_c c^0 f'_{\text{act}}\left(c^0\right)\frac{3\left(R_0^2 - R_{\text{nucl}}^2\right)}{8\pi R_0^2} + \frac{a\chi_c c^0 f'_{\text{act}}\left(c^0\right) - 1}{2\pi}\ln\left(\frac{R_0}{R_{\text{nucl}}}\right) < 0 \\
\iff &\left[a\chi_c c^0 f'_{\text{act}}\left(c^0\right) < \frac{3\left(R_0^4 - R_{\text{nucl}}^4\right) + 4R_0^2 R_{\text{nucl}}^2 \ln\left(\frac{R_0}{R_{\text{nucl}}}\right)}{R_{\text{nucl}}^2\left(3\left(R_{\text{nucl}}^2 - R_0^2\right) + 4R_0^2\ln\left(\frac{R_0}{R_{\text{nucl}}}\right)\right)}\right. \\
&\quad \left.\text{and } 3\left(R_{\text{nucl}}^2 - R_0^2\right) + 4R_0^2\ln\left(\frac{R_0}{R_{\text{nucl}}}\right) > 0\right] \text{ or } 3\left(R_{\text{nucl}}^2 - R_0^2\right) + 4R_0^2\ln\left(\frac{R_0}{R_{\text{nucl}}}\right) < 0.
\end{aligned}$$

Moreover, if $3\left(R_{\text{nucl}}^2 - R_0^2\right) + 4R_0^2\ln\left(\frac{R_0}{R_{\text{nucl}}}\right) > 0$ then $\frac{3\left(R_0^4 - R_{\text{nucl}}^4\right) + 4R_0^2 R_{\text{nucl}}^2\ln\left(\frac{R_0}{R_{\text{nucl}}}\right)}{R_{\text{nucl}}^2\left(3\left(R_{\text{nucl}}^2 - R_0^2\right) + 4R_0^2\ln\left(\frac{R_0}{R_{\text{nucl}}}\right)\right)} > 1$. Thus λ_1 changes sign from negative to positive as χ_c exceeds χ_c^*. We can note that λ_1 approximates well a root of G_1 and that we have:

$$\lambda_1 = \left(a\chi_c c^0 f'_{\text{act}}\left(c^0\right) - 1\right)\frac{8\left(R_0^2 - R_{\text{nucl}}^2\right)}{3a\chi_c c^0 f'_{\text{act}}\left(c^0\right)\left(R_0^4 + R_0^2 R_{\text{nucl}}^2 - 2R_{\text{nucl}}^4\right)} + o\left(\left|a\chi_c c^0 f'_{\text{act}}\left(c^0\right) - 1\right|\right).$$

This eigenvalue is associated with a non-trivial eigenfunction:

$$c\left(r\right) = \beta_{\lambda_1} J_1\left(-\mathrm{i}\lambda_1^{\frac{1}{2}} r\right) + \gamma_{\lambda_1} Y_1\left(-\mathrm{i}\lambda_1^{\frac{1}{2}} r\right),$$

with

$$\beta_{\lambda_1} = \mathrm{i}\lambda_1^{\frac{1}{2}} Y_1'\left(-\mathrm{i}\lambda_1^{\frac{1}{2}} R_0\right) + \frac{\chi_c}{\chi_c^*} Y_1\left(-\mathrm{i}\lambda_1^{\frac{1}{2}} R_0\right),$$

and

$$\gamma_{\lambda_1} = -\left(\mathrm{i}\lambda_1^{\frac{1}{2}} J_1'\left(-\mathrm{i}\lambda_1^{\frac{1}{2}} R_0\right) + \frac{\chi_c}{\chi_c^*} J_1\left(-\mathrm{i}\lambda_1^{\frac{1}{2}} R_0\right)\right).$$

To conclude the proof of the theorem, we need to show that when $\chi_c < \chi_c^*$ all the eigenvalues associated to (4.8) have negative real part. We give only a graphical illustration here. For several values of R_0, R_{nucl} and $\frac{\chi_c}{\chi_c^*}$, we represent the function G_1 by representing its real part, its imaginary part and its modulus (see fig. 4.2 for an example). We then observe that the root of G_1 with the largest real part seems to be a real root of G_1, which is confirmed by studying the imaginary part of G_1. Indeed, we notice that if $\lambda \in \mathbb{R}$ then $G_1\left(\lambda\right) \in \mathbb{R}$.

We can therefore restrict the graphical study of G_1 to the graphical study of G_1 when $\lambda \in \mathbb{R}$. For R_0 and R_{nucl} fixed and for different values of $\frac{\chi_c}{\chi_c^*}$, we plot G_1 as a function of $\lambda \in \mathbb{R}$ (see fig. 4.3). This allows us to observe the largest real root of G_1 and we notice that when $\chi_c < \chi_c^*$ then this one is negative.

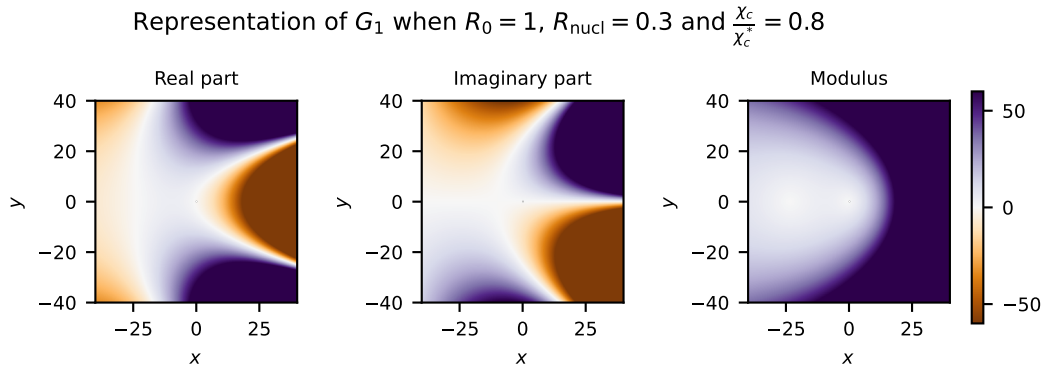

Figure 4.2: **Representation of G_1 in the complex framework for $R_0 = 1$, $R_{\text{nucl}} = 0.3$ and $\frac{\chi_c}{\chi_c^*} = 0.8$.** *Plots of the real part (left), the imaginary part (middle) and the modulus (right) of the function G_1 for $\lambda = x + \mathrm{i}y \in \mathbb{C}$ with $x, y \in [-40, 40]$. We observe that the root of G_1 with the greatest real part is a real root.*

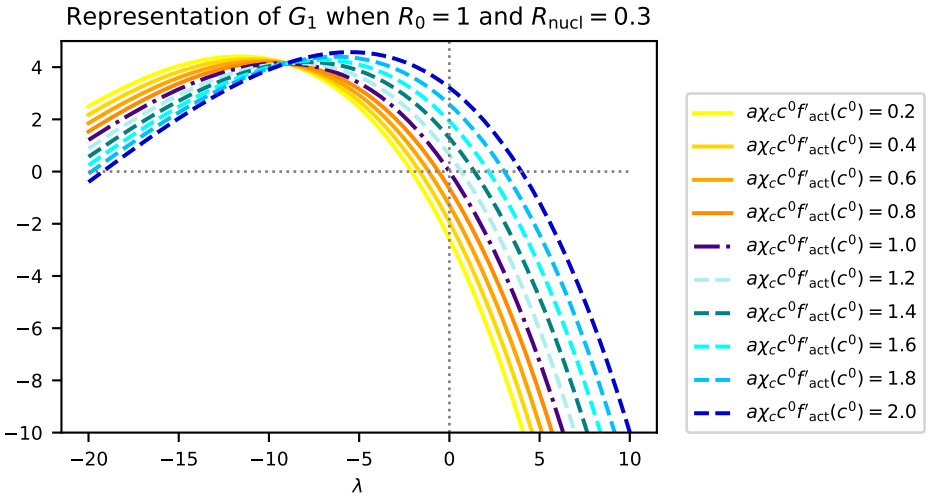

Figure 4.3: **Graphs of $\lambda \mapsto G_1(\lambda)$ for $\lambda \in \mathbb{R}$ when $R_0 = 1$ and $R_{\text{nucl}} = 0.3$ for different values of $\frac{\chi_c}{\chi_c^*} = a\chi_c c^0 f'\left(c^0\right)$.** *Each curve corresponds to a different value of χ_c. The solid yellow-orange curves correspond to the case where $\chi_c < \chi_c^*$, the dashed blue curves correspond to the case where $\chi_c > \chi_c^*$ and the dark dashdotted curve corresponds to the case where $\chi_c = 1\chi_c^*$. The grey dotted lines are the lines of equation $\lambda = 0$ and $y = 0$. In the case where $\chi_c < \chi_c^*$ we notice that G_1 seems to admit no positive root.*

4.2.2 . Travelling waves

Travelling waves correspond to the cell moving by translation with a constant velocity in a given direction. Without loss of generality, we can assume that the velocity of a travelling wave is given by $\mathbf{u}_{\mathrm{tw}} = (V, 0)$ with $V > 0$. In the substrate frame of reference, using the travelling wave ansatz :

$$c\left(t, (x, y)\right) = c\left(x - Vt, y\right),$$

we have that, in the cell frame of reference, a travelling wave solution of eq. (4.3) is solution of the following problem:

$$\begin{cases} \operatorname{div}\left(\nabla c + a\left(V, 0\right) c\right) = 0 & \text{in } \Omega \setminus N, \quad (4.11a) \\ \left(\nabla c + a\left(V, 0\right) c\right) \cdot \mathbf{n} = 0 & \text{on } \partial\left(\Omega \setminus N\right), \quad (4.11b) \\ V = \dfrac{-\chi_c}{A_\Omega} \displaystyle\int_{\partial\Omega} f_{\mathrm{act}}\left(c\right) n_x. & (4.11c) \end{cases}$$

Proposition 4.2.5. *If c is a solution of eq. (4.11), then c is of the form:*

$$c\left(x, y\right) = \frac{M}{\int_{\Omega \setminus N} e^{-aVx'} \,\mathrm{d}x' \,\mathrm{d}y'} e^{-aVx},$$

with $(x, y) \in \Omega \setminus N$.

Proof. Any non-negative solution of eqs. (4.11a) and (4.11b) is given by:

$$\tilde{c}\left(x, y\right) = c_1 e^{-aVx}, \qquad (x, y) \in \Omega \setminus N,$$

with $c_1 > 0$. Indeed, as for all $(x, y) \in \Omega \setminus N$, $\nabla \tilde{c}\left(x, y\right) = -a\left(V, 0\right) \tilde{c}\left(x, y\right)$, then $\tilde{c}$ is a solution of eqs. (4.11a) and (4.11b). Moreover, if we assume that for all $(x, y) \in \Omega \setminus N$ we have $\tilde{c} = c_1\left(x, y\right) e^{-aVx}$ then, multiplying eq. (4.11a) by $c_1\left(x, y\right)$ and integrating by parts, we have:

$$\int_{\Omega \setminus N} \nabla c_1\left(x, y\right) \cdot \left(\nabla c\left(x, y\right) + a\left(V, 0\right) c\left(x, y\right)\right) \,\mathrm{d}x \,\mathrm{d}y = 0,$$

and it follows that:

$$\int_{\Omega \setminus N} \left|\nabla c_1\left(x, y\right)\right|^2 e^{-aVx} \,\mathrm{d}x \,\mathrm{d}y = 0.$$

Then, necessarily, we have for all $(x, y) \in \Omega \setminus N$ that:

$$\nabla c_1\left(x, y\right) = 0.$$

Finally, using the condition on the total number of markers, we have that:

$$c_1 = \frac{M}{\int_{\Omega \setminus N} e^{-aVx'} \,\mathrm{d}x' \,\mathrm{d}y'}.$$

□

4.3 . Finite element scheme of the model

In this section we write a finite element scheme to run simulations of the rigid model eq. (4.1). This scheme is obtained after an implicit time discretization and a finite element discretization in space.

4.3.1 . Time discretization

We discretize in time our model eq. (4.1). Let Δt be the time step. For $i \in \{0, \dots, N_f\}$ with $N_f \in \mathbb{N}$, we denote $t^i = i\Delta t$, $\mathbf{u}^i = \mathbf{u}\left(t^i\right)$ and $c^i = c\left(t^i, \cdot\right)$. We also denote $\mathbf{x}^i_{\text{nucl}} = \mathbf{x}_{\text{nucl}}\left(t^i\right)$ and $\mathbf{x}^i_{\text{cell}} = \mathbf{x}_{\text{cell}}\left(t^i\right)$. Moreover, we denote by $\dot{W}^{Q,i}$ an approximation of the coloured noise at time t^i.

The implicit discretization of the problem is given by:

$$\begin{cases} \dfrac{c^{i+1} - c^i}{\Delta t} = \operatorname{div}\left(\nabla c^{i+1} + a\mathbf{u}^{i+1}c^{i+1} - \alpha\dot{W}^{Q,i+1}c^{i+1}\right) & \text{in } \Omega \setminus N, \quad (4.12a) \\ \left(\nabla c^{i+1} + a\mathbf{u}^{i+1}c^{i+1} - \alpha\dot{W}^{Q,i+1}c^{i+1}\right) \cdot \mathbf{n} = 0 & \text{on } \partial\Omega \cup \partial N, \quad (4.12b) \\ \mathbf{u}^i = \dfrac{-\chi_c}{A_\Omega} \displaystyle\int_{\partial\Omega} f_{\text{act}}\left(c^i\right)\mathbf{n}\,\mathrm{d}\sigma. & (4.12c) \end{cases}$$

with

$$\begin{cases} \mathbf{x}^{i+1}_{\text{cell}} = \mathbf{x}^i_{\text{cell}} + \Delta t\,\mathbf{u}^i, & (4.13a) \\ \mathbf{x}^{i+1}_{\text{nucl}} = \mathbf{x}^i_{\text{nucl}} + \Delta t\,\mathbf{u}^i. & (4.13b) \end{cases}$$

4.3.2 . Spatial discretization

We discretize in space our time-discrete model eqs. (4.12) and (4.13). We use a finite element discretization. Let $\mathcal{T}$ be a triangulation of $\Omega \setminus N$. For all triangle $K \in \mathcal{T}$ we note $\left(\lambda_1^K, \lambda_2^K, \lambda_3^K\right)$ the barycentric coordinate functions of K. First we define the functional spaces needed. Let $\mathbb{P}_k$ be the set of polynomials of $\mathbb{R}^2$ of degrees less or equal k. Let $\mathcal{H}_c$ be the functional space define by:

$$\mathcal{H}_c = \left\{\psi \in H^1\left(\Omega \setminus N\right) \mid \forall K \in \mathcal{T}, \psi|_K \in \mathbb{P}_1 \oplus \operatorname{Span}\left\{\lambda_1^K, \lambda_2^K, \lambda_3^K\right\}\right\}.$$

4.3.3 . Discretization of the noise

To discretize the coloured noise, we use the one done by Boulakia et al. (2015). We recall that $\dot{W}^{Q,i}$ denotes an approximation of the coloured noise at time t^i, $i \in \{1, \dots, N_f\}$. We set:

$$\dot{W}^{Q,i} = \frac{W^Q_{t^i} - W^Q_{t^{i-1}}}{\Delta t}.$$

From the definition of W^Q_t, we know that $\dot{W}^{Q,i}$ is equal in law to $\dfrac{1}{\sqrt{\Delta t}} W^Q_1$ and that the $\left\{\dot{W}^{Q,i}\right\}_{1 \le i \le N_f}$ are independent.

From Boulakia et al. (2015), a way to approximate the noise and to compute $W^{Q,i}_1 = \left(\omega^i_1, \omega^i_2\right)$ relies on the computation of a covariance matrix. Indeed, let $\{P_j, 1 \le j \le N_h\}$ be the set of all the nodes of the triangulation $\mathcal{T}$, where N_h is the number of nodes of the triangulation, and $\{\psi_j, 1 \le j \le N_h\}$ be a basis of the Lagrangian $P1$ finite element. ψ_j is a continuous affine function on $\Omega \setminus N$ such that for all $1 \le j, k \le N_h$, we have $\psi_j\left(P_k\right) = \delta_{jk}$. For $m \in \{1, 2\}$, the $P1$ discretization of ω^i_m is given by

$$\omega^i_m = \sum_{j=1}^{N_h} x^i_j \psi_j.$$

with $\left\{x_j^i, 1 \leq j \leq N_h\right\}$ a realisation of a centred Gaussian vector of covariance matrix Σ. We have $\Sigma = \left(q\left(P_j, P_k\right)\right)_{1 \leq j,k \leq N_h}$. Let X be a centred Gaussian vector of covariance matrix Σ. We have

$$X = SY,$$

with Y a Gaussian vector such that for all $1 \leq j \leq N_h$, $Y_j \sim \mathcal{N}(0,1)$ and S such that $\Sigma = SS^T$. Thus to compute $W_1^{Q,i}$, we just have to simulate a realization of a standard Gaussian vector and to compute the Cholesky decomposition S of the covariance matrix Σ.

4.3.4 . Variational formulation of the discrete problem on the concentration

The variational formulation of eq. (4.12) is given by:

$$\begin{cases} \text{Find } c^{i+1} \in \mathcal{H}_c \text{ such that for all } \psi \in \mathcal{H}_c, \text{ we have:} \\ \displaystyle\int_{\Omega \setminus N} \left(\frac{c^{i+1} - c^i}{\Delta t}\right) \psi \, \mathrm{d}\mathbf{x} \\ \qquad \displaystyle + \int_{\Omega \setminus N} \left(\left(a\mathbf{u}^{i+1} - \frac{\alpha}{\sqrt{\Delta t}} \dot{W}_1^{Q,i+1}\right) c^{i+1} + \nabla c^{i+1}\right) \cdot \nabla \psi \, \mathrm{d}\mathbf{x} = 0, \end{cases} \tag{4.14}$$

where $\left(W_1^{Q,i}\right)_{1 \leq i \leq N_f}$ is a sequence of independent Q-Wiener processes evaluated at time 1.

4.3.5 . Numerical scheme

After initialization with c^{in} given, a time iteration of the numerical scheme to simulate the problem (4.1) is given by the following algorithm:

Algorithm 4.1 : Numerical scheme to simulate the model eq. (4.1) obtained after time discretization and space discretization with a finite element method.

1. Initialisation: $c^0 = c^{\text{in}}$ the given initial condition and definition of the mesh.
2. Computation of S the Cholesky decomposition of the covariance matrix Σ.
3. Time iteration:
   (a) Compute $\mathbf{u}^{i+1} = \dfrac{-\chi_c}{A_\Omega} \int_{\partial\Omega} f_{\text{act}}\left(c^i\right) \mathbf{n} \, \mathrm{d}\sigma$.
   (b) Compute $\dot{W}_1^{Q,i+1} = SY$, where Y is a realisation of a standard normal gaussian vector.
   (c) Computation of the markers concentration c^{i+1} using $\mathbf{u}^{i+1}$ and $\dot{W}_1^{Q,i+1}$ by solving the variational formulation eq. (4.14).
   (d) Update of the domain:
   $$\mathbf{x}_{\text{cell}}^{i+1} = \mathbf{x}_{\text{cell}}^i + \Delta t \, \mathbf{u}^i,$$
   $$\mathbf{x}_{\text{nucl}}^{i+1} = \mathbf{x}_{\text{nucl}}^i + \Delta t \, \mathbf{u}^i.$$

4.4 . Numerical results

4.4.1 . Numerical verifications

In this section, we check that the numerical scheme proposed in algorithm 4.1 is consistent with the mathematical study of the model in the deterministic case $\alpha = 0$. We therefore check

that if $\alpha = 0$ then we recover numerically the stationary state (4.4) as well as the result on the stability of the latter stated in theorem 4.2.2.

First, we check that the numerical scheme captures the stationary state. We then set a time step Δt, then R_0 and R_{nucl} in order to define the geometry of the cell, and we choose as the initial condition for the markers concentration $c^{\text{in}}(\mathbf{x}) = \dfrac{M}{|\Omega \setminus N|}$.

In this case, we observe that whatever the values of R_0, R_{nucl} and χ_c, we find a stationary state (see fig. 4.4 for an example). Indeeed, we observe that the velocity of the cell remains zero over time. We also observe that the distribution of markers is well conserved over time. Moreover, we can observe that the quantity of markers is well conserved over time (see fig. 4.4 right), which is in agreement with eq. (4.2).

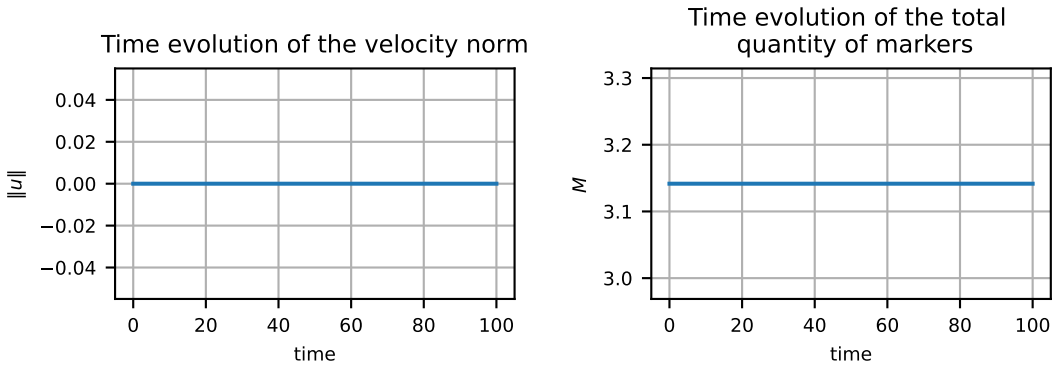

Figure 4.4: **Example of capturing the stationary state using the numerical scheme.** *The curve on the left represents the evolution of the velocity norm over time. We can observe that this remains zero throughout the study interval* $[0, 100]$*. The curve on the right represents the evolution of the total quantity of markers over time. We note that this remains constant over time.*
The results presented here are obtained with the parameters $\Delta t = 0.00005$, $R_0 = 1$, $R_{\text{nucl}} = 0.3$, $c^{\text{in}}(\mathbf{x}) = \frac{M}{|\Omega \setminus N|}$, $M = \pi$, $a = 1$, $\chi_c = 1.5$, $f_{\text{act}}(c) = \frac{c(1+c_s)^2}{c_s(c+c_s)}$ *with* $c_s = 0.5$ *and* $\alpha = 0$.

Secondly, we check that the numerical scheme gives results in accordance with theorem 4.2.2. We therefore study the linear stability of the stationary state numerically. To do this, we choose a perturbation of the stationary state as the initial condition and observe, depending on the value of χ_c, whether the system returns to the stationary state.

The chosen stationary state perturbation is given by:

$$c^{\text{in}}(\mathbf{x}) = K(1 + X(\mathbf{x}))\, \mathbb{1}_{1+X(\mathbf{x})>0} \tag{4.15}$$

where for all $\mathbf{x} \in \Omega \setminus N$ we have $X(\mathbf{x}) \sim \mathcal{N}(0, 1)$ and K such that $\int_{\Omega \setminus N} c^{\text{in}}(\mathbf{x})\, \mathrm{d}\mathbf{x} = M$.

As illustrated in fig. 4.5 for the case where $R_0 = 1$ and $R_{\text{nucl}} = 0.3$, we correctly find the criterion on the linear stablity of the stationary state. Indeed, when $\chi_c < \chi_c^*$, we have that the norm of the velocity decreases very quickly towards 0 then is constant equal to 0. This illustrates that when $\chi_c < \chi_c^*$ the stationary state is stable. Also, when $\chi_c > \chi_c^*$, we observe that the norm increases rapidly towards a strictly positive value and then becomes constant. This suggests that when $\chi_c > \chi_c^*$ there are stable travelling waves.

The trajectory study confirms that we are indeed capturing travelling waves (see fig. 4.6). Each cell maintains its orientation over time, which, coupled with the fact that the norm of

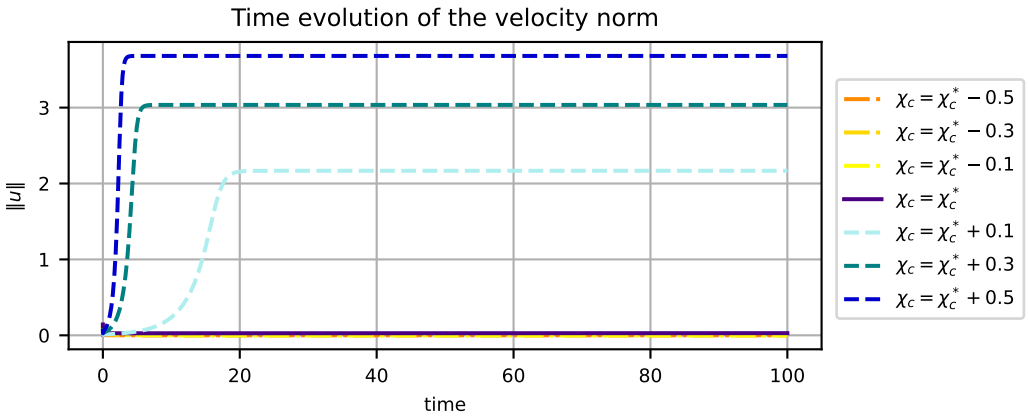

Figure 4.5: **Numerical illustration of theorem 4.2.2.** *Each curve represents the evolution of the norm of the velocity of a cell for different values of χ_c (see legend on the right). When $\chi_c < \chi_c^*$ the norm of the velocity decreases very rapidly towards 0 (dashdotted curves in overlapping shades of orange), whereas when $\chi_c > \chi_c^*$ it increases rapidly towards a non-zero value (dashed curves in shades of blue) . The critical case $\chi_c = \chi_c^*$ is also represented (dark curve), here the velocity is close to zero.*
The results presented here are obtained with the parameters $\Delta t = 0.005$, $R_0 = 1$, $R_{\text{nucl}} = 0.3$, $M = \pi$, $a = 1$, c^{in} given by eq. (4.15) and χ_c^* given by (4.5) and $f_{\text{act}}(c) = \frac{c(1+c_s)^2}{c_s(c+c_s)}$ with $c_s = 0.5$ and $\alpha = 0$.

the velocity is constant, leads to a progressive wave. The result is not surprising and is in agreement with Lavi et al. (2020) results in the case of a rigid cell.

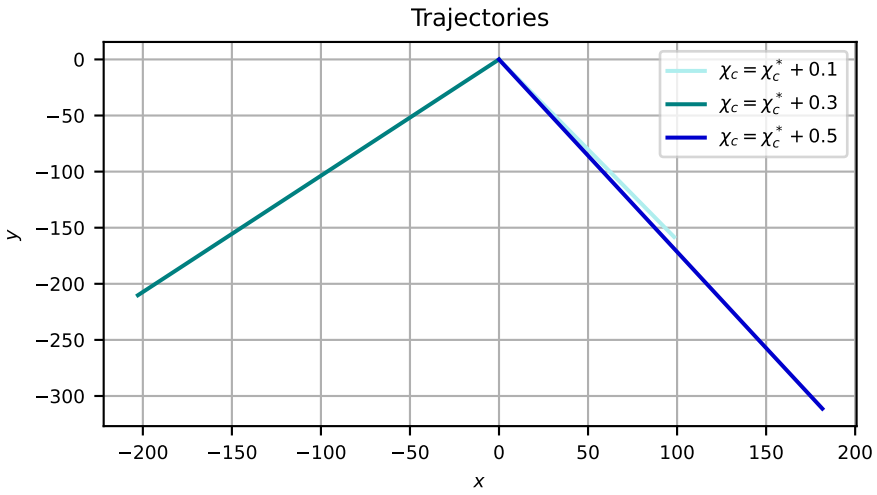

Figure 4.6: **Trajectories associated with the cells in fig. 4.5 in the case where $\chi_c > \chi_c^*$.** *Each curve represents the trajectory of one of the cells studied in fig. 4.5. Only those where $\chi_c > \chi_c^*$ are represented, keeping the same colour coding (see legend on the right). We can therefore see that here the cells do not change orientation over time.*
The results presented here are obtained with the parameters $\Delta t = 0.005$, $R_0 = 1$, $R_{\text{nucl}} = 0.3$, $M = \pi$, $a = 1$, c^{in} given by eq. (4.15), χ_c^* given by (4.5), $f_{\text{act}}(c) = \frac{c(1+c_s)^2}{c_s(c+c_s)}$ with $c_s = 0.5$ and $\alpha = 0$.

4.4.2 . Verification of agreement with the UCSP law and capture of the different types of trajectory

In this section, we illustrate that although the rigid crown model is only a toy model, it exhibits rich behaviour. Indeed, we illustrate that the trajectories obtained via algorithm 4.1 satisfy the UCSP law. Also, there exists a range of parameters in order to find the three types of trajectories: Brownian, intermittent and persistent.

By fixing all the model parameters and varying only χ_c, we observe Brownian trajectories when $\chi_c < \chi_c^*$, intermittent trajectories when $\chi_c = \chi_c^*$ and persistent trajectories when $\chi_c > \chi_c^*$.

In this section, for the numerical results presented, $R_0 = 1$, $R_{\text{nucl}} = 0.3$, $M = \pi$ and $a = 1$. As an initial condition c^{in} for the concentration of markers, we choose the function defined for all $\mathbf{x} \in \Omega \setminus N$ by $c^{\text{in}}(\mathbf{x}) = \dfrac{M}{|\Omega \setminus N|}$. The noise parameters are set to $\alpha = 0.3$ and $\zeta = 0.2$. Finally, the numerical simulations are performed over the time interval $[0, 15]$ with $\Delta t = 0.005$. Here are the results when $\chi_c = \chi_c^* - 0.3$, $\chi_c = \chi_c^*$ and $\chi_c = \chi_c^* + 0.5$ with χ_c^* defined in eq. (4.5).

4.4.2.1 . Illustration of the Brownian trajectories

In this subsection, we present the results when $\chi_c = \chi_c^* - 0.3$. We then observe that the trajectories are Brownian. This can be seen visually in fig. 4.7 and is confirmed by the study of the EASD and MSD, which are close to 1 (see fig. 4.9). In addition, we can see that the trajectories satisfy the UCSP (see fig. 4.8). We also observe that the cells have a low velocity: the mean norm is close to the intensity α of the noise (see fig. 4.10). These observations are in good agreement with those made about Brownian behaviour in Maiuri et al. (2015).

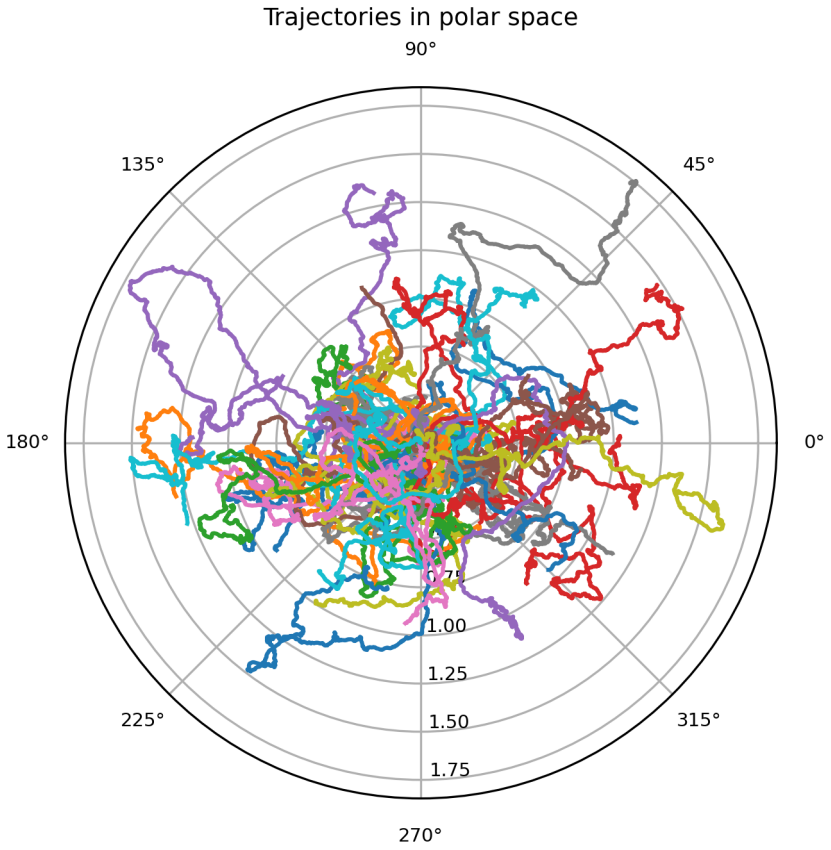

Figure 4.7: **Trajectories in polar coordinates in the case where $\chi_c < \chi_c^*$.** *Each curve represents, in polar coordinates, the trajectory of one cell simulated by algorithm 4.1 on the time interval $[0, 15]$. Visually, the trajectories seem to be Brownian. Fifty cells are represented.*
The results presented here are obtained with the parameters $\Delta t = 0.005$, $R_0 = 1$, $R_{\text{nucl}} = 0.3$, $M = \pi$, $a = 1$, $c^{\text{in}} = \dfrac{M}{|\Omega \setminus N|}$, $\chi_c = \chi_c^* - 0.3$ with χ_c^* given by (4.5), $f_{\text{act}}(c) = \frac{c(1+c_s)^2}{c_s(c+c_s)}$ with $c_s = 0.5$, $\alpha = 0.3$ and $\zeta = 0.2$.

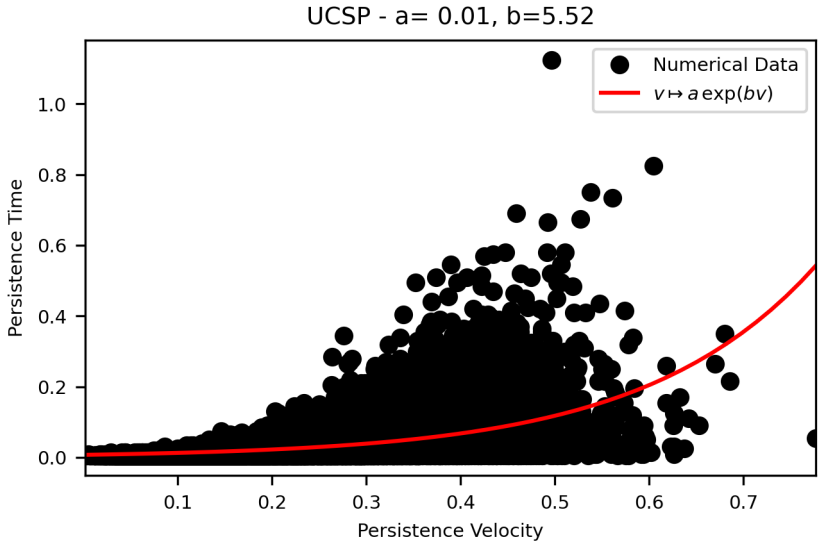

Figure 4.8: **Verification that the trajectories in fig. 4.7 satisfy the UCSP law (case when $\chi_c < \chi_c^*$).** *The persistence time of a locally persistent trajectory portion is plotted as a function of the persistence velocity. Each black dot corresponds to a datum. In red is plotted an interpolation of the points, of form $v \mapsto ae^{bv}$, which corresponds to the UCSP law. We can see that the data corresponds well to the interpolation and that the trajectories satisfy the UCSP law.*
The results presented here are obtained with the parameters $\Delta t = 0.005$, $R_0 = 1$, $R_{\text{nucl}} = 0.3$, $M = \pi$, $a = 1$, $c^{\text{in}} = \dfrac{M}{|\Omega \setminus N|}$, $\chi_c = \chi_c^* - 0.3$ with χ_c^* given by (4.5), $f_{\text{act}}(c) = \frac{c(1+c_s)^2}{c_s(c+c_s)}$ with $c_s = 0.5$, $\alpha = 0.3$ and $\zeta = 0.2$.

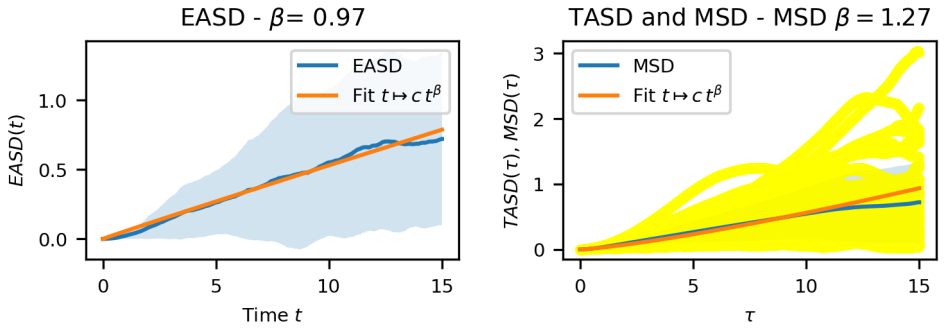

Figure 4.9: **Verification that the trajectories in fig. 4.7 are Brownian (case when $\chi_c < \chi_c^*$).** *On the left is shown in blue the EASD associated with the trajectories in fig. 4.7 and in orange the interpolation of the EASD, in the form $t \mapsto ct^\beta$. By the properties of the EASD, as β close to 1, the trajectories in fig. 4.7 are indeed Brownian. This is confirmed by the study of the MSD, which is shown in blue on the right. Also shown on the right are the TASD of each cell in yellow and the interpolation of the MSD in form $t \mapsto ct^\beta$ in orange.*
The results presented here are obtained with the parameters $\Delta t = 0.005$, $R_0 = 1$, $R_{\text{nucl}} = 0.3$, $M = \pi$, $a = 1$, $c^{\text{in}} = \dfrac{M}{|\Omega \setminus N|}$, $\chi_c = \chi_c^* - 0.3$ with χ_c^* given by (4.5), $f_{\text{act}}(c) = \frac{c(1+c_s)^2}{c_s(c+c_s)}$ with $c_s = 0.5$, $\alpha = 0.3$ and $\zeta = 0.2$.

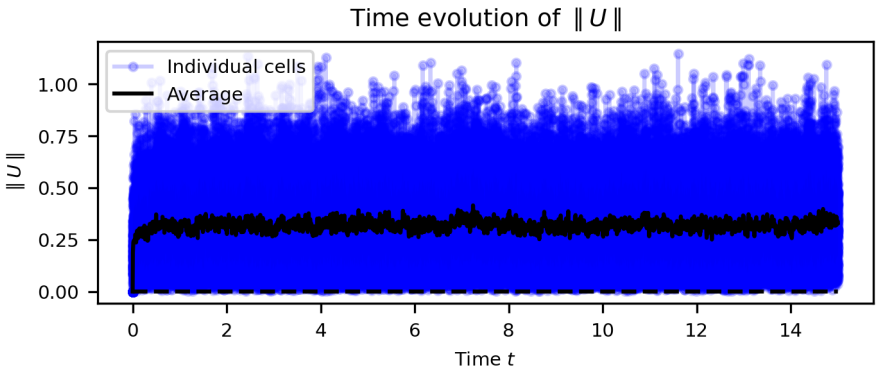

Figure 4.10: **Time evolution of the norm of the velocity of the cells whose trajectories are shown in fig. 4.7 (case when $\chi_c < \chi_c^*$).** *The blue lines show the evolution over time of the norm of the velocity of each cell and the black line shows the evolution of the mean of the norms of the velocities of the cells. We can see that the value of the mean of the norms of the cell velocities corresponds to the choice of α.*
The results presented here are obtained with the parameters $\Delta t = 0.005$, $R_0 = 1$, $R_{\text{nucl}} = 0.3$, $M = \pi$, $a = 1$, $c^{\text{in}} = \dfrac{M}{|\Omega \setminus N|}$, $\chi_c = \chi_c^* - 0.3$ with χ_c^* given by (4.5), $f_{\text{act}}(c) = \frac{c(1+c_s)^2}{c_s(c+c_s)}$ with $c_s = 0.5$, $\alpha = 0.3$ and $\zeta = 0.2$.

4.4.2.2 . Illustration of the persistent trajectories

In this subsection, we present the results when $\chi_c = \chi_c^* + 0.5$. We then observe that the trajectories are persistent. This can be seen visually in fig. 4.11 and is confirmed by the study of the EASD and MSD, which are equal or close to 2 (see fig. 4.13). In addition, we can see that the trajectories satisfy the UCSP (see fig. 4.12). We also observe that the cells have a high velocity (see fig. 4.14). These observations are in good agreement with those made about persistent behaviour in Maiuri et al. (2015).

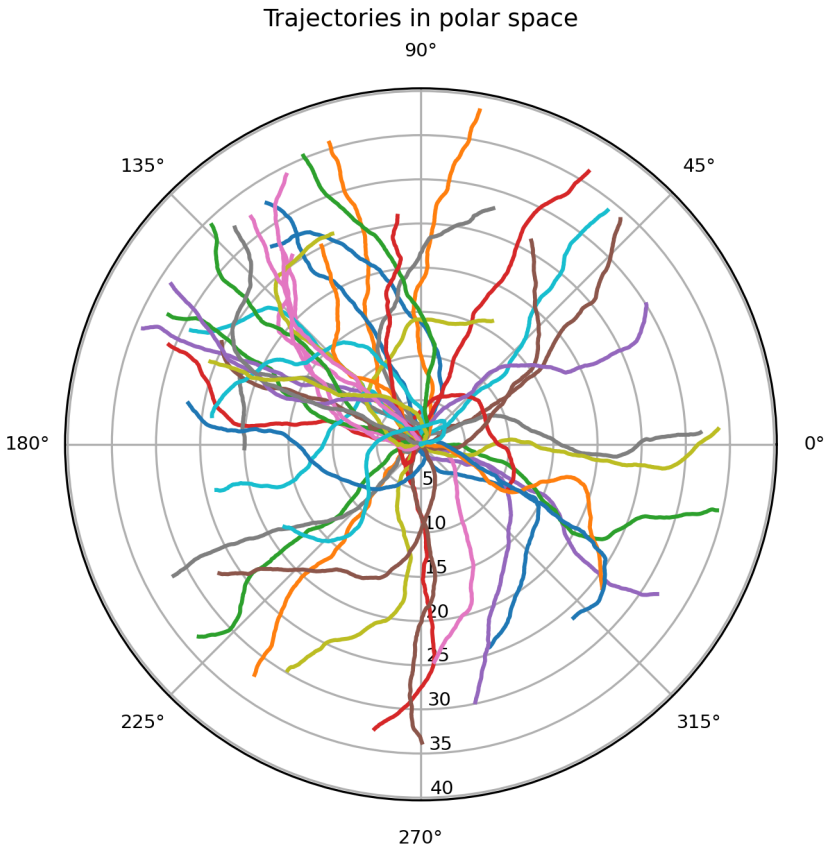

Figure 4.11: **Trajectories in polar coordinates in the case where $\chi_c > \chi_c^*$.** *Each curve represents, in polar coordinates, the trajectory of one cell simulated by algorithm 4.1 on the time interval $[0, 15]$. Visually, the trajectories seem to be persistent. Fifty cells are represented.*
The results presented here are obtained with the parameters $\Delta t = 0.005$, $R_0 = 1$, $R_{\text{nucl}} = 0.3$, $M = \pi$, $a = 1$, $c^{\text{in}} = \dfrac{M}{|\Omega \setminus N|}$, $\chi_c = \chi_c^* + 0.5$ with χ_c^* given by (4.5), $f_{\text{act}}(c) = \frac{c(1+c_s)^2}{c_s(c+c_s)}$ with $c_s = 0.5$, $\alpha = 0.3$ and $\zeta = 0.2$.

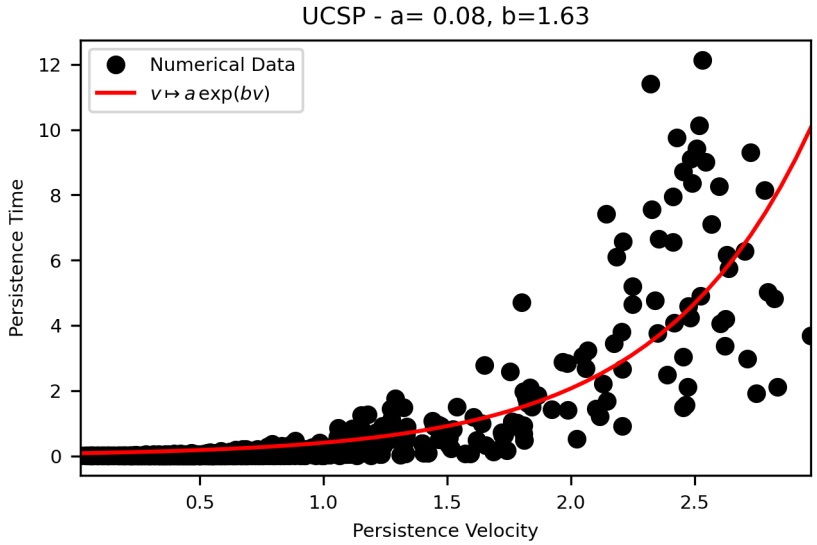

Figure 4.12: **Verification that the trajectories in fig. 4.11 satisfy the UCSP law (case when $\chi_c > \chi_c^*$).** *The persistence time of a locally persistent trajectory portion is plotted as a function of the persistence velocity. Each black dot corresponds to a datum. In red is plotted an interpolation of the points, of form $v \mapsto ae^{bv}$, which corresponds to the UCSP law. We can see that the data corresponds well to the interpolation and that the trajectories satisfy the UCSP law.*
The results presented here are obtained with the parameters $\Delta t = 0.005$, $R_0 = 1$, $R_{\text{nucl}} = 0.3$, $M = \pi$, $a = 1$, $c^{\text{in}} = \dfrac{M}{|\Omega \setminus N|}$, $\chi_c = \chi_c^* + 0.5$ with χ_c^* given by (4.5), $f_{\text{act}}(c) = \frac{c(1+c_s)^2}{c_s(c+c_s)}$ with $c_s = 0.5$, $\alpha = 0.3$ and $\zeta = 0.2$.

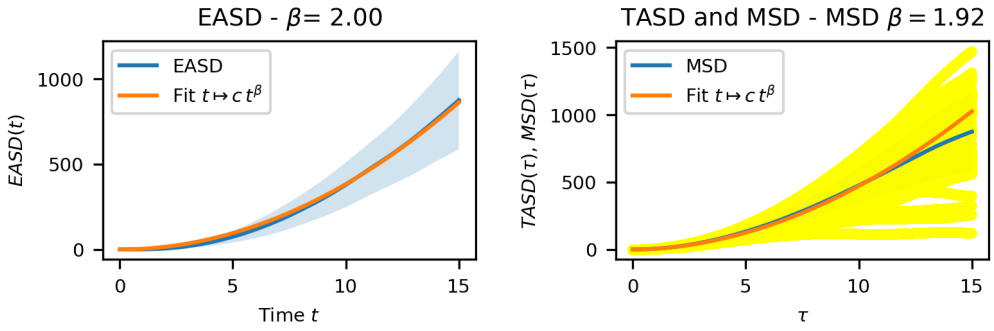

Figure 4.13: **Verification that the trajectories in fig. 4.11 are Brownian (case when $\chi_c > \chi_c^*$).** *On the left is shown in blue the EASD associated with the trajectories in fig. 4.11 and in orange the interpolation of the EASD, in the form $t \mapsto ct^{\beta}$. By the properties of the EASD, as β equals to 2, the trajectories in fig. 4.11 are indeed persistent. This is confirmed by the study of the MSD, which is shown in blue on the right. Also shown on the right are the TASD of each cell in yellow and the interpolation of the MSD in form $t \mapsto ct^{\beta}$ in orange.*
The results presented here are obtained with the parameters $\Delta t = 0.005$, $R_0 = 1$, $R_{\text{nucl}} = 0.3$, $M = \pi$, $a = 1$, $c^{\text{in}} = \dfrac{M}{|\Omega \setminus N|}$, $\chi_c = \chi_c^* + 0.5$ with χ_c^* given by (4.5), $f_{\text{act}}(c) = \frac{c(1+c_s)^2}{c_s(c+c_s)}$ with $c_s = 0.5$, $\alpha = 0.3$ and $\zeta = 0.2$.

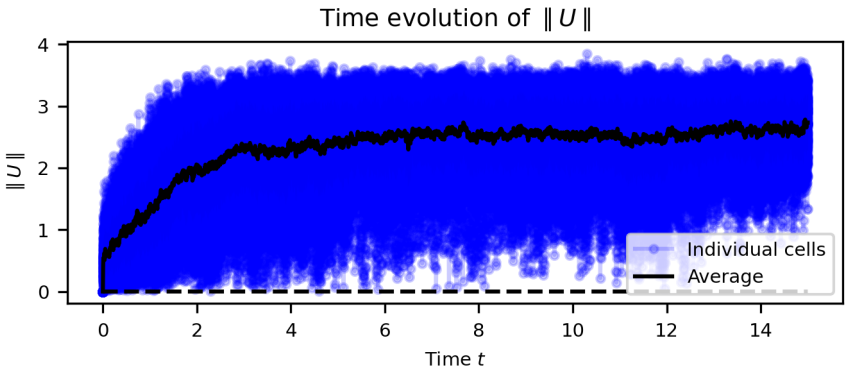

Figure 4.14: **Time evolution of the norm of the velocity of the cells whose trajectories are shown in fig. 4.11 (case when $\chi_c > \chi_c^*$).** *The blue lines show the evolution over time of the norm of the velocity of each cell and the black line shows the evolution of the mean of the norms of the velocities of the cells.*
The results presented here are obtained with the parameters $\Delta t = 0.005$, $R_0 = 1$, $R_{\text{nucl}} = 0.3$, $M = \pi$, $a = 1$, $c^{\text{in}} = \dfrac{M}{|\Omega \setminus N|}$, $\chi_c = \chi_c^* + 0.5$ *with* χ_c^* *given by* (4.5), $f_{\text{act}}(c) = \frac{c(1+c_s)^2}{c_s(c+c_s)}$ *with* $c_s = 0.5$, $\alpha = 0.3$ *and* $\zeta = 0.2$.

4.4.2.3 . Illustration of the intermittent trajectories

In this subsection, we present the results when $\chi_c = \chi_c^*$. We then observe that the trajectories are intermittent. This can be seen visually in fig. 4.15 and is confirmed by the study of the EASD and MSD, which are between 1 and 2 (see fig. 4.17). In addition, we can see that the trajectories satisfy the UCSP (see fig. 4.16). We also observe that the cells have a intermediate velocity: the velocity norm is between the velocities of the case $\chi_c = \chi_c^* - 0.3$ and $\chi_c = \chi_c^* + 0.5$ (see fig. 4.18). These observations are in good agreement with those made about intermittent behaviour in Maiuri et al. (2015).

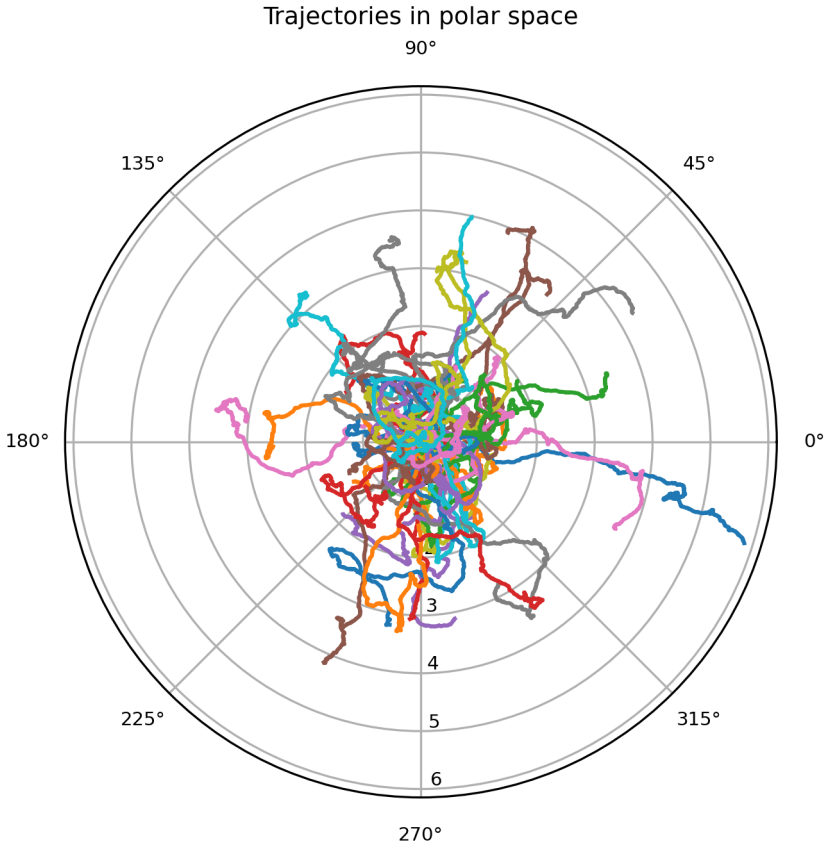

Figure 4.15: **Trajectories in polar coordinates in the case where $\chi_c = \chi_c^*$.** *Each curve represents, in polar coordinates, the trajectory of one cell simulated by algorithm 4.1 on the time interval $[0, 15]$. Visually, the trajectories seem to be intermittent. Fifty cells are represented.*
The results presented here are obtained with the parameters $\Delta t = 0.005$, $R_0 = 1$, $R_{\text{nucl}} = 0.3$, $M = \pi$, $a = 1$, $c^{\text{in}} = \dfrac{M}{|\Omega \setminus N|}$, $\chi_c = \chi_c^*$ with χ_c^* given by (4.5), $f_{\text{act}}(c) = \frac{c(1+c_s)^2}{c_s(c+c_s)}$ with $c_s = 0.5$, $\alpha = 0.3$ and $\zeta = 0.2$.

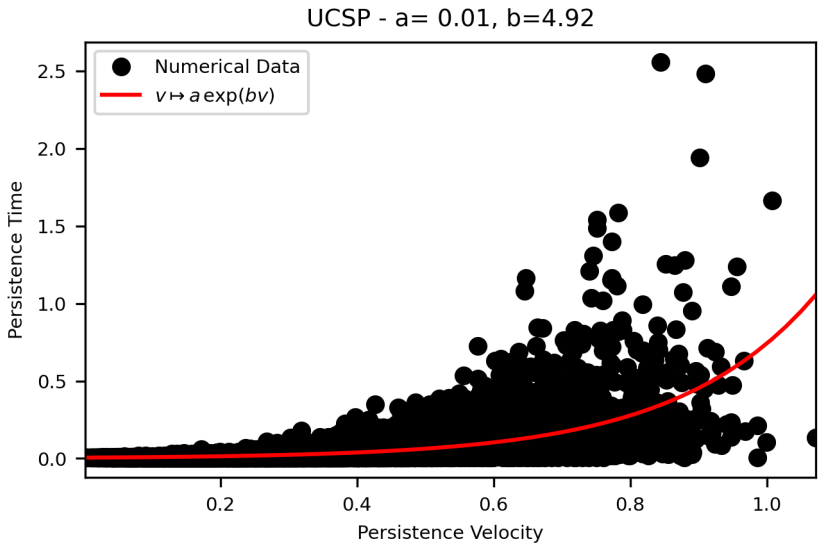

Figure 4.16: **Verification that the trajectories in fig. 4.15 satisfy the UCSP law (case when $\chi_c = \chi_c^*$).** *The persistence time of a locally persistent trajectory portion is plotted as a function of the persistence velocity. Each black dot corresponds to a datum. In red is plotted an interpolation of the points, of form $v \mapsto ae^{bv}$, which corresponds to the UCSP law. We can see that the data corresponds well to the interpolation and that the trajectories satisfy the UCSP law.*
The results presented here are obtained with the parameters $\Delta t = 0.005$, $R_0 = 1$, $R_{\text{nucl}} = 0.3$, $M = \pi$, $a = 1$, $c^{\text{in}} = \dfrac{M}{|\Omega \setminus N|}$, $\chi_c = \chi_c^*$ with χ_c^* given by (4.5), $f_{\text{act}}(c) = \frac{c(1+c_s)^2}{c_s(c+c_s)}$ with $c_s = 0.5$, $\alpha = 0.3$ and $\zeta = 0.2$.

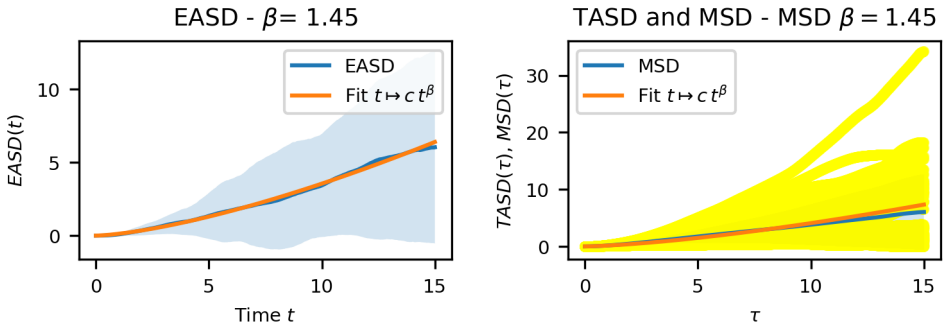

Figure 4.17: **Verification that the trajectories in fig. 4.15 are intermittent (case when $\chi_c = \chi_c^*$).** *On the left is shown in blue the EASD associated with the trajectories in fig. 4.15 and in orange the interpolation of the EASD, in the form $t \mapsto ct^\beta$. By the properties of the EASD, as β between 1 and 2, the trajectories in fig. 4.15 are neither Brownian neither persistent. This is confirmed by the study of the MSD, which is shown in blue on the right. Also shown on the right are the TASD of each cell in yellow and the interpolation of the MSD in form $t \mapsto ct^\beta$ in orange.*
The results presented here are obtained with the parameters $\Delta t = 0.005$, $R_0 = 1$, $R_{\text{nucl}} = 0.3$, $M = \pi$, $a = 1$, $c^{\text{in}} = \dfrac{M}{|\Omega \setminus N|}$, $\chi_c = \chi_c^*$ with χ_c^* given by (4.5), $f_{\text{act}}(c) = \frac{c(1+c_s)^2}{c_s(c+c_s)}$ with $c_s = 0.5$, $\alpha = 0.3$ and $\zeta = 0.2$.

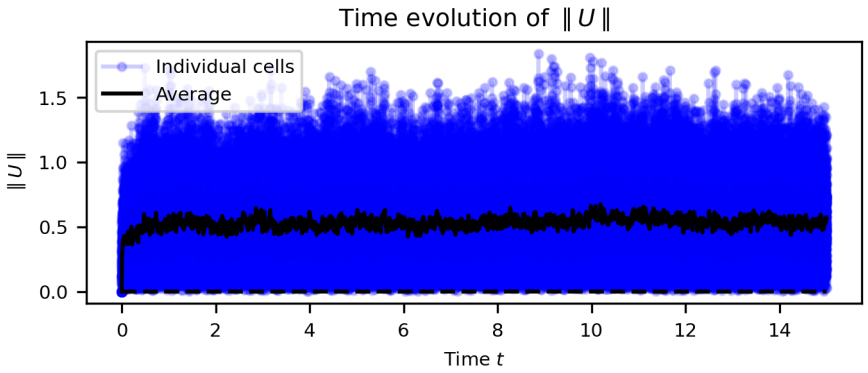

Figure 4.18: **Time evolution of the norm of the velocity of the cells whose trajectories are shown in fig. 4.15 (case when $\chi_c = \chi_c^*$).** *The blue lines show the evolution over time of the norm of the velocity of each cell and the black line shows the evolution of the mean of the norms of the velocities of the cells. We can see that the value of the mean of the norms of the cell velocities corresponds to the choice of α.*
The results presented here are obtained with the parameters $\Delta t = 0.005$, $R_0 = 1$, $R_{\text{nucl}} = 0.3$, $M = \pi$, $a = 1$, $c^{\text{in}} = \dfrac{M}{|\Omega \setminus N|}$, $\chi_c = \chi_c^*$ with χ_c^* given by (4.5), $f_{\text{act}}(c) = \frac{c(1+c_s)^2}{c_s(c+c_s)}$ with $c_s = 0.5$, $\alpha = 0.3$ and $\zeta = 0.2$.

We have therefore highlighted the fact that the model allows all three types of trajectory to be found. We note that if the nucleus is fixed in the cell, then the results are similar to those obtained when we do not consider the nucleus (see chapter 3). The results obtained numerically in this chapter will be analysed in comparison with those obtained in chapter 6 when the dynamics of the nucleus are taken into account.

Conclusion and perspectives. The model allows all three types of trajectory to be found. The results obtained seem similar to those obtained when considering a rigid cell with a fluid domain having a disk domain (see chapter 3). However, the study of the linear stability of the stationary state proves that, for the choice of $f_{\text{act}}(c) = \frac{c(1+c_s)^2}{c_s(c+c_s)}$, the crown geometry of the fluid domain tends to stabilise the model. Indeed, as soon as $c_s < \frac{M}{\pi R_0^2}$, we have that for the same choice of parameters, the threshold above which the stationary state is unstable is greater in the case of the crown model. Let us denote $c^0(r)$ the stationary concentration associated with the domain where the inner disk of the crown domain has radius $r \in (0, R_0)$ and $\chi_c^*(r)$ the associated critical threshold. We know that c^0 is an increasing function on $[0, R_0]$. Also, as we have assumed that $c_s < \frac{M}{\pi R_0^2} = c^0(0)$ and that the function $x \mapsto \frac{1}{axf'_{\text{act}}(x)}$ is increasing on $[c_s, +\infty)$, we obtain that χ_c^* is an increasing function on $[0, R_0]$. The results obtained numerically in this chapter will be analysed in comparison with those obtained in chapter 6 when the dynamics of the nucleus are taken into account.

In a future project, we aim to study the long-term dynamics of the model. We pursue the characterisation of travelling waves initiated in section 4.2.2. An explicit expression for the travelling wave velocity shall be given. We will show the existence of travelling waves and the convergence in long time to a travelling wave or the stationary state. Finally, we aim to show a bifurcation result from the stationary state to a travelling wave when χ_c becomes larger than χ_c^*.

Bibliography

Alazard, T., Magliocca, M., and Meunier, N. (2022). Traveling wave solution for a coupled incompressible Darcy's free boundary problem with surface tension. arXiv:2205.04365 [math]. 103

Boulakia, M., Genadot, A., and Thieullen, M. (2015). Simulation of SPDEs for Excitable Media Using Finite Elements. Journal of Scientific Computing, 65(1):171–195. 110

Lavi, I., Meunier, N., Voituriez, R., and Casademunt, J. (2020). Motility and morphodynamics of confined cells. Physical Review E, 101(2):022404. Publisher: American Physical Society. 103, 113

Maiuri, P., Rupprecht, J.-F., Wieser, S., Ruprecht, V., Bénichou, O., Carpi, N., Coppey, M., De Beco, S., Gov, N., Heisenberg, C.-P., Lage Crespo, C., Lautenschlaeger, F., Le Berre, M., Lennon-Dumenil, A.-M., Raab, M., Thiam, H.-R., Piel, M., Sixt, M., and Voituriez, R. (2015). Actin Flows Mediate a Universal Coupling between Cell Speed and Cell Persistence. Cell, 161(2):374–386. 114, 118, 121

5 - Rigid cell model with a particle

In this chapter, we present a second toy model which will be useful for highlighting the properties of the nucleus in chapter 6. This model is a simplification of the general model (1.1) in which the cell is assumed to be rigid and has a rigid particle which is transported by the fluid contained in the cell. This makes it possible to study the impact of the presence of the nucleus in the cell when its dynamics are neglected and thus to highlight the impact of the dynamics of the nucleus on the trajectories of the cells (see chapter 6). First we present the model studied. We then study the stationary states of the model and their stability. Finally, we discretise the model in order to write a numerical scheme based on finite element method for simulating the model. Contrary to the model presented in chapter 4, the fluid domain is a deformable domain. The particle can move inside the cell. The numerical scheme takes this into account. In order to handle the different boundary conditions, a decomposition method is proposed. Potential contacts between the cell boundary and the nucleus are avoided using an Uzawa algorithm. We then study the trajectories obtained by simulating the model. We illustrate that the model can simulate Brownian, intermittent and persistent trajectories.

5.1 . Modelling

In this section, we aim to derive a cell motility model from the deformable model, taking into account a rigid particle transported by the fluid and assuming that the cell is rigid. Considering a rigid particle transported by the fluid means neglecting the forces characterising the nucleus f_{NB} and $\mathbf{f}_{\mathrm{BN}}$ by assuming them to be zero. First, we define the deformable model with a rigid particle. Next, we study the dynamics of the centre of mass of the cell given by the deformable model. Finally, we derive a rigid model analogous to the deformable model.

5.1.1 . Deformable model

We restrict ourselves to the case where the cell's environment presents no obstacle and where there is no external signal. We neglect the effects of undercooling and assume that the substrate is homogeneous, i.e. that ξ_{M} is independent of space and we set for all $\mathbf{x} \in \mathbb{R}^2$, $\xi_{\mathrm{M}}(\mathbf{x}) = 1$. Then we have ξ_{nucl} independent of time. We also assume that f_{NB} and $\mathbf{f}_{\mathrm{BN}}$ to be zero. Under these assumptions and keeping the notations from chapter 1, the deformable

model (1.1) is written as follows:

$$\begin{cases} \mathbf{u} + \nabla P = 0 & \text{in } \Omega(t) \setminus N(t), & \text{(5.1a)} \\ \operatorname{div}(\mathbf{u}) = 0 & \text{in } \Omega(t) \setminus N(t), & \text{(5.1b)} \\ V_n = \mathbf{u} \cdot \mathbf{n} & \text{on } \partial\Omega(t), & \text{(5.1c)} \\ P = \gamma\kappa + \chi_c f_{\text{act}}(c) & \text{on } \partial\Omega(t), & \text{(5.1d)} \\ \mathbf{u}_{\text{nucl}}(t) = \dfrac{1}{\xi_{\text{nucl}} |N|} \displaystyle\int_{\partial N(t)} P(t, \mathbf{x}) \mathbf{n} \, \mathrm{d}\sigma & & \text{(5.1e)} \\ \mathbf{u} \cdot \mathbf{n} = \mathbf{u}_{\text{nucl}} \cdot \mathbf{n} & \text{on } \partial N(t), & \text{(5.1f)} \\ \partial_t c = \operatorname{div}\left(\nabla c - (1-a)\mathbf{u}c - \alpha \dot{W}_t^Q c\right) & \text{in } \Omega(t) \setminus N(t), & \text{(5.1g)} \\ \left(\nabla c + a\mathbf{u}c - \alpha \dot{W}_t^Q c\right) \cdot \mathbf{n} = 0 & \text{on } \partial(\Omega(t) \setminus N(t)), & \text{(5.1h)} \\ c(0, \mathbf{x}) = c^{\text{in}}(\mathbf{x}) & \text{in } \Omega(0) \setminus N(0). & \text{(5.1i)} \end{cases}$$

5.1.2 . Force balance

Let $\mathbf{x}_{\text{cm}}(t)$ be the centre of mass of $\Omega(t)$ at time $t \geq 0$. We have:

$$\mathbf{x}_{\text{cm}}(t) = \frac{1}{A_\Omega} \int_{\Omega(t)} (x, y) \, \mathrm{d}x \, \mathrm{d}y.$$

We also define the velocity of the centre of mass $\mathbf{u}_{\text{cm}}$. For all $t \geq 0$, we have:

$$\mathbf{u}_{\text{cm}}(t) = \frac{\mathrm{d}}{\mathrm{d}t} \mathbf{x}_{\text{cm}}(t).$$

For all $t \geq 0$, we have:

$$\begin{aligned} \frac{\mathrm{d}}{\mathrm{d}t} \int_{\Omega(t)} x \, \mathrm{d}x \, \mathrm{d}y &= \int_{\partial\Omega(t)} x V_n \, \mathrm{d}\sigma = \int_{\partial\Omega(t)} x \mathbf{u} \cdot \mathbf{n} \, \mathrm{d}\sigma \\ &= \int_{\Omega(t) \setminus N(t)} \operatorname{div}(x\mathbf{u}) \, \mathrm{d}x \, \mathrm{d}y + \int_{N(t)} \operatorname{div}(x\mathbf{u}_{\text{nucl}}) \, \mathrm{d}x \, \mathrm{d}y \\ &= \int_{\Omega(t) \setminus N(t)} \nabla x \cdot \mathbf{u} \, \mathrm{d}x \, \mathrm{d}y + \mathbf{u}_{\text{nucl}} \cdot \int_{N(t)} \nabla x \, \mathrm{d}x \, \mathrm{d}y \\ &= -\int_{\Omega(t) \setminus N(t)} \operatorname{div}(P \nabla x) \, \mathrm{d}x \, \mathrm{d}y + \mathbf{u}_{\text{nucl},x} \\ &= -\int_{\partial\Omega(t)} P \nabla x \cdot \mathbf{n} \, \mathrm{d}\sigma - \int_{\partial N(t)} P \nabla x \cdot \mathbf{n} \, \mathrm{d}\sigma + \mathbf{u}_{\text{nucl},x} \\ &= -\int_{\partial\Omega(t)} (\gamma\kappa + \chi_c f_{\text{act}}(c)) \mathbf{n}_x \, \mathrm{d}\sigma - \int_{\partial\Omega(t)} P \mathbf{n}_x \, \mathrm{d}\sigma + \mathbf{u}_{\text{nucl},x} \\ &= -\int_{\partial\Omega(t)} (\gamma\kappa + \chi_c f_{\text{act}}(c)) \mathbf{n}_x \, \mathrm{d}\sigma - \xi_{\text{nucl}} |N| \mathbf{u}_{\text{nucl},x} + \mathbf{u}_{\text{nucl},x} \end{aligned}$$

where we used the incompresisbility constraint (5.1b), the darcy law (5.1a), the boundary condition (5.1d) and the nucleus velocity expression (5.1e). Analogously, we have:

$$\frac{\mathrm{d}}{\mathrm{d}t} \int_{\Omega(t)} y \, \mathrm{d}x \, \mathrm{d}y = -\int_{\partial\Omega(t)} (\gamma\kappa + \chi_c f_{\text{act}}(c)) \mathbf{n}_y \, \mathrm{d}\sigma - \xi_{\text{nucl}} |N| \mathbf{u}_{\text{nucl},y} + \mathbf{u}_{\text{nucl},y}.$$

Since $\int_{\partial\Omega(t)} \kappa \mathbf{n} \, \mathrm{d}\sigma = 0$, it follows:

$$\mathbf{u}_{\text{cm}}(t) = -\frac{1}{A_\Omega} \int_{\partial\Omega(t)} \chi_c f_{\text{act}}(c) \mathbf{n} \, \mathrm{d}\sigma + \frac{|N|}{A_\Omega} (1 - \xi_{\text{nucl}}) \mathbf{u}_{\text{nucl}}(t). \tag{5.2}$$

5.1.3 . Rigid formulation

We want to write the rigid model associated with the deformable model eqs. (5.1) and (5.2). We assume the cell to be rigid and the cell to have a circular shape: $\Omega(t)$ is a disk of radius $R_0 > 0$. We assume that the velocity of the centre of mass in the rigid case is the same as in the deformable case. Thus, the external boundary of the cell moves at the velocity of the centre of mass. As in the deformable case, the cell is filled by a Darcy fluid with velocity $\mathbf{u}$ and pressure P. Thus, with the assumption that the cell boundary normal velocity is equal to the inside fluid normal velocity and with velocities continuity at the nucleus boundary, we have:

$$\begin{cases} \mathbf{u} + \nabla P = 0 & \text{in } \Omega(t) \setminus N(t), \\ \operatorname{div}(\mathbf{u}) = 0 & \text{in } \Omega(t) \setminus N(t), \\ \mathbf{u} \cdot \mathbf{n} = \mathbf{u}_{\mathrm{cm}} \cdot \mathbf{n} & \text{on } \partial\Omega(t), \\ \mathbf{u} \cdot \mathbf{n} = \mathbf{u}_{\mathrm{nucl}} \cdot \mathbf{n} & \text{on } \partial N(t), \\ \Omega(t) = B(0, R_0) + \displaystyle\int_0^t \mathbf{u}_{\mathrm{cm}}(s)\, \mathrm{d}s, & \\ N(t) = B(0, R_{\mathrm{nucl}}) + \displaystyle\int_0^t \mathbf{u}_{\mathrm{nucl}}(s)\, \mathrm{d}s. & \end{cases}$$

The rigid particle is modelled as in the deformable case. We assume it to have a rigid movement. The force balance on the nucleus leads to the following expression for the particle velocity:

$$\mathbf{u}_{\mathrm{nucl}} = \frac{1}{\xi_{\mathrm{nucl}} |N|} \int_{\partial N(t)} P(t, \mathbf{x})\, \mathbf{n}\, \mathrm{d}\sigma.$$

Finally, as in the deformable case, we assume that rear markers are inside the cell, that they can diffuse inside the cell and be transported by the fluid or attached to the plate, and that in addition they are subject to stochastic fluctuations (modelled as in the section 1.3.7), which leads to:

$$\begin{cases} \partial_t c = \operatorname{div}\left(\nabla c - (1-a)\, \mathbf{u} c - \alpha \dot{W}_t^Q c\right) & \text{in } \Omega(t) \setminus N(t), \\ \left(\nabla c + a \mathbf{u} c - \alpha \dot{W}_t^Q c\right) \cdot \mathbf{n} = 0 & \text{on } \partial\left(\Omega(t) \setminus N(t)\right). \end{cases}$$

Thus, the rigid cell model with a rigid nucleus inside the cell that can move is given by:

$$
\begin{cases}
\mathbf{u} + \nabla P = 0 & \text{in } \Omega(t) \setminus N(t), \quad (5.3a)\\
\operatorname{div}(\mathbf{u}) = 0 & \text{in } \Omega(t) \setminus N(t), \quad (5.3b)\\
\mathbf{u} \cdot \mathbf{n} = \mathbf{u}_{\text{cm}} \cdot \mathbf{n} & \text{on } \partial\Omega(t), \quad (5.3c)\\
\mathbf{u} \cdot \mathbf{n} = \mathbf{u}_{\text{nucl}} \cdot \mathbf{n} & \text{on } \partial N(t), \quad (5.3d)\\
\mathbf{u}_{\text{nucl}}(t) = \dfrac{1}{\xi_{\text{nucl}} |N|} \displaystyle\int_{\partial N(t)} P(t, \mathbf{x}) \mathbf{n} \, \mathrm{d}\sigma, & (5.3e)\\
\mathbf{u}_{\text{cm}}(t) = \dfrac{-\chi_c}{A_\Omega} \displaystyle\int_{\partial\Omega(t)} f_{\text{act}}(c) \, \mathbf{n} \, \mathrm{d}\sigma + \dfrac{|N|}{A_\Omega} (1 - \xi_{\text{nucl}}) \, \mathbf{u}_{\text{nucl}}(t), & (5.3f)\\
\partial_t c = \operatorname{div}\left(\nabla c - (1-a)\,\mathbf{u} c - \alpha \dot{W}_t^Q c\right) & \text{in } \Omega(t) \setminus N(t), \quad (5.3g)\\
\left(\nabla c + a \mathbf{u} c - \alpha \dot{W}_t^Q c\right) \cdot \mathbf{n} = 0 & \text{on } \partial(\Omega(t) \setminus N(t)), \quad (5.3h)\\
\Omega(t) = B(0, R_0) + \displaystyle\int_0^t \mathbf{u}_{\text{cm}}(s) \, \mathrm{d}s, & (5.3i)\\
N(t) = B(0, R_{\text{nucl}}) + \displaystyle\int_0^t \mathbf{u}_{\text{nucl}}(s) \, \mathrm{d}s. & (5.3j)
\end{cases}
$$

We can note that, in general, since $\mathbf{u}_{\text{cm}} \neq \mathbf{u}_{\text{nucl}}$, the fluid domain is not a rigid domain but a deformable domain. In accordance with the modelling of noise in section 1.3.7, the space coloured noise $\dot{W}_t^Q$ is defined on a probability space associated with the open $\Omega(0) = B(0, R_0)$.

As in the deformable case, the total quantity of markers M is conserved over time and we have:

$$M = \int_{\Omega(t) \setminus N(t)} c(t, \mathbf{x}) \, \mathrm{d}\mathbf{x}. \quad (5.4)$$

Remark 5.1.1. *In the model (5.3), P is defined up to a constant. Indeed, if $(P, \mathbf{u}, c)$ is a solution of (5.3), then for all $P_0 \in \mathbb{R}$, $(P + P_0, \mathbf{u}, c)$ is also a solution of (5.3). Thus, in order to define a form of uniqueness of solutions, we can define an equivalence class and state that $(P_1, \mathbf{u}_1, c_1)$ and $(P_2, \mathbf{u}_2, c_2)$ are equivalent solutions if and only if $\mathbf{u}_1 = \mathbf{u}_2$, $c_1 = c_2$ and there exists $Q \in \mathbb{R}$ such that $P_1 = P_2 + Q$.*

5.2 . Study of the model

In this section, we study the stationary state of model (5.3) in the case where we neglect the noise and take $\alpha = 0$ in eqs. (5.3g) and (5.3h). First, we prove that the model admits a stationary state. Secondly, we study its linear stability and give a criterion for its stability. There exists χ_c^* such that if $\chi_c < \chi_c^*$ then the stationary state is stable and unstable otherwise.

Considering $\alpha = 0$, the model under study in this section is as follows:

$$\begin{cases} \mathbf{u} + \nabla P = 0 & \text{in } \Omega(t) \setminus N(t), & \text{(5.5a)} \\ \operatorname{div}(\mathbf{u}) = 0 & \text{in } \Omega(t) \setminus N(t), & \text{(5.5b)} \\ \mathbf{u} \cdot \mathbf{n} = \mathbf{u}_{\text{cm}} \cdot \mathbf{n} & \text{on } \partial\Omega(t), & \text{(5.5c)} \\ \mathbf{u} \cdot \mathbf{n} = \mathbf{u}_{\text{nucl}} \cdot \mathbf{n} & \text{on } \partial N(t), & \text{(5.5d)} \\ \mathbf{u}_{\text{nucl}}(t) = \dfrac{1}{\xi_{\text{nucl}} |N|} \displaystyle\int_{\partial N(t)} P(t, \mathbf{x}) \mathbf{n} \, \mathrm{d}\sigma, & & \text{(5.5e)} \\ \mathbf{u}_{\text{cm}}(t) = \dfrac{-\chi_c}{A_\Omega} \displaystyle\int_{\partial\Omega(t)} f_{\text{act}}(c) \, \mathbf{n} \, \mathrm{d}\sigma + \dfrac{|N|}{A_\Omega} (1 - \xi_{\text{nucl}}) \, \mathbf{u}_{\text{nucl}}(t), & & \text{(5.5f)} \\ \partial_t c = \operatorname{div}(\nabla c - (1 - a) \, \mathbf{u} c) & \text{in } \Omega(t) \setminus N(t), & \text{(5.5g)} \\ (\nabla c + a \mathbf{u} c) \cdot \mathbf{n} = 0 & \text{on } \partial(\Omega(t) \setminus N(t)), & \text{(5.5h)} \\ \Omega(t) = B(0, R_0) + \displaystyle\int_0^t \mathbf{u}_{\text{cm}}(s) \, \mathrm{d}s, & & \text{(5.5i)} \\ N(t) = B(0, R_{\text{nucl}}) + \displaystyle\int_0^t \mathbf{u}_{\text{nucl}}(s) \, \mathrm{d}s. & & \text{(5.5j)} \end{cases}$$

5.2.1 . Stationary state

Proposition 5.2.1. *The model eq. (5.5) admits an unique radially symmetric stationary state given by:*

$$\begin{cases} \mathbf{u}^0(\mathbf{x}) = 0, & \mathbf{x} \in \Omega^0 \setminus N^0, & \text{(5.6a)} \\ P^0(\mathbf{x}) = 0, & \mathbf{x} \in \Omega^0 \setminus N^0, & \text{(5.6b)} \\ \mathbf{u}^0_{\text{nucl}} = 0, & & \text{(5.6c)} \\ \mathbf{u}^0_{\text{cm}} = 0, & & \text{(5.6d)} \\ c^0(\mathbf{x}) = \dfrac{M}{|\Omega^0 \setminus N^0|}, & \mathbf{x} \in \Omega^0 \setminus N^0, & \text{(5.6e)} \\ \Omega^0 = B(0, R_0) \text{ and } N^0 = B(0, R_{\text{nucl}}). & & \text{(5.6f)} \end{cases}$$

Uniqueness is defined according to the remark 5.1.1.

Proof. We are looking for a radially symmetric stationnary state. Thus necessarily the cell geometry is given by $\Omega^0 = B(0, R_0)$ and $N^0 = B(0, R_{\text{nucl}})$.

With this geometry, the stationary problem asssociated with the model (5.5) is given as follows:

$$\begin{cases} \mathbf{u} + \nabla P = 0 & \text{in } \Omega^0 \setminus N^0, \\ \operatorname{div}(\mathbf{u}) = 0 & \text{in } \Omega^0 \setminus N^0, \\ \mathbf{u} \cdot \mathbf{n} = 0 & \text{on } \partial\Omega^0 \cup \partial N^0, \\ \Delta c - (1 - a) \, \mathbf{u} \cdot \nabla c = 0 & \text{in } \Omega^0 \setminus N^0, \\ (\nabla c + a \mathbf{u} c) \cdot \mathbf{n} = 0 & \text{on } \partial\Omega^0 \cup \partial N^0. \end{cases}$$

Thus the problem on P reads:

$$\begin{cases} -\Delta P = 0 & \text{in } \Omega^0 \setminus N^0, \\ -\nabla P \cdot \mathbf{n} = 0 & \text{on } \partial\Omega^0 \cup \partial N^0, \end{cases}$$

which leads to the fact that P is such that $\nabla P = 0$ over $\Omega^0 \setminus N^0$ and thus P is constant over $\Omega^0 \setminus N^0$. Moreover, we deduce that $\mathbf{u} = 0$ over $\Omega^0 \setminus N^0$.

Substituting the value of $\mathbf{u}$ into the dynamics of concentration c, we obtain:

$$\begin{cases} -\Delta c = 0 & \text{in } \Omega^0 \setminus N^0, \\ -\nabla c \cdot \mathbf{n} = 0 & \text{on } \partial\Omega^0 \cup \partial N^0, \end{cases}$$

and c is constant over $\Omega^0 \setminus N^0$. Using the constraint on the total quantity of markers (5.4), we deduce that for all $\mathbf{x} \in \Omega^0 \setminus N^0$, $c(\mathbf{x}) = \dfrac{M}{|\Omega^0 \setminus N^0|}$. □

Remark 5.2.2. *We can note that for all $\mathbf{x}_{\text{nucl}} \in \mathbb{R}^2$ such that $N = B(\mathbf{x}_{\text{nucl}}, R_{\text{nucl}})$ is a subset of $\Omega = B(0, R_0)$ then*

$$\begin{cases} \mathbf{u}^0(\mathbf{x}) = 0, & \mathbf{x} \in \Omega \setminus N, \\ P^0(\mathbf{x}) = 0, & \mathbf{x} \in \Omega \setminus N, \\ \mathbf{u}^0_{\text{nucl}} = 0, & \\ \mathbf{u}^0_{\text{cm}} = 0, & \\ c^0(\mathbf{x}) = \dfrac{M}{|\Omega \setminus N|}, & \mathbf{x} \in \Omega \setminus N, \end{cases}$$

is a stationary of the problem (5.5).

In the sequel we denote:

$$\chi_c^* = \frac{1}{ac^0 f'_{\text{act}}(c^0)}. \tag{5.7}$$

Theorem 5.2.3. *In the case where $\xi_{\text{nucl}} = 1$, if $\chi_c < \chi_c^*$, then the stationary state (5.6) is linearly stable. On the opposite, if $\chi_c > \chi_c^*$, then the stationary state is linearly unstable.*

5.2.2 . Proof of theorem 5.2.3

The theorem is proved in three steps. The first consists of computing the linearised problem of problem (5.5) around the stationary state (5.6) and deducing an eigenvalue problem. The stationary state will then be stable if all the eigenvalues of the eigenvalue problem have a negative real part. The second step consists to establish that the eigenvalue problem admits a positive real part eigenvalue, is equivalent to the fact that a simpler problem admits a real part eigenvalue. This step is based on the radially symmetric nature of the problem and Fourier analysis. The third step consists in studying this simpler problem. We can then exhibit a positive real part eigenvalue of it when $\chi_c > \chi_c^*$. Also, using a graphical argument, it consists in illustrating that if $\chi_c < \chi_c^*$ then the eigenvalues of this problem have a negative real part. The arguments used are inspired by those of Lavi et al. (2020); Alazard et al. (2022) and are similar to those of section 4.2.1.2.

Step 1. The following lemma gives the expression for the linearised problem associated with problem (5.5) around the stationary state (5.6).

Lemma 5.2.4. *The linearised problem associated to eq. (5.5) around the stationary state (5.6) is given by:*

$$\begin{cases} -\Delta\tilde{P} = 0 & \text{in } \Omega^0 \setminus N^0, \quad (5.8a) \\ -\nabla\tilde{P}\cdot\mathbf{n} = \tilde{\mathbf{u}}_{\mathrm{cm}}\cdot\mathbf{n} & \text{on } \partial\Omega^0, \quad (5.8b) \\ -\nabla\tilde{P}\cdot\mathbf{n} = \tilde{\mathbf{u}}_{\mathrm{nucl}}\cdot\mathbf{n} & \text{on } \partial N^0, \quad (5.8c) \\ \partial_t\tilde{c} = \Delta\tilde{c} & \text{in } \Omega^0 \setminus N^0, \quad (5.8d) \\ \left(\nabla\tilde{c} + a\tilde{\mathbf{u}}_{\mathrm{cm}}c^0\right)\cdot\mathbf{n} = 0 & \text{on } \partial\Omega^0, \quad (5.8e) \\ \left(\nabla\tilde{c} + a\tilde{\mathbf{u}}_{\mathrm{nucl}}c^0\right)\cdot\mathbf{n} = 0 & \text{on } \partial N^0, \quad (5.8f) \end{cases}$$

with

$$\tilde{\mathbf{u}}_{\mathrm{cm}}(t) = \frac{-\chi_c f'_{\mathrm{act}}\left(c^0\right)}{A_\Omega}\int_{\partial\Omega^0}\tilde{c}(t,\mathbf{x})\,\mathbf{n}\,\mathrm{d}\sigma, \quad (5.9a)$$

$$\tilde{\mathbf{u}}_{\mathrm{nucl}}(t) = \frac{1}{|N|}\int_{\partial N^0}\tilde{P}(t,\mathbf{x})\,\mathbf{n}\,\mathrm{d}\sigma. \quad (5.9b)$$

Proof. We perform a formal expansion of the solutions of model (5.5) around the stationary state (5.6). Let $\varepsilon > 0$ small. For all $t \geq 0$, we set:

$$\Omega(t) = B\left(\mathbf{x}_{\mathrm{cell}}(t), R_0\right) \quad \text{and} \quad N(t) = B\left(\mathbf{x}_{\mathrm{nucl}}(t), R_{\mathrm{nucl}}\right),$$

with

$$\mathbf{x}_{\mathrm{cell}}(t) = \varepsilon\tilde{\mathbf{x}}_{\mathrm{cell}}(t) + \mathcal{O}\left(\varepsilon^2\right),$$
$$\mathbf{x}_{\mathrm{nucl}}(t) = \varepsilon\tilde{\mathbf{x}}_{\mathrm{nucl}}(t) + \mathcal{O}\left(\varepsilon^2\right).$$

Thus we can set for all $t \geq 0$:

$$\mathbf{u}_{\mathrm{cm}}(t) = \mathbf{u}^0_{\mathrm{cm}} + \varepsilon\tilde{\mathbf{u}}_{\mathrm{cm}}(t) + \mathcal{O}\left(\varepsilon^2\right),$$
$$\mathbf{u}_{\mathrm{nucl}}(t) = \mathbf{u}^0_{\mathrm{nucl}} + \varepsilon\tilde{\mathbf{u}}_{\mathrm{nucl}}(t) + \mathcal{O}\left(\varepsilon^2\right).$$

Moreover, for all $t \geq 0$ and $\mathbf{x} \in \Omega^0 \setminus N^0$, we set:

$$P(t) = P^0 + \varepsilon\tilde{P}(t) + \mathcal{O}\left(\varepsilon^2\right),$$

and

$$c(t,\mathbf{x}) = c^0 + \varepsilon\tilde{c}(t,\mathbf{x}) + \mathcal{O}\left(\varepsilon^2\right).$$

As P_0 satisfies eq. (5.6b) and P satisfies eqs. (5.5a) and (5.5b), we have that in $\Omega^0 \setminus N^0$:

$$-\Delta\tilde{P} = 0.$$

In addition, since P satisfies eq. (5.5b) and $\mathbf{u}$ satisfies the boundary conditions eqs. (5.5c) and (5.5d), we deduce that $\tilde{P}$ satisfies the following boundary conditions:

$$-\nabla\tilde{P}\cdot\mathbf{n} = \tilde{\mathbf{u}}_{\mathrm{cm}}\cdot\mathbf{n} \quad \text{on } \partial\Omega^0,$$
$$-\nabla\tilde{P}\cdot\mathbf{n} = \tilde{\mathbf{u}}_{\mathrm{nucl}}\cdot\mathbf{n} \quad \text{on } \partial N^0.$$

Using the fact that c^0 satisfies eq. (5.6e) and c satisfies (5.5g), we deduce that in $\Omega^0 \setminus N^0$:

$$\partial_t\tilde{c} = \Delta\tilde{c}.$$

We also have on $\partial\Omega^0$ that:

$$\begin{aligned}(\nabla c + a\mathbf{u}_{\mathrm{cm}} c)\cdot\mathbf{n} &= \left(\nabla c^0 + \varepsilon\nabla\tilde{c} + a\mathbf{u}^0_{\mathrm{cm}}c^0 + \varepsilon a\mathbf{u}^0_{\mathrm{cm}}\tilde{c} + \varepsilon a\tilde{\mathbf{u}}_{\mathrm{cm}}c^0\right)\cdot\mathbf{n} + \mathcal{O}\left(\varepsilon^2\right)\\ &= \varepsilon\left(\nabla\tilde{c} + a\tilde{\mathbf{u}}_{\mathrm{cm}}c^0\right)\cdot\mathbf{n} + \mathcal{O}\left(\varepsilon^2\right),\end{aligned}$$

which leads to the boundary condition:

$$\left(\nabla\tilde{c} + a\tilde{\mathbf{u}}_{\mathrm{cm}}c^0\right)\cdot\mathbf{n} = 0 \qquad \text{on } \partial\Omega^0.$$

Similarly, we obtain the boundary condition on N^0:

$$\left(\nabla\tilde{c} + a\tilde{\mathbf{u}}_{\mathrm{nucl}}c^0\right)\cdot\mathbf{n} = 0.$$

Moreover, we have:

$$\begin{aligned}\int_{\partial\Omega(t)} f_{\mathrm{act}}(c)\,\mathbf{n}\,\mathrm{d}\sigma &= \int_{\partial\Omega(t)} f_{\mathrm{act}}\left(c^0\right) + \varepsilon\tilde{c}f'_{\mathrm{act}}\left(c^0\right)\mathbf{n}\,\mathrm{d}\sigma + \mathcal{O}\left(\varepsilon^2\right)\\ &= \varepsilon f'_{\mathrm{act}}\left(c^0\right)\int_{\partial\Omega(t)}\tilde{c}\mathbf{n}\,\mathrm{d}\sigma + \mathcal{O}\left(\varepsilon^2\right)\\ &= \varepsilon f'_{\mathrm{act}}\left(c^0\right)\int_{\partial\Omega^0}\tilde{c}\mathbf{n}\,\mathrm{d}\sigma + \mathcal{O}\left(\varepsilon^2\right).\end{aligned}$$

Thus we deduce that

$$\tilde{\mathbf{u}}_{\mathrm{cm}} = \frac{-\chi_c f'_{\mathrm{act}}\left(c^0\right)}{A_\Omega}\int_{\partial\Omega^0}\tilde{c}\mathbf{n}\,\mathrm{d}\sigma.$$

Similarly, we have:

$$\int_{\partial N(t)} P\mathbf{n}\,\mathrm{d}\sigma = \varepsilon\int_{\partial N^0}\tilde{P}\mathbf{n}\,\mathrm{d}\sigma + \mathcal{O}\left(\varepsilon^2\right),$$

which leads to:

$$\tilde{\mathbf{u}}_{\mathrm{nucl}} = \frac{1}{|N|}\int_{\partial N^0}\tilde{P}\mathbf{n}\,\mathrm{d}\sigma.$$

□

The eigenvalue problem associated with eqs. (5.8) and (5.9) is given by:

$$\begin{cases} -\Delta\tilde{P} = 0 & \text{in } \Omega^0\setminus N^0, & \text{(5.10a)}\\ -\nabla\tilde{P}\cdot\mathbf{n} = \tilde{\mathbf{u}}_{\mathrm{cm}}\cdot\mathbf{n} & \text{on } \partial\Omega^0, & \text{(5.10b)}\\ -\nabla\tilde{P}\cdot\mathbf{n} = \tilde{\mathbf{u}}_{\mathrm{nucl}}\cdot\mathbf{n} & \text{on } \partial N^0, & \text{(5.10c)}\\ \lambda\tilde{c} = \Delta\tilde{c} & \text{in } \Omega^0\setminus N^0, & \text{(5.10d)}\\ \left(\nabla\tilde{c} + a\tilde{\mathbf{u}}_{\mathrm{cm}}c^0\right)\cdot\mathbf{n} = 0 & \text{on } \partial\Omega^0, & \text{(5.10e)}\\ \left(\nabla\tilde{c} + a\tilde{\mathbf{u}}_{\mathrm{nucl}}c^0\right)\cdot\mathbf{n} = 0 & \text{on } \partial N^0, & \text{(5.10f)}\end{cases}$$

where $\lambda\in\mathbb{C}$ and $\tilde{\mathbf{u}}_{\mathrm{cm}}$, $\tilde{\mathbf{u}}_{\mathrm{nucl}}$ defined by eq. (5.9).

Step 2. Using Fourier analysis and the radially symmetric nature of the problem (5.10), we prove the following lemma, which reduces the spectral study of eq. (5.10) to that of a simpler eigenvalue problem.

Lemma 5.2.5. *The problem (5.10) admits an eigenvalue with a positive real part if and only if the following problem eq. (5.11) admits one.*

$$\begin{cases} \lambda c = \left(\partial_{rr}^2 + \dfrac{1}{r}\partial_r - \dfrac{1}{r^2}\right) c & r \in (R_{\mathrm{nucl}}, R_0)\,, \quad (5.11a) \\ \partial_r c\,(R_0) + a\tilde{u}_{\mathrm{cm}} c^0 = 0, & (5.11b) \\ \partial_r c\,(R_{\mathrm{nucl}}) + a\tilde{u}_{\mathrm{nucl}} c^0 = 0, & (5.11c) \end{cases}$$

with

$$\tilde{u}_{\mathrm{cm}} = \tilde{u}_{\mathrm{nucl}} = \frac{-\chi_c f'_{\mathrm{act}}\left(c^0\right)}{R_0} c\,(R_0)\,. \quad (5.12)$$

Proof. Since problem (5.10) is radially symmetrical, we can use Fourier analysis to study its spectra. Let $\lambda \in \mathbb{C}$ and let $\left(\tilde{P}, \tilde{c}, \tilde{\mathbf{u}}_{\mathrm{cm}}, \tilde{\mathbf{u}}_{\mathrm{nucl}}\right)$ be an eigenfunction associated with λ. In polar coordinates, for all $r \in (R_{\mathrm{nucl}}, R_0)$ and $\theta \in (-\pi, \pi]$, the Fourier decomposition of $\tilde{P}$ is given by:

$$\tilde{P}\,(r,\theta) = \sum_{m\in\mathbb{N}} P_{cm}\,(r)\cos\,(m\theta) + P_{sm}\,(r)\sin\,(m\theta)\,,$$

and the one of $\tilde{c}$ by:

$$\tilde{c}\,(r,\theta) = \sum_{m\in\mathbb{N}} c_{cm}\,(r)\cos\,(m\theta) + \sum_{m\in\mathbb{N}} c_{sm}\,(r)\sin\,(m\theta)\,.$$

For all $m \in \mathbb{N}$ with $m \neq 1$, we have:

$$\int_{-\pi}^{\pi} \cos\,(m\theta)\cos\,(\theta) = \int_{-\pi}^{\pi} \sin\,(m\theta)\sin\,(\theta) = 0$$

and

$$\int_{-\pi}^{\pi} \cos\,(m\theta)\sin\,(\theta) = \int_{-\pi}^{\pi} \sin\,(m\theta)\cos\,(\theta) = 0.$$

We also have:

$$\int_{-\pi}^{\pi} \cos^2\,(\theta) = \int_{-\pi}^{\pi} \sin^2\,(\theta) = \pi$$

and

$$\int_{-\pi}^{\pi} \cos\,(\theta)\sin\,(\theta) = 0.$$

Thus, in particular, we have:

$$\int_{\partial N^0} \tilde{P}\mathbf{n}\,\mathrm{d}\sigma = -\pi R_{\mathrm{nucl}} \begin{pmatrix} P_{c1}\,(R_{\mathrm{nucl}}) \\ P_{s1}\,(R_{\mathrm{nucl}}) \end{pmatrix}$$

and

$$\int_{\partial\Omega} \tilde{c}\mathbf{n}\,\mathrm{d}\sigma = \pi R_0 \begin{pmatrix} c_{c1}\,(R_0) \\ c_{s1}\,(R_0) \end{pmatrix}.$$

By linearity of eq. (5.10) and independence of the cosine and sine modes, we deduce that for all $m \neq 1$, (P_{cm}, c_{cm}) and (P_{sm}, c_{sm}) satisfy:

$$\begin{cases} -\left(\partial_{rr}^2 + \dfrac{1}{r}\partial_r - \dfrac{m^2}{r^2}\right) P_m = 0 & r \in (R_{\mathrm{nucl}}, R_0)\,, \quad (5.13a) \\ -\partial_r P_m = 0 & r \in \{R_{\mathrm{nucl}}, R_0\}\,, \quad (5.13b) \\ \lambda c_m = \left(\partial_{rr}^2 + \dfrac{1}{r}\partial_r - \dfrac{m^2}{r^2}\right) c_m & r \in (R_{\mathrm{nucl}}, R_0)\,, \quad (5.13c) \\ \partial_r c_m = 0 & r \in \{R_{\mathrm{nucl}}, R_0\}\,. \quad (5.13d) \end{cases}$$

Moreover, in the case where $m = 1$, we have that (P_{c1}, c_{c1}) satisfies:

$$\begin{cases} -\left(\partial_{rr}^2 + \frac{1}{r}\partial_r - \frac{m^2}{r^2}\right) P_{c1} = 0 & r \in (R_{\text{nucl}}, R_0), \quad (5.14a) \\ -\partial_r P_{c1}(R_0) = \tilde{\mathbf{u}}_{\text{cm},x}, & (5.14b) \\ \partial_r P_{c1}(R_{\text{nucl}}) = \tilde{\mathbf{u}}_{\text{nucl},x}, & (5.14c) \\ \lambda c_{c1} = \left(\partial_{rr}^2 + \frac{1}{r}\partial_r - \frac{m^2}{r^2}\right) c_{c1} & r \in (R_{\text{nucl}}, R_0), \quad (5.14d) \\ \partial_r c_{c1}(R_0) + a\tilde{\mathbf{u}}_{\text{cm},x} c^0 = 0, & (5.14e) \\ \partial_r c_{c1}(R_{\text{nucl}}) + a\tilde{\mathbf{u}}_{\text{nucl},x} c^0 = 0, & (5.14f) \end{cases}$$

and similarly, (P_{s1}, c_{s1}) satisfies:

$$\begin{cases} -\left(\partial_{rr}^2 + \frac{1}{r}\partial_r - \frac{m^2}{r^2}\right) P_{s1} = 0 & r \in (R_{\text{nucl}}, R_0), \quad (5.15a) \\ -\partial_r P_{s1}(R_0) = \tilde{\mathbf{u}}_{\text{cm},y}, & (5.15b) \\ \partial_r P_{s1}(R_{\text{nucl}}) = \tilde{\mathbf{u}}_{\text{nucl},y}, & (5.15c) \\ \lambda c_{s1} = \left(\partial_{rr}^2 + \frac{1}{r}\partial_r - \frac{m^2}{r^2}\right) c_{s1} & r \in (R_{\text{nucl}}, R_0), \quad (5.15d) \\ \partial_r c_{s1}(R_0) + a\tilde{\mathbf{u}}_{\text{cm},y} c^0 = 0, & (5.15e) \\ \partial_r c_{s1}(R_{\text{nucl}}) + a\tilde{\mathbf{u}}_{\text{nucl},y} c^0 = 0, & (5.15f) \end{cases}$$

where $\tilde{\mathbf{u}}_{\text{nucl},x}$ and $\tilde{\mathbf{u}}_{\text{nucl},y}$ denotes the two coordinates of $\tilde{\mathbf{u}}_{\text{nucl}}$ and $\tilde{\mathbf{u}}_{\text{cm},x}$ and $\tilde{\mathbf{u}}_{\text{cm},y}$ the ones of $\tilde{\mathbf{u}}_{\text{cm}}$. We can note that $\tilde{\mathbf{u}}_{\text{cm}}$ and $\tilde{\mathbf{u}}_{\text{nucl}}$ depends only on the mode $m = 1$ which allows us to use the independence of the cosine and sine modes.

From the independence of the cosine and sine modes, we also deduce that studying the spectrum of problem (5.10) is equivalent to study the spectrum of problem (5.13) for all $m \neq 1$, (5.14) and (5.15).

For $m \neq 1$, as c_m and P_m satisfying eq. (5.13) are not coupled and the functions $(r, \theta) \mapsto c_{cm}(r)\cos(m\theta)$ and $(r, \theta) \mapsto c_{sm}(r)\sin(m\theta)$ satisfy:

$$\begin{cases} \lambda c = \Delta c & \text{in } \Omega \setminus N, \\ \nabla c \cdot \mathbf{n} = 0 & \text{on } \partial\Omega \cup \partial N, \end{cases}$$

the eigenvalue problem associated with the heat equation, the problem (5.13) only admits non positive eigenvalues.

By symmetry, we see that problems (5.14) and (5.15) are analogous. We therefore restrict our spectral study of problem (5.10) to the spectral study of the problem (5.14).

Finally, since $\tilde{P}$ satisfies the laplacian equation (5.10a), we have that for all $m \in \mathbb{N}$, there exists A_m, B_m, C_m and $D_m \in \mathbb{R}$ such that for all $r \in (R_{\text{nucl}}, R_0)$:

$$\begin{cases} P_{cm}(r) = A_m r^m + C_m r^{-m}, \\ P_{sm}(r) = B_m r^m + D_m r^{-m}. \end{cases}$$

In particular, we have $P_{c1}(R_{\text{nucl}}) = A_1 R_{\text{nucl}} + C_1 R_{\text{nucl}}^{-1}$ and thus:

$$\tilde{\mathbf{u}}_{\text{nucl},x} = -\left(A_1 + C_1 R_{\text{nucl}}^{-2}\right).$$

From the boundary conditions eqs. (5.14b) and (5.14c), it follows that:

$$\begin{cases} -\left(A_1 - \dfrac{C_1}{R_0^2}\right) = \dfrac{-\chi_c f'_{\mathrm{act}}\left(c^0\right)}{R_0} c_{c1}\left(R_0\right), \\ -\left(A_1 - \dfrac{C_1}{R_{\mathrm{nucl}}^2}\right) = -\left(A_1 + \dfrac{C_1}{R_{\mathrm{nucl}}^2}\right). \end{cases}$$

We thus have:

$$\begin{cases} A_1 = \dfrac{\chi_c f'_{\mathrm{act}}\left(c^0\right)}{R_0} c_{c1}\left(R_0\right), \\ C_1 = 0. \end{cases}$$

We can conclude that:

$$\tilde{\mathbf{u}}_{\mathrm{nucl},x} = -\frac{\chi_c f'_{\mathrm{act}}\left(c^0\right)}{R_0} c_{c1}\left(R_0\right).$$

□

Step 3. We study the spectrum of problem (5.11). The following lemma gives the form of the eigenfunctions of eq. (5.11).

Lemma 5.2.6. *Let $\lambda \in \mathbb{C}$. The eigenfunctions of eq. (5.11) associated with the eigenvalue $\lambda \in \mathbb{C}$ are given by:*

$$c\left(r\right) = \beta_\lambda J_1\left(-\mathrm{i}\lambda^{\frac{1}{2}} r\right) + \gamma_\lambda Y_1\left(-\mathrm{i}\lambda^{\frac{1}{2}} r\right), \tag{5.16}$$

where $r \in \left(R_{\mathrm{nucl}}, R_0\right)$, J_1 and Y_1 denote respectively the Bessel function of the first kind of order 1 and that of the second kind of order 1 and $\left(\beta_\lambda, \gamma_\lambda\right) \in \mathbb{C}^2$ solution of:

$$\begin{aligned} &-\mathrm{i}\lambda^{\frac{1}{2}}\left(\beta_\lambda J_1'\left(-\mathrm{i}\lambda^{\frac{1}{2}} R_0\right) + \gamma_\lambda Y_1'\left(-\mathrm{i}\lambda^{\frac{1}{2}} R_0\right)\right) \\ &\qquad = \frac{a\chi_c c^0 f'_{\mathrm{act}}\left(c^0\right)}{R_0}\left(\beta_\lambda J_1\left(-\mathrm{i}\lambda^{\frac{1}{2}} R_0\right) + \gamma_\lambda Y_1\left(-\mathrm{i}\lambda^{\frac{1}{2}} R_0\right)\right), \end{aligned} \tag{5.17}$$

and

$$\begin{aligned} &-\mathrm{i}\lambda^{\frac{1}{2}}\left(\beta_\lambda J_1'\left(-\mathrm{i}\lambda^{\frac{1}{2}} R_{\mathrm{nucl}}\right) + \gamma_\lambda Y_1'\left(-\mathrm{i}\lambda^{\frac{1}{2}} R_{\mathrm{nucl}}\right)\right) \\ &\qquad = \frac{a\chi_c c^0 f'_{\mathrm{act}}\left(c^0\right)}{R_0}\left(\beta_\lambda J_1\left(-\mathrm{i}\lambda^{\frac{1}{2}} R_0\right) + \gamma_\lambda Y_1\left(-\mathrm{i}\lambda^{\frac{1}{2}} R_0\right)\right). \end{aligned} \tag{5.18}$$

Proof. From the definition of the Bessel functions, there exists β_λ and $\gamma_\lambda \in \mathbb{C}$ such that the solutions c of eq. (5.11a) are given, for all $r \in \left(R_{\mathrm{nucl}}, R_0\right)$, by:

$$c\left(r\right) = \beta_\lambda J_1\left(-\mathrm{i}\lambda^{\frac{1}{2}} r\right) + \gamma_\lambda Y_1\left(-\mathrm{i}\lambda^{\frac{1}{2}} r\right).$$

Then the boundary condition eq. (5.11b) reads eq. (5.17) and the boundary condition eq. (5.11c) reads eq. (5.18). □

From the previous lemma we derive the following lemma giving an explicit condition on the eigenvalues of eq. (5.11).

Lemma 5.2.7. *Let $\lambda \in \mathbb{C}$ be an eigenvalue of eq. (5.11). Then λ is such that $G_1(\lambda) = 0$ with G_1 defined for all $z \in \mathbb{C}$ by:*

$$\begin{aligned} G_1(z) = z\left(J_1'\left(-\mathrm{i}z^{\frac{1}{2}}R_0\right)Y_1'\left(-\mathrm{i}z^{\frac{1}{2}}R_{\mathrm{nucl}}\right) - J_1'\left(-\mathrm{i}z^{\frac{1}{2}}R_{\mathrm{nucl}}\right)Y_1'\left(-\mathrm{i}z^{\frac{1}{2}}R_0\right)\right) \\ + \frac{\mathrm{i}z^{\frac{1}{2}}a\chi_c c^0 f'_{\mathrm{act}}(c^0)}{R}\left[J_1\left(-\mathrm{i}z^{\frac{1}{2}}R_0\right)Y_1'\left(-\mathrm{i}z^{\frac{1}{2}}R_0\right) - J_1'\left(-\mathrm{i}z^{\frac{1}{2}}R_0\right)Y_1\left(-\mathrm{i}z^{\frac{1}{2}}R_0\right)\right. \\ \left. + J_1'\left(-\mathrm{i}z^{\frac{1}{2}}R_{\mathrm{nucl}}\right)Y_1\left(-\mathrm{i}z^{\frac{1}{2}}R_0\right) - J_1\left(-\mathrm{i}z^{\frac{1}{2}}R_0\right)Y_1'\left(-\mathrm{i}z^{\frac{1}{2}}R_{\mathrm{nucl}}\right)\right]. \end{aligned}$$

Lemma 5.2.8. *If $\chi_c > \chi_c^*$, then the eigenvalue problem defined by eq. (5.11) admits an eigenvalue with a positive real part.*

Proof. Let $\lambda \in \mathbb{C}$ be an eigenvalue of the problem (5.11) From lemma 5.2.7, we have that λ is such that $G_1(\lambda) = 0$. We perform the expansion of G_1 around 0. Using the properties of the Bessel functions, for λ close to zero, we have:

$$\begin{aligned} J_1\left(-\mathrm{i}\lambda^{\frac{1}{2}}R_0\right) &= \frac{-\mathrm{i}\lambda^{\frac{1}{2}}R_0}{2} + o(\lambda), \\ J_1'\left(-\mathrm{i}\lambda^{\frac{1}{2}}R_0\right) &= \frac{1}{2} + \frac{3R_0^2\lambda}{16} + o(\lambda), \\ Y_1\left(-\mathrm{i}\lambda^{\frac{1}{2}}R_0\right) &= \frac{-2\mathrm{i}}{\pi\lambda^{\frac{1}{2}}R_0} + \frac{\mathrm{i}(1-2\gamma)\lambda^{\frac{1}{2}}R_0}{2\pi} + \frac{2}{\pi}J_1\left(-\mathrm{i}\lambda^{\frac{1}{2}}R_0\right)\log\left(\frac{-\mathrm{i}\lambda^{\frac{1}{2}}R_0}{2}\right) + o(\lambda), \\ Y_1'\left(-\mathrm{i}\lambda^{\frac{1}{2}}R_0\right) &= \frac{-2}{\lambda R_0^2\pi} + \frac{1+2\gamma}{2\pi} - \frac{R_0^2\lambda(11-12\gamma)}{32\pi} + \frac{2}{\pi}J_1'\left(-\mathrm{i}\lambda^{\frac{1}{2}}R\right)\log\left(\frac{-\mathrm{i}\lambda^{\frac{1}{2}}R}{2}\right) + o(\lambda), \end{aligned}$$

where γ denotes the Euler's constant. Thus for λ close to zero, we have:

$$\begin{aligned} G_1(\lambda) &= \left(1 - a\chi_c c^0 f'_{\mathrm{act}}(c^0)\right)\left(\frac{1}{R_0^2\pi} - \frac{1}{R_{\mathrm{nucl}}^2\pi}\right) \\ &\quad + \frac{3\left(R_{\mathrm{nucl}}^4 - R_0^4\right)}{8\pi R_0^2 R_{\mathrm{nucl}}^2}\lambda - a\chi_c c^0 f'_{\mathrm{act}}(c^0)\frac{3\left(R_0^2 - R_{\mathrm{nucl}}^2\right)}{8\pi R_0^2}\lambda \\ &\quad + \frac{a\chi_c c^0 f'_{\mathrm{act}}(c^0) - 1}{2\pi}\ln\left(\frac{R_0}{R_{\mathrm{nucl}}}\right)\lambda + o(\lambda), \\ &= g(\lambda) + o(\lambda). \end{aligned}$$

The function g admits $\lambda_1 \in \mathbb{R}$ as root with λ_1 defined by:

$$\lambda_1 = -\frac{\left(1 - a\chi_c c^0 f'_{\mathrm{act}}(c^0)\right)\left(\frac{1}{R_0^2\pi} - \frac{1}{R_{\mathrm{nucl}}^2\pi}\right)}{\frac{3\left(R_{\mathrm{nucl}}^4 - R_0^4\right)}{8\pi R_0^2 R_{\mathrm{nucl}}^2} - a\chi_c c^0 f'_{\mathrm{act}}(c^0)\frac{3\left(R_0^2 - R_{\mathrm{nucl}}^2\right)}{8\pi R_0^2} + \frac{a\chi_c c^0 f'_{\mathrm{act}}(c^0) - 1}{2\pi}\ln\left(\frac{R_0}{R_{\mathrm{nucl}}}\right)}.$$

We have:

$$\left(1 - a\chi_c c^0 f'_{\mathrm{act}}(c^0)\right)\left(\frac{1}{R_0^2\pi} - \frac{1}{R_{\mathrm{nucl}}^2\pi}\right) > 0 \iff \chi_c > \chi_c^*.$$

We also have:

$$\frac{3\left(R_{\text{nucl}}^4-R_0^4\right)}{8\pi R_0^2R_{\text{nucl}}^2}-a\chi_c c^0 f'_{\text{act}}\left(c^0\right)\frac{3\left(R_0^2-R_{\text{nucl}}^2\right)}{8\pi R_0^2}+\frac{a\chi_c c^0 f'_{\text{act}}\left(c^0\right)-1}{2\pi}\ln\left(\frac{R_0}{R_{\text{nucl}}}\right)<0$$

$$\iff\left[a\chi_c c^0 f'_{\text{act}}\left(c^0\right)<\frac{3\left(R_0^4-R_{\text{nucl}}^4\right)+4R_0^2R_{\text{nucl}}^2\ln\left(\frac{R_0}{R_{\text{nucl}}}\right)}{R_{\text{nucl}}^2\left(3\left(R_{\text{nucl}}^2-R_0^2\right)+4R_0^2\ln\left(\frac{R_0}{R_{\text{nucl}}}\right)\right)}\right.$$

$$\left.\text{and } 3\left(R_{\text{nucl}}^2-R_0^2\right)+4R_0^2\ln\left(\frac{R_0}{R_{\text{nucl}}}\right)>0\right]\text{ or } 3\left(R_{\text{nucl}}^2-R_0^2\right)+4R_0^2\ln\left(\frac{R_0}{R_{\text{nucl}}}\right)<0.$$

Moreover, if $3\left(R_{\text{nucl}}^2-R_0^2\right)+4R_0^2\ln\left(\frac{R_0}{R_{\text{nucl}}}\right)>0$ then $\frac{3\left(R_0^4-R_{\text{nucl}}^4\right)+4R_0^2R_{\text{nucl}}^2\ln\left(\frac{R_0}{R_{\text{nucl}}}\right)}{R_{\text{nucl}}^2\left(3\left(R_{\text{nucl}}^2-R_0^2\right)+4R_0^2\ln\left(\frac{R_0}{R_{\text{nucl}}}\right)\right)}>1$. Thus λ_1 changes sign from negative to positive as χ_c exceeds χ_c^*. We can note that λ_1 approximates well a root of G_1 and that we have:

$$\lambda_1=\left(a\chi_c c^0 f'_{\text{act}}\left(c^0\right)-1\right)\frac{8\left(R_0^2-R_{\text{nucl}}^2\right)}{3a\chi_c c^0 f'_{\text{act}}\left(c^0\right)\left(R_0^4+R_0^2R_{\text{nucl}}^2-2R_{\text{nucl}}^4\right)}+o\left(\left|a\chi_c c^0 f'_{\text{act}}\left(c^0\right)-1\right|\right).$$

This eigenvalue is associated with the non-trivial eigenfunction:

$$c\left(r\right)=\beta_{\lambda_1}J_1\left(-\mathrm{i}\lambda_1^{\frac{1}{2}}r\right)+\gamma_{\lambda_1}Y_1\left(-\mathrm{i}\lambda_1^{\frac{1}{2}}r\right),$$

with

$$\beta_{\lambda_1}=\mathrm{i}\lambda_1^{\frac{1}{2}}Y_1'\left(-\mathrm{i}\lambda_1^{\frac{1}{2}}R_0\right)+\frac{a\chi_c c^0 f'_{\text{act}}\left(c^0\right)}{R_0}Y_1\left(-\mathrm{i}\lambda_1^{\frac{1}{2}}R_0\right),$$

$$\gamma_{\lambda_1}=-\left(\mathrm{i}\lambda_1^{\frac{1}{2}}J_1'\left(-\mathrm{i}\lambda_1^{\frac{1}{2}}R_0\right)+\frac{a\chi_c c^0 f'_{\text{act}}\left(c^0\right)}{R_0}J_1\left(-\mathrm{i}\lambda_1^{\frac{1}{2}}R_0\right)\right).$$

□

From the lemma 5.2.8, we deduce that when $\chi_c>\chi_c^*$, the eigenvalue problem defined by eq. (5.10) admits an eigenvalue with a positive real part and thus the stationary state is linearly unstable.

To conclude the proof of the theorem, we need to show that when $\chi_c<\chi_c^*$ all the eigenvalues associated to (5.11) have negative real part. We give only a graphical illustration here. For several values of R_0, R_{nucl} and $\frac{\chi_c}{\chi_c^*}$, we represent the function G_1 by representing its real part, its imaginary part and its modulus (see fig. 5.1 for an example). We then observe that the root of G_1 with the largest real part seems to be a real root of G_1, which is confirmed by studying the imaginary part of G_1. Indeed, we notice that if $\lambda\in\mathbb{R}$ then $G_1\left(\lambda\right)\in\mathbb{R}$.

We can therefore restrict the graphical study of G_1 to the graphical study of G_1 when $\lambda\in\mathbb{R}$. For R_0 and R_{nucl} fixed and for different values of $\frac{\chi_c}{\chi_c^*}$, we plot G_1 as a function of $\lambda\in\mathbb{R}$ (see fig. 5.2). This allows us to observe the largest real root of G_1 and we notice that when $\chi_c<\chi_c^*$ then this one is negative.

Moreover, we observe numerically that as soon as $\chi_c<\chi_c^*$ then the stationary state is stable, this will be illustrated in section 5.4.1.

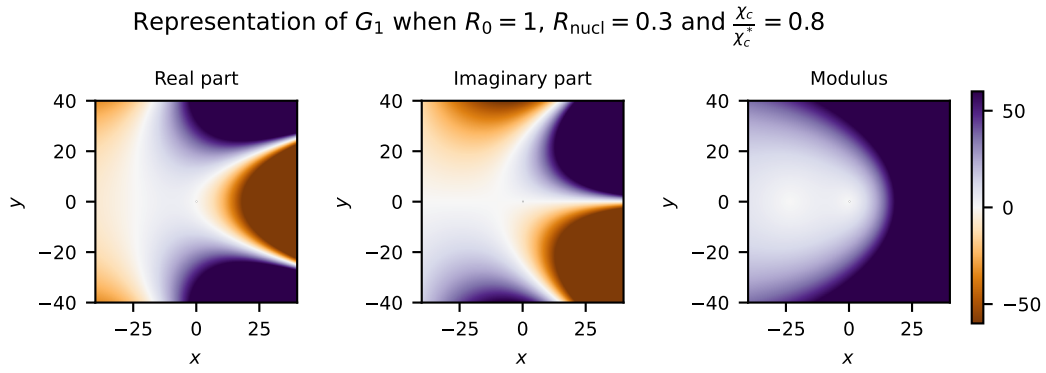

Figure 5.1: **Representation of G_1 in the complex framework for $R_0 = 1$, $R_{\text{nucl}} = 0.3$ and $\frac{\chi_c}{\chi_c^*} = 0.8$.** *Plots of the real part (left), the imaginary part (middle) and the modulus (right) of the function G_1 for $\lambda = x + \mathrm{i}y \in \mathbb{C}$ with $x, y \in [-40, 40]$. We observe that the root of G_1 with the greatest real part is a real root.*

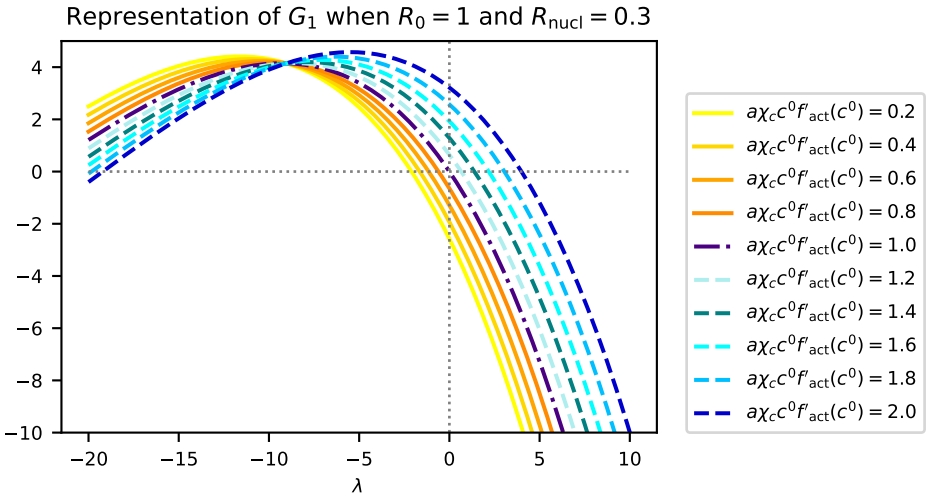

Figure 5.2: **Graphs of $\lambda \mapsto G_1(\lambda)$ for $\lambda \in \mathbb{R}$ when $R_0 = 1$ and $R_{\text{nucl}} = 0.3$ for different values of $\frac{\chi_c}{\chi_c^*} = a\chi_c c^0 f'\left(c^0\right)$.** *Each curve corresponds to a different value of χ_c. The solid yellow-orange curves correspond to the case where $\chi_c < \chi_c^*$, the dashed blue curves correspond to the case where $\chi_c > \chi_c^*$ and the dark dashdotted curve corresponds to the case where $\chi_c = 1\chi_c^*$. The grey dotted lines are the lines of equation $\lambda = 0$ and $y = 0$. In the case where $\chi_c < \chi_c^*$ we notice that G_1 seems to admit no positive root.*

5.3 . Finite element scheme of the rigid model

In this section we write a finite element scheme to run simulations of the rigid model eq. (5.3). The proposed scheme is based on a semi-implicit discretization in time and a discretisation in space using a finite element method.

5.3.1 . Time discretization

We discretize in time our model eq. (5.3). Let Δt be the time step. For $i \in \{0, \dots, N_f\}$ with $N_f \in \mathbb{N}$, we denote $t^i = i\Delta t$, $\mathbf{u}^i = \mathbf{u}\left(t^i, \cdot\right)$, $P^i = P\left(t^i, \cdot\right)$ and $c^i = c\left(t^i, \cdot\right)$. We also denote $\Omega^i = \Omega\left(t^i\right)$ and $N^i = N\left(t^i\right)$. In addition, we denote $\mathbf{f}^i_{\mathrm{BN}}$ the force induced by the boundary onto the nucleus associated with the cell geometry at time t^i and anagously we denote f^i_{NB} the force induced by the nucleus on a point of $\partial\Omega^i$ at time t^i.

The implicit discretization of the problem about velocities is given by:

$$\begin{cases} \mathbf{u}^{i+1} + \nabla P^{i+1} = 0 & \text{in } \Omega^i \setminus N^i, \quad (5.19a) \\ \operatorname{div}\left(\mathbf{u}^{i+1}\right) = 0 & \text{in } \Omega^i \setminus N^i, \quad (5.19b) \\ \mathbf{u}^{i+1} \cdot \mathbf{n} = \mathbf{u}^{i+1}_{\mathrm{cm}} \cdot \mathbf{n} & \text{on } \partial\Omega^i, \quad (5.19c) \\ \mathbf{u}^{i+1} \cdot \mathbf{n} = \mathbf{u}^{i+1}_{\mathrm{nucl}} \cdot \mathbf{n} & \text{on } \partial N^i, \quad (5.19d) \\ \mathbf{u}^{i+1}_{\mathrm{nucl}} = \dfrac{1}{\xi_{\mathrm{nucl}} \left|N^i\right|} \displaystyle\int_{\partial N^i} P^{i+1} \mathbf{n} \, \mathrm{d}\sigma, & (5.19e) \\ \mathbf{u}^{i+1}_{\mathrm{cm}} = \dfrac{-1}{\left|\Omega^i\right|} \displaystyle\int_{\partial\Omega^i} \chi_c f_{\mathrm{act}}\left(c^i\right) \mathbf{n} \, \mathrm{d}\sigma + \dfrac{\left|N^i\right|}{\left|\Omega^i\right|} \left(1 - \xi_{\mathrm{nucl}}\right) \mathbf{u}^{i+1}_{\mathrm{nucl}}, & (5.19f) \end{cases}$$

and

$$\begin{cases} \dfrac{c^{i+1} - c^i}{\Delta t} = \operatorname{div}\left(\nabla c^{i+1} - (1-a)\, \mathbf{u}^{i+1} c^{i+1} - \alpha \dot{W}^{Q,i} c^{i+1}\right) & \text{in } \Omega^i \setminus N^i, \quad (5.20a) \\ \left(\nabla c^{i+1} + a \mathbf{u}^{i+1} c^{i+1} - \alpha \dot{W}^{Q,i} c^{i+1}\right) \cdot \mathbf{n} = 0 & \text{on } \partial\Omega^i \cup \partial N^i, \quad (5.20b) \end{cases}$$

with

$$\begin{cases} \Omega^{i+1} = \left(\mathrm{Id} + \Delta t\, \mathbf{u}^{i+1}_{\mathrm{cm}}\right)\left(\Omega^i\right), & (5.21a) \\ N^{i+1} = \left(\mathrm{Id} + \Delta t\, \mathbf{u}^{i+1}_{\mathrm{nucl}}\right)\left(N^i\right). & (5.21b) \end{cases}$$

5.3.2 . Decomposition of the fluid problem

We focus on the fluid velocity and pressure eq. (5.19). Instead to solve numerically this problem (5.19), we solve the following:

$$\begin{cases} -\Delta P^{i+1} = 0 & \text{in } \Omega^i \setminus N^i, \quad (5.22a) \\ -\nabla P^{i+1} \cdot \mathbf{n} = \mathbf{u}^{i+1}_{\mathrm{cm}} \cdot \mathbf{n} & \text{on } \partial\Omega^i, \quad (5.22b) \\ -\nabla P^{i+1} \cdot \mathbf{n} = \mathbf{u}^{i+1}_{\mathrm{nucl}} \cdot \mathbf{n} & \text{on } \partial N^i, \quad (5.22c) \end{cases}$$

with

$$\mathbf{u}^{i+1}_{\mathrm{nucl}} = \frac{1}{\xi_{\mathrm{nucl}} \left|N^i\right|} \int_{\partial N^i} P^{i+1} \mathbf{n} \, \mathrm{d}\sigma$$

and

$$\mathbf{u}^{i+1}_{\mathrm{cm}} = \frac{-1}{\left|\Omega^i\right|} \int_{\partial\Omega^i} \chi_c f_{\mathrm{act}}\left(c^i\right) \mathbf{n} \, \mathrm{d}\sigma + \frac{\left|N^i\right|}{\left|\Omega^i\right|} \left(1 - \xi_{\mathrm{nucl}}\right) \mathbf{u}^{i+1}_{\mathrm{nucl}}.$$

We then set $\mathbf{u}^{i+1} = -\nabla P^{i+1}$. We decompose eq. (5.22) in four independent problems to separate the boundary conditions on $\partial\Omega^i$ and ∂N^i. We define as follows the four problems:

$$\begin{cases} -\Delta P_1 = 0 & \text{in } \Omega^i \setminus N^i, \quad (5.23a) \\ \nabla P_1 \cdot \mathbf{n} = n_x & \text{on } \partial\Omega^i, \quad (5.23b) \\ \nabla P_1 \cdot \mathbf{n} = 0 & \text{on } \partial N^i, \quad (5.23c) \end{cases}$$

$$\begin{cases} -\Delta P_2 = 0 & \text{in } \Omega^i \setminus N^i, \quad (5.24a) \\ \nabla P_2 \cdot \mathbf{n} = n_y & \text{on } \partial\Omega^i, \quad (5.24b) \\ \nabla P_2 \cdot \mathbf{n} = 0 & \text{on } \partial N^i, \quad (5.24c) \end{cases}$$

$$\begin{cases} -\Delta P_3 = 0 & \text{in } \Omega^i \setminus N^i, \quad (5.25a) \\ \nabla P_3 \cdot \mathbf{n} = 0 & \text{on } \partial\Omega\left(t\right), \quad (5.25b) \\ \nabla P_3 \cdot \mathbf{n} = n_x & \text{on } \partial N^i, \quad (5.25c) \end{cases}$$

$$\begin{cases} -\Delta P_4 = 0 & \text{in } \Omega^i \setminus N^i, \quad (5.26a) \\ \nabla P_4 \cdot \mathbf{n} = 0 & \text{on } \partial\Omega\left(t\right), \quad (5.26b) \\ \nabla P_4 \cdot \mathbf{n} = n_y & \text{on } \partial N^i, \quad (5.26c) \end{cases}$$

where n_x and n_y are the coordinates of the normal outward vector of $\Omega^i \setminus N^i$.

We want to find μ_1, μ_2, μ_3 and $\mu_4 \in \mathbb{R}$ such that $P^{i+1} = \mu_1 P_1 + \mu_2 P_2 + \mu_3 P_3 + \mu_4 P_4$ with P_1, p_2, P_3 and P_4 respectively solutions to eqs. (5.23) to (5.26). This is equivalent to find $\boldsymbol{\mu} = (\mu_1, \mu_2, \mu_3, \mu_4)^T$ such that $A_\mu \boldsymbol{\mu} = B_\mu$ where A_μ is the following matrix

$$A_\mu = \begin{pmatrix} 1 + \frac{1-\xi_{\text{nucl}}}{\xi_{\text{nucl}}|\Omega^i|} P_1^x & \frac{1-\xi_{\text{nucl}}}{\xi_{\text{nucl}}|\Omega^i|} P_2^x & \frac{1-\xi_{\text{nucl}}}{\xi_{\text{nucl}}|\Omega^i|} P_3^x & \frac{1-\xi_{\text{nucl}}}{\xi_{\text{nucl}}|\Omega^i|} P_4^x \\ \frac{1-\xi_{\text{nucl}}}{\xi_{\text{nucl}}|\Omega^i|} P_1^y & 1 + \frac{1-\xi_{\text{nucl}}}{\xi_{\text{nucl}}|\Omega^i|} P_2^y & \frac{1-\xi_{\text{nucl}}}{\xi_{\text{nucl}}|\Omega^i|} P_3^y & \frac{1-\xi_{\text{nucl}}}{\xi_{\text{nucl}}|\Omega^i|} P_4^y \\ \frac{1}{\xi_{\text{nucl}}|N^i|} P_1^x & \frac{1}{\xi_{\text{nucl}}|N^i|} P_2^x & 1 + \frac{1}{\xi_{\text{nucl}}|N^i|} P_3^x & \frac{1}{\xi_{\text{nucl}}|N^i|} P_4^x \\ \frac{1}{\xi_{\text{nucl}}|N^i|} P_1^y & \frac{1}{\xi_{\text{nucl}}|N^i|} P_2^y & \frac{1}{\xi_{\text{nucl}}|N^i|} P_3^y & 1 + \frac{1}{\xi_{\text{nucl}}|N^i|} P_4^y \end{pmatrix} \quad (5.27)$$

and B the following vector

$$B_\mu = \begin{pmatrix} \frac{1}{|\Omega^i|} \int_{\partial\Omega^i} \chi_c f_{\text{act}}\left(c^i\right) n_x \, \mathrm{d}\sigma \\ \frac{1}{|\Omega^i|} \int_{\partial\Omega^i} \chi_c f_{\text{act}}\left(c^i\right) n_y \, \mathrm{d}\sigma \\ 0 \\ 0 \end{pmatrix} \quad (5.28)$$

with $P_j^x = \int_{\partial N^i} P_j \, n_x \, \mathrm{d}\sigma$ and $P_j^y = \int_{\partial N^i} P_j \, n_y \, \mathrm{d}\sigma$ for $j \in \{1, 2, 3, 4\}$ and $\mathbf{f}_{\text{BN},x}^i$, $\mathbf{f}_{\text{BN},y}^i$ the coordinates of $\mathbf{f}_{\text{BN}}^i$.

5.3.3 . Spatial discretization

We discretize in space our time-discrete model eqs. (5.19) to (5.21). We use a finite element discretization. Let $\mathcal{T}$ be a triangulation of $\Omega^i \setminus N^i$. For all triangle $K \in \mathcal{T}$ we note $\left(\lambda_1^K, \lambda_2^K, \lambda_3^K\right)$ the barycentric coordinate functions of K. First we define the functional spaces needed. Let $\mathbb{P}_k$ be the set of polynomials of $\mathbb{R}^2$ of degrees less or equal k. Let $\mathcal{H}_P$ be the functional space define by:

$$\mathcal{H}_P = \left\{ Q \in H^1\left(\Omega^i \setminus N^i\right) \mid \forall K \in \mathcal{T}, Q|_K \in \mathbb{P}_1 \right\}.$$

Let $\mathcal{H}_c$ be the functional space define by:

$$\mathcal{H}_c = \left\{ \psi \in H^1\left(\Omega^i \setminus N^i\right) \mid \forall K \in \mathcal{T}, \psi|_K \in \mathbb{P}_1 \oplus \text{Span}\left\{\lambda_1^K, \lambda_2^K, \lambda_3^K\right\} \right\}.$$

5.3.4 . Variational formulation of the fluid problem

Instead of writing the variational formulation of eq. (5.19), we use the decomposition result and write the variational formulation of the four independent problems eqs. (5.23) to (5.26).

The variational formulation of the problem eq. (5.23) is given by:

$$\begin{cases} \text{Find } P_1 \in \mathcal{H}_P \text{ such that for all } Q \in \mathcal{H}_P, \text{ we have:} \\ \displaystyle\int_{\Omega^i \setminus N^i} \nabla P_1 \cdot \nabla Q \, \mathrm{d}\mathbf{x} - \int_{\partial\Omega^i} Q n_x \, \mathrm{d}\sigma = 0. \end{cases} \tag{5.29}$$

The variational formulation of the problem eq. (5.24) is given by:

$$\begin{cases} \text{Find } P_2 \in \mathcal{H}_P \text{ such that for all } Q \in \mathcal{H}_P, \text{ we have:} \\ \displaystyle\int_{\Omega^i \setminus N^i} \nabla P_2 \cdot \nabla Q \, \mathrm{d}\mathbf{x} - \int_{\partial\Omega^i} Q n_y \, \mathrm{d}\sigma = 0. \end{cases} \tag{5.30}$$

The variational formulation of the problem eq. (5.25) is given by:

$$\begin{cases} \text{Find } P_3 \in \mathcal{H}_P \text{ such that for all } Q \in \mathcal{H}_P, \text{ we have:} \\ \displaystyle\int_{\Omega^i \setminus N^i} \nabla P_3 \cdot \nabla Q \, \mathrm{d}\mathbf{x} - \int_{\partial N^i} Q n_x \, \mathrm{d}\sigma = 0. \end{cases} \tag{5.31}$$

The variational formulation of the problem eq. (5.26) is given by:

$$\begin{cases} \text{Find } P_3 \in \mathcal{H}_P \text{ such that for all } Q \in \mathcal{H}_P, \text{ we have:} \\ \displaystyle\int_{\Omega^i \setminus N^i} \nabla P_3 \cdot \nabla Q \, \mathrm{d}\mathbf{x} - \int_{\partial N^i} Q n_y \, \mathrm{d}\sigma = 0. \end{cases} \tag{5.32}$$

5.3.5 . Discretization of the noise

The discretization of the noise is based on the method developed in Boulakia et al. (2015). Instead of simulating $\dot{W}_t^Q$ over its entire domain of definition, we want to restrict its simulation to the current fluid domain. We recall that $\dot{W}^{Q,i}$ denotes an approximation of the coloured noise at time t^i, $i \in \{1, \ldots, N_f\}$. We set:

$$\dot{W}^{Q,i} = \frac{W_{t^i}^Q - W_{t^{i-1}}^Q}{\Delta t}.$$

From the definition of W_t^Q, we know that $\dot{W}^{Q,i}$ is equal in law to $\frac{1}{\sqrt{\Delta t}} W_1^Q$ and that the $\left\{\dot{W}^{Q,i}\right\}_{1 \leq i \leq N_f}$ are independent. Therefore, to simulate $\dot{W}^{Q,i}$, we simulate $W_1^{Q,i}$. For all i, $W_1^{Q,i}$ is a realisation of the Q-Wiener process at time t^i restricted to the discrete current fluid domain $\Omega^i \setminus N^i$.

A way to compute $W_1^{Q,i} = \left(\omega_1^i, \omega_2^i\right)$, the discrete noise, relies on the computation of a covariance matrix (Boulakia et al., 2015). The computation of the covariance matrix is restricted to the computation of the covariance matrix restricted to the current domain. At time t^i, let $\left\{P_j^i, 1 \leq j \leq N_h^i\right\}$ be the set of all the nodes of the triangulation $\mathcal{T}_h^i$ of $\Omega^i \setminus N^i$, where N_h^i is the number of nodes of the triangulation, and $\left\{\psi_j^i, 1 \leq j \leq N_h^i\right\}$ be a basis of the Lagrangian $P1$

finite element. ψ_j^i is a continuous affine function on $\Omega^i \setminus N^i$ such that for all $1 \leq j,k \leq N_h^i$, we have $\psi_j^i\left(P_k^i\right) = \delta_{jk}$. For $m \in \{1,2\}$, the $P1$ discretization of ω_m^i is given by

$$\omega_m^i = \sum_{j=1}^{N_h^i} x_j^i \psi_j^i.$$

with $\left\{x_j^i, 1 \leq j \leq N_h^i\right\}$ a realisation of a centred Gaussian vector of covariance matrix Σ^i. We have $\Sigma^i = \left(q\left(P_j^i, P_k^i\right)\right)_{1\leq j,k\leq N_h^i}$. Let X be a centred Gaussian vector of covariance matrix Σ^i. We have

$$X = S^i Y,$$

with Y a Gaussian vector such that for all $1 \leq j \leq N_h^i$, $Y_j \sim \mathcal{N}(0,1)$ and S^i such that $\Sigma^i = S^i\left(S^i\right)^T$. Thus to compute $W_1^{Q,i}$, we just have to simulate a realization of a standard Gaussian vector and to compute the Cholesky decomposition S^i of the covariance matrix Σ^i. Note that since the domain is deformable, the space-dependent Σ^i matrix is time-dependent and must be computed along with its Cholesky decomposition S^i at each time step.

5.3.6 . Discretization of the concentration problem

At each step of the numerical simulations, the mesh is propagating with the velocity $\mathbf{u}_{\text{mesh}}$ which satisfies:

$$\begin{cases} \Delta \mathbf{u}_{\text{mesh}} = 0 & \text{in } \Omega^i \setminus N^i, \\ \mathbf{u}_{\text{mesh}} = \mathbf{u}_{\text{cm}}^{i+1} & \text{on } \partial\Omega^i, \\ \mathbf{u}_{\text{mesh}} = \mathbf{u}_{\text{nucl}}^{i+1} & \text{on } \partial N^i. \end{cases}$$

Thus the mesh propagation induces advection at velocity $\mathbf{u}_{\text{mesh}}$ of the markers concentration. Taking it into account leads to modify the discrete concentration problem eq. (5.20) as follows:

$$\begin{cases} \dfrac{c^{i+1}-c^i}{\Delta t} + (1-a)\,\mathbf{u}^{i+1}\cdot\nabla c^{i+1} - \dfrac{\alpha}{\sqrt{\Delta t}} W_1^{Q,i} c^{i+1} \\ \qquad\qquad - \mathbf{u}_{\text{mesh}}\cdot\nabla c^{i+1} - \Delta c^{i+1} = 0 & \text{in } \Omega^i \setminus N^i, \quad (5.33a) \\ \left(\nabla c^{i+1} + a c^{i+1}\mathbf{u}^{i+1} - \alpha \dot{W}^{Q,i+1} c^{i+1}\right)\cdot \mathbf{n} = 0 & \text{on } \partial\Omega^i \cup \partial N^i. \quad (5.33b) \end{cases}$$

The variational formulation of eq. (5.33) is given by:

$$\begin{cases} \text{Find } c^{i+1} \in \mathcal{H}_c \text{ such that for all } \psi \in \mathcal{H}_c, \text{ we have:} \\ \displaystyle\int_{\Omega^i\setminus N^i} \left(\frac{c^{i+1}-c^i}{\Delta t}\right)\psi \,\mathrm{d}\mathbf{x} + \int_{\Omega^i\setminus N^i} \operatorname{div}\left(\mathbf{u}_{\text{mesh}}\right) c^{i+1}\psi \,\mathrm{d}\mathbf{x} \\ \qquad - \displaystyle\int_{\Omega^i\setminus N^i} \left((1-a)\,\mathbf{u}^{i+1}c^{i+1} - \mathbf{u}_{\text{mesh}} c^{i+1} - \nabla c^{i+1}\right)\cdot\nabla\psi \,\mathrm{d}\mathbf{x} \\ \qquad + \displaystyle\int_{\Omega^i\setminus N^i} \frac{\alpha}{\sqrt{\Delta t}} c^{i+1} W_1^{Q,i}\cdot\nabla\psi \,\mathrm{d}\mathbf{x} = 0. \end{cases} \quad (5.34)$$

5.3.7 . Avoid contact between cell boundary and particle

The discretization steps described above can be used to simulate eq. (5.3). However, these steps do not ensure that the particle remains inside the cell. To ensure this, we add a step to

the computation of the cell and nucleus velocities. Using a Uzawa algorithm, we project the velocities of the cell and the nucleus onto a space of so-called admissible velocities, chosen to ensure that the nucleus and the boundary of the cell are not in contact. The numerical scheme used to simulate eq. (5.3) is given by the following algorithm.

Algorithm 5.1 : Numerical scheme to simulate eq. (5.3) obtained after time discretization and space discretization with a finite element method.

1. Initialisation: $c^0 = c^{\text{in}}$ the given initial condition and definition of the mesh with Ω^0 and N^0 given.
2. Time iteration:
   (a) Compute $\mathbf{u}^{i+1}$ and P^{i+1} using c^i and the decomposition method:
      i. Solve the variational formulation eq. (5.29) to compute P_1.
      ii. Solve the variational formulation eq. (5.30) to compute P_2.
      iii. Solve the variational formulation eq. (5.31) to compute P_3.
      iv. Solve the variational formulation eq. (5.32) to compute P_4.
      v. Compute $\boldsymbol{\mu} = (\mu_1, \mu_2, \mu_3, \mu_4)^T$ by solving $A_\mu \boldsymbol{\mu} = B_\mu$ with A_μ given by eq. (5.27) and B_μ given by eq. (5.28).
      vi. Deduce $P^{i+1} = \mu_1 P_1 + \mu_2 P_2 + \mu_3 P_3 + \mu_4 P_4$ and compute $\mathbf{u}^{i+1} = -\nabla P^{i+1}$.
   (b) Computation of the *a priori* nucleus velocity: $\mathbf{u}_{\text{nucl}}^{i+\frac{1}{2}} = \dfrac{1}{\xi_{\text{nucl}} |N^i|} \displaystyle\int_{\partial N^i} P^{i+1} \mathbf{n} \, \mathrm{d}\sigma$.
   (c) Computation of the *a priori* cell velocity:
   $\mathbf{u}_{\text{cm}}^{i+\frac{1}{2}} = \dfrac{-1}{|\Omega^i|} \displaystyle\int_{\partial \Omega^i} \chi_c f_{\text{act}} \left(c^i\right) \mathbf{n} \, \mathrm{d}\sigma + \dfrac{|N^i|}{|\Omega^i|} \left(1 - \xi_{\text{nucl}}\right) \mathbf{u}_{\text{nucl}}^{i+1}$.
   (d) Using a Uzawa algorithm, computation of $\mathbf{u}_{\text{nucl}}^{i+1}$ and $\mathbf{u}_{\text{cm}}^{i+1}$ which are the projection of the *a priori* velocities $\mathbf{u}_{\text{nucl}}^{i+\frac{1}{2}}$ and $\mathbf{u}_{\text{cm}}^{i+\frac{1}{2}}$ on an admissible velocities space (see algorithm 5.2 for more details).
   (e) Computation of the mesh velocity $\mathbf{u}_{\text{mesh}}$.
   (f) Computation of the covariance matrix Σ^i and S^i its Cholesky decomposition and deduction of the discrete noise $W_1^{Q,i} = S^i Y$ where Y a realisation of a standard normal Gaussian vector.
   (g) Computation of the markers concentration c^{i+1} using $\mathbf{u}^{i+1}$, $W_1^{Q,i}$ and $\mathbf{u}_{\text{mesh}}$ by solving the variational formulation eq. (5.34).
   (h) Update of the domain:

$$\Omega^{i+1} = \left(\mathrm{Id} + \Delta t \, \mathbf{u}_{\text{mesh}}\right) \left(\Omega^i\right),$$
$$N^{i+1} = \left(\mathrm{Id} + \Delta t \, \mathbf{u}_{\text{mesh}}\right) \left(N^i\right)$$

Next, we give details concerning Uzawa's algorithm for handling the potential contact between the cell boundary and the nucleus. Let $i \in \{0, \ldots, N_f\}$. We denote by $\mathbf{X} = \left(\mathbf{x}_{\text{nucl}}^i, \mathbf{x}_{\text{cell}}^i\right)$ the vector with the coordinate of the particle and cell centres at time t^i. The distance $D\left(\mathbf{X}\right)$ between the particle and the cell boundary is given by:

$$D\left(\mathbf{X}\right) = R_0 - R_{\text{nucl}} - \left|\mathbf{x}_{\text{nucl}}^i - \mathbf{x}_{\text{cell}}^i\right|.$$

The gradient G of the distance D is given by:

$$G(\mathbf{X}) = (-\mathbf{e}(\mathbf{X}), \mathbf{e}(\mathbf{X})),$$

where $\mathbf{e}(\mathbf{X}) = \dfrac{\mathbf{x}_{\text{nucl}}^{i+\frac{1}{2}} - \mathbf{x}_{\text{cell}}^{i}}{\left|\mathbf{x}_{\text{nucl}}^{i} - \mathbf{x}_{\text{cell}}^{i}\right|}$. Let $\mathbf{V} = \left(\mathbf{u}_{\text{nucl}}^{i+\frac{1}{2}}, \mathbf{u}_{\text{cm}}^{i+\frac{1}{2}}\right)$ be the vector containing the velocities of the particle and the cell. The vector $\mathbf{V}$ is said to be admissible if the velocities $\mathbf{u}_{\text{nucl}}^{i+\frac{1}{2}}$ and $\mathbf{u}_{\text{cm}}^{i+\frac{1}{2}}$ ensure that, at the next time step, the nucleus and the boundary of the cell are not in contact. This condition is expressed as:

$$D(\mathbf{X} + \Delta t\, \mathbf{V}) \geq \varepsilon,$$

with $\varepsilon > 0$ small. By linearising this condition, it can be approximated by:

$$D(\mathbf{X}) + \Delta t G(\mathbf{X}) \cdot \mathbf{V} \geq \varepsilon.$$

From this linearized condition and the expression of the gradient G, we derive a space of admissible velocities defined by:

$$\mathcal{K}(\mathbf{X}) = \left\{(\mathbf{v}_n, \mathbf{v}_c) \in \mathbb{R}^2 \times \mathbb{R}^2 \text{ s.t. } \Delta t\left(\mathbf{e}(\mathbf{X}) \cdot \mathbf{v}_n - \mathbf{e}(\mathbf{X}) \cdot \mathbf{v}_c\right) \leq D(\mathbf{X}) - \varepsilon\right\}.$$

Let $\left(\mathbf{u}_{\text{nucl}}^{i+1}, \mathbf{u}_{\text{cm}}^{i+1}\right)$ be the projection of $\mathbf{V}$ onto $\mathcal{K}(\mathbf{X})$. Then $\left(\mathbf{u}_{\text{nucl}}^{i+1}, \mathbf{u}_{\text{cm}}^{i+1}\right)$ satifies the following minimisation problem:

$$\begin{aligned}\left|\left(\mathbf{u}_{\text{nucl}}^{i+1}, \mathbf{u}_{\text{cm}}^{i+1}\right)\right|^2 - 2\left\langle \left(\mathbf{u}_{\text{nucl}}^{i+1}, \mathbf{u}_{\text{cm}}^{i+1}\right), \left(\mathbf{u}_{\text{nucl}}^{i+\frac{1}{2}}, \mathbf{u}_{\text{cm}}^{i+\frac{1}{2}}\right)\right\rangle \\ = \min_{(\mathbf{v}_n, \mathbf{v}_c) \in \mathcal{K}(\mathbf{X})} \left(\left|(\mathbf{v}_n, \mathbf{v}_c)\right|^2 - 2\left\langle (\mathbf{v}_n, \mathbf{v}_c), \left(\mathbf{u}_{\text{nucl}}^{i+\frac{1}{2}}, \mathbf{u}_{\text{cm}}^{i+\frac{1}{2}}\right)\right\rangle\right)\end{aligned}$$

It follows that there exists $\lambda \geq 0$ such that $\left(\mathbf{u}_{\text{nucl}}^{i+1}, \mathbf{u}_{\text{cm}}^{i+1}\right)$ satisfies (Lefebvre, 2007):

$$\begin{cases} 2\left(\mathbf{u}_{\text{nucl}}^{i+1}, \mathbf{u}_{\text{cm}}^{i+1}\right) + \lambda\left(\Delta t\, \mathbf{e}(\mathbf{X}), -\Delta t\, \mathbf{e}(\mathbf{X})\right) = 2\left(\mathbf{u}_{\text{nucl}}^{i+\frac{1}{2}}, \mathbf{u}_{\text{cm}}^{i+\frac{1}{2}}\right), \\ \Delta t\left(\mathbf{e}(\mathbf{X}) \cdot \mathbf{u}_{\text{nucl}}^{i+1} - \mathbf{e}(\mathbf{X}) \cdot \mathbf{u}_{\text{cm}}^{i+1}\right) \leq D(\mathbf{X}) - \varepsilon, \\ \lambda\left(\Delta t\left(\mathbf{e}(\mathbf{X}) \cdot \mathbf{u}_{\text{nucl}}^{i+1} - \mathbf{e}(\mathbf{X}) \cdot \mathbf{u}_{\text{cm}}^{i+1}\right) - D(\mathbf{X}) + \varepsilon\right) = 0. \end{cases}$$

To solve this dual problem, we use a Uzawa algorithm, which is a projected fixed-step gradient descent algorithm. The algorithm used is described in algorithm 5.2.

Algorithm 5.2 : Uzawa algorithm for projecting particle and cell velocities to ensure no contact between the cell boundary and the particle.

Assume $\mathbf{u}_{\text{nucl}}^{i+\frac{1}{2}}$ and $\mathbf{u}_{\text{cm}}^{i+\frac{1}{2}}$ given.

1. Let $\mathbf{v}_n^0 \in \mathbb{R}^2$ and $\mathbf{v}_c^0 \in \mathbb{R}^2$. Let $\lambda^0 \geq 0$. Let $\eta > 0$ small and $\rho > 0$ a projection step.
2. While $\left|\left(\mathbf{v}_n^{k+1}, \mathbf{v}_c^{k+1}\right) - \left(\mathbf{v}_n^k, \mathbf{v}_c^k\right)\right| > \eta$ or $\left|\lambda^{k+1} - \lambda^k\right| > \eta$ do:
   (a) $\mathbf{v}_n^{k+1} = \mathbf{u}_{\text{nucl}}^{i+\frac{1}{2}} - \frac{1}{2}\lambda^k \Delta t\, \mathbf{e}\left(\mathbf{X}\right)$.
   (b) $\mathbf{v}_c^{k+1} = \mathbf{u}_{\text{cm}}^{i+\frac{1}{2}} + \frac{1}{2}\lambda^k \Delta t\, \mathbf{e}\left(\mathbf{X}\right)$.
   (c) $\lambda^{k+1} = \Pi_{\mathbb{R}_+}\left[\lambda^k + \rho\left(\Delta t\, \left(\mathbf{e}\left(\mathbf{X}\right) \cdot \mathbf{v}_n^{k+1} - \mathbf{e}\left(\mathbf{X}\right) \cdot \mathbf{v}_c^{k+1}\right) - D\left(\mathbf{X}\right) + \varepsilon\right)\right]$.
3. Update of the particle and the cell velocities:

$$\mathbf{u}_{\text{nucl}}^{i+1} = \mathbf{v}_n^{k+1}$$

and

$$\mathbf{u}_{\text{cm}}^{i+1} = \mathbf{v}_c^{k+1}.$$

5.4 . Numerical results

In this section, after checking that the proposed numerical scheme is consistent with the study of the model, we illustrate that numerically the model makes it possible to obtain the three types of trajectories: persistent, Brownian and intermittent. The numerical scheme is implemented using FreeFEM++ (Hecht, 2012).

5.4.1 . Numerical verification

In this section, we check that the numerical scheme proposed in algorithm 5.1 is consistent with the mathematical study of the model. We therefore check that if $\alpha = 0$ then we recover the stationary state (5.6) as well as the result on the stability of the latter stated in theorem 5.2.3.

First, we check that the numerical scheme captures the stationary state. We then set a time step Δt, then R_0 and R_{nucl} in order to define the geometry of the cell, and we choose as the initial condition for the markers concentration $c^0\left(\mathbf{x}\right) = \dfrac{M}{|\Omega \setminus N|}$.

In this case, we observe that whatever the values of R_0, R_{nucl} and χ_c, we find a stationary state (see fig. 6.5 for an example). Indeed, the velocity of the cell remains zero over time and the position of the nucleus at the centre of the cell is maintained. We also observe that the distribution of markers is weel conserved over time.Moreover, we can observe that the quantity of markers is well conserved over time (see fig. 5.3 right), which is in agreement with eq. (5.4) (see fig. 5.4).

Secondly, we check that the numerical scheme gives results in accordance with theorem 5.2.3. We therefore study the linear stability of the stationary state numerically. To do this, we choose a perturbation of the stationary state as the initial condition and observe, depending on the value of χ_c, whether the system returns to the stationary state. In accordance with remark 5.1.1, we only consider stationary state perturbations where only the marker distribution is perturbed and not the position of the nucleus.

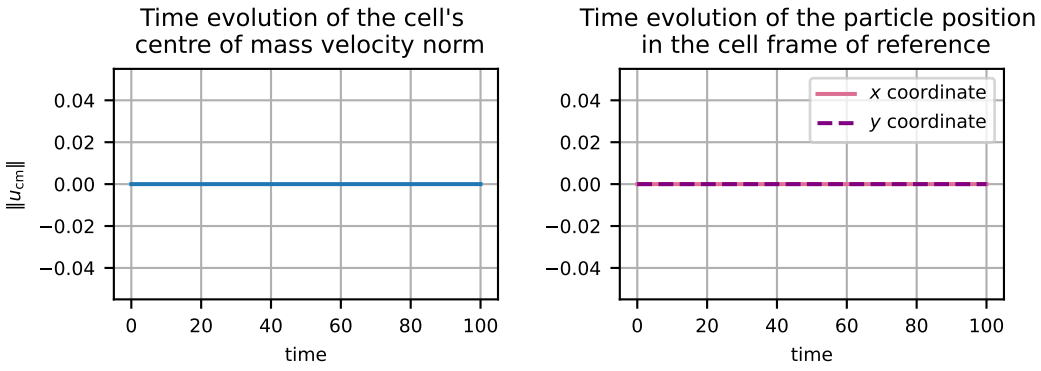

Figure 5.3: **Example of capturing the stationary state using the numerical scheme.** *The curve on the left represents the evolution of the velocity norm over time. We can observe that this remains zero throughout the study interval* $[0, 100]$*. The curves on the right represent the evolution over time of the coordinates of the nucleus position. We can see that the position of the particle is preserved over the study interval.*
The results presented here are obtained with the parameters $\Delta t = 0.005$, $R_0 = 1$, $R_{\text{nucl}} = 0.3$, $\mathbf{x}_{\text{nucl}}^{\text{in}} = (0; 0)$, $c^{\text{in}}(\mathbf{x}) = \frac{M}{\pi\left(R_0^2 - R_{\text{nucl}}^2\right)}$, $M = \pi$, $a = 1$, $\chi_c = 0.5$, $f_{\text{act}}(c) = \frac{c(1+c_s)^2}{c_s(c+c_s)}$ *with* $c_s = 0.5$.

The chosen stationary state perturbation is given by:

$$c^{\text{in}}(\mathbf{x}) = K\left(1 + X(\mathbf{x})\right) \mathbb{1}_{1+X(\mathbf{x})>0} \tag{5.35}$$

where for all $\mathbf{x} \in \Omega \setminus N$ we have $X(\mathbf{x}) \sim \mathcal{N}(0, 1)$ and K such that $\int_{\Omega\setminus N} c^{\text{in}}(\mathbf{x})\, \mathrm{d}\mathbf{x} = M$.The nucleus position is perturbed by choosing:

$$\mathbf{x}_{\text{nucl}}^{\text{in}} = (0; 0)\,.$$

As illustrated in fig. 5.5 for the case where $R_0 = 1$ and $R_{\text{nucl}} = 0.3$, we correctly find the criterion on the linear stablity of the stationary state. Indeed, when $\chi_c < \chi_c^*$, we have that the norm of the velocity decreases very quickly towards 0 then is constant equal to 0. This illustrates that when $\chi_c < \chi_c^*$ the stationary state is stable. Also, when $\chi_c > \chi_c^*$, we observe that the norm increases rapidly towards a strictly positive value and then becomes constant. This suggests that when $\chi_c > \chi_c^*$ there are stable travelling waves.

The trajectory study confirms that we are indeed capturing travelling waves (see fig. 5.6). Each cell maintains its orientation over time, which, coupled with the fact that the norm of the velocity is constant, leads to a progressive wave. The result is not surprising and is in agreement with Lavi et al. (2020) results in the case of a rigid cell.

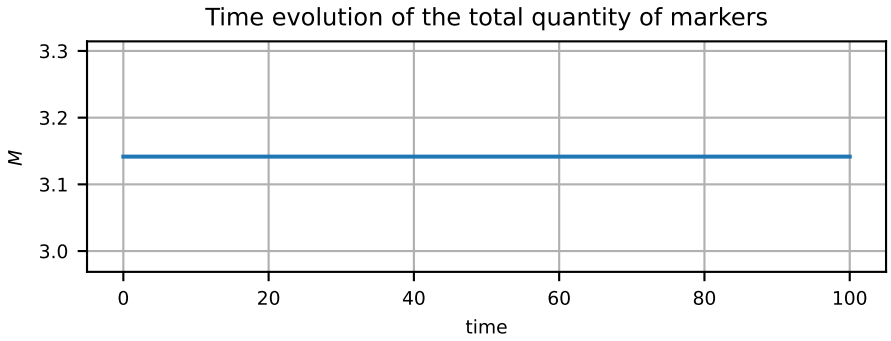

Figure 5.4: **Illustration of the conservation of the total quantity of markers.** *The curve represents the evolution of the total quantity of markers over time. We note that this remains constant throughout the study interval* $[0, 100]$.
The results presented here are obtained with the parameters $\Delta t = 0.005$, $R_0 = 1$, $R_{\text{nucl}} = 0.3$, $\mathbf{x}_{\text{nucl}}^{\text{in}} = (0; 0)$, $c^{\text{in}}(\mathbf{x}) = \frac{M}{\pi\left(R_0^2 - R_{\text{nucl}}^2\right)}$, $M = \pi$, $a = 1$, $\chi_c = 0.5$, $f_{\text{act}}(c) = \frac{c(1+c_s)^2}{c_s(c+c_s)}$ *with* $c_s = 0.5$.

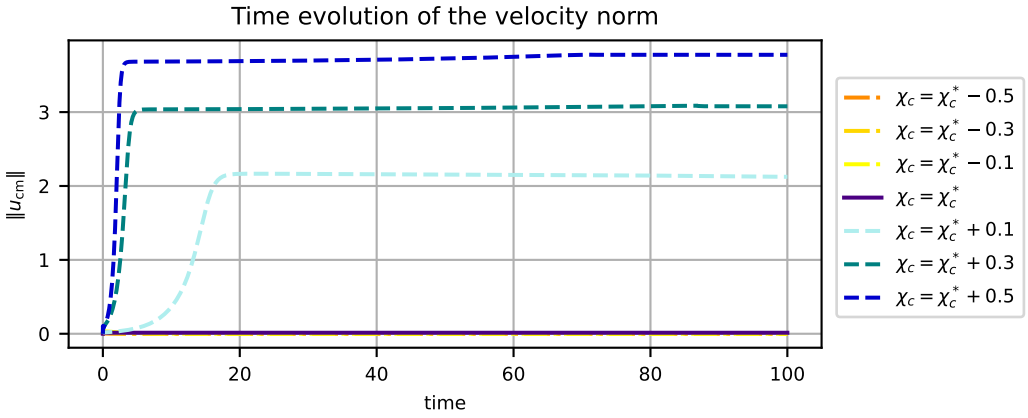

Figure 5.5: **Numerical illustration of theorem 5.2.3.** *Each curve represents the evolution of the cell's centre of mass velocity norm of a cell for different values of* χ_c *(see legend on the right). When* $\chi_c < \chi_c^*$ *the norm of the velocity decreases very rapidly towards* 0 *(dashdotted curves in overlapping shades of orange), whereas when* $\chi_c > \chi_c^*$ *it increases rapidly towards a non-zero value (dashed curves in shades of blue) . The critical case* $\chi_c = \chi_c^*$ *is also represented (dark curve), here the norm of the velocity is close to zero and decreases.*
The results presented here are obtained with the parameters $\Delta t = 0.005$, $R_0 = 1$, $R_{\text{nucl}} = 0.3$, $\mathbf{x}_{\text{nucl}}^{\text{in}} = (0; 0)$, $M = \pi$, $a = 1$, c^{in} *given by eq. (5.35) and* χ_c^* *given by (5.7),* $f_{\text{act}}(c) = \frac{c(1+c_s)^2}{c_s(c+c_s)}$ *with* $c_s = 0.5$, $\beta = 1.5$ *and* $\delta = 0.5$.

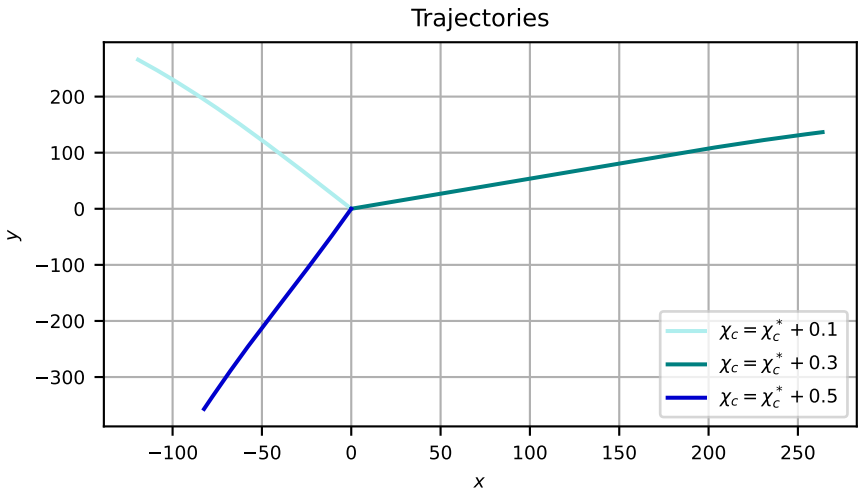

Figure 5.6: **Trajectories associated with the cells in fig. 5.5 in the case where $\chi_c > \chi_c^*$.** *Each curve represents the trajectory of one of the cells studied in figure 3. Only those where $\chi_c > \chi_c^*$ are represented, keeping the same colour coding (see legend on the right). We can therefore see that here the cells do not change orientation over time.*
The results presented here are obtained with the parameters $\Delta t = 0.005$, $R_0 = 1$, $R_{\text{nucl}} = 0.3$, $\mathbf{x}_{\text{nucl}}^{\text{in}} = (0;0)$, $M = \pi$, $a = 1$, c^{in} given by eq. (5.35), χ_c^* given by (5.7), $f_{\text{act}}(c) = \frac{c(1+c_s)^2}{c_s(c+c_s)}$ with $c_s = 0.5$.

Figure 5.7 illustrates the evolution of the organisation of the cell of the trajectory shown in fig. 5.6 when $\chi_c = \chi_c^* + 0.1$. We can see that the particle is at the rear of the cell at the end of the simulation. Note also that the shape of the fluid domain changes over time.

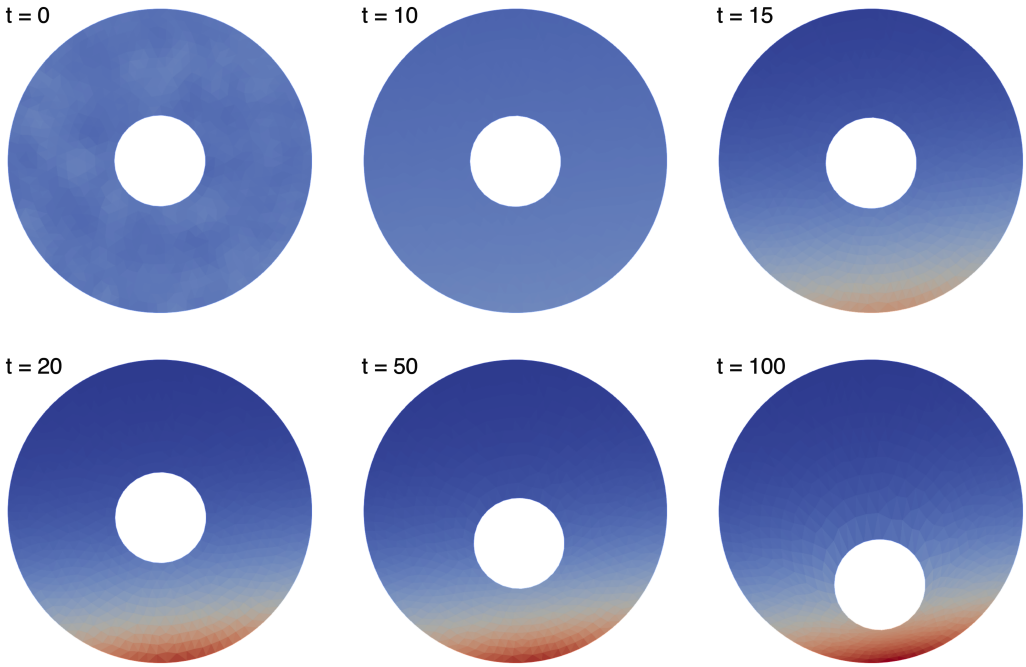

Figure 5.7: **Snapshots of the cell organisation for the case $\chi_c = \chi_c^* + 0.1$ of the fig. 5.6.** *Snapshots at time $t = 0$, $t = 10$, $t = 15$, $t = 20$, $t = 50$, and $t = 100$ of the cell organisation of the cell whose trajectory is represented in fig. 5.6. The red area represents the area with high markers concentration and the area in dark blue the one with low markers concentration. We can observe that the particle moves inside the cell.*
The results presented here are obtained with the parameters $\Delta t = 0.005$, $R_0 = 1$, $R_{\text{nucl}} = 0.3$, $\mathbf{x}_{\text{nucl}}^{\text{in}} = (0;0)$, $M = \pi$, $a = 1$, c^{in} given by eq. (5.35), $\chi_c = \chi_c^* + 0.1$ with χ_c^* given by (5.7), $f_{\text{act}}(c) = \frac{c(1+c_s)^2}{c_s(c+c_s)}$ with $c_s = 0.5$.

5.4.2 . Verification of agreement with the UCSP law and capture of the different types of trajectory

In this section, we illustrate that although the rigid crown model is only a toy model, it exhibits rich behaviour. Indeed, we illustrate that the trajectories obtained via algorithm 5.1 satisfy the UCSP law. Also, there exists a range of parameters in order to find the three types of trajectories: Brownian, intermittent and persistent.

By fixing all the model parameters and varying only χ_c, we observe Brownian trajectories when $\chi_c < \chi_c^*$, intermittent trajectories when $\chi_c = \chi_c^*$ and persistent trajectories when $\chi_c > \chi_c^*$.

In this section, for the numerical results presented, $R_0 = 1$, $R_{\text{nucl}} = 0.3$, $M = \pi$ and $a = 1$. As an initial condition c^{in} for the concentration of markers, we choose the function defined for all $\mathbf{x} \in \Omega \setminus N$ by $c^{\text{in}}(\mathbf{x}) = \dfrac{M}{|\Omega \setminus N|}$. The noise parameters are set to $\alpha = 0.3$ and $\zeta = 0.2$. Finally,

the numerical simulations are performed over the time interval $[0, 15]$ with $\Delta t = 0.005$. Here are the results when $\chi_c = \chi_c^* - 0.3$, $\chi_c = \chi_c^*$ and $\chi_c = \chi_c^* + 0.5$ with χ_c^* defined in eq. (4.5).

5.4.2.1 . Illustration of the Brownian trajectories

In this subsection, we present the results when $\chi_c = \chi_c^* - 0.3$. We then observe that the trajectories are Brownian. This can be seen visually in fig. 5.8 and is confirmed by the study of the EASD and MSD, which are close to 1 (see fig. 5.10). In addition, we can see that the trajectories satisfy the UCSP (see fig. 5.9). We also observe that the cells have a low velocity: the mean norm is close to the intensity α of the noise (see fig. 5.11). These observations are in good agreement with those made about Brownian behaviour in Maiuri et al. (2015).

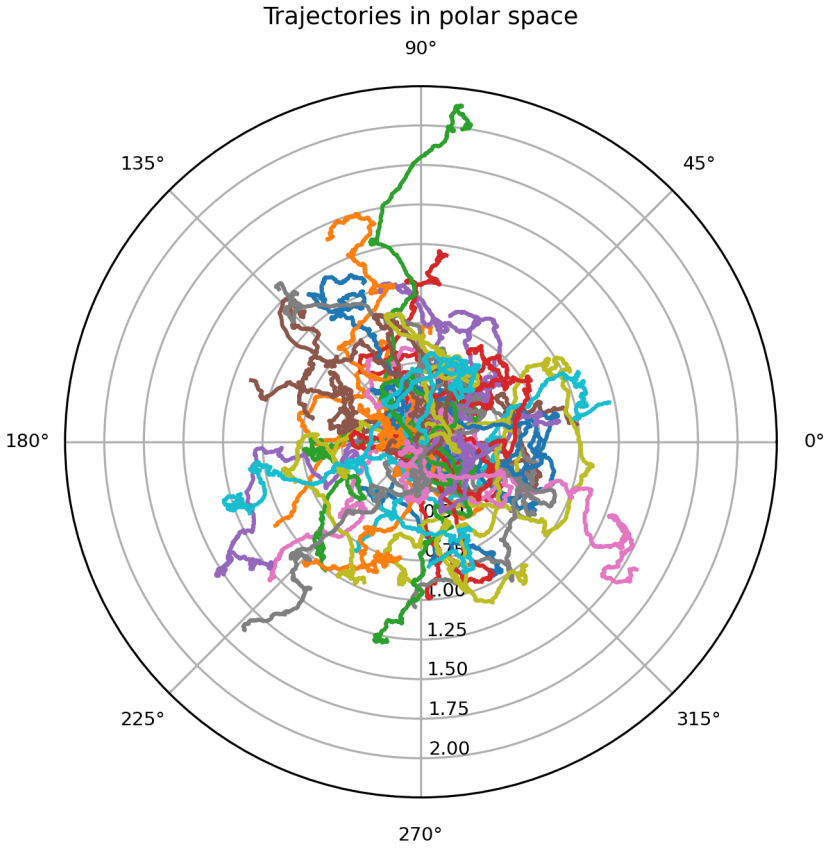

Figure 5.8: **Trajectories in polar coordinates in the case where $\chi_c < \chi_c^*$.** *Each curve represents, in polar coordinates, the trajectory of one cell simulated by algorithm 5.1 on the time interval $[0, 15]$. Visually, the trajectories seem to be Brownian. Fifty cells are represented.*
The results presented here are obtained with the parameters $\Delta t = 0.005$, $R_0 = 1$, $R_{\text{nucl}} = 0.3$, $\mathbf{x}_{\text{nucl}}^{\text{in}} = (0; 0)$, $M = \pi$, $a = 1$, $c^{\text{in}} = \dfrac{M}{|\Omega \setminus N|}$, $\chi_c = \chi_c^* - 0.3$ with χ_c^* given by (5.7), $f_{\text{act}}(c) = \frac{c(1+c_s)^2}{c_s(c+c_s)}$ with $c_s = 0.5$, $\alpha = 0.3$, $\zeta = 0.2$ and $\xi_{\text{nucl}} = 1$.

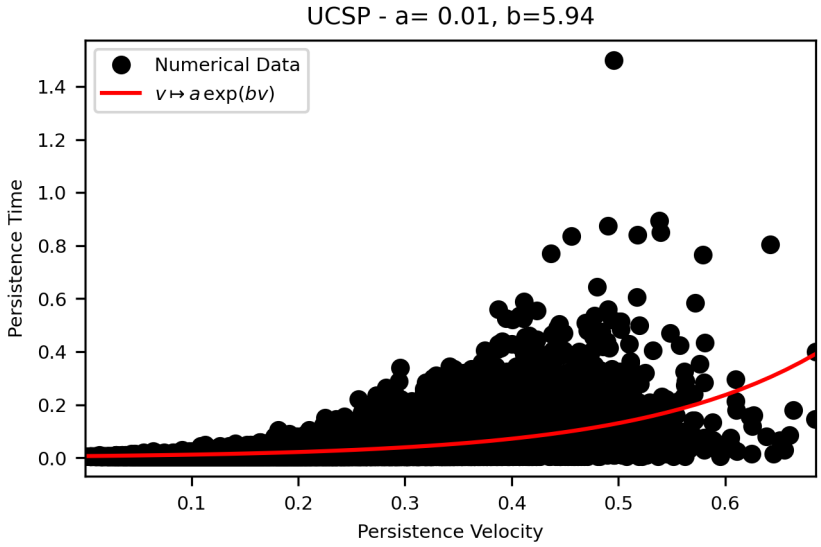

Figure 5.9: **Verification that the trajectories in fig. 5.8 satisfy the UCSP law (case when $\chi_c < \chi_c^*$).** *The persistence time of a locally persistent trajectory portion is plotted as a function of the persistence velocity. Each black dot corresponds to a datum. In red is plotted an interpolation of the points, of form $v \mapsto ae^{bv}$, which corresponds to the UCSP law. We can see that the data corresponds well to the interpolation and that the trajectories satisfy the UCSP law.*
The results presented here are obtained with the parameters $\Delta t = 0.005$, $R_0 = 1$, $R_{\text{nucl}} = 0.3$, $\mathbf{x}_{\text{nucl}}^{\text{in}} = (0;0)$, $M = \pi$, $a = 1$, $c^{\text{in}} = \dfrac{M}{|\Omega \setminus N|}$, $\chi_c = \chi_c^* - 0.3$ *with* χ_c^* *given by* (5.7), $f_{\text{act}}(c) = \frac{c(1+c_s)^2}{c_s(c+c_s)}$ *with* $c_s = 0.5$, $\alpha = 0.3$, $\zeta = 0.2$ *and* $\xi_{\text{nucl}} = 1$.

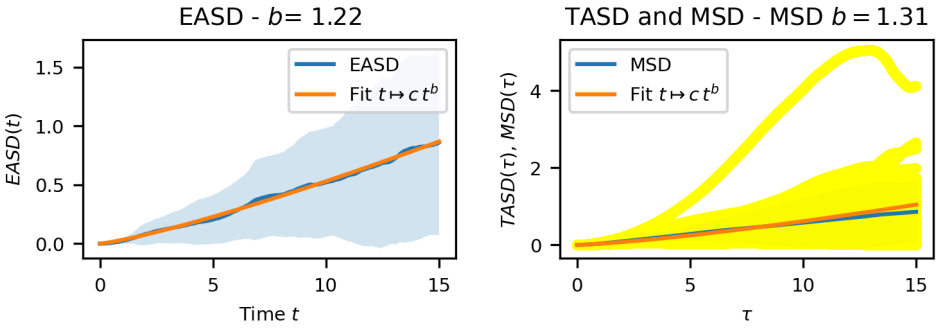

Figure 5.10: **Verification that the trajectories in fig. 5.8 are Brownian (case when $\chi_c < \chi_c^*$).** *On the left is shown in blue the EASD associated with the trajectories in fig. 4.7 and in orange the interpolation of the EASD, in the form $t \mapsto ct^b$. By the properties of the EASD, as b close to 1, the trajectories in fig. 5.8 are indeed Brownian. This is confirmed by the study of the MSD, which is shown in blue on the right. Also shown on the right are the TASD of each cell in yellow and the interpolation of the MSD in form $t \mapsto ct^b$ in orange.*
The results presented here are obtained with the parameters $\Delta t = 0.005$, $R_0 = 1$, $R_{\text{nucl}} = 0.3$, $\mathbf{x}_{\text{nucl}}^{\text{in}} = (0;0)$, $M = \pi$, $a = 1$, $c^{\text{in}} = \dfrac{M}{|\Omega \setminus N|}$, $\chi_c = \chi_c^* - 0.3$ *with* χ_c^* *given by* (5.7), $f_{\text{act}}(c) = \frac{c(1+c_s)^2}{c_s(c+c_s)}$ *with* $c_s = 0.5$, $\alpha = 0.3$, $\zeta = 0.2$ *and* $\xi_{\text{nucl}} = 1$.

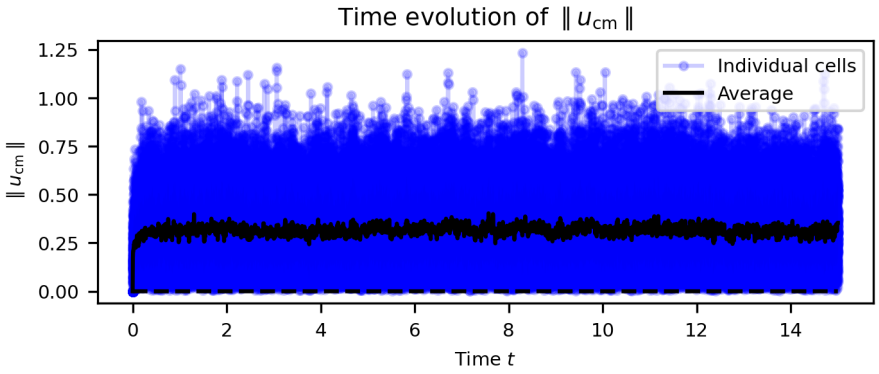

Figure 5.11: **Time evolution of the norm of the velocity of the cells whose trajectories are shown in fig. 5.8 (case when $\chi_c < \chi_c^*$).** *The blue lines show the evolution over time of the norm of the velocity of each cell and the black line shows the evolution of the mean of the norms of the velocities of the cells. We can see that the value of the mean of the norms of the cell velocities corresponds to the choice of α.*
The results presented here are obtained with the parameters $\Delta t = 0.005$, $R_0 = 1$, $R_{\text{nucl}} = 0.3$, $\mathbf{x}_{\text{nucl}}^{\text{in}} = (0;0)$, $M = \pi$, $a = 1$, $c^{\text{in}} = \dfrac{M}{|\Omega \setminus N|}$, $\chi_c = \chi_c^* - 0.3$ with χ_c^* given by (5.7), $f_{\text{act}}(c) = \frac{c(1+c_s)^2}{c_s(c+c_s)}$ with $c_s = 0.5$, $\alpha = 0.3$, $\zeta = 0.2$ and $\xi_{\text{nucl}} = 1$.

5.4.2.2 . Illustration of the persistent trajectories

In this subsection, we present the results when $\chi_c = \chi_c^* + 0.5$. We then observe that the trajectories are persistent. This can be seen visually in fig. 5.12 and is confirmed by the study of the EASD and MSD, which are equal or close to 2 (see fig. 5.14). In addition, we can see that the trajectories satisfy the UCSP (see fig. 5.13). We also observe that the cells have a high velocity (see fig. 5.15). These observations are in good agreement with those made about persistent behaviour in Maiuri et al. (2015).

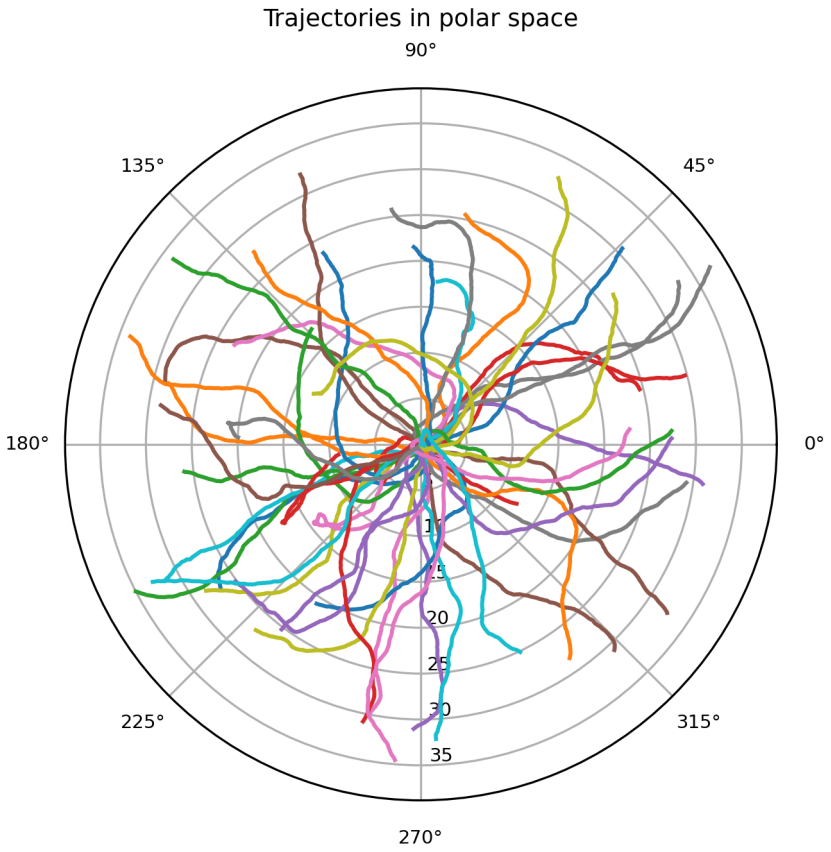

Figure 5.12: **Trajectories in polar coordinates in the case where $\chi_c > \chi_c^*$.** *Each curve represents, in polar coordinates, the trajectory of one cell simulated by algorithm 5.1 on the time interval $[0, 15]$. Visually, the trajectories seem to be persistent. Fifty cells are represented.*
The results presented here are obtained with the parameters $\Delta t = 0.005$, $R_0 = 1$, $R_{\text{nucl}} = 0.3$, $\mathbf{x}_{\text{nucl}}^{\text{in}} = (0; 0)$, $M = \pi$, $a = 1$, $c^{\text{in}} = \dfrac{M}{|\Omega \setminus N|}$, $\chi_c = \chi_c^* + 0.5$ with χ_c^* given by (5.7), $f_{\text{act}}(c) = \frac{c(1+c_s)^2}{c_s(c+c_s)}$ with $c_s = 0.5$, $\alpha = 0.3$, $\zeta = 0.2$ and $\xi_{\text{nucl}} = 1$.

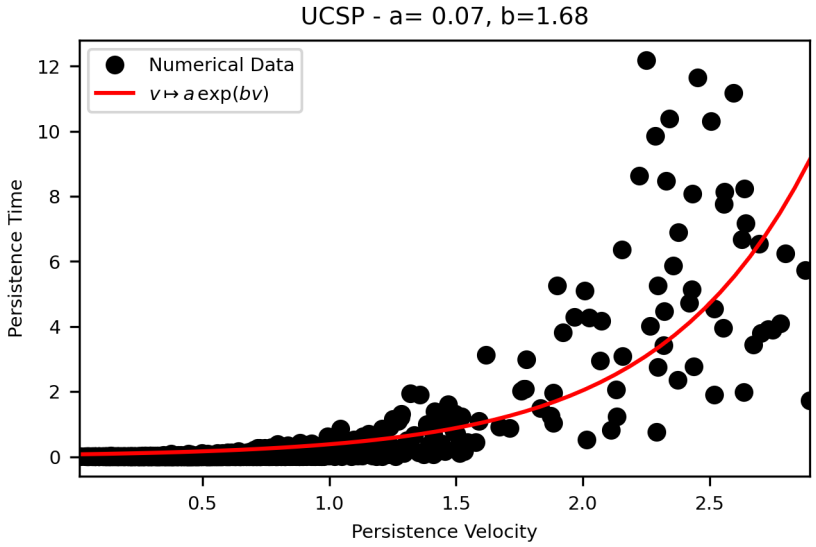

Figure 5.13: **Verification that the trajectories in fig. 5.12 satisfy the UCSP law (case when $\chi_c > \chi_c^*$).** *The persistence time of a locally persistent trajectory portion is plotted as a function of the persistence velocity. Each black dot corresponds to a datum. In red is plotted an interpolation of the points, of form $v \mapsto ae^{bv}$, which corresponds to the UCSP law. We can see that the data corresponds well to the interpolation and that the trajectories satisfy the UCSP law.*
The results presented here are obtained with the parameters $\Delta t = 0.005$, $R_0 = 1$, $R_{\text{nucl}} = 0.3$, $\mathbf{x}_{\text{nucl}}^{\text{in}} = (0;0)$, $M = \pi$, $a = 1$, $c^{\text{in}} = \dfrac{M}{|\Omega \setminus N|}$, $\chi_c = \chi_c^* + 0.5$ *with* χ_c^* *given by* (5.7), $f_{\text{act}}(c) = \frac{c(1+c_s)^2}{c_s(c+c_s)}$ *with* $c_s = 0.5$, $\alpha = 0.3$, $\zeta = 0.2$ *and* $\xi_{\text{nucl}} = 1$.

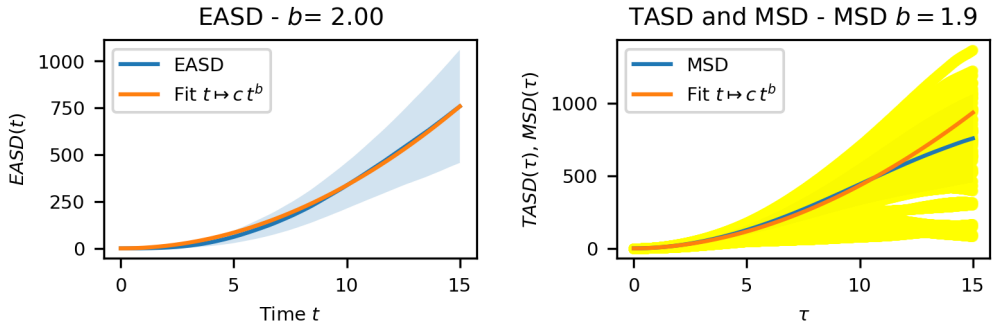

Figure 5.14: **Verification that the trajectories in fig. 5.12 are Brownian (case when $\chi_c > \chi_c^*$).** *On the left is shown in blue the EASD associated with the trajectories in fig. 5.12 and in orange the interpolation of the EASD, in the form $t \mapsto ct^b$. By the properties of the EASD, as b equals to 2, the trajectories in fig. 5.12 are indeed persistent. This is confirmed by the study of the MSD, which is shown in blue on the right. Also shown on the right are the TASD of each cell in yellow and the interpolation of the MSD in form $t \mapsto ct^b$ in orange.*
The results presented here are obtained with the parameters $\Delta t = 0.005$, $R_0 = 1$, $R_{\text{nucl}} = 0.3$, $\mathbf{x}_{\text{nucl}}^{\text{in}} = (0;0)$, $M = \pi$, $a = 1$, $c^{\text{in}} = \dfrac{M}{|\Omega \setminus N|}$, $\chi_c = \chi_c^* + 0.5$ *with* χ_c^* *given by* (5.7), $f_{\text{act}}(c) = \frac{c(1+c_s)^2}{c_s(c+c_s)}$ *with* $c_s = 0.5$, $\alpha = 0.3$, $\zeta = 0.2$ *and* $\xi_{\text{nucl}} = 1$.

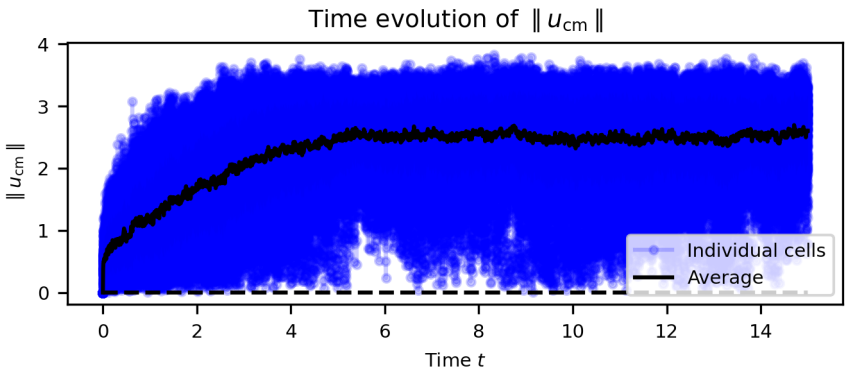

Figure 5.15: **Time evolution of the norm of the velocity of the cells whose trajectories are shown in fig. 5.12 (case when $\chi_c > \chi_c^*$).** *The blue lines show the evolution over time of the norm of the velocity of each cell and the black line shows the evolution of the mean of the norms of the velocities of the cells.*
The results presented here are obtained with the parameters $\Delta t = 0.005$, $R_0 = 1$, $R_{\text{nucl}} = 0.3$, $\mathbf{x}_{\text{nucl}}^{\text{in}} = (0;0)$, $M = \pi$, $a = 1$, $c^{\text{in}} = \dfrac{M}{|\Omega \setminus N|}$, $\chi_c = \chi_c^* + 0.5$ *with* χ_c^* *given by* (5.7), $f_{\text{act}}(c) = \frac{c(1+c_s)^2}{c_s(c+c_s)}$ *with* $c_s = 0.5$, $\alpha = 0.3$, $\zeta = 0.2$ *and* $\xi_{\text{nucl}} = 1$.

5.4.2.3 . Illustration of the intermittent trajectories

In this subsection, we present the results when $\chi_c = \chi_c^*$. We then observe that the trajectories are intermittent. This can be seen visually in fig. 5.16 and is confirmed by the study of the EASD and MSD, which are between 1 and 2 (see fig. 5.18). In addition, we can see that the trajectories satisfy the UCSP (see fig. 5.17). We also observe that the cells have a intermediate velocity: the velocity norm is between the velocities of the case $\chi_c = \chi_c^* - 0.3$ and $\chi_c = \chi_c^* + 0.5$ (see fig. 5.19). These observations are in good agreement with those made about intermittent behaviour in Maiuri et al. (2015).

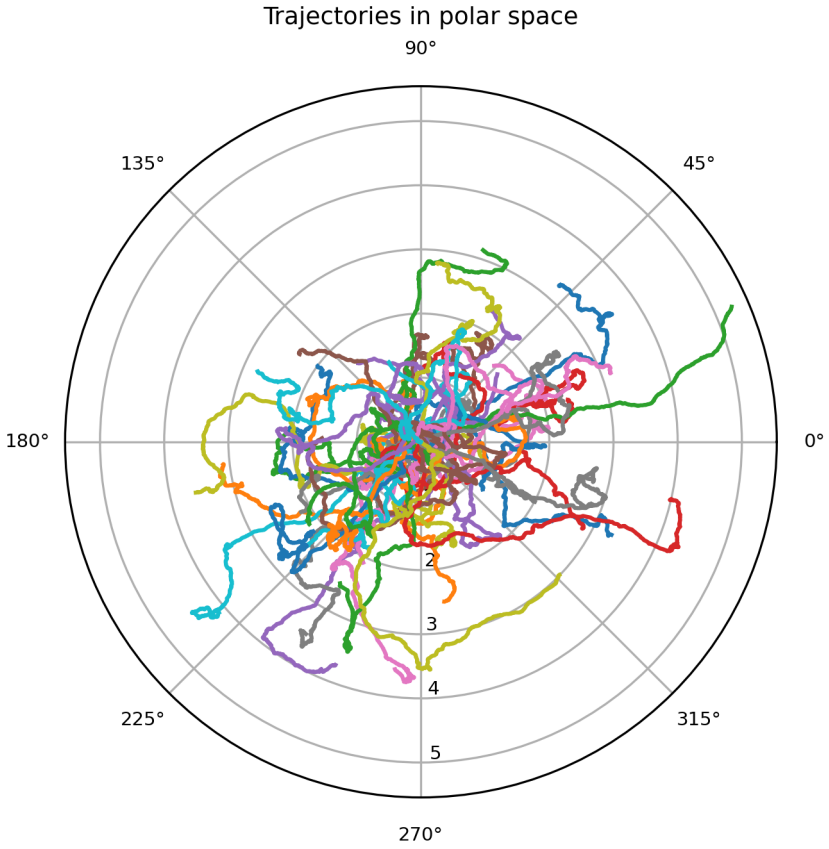

Figure 5.16: **Trajectories in polar coordinates in the case where $\chi_c = \chi_c^*$.** *Each curve represents, in polar coordinates, the trajectory of one cell simulated by algorithm 5.1 on the time interval $[0, 15]$. Visually, the trajectories seem to be intermittent. Fifty cells are represented.*
The results presented here are obtained with the parameters $\Delta t = 0.005$, $R_0 = 1$, $R_{\text{nucl}} = 0.3$, $\mathbf{x}_{\text{nucl}}^{\text{in}} = (0; 0)$, $M = \pi$, $a = 1$, $c^{\text{in}} = \dfrac{M}{|\Omega \setminus N|}$, $\chi_c = \chi_c^*$ with χ_c^* given by (5.7), $f_{\text{act}}(c) = \frac{c(1+c_s)^2}{c_s(c+c_s)}$ with $c_s = 0.5$, $\alpha = 0.3$, $\zeta = 0.2$ and $\xi_{\text{nucl}} = 1$.

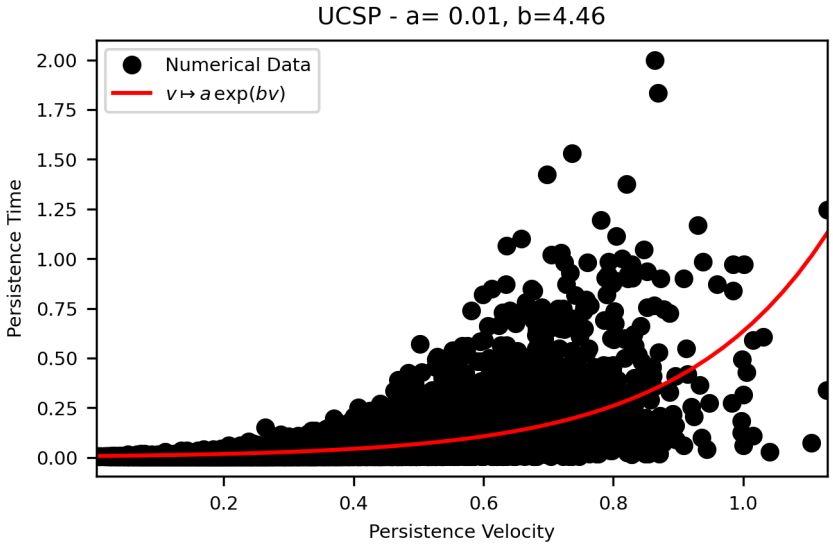

Figure 5.17: **Verification that the trajectories in fig. 5.16 satisfy the UCSP law (case when $\chi_c = \chi_c^*$).** *The persistence time of a locally persistent trajectory portion is plotted as a function of the persistence velocity. Each black dot corresponds to a datum. In red is plotted an interpolation of the points, of form $v \mapsto ae^{bv}$, which corresponds to the UCSP law. We can see that the data corresponds well to the interpolation and that the trajectories satisfy the UCSP law.*
The results presented here are obtained with the parameters $\Delta t = 0.005$, $R_0 = 1$, $R_{\text{nucl}} = 0.3$, $\mathbf{x}_{\text{nucl}}^{\text{in}} = (0;0)$, $M = \pi$, $a = 1$, $c^{\text{in}} = \dfrac{M}{|\Omega \setminus N|}$, $\chi_c = \chi_c^*$ with χ_c^* given by (5.7), $f_{\text{act}}(c) = \frac{c(1+c_s)^2}{c_s(c+c_s)}$ with $c_s = 0.5$, $\alpha = 0.3$, $\zeta = 0.2$ and $\xi_{\text{nucl}} = 1$.

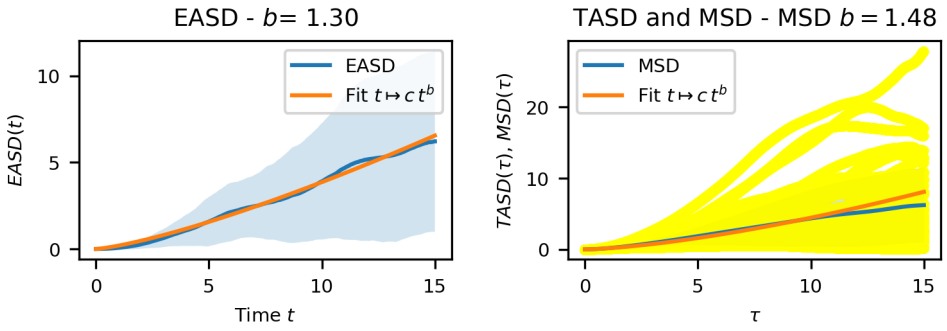

Figure 5.18: **Verification that the trajectories in fig. 5.16 are intermittent (case when $\chi_c = \chi_c^*$).** *On the left is shown in blue the EASD associated with the trajectories in fig. 5.16 and in orange the interpolation of the EASD, in the form $t \mapsto ct^b$. By the properties of the EASD, as b between 1 and 2, the trajectories in fig. 5.16 are neither Brownian neither persistent. This is confirmed by the study of the MSD, which is shown in blue on the right. Also shown on the right are the TASD of each cell in yellow and the interpolation of the MSD in form $t \mapsto ct^b$ in orange.*
The results presented here are obtained with the parameters $\Delta t = 0.005$, $R_0 = 1$, $R_{\text{nucl}} = 0.3$, $\mathbf{x}_{\text{nucl}}^{\text{in}} = (0;0)$, $M = \pi$, $a = 1$, $c^{\text{in}} = \dfrac{M}{|\Omega \setminus N|}$, $\chi_c = \chi_c^*$ with χ_c^* given by (5.7), $f_{\text{act}}(c) = \frac{c(1+c_s)^2}{c_s(c+c_s)}$ with $c_s = 0.5$, $\alpha = 0.3$, $\zeta = 0.2$ and $\xi_{\text{nucl}} = 1$.

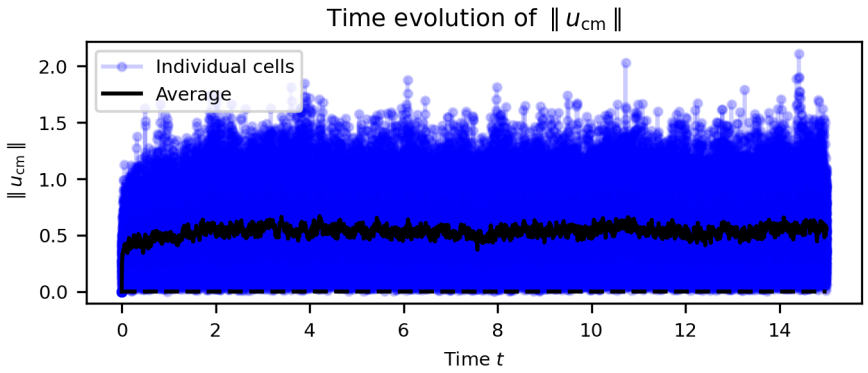

Figure 5.19: **Time evolution of the norm of the velocity of the cells whose trajectories are shown in fig. 5.16 (case when $\chi_c = \chi_c^*$).** *The blue lines show the evolution over time of the norm of the velocity of each cell and the black line shows the evolution of the mean of the norms of the velocities of the cells. We can see that the value of the mean of the norms of the cell velocities corresponds to the choice of α.*
The results presented here are obtained with the parameters $\Delta t = 0.005$, $R_0 = 1$, $R_{\text{nucl}} = 0.3$, $\mathbf{x}_{\text{nucl}}^{\text{in}} = (0; 0)$, $M = \pi$, $a = 1$, $c^{\text{in}} = \dfrac{M}{|\Omega \setminus N|}$, $\chi_c = \chi_c^*$ with χ_c^* given by (5.7), $f_{\text{act}}(c) = \frac{c(1+c_s)^2}{c_s(c+c_s)}$ with $c_s = 0.5$, $\alpha = 0.3$, $\zeta = 0.2$ and $\xi_{\text{nucl}} = 1$.

Conclusion and perspectives. The model allows all three types of trajectory to be found. The results obtained seem similar to those obtained when considering a rigid cell without particle (see chapter 3). Nevertheless, the study of the linear stability of the stationary state proves that, for the choice of $f_{\text{act}}(c) = \frac{c(1+c_s)^2}{c_s(c+c_s)}$, the presence of a particle tends to stabilise the model. Indeed, as soon as $c_s < \frac{M}{\pi R_0^2}$, we have that for the same choice of parameters, the threshold above which the stationary state is unstable is greater when the particle is present. Similarly, the larger the particle, the more stable the stationary state. Let us denote $c^0(r)$ the stationary concentration associated with the domain where the particle has radius $r \in (0, R_0)$ and $\chi_c^*(r)$ the associated critical threshold. We know that c^0 is an increasing function on $[0, R_0]$. Also, as we have assumed that $c_s < \frac{M}{\pi R_0^2} = c^0(0)$ and that the function $x \mapsto \frac{1}{a x f'_{\text{act}}(x)}$ is increasing on $[c_s, +\infty)$, we obtain that χ_c^* is an increasing function on $[0, R_0]$. The results obtained numerically in this chapter will be analysed in comparison with those obtained in chapter 6 when the dynamics of the nucleus are taken into account.

Finally, in future work we aim to study the impact on trajectories of the parameter ξ_{nucl}. The results presented in this chapter are obtained with $\xi_{\text{nucl}} = 1$. Numerically, when $\xi_{\text{nucl}} \neq 1$, the particle initially positioned at the centre of the cell moves further away from the centre of the cell when $\xi_{\text{nucl}} = 1$ (see fig. 5.20). This justifies the addition of the Uzawa algorithm to the numerical scheme to manage potential contacts between the nucleus and the boundary of the cell. Investigating the case of $xi_{mathrmnucl} \neq 1$ will enable us to understand the impact of the particle's position on trajectories and cell motility. This will be done in a future work. We will also study the impact of this parameter on the stability of the stationary state.

We also plan to demonstrate a bifurcation result from the stationary state to travelling waves when $\chi_c > \chi_c^*$ and to study the convergence in long time to a travelling wave.

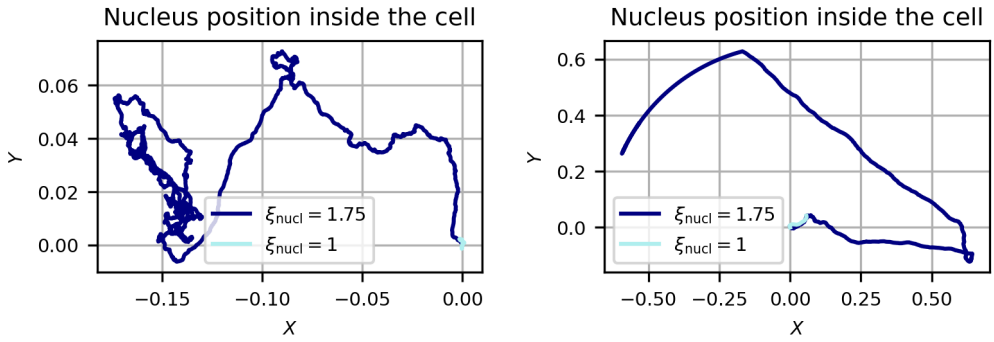

Figure 5.20: **Representation of nucleus position in the cell frame of reference for different value of χ_c and ξ_{nucl}.** *On the left is represented the nucleus position in the cell frame of reference when $\chi_c = \chi_c^* - 0.3$ and on the right when $\chi_c = \chi_c^* + 0.5$. The curves in dark blue correspond to $\xi_{\text{nucl}} = 1.75$ and the one in turquoise correspond to $\xi_{\text{nucl}} = 1$. We observe that in the case where $\xi_{\text{nucl}} = 1.75$, the particle moves away from the centre of the cell.*
The results presented here are obtained with the parameters $\Delta t = 0.005$, $R_0 = 1$, $R_{\text{nucl}} = 0.3$, $\mathbf{x}_{\text{nucl}}^{\text{in}} = (0;0)$, $M = \pi$, $a = 1$, $c^{\text{in}} = \dfrac{M}{|\Omega \setminus N|}$, $f_{\text{act}}(c) = \frac{c(1+c_s)^2}{c_s(c+c_s)}$ with $c_s = 0.5$, $\alpha = 0.3$, and $\zeta = 0.2$.

Bibliography

Alazard, T., Magliocca, M., and Meunier, N. (2022). Traveling wave solution for a coupled incompressible Darcy's free boundary problem with surface tension. arXiv:2205.04365 [math]. 130

Boulakia, M., Genadot, A., and Thieullen, M. (2015). Simulation of SPDEs for Excitable Media Using Finite Elements. Journal of Scientific Computing, 65(1):171–195. 141

Hecht, F. (2012). New development in freefem++. J. Numer. Math., 20(3-4):251–265. 145

Lavi, I., Meunier, N., Voituriez, R., and Casademunt, J. (2020). Motility and morphodynamics of confined cells. Physical Review E, 101(2):022404. Publisher: American Physical Society. 130, 146

Lefebvre, A. (2007). Modélisation numérique d'écoulements fluide/particules. phdthesis, Université Paris Sud. 144

Maiuri, P., Rupprecht, J.-F., Wieser, S., Ruprecht, V., Bénichou, O., Carpi, N., Coppey, M., De Beco, S., Gov, N., Heisenberg, C.-P., Lage Crespo, C., Lautenschlaeger, F., Le Berre, M., Lennon-Dumenil, A.-M., Raab, M., Thiam, H.-R., Piel, M., Sixt, M., and Voituriez, R. (2015). Actin Flows Mediate a Universal Coupling between Cell Speed and Cell Persistence. Cell, 161(2):374–386. 150, 153, 156

6 - Rigid cell model with a rigid nucleus

In this chapter, in the first section we introduce an analogous two dimensional rigid model to the model (1.1) in the case where we assume the substrate to be homogeneous (ξ_{M} is independent of the space and time) and there is no external signal. In the second section, we design a finite element scheme to simulate our model. In the third one, we present some numerical results. By comparing the results obtained with those obtained in chapters 4 and 5, we show that taking the nucleus into account enables intermittent trajectories to be recovered. We also study numerically the heuristic approach proposed in section 1.3.9 to model the forces induced by the nucleus on the cell boundary and by the cell boundary on the nucleus. We show that the heuristic approach yields results similar to the former.

6.1 . From deformable to rigid model

In this section, we aim to derive a model of cell motility from the deformable model, taking into account the nucleus and assuming that the cell is rigid. First, we recall the deformable model. Then we study the dynamics of the cell's centre of mass given by the deformable model. Finally, we derive a rigid model analogous to the deformable model.

6.1.1 . Deformable model

We restrict ourselves to the case where the cell's environment presents no obstacle and where there is no external signal. We neglect the effects of undercooling and assume that the substrate is homogeneous, i.e. that ξ_{M} is independent of space and we set for all $\mathbf{x} \in \mathbb{R}^2$, $\xi_{\mathrm{M}}(\mathbf{x}) = 1$. Then we have ξ_{nucl} independent of time. Under these assumptions and keeping the notations from chapter 1, the deformable model (1.1) is written as follows:

$$
\begin{cases}
\mathbf{u} + \nabla P = 0 & \text{in } \Omega(t) \setminus N(t), & \text{(6.1a)}\\
\operatorname{div}(\mathbf{u}) = 0 & \text{in } \Omega(t) \setminus N(t), & \text{(6.1b)}\\
V_n = \mathbf{u} \cdot \mathbf{n} & \text{on } \partial\Omega(t), & \text{(6.1c)}\\
P = \gamma\kappa + \chi_c f_{\mathrm{act}}(c) - f_{\mathrm{NB}} & \text{on } \partial\Omega(t), & \text{(6.1d)}\\
\mathbf{u}_{\mathrm{nucl}}(t) = \dfrac{1}{\xi_{\mathrm{nucl}}|N|}\left(\displaystyle\int_{\partial N(t)} P(t,\mathbf{x})\mathbf{n}\,\mathrm{d}\sigma + \mathbf{f}_{\mathrm{BN}}\right) & & \text{(6.1e)}\\
\mathbf{u}\cdot\mathbf{n} = \mathbf{u}_{\mathrm{nucl}}\cdot\mathbf{n} & \text{on } \partial N(t), & \text{(6.1f)}\\
\partial_t c = \operatorname{div}\left(\nabla c - (1-a)\,\mathbf{u}c - \alpha\dot{W}_t^Q c\right) & \text{in } \Omega(t)\setminus N(t), & \text{(6.1g)}\\
\left(\nabla c + a\mathbf{u}c - \alpha\dot{W}_t^Q c\right)\cdot\mathbf{n} = 0 & \text{on } \partial\left(\Omega(t)\setminus N(t)\right), & \text{(6.1h)}\\
c(0,\mathbf{x}) = c0(\mathbf{x}) & \text{in } \Omega(0)\setminus N(0). & \text{(6.1i)}
\end{cases}
$$

6.1.2 . Force balance

Let $\mathbf{x}_{\mathrm{cm}}(t)$ be the centre of mass of $\Omega(t)$ at time $t \geq 0$. We have:

$$\mathbf{x}_{\mathrm{cm}}(t) = \frac{1}{A_\Omega}\int_{\Omega(t)} (x,y)\,\mathrm{d}x\,\mathrm{d}y.$$

We also define the velocity of the centre of mass $\mathbf{u}_{\mathrm{cm}}$. For all $t \geq 0$, we have:

$$\mathbf{u}_{\mathrm{cm}}(t) = \frac{\mathrm{d}}{\mathrm{d}t}\mathbf{x}_{\mathrm{cm}}(t).$$

For all $t \geq 0$, we have:

$$\begin{aligned}
\frac{\mathrm{d}}{\mathrm{d}t}\int_{\Omega(t)} x\,\mathrm{d}x\,\mathrm{d}y &= \int_{\partial\Omega(t)} xV_n\,\mathrm{d}\sigma = \int_{\partial\Omega(t)} x\mathbf{u}\cdot\mathbf{n}\,\mathrm{d}\sigma \\
&= \int_{\Omega(t)\setminus N(t)} \mathrm{div}\,(x\mathbf{u})\,\mathrm{d}x\,\mathrm{d}y + \int_{N(t)} \mathrm{div}\,(x\mathbf{u}_{\mathrm{nucl}})\,\mathrm{d}x\,\mathrm{d}y \\
&= \int_{\Omega(t)\setminus N(t)} \nabla x\cdot\mathbf{u}\,\mathrm{d}x\,\mathrm{d}y + \mathbf{u}_{\mathrm{nucl}}\cdot\int_{N(t)} \nabla x\,\mathrm{d}x\,\mathrm{d}y \\
&= -\int_{\Omega(t)\setminus N(t)} \mathrm{div}\,(P\nabla x)\,\mathrm{d}x\,\mathrm{d}y + \mathbf{u}_{\mathrm{nucl},x} \\
&= -\int_{\partial\Omega(t)} P\nabla x\cdot\mathbf{n}\,\mathrm{d}\sigma - \int_{\partial N(t)} P\nabla x\cdot\mathbf{n}\,\mathrm{d}\sigma + \mathbf{u}_{\mathrm{nucl},x} \\
&= -\int_{\partial\Omega(t)} (\gamma\kappa + \chi_c f_{\mathrm{act}}(c) - f_{\mathrm{NB}})\,\mathbf{n}_x\,\mathrm{d}\sigma - \int_{\partial\Omega(t)} P\mathbf{n}_x\,\mathrm{d}\sigma + \mathbf{u}_{\mathrm{nucl},x} \\
&= -\int_{\partial\Omega(t)} (\gamma\kappa + \chi_c f_{\mathrm{act}}(c) - f_{\mathrm{NB}})\,\mathbf{n}_x\,\mathrm{d}\sigma - \xi_{\mathrm{nucl}}|N|\,\mathbf{u}_{\mathrm{nucl},x} + \mathbf{f}_{\mathrm{BN},x} + \mathbf{u}_{\mathrm{nucl},x}
\end{aligned}$$

where we used the incompresisbility constraint (6.1b), the darcy law (6.1a), the boundary condition (6.1d) and the nucleus velocity expression (6.1e). Analogously, we have:

$$\frac{\mathrm{d}}{\mathrm{d}t}\int_{\Omega(t)} y\,\mathrm{d}x\,\mathrm{d}y = -\int_{\partial\Omega(t)} (\gamma\kappa + \chi_c f_{\mathrm{act}}(c) - f_{\mathrm{NB}})\,\mathbf{n}_y\,\mathrm{d}\sigma - \xi_{\mathrm{nucl}}|N|\,\mathbf{u}_{\mathrm{nucl},y} + \mathbf{f}_{\mathrm{BN},y} + \mathbf{u}_{\mathrm{nucl},y}.$$

Since $\int_{\partial\Omega(t)} \kappa\mathbf{n}\,\mathrm{d}\sigma = 0$, it follows:

$$\mathbf{u}_{\mathrm{cm}}(t) = -\frac{1}{A_\Omega}\int_{\partial\Omega(t)} (\chi_c f_{\mathrm{act}}(c) - f_{\mathrm{NB}})\,\mathbf{n}\,\mathrm{d}\sigma + \frac{1}{A_\Omega}\left(|N|(1-\xi_{\mathrm{nucl}})\,\mathbf{u}_{\mathrm{nucl}}(t) + \mathbf{f}_{\mathrm{BN}}\right).$$

Recalling that $\displaystyle\int_{\partial\Omega(t)} f_{NB}\mathbf{n}\,\mathrm{d}\sigma + \mathbf{f}_{BN} = 0$, we have:

$$\mathbf{u}_{\mathrm{cm}}(t) = -\frac{1}{A_\Omega}\int_{\partial\Omega(t)} \chi_c f_{\mathrm{act}}(c)\,\mathbf{n}\,\mathrm{d}\sigma + \frac{|N|}{A_\Omega}(1-\xi_{\mathrm{nucl}})\,\mathbf{u}_{\mathrm{nucl}}(t). \tag{6.2}$$

6.1.3 . Rigid formulation

We want to write the rigid model associated with the deformable model eqs. (6.1) and (6.2). We assume the cell to be rigid and the cell to have a circular shape: $\Omega(t)$ is a disk of radius $R_0 > 0$. We assume that the velocity of the centre of mass in the rigid case is the same as in the deformable case. Thus, the external boundary of the cell moves at the velocity of the centre of mass. As in the deformable case, the cell is filled by a Darcy fluid with velocity $\mathbf{u}$ and pressure P. Thus, with the assumption that the cell boundary normal velocity is equal to the

inside fluid normal velocity and with velocities continuity at the nucleus boundary, we have:

$$\begin{cases} \mathbf{u} + \nabla P = 0 & \text{in } \Omega(t) \setminus N(t), \\ \operatorname{div}(\mathbf{u}) = 0 & \text{in } \Omega(t) \setminus N(t), \\ \mathbf{u} \cdot \mathbf{n} = \mathbf{u}_{\mathrm{cm}} \cdot \mathbf{n} & \text{on } \partial\Omega(t), \\ \mathbf{u} \cdot \mathbf{n} = \mathbf{u}_{\mathrm{nucl}} \cdot \mathbf{n} & \text{on } \partial N(t), \\ \Omega(t) = B(0, R_0) + \displaystyle\int_0^t \mathbf{u}_{\mathrm{cm}}(s)\, \mathrm{d}s, & \\ N(t) = B(0, R_{\mathrm{nucl}}) + \displaystyle\int_0^t \mathbf{u}_{\mathrm{nucl}}(s)\, \mathrm{d}s. & \end{cases}$$

The nucleus is modelled as in the deformable case. We assume it to have a rigid movement. The force balance on the nucleus leads to the following expression for the nucleus velocity:

$$\mathbf{u}_{\mathrm{nucl}} = \frac{1}{\xi_{\mathrm{nucl}} |N|} \left(\int_{\partial N(t)} P(t, \mathbf{x})\, \mathbf{n}\, \mathrm{d}\sigma + \mathbf{f}_{\mathrm{BN}} \right).$$

Finally, as in the deformable case, we assume that rear markers are inside the cell, that they can diffuse inside the cell and be transported by the fluid or attached to the plate, and that in addition they are subject to stochastic fluctuations (modelled as in the section 1.3.7), which leads to:

$$\begin{cases} \partial_t c = \operatorname{div}\left(\nabla c - (1-a)\, \mathbf{u} c - \alpha \dot{W}_t^Q c \right) & \text{in } \Omega(t) \setminus N(t), \\ \left(\nabla c + a \mathbf{u} c - \alpha \dot{W}_t^Q c \right) \cdot \mathbf{n} = 0 & \text{on } \partial\left(\Omega(t) \setminus N(t)\right). \end{cases}$$

Thus, the rigid cell model with a rigid nucleus inside the cell that can move is given by:

$$\begin{cases} \mathbf{u} + \nabla P = 0 & \text{in } \Omega(t) \setminus N(t), \quad (6.3a) \\ \operatorname{div}(\mathbf{u}) = 0 & \text{in } \Omega(t) \setminus N(t), \quad (6.3b) \\ \mathbf{u}_{\mathrm{nucl}}(t) = \dfrac{1}{\xi_{\mathrm{nucl}} |N|} \left(\displaystyle\int_{\partial N(t)} P(t, \mathbf{x}) \mathbf{n}\, \mathrm{d}\sigma + \mathbf{f}_{\mathrm{BN}} \right), & (6.3c) \\ \mathbf{u}_{\mathrm{cm}}(t) = \dfrac{-\chi_c}{A_\Omega} \displaystyle\int_{\partial\Omega(t)} f_{\mathrm{act}}(c)\, \mathbf{n}\, \mathrm{d}\sigma + \dfrac{|N|}{A_\Omega} (1 - \xi_{\mathrm{nucl}})\, \mathbf{u}_{\mathrm{nucl}}(t), & (6.3d) \\ \mathbf{u} \cdot \mathbf{n} = \mathbf{u}_{\mathrm{cm}} \cdot \mathbf{n} & \text{on } \partial\Omega(t), \quad (6.3e) \\ \mathbf{u} \cdot \mathbf{n} = \mathbf{u}_{\mathrm{nucl}} \cdot \mathbf{n} & \text{on } \partial N(t), \quad (6.3f) \\ \partial_t c = \operatorname{div}\left(\nabla c - (1-a)\, \mathbf{u} c - \alpha \dot{W}_t^Q c \right) & \text{in } \Omega(t) \setminus N(t), \quad (6.3g) \\ \left(\nabla c + a \mathbf{u} c - \alpha \dot{W}_t^Q c \right) \cdot \mathbf{n} = 0 & \text{on } \partial\left(\Omega(t) \setminus N(t)\right), \quad (6.3h) \\ \Omega(t) = B(0, R_0) + \displaystyle\int_0^t \mathbf{u}_{\mathrm{cm}}(s)\, \mathrm{d}s, & (6.3i) \\ N(t) = B(0, R_{\mathrm{nucl}}) + \displaystyle\int_0^t \mathbf{u}_{\mathrm{nucl}}(s)\, \mathrm{d}s. & (6.3j) \end{cases}$$

We recall that $\mathbf{f}_{\mathrm{BN}}$ is defined by eq. (1.22) in this case we have for all $t \geq 0$:

$$\mathbf{f}_{\mathrm{BN}}(t) = \delta \int_{\partial\Omega(t)} \frac{\mathbf{v}_{\mathrm{BN}} \cdot \mathbf{n}}{\left(\|\mathbf{v}_{\mathrm{BN}}\| - R_{\mathrm{nucl}} \right)^\beta} \mathbf{n}\, \mathrm{d}\sigma, \tag{6.4}$$

with $\beta > 1$, $\delta > 0$ and $\mathbf{v}_{\mathrm{BN}} = \mathbf{x}_{\mathrm{nucl}} - \mathbf{x}_B$ where $\mathbf{x}_B \in \partial\Omega(t)$.

We also recall that $\mathbf{f}_{\mathrm{BN}}$ can also be defined by eq. (1.24) and we recall that in this case, for all $t \geq 0$ we have:

$$\mathbf{f}_{\mathrm{BN}}(t) = -k\left(\mathbf{x}_{\mathrm{nucl}}(t) - \mathbf{x}_{\mathrm{cm}}(t)\right), \tag{6.5}$$

with $k > 0$ and $\mathbf{x}_{\mathrm{cm}}$ the centre of the cell.

We can note that, in general, since $\mathbf{u}_{\mathrm{cm}} \neq \mathbf{u}_{\mathrm{nucl}}$, the fluid domain is not a rigid domain but a deformable domain. In accordance with the modelling of noise in section 1.3.7, the space coloured noise $\dot{W}_t^Q$ is defined on a probability space associated with the bounded open $\Omega(0) = B(0, R_0)$.

Moreover, the total quantity of markers M inside the cell remains constant over the time and we have:

$$M = \int_{\Omega(t)\setminus N(t)} c(t, \mathbf{x})\, \mathrm{d}\mathbf{x}. \tag{6.6}$$

Remark 6.1.1. *In the model (6.3), P is defined up to a constant. Indeed, if $(P, \mathbf{u}, c)$ is a solution of (6.3), then for all $P_0 \in \mathbb{R}$, $(P + P_0, \mathbf{u}, c)$ is also a solution of (6.3). Thus, in order to define a form of uniqueness of solutions, we can define an equivalence class and state that $(P_1, \mathbf{u}_1, c_1)$ and $(P_2, \mathbf{u}_2, c_2)$ are equivalent solutions if and only if $\mathbf{u}_1 = \mathbf{u}_2$, $c_1 = c_2$ and there exists $Q \in \mathbb{R}$ such that $P_1 = P_2 + Q$.*

6.2 . Study of the model

In this section, we study the stationary state of model (6.3) in the case where we neglect the noise and take $\alpha = 0$ in eqs. (6.3g) and (6.3h). First, we prove that the model admits a stationary state. Secondly, we study its linear stability and give a criterion for its stability. There exists χ_c^* such that if $\chi_c < \chi_c^*$ then the stationary state is stable and unstable otherwise.

6.2.1 . Stationary state

Proposition 6.2.1. *The model eq. (6.3) admits unique stationary state given by:*

$$\begin{cases} \mathbf{u}^0(\mathbf{x}) = 0, & \text{(6.7a)} \\ P^0(\mathbf{x}) = 0, & \text{(6.7b)} \\ \mathbf{u}_{\mathrm{nucl}}^0 = 0, & \text{(6.7c)} \\ \mathbf{u}_{\mathrm{cm}}^0 = 0, & \text{(6.7d)} \\ c^0(\mathbf{x}) = \dfrac{M}{|\Omega \setminus N|}, & \text{(6.7e)} \\ \Omega^0 = B(0, R_0) \text{ and } N^0 = B(0, R_{\mathrm{nucl}}). & \text{(6.7f)} \end{cases}$$

Uniqueness is defined according to the remark 6.1.1.

Proof. The stationary problem asssociated with the model (6.3) is given as follows:

$$\begin{cases} \mathbf{u} + \nabla P = 0 & \text{in } \Omega \setminus N, \\ \operatorname{div}(\mathbf{u}) = 0 & \text{in } \Omega \setminus N, \\ \mathbf{u} \cdot \mathbf{n} = 0 & \text{on } \partial\Omega \cup \partial N, \\ \displaystyle\int_{\partial N} P\mathbf{n}\, \mathrm{d}\sigma + \mathbf{f}_{\mathrm{BN}} = 0, & \\ \Delta c - (1-a)\, \mathbf{u} \cdot \nabla c = 0 & \text{in } \Omega \setminus N, \\ (\nabla c + a\mathbf{u}c) \cdot \mathbf{n} = 0 & \text{on } \partial\Omega \cup \partial N, \\ \Omega = B(0, R_0) \text{ and } N = B(\mathbf{x}_{\mathrm{nucl}}, R_{\mathrm{nucl}}). & \end{cases}$$

Thus the problem on P reads:

$$\begin{cases} -\Delta P = 0 & \text{in } \Omega \setminus N, \\ -\nabla P \cdot \mathbf{n} = 0 & \text{on } \partial\Omega \cup \partial N, \end{cases}$$

which leads to the fact that P is such that $\nabla P = 0$ over $\Omega \setminus N$ and thus P is constant over $\Omega \setminus N$. Moreover, we deduce that $\mathbf{u} = 0$ over $\Omega \setminus N$.

Substituting the value of $\mathbf{u}$ into the dynamics of concentration c, we obtain:

$$\begin{cases} -\Delta c = 0 & \text{in } \Omega \setminus N, \\ -\nabla c \cdot \mathbf{n} = 0 & \text{on } \partial\Omega \cup \partial N, \end{cases}$$

and c is constant over $\Omega \setminus N$. Using the constraint on the total quantity of markers, we deduce that for all $\mathbf{x} \in \Omega \setminus N$, $c(\mathbf{x}) = \dfrac{M}{|\Omega \setminus N|}$.

As P is constant over $\Omega \setminus N$, then necessarily $\mathbf{f}_{\mathrm{BN}} = 0$. For both possible choices for $\mathbf{f}_{\mathrm{BN}} = 0$ given by eqs. (6.4) and (6.5), it follows that $\mathbf{x}_{\mathrm{nucl}} = 0$ and $N = B(0, R_{\mathrm{nucl}})$ for . □

In the sequel we denote:

$$\chi_c^* = \frac{1}{ac^0 f'_{\mathrm{act}}(c^0)}. \tag{6.8}$$

Theorem 6.2.2. *Let $\mathbf{f}_{\mathrm{BN}}$ be defined either by eq. (6.4) or by eq. (6.5). In the case where $\xi_{\mathrm{nucl}} = 1$, if $\chi_c < \chi_c^*$, then the stationary state (6.7) is linearly stable. On the opposite, if $\chi_c > \chi_c^*$, then the stationary state is linearly unstable.*

6.2.2 . Proof of theorem 6.2.2

To study the linear stability of the stationary state (6.7) and proof theorem 6.2.2, we proceed in three steps. First, we linearise the problem (6.3) around this stationary state. From the linearisation of the problem, we derive an eigenvalue problem. Secondly, we study this eigenvalue problem. We study the sign of the real part of the eigenvalues: when there is an eigenvalue with a positive real part, the stationary state is linearly unstable, whereas when all the eigenvalues have a negative real part, the stationary state is linearly stable. To do this, we use Fourier analysis to decompose the eigenvalue problem into simpler problems. Finally, we derive an explicit condition on the eigenvalues. We exhibit an eigenvalue with a positive real part when $\chi_c > \chi_c^*$ and with a graphical argument, we illustrate that when $\chi_c < \chi_c^*$ all the eigenvalues have a negative real part. The arguments used are inspired by those of Lavi et al. (2020); Alazard et al. (2022) and are similar to those of sections 4.2.1.2 and 5.2.2. The proof is detailed for $\mathbf{f}_{\mathrm{BN}}$ defined by eq. (6.4). For the case where $\mathbf{f}_{\mathrm{BN}}$ is defined by eq. (6.5) see remark 6.2.9.

Step 1. The linearised problem associated with the model (6.3) around the stationary state (6.7) in the following lemma. Then we deduce an eigenvalue problem associated to this linearised problem.

Lemma 6.2.3. *The linearised problem associated to eq.* (6.3) *around the stationary state* (6.7) *is given by:*

$$\begin{cases} -\Delta\tilde{P} = 0 & \text{in } \Omega^0 \setminus N^0, & \text{(6.9a)} \\ -\nabla\tilde{P}\cdot\mathbf{n} = \tilde{\mathbf{u}}_{\mathrm{cm}}\cdot\mathbf{n} & \text{on } \partial\Omega^0, & \text{(6.9b)} \\ -\nabla\tilde{P}\cdot\mathbf{n} = \tilde{\mathbf{u}}_{\mathrm{nucl}}\cdot\mathbf{n} & \text{on } \partial N^0, & \text{(6.9c)} \\ \partial_t\tilde{c} = \Delta\tilde{c} & \text{in } \Omega^0 \setminus N^0, & \text{(6.9d)} \\ \left(\nabla\tilde{c} + a\tilde{\mathbf{u}}_{\mathrm{cm}}c^0\right)\cdot\mathbf{n} = 0 & \text{on } \partial\Omega^0, & \text{(6.9e)} \\ \left(\nabla\tilde{c} + a\tilde{\mathbf{u}}_{\mathrm{nucl}}c^0\right)\cdot\mathbf{n} = 0 & \text{on } \partial N^0, & \text{(6.9f)} \end{cases}$$

with

$$\tilde{\mathbf{u}}_{\mathrm{cm}}(t) = \frac{-\chi_c f'_{\mathrm{act}}\left(c^0\right)}{A_\Omega}\int_{\partial\Omega^0}\tilde{c}(t,\mathbf{x})\,\mathbf{n}\,\mathrm{d}\sigma,$$

$$\tilde{\mathbf{u}}_{\mathrm{nucl}}(t) = \frac{1}{|N|}\left(\int_{\partial N^0}\tilde{P}(t,\mathbf{x})\,\mathbf{n}\,\mathrm{d}\sigma + \frac{\delta R_0\pi\left(R_0(1-\beta) - R_{\mathrm{nucl}}\right)}{\left(R_0 - R_{\mathrm{nucl}}\right)^{\beta+1}}\left(\tilde{\mathbf{x}}_{\mathrm{nucl}}(t) - \tilde{\mathbf{x}}_{\mathrm{cell}}(t)\right)\right), \quad \text{(6.10a)}$$

(6.10b)

and $\tilde{\mathbf{x}}_{\mathrm{cell}} = (\tilde{x}_{\mathrm{cell}}, \tilde{y}_{\mathrm{cell}})$ *and* $\tilde{\mathbf{x}}_{\mathrm{nucl}} = (\tilde{x}_{\mathrm{nucl}}, \tilde{y}_{\mathrm{nucl}})$ *such that for all* $t \geq 0$*:*

$$\frac{\mathrm{d}}{\mathrm{d}t}\tilde{\mathbf{x}}_{\mathrm{cell}}(t) = \tilde{\mathbf{u}}_{\mathrm{cm}}(t) \quad \textit{and} \quad \frac{\mathrm{d}}{\mathrm{d}t}\tilde{\mathbf{x}}_{\mathrm{nucl}}(t) = \tilde{\mathbf{u}}_{\mathrm{nucl}}(t).$$

Proof. We perform a formal expansion of the solutions of model (6.3) around the stationary state (6.7). Let $\varepsilon > 0$ small. For all $t \geq 0$, we set:

$$\Omega(t) = B\left(\mathbf{x}_{\mathrm{cell}}(t), R_0\right) \quad \text{and} \quad N(t) = B\left(\mathbf{x}_{\mathrm{nucl}}(t), R_{\mathrm{nucl}}\right),$$

with

$$\mathbf{x}_{\mathrm{cell}}(t) = \varepsilon\tilde{\mathbf{x}}_{\mathrm{cell}}(t) + \mathcal{O}\left(\varepsilon^2\right),$$
$$\mathbf{x}_{\mathrm{nucl}}(t) = \varepsilon\tilde{\mathbf{x}}_{\mathrm{nucl}}(t) + \mathcal{O}\left(\varepsilon^2\right).$$

Thus we can set for all $t \geq 0$:

$$\mathbf{u}_{\mathrm{cm}}(t) = \mathbf{u}^0_{\mathrm{cm}} + \varepsilon\tilde{\mathbf{u}}_{\mathrm{cm}}(t) + \mathcal{O}\left(\varepsilon^2\right),$$
$$\mathbf{u}_{\mathrm{nucl}}(t) = \mathbf{u}^0_{\mathrm{nucl}} + \varepsilon\tilde{\mathbf{u}}_{\mathrm{nucl}}(t) + \mathcal{O}\left(\varepsilon^2\right).$$

Moreover, for all $t \geq 0$ and $\mathbf{x} \in \Omega^0 \setminus N^0$, we set:

$$P(t) = P^0 + \varepsilon\tilde{P}(t) + \mathcal{O}\left(\varepsilon^2\right),$$

and

$$c(t,\mathbf{x}) = c^0 + \varepsilon\tilde{c}(t,\mathbf{x}) + \mathcal{O}\left(\varepsilon^2\right).$$

As P_0 satisfies eq. (6.7b) and P satisfies eqs. (6.3a) and (6.3b), we have that in $\Omega^0 \setminus N^0$:

$$-\Delta \tilde{P} = 0.$$

In addition, since P satisfies eq. (6.3b) and $\mathbf{u}$ satisfies the boundary conditions eqs. (6.3e) and (6.3f), we deduce that $\tilde{P}$ satisfies the following boundary conditions:

$$\begin{aligned} -\nabla \tilde{P} \cdot \mathbf{n} &= \tilde{\mathbf{u}}_{\mathrm{cm}} \cdot \mathbf{n} && \text{on } \partial\Omega^0, \\ -\nabla \tilde{P} \cdot \mathbf{n} &= \tilde{\mathbf{u}}_{\mathrm{nucl}} \cdot \mathbf{n} && \text{on } \partial N^0. \end{aligned}$$

Using the fact that c^0 satisfies eq. (6.7e) and c satisfies (6.3g), we deduce that in $\Omega^0 \setminus N^0$:

$$\partial_t \tilde{c} = \Delta \tilde{c}.$$

We also have on $\partial\Omega^0$ that:

$$\begin{aligned} (\nabla c + a\mathbf{u}_{\mathrm{cm}} c) \cdot \mathbf{n} &= \left(\nabla c^0 + \varepsilon \nabla \tilde{c} + a\mathbf{u}_{\mathrm{cm}}^0 c^0 + \varepsilon a \mathbf{u}_{\mathrm{cm}}^0 \tilde{c} + \varepsilon a \tilde{\mathbf{u}}_{\mathrm{cm}} c^0\right) \cdot \mathbf{n} + \mathcal{O}\left(\varepsilon^2\right) \\ &= \varepsilon \left(\nabla \tilde{c} + a\tilde{\mathbf{u}}_{\mathrm{cm}} c^0\right) \cdot \mathbf{n} + \mathcal{O}\left(\varepsilon^2\right), \end{aligned}$$

which leads to the boundary condition:

$$\left(\nabla \tilde{c} + a\tilde{\mathbf{u}}_{\mathrm{cm}} c^0\right) \cdot \mathbf{n} = 0 \qquad \text{on } \partial\Omega^0.$$

Similarly, we obtain the boundary condition on N^0:

$$\left(\nabla \tilde{c} + a\tilde{\mathbf{u}}_{\mathrm{nucl}} c^0\right) \cdot \mathbf{n} = 0.$$

Moreover, we have:

$$\begin{aligned} \int_{\partial\Omega(t)} f_{\mathrm{act}}(c)\, \mathbf{n}\, \mathrm{d}\sigma &= \int_{\partial\Omega(t)} f_{\mathrm{act}}\left(c^0\right) + \varepsilon \tilde{c} f'_{\mathrm{act}}\left(c^0\right) \mathbf{n}\, \mathrm{d}\sigma + \mathcal{O}\left(\varepsilon^2\right) \\ &= \varepsilon f'_{\mathrm{act}}\left(c^0\right) \int_{\partial\Omega(t)} \tilde{c}\mathbf{n}\, \mathrm{d}\sigma + \mathcal{O}\left(\varepsilon^2\right) \\ &= \varepsilon f'_{\mathrm{act}}\left(c^0\right) \int_{\partial\Omega^0} \tilde{c}\mathbf{n}\, \mathrm{d}\sigma + \mathcal{O}\left(\varepsilon^2\right). \end{aligned}$$

Thus we deduce that

$$\tilde{\mathbf{u}}_{\mathrm{cm}} = \frac{-\chi_c f'_{\mathrm{act}}\left(c^0\right)}{A_\Omega} \int_{\partial\Omega^0} \tilde{c}\mathbf{n}\, \mathrm{d}\sigma.$$

Finally, as $\mathbf{f}_{\mathrm{BN}} = \delta \displaystyle\int_{\partial\Omega(t)} \frac{\mathbf{v}_{\mathrm{BN}} \cdot \mathbf{n}}{\left(\|\mathbf{v}_{\mathrm{BN}}\| - R_{\mathrm{nucl}}\right)^\beta} \mathbf{n}\, \mathrm{d}\sigma$ and for all $\theta \in (-\pi, \pi]$, in polar coordinates, we have:

$$\begin{aligned} \frac{\mathbf{v}_{\mathrm{BN}} \cdot \mathbf{n}}{\left(\|\mathbf{v}_{\mathrm{BN}}\| - R_{\mathrm{nucl}}\right)^\beta} &= \frac{-R_0}{\left(R_0 - R_{\mathrm{nucl}}\right)^\beta} \\ &\quad + \varepsilon \frac{R_0 - R_{\mathrm{nucl}} - \beta R_0}{\left(R_0 - R_{\mathrm{nucl}}\right)^{\beta+1}} \left(\left(\tilde{x}_{\mathrm{nucl}} - \tilde{x}_{\mathrm{cell}}\right)\cos\theta + \left(\tilde{y}_{\mathrm{nucl}} - \tilde{y}_{\mathrm{cell}}\right)\sin\theta\right) + \mathcal{O}\left(\varepsilon^2\right). \end{aligned}$$

Thus it follows that:

$$\begin{aligned} \mathbf{f}_{\mathrm{BN}} &= \delta\varepsilon \frac{R_0 - R_{\mathrm{nucl}} - \beta R_0}{\left(R_0 - R_{\mathrm{nucl}}\right)^{\beta+1}} \int_{-\pi}^{\pi} \left(\left(\tilde{x}_{\mathrm{nucl}} - \tilde{x}_{\mathrm{cell}}\right)\cos\theta + \left(\tilde{y}_{\mathrm{nucl}} - \tilde{y}_{\mathrm{cell}}\right)\sin\theta\right) \begin{pmatrix}\cos\theta \\ \sin\theta\end{pmatrix} \mathrm{d}\theta + \mathcal{O}\left(\varepsilon^2\right) \\ &= \delta\varepsilon \frac{R_0 - R_{\mathrm{nucl}} - \beta R_0}{\left(R_0 - R_{\mathrm{nucl}}\right)^{\beta+1}} \left(\tilde{\mathbf{x}}_{\mathrm{nucl}} - \tilde{\mathbf{x}}_{\mathrm{cell}}\right) + \mathcal{O}\left(\varepsilon^2\right). \end{aligned}$$

Finally we have:

$$\tilde{\mathbf{u}}_{\mathrm{nucl}}(t) = \frac{1}{|N|}\left(\int_{\partial N^0} \tilde{P}(t,\mathbf{x})\,\mathbf{n}\,\mathrm{d}\sigma + \frac{\delta R_0 \pi \left(R_0(1-\beta) - R_{\mathrm{nucl}}\right)}{\left(R_0 - R_{\mathrm{nucl}}\right)^{\beta+1}}\left(\tilde{\mathbf{x}}_{\mathrm{nucl}}(t) - \tilde{\mathbf{x}}_{\mathrm{cell}}(t)\right)\right).$$

□

The eigenvalue problem associated with eqs. (6.9) and (6.10) is given by:

$$\begin{cases} -\Delta\tilde{P} = 0 & \text{in } \Omega^0 \setminus N^0, & \text{(6.11a)}\\ -\nabla\tilde{P}\cdot\mathbf{n} = \tilde{\mathbf{u}}_{\mathrm{cm}}\cdot\mathbf{n} & \text{on } \partial\Omega^0, & \text{(6.11b)}\\ -\nabla\tilde{P}\cdot\mathbf{n} = \tilde{\mathbf{u}}_{\mathrm{nucl}}\cdot\mathbf{n} & \text{on } \partial N^0, & \text{(6.11c)}\\ \lambda\tilde{c} = \Delta\tilde{c} & \text{in } \Omega^0 \setminus N^0, & \text{(6.11d)}\\ \left(\nabla\tilde{c} + a\tilde{\mathbf{u}}_{\mathrm{cm}}c^0\right)\cdot\mathbf{n} = 0 & \text{on } \partial\Omega^0, & \text{(6.11e)}\\ \left(\nabla\tilde{c} + a\tilde{\mathbf{u}}_{\mathrm{nucl}}c^0\right)\cdot\mathbf{n} = 0 & \text{on } \partial N^0, & \text{(6.11f)} \end{cases}$$

with

$$\lambda\tilde{\mathbf{x}}_{\mathrm{cm}} = \frac{-\chi_c f'_{\mathrm{act}}\left(c^0\right)}{A_\Omega}\int_{\partial\Omega^0}\tilde{c}(\mathbf{x})\,\mathbf{n}\,\mathrm{d}\sigma, \qquad \text{(6.12a)}$$

$$\lambda\tilde{\mathbf{x}}_{\mathrm{nucl}} = \frac{1}{|N|}\left(\int_{\partial N^0}\tilde{P}(\mathbf{x})\,\mathbf{n}\,\mathrm{d}\sigma + \frac{\delta R_0\pi\left(R_0(1-\beta) - R_{\mathrm{nucl}}\right)}{\left(R_0 - R_{\mathrm{nucl}}\right)^{\beta+1}}\left(\tilde{\mathbf{x}}_{\mathrm{nucl}} - \tilde{\mathbf{x}}_{\mathrm{cell}}\right)\right), \qquad \text{(6.12b)}$$

where $\lambda \in \mathbb{C}$.

Step 2. Using Fourier analysis and the radially symmetric nature of the problem (6.12), we show the following lemma, which reduces the spectral study of eq. (6.12) to a simpler problem.

Lemma 6.2.4. *The problem* (6.11)-(6.12) *admits an eigenvalue with a positive real part if and only if the following problem eqs.* (6.13) *to* (6.15) *admits one.*

$$\begin{cases} \lambda c = \left(\partial^2_{rr} + \frac{1}{r}\partial_r - \frac{1}{r^2}\right)c & r \in (R_{\mathrm{nucl}}, R_0), & \text{(6.13a)}\\ \partial_r c(R_0) + a\tilde{u}_{\mathrm{cm}}c^0 = 0, & & \text{(6.13b)}\\ \partial_r c(R_{\mathrm{nucl}}) + a\tilde{u}_{\mathrm{nucl}}c^0 = 0, & & \text{(6.13c)}\\ \lambda\tilde{x}_{\mathrm{cell}} = \tilde{u}_{\mathrm{cm}}, & & \text{(6.13d)}\\ \lambda\tilde{x}_{\mathrm{nucl}} = \tilde{u}_{\mathrm{nucl}}, & & \text{(6.13e)} \end{cases}$$

with

$$\tilde{u}_{\mathrm{cm}} = \frac{-\chi_c f'_{\mathrm{act}}\left(c^0\right)}{R_0}c(R_0) \qquad \text{(6.14)}$$

and

$$\tilde{u}_{\mathrm{nucl}} = \frac{-\chi_c f'_{\mathrm{act}}\left(c^0\right)}{R_0}c(R_0) + \frac{\delta\left(R_0^2 - R_{\mathrm{nucl}}^2\right)\left(R_0(1-\beta) - R_{\mathrm{nucl}}\right)}{2R_0R_{\mathrm{nucl}}^2\left(R_0 - R_{\mathrm{nucl}}\right)^{\beta+1}}\left(\tilde{x}_{\mathrm{nucl}} - \tilde{x}_{\mathrm{cell}}\right). \qquad \text{(6.15)}$$

Proof. Since problem (6.11) and (6.12) is radially symmetrical, we can use Fourier analysis to study its spectra. Let $\lambda \in \mathbb{C}$ and let $\left(\tilde{P}, \tilde{c}, \tilde{\mathbf{u}}_{\mathrm{cm}}, \tilde{\mathbf{u}}_{\mathrm{nucl}}\right)$ be an eigenfunction associated with λ. In polar coordinates, for all $r \in (R_{\mathrm{nucl}}, R_0)$ and $\theta \in (-\pi, \pi]$, the Fourier decomposition of $\tilde{P}$ is given by:

$$\tilde{P}(r,\theta) = \sum_{m\in\mathbb{N}} P_{cm}(r)\cos(m\theta) + P_{sm}(r)\sin(m\theta),$$

and the one of $\tilde{c}$ by:

$$\tilde{c}(r,\theta) = \sum_{m\in\mathbb{N}} c_{cm}(r)\cos(m\theta) + \sum_{m\in\mathbb{N}} c_{sm}(r)\sin(m\theta).$$

For all $m \in \mathbb{N}$ with $m \neq 1$, we have:

$$\int_{-\pi}^{\pi} \cos(m\theta)\cos(\theta) = \int_{-\pi}^{\pi} \sin(m\theta)\sin(\theta) = 0$$

and

$$\int_{-\pi}^{\pi} \cos(m\theta)\sin(\theta) = \int_{-\pi}^{\pi} \sin(m\theta)\cos(\theta) = 0.$$

We also have:

$$\int_{-\pi}^{\pi} \cos^2(\theta) = \int_{-\pi}^{\pi} \sin^2(\theta) = \pi$$

and

$$\int_{-\pi}^{\pi} \cos(\theta)\sin(\theta) = 0.$$

Thus, in particular, we have:

$$\int_{\partial N^0} \tilde{P}\mathbf{n}\,\mathrm{d}\sigma = -\pi R_{\mathrm{nucl}} \begin{pmatrix} P_{c1}(R_{\mathrm{nucl}}) \\ P_{s1}(R_{\mathrm{nucl}}) \end{pmatrix}$$

and

$$\int_{\partial\Omega} \tilde{c}\mathbf{n}\,\mathrm{d}\sigma = \pi R_0 \begin{pmatrix} c_{c1}(R_0) \\ c_{s1}(R_0) \end{pmatrix}.$$

By linearity of eq. (6.11) and independence of the cosine and sine modes, we deduce that for all $m \neq 1$, (P_{cm}, c_{cm}) and (P_{sm}, c_{sm}) satisfy:

$$\begin{cases} -\left(\partial_{rr}^2 + \dfrac{1}{r}\partial_r - \dfrac{m^2}{r^2}\right) P_m = 0 & r \in (R_{\mathrm{nucl}}, R_0), \quad (6.16a) \\ -\partial_r P_m = 0 & r \in \{R_{\mathrm{nucl}}, R_0\}, \quad (6.16b) \\ \lambda c_m = \left(\partial_{rr}^2 + \dfrac{1}{r}\partial_r - \dfrac{m^2}{r^2}\right) c_m & r \in (R_{\mathrm{nucl}}, R_0), \quad (6.16c) \\ \partial_r c_m = 0 & r \in \{R_{\mathrm{nucl}}, R_0\}. \quad (6.16d) \end{cases}$$

Moreover, in the case where $m = 1$, we have that (P_{c1}, c_{c1}) satisfies:

$$\begin{cases} -\left(\partial_{rr}^2 + \frac{1}{r}\partial_r - \frac{m^2}{r^2}\right) P_{c1} = 0 & r \in (R_{\text{nucl}}, R_0)\,, \quad (6.17a) \\ -\partial_r P_{c1}\,(R_0) = \tilde{\mathbf{u}}_{\text{cm},x}, & (6.17b) \\ \partial_r P_{c1}\,(R_{\text{nucl}}) = \tilde{\mathbf{u}}_{\text{nucl},x}, & (6.17c) \\ \lambda c_{c1} = \left(\partial_{rr}^2 + \frac{1}{r}\partial_r - \frac{m^2}{r^2}\right) c_{c1} & r \in (R_{\text{nucl}}, R_0)\,, \quad (6.17d) \\ \partial_r c_{c1}\,(R_0) + a\tilde{\mathbf{u}}_{\text{cm},x} c^0 = 0, & (6.17e) \\ \partial_r c_{c1}\,(R_{\text{nucl}}) + a\tilde{\mathbf{u}}_{\text{nucl},x} c^0 = 0, & (6.17f) \end{cases}$$

and similarly, (P_{s1}, c_{s1}) satisfies:

$$\begin{cases} -\left(\partial_{rr}^2 + \frac{1}{r}\partial_r - \frac{m^2}{r^2}\right) P_{s1} = 0 & r \in (R_{\text{nucl}}, R_0)\,, \quad (6.18a) \\ -\partial_r P_{s1}\,(R_0) = \tilde{\mathbf{u}}_{\text{cm},y}, & (6.18b) \\ \partial_r P_{s1}\,(R_{\text{nucl}}) = \tilde{\mathbf{u}}_{\text{nucl},y}, & (6.18c) \\ \lambda c_{s1} = \left(\partial_{rr}^2 + \frac{1}{r}\partial_r - \frac{m^2}{r^2}\right) c_{s1} & r \in (R_{\text{nucl}}, R_0)\,, \quad (6.18d) \\ \partial_r c_{s1}\,(R_0) + a\tilde{\mathbf{u}}_{\text{cm},y} c^0 = 0, & (6.18e) \\ \partial_r c_{s1}\,(R_{\text{nucl}}) + a\tilde{\mathbf{u}}_{\text{nucl},y} c^0 = 0, & (6.18f) \end{cases}$$

where $\tilde{\mathbf{u}}_{\text{nucl},x}$ and $\tilde{\mathbf{u}}_{\text{nucl},y}$ denotes the two coordinates of $\tilde{\mathbf{u}}_{\text{nucl}}$ and $\tilde{\mathbf{u}}_{\text{cm},x}$ and $\tilde{\mathbf{u}}_{\text{cm},y}$ the ones of $\tilde{\mathbf{u}}_{\text{cm}}$. We can note that $\tilde{\mathbf{u}}_{\text{cm}}$ and $\tilde{\mathbf{u}}_{\text{nucl}}$ depends only on the mode $m = 1$ which allows us to use the independence of the cosine and sine modes.

We then have that studying the spectrum of problem (6.11) is equivalent to studying, for all $m \neq 1$, the spectrum of problem (6.16) and those of problems (6.17) and (6.18). We note that for all $m \neq 1$, the eigenvalues of problem (6.16), which corresponds to the heat equation, have negative real parts. Thus, if problem (6.11) has a positive real part eigenvalue, then problem (6.17) or problem (6.18) has a positive real part eigenvalue. By symmetry, we see that problems (6.17) and (6.18) are analogous. We therefore restrict our spectral study of problem (6.11)-(6.12) to the spectral study of the problem (6.17).

Finally, since $\tilde{P}$ satisfies the laplacian equation (6.11a), we have that for all $m \in \mathbb{N}$, there exists A_m, B_m, C_m and $D_m \in \mathbb{R}$ such that for all $r \in (R_{\text{nucl}}, R_0)$:

$$\begin{cases} P_{cm}\,(r) = A_m r^m + C_m r^{-m}, \\ P_{sm}\,(r) = B_m r^m + D_m r^{-m}. \end{cases}$$

In particular, we have $P_{c1}\,(R_{\text{nucl}}) = A_1 R_{\text{nucl}} + C_1 R_{\text{nucl}}^{-1}$ and thus:

$$\tilde{\mathbf{u}}_{\text{nucl},x} = -\left(A_1 + C_1 R_{\text{nucl}}^{-2}\right) + \frac{\delta R_0\,(R_0\,(1-\beta) - R_{\text{nucl}})}{R_{\text{nucl}}^2\,(R_0 - R_{\text{nucl}})^{\beta+1}}\,(\tilde{x}_{\text{nucl}} - \tilde{x}_{\text{cell}})\,.$$

From the boundary conditions eqs. (6.17b) and (6.17c), it follows that:

$$\begin{cases} -\left(A_1 - \frac{C_1}{R_0^2}\right) = \frac{-\chi_c f'_{\text{act}}\,(c^0)}{R_0} c_{c1}\,(R_0)\,, \\ -\left(A_1 - \frac{C_1}{R_{\text{nucl}}^2}\right) = -\left(A_1 + \frac{C_1}{R_{\text{nucl}}^2}\right) + \frac{\delta R_0\,(R_0\,(1-\beta) - R_{\text{nucl}})}{R_{\text{nucl}}^2\,(R_0 - R_{\text{nucl}})^{\beta+1}}\,(\tilde{x}_{\text{nucl}} - \tilde{x}_{\text{cell}})\,. \end{cases}$$

We thus have:

$$\begin{cases} A_1 = \dfrac{\chi_c f'_{\text{act}}\left(c^0\right)}{R_0} c_{c1}\left(R_0\right) + \dfrac{\delta\left(R_0\left(1-\beta\right) - R_{\text{nucl}}\right)}{2R_0\left(R_0 - R_{\text{nucl}}\right)^{\beta+1}}\left(\tilde{x}_{\text{nucl}} - \tilde{x}_{\text{cell}}\right), \\ C_1 = \dfrac{R_0\left(R_0\left(1-\beta\right) - R_{\text{nucl}}\right)}{2\left(R_0 - R_{\text{nucl}}\right)^{\beta+1}}\left(\tilde{x}_{\text{nucl}} - \tilde{x}_{\text{cell}}\right). \end{cases}$$

We can conclude that:

$$\tilde{\mathbf{u}}_{\text{nucl},x} = -\frac{\chi_c f'_{\text{act}}\left(c^0\right)}{R_0} c_{c1}\left(R_0\right) + \frac{\delta\left(R_0^2 - R_{\text{nucl}}^2\right)\left(R_0\left(1-\beta\right) - R_{\text{nucl}}\right)}{2R_0 R_{\text{nucl}}^2\left(R_0 - R_{\text{nucl}}\right)^{\beta+1}}\left(\tilde{x}_{\text{nucl}} - \tilde{x}_{\text{cell}}\right).$$

□

Step 3. We study the spectral problem (6.13) and show with a graphical argument that when $\chi_c < \chi_c^*$ then all the eigenvalues of eq. (6.13) are of negative real part and that if $\chi_c > \chi_c^*$ then there exists an eigenvalue of eq. (6.13) of positive real part.

Lemma 6.2.5. *Let $\lambda \in \mathbb{C}$. The eigenfunctions of eqs. (6.13) to (6.15) associated with the eigenvalue $\lambda \in \mathbb{C}$ are given by:*

$$\begin{pmatrix} c\left(r\right) \\ x_{\text{cell}} \\ x_{\text{nucl}} \end{pmatrix} = \begin{pmatrix} \beta_\lambda J_1\left(-\mathrm{i}\lambda^{\frac{1}{2}} r\right) + \gamma_\lambda Y_1\left(-\mathrm{i}\lambda^{\frac{1}{2}} r\right) \\ \hat{x}_{\text{cell},\lambda} \\ \hat{x}_{\text{nucl},\lambda} \end{pmatrix}, \tag{6.19}$$

where $r \in \left(R_{\text{nucl}}, R_0\right)$, J_1 and Y_1 denote respectively the Bessel function of the first kind of order 1 and that of the second kind of order 1 and $\left(\beta_\lambda, \gamma_\lambda, \hat{x}_{\text{cell},\lambda}, \hat{x}_{\text{nucl},\lambda}\right) \in \mathbb{C}^4$ solution of:

$$\begin{aligned} &-\mathrm{i}\lambda^{\frac{1}{2}}\left(\beta_\lambda J_1'\left(-\mathrm{i}\lambda^{\frac{1}{2}} R_0\right) + \gamma_\lambda Y_1'\left(-\mathrm{i}\lambda^{\frac{1}{2}} R_0\right)\right) \\ &\qquad = \frac{a\chi_c c^0 f'_{\text{act}}\left(c^0\right)}{R_0}\left(\beta_\lambda J_1\left(-\mathrm{i}\lambda^{\frac{1}{2}} R_0\right) + \gamma_\lambda Y_1\left(-\mathrm{i}\lambda^{\frac{1}{2}} R_0\right)\right), \end{aligned} \tag{6.20}$$

$$\begin{aligned} &-\mathrm{i}\lambda^{\frac{1}{2}}\left(\beta_\lambda J_1'\left(-\mathrm{i}\lambda^{\frac{1}{2}} R_{\text{nucl}}\right) + \gamma_\lambda Y_1'\left(-\mathrm{i}\lambda^{\frac{1}{2}} R_{\text{nucl}}\right)\right) \\ &\qquad = \frac{a\chi_c c^0 f'_{\text{act}}\left(c^0\right)}{R_0}\left(\beta_\lambda J_1\left(-\mathrm{i}\lambda^{\frac{1}{2}} R_0\right) + \gamma_\lambda Y_1\left(-\mathrm{i}\lambda^{\frac{1}{2}} R_0\right)\right) \\ &\qquad\qquad - ac^0 \frac{\delta\left(R_0^2 - R_{\text{nucl}}^2\right)\left(R_0\left(1-\beta\right) - R_{\text{nucl}}\right)}{2R_0 R_{\text{nucl}}^2\left(R_0 - R_{\text{nucl}}\right)^{\beta+1}}\left(\hat{x}_{\text{nucl},\lambda} - \hat{x}_{\text{cell},\lambda}\right) \end{aligned} \tag{6.21}$$

and

$$\lambda\left(\hat{x}_{\text{nucl},\lambda} - \hat{x}_{\text{cell},\lambda}\right) = \frac{\delta\left(R_0^2 - R_{\text{nucl}}^2\right)\left(R_0\left(1-\beta\right) - R_{\text{nucl}}\right)}{2R_0 R_{\text{nucl}}^2\left(R - R_{\text{nucl}}\right)^{\beta+1}}\left(\hat{x}_{\text{nucl},\lambda} - \hat{x}_{\text{cell},\lambda}\right). \tag{6.22}$$

Proof. From eqs. (6.13d) and (6.13e), we deduce that:

$$x_{\text{cell}} = \hat{x}_{\text{cell},\lambda} \in \mathbb{C} \quad \text{and} \quad x_{\text{nucl}} = \hat{x}_{\text{nucl},\lambda} \in \mathbb{C}$$

satisfy

$$\lambda\left(x_{\text{nucl}} - x_{\text{cell}}\right) = \tilde{u}_{\text{nucl}} - \tilde{u}_{\text{cm}}.$$

Combining it with eqs. (6.14) and (6.15), the expressions of $\tilde{u}_{\mathrm{nucl}}$ and $\tilde{u}_{\mathrm{cm}}$, we deduce that:

$$\lambda\left(\hat{x}_{\mathrm{nucl},\lambda}-\hat{x}_{\mathrm{cell},\lambda}\right)=\frac{\delta\left(R_0^2-R_{\mathrm{nucl}}^2\right)\left(R_0\left(1-\beta\right)-R_{\mathrm{nucl}}\right)}{2R_0R_{\mathrm{nucl}}^2\left(R_0-R_{\mathrm{nucl}}\right)^{\beta+1}}\left(\hat{x}_{\mathrm{nucl},\lambda}-\hat{x}_{\mathrm{cell},\lambda}\right).$$

From the definition of the Bessel functions, there exists β_λ and $\gamma_\lambda \in \mathbb{C}$ such that the solutions c of eq. (6.13a) are given, for all $r \in (R_{\mathrm{nucl}}, R_0)$, by:

$$c\left(r\right)=\beta_\lambda J_1\left(-\mathrm{i}\lambda^{\frac{1}{2}}r\right)+\gamma_\lambda Y_1\left(-\mathrm{i}\lambda^{\frac{1}{2}}r\right).$$

Then the boundary condition eq. (6.13b) reads eq. (6.20) and the boundary condition eq. (6.13c) reads eq. (6.21). □

Lemma 6.2.6. *Let $\lambda \in \mathbb{C}$ be an eigenvalue of eqs. (6.13) to (6.15). Then either*

$$\lambda=\frac{\delta\left(R_0^2-R_{\mathrm{nucl}}^2\right)\left(R_0\left(1-\beta\right)-R_{\mathrm{nucl}}\right)}{2R_0R_{\mathrm{nucl}}^2\left(R-R_{\mathrm{nucl}}\right)^{\beta+1}}$$

or λ is such that $G_1(\lambda)=0$ with G_1 defined for all $z \in \mathbb{C}$ by:

$$\begin{aligned}G_1\left(z\right)=&\,z\left(J_1'\left(-\mathrm{i}z^{\frac{1}{2}}R_0\right)Y_1'\left(-\mathrm{i}z^{\frac{1}{2}}R_{\mathrm{nucl}}\right)-J_1'\left(-\mathrm{i}z^{\frac{1}{2}}R_{\mathrm{nucl}}\right)Y_1'\left(-\mathrm{i}z^{\frac{1}{2}}R_0\right)\right)\\&+\frac{\mathrm{i}z^{\frac{1}{2}}a\chi_c c^0 f_{\mathrm{act}}'\left(c^0\right)}{R}\left[J_1\left(-\mathrm{i}z^{\frac{1}{2}}R_0\right)Y_1'\left(-\mathrm{i}z^{\frac{1}{2}}R_0\right)-J_1'\left(-\mathrm{i}z^{\frac{1}{2}}R_0\right)Y_1\left(-\mathrm{i}z^{\frac{1}{2}}R_0\right)\right.\\&\left.+J_1'\left(-\mathrm{i}z^{\frac{1}{2}}R_{\mathrm{nucl}}\right)Y_1\left(-\mathrm{i}z^{\frac{1}{2}}R_0\right)-J_1\left(-\mathrm{i}z^{\frac{1}{2}}R_0\right)Y_1'\left(-\mathrm{i}z^{\frac{1}{2}}R_{\mathrm{nucl}}\right)\right].\end{aligned}$$

Proof. Let $\lambda \in \mathbb{C}$ be an eigenvalue of eqs. (6.13) to (6.15). Then by lemma 6.2.5, λ is associate with an eigenfunction $(c, x_{\mathrm{cell}}, x_{\mathrm{nucl}})$ of the form (6.19). In particular it satisfies eq. (6.22). Then either we have

$$\lambda=\frac{\delta\left(R^2-R_{\mathrm{nucl}}^2\right)\left(R\left(1-\beta\right)-R_{\mathrm{nucl}}\right)}{2R_0R_{\mathrm{nucl}}^2\left(R-R_{\mathrm{nucl}}\right)^{\beta+1}}$$

and $x_{\mathrm{nucl}}-x_{\mathrm{cell}} \neq 0$, or

$$x_{\mathrm{nucl}}-x_{\mathrm{cell}}=0$$

and $\lambda \neq 0$ such that

$$\begin{aligned}&-\mathrm{i}\lambda^{\frac{1}{2}}\left(\beta_\lambda J_1'\left(-\mathrm{i}\lambda^{\frac{1}{2}}R_0\right)+\gamma_\lambda Y_1'\left(-\mathrm{i}\lambda^{\frac{1}{2}}R_0\right)\right)\\&\qquad=\frac{a\chi_c c^0 f_{\mathrm{act}}'\left(c^0\right)}{R}\left(\beta_\lambda J_1\left(-\mathrm{i}\lambda^{\frac{1}{2}}R_0\right)+\gamma_\lambda Y_1\left(-\mathrm{i}\lambda^{\frac{1}{2}}R_0\right)\right),\\&-\mathrm{i}\lambda^{\frac{1}{2}}\left(\beta_\lambda J_1'\left(-\mathrm{i}\lambda^{\frac{1}{2}}R_{\mathrm{nucl}}\right)+\gamma_\lambda Y_1'\left(-\mathrm{i}\lambda^{\frac{1}{2}}R_{\mathrm{nucl}}\right)\right)\\&\qquad=\frac{a\chi_c c^0 f_{\mathrm{act}}'\left(c^0\right)}{R}\left(\beta_\lambda J_1\left(-\mathrm{i}\lambda^{\frac{1}{2}}R_0\right)+\gamma_\lambda Y_1\left(-\mathrm{i}\lambda^{\frac{1}{2}}R_0\right)\right).\end{aligned}$$

Combining these two conditions leads to the condition $G_1(\lambda)=0$. □

Remark 6.2.7. *Since $\beta > 1$, we can note that* $\dfrac{\delta\left(R^2-R_{\mathrm{nucl}}^2\right)\left(R\left(1-\beta\right)-R_{\mathrm{nucl}}\right)}{2R_0R_{\mathrm{nucl}}^2\left(R-R_{\mathrm{nucl}}\right)^{\beta+1}}<0.$

Lemma 6.2.8. *If $\chi_c > \chi_c^*$, then the eigenvalue problem defined by eqs. (6.13) to (6.15) admits an eigenvalue with a positive real part.*

Proof. Let $\lambda \neq \dfrac{\delta\left(R^2 - R_{\text{nucl}}^2\right)\left(R\left(1-\beta\right) - R_{\text{nucl}}\right)}{2R_0 R_{\text{nucl}}^2 \left(R - R_{\text{nucl}}\right)^{\beta+1}}$ be an eigenvalue of the problem defined by eqs. (6.13) to (6.15) From lemma 6.2.6, we have that λ is such that $G_1\left(\lambda\right) = 0$. We perform the expansion of G_1 around 0. Using the properties of the Bessel functions, for λ close to zero, we have:

$$
\begin{aligned}
J_1\left(-\mathrm{i}\lambda^{\frac{1}{2}} R_0\right) &= \frac{-\mathrm{i}\lambda^{\frac{1}{2}} R_0}{2} + o\left(\lambda\right), \\
J_1'\left(-\mathrm{i}\lambda^{\frac{1}{2}} R_0\right) &= \frac{1}{2} + \frac{3R_0^2\lambda}{16} + o\left(\lambda\right), \\
Y_1\left(-\mathrm{i}\lambda^{\frac{1}{2}} R_0\right) &= \frac{-2\mathrm{i}}{\pi\lambda^{\frac{1}{2}} R_0} + \frac{\mathrm{i}\left(1-2\gamma\right)\lambda^{\frac{1}{2}} R_0}{2\pi} + \frac{2}{\pi} J_1\left(-\mathrm{i}\lambda^{\frac{1}{2}} R_0\right) \log\left(\frac{-\mathrm{i}\lambda^{\frac{1}{2}} R_0}{2}\right) + o\left(\lambda\right), \\
Y_1'\left(-\mathrm{i}\lambda^{\frac{1}{2}} R_0\right) &= \frac{-2}{\lambda R_0^2 \pi} + \frac{1+2\gamma}{2\pi} - \frac{R_0^2\lambda\left(11-12\gamma\right)}{32\pi} + \frac{2}{\pi} J_1'\left(-\mathrm{i}\lambda^{\frac{1}{2}} R\right) \log\left(\frac{-\mathrm{i}\lambda^{\frac{1}{2}} R}{2}\right) + o\left(\lambda\right),
\end{aligned}
$$

where γ denotes the Euler's constant. Thus for λ close to zero, we have:

$$
\begin{aligned}
G_1\left(\lambda\right) &= \left(1 - a\chi_c c^0 f_{\text{act}}'\left(c^0\right)\right)\left(\frac{1}{R_0^2\pi} - \frac{1}{R_{\text{nucl}}^2\pi}\right) \\
&\quad + \frac{3\left(R_{\text{nucl}}^4 - R_0^4\right)}{8\pi R_0^2 R_{\text{nucl}}^2}\lambda - a\chi_c c^0 f_{\text{act}}'\left(c^0\right)\frac{3\left(R_0^2 - R_{\text{nucl}}^2\right)}{8\pi R_0^2}\lambda \\
&\quad + \frac{a\chi_c c^0 f_{\text{act}}'\left(c^0\right) - 1}{2\pi}\ln\left(\frac{R_0}{R_{\text{nucl}}}\right)\lambda + o\left(\lambda\right), \\
&= g\left(\lambda\right) + o\left(\lambda\right).
\end{aligned}
$$

The function g admits $\lambda_1 \in \mathbb{R}$ as root with λ_1 defined by:

$$
\lambda_1 = -\frac{\left(1 - a\chi_c c^0 f_{\text{act}}'\left(c^0\right)\right)\left(\frac{1}{R_0^2\pi} - \frac{1}{R_{\text{nucl}}^2\pi}\right)}{\frac{3\left(R_{\text{nucl}}^4 - R_0^4\right)}{8\pi R_0^2 R_{\text{nucl}}^2} - a\chi_c c^0 f_{\text{act}}'\left(c^0\right)\frac{3\left(R_0^2 - R_{\text{nucl}}^2\right)}{8\pi R_0^2} + \frac{a\chi_c c^0 f_{\text{act}}'\left(c^0\right) - 1}{2\pi}\ln\left(\frac{R_0}{R_{\text{nucl}}}\right)}.
$$

We have:

$$
\left(1 - a\chi_c c^0 f_{\text{act}}'\left(c^0\right)\right)\left(\frac{1}{R_0^2\pi} - \frac{1}{R_{\text{nucl}}^2\pi}\right) > 0 \iff \chi_c > \chi_c^*.
$$

We also have:

$$
\begin{aligned}
&\frac{3\left(R_{\text{nucl}}^4 - R_0^4\right)}{8\pi R_0^2 R_{\text{nucl}}^2} - a\chi_c c^0 f_{\text{act}}'\left(c^0\right)\frac{3\left(R_0^2 - R_{\text{nucl}}^2\right)}{8\pi R_0^2} + \frac{a\chi_c c^0 f_{\text{act}}'\left(c^0\right) - 1}{2\pi}\ln\left(\frac{R_0}{R_{\text{nucl}}}\right) < 0 \\
\iff &\left[a\chi_c c^0 f_{\text{act}}'\left(c^0\right) < \frac{3\left(R_0^4 - R_{\text{nucl}}^4\right) + 4R_0^2 R_{\text{nucl}}^2 \ln\left(\frac{R_0}{R_{\text{nucl}}}\right)}{R_{\text{nucl}}^2\left(3\left(R_{\text{nucl}}^2 - R_0^2\right) + 4R_0^2\ln\left(\frac{R_0}{R_{\text{nucl}}}\right)\right)}\right. \\
&\qquad \left.\text{and } 3\left(R_{\text{nucl}}^2 - R_0^2\right) + 4R_0^2\ln\left(\frac{R_0}{R_{\text{nucl}}}\right) > 0\right] \text{ or } 3\left(R_{\text{nucl}}^2 - R_0^2\right) + 4R_0^2\ln\left(\frac{R_0}{R_{\text{nucl}}}\right) < 0.
\end{aligned}
$$

Moreover, if $3\left(R_{\text{nucl}}^2 - R_0^2\right) + 4R_0^2\ln\left(\frac{R_0}{R_{\text{nucl}}}\right) > 0$ then $\dfrac{3\left(R_0^4 - R_{\text{nucl}}^4\right) + 4R_0^2 R_{\text{nucl}}^2\ln\left(\frac{R_0}{R_{\text{nucl}}}\right)}{R_{\text{nucl}}^2\left(3\left(R_{\text{nucl}}^2 - R_0^2\right) + 4R_0^2\ln\left(\frac{R_0}{R_{\text{nucl}}}\right)\right)} > 1$. Thus λ_1 changes sign from negative to positive as χ_c exceeds χ_c^*. We can note that λ_1 approximates well a root of G_1 and that we have:

$$
\lambda_1 = \left(a\chi_c c^0 f_{\text{act}}'\left(c^0\right) - 1\right)\frac{8\left(R_0^2 - R_{\text{nucl}}^2\right)}{3a\chi_c c^0 f_{\text{act}}'\left(c^0\right)\left(R_0^4 + R_0^2 R_{\text{nucl}}^2 - 2R_{\text{nucl}}^4\right)} + o\left(\left|a\chi_c c^0 f_{\text{act}}'\left(c^0\right) - 1\right|\right).
$$

This eigenvalue is associated with the non-trivial eigenfunction:

$$\begin{pmatrix} c\left(r\right) \\ \rho \\ x_{\text{nucl}} \end{pmatrix} = \begin{pmatrix} \beta_{\lambda_1} J_1\left(-\mathrm{i}\lambda_1^{\frac{1}{2}} r\right) + \gamma_{\lambda_1} Y_1\left(-\mathrm{i}\lambda_1^{\frac{1}{2}} r\right) \\ 0 \\ 0 \end{pmatrix},$$

with

$$\beta_{\lambda_1} = \left(\mathrm{i}\lambda_1^{\frac{1}{2}} Y_1'\left(-\mathrm{i}\lambda_1^{\frac{1}{2}} R_0\right) + \frac{a\chi_c c^0 f'_{\text{act}}\left(c^0\right)}{R_0} Y_1\left(-\mathrm{i}\lambda_1^{\frac{1}{2}} R_0\right)\right),$$

$$\gamma_{\lambda_1} = -\left(\mathrm{i}\lambda_1^{\frac{1}{2}} J_1'\left(-\mathrm{i}\lambda_1^{\frac{1}{2}} R_0\right) + \frac{a\chi_c c^0 f'_{\text{act}}\left(c^0\right)}{R_0} J_1\left(-\mathrm{i}\lambda_1^{\frac{1}{2}} R_0\right)\right).$$

□

From the lemma 6.2.8, we deduce that when $\chi_c > \chi_c^*$, the eigenvalue problem defined by equations eqs. (6.11) and (6.12) admits an eigenvalue with a positive real part and thus the stationary state is linearly unstable.

To conclude the proof of the theorem, we need to show that when $\chi_c < \chi_c^*$ all the eigenvalues associated to (5.11) have negative real part. We give only a graphical illustration here. For several values of R_0, R_{nucl} and $\frac{\chi_c}{\chi_c^*}$, we represent the function G_1 by representing its real part, its imaginary part and its modulus (see fig. 6.1 for an example). We then observe that the root of G_1 with the largest real part seems to be a real root of G_1, which is confirmed by studying the imaginary part of G_1. Indeed, we notice that if $\lambda \in \mathbb{R}$ then $G_1\left(\lambda\right) \in \mathbb{R}$.

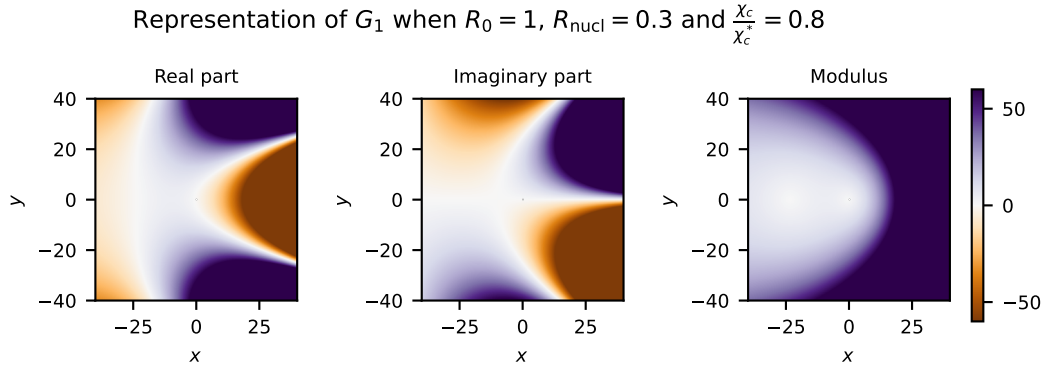

Figure 6.1: **Representation of G_1 in the complex framework for $R_0 = 1$, $R_{\text{nucl}} = 0.3$ and $\frac{\chi_c}{\chi_c^*} = 0.8$.** *Plots of the real part (left), the imaginary part (middle) and the modulus (right) of the function G_1 for $\lambda = x + \mathrm{i}y \in \mathbb{C}$ with $x, y \in [-40, 40]$. We observe that the root of G_1 with the greatest real part is a real root.*

We can therefore restrict the graphical study of G_1 to the graphical study of G_1 when $\lambda \in \mathbb{R}$. For R_0 and R_{nucl} fixed and for different values of $\frac{\chi_c}{\chi_c^*}$, we plot G_1 as a function of $\lambda \in \mathbb{R}$ (see fig. 6.2). This allows us to observe the largest real root of G_1 and we notice that when $\chi_c < \chi_c^*$ then this one is negative.

Moreover, we observe numerically that as soon as $\chi_c < \chi_c^*$ then the stationary state is stable, this will be illustrated in section 6.4.2.

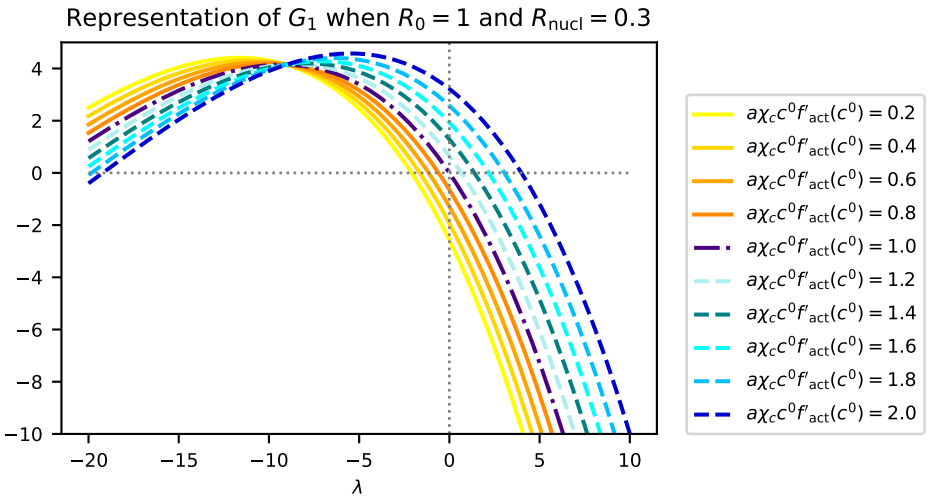

Figure 6.2: **Graphs of $\lambda \mapsto G_1(\lambda)$ for $\lambda \in \mathbb{R}$ when $R_0 = 1$ and $R_{\text{nucl}} = 0.3$ for different values of $\frac{\chi_c}{\chi_c^*} = a\chi_c c^0 f'\left(c^0\right)$.** *Each curve corresponds to a different value of χ_c. The solid yellow-orange curves correspond to the case where $\chi_c < \chi_c^*$, the dashed blue curves correspond to the case where $\chi_c > \chi_c^*$ and the dark dashdotted curve corresponds to the case where $\chi_c = 1\chi_c^*$. The grey dotted lines are the lines of equation $\lambda = 0$ and $y = 0$. In the case where $\chi_c < \chi_c^*$ we notice that G_1 seems to admit no positive root.*

Remark 6.2.9. *If for the force $\mathbf{f}_{\text{BN}}$ we choose the expression eq. (6.5) given by the heuristic approach, we then have for all $t \geq 0$:*

$$\mathbf{f}_{\text{BN}}(t) = -k\left(\mathbf{x}_{\text{nucl}}(t) - \mathbf{x}_{\text{cm}}(t)\right).$$

To proof the result on the stability of the stationary state of theorem 7.2.4, we can use the same the proof as the one in the case where $\mathbf{f}_{\text{BN}}$ defined by eq. (6.4). It suffices to follow the same procedure as that detailed in this section with $-k = \dfrac{\delta\pi R_0\left(R_0(1-\beta) - R_{\text{nucl}}\right)}{\left(R_0 - R_{\text{nucl}}\right)^{\beta+1}}$.

6.3 . Finite element scheme of the rigid model

In this section, we write a numerical scheme to simulate model (6.3). The procedure for obtaining this is very similar to that developed in section 5.3 for the model with a rigid particle. The proposed scheme is based on a semi-implicit discretization in time and a discretization in space using a finite element method.

6.3.1 . Time discretization

We discretize in time our model eq. (6.3). Let Δt be the time step. For $i \in \{0, \ldots, N_f\}$ with $N_f \in \mathbb{N}$, we denote $t^i = i\Delta t$, $\mathbf{u}^i = \mathbf{u}\left(t^i, \cdot\right)$, $P^i = P\left(t^i, \cdot\right)$ and $c^i = c\left(t^i, \cdot\right)$. We also denote $\Omega^i = \Omega\left(t^i\right)$ and $N^i = N\left(t^i\right)$. In addition, we denote $\mathbf{f}_{\text{BN}}^i$ the force induced by the boundary onto the nucleus associated with the cell geometry at time t^i and anagously we denote f_{NB}^i the force induced by the nucleus on a point of $\partial\Omega^i$ at time t^i. Moreover, we denote by $\dot{W}^{Q,i}$ an approximation of the coloured noise at time t^i.

The implicit discretization of the problem about velocities is given by:

$$\begin{cases} \mathbf{u}^{i+1} + \nabla P^{i+1} = 0 & \text{in } \Omega^i \setminus N^i, \quad (6.23a) \\ \operatorname{div}\left(\mathbf{u}^{i+1}\right) = 0 & \text{in } \Omega^i \setminus N^i, \quad (6.23b) \\ \mathbf{u}^{i+1} \cdot \mathbf{n} = \mathbf{u}_{\mathrm{cm}}^{i+1} \cdot \mathbf{n} & \text{on } \partial\Omega^i, \quad (6.23c) \\ \mathbf{u}^{i+1} \cdot \mathbf{n} = \mathbf{u}_{\mathrm{nucl}}^{i+1} \cdot \mathbf{n} & \text{on } \partial N^i, \quad (6.23d) \\ \mathbf{u}_{\mathrm{nucl}}^{i+1} = \dfrac{1}{\xi_{\mathrm{nucl}} \left|N^i\right|} \left(\displaystyle\int_{\partial N^i} P^{i+1} \mathbf{n} \, \mathrm{d}\sigma + \left|N^i\right| \mathbf{f}_{\mathrm{BN}}^i \right), & (6.23e) \\ \mathbf{u}_{\mathrm{cm}}^{i+1} = \dfrac{-1}{\left|\Omega^i\right|} \displaystyle\int_{\partial\Omega^i} \chi_c f_{\mathrm{act}}\left(c^i\right) \mathbf{n} \, \mathrm{d}\sigma + \dfrac{\left|N^i\right|}{\left|\Omega^i\right|} \left(1 - \xi_{\mathrm{nucl}}\right) \mathbf{u}_{\mathrm{nucl}}^{i+1}, & (6.23f) \end{cases}$$

and

$$\begin{cases} \dfrac{c^{i+1} - c^i}{\Delta t} = \operatorname{div}\left(\nabla c^{i+1} - (1-a)\, \mathbf{u}^{i+1} c^{i+1} - \alpha \dot{W}^{Q,i} c^{i+1} \right) & \text{in } \Omega^i \setminus N^i, \quad (6.24a) \\ \left(\nabla c^{i+1} + a \mathbf{u}^{i+1} c^{i+1} - \alpha \dot{W}^{Q,i} c^{i+1} \right) \cdot \mathbf{n} = 0 & \text{on } \partial\Omega^i \cup \partial N^i, \quad (6.24b) \end{cases}$$

with

$$\begin{cases} \Omega^{i+1} = \left(\mathrm{Id} + \Delta t\, \mathbf{u}_{\mathrm{cm}}^{i+1}\right)\left(\Omega^i\right), & (6.25a) \\ N^{i+1} = \left(\mathrm{Id} + \Delta t\, \mathbf{u}_{\mathrm{nucl}}^{i+1}\right)\left(N^i\right). & (6.25b) \end{cases}$$

6.3.2 . Decomposition of the fluid problem

We focus on the fluid velocity and pressure eq. (6.23). Instead to solve numerically this problem (6.23), we solve the following:

$$\begin{cases} -\Delta P^{i+1} = 0 & \text{in } \Omega^i \setminus N^i, \quad (6.26a) \\ -\nabla P^{i+1} \cdot \mathbf{n} = \mathbf{u}_{\mathrm{cm}}^{i+1} \cdot \mathbf{n} & \text{on } \partial\Omega^i, \quad (6.26b) \\ -\nabla P^{i+1} \cdot \mathbf{n} = \mathbf{u}_{\mathrm{nucl}}^{i+1} \cdot \mathbf{n} & \text{on } \partial N^i, \quad (6.26c) \end{cases}$$

with

$$\mathbf{u}_{\mathrm{nucl}}^{i+1} = \frac{1}{\xi_{\mathrm{nucl}} \left|N^i\right|} \left(\int_{\partial N^i} P^{i+1} \mathbf{n} \, \mathrm{d}\sigma + \left|N^i\right| \mathbf{f}_{\mathrm{BN}}^i \right)$$

and

$$\mathbf{u}_{\mathrm{cm}}^{i+1} = \frac{-1}{\left|\Omega^i\right|} \int_{\partial\Omega^i} \chi_c f_{\mathrm{act}}\left(c^i\right) \mathbf{n} \, \mathrm{d}\sigma + \frac{\left|N^i\right|}{\left|\Omega^i\right|} \left(1 - \xi_{\mathrm{nucl}}\right) \mathbf{u}_{\mathrm{nucl}}^{i+1}.$$

We then set $\mathbf{u}^{i+1} = -\nabla P^{i+1}$. We decompose eq. (6.26) in four independent problems to separate the boundary conditions on $\partial\Omega^i$ and ∂N^i. We define as follows the four problems:

$$\begin{cases} -\Delta P_1 = 0 & \text{in } \Omega^i \setminus N^i, \quad (6.27a) \\ \nabla P_1 \cdot \mathbf{n} = n_x & \text{on } \partial\Omega^i, \quad (6.27b) \\ \nabla P_1 \cdot \mathbf{n} = 0 & \text{on } \partial N^i, \quad (6.27c) \end{cases}$$

$$\begin{cases} -\Delta P_2 = 0 & \text{in } \Omega^i \setminus N^i, \quad (6.28a) \\ \nabla P_2 \cdot \mathbf{n} = n_y & \text{on } \partial\Omega^i, \quad (6.28b) \\ \nabla P_2 \cdot \mathbf{n} = 0 & \text{on } \partial N^i, \quad (6.28c) \end{cases}$$

$$\begin{cases} -\Delta P_3 = 0 & \text{in } \Omega^i \setminus N^i, \quad (6.29a) \\ \nabla P_3 \cdot \mathbf{n} = 0 & \text{on } \partial\Omega^i, \quad (6.29b) \\ \nabla P_3 \cdot \mathbf{n} = n_x & \text{on } \partial N^i, \quad (6.29c) \end{cases}$$

$$\begin{cases} -\Delta P_4 = 0 & \text{in } \Omega^i \setminus N^i, \quad (6.30a) \\ \nabla P_4 \cdot \mathbf{n} = 0 & \text{on } \partial\Omega^i, \quad (6.30b) \\ \nabla P_4 \cdot \mathbf{n} = n_y & \text{on } \partial N^i, \quad (6.30c) \end{cases}$$

where n_x and n_y are the coordinates of the normal outward vector of $\Omega^i \setminus N^i$.

We want to find μ_1, μ_2, μ_3 and $\mu_4 \in \mathbb{R}$ such that $P^{i+1} = \mu_1 P_1 + \mu_2 P_2 + \mu_3 P_3 + \mu_4 P_4$ with P_1, P_2, P_3 and P_4 respectively solutions to eqs. (6.27) to (6.30). This is equivalent to find $\boldsymbol{\mu} = (\mu_1, \mu_2, \mu_3, \mu_4)^T$ such that $A_\mu \boldsymbol{\mu} = B_\mu$ where A_μ is the following matrix

$$A_\mu = \begin{pmatrix} 1 + \frac{1-\xi_{\text{nucl}}}{\xi_{\text{nucl}}|\Omega^i|} P_1^x & \frac{1-\xi_{\text{nucl}}}{\xi_{\text{nucl}}|\Omega^i|} P_2^x & \frac{1-\xi_{\text{nucl}}}{\xi_{\text{nucl}}|\Omega^i|} P_3^x & \frac{1-\xi_{\text{nucl}}}{\xi_{\text{nucl}}|\Omega^i|} P_4^x \\ \frac{1-\xi_{\text{nucl}}}{\xi_{\text{nucl}}|\Omega^i|} P_1^y & 1 + \frac{1-\xi_{\text{nucl}}}{\xi_{\text{nucl}}|\Omega^i|} P_2^y & \frac{1-\xi_{\text{nucl}}}{\xi_{\text{nucl}}|\Omega^i|} P_3^y & \frac{1-\xi_{\text{nucl}}}{\xi_{\text{nucl}}|\Omega^i|} P_4^y \\ \frac{1}{\xi_{\text{nucl}}|N^i|} P_1^x & \frac{1}{\xi_{\text{nucl}}|N^i|} P_2^x & 1 + \frac{1}{\xi_{\text{nucl}}|N^i|} P_3^x & \frac{1}{\xi_{\text{nucl}}|N^i|} P_4^x \\ \frac{1}{\xi_{\text{nucl}}|N^i|} P_1^y & \frac{1}{\xi_{\text{nucl}}|N^i|} P_2^y & \frac{1}{\xi_{\text{nucl}}|N^i|} P_3^y & 1 + \frac{1}{\xi_{\text{nucl}}|N^i|} P_4^y \end{pmatrix} \quad (6.31)$$

and B the following vector

$$B_\mu = \begin{pmatrix} \frac{1}{|\Omega^i|} \int_{\partial\Omega^i} \left(\chi_c f_{\text{act}}\left(c^i\right) - f_{NB}^i\right) n_x \, \mathrm{d}\sigma - \frac{|N^i|}{\xi_{\text{nucl}}|\Omega^i|} \mathbf{f}_{\text{BN},x}^i \\ \frac{1}{|\Omega^i|} \int_{\partial\Omega^i} \left(\chi_c f_{\text{act}}\left(c^i\right) - f_{NB}^i\right) n_y \, \mathrm{d}\sigma - \frac{|N^i|}{\xi_{\text{nucl}}|\Omega^i|} \mathbf{f}_{\text{BN},y}^i \\ -\frac{\mathbf{f}_{\text{BN},x}^i}{\xi_{\text{nucl}}} \\ -\frac{\mathbf{f}_{\text{BN},y}^i}{\xi_{\text{nucl}}} \end{pmatrix} \quad (6.32)$$

with $P_j^x = \int_{\partial N^i} P_j \, n_x \, \mathrm{d}\sigma$ and $P_j^y = \int_{\partial N^i} P_j \, n_y \, \mathrm{d}\sigma$ for $j \in \{1, 2, 3, 4\}$ and $\mathbf{f}_{\text{BN},x}^i$, $\mathbf{f}_{\text{BN},y}^i$ the coordinates of $\mathbf{f}_{\text{BN}}^i$.

6.3.3 . Spatial discretization

We discretize in space our time-discrete model eqs. (6.23) to (6.25). We use a finite element discretization. Let $\mathcal{T}$ be a triangulation of $\Omega^i \setminus N^i$ (see fig. 6.3). For all triangle $K \in \mathcal{T}$ we note $\left(\lambda_1^K, \lambda_2^K, \lambda_3^K\right)$ the barycentric coordinate functions of K. First we define the functional spaces needed. Let $\mathbb{P}_k$ be the set of polynomials of $\mathbb{R}^2$ of degrees less or equal k. Let $\mathcal{H}_P$ be the functional space define by:

$$\mathcal{H}_P = \left\{ Q \in H^1\left(\Omega^i \setminus N^i\right) \mid \forall K \in \mathcal{T}, Q|_K \in \mathbb{P}_1 \right\}.$$

Let $\mathcal{H}_c$ be the functional space define by:

$$\mathcal{H}_c = \left\{ \psi \in H^1\left(\Omega^i \setminus N^i\right) \mid \forall K \in \mathcal{T}, \psi|_K \in \mathbb{P}_1 \oplus \text{Span}\left\{\lambda_1^K, \lambda_2^K, \lambda_3^K\right\} \right\}.$$

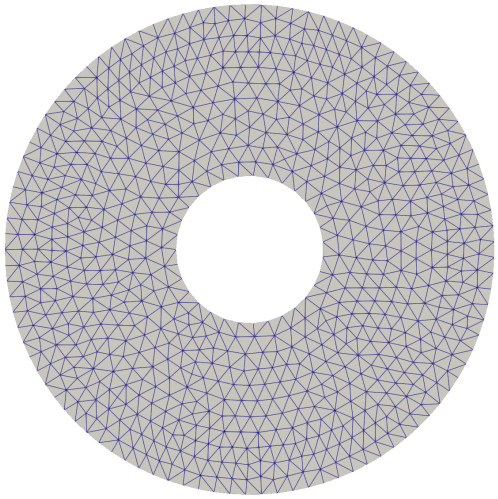

Figure 6.3: **Illustration of the initial mesh of the fluid domain when the nucleus is at the cell centre.**

6.3.4 . Variational formulation of the fluid problem

Instead of writing the variational formulation of eq. (6.23), we use the decomposition result and write the variational formulation of the four independent problems eqs. (6.27) to (6.30).

The variational formulation of the problem eq. (6.27) is given by:

$$\begin{cases} \text{Find } P_1 \in \mathcal{H}_P \text{ such that for all } Q \in \mathcal{H}_P, \text{ we have:} \\ \displaystyle\int_{\Omega^i \setminus N^i} \nabla P_1 \cdot \nabla Q \, \mathrm{d}\mathbf{x} - \int_{\partial\Omega^i} Q n_x \, \mathrm{d}\sigma = 0. \end{cases} \tag{6.33}$$

The variational formulation of the problem eq. (6.28) is given by:

$$\begin{cases} \text{Find } P_2 \in \mathcal{H}_P \text{ such that for all } Q \in \mathcal{H}_P, \text{ we have:} \\ \displaystyle\int_{\Omega^i \setminus N^i} \nabla P_2 \cdot \nabla Q \, \mathrm{d}\mathbf{x} - \int_{\partial\Omega^i} Q n_y \, \mathrm{d}\sigma = 0. \end{cases} \tag{6.34}$$

The variational formulation of the problem eq. (6.29) is given by:

$$\begin{cases} \text{Find } P_3 \in \mathcal{H}_P \text{ such that for all } Q \in \mathcal{H}_P, \text{ we have:} \\ \displaystyle\int_{\Omega^i \setminus N^i} \nabla P_3 \cdot \nabla Q \, \mathrm{d}\mathbf{x} - \int_{\partial N^i} Q n_x \, \mathrm{d}\sigma = 0. \end{cases} \tag{6.35}$$

The variational formulation of the problem eq. (6.30) is given by:

$$\begin{cases} \text{Find } P_3 \in \mathcal{H}_P \text{ such that for all } Q \in \mathcal{H}_P, \text{ we have:} \\ \displaystyle\int_{\Omega^i \setminus N^i} \nabla P_3 \cdot \nabla Q \, \mathrm{d}\mathbf{x} - \int_{\partial N^i} Q n_y \, \mathrm{d}\sigma = 0. \end{cases} \tag{6.36}$$

6.3.5 . Discretization of the noise

The discretization of the noise is based on the method developed in Boulakia et al. (2015). Instead of simulating $\dot{W}_t^Q$ over its entire domain of definition, we want to restrict its simulation to the current fluid domain. We recall that $\dot{W}^{Q,i}$ denotes an approximation of the coloured noise at time t^i, $i \in \{1, \dots, N_f\}$. We set:

$$\dot{W}^{Q,i} = \frac{W_{t^i}^Q - W_{t^{i-1}}^Q}{\Delta t}.$$

From the definition of W_t^Q, we know that $\dot{W}^{Q,i}$ is equal in law to $\frac{1}{\sqrt{\Delta t}} W_1^Q$ and that the $\left\{\dot{W}^{Q,i}\right\}_{1 \leq i \leq N_f}$ are independent. Therefore, to simulate $\dot{W}^{Q,i}$, we simulate $W_1^{Q,i}$. For all i, $W_1^{Q,i}$ is a realisation of the Q-Wiener process at time 1 restricted to the discrete current fluid domain $\Omega^i \setminus N^i$.

A way to compute $W_1^{Q,i} = \left(\omega_1^i, \omega_2^i\right)$, the discrete noise, relies on the computation of a covariance matrix (Boulakia et al., 2015). The computation of the covariance matrix is restricted to the computation of the covariance matrix restricted to the current domain. At time t^i, let $\left\{P_j^i, 1 \leq j \leq N_h^i\right\}$ be the set of all the nodes of the triangulation $\mathcal{T}_h^i$ of $\Omega^i \setminus N^i$, where N_h^i is the number of nodes of the triangulation, and $\left\{\psi_j^i, 1 \leq j \leq N_h^i\right\}$ be a basis of the Lagrangian $P1$ finite element. ψ_j^i is a continuous affine function on $\Omega^i \setminus N^i$ such that for all $1 \leq j, k \leq N_h^i$, we have $\psi_j^i\left(P_k^i\right) = \delta_{jk}$. For $m \in \{1, 2\}$, the $P1$ discretization of ω_m^i is given by

$$\omega_m^i = \sum_{j=1}^{N_h^i} x_j^i \psi_j^i.$$

with $\left\{x_j^i, 1 \leq j \leq N_h^i\right\}$ a realisation of a centred Gaussian vector of covariance matrix Σ^i. We have $\Sigma^i = \left(q\left(P_j^i, P_k^i\right)\right)_{1 \leq j,k \leq N_h^i}$. Let X be a centred Gaussian vector of covariance matrix Σ^i. We have

$$X = S^i Y,$$

with Y a Gaussian vector such that for all $1 \leq j \leq N_h^i$, $Y_j \sim \mathcal{N}(0, 1)$ and S^i such that $\Sigma^i = S^i \left(S^i\right)^T$. Thus to compute $W_1^{Q,i}$, we just have to simulate a realization of a standard Gaussian vector and to compute the Cholesky decomposition S^i of the covariance matrix Σ^i. Note that since the domain is deformable, the space-dependent Σ^i matrix is time-dependent and must be computed along with its Cholesky decomposition S^i at each time step.

6.3.6 . Discretization of the concentration problem

At each step of the numerical simulations, the mesh is propagating with the velocity $\mathbf{u}_{\text{mesh}}$ which satisfies:

$$\begin{cases} \Delta \mathbf{u}_{\text{mesh}} = 0 & \text{in } \Omega^i \setminus N^i, \\ \mathbf{u}_{\text{mesh}} = \mathbf{u}_{\text{cm}}^{i+1} & \text{on } \partial\Omega^i, \\ \mathbf{u}_{\text{mesh}} = \mathbf{u}_{\text{nucl}}^{i+1} & \text{on } \partial N^i. \end{cases}$$

Thus the mesh propagation induces advection at velocity $\mathbf{u}_{\text{mesh}}$ of the markers concentration. Taking it into account leads to modify the discrete concentration problem eq. (6.24) as

follows:

$$\begin{cases} \dfrac{c^{i+1}-c^i}{\Delta t} + (1-a)\,\mathbf{u}^{i+1}\cdot\nabla c^{i+1} - \dfrac{\alpha}{\sqrt{\Delta t}} W_1^{Q,i} c^{i+1} \\ \qquad\qquad - \mathbf{u}_{\text{mesh}}\cdot\nabla c^{i+1} - \Delta c^{i+1} = 0 & \text{in } \Omega^i \setminus N^i, \quad (6.37a) \\ \left(\nabla c^{i+1} + a c^{i+1}\mathbf{u}^{i+1}\right)\cdot\mathbf{n} = 0 & \text{on } \partial\Omega^i \cup \partial N^i. \quad (6.37b) \end{cases}$$

The variational formulation of eq. (6.37) is given by:

$$\begin{cases} \text{Find } c^{i+1} \in \mathcal{H}_c \text{ such that for all } \psi \in \mathcal{H}_c, \text{ we have:} \\ \displaystyle\int_{\Omega^i\setminus N^i} \left(\frac{c^{i+1}-c^i}{\Delta t}\right)\psi\,\mathrm{d}\mathbf{x} + \int_{\Omega^i\setminus N^i} \operatorname{div}\left(\mathbf{u}_{\text{mesh}}\right) c^{i+1}\psi\,\mathrm{d}\mathbf{x} \\ \qquad - \displaystyle\int_{\Omega^i\setminus N^i} \left((1-a)\,\mathbf{u}^{i+1}c^{i+1} - \mathbf{u}_{\text{mesh}}c^{i+1} - \nabla c^{i+1}\right)\cdot\nabla\psi\,\mathrm{d}\mathbf{x} \\ \qquad + \displaystyle\int_{\Omega^i\setminus N^i} \frac{\alpha}{\sqrt{\Delta t}} c^{i+1} W_1^{Q,i}\cdot\nabla\psi\,\mathrm{d}\mathbf{x} = 0. \end{cases} \quad (6.38)$$

6.3.7 . Avoid contact between cell boundary and nucleus

The discretization steps described above can be used to simulate eq. (5.3). However, these steps do not ensure that the particle remains inside the cell. To ensure this, we add a step to the computation of the cell and nucleus velocities. Using a Uzawa algorithm, we project the velocities of the cell and the nucleus onto a space of so-called admissible velocities, chosen to ensure that the nucleus and the boundary of the cell are not in contact. The numerical scheme used to simulate eq. (5.3) is given by the following algorithm.

Algorithm 6.1 : Numerical scheme to simulate eq. (6.3) obtained after time discretization and space discretization with a finite element method.

1. Initialisation: $c^0 = c^{\text{in}}$ the given initial condition and definition of the mesh with Ω^0 and N^0 given.
2. Time iteration:
   (a) Compute $\mathbf{u}^{i+1}$ and P^{i+1} using c^i and the decomposition method:
      i. Solve the variational formulation eq. (6.33) to compute P_1.
      ii. Solve the variational formulation eq. (6.34) to compute P_2.
      iii. Solve the variational formulation eq. (6.35) to compute P_3.
      iv. Solve the variational formulation eq. (6.36) to compute P_4.
      v. Compute $\boldsymbol{\mu} = (\mu_1, \mu_2, \mu_3, \mu_4)^T$ by solving $A_\mu \boldsymbol{\mu} = B_\mu$ with A_μ given by eq. (6.31) and B_μ given by eq. (6.32).
      vi. Deduce $P^{i+1} = \mu_1 P_1 + \mu_2 P_2 + \mu_3 P_3 + \mu_4 P_4$ and compute $\mathbf{u}^{i+1} = -\nabla P^{i+1}$.
   (b) Computation of the *a priori* nucleus velocity:
   $$\mathbf{u}_{\text{nucl}}^{i+\frac{1}{2}} = \frac{1}{\xi_{\text{nucl}} \left|N^i\right|} \left(\int_{\partial N^i} P^{i+1} \mathbf{n} \, \mathrm{d}\sigma + \left|N^i\right| \mathbf{f}_{\text{BN}} \right).$$
   (c) Computation of the *a priori* cell velocity:
   $$\mathbf{u}_{\text{cm}}^{i+\frac{1}{2}} = \frac{-1}{|\Omega^i|} \int_{\partial \Omega^i} \chi_c f_{\text{act}} \left(c^i\right) \mathbf{n} \, \mathrm{d}\sigma + \frac{\left|N^i\right|}{|\Omega^i|} \left(1 - \xi_{\text{nucl}}\right) \mathbf{u}_{\text{nucl}}^{i+\frac{1}{2}}.$$
   (d) Using a Uzawa algorithm, computation of $\mathbf{u}_{\text{nucl}}^{i+1}$ and $\mathbf{u}_{\text{cm}}^{i+1}$ which are the projection of the *a priori* velocities $\mathbf{u}_{\text{nucl}}^{i+\frac{1}{2}}$ and $\mathbf{u}_{\text{cm}}^{i+\frac{1}{2}}$ on an admissible velocities space (see algorithm 6.2 for more details).
   (e) Computation of the mesh velocity $\mathbf{u}_{\text{mesh}}$.
   (f) Computation of the covariance matrix Σ^i and S^i its Cholesky decomposition and deduction of the discrete noise $W_1^{Q,i} = S^i Y$ where Y a realisation of a standard normal Gaussian vector.
   (g) Computation of the markers concentration c^{i+1} using $\mathbf{u}^{i+1}$, $W_1^{Q,i}$ and $\mathbf{u}_{\text{mesh}}$ by solving the variational formulation eq. (5.34).
   (h) Update of the domain:
   $$\Omega^{i+1} = \left(\mathrm{Id} + \Delta t \, \mathbf{u}_{\text{mesh}}\right) \left(\Omega^i\right),$$
   $$N^{i+1} = \left(\mathrm{Id} + \Delta t \, \mathbf{u}_{\text{mesh}}\right) \left(N^i\right)$$

Next, we give details concerning Uzawa's algorithm for handling the potential contact between the cell boundary and the nucleus. Let $i \in \{0, \ldots, N_f\}$. We denote by $\mathbf{X} = \left(\mathbf{x}_{\text{nucl}}^i, \mathbf{x}_{\text{cell}}^i\right)$ the vector with the coordinate of the particle and cell centres at time t^i. The distance $D\left(\mathbf{X}\right)$ between the nucleus and the cell boundary is given by:

$$D\left(\mathbf{X}\right) = R_0 - R_{\text{nucl}} - \left|\mathbf{x}_{\text{nucl}}^i - \mathbf{x}_{\text{cell}}^i\right|.$$

The gradient G of the distance D is given by:

$$G\left(\mathbf{X}\right) = \left(-\mathbf{e}\left(\mathbf{X}\right), \mathbf{e}\left(\mathbf{X}\right)\right),$$

where $\mathbf{e}\left(\mathbf{X}\right) = \dfrac{\mathbf{x}_{\text{nucl}}^{i+\frac{1}{2}} - \mathbf{x}_{\text{cell}}^i}{\left|\mathbf{x}_{\text{nucl}}^i - \mathbf{x}_{\text{cell}}^i\right|}$. Let $\mathbf{V} = \left(\mathbf{u}_{\text{nucl}}^{i+\frac{1}{2}}, \mathbf{u}_{\text{cm}}^{i+\frac{1}{2}}\right)$ be the vector containing the velocities

of the nucleus and the cell. The vector $\mathbf{V}$ is said to be admissible if the velocities $\mathbf{u}_{\text{nucl}}^{i+\frac{1}{2}}$ and $\mathbf{u}_{\text{cm}}^{i+\frac{1}{2}}$ ensure that, at the next time step, the nucleus and the boundary of the cell are not in contact. This condition is expressed as:

$$D\left(\mathbf{X}+\Delta t\,\mathbf{V}\right)\geq\varepsilon,$$

with $\varepsilon>0$ small. By linearising this condition, it can be approximated by:

$$D\left(\mathbf{X}\right)+\Delta t G\left(\mathbf{X}\right)\cdot\mathbf{V}\geq\varepsilon.$$

From this linearized condition and the expression of the gradient G, we derive a space of admissible velocities defined by:

$$\mathcal{K}\left(\mathbf{X}\right)=\left\{(\mathbf{v}_n,\mathbf{v}_c)\in\mathbb{R}^2\times\mathbb{R}^2 \text{ s.t. } \Delta t\left(\mathbf{e}\left(\mathbf{X}\right)\cdot\mathbf{v}_n-\mathbf{e}\left(\mathbf{X}\right)\cdot\mathbf{v}_c\right)\leq D\left(\mathbf{X}\right)-\varepsilon\right\}.$$

Let $\left(\mathbf{u}_{\text{nucl}}^{i+1},\,\mathbf{u}_{\text{cm}}^{i+1}\right)$ be the projection of $\mathbf{V}$ onto $\mathcal{K}\left(\mathbf{X}\right)$. Then $\left(\mathbf{u}_{\text{nucl}}^{i+1},\,\mathbf{u}_{\text{cm}}^{i+1}\right)$ satifies the following minimisation problem:

$$\begin{aligned}\left|\left(\mathbf{u}_{\text{nucl}}^{i+1},\,\mathbf{u}_{\text{cm}}^{i+1}\right)\right|^2-2\left\langle\left(\mathbf{u}_{\text{nucl}}^{i+1},\,\mathbf{u}_{\text{cm}}^{i+1}\right),\left(\mathbf{u}_{\text{nucl}}^{i+\frac{1}{2}},\,\mathbf{u}_{\text{cm}}^{i+\frac{1}{2}}\right)\right\rangle&\\ =\min_{(\mathbf{v}_n\,,\mathbf{v}_c)\in\mathcal{K}(\mathbf{X})}\left(\left|(\mathbf{v}_n\,,\,\mathbf{v}_c)\right|^2-2\left\langle(\mathbf{v}_n\,,\,\mathbf{v}_c),\left(\mathbf{u}_{\text{nucl}}^{i+\frac{1}{2}},\,\mathbf{u}_{\text{cm}}^{i+\frac{1}{2}}\right)\right\rangle\right)&\end{aligned}$$

It follows that there exists $\lambda\geq0$ such that $\left(\mathbf{u}_{\text{nucl}}^{i+1},\,\mathbf{u}_{\text{cm}}^{i+1}\right)$ satisfies (Lefebvre, 2007):

$$\begin{cases}2\left(\mathbf{u}_{\text{nucl}}^{i+1},\,\mathbf{u}_{\text{cm}}^{i+1}\right)+\lambda\left(\Delta t\,\mathbf{e}\left(\mathbf{X}\right)\,,\,-\Delta t\,\mathbf{e}\left(\mathbf{X}\right)\right)=2\left(\mathbf{u}_{\text{nucl}}^{i+\frac{1}{2}},\,\mathbf{u}_{\text{cm}}^{i+\frac{1}{2}}\right),\\ \Delta t\left(\mathbf{e}\left(\mathbf{X}\right)\cdot\mathbf{u}_{\text{nucl}}^{i+1}-\mathbf{e}\left(\mathbf{X}\right)\cdot\mathbf{u}_{\text{cm}}^{i+1}\right)\leq D\left(\mathbf{X}\right)-\varepsilon,\\ \lambda\left(\Delta t\left(\mathbf{e}\left(\mathbf{X}\right)\cdot\mathbf{u}_{\text{nucl}}^{i+1}-\mathbf{e}\left(\mathbf{X}\right)\cdot\mathbf{u}_{\text{cm}}^{i+1}\right)-D\left(\mathbf{X}\right)+\varepsilon\right)=0.\end{cases}$$

To solve this dual problem, we use a Uzawa algorithm, which is a projected fixed-step gradient descent algorithm. The algorithm used is described in algorithm 6.2.

Algorithm 6.2 : Uzawa algorithm for projecting nucleus and cell velocities to ensure no contact between the cell boundary and the nucleus.

Assume $\mathbf{u}_{\text{nucl}}^{i+\frac{1}{2}}$ and $\mathbf{u}_{\text{cm}}^{i+\frac{1}{2}}$ given.

1. Let $\mathbf{v}_n^0\in\mathbb{R}^2$ and $\mathbf{v}_c^0\in\mathbb{R}^2$. Let $\lambda^0\geq0$. Let $\eta>0$ small and $\rho>0$ a projection step.
2. While $\left|\left(\mathbf{v}_n^{k+1},\mathbf{v}_c^{k+1}\right)-\left(\mathbf{v}_n^{k},\mathbf{v}_c^{k}\right)\right|>\eta$ or $\left|\lambda^{k+1}-\lambda^k\right|>\eta$ do:
   (a) $\mathbf{v}_n^{k+1}=\mathbf{u}_{\text{nucl}}^{i+\frac{1}{2}}-\frac{1}{2}\lambda^k\Delta t\,\mathbf{e}\left(\mathbf{X}\right)$.
   (b) $\mathbf{v}_c^{k+1}=\mathbf{u}_{\text{cm}}^{i+\frac{1}{2}}+\frac{1}{2}\lambda^k\Delta t\,\mathbf{e}\left(\mathbf{X}\right)$.
   (c) $\lambda^{k+1}=\Pi_{\mathbb{R}_+}\left[\lambda^k+\rho\left(\Delta t\,\left(\mathbf{e}\left(\mathbf{X}\right)\cdot\mathbf{v}_n^{k+1}-\mathbf{e}\left(\mathbf{X}\right)\cdot\mathbf{v}_c^{k+1}\right)-D\left(\mathbf{X}\right)+\varepsilon\right)\right]$.
3. Update of the nucleus and the cell velocities:

$$\mathbf{u}_{\text{nucl}}^{i+1}=\mathbf{v}_n^{k+1}$$

and

$$\mathbf{u}_{\text{cm}}^{i+1}=\mathbf{v}_c^{k+1}.$$

6.4 . Numerical results

Using FreeFEM++ (Hecht, 2012), the algorithm 6.1 is implemented in order to run numerical simulations of the model (6.3). Firstly, considering $\mathbf{f}_{\mathrm{BN}}$ defined by eq. (6.4), we check that the proposed algorithm is in agreement with the results obtained during the analysis of the model. We therefore check that the scheme enables to recover the model's stationary state (6.7) and its stability according to the criterion given in the theorem 6.2.2 (see section 6.4.2). We also show that the modelling of the force between the boundary of the cell and the nucleus is in good agreement with the fact that the nucleus returns towards the centre of the cell (see section 6.4.1). We then investigate the role of the nucleus in cell motility (see section 6.4.3). Finally, we illustrate that if $\mathbf{f}_{\mathrm{BN}}$ is defined by eq. (6.5) then we obtain similar results (see section 6.4.4). This allows us to justify numerically the heuristic we have developed concerning the forces between the cell boundary and the nucleus, and to say that it is a good approximation to the case where $\mathbf{f}_{\mathrm{BN}}$ is defined by eq. (6.4).

6.4.1 . Illustration of the action of the restoring force on the nucleus

In this subsection, we illustrate, numerically, the effect of the restoring force on the nucleus. This force is supposed to return the nucleus to the centre of the cell. We also aim to verify that the nucleus represents a system isolated from the cell. This means checking that the action of the nucleus alone does not modify the cell centre of mass's velocity. To verify these two points, we remove the coupling between marker concentration and fluid dynamics by assuming that $\chi_c = 0$ and study the evolution of the nucleus position in the cell reference frame as well as the evolution of the cell velocity.

To ensure this, for different values of R_0 and R_{nucl}, β and δ, we initially place the nucleus outside its equilibrium position and plot the evolution over time of the position of the nucleus in the cell reference frame. Whatever the initial position of the nucleus $\mathbf{x}_{\mathrm{nucl}}^{\mathrm{in}}$, whatever R_0 and R_{nucl} such that $B\left(\mathbf{x}_{\mathrm{nucl}}^{\mathrm{in}}, R_{\mathrm{nucl}}\right) \subset B\left(0, R_0\right)$, we observe that as long as $\beta > 1$ and $\delta > 0$, the nucleus returns to its equilibrium position and the cell's centre of mass velocity is equal to zero (see fig. 6.4). This confirms the modelling assumptions.

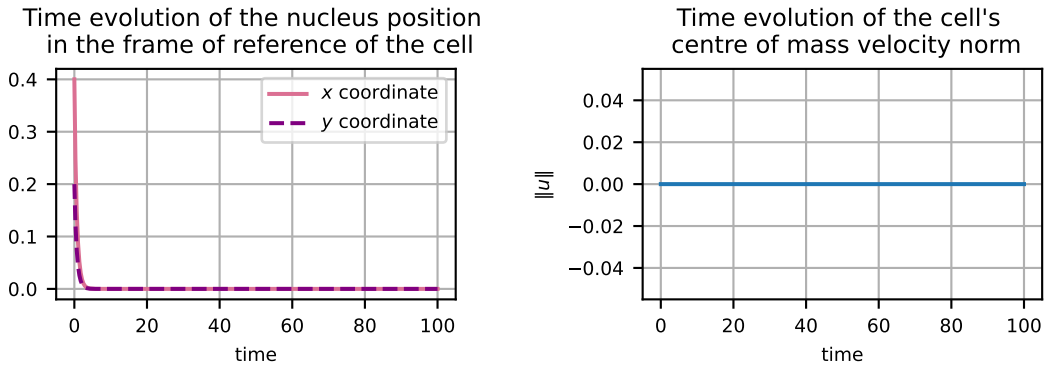

Figure 6.4: **Illustration of the nucleus dynamic without coupling with the markers concentration.** *On the left is the time evolution of the nucleus position in the cell frame of reference. We can observe that the nucleus quickly returns to the centre of the cell, as desired. On the right is the time evolution of the norm of the velocity of the centre of mass of the cell. We can note that this is constant and equal to zero, which means that the cell is not moving.*
The results presented here are obtained with the parameters $\Delta t = 0.005$, $R_0 = 1$, $R_{\text{nucl}} = 0.3$, $\mathbf{x}_{\text{nucl}}^{\text{in}} = (0.4; 0.2)$, $\chi_c = 0$, $\beta = 1.5$, $\delta = 0.141372$ *and* $\xi_{\text{nucl}} = 1$.

6.4.2 . Illustration of the theorem 6.2.2

In this section, we check that the numerical scheme proposed in algorithm 6.1 is consistent with the mathematical study of the model. We therefore check that if $\alpha = 0$ then we recover the stationary state (6.7) as well as the result on the stability of the latter stated in theorem 6.2.2.

First, we check that the model captures the stationary state. We then set a time step Δt, then R_0 and R_{nucl} in order to define the geometry of the cell, and we choose as the initial condition for the markers concentration $c^{\text{in}}(\mathbf{x}) = \dfrac{M}{|\Omega \setminus N|}$.

In this case, we observe that whatever the values of R_0, R_{nucl} and χ_c, we find a stationary state (see fig. 6.5 for an example). Indeed, the velocity of the cell remains zero over time and the position of the nucleus at the centre of the cell is maintained. We also observe that the distribution of markers is weel conserved over time. Moreover, we can observe that the quantity of markers is well conserved over time, which is in agreement with eq. (6.6) (see fig. 6.6).

Secondly, we check that the numerical scheme gives results in accordance with theorem 6.2.2. We therefore study the linear stability of the stationary state numerically. To do this, we choose a perturbation of the stationary state as the initial condition and observe, depending on the value of χ_c, whether the system returns to the stationary state.

The chosen stationary state perturbation is given by:

$$c^{\text{in}}(\mathbf{x}) = K(1 + X(\mathbf{x}))\,\mathbb{1}_{1+X(\mathbf{x})>0} \tag{6.39}$$

where for all $\mathbf{x} \in \Omega \setminus N$ we have $X(\mathbf{x}) \sim \mathcal{N}(0,1)$ and K such that $\int_{\Omega\setminus N} c^{\text{in}}(\mathbf{x})\,\mathrm{d}\mathbf{x} = M$. The nucleus position is perturbed by choosing:

$$\mathbf{x}_{\text{nucl}}^{\text{in}} = (0.1; 0)\,.$$

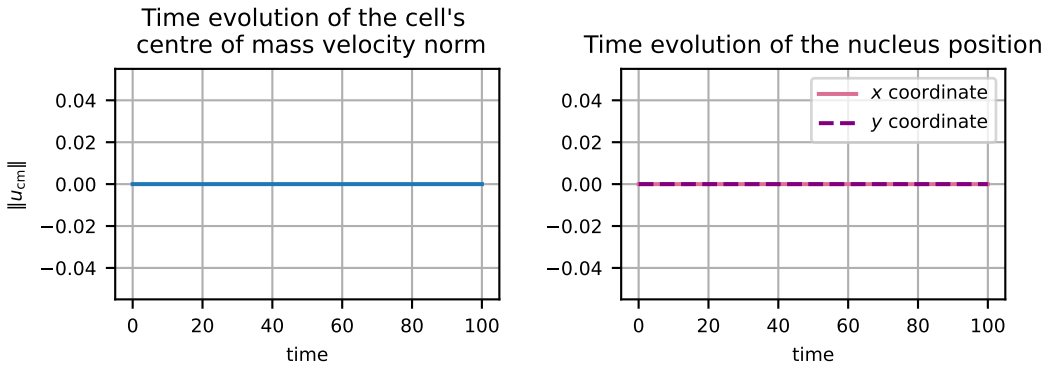

Figure 6.5: **Example of capturing the stationary state using the numerical scheme.** *The curve on the left represents the evolution of the velocity norm over time. We can observe that this remains zero throughout the study interval* $[0, 100]$*. The curves on the right represent the evolution over time of the coordinates of the nucleus position. We can see that the position of the nucleus is preserved over the study interval.*
The results presented here are obtained with the parameters $\Delta t = 0.005$, $R_0 = 1$, $R_{\text{nucl}} = 0.3$, $\mathbf{x}_{\text{nucl}}^{\text{in}} = (0; 0)$, $c^{\text{in}}(\mathbf{x}) = \frac{M}{\pi\left(R_0^2 - R_{\text{nucl}}^2\right)}$, $M = \pi$, $a = 1$, $\chi_c = 0.733956$, $f_{\text{act}}(c) = \frac{c(1+c_s)^2}{c_s(c+c_s)}$ *with* $c_s = 0.5$, $\beta = 1.5$, $\delta = 0.5$, *and* ξ_{nucl}.

As illustrated in fig. 6.7 for the case where $R_0 = 1$ and $R_{\text{nucl}} = 0.3$, we correctly find the criterion on the linear stablity of the stationary state. Indeed, when $\chi_c < \chi_c^*$, we have that the norm of the velocity decreases very quickly towards 0 then is constant equal to 0. This illustrates that when $\chi_c < \chi_c^*$ the stationary state is stable. Also, when $\chi_c > \chi_c^*$, we observe that the norm increases rapidly towards a strictly positive value and then becomes constant. This suggests that when $\chi_c > \chi_c^*$ there are stable travelling waves.

The trajectory study confirms that we are indeed capturing travelling waves (see fig. 6.8). Each cell maintains its orientation over time, which, coupled with the fact that the norm of the velocity is constant, leads to a progressive wave. The result is not surprising and is in agreement with Lavi et al. (2020) results in the case of a rigid cell.

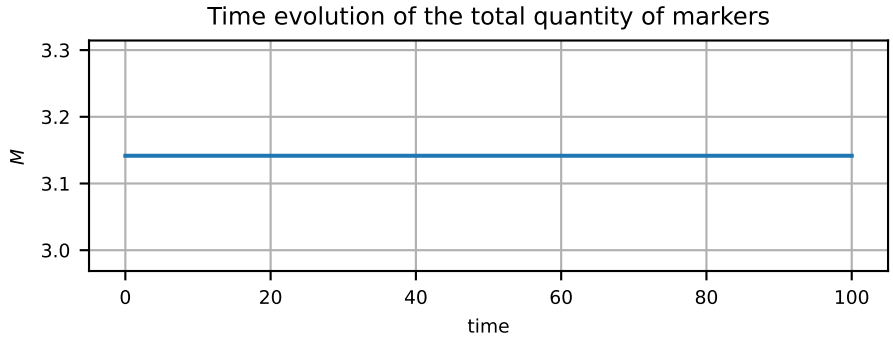

Figure 6.6: **Illustration of the conservation of the total quantity of markers.** *The curve represents the evolution of the total quantity of markers over time. We note that this remains constant throughout the study interval* $[0, 100]$.
The results presented here are obtained with the parameters $\Delta t = 0.005$, $R_0 = 1$, $R_{\text{nucl}} = 0.3$, $\mathbf{x}_{\text{nucl}}^{\text{in}} = (0; 0)$, $c^{\text{in}}(\mathbf{x}) = \frac{M}{\pi\left(R_0^2 - R_{\text{nucl}}^2\right)}$, $M = \pi$, $a = 1$, $\chi_c = 0.5$, $f_{\text{act}}(c) = \frac{c(1+c_s)^2}{c_s(c+c_s)}$ *with* $c_s = 0.5$, $\beta = 1.5$, $\delta = 0.141372$ *and* $\xi_{\text{nucl}} = 1$.

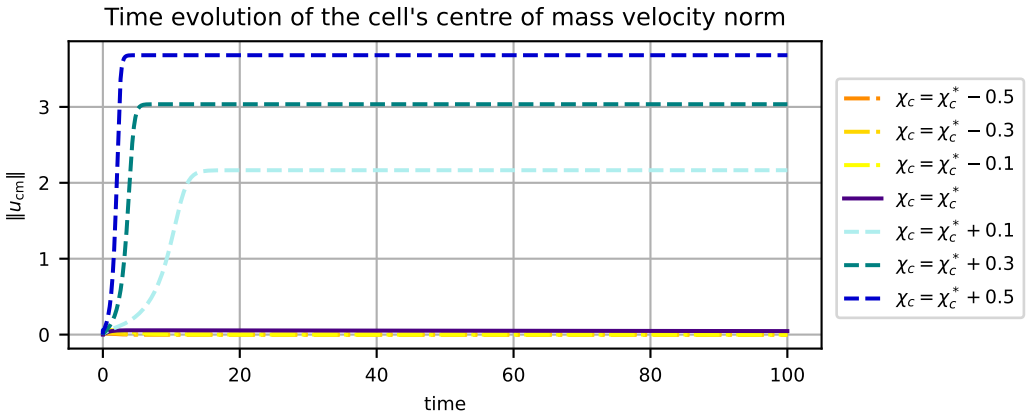

Figure 6.7: **Numerical illustration of theorem 6.2.2.** *Each curve represents the evolution of the cell's centre of mass velocity norm of a cell for different values of* χ_c *(see legend on the right). When* $\chi_c < \chi_c^*$ *the norm of the velocity decreases very rapidly towards* 0 *(dashdotted curves in overlapping shades of orange), whereas when* $\chi_c > \chi_c^*$ *it increases rapidly towards a non-zero value (dashed curves in shades of blue) . The critical case* $\chi_c = \chi_c^*$ *is also represented (dark curve), here the norm of the velocity is close to zero and decreases.*
The results presented here are obtained with the parameters $\Delta t = 0.005$, $R_0 = 1$, $R_{\text{nucl}} = 0.3$, $\mathbf{x}_{\text{nucl}}^{\text{in}} = (0.1; 0)$, $M = \pi$, $a = 1$, c^{in} *given by eq. (6.39) and* χ_c^* *given by (6.8),* $f_{\text{act}}(c) = \frac{c(1+c_s)^2}{c_s(c+c_s)}$ *with* $c_s = 0.5$, $\beta = 1.5$, $\delta = 0.141372$ *and* $\xi_{\text{nucl}} = 1$.

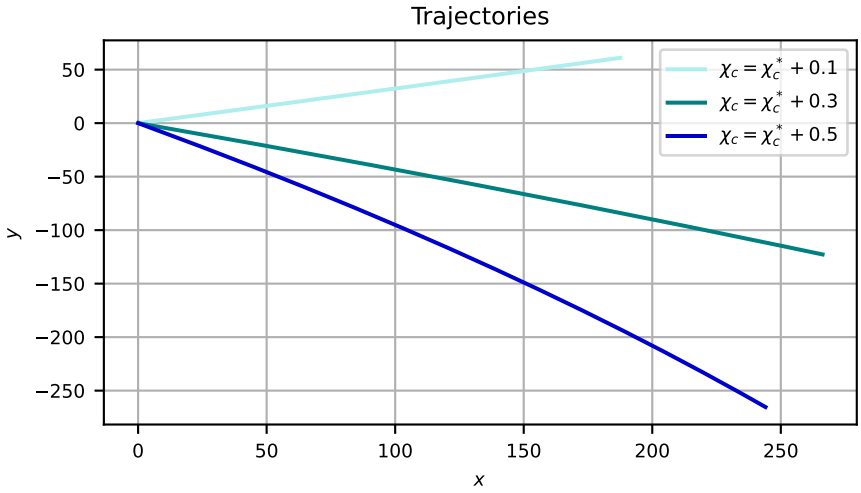

Figure 6.8: **Trajectories associated with the cells in fig. 6.7 in the case where $\chi_c > \chi_c^*$.** *Each curve represents the trajectory of one of the cells studied in figure 3. Only those where $\chi_c > \chi_c^*$ are represented, keeping the same colour coding (see legend on the right). We can therefore see that here the cells do not change orientation over time.*
The results presented here are obtained with the parameters $\Delta t = 0.005$, $R_0 = 1$, $R_{\text{nucl}} = 0.3$, $\mathbf{x}_{\text{nucl}}^{\text{in}} = (0.1; 0)$, $M = \pi$, $a = 1$, c^{in} given by eq. (6.39), χ_c^* given by (6.8), $f_{\text{act}}(c) = \frac{c(1+c_s)^2}{c_s(c+c_s)}$ with $c_s = 0.5$, $\beta = 1.5$, $\delta = 0.141372$ and $\xi_{\text{nucl}} = 1$.

6.4.3 . Role of the nucleus

In this section we numerically study the impact of the nucleus on cell motility. To do this, we highlight the properties of the nucleus and show that our model gives results in line with biological observations. First, we verify that the trajectories simulated via algorithm 6.1 satisfy the UCSP law. By comparing the results obtained with the crown model (see section 4.4.2) and the model with a rigid particle (see section 5.4.2), we highlight the effect of the nucleus on the trajectories. Finally, we highlight the link between cell polarisation and the dynamic of the nucleus

6.4.3.1 . Impact of the nucleus on the trajectories

In this section, we want to illustrate the impact of the nucleus on trajectories. In order to be able to compare with the results of sections 4.4.2 and 5.4.2 obtained respectively in the case of the crown model and the model with a rigid particle, we follow the same procedure. We fix all the parameters and vary only χ_c. We thus set for the numerical results presented, $R_0 = 1$, $R_{\text{nucl}} = 0.3$, $M = \pi$ and $a = 1$. The initial position of the nucleus is set to $\mathbf{x}_{\text{nucl}}^{\text{in}} = (0; 0)$. As an initial condition c^{in} for the concentration of markers, we choose the function defined for all $\mathbf{x} \in \Omega \setminus N$ by $c^{\text{in}}(\mathbf{x}) = \dfrac{M}{|\Omega \setminus N|}$. The noise parameters are set to $\alpha = 0.3$ and $\zeta = 0.2$. The nucleus dynamic parameters are set to $\xi_{\text{nucl}} = 1$, $\alpha = 0.3$, $\zeta = 0.2$, $\beta = 1.5$ and $\delta = 0.141372$. Finally, the numerical simulations are performed over the time interval $[0, 15]$ with $\Delta t = 0.005$.

Here are the results when $\chi_c = \chi_c^* - 0.3$, $\chi_c = \chi_c^*$ and $\chi_c = \chi_c^* + 0.5$ with χ_c^* defined in eq. (6.8).

Case where $\chi_c = \chi_c^* - 0.3$ In this paragraph, we present the results when $\chi_c = \chi_c^* - 0.3$. Visually, and unlike the cases of the crown model and the model with a rigid particle, the trajectories do not seem Brownian. We can observe trajectories with parts that appear to be persistent. The trajectories look intermittent (see fig. 6.9). This is confirmed by the study of the EASD and MSD, which are between 1 and 2 (see fig. 6.11). The UCSP law is always satisfied by the trajectories (see fig. 6.10).

As in the case of the crown model and the rigid particle, we observe that the velocity of the centre of mass is low (see fig. 6.12). However, we can observe that the dynamics of the velocity of the centre of mass is different. It seems that the mean of the norms of the velocities of the centre of mass increases over time and is no longer equal to the intensity of the noise. This means that the cell is not moving just because of the noise.

It seems that, with this choice of parameter $\chi_c = \chi_c^* - 0.3$, the nucleus makes the trajectories more directional than when its dynamics are not taken into account. One possible explanation is that as soon as the nucleus is no longer located at the centre of the cell, the cell starts to polarise, which induces directional movement until the nucleus is once again located at the centre of the cell. As the noise is present all the time, the position of the nucleus, via the coupling between the markers and the fluid, is permanently perturbed, leading to these intermittent trajectories.

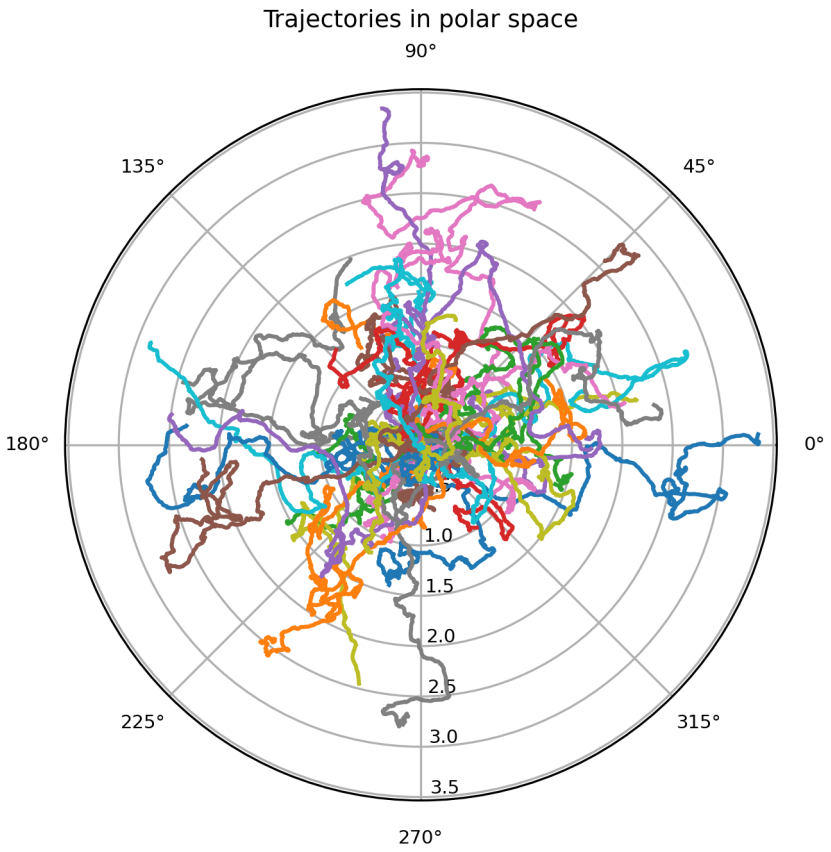

Figure 6.9: **Trajectories in polar coordinates in the case where $\chi_c < \chi_c^*$.** *Each curve represents, in polar coordinates, the trajectory of one cell simulated by algorithm 6.1 on the time interval $[0, 15]$. Visually, the trajectories seem to be intermittent. Fifty cells are represented.*
The results presented here are obtained with the parameters $\Delta t = 0.005$, $R_0 = 1$, $R_{\text{nucl}} = 0.3$, $\mathbf{x}_{\text{nucl}}^{\text{in}} = (0; 0)$, $M = \pi$, $a = 1$, $c^{\text{in}} = \dfrac{M}{|\Omega \setminus N|}$, $\chi_c = \chi_c^* - 0.3$ with χ_c^* given by (6.8), $f_{\text{act}}(c) = \frac{c(1+c_s)^2}{c_s(c+c_s)}$ with $c_s = 0.5$, $\alpha = 0.3$, $\zeta = 0.2$, $\beta = 1.5$, $\delta = 0.141372$ and $\xi_{\text{nucl}} = 1$.

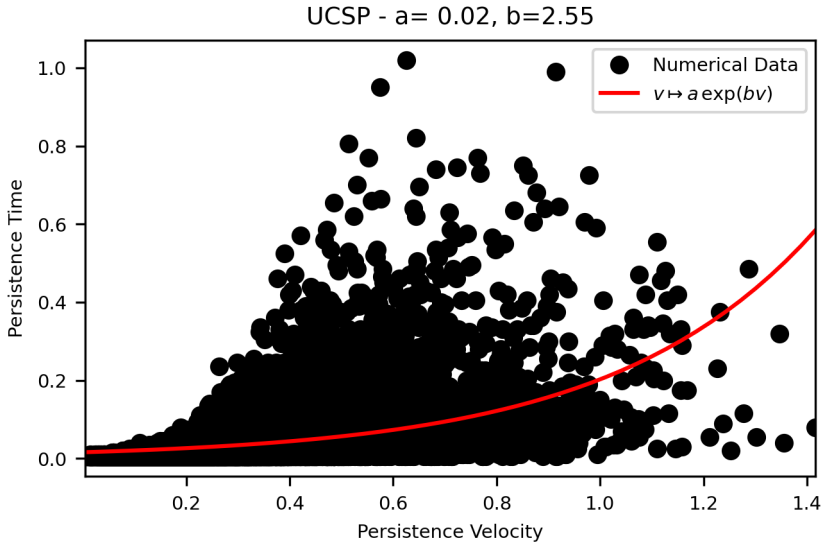

Figure 6.10: **Verification that the trajectories in fig. 6.9 satisfy the UCSP law (case when $\chi_c < \chi_c^*$).** *The persistence time of a locally persistent trajectory portion is plotted as a function of the persistence velocity. Each black dot corresponds to a datum. In red is plotted an interpolation of the points, of form $v \mapsto ae^{bv}$, which corresponds to the UCSP law. We can see that the data corresponds well to the interpolation and that the trajectories satisfy the UCSP law.*
The results presented here are obtained with the parameters $\Delta t = 0.005$, $R_0 = 1$, $R_{\text{nucl}} = 0.3$, $\mathbf{x}_{\text{nucl}}^{\text{in}} = (0;0)$, $M = \pi$, $a = 1$, $c^{\text{in}} = \dfrac{M}{|\Omega \setminus N|}$, $\chi_c = \chi_c^* - 0.3$ *with* χ_c^* *given by* (6.8), $f_{\text{act}}(c) = \frac{c(1+c_s)^2}{c_s(c+c_s)}$ *with* $c_s = 0.5$, $\alpha = 0.3$, $\zeta = 0.2$, $\beta = 1.5$, $\delta = 0.141372$ *and* $\xi_{\text{nucl}} = 1$.

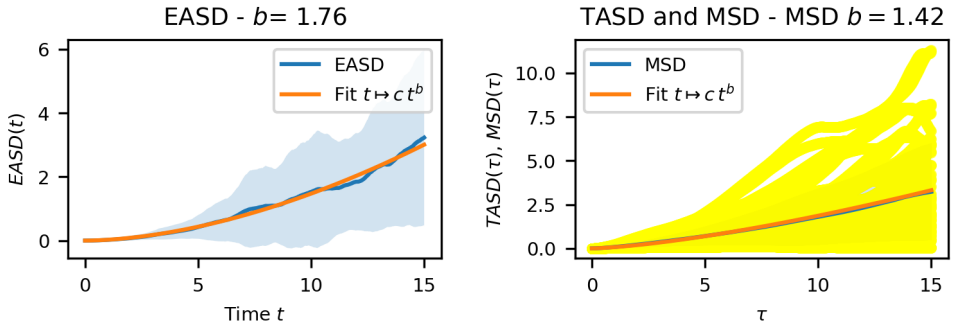

Figure 6.11: **Verification that the trajectories in fig. 6.9 are Brownian (case when $\chi_c < \chi_c^*$).** *On the left is shown in blue the EASD associated with the trajectories in fig. 6.9 and in orange the interpolation of the EASD, in the form $t \mapsto ct^b$. By the properties of the EASD, as b between 1 and 2, the trajectories in fig. 6.9 may be intermittent. This is confirmed by the study of the MSD, which is shown in blue on the right. Also shown on the right are the TASD of each cell in yellow and the interpolation of the MSD in form $t \mapsto ct^b$ in orange.*
The results presented here are obtained with the parameters $\Delta t = 0.005$, $R_0 = 1$, $R_{\text{nucl}} = 0.3$, $\mathbf{x}_{\text{nucl}}^{\text{in}} = (0;0)$, $M = \pi$, $a = 1$, $c^{\text{in}} = \dfrac{M}{|\Omega \setminus N|}$, $\chi_c = \chi_c^* - 0.3$ *with* χ_c^* *given by* (6.8), $f_{\text{act}}(c) = \frac{c(1+c_s)^2}{c_s(c+c_s)}$ *with* $c_s = 0.5$, $\alpha = 0.3$, $\zeta = 0.2$, $\beta = 1.5$, $\delta = 0.141372$ *and* $\xi_{\text{nucl}} = 1$.

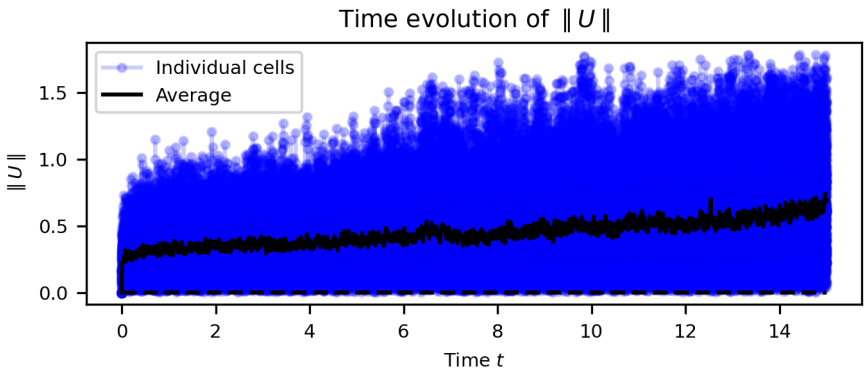

Figure 6.12: **Time evolution of the norm of the velocity of the cells whose trajectories are shown in fig. 6.9 (case when $\chi_c < \chi_c^*$).** *The blue lines show the evolution over time of the norm of the centre of mass velocity of each cell and the black line shows the evolution of the mean of the norms of the velocities of the cells.*
The results presented here are obtained with the parameters $\Delta t = 0.005$, $R_0 = 1$, $R_{\text{nucl}} = 0.3$, $\mathbf{x}_{\text{nucl}}^{\text{in}} = (0;0)$, $M = \pi$, $a = 1$, $c^{\text{in}} = \dfrac{M}{|\Omega \setminus N|}$, $\chi_c = \chi_c^* - 0.3$ *with* χ_c^* *given by* (6.8), $f_{\text{act}}(c) = \frac{c(1+c_s)^2}{c_s(c+c_s)}$ *with* $c_s = 0.5$, $\alpha = 0.3$, $\zeta = 0.2$, $\beta = 1.5$, $\delta = 0.141372$ *and* $\xi_{\text{nucl}} = 1$.

Case where $\chi_c = \chi_c^* + 0.5$ In this paragraph, we present the results when $\chi_c = \chi_c^* + 0.5$. Visually, the trajectories seem intermittent (see fig. 6.13), which is in agreement with the EASD and MSD study, which is between 1 and 2 (see fig. 6.15). This observation is very different from that made for the same parameters in the case of the crown model or the model with the rigid particle, where the trajectories were persistent. In addition, we can see that the trajectories satisfy the UCSP (see fig. 6.14).

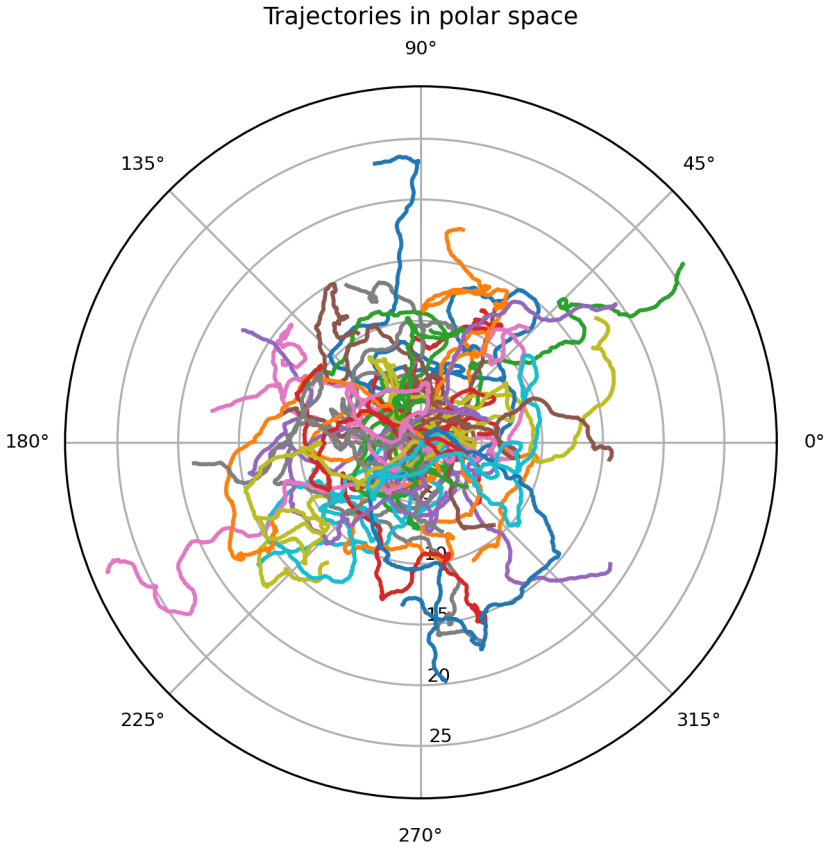

Figure 6.13: **Trajectories in polar coordinates in the case where $\chi_c > \chi_c^*$.** *Each curve represents, in polar coordinates, the trajectory of one cell simulated by algorithm 6.1 on the time interval $[0, 15]$. Visually, the trajectories seem to be intermittent. Fifty cells are represented.*
The results presented here are obtained with the parameters $\Delta t = 0.005$, $R_0 = 1$, $R_{\text{nucl}} = 0.3$, $\mathbf{x}_{\text{nucl}}^{\text{in}} = (0; 0)$, $M = \pi$, $a = 1$, $c^{\text{in}} = \dfrac{M}{|\Omega \setminus N|}$, $\chi_c = \chi_c^* + 0.5$ with χ_c^* given by (6.8), $f_{\text{act}}(c) = \frac{c(1+c_s)^2}{c_s(c+c_s)}$ with $c_s = 0.5$, $\alpha = 0.3$, $\zeta = 0.2$, $\beta = 1.5$, $\delta = 0.141372$ and $\xi_{\text{nucl}} = 1$.

Finally, we can observe that, with these parameters, the mean velocity of the centre of mass is high (see fig. 6.16). This is higher than in the case of the crown model and the model with the rigid particle. In addition, it is interesting to note that, although they move faster, in the case of the model with the nucleus the cells move less far from their initial position. In fact, we can see in fig. 6.13 that on average the cells have moved away from their initial position by a distance of 20, whereas in the case of the crown model they have moved away by a distance

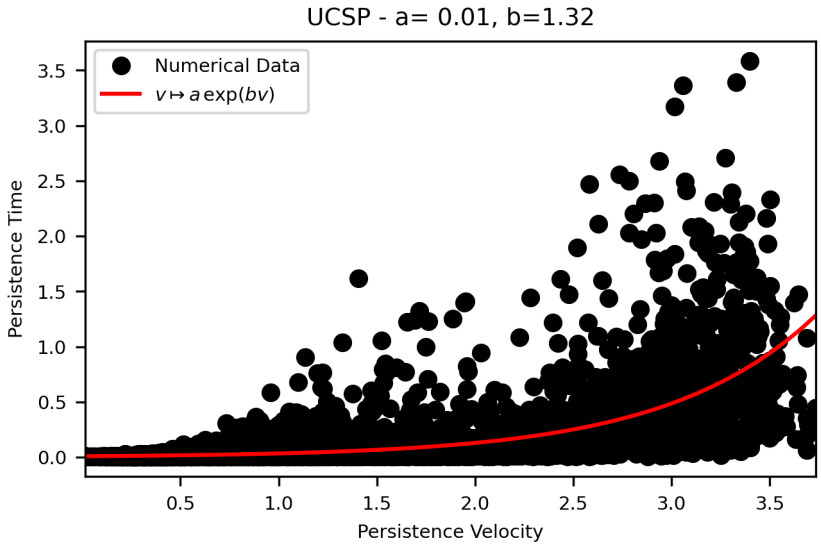

Figure 6.14: **Verification that the trajectories in fig. 6.13 satisfy the UCSP law (case when $\chi_c > \chi_c^*$).** *The persistence time of a locally persistent trajectory portion is plotted as a function of the persistence velocity. Each black dot corresponds to a datum. In red is plotted an interpolation of the points, of form $v \mapsto ae^{bv}$, which corresponds to the UCSP law. We can see that the data corresponds well to the interpolation and that the trajectories satisfy the UCSP law.*
The results presented here are obtained with the parameters $\Delta t = 0.005$, $R_0 = 1$, $R_{\text{nucl}} = 0.3$, $\mathbf{x}_{\text{nucl}}^{\text{in}} = (0;0)$, $M = \pi$, $a = 1$, $c^{\text{in}} = \dfrac{M}{|\Omega \setminus N|}$, $\chi_c = \chi_c^* + 0.5$ with χ_c^* given by (6.8), $f_{\text{act}}(c) = \frac{c(1+c_s)^2}{c_s(c+c_s)}$ with $c_s = 0.5$, $\alpha = 0.3$, $\zeta = 0.2$, $\beta = 1.5$, $\delta = 0.141372$ and $\xi_{\text{nucl}} = 1$.

of 25. This is consistent with the intermittent behaviour observed and with the capture of the stop-and-go phenomenon.

It seems that, with this choice of parameter $\chi_c = \chi_c^* + 0.5$, the nucleus makes the trajectories less directional than when its dynamics are not taken into account. One possible explanation for this is based on the fact that the dynamics of the nucleus bring it back to the centre of the cell. If the cell is polarised, with the nucleus at the back, then this dynamic depolarises the cell. Fluctuations due to noise disturb the position of the nucleus, leading to polarisation of the cell and again to persistent movement. Note that this explanation is the same as that proposed for the case $\chi_c = \chi_c^* - 0.3$. This means that the dynamics of the nucleus tends to make the dynamics of the cell intermittent, which is interesting from the point of view of observing the stop-and-go phenomenon.

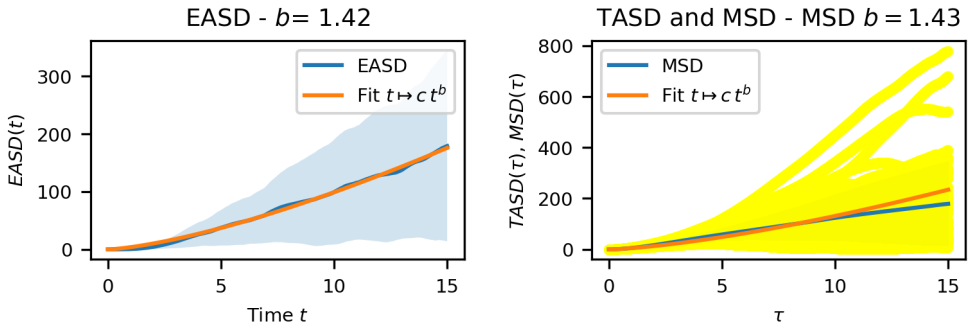

Figure 6.15: **Verification that the trajectories in fig. 6.13 are Brownian (case when $\chi_c > \chi_c^*$).** *On the left is shown in blue the EASD associated with the trajectories in fig. 6.13 and in orange the interpolation of the EASD, in the form $t \mapsto ct^b$. By the properties of the EASD, as b between 1 and 2, the trajectories in fig. 6.13 may be intermittent. This is confirmed by the study of the MSD, which is shown in blue on the right. Also shown on the right are the TASD of each cell in yellow and the interpolation of the MSD in form $t \mapsto ct^b$ in orange.*
The results presented here are obtained with the parameters $\Delta t = 0.005$, $R_0 = 1$, $R_{\text{nucl}} = 0.3$, $\mathbf{x}_{\text{nucl}}^{\text{in}} = (0;0)$, $M = \pi$, $a = 1$, $c^{\text{in}} = \dfrac{M}{|\Omega \setminus N|}$, $\chi_c = \chi_c^* + 0.5$ with χ_c^* given by (6.8), $f_{\text{act}}(c) = \frac{c(1+c_s)^2}{c_s(c+c_s)}$ with $c_s = 0.5$, $\alpha = 0.3$, $\zeta = 0.2$, $\beta = 1.5$, $\delta = 0.141372$ and $\xi_{\text{nucl}} = 1$.

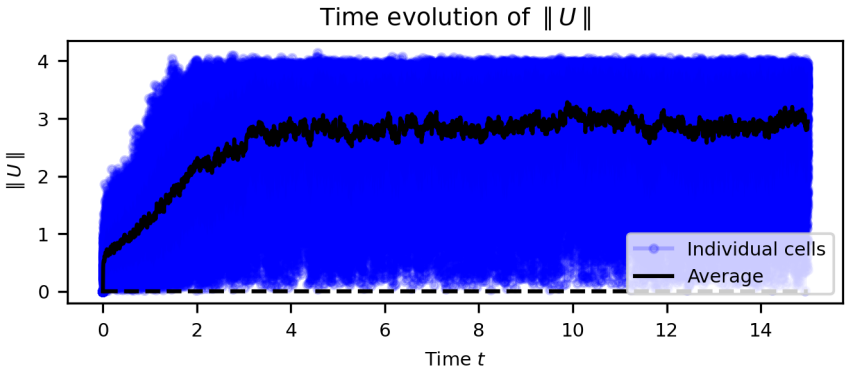

Figure 6.16: **Time evolution of the norm of the centre of mass velocity of the cells whose trajectories are shown in fig. 6.13 (case when $\chi_c > \chi_c^*$).** *The blue lines show the evolution over time of the norm of the velocity of each cell and the black line shows the evolution of the mean of the norms of the velocities of the cells.*
The results presented here are obtained with the parameters $\Delta t = 0.005$, $R_0 = 1$, $R_{\text{nucl}} = 0.3$, $\mathbf{x}_{\text{nucl}}^{\text{in}} = (0;0)$, $M = \pi$, $a = 1$, $c^{\text{in}} = \dfrac{M}{|\Omega \setminus N|}$, $\chi_c = \chi_c^* + 0.5$ with χ_c^* given by (6.8), $f_{\text{act}}(c) = \frac{c(1+c_s)^2}{c_s(c+c_s)}$ with $c_s = 0.5$, $\alpha = 0.3$, $\zeta = 0.2$, $\beta = 1.5$, $\delta = 0.141372$ and $\xi_{\text{nucl}} = 1$.

Case where $\chi_c = \chi_c^*$ In this paragraph, we present the results when $\chi_c = \chi_c^*$. Visually, and like the cases of the crown model and the model with a rigid particle, the trajectories seem intermittent (see fig. 6.17). This is confirmed by the study of the EASD and MSD, which are between 1 and 2 (see fig. 6.19). The UCSP law is always satisfied by the trajectories (see fig. 6.18).

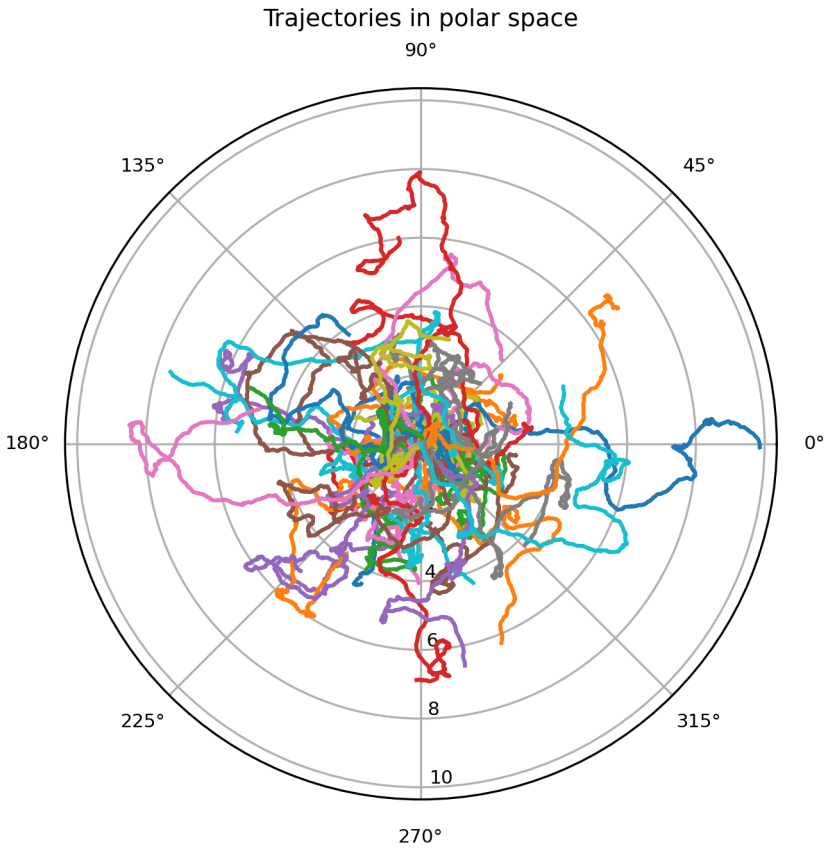

Figure 6.17: **Trajectories in polar coordinates in the case where $\chi_c = \chi_c^*$.** *Each curve represents, in polar coordinates, the trajectory of one cell simulated by algorithm 6.1 on the time interval $[0, 15]$. Visually, the trajectories seem to be intermittent. Fifty cells are represented. The results presented here are obtained with the parameters $\Delta t = 0.005$, $R_0 = 1$, $R_{\text{nucl}} = 0.3$, $\mathbf{x}_{\text{nucl}}^{\text{in}} = (0; 0)$, $M = \pi$, $a = 1$, $c^{\text{in}} = \dfrac{M}{|\Omega \setminus N|}$, $\chi_c = \chi_c^*$ with χ_c^* given by (6.8), $f_{\text{act}}(c) = \frac{c(1+c_s)^2}{c_s(c+c_s)}$ with $c_s = 0.5$, $\alpha = 0.3$, $\zeta = 0.2$, $\beta = 1.5$, $\delta = 0.141372$ and $\xi_{\text{nucl}} = 1$.*

As in the case of the crown model and the rigid particle, we observe that the velocity of the centre of mass is intermediate (see fig. 6.20) but is higher than in the case of the crown model and the model with the rigid particle.

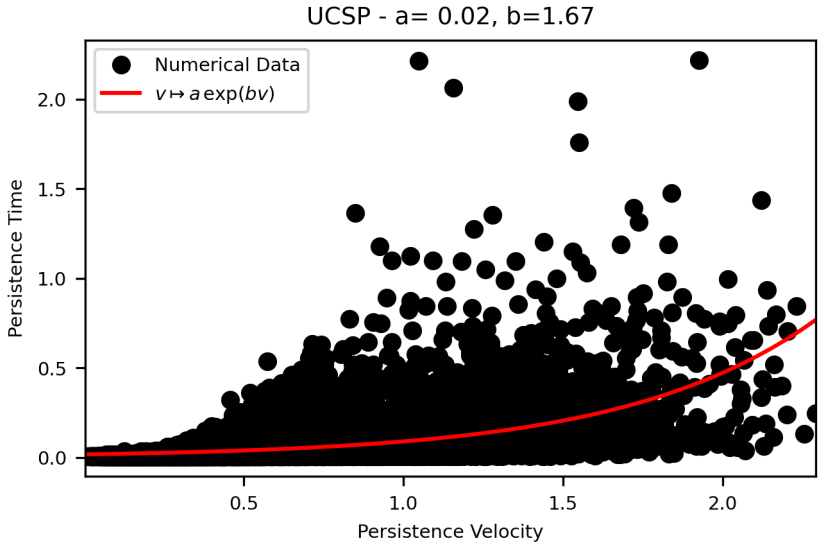

Figure 6.18: **Verification that the trajectories in fig. 6.17 satisfy the UCSP law (case when $\chi_c = \chi_c^*$).** *The persistence time of a locally persistent trajectory portion is plotted as a function of the persistence velocity. Each black dot corresponds to a datum. In red is plotted an interpolation of the points, of form $v \mapsto ae^{bv}$, which corresponds to the UCSP law. We can see that the data corresponds well to the interpolation and that the trajectories satisfy the UCSP law.*
The results presented here are obtained with the parameters $\Delta t = 0.005$, $R_0 = 1$, $R_{\text{nucl}} = 0.3$, $\mathbf{x}_{\text{nucl}}^{\text{in}} = (0;0)$, $M = \pi$, $a = 1$, $c^{\text{in}} = \dfrac{M}{|\Omega \setminus N|}$, $\chi_c = \chi_c^*$ with χ_c^* given by (6.8), $f_{\text{act}}(c) = \frac{c(1+c_s)^2}{c_s(c+c_s)}$ with $c_s = 0.5$, $\alpha = 0.3$, $\zeta = 0.2$, $\beta = 1.5$, $\delta = 0.141372$ and $\xi_{\text{nucl}} = 1$.

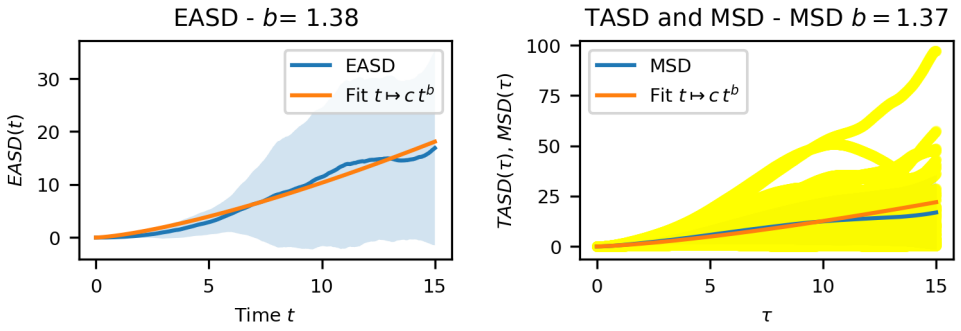

Figure 6.19: **Verification that the trajectories in fig. 6.17 are intermittent (case when $\chi_c = \chi_c^*$).** *On the left is shown in blue the EASD associated with the trajectories in fig. 6.17 and in orange the interpolation of the EASD, in the form $t \mapsto ct^b$. By the properties of the EASD, as b between 1 and 2, the trajectories in fig. 6.17 are neither Brownian neither persistent. This is confirmed by the study of the MSD, which is shown in blue on the right. Also shown on the right are the TASD of each cell in yellow and the interpolation of the MSD in form $t \mapsto ct^b$ in orange.*
The results presented here are obtained with the parameters $\Delta t = 0.005$, $R_0 = 1$, $R_{\text{nucl}} = 0.3$, $\mathbf{x}_{\text{nucl}}^{\text{in}} = (0;0)$, $M = \pi$, $a = 1$, $c^{\text{in}} = \dfrac{M}{|\Omega \setminus N|}$, $\chi_c = \chi_c^*$ with χ_c^* given by (6.8), $f_{\text{act}}(c) = \frac{c(1+c_s)^2}{c_s(c+c_s)}$ with $c_s = 0.5$, $\alpha = 0.3$, $\zeta = 0.2$, $\beta = 1.5$, $\delta = 0.141372$ and $\xi_{\text{nucl}} = 1$.

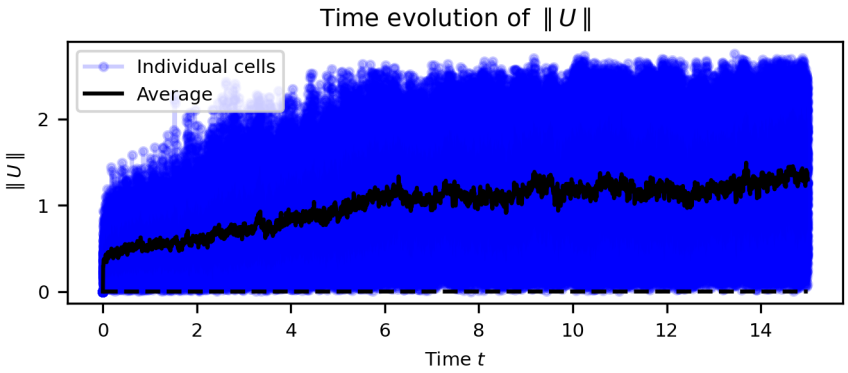

Figure 6.20: **Time evolution of the norm of the velocity of the cells whose trajectories are shown in fig. 6.17 (case when $\chi_c = \chi_c^*$).** *The blue lines show the evolution over time of the norm of the velocity of each cell and the black line shows the evolution of the mean of the norms of the velocities of the cells.*
The results presented here are obtained with the parameters $\Delta t = 0.005$, $R_0 = 1$, $R_{\text{nucl}} = 0.3$, $\mathbf{x}_{\text{nucl}}^{\text{in}} = (0; 0)$, $M = \pi$, $a = 1$, $c^{\text{in}} = \dfrac{M}{|\Omega \setminus N|}$, $\chi_c = \chi_c^*$ *with* χ_c^* *given by (6.8),* $f_{\text{act}}(c) = \frac{c(1+c_s)^2}{c_s(c+c_s)}$ *with* $c_s = 0.5$, $\alpha = 0.3$, $\zeta = 0.2$, $\beta = 1.5$, $\delta = 0.141372$ *and* $\xi_{\text{nucl}} = 1$.

Thus, the comparison with the results obtained with the crown model and the model with a rigid particle shows that taking into account the dynamics of the nucleus allows us to accurately capture the intermittent behaviour of the cells. The cells alternate between phases in which they are polarised and phases in which they are not. This shows that the nucleus and its dynamics play a very important role in cell polarisation and depolarisation. We investigate this in the next section.

6.4.3.2 . Cell polarisation is linked with the dynamic of the nucleus

In this section, we illustrate that the dynamics of the nucleus are linked to the polarisation of the cell. Since the model is rigid, a polarised cell is characterised by an asymmetric distribution of markers and the nucleus located at the rear of the cell. The more asymmetrically the marker concentration is distributed, the greater the norm of the velocity of the cell's centre of mass. Our model therefore shows that a cell is polarised if its velocity is high and its nucleus is at the rear.

In order to highlight the effect of the nucleus on the intermittent nature of a cell's trajectory, we represent the trajectories by subdividing them according to the relative position of the nucleus and the cell's velocity. An example of this is shown in fig. 6.21.

We observe that before a change of direction, the velocity decreases. Then, the nucleus moves closer to the centre of the cell. This leads to depolarisation of the cell. When the cell takes a new direction, it polarises again. The nucleus moves away from the centre of the cell and towards the back of the cell (see fig. 6.22). The cell's velocity increases again. We also observe that before taking another direction, the cell stops. We then observe a diffusive movement with a very low velocity. We can see that in the areas where the cell is polarised, it maintains its direction. This accurately illustrates the intermittent nature of a trajectory.

This suggests that the positioning of the nucleus at the rear of the cell is important in the phenomenon of polarisation. It also indicates that the positioning of the nucleus is crucial in the phenomenon of depolarisation. For the cell to be in a depolarised state, the nucleus must be at its center.

We note that the presented result is obtained when the friction of the nucleus on the substrate is higher than that of the cytoplasm. We obtain a similar result when assuming the frictions are the same ($\xi_{\mathrm{nucl}} = 1$), though it is less apparent that the nucleus moves to the rear of the cell, as it remains very close to the center.

These results are interesting because the considered model, despite its simplicity, highlights the role of the nucleus in cell motility. This role is clearly highlighted by the numerical results concerning the polarisation of the cell and the positioning of the nucleus within the cell. Additionally, we note that when the cell migrates, the nucleus maintains its position at the rear of the cell.

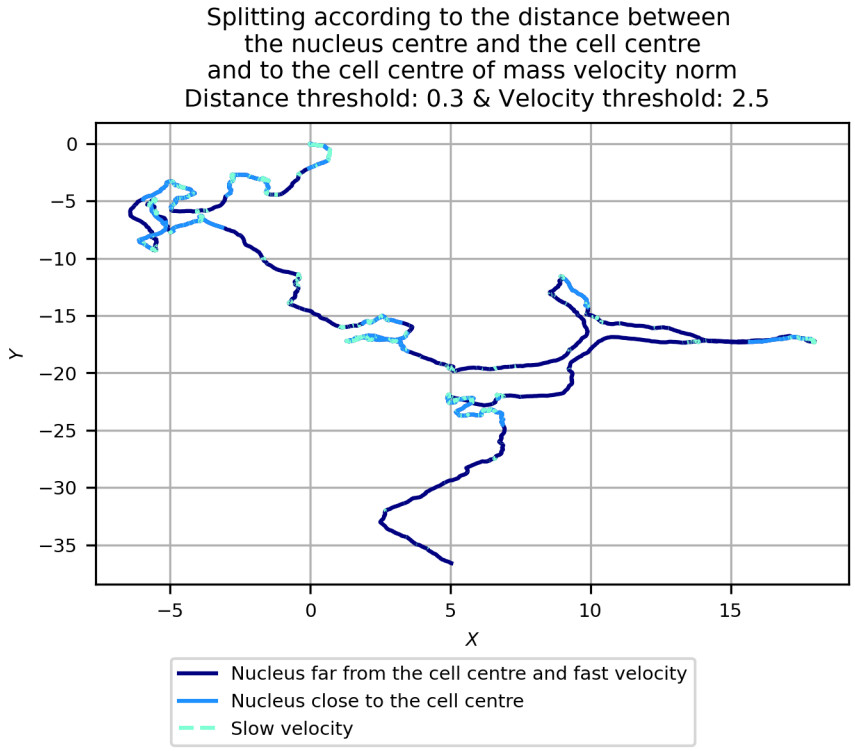

Figure 6.21: **Representation of the trajectory of cell split according to the relative position of the nucleus and the cell's velocity.** *A trajectory of a cell is represented. The part shown in dark blue corresponds to the moments when the nucleus is positioned at the back of the cell and the cell velocity is high. The sky-blue area corresponds to moments when the nucleus is no longer positioned at the back of the cell and is close to the centre of the cell. The part shown in cyan corresponds to moments when the cell velocity is low. We observe that before a change of direction, the velocity decreases. The nucleus then moves closer to the centre. This leads to depolarisation of the cell. When the cell takes a new direction, the nucleus moves towards the rear of the cell and the cell velocity increases. The cell becomes polarised. We can see that in the areas where the cell is polarised, it maintains its direction.*
The results presented here are obtained with the parameters $\Delta t = 0.005$, $R_0 = 1$, $R_{\text{nucl}} = 0.3$, $\mathbf{x}_{\text{nucl}}^{\text{in}} = (0;0)$, $M = \pi$, $a = 1$, $c^{\text{in}} = \dfrac{M}{|\Omega \setminus N|}$, $\chi_c = \chi_c^* + 0.5$ *with* χ_c^* *given by* (6.8), $f_{\text{act}}(c) = \frac{c(1+c_s)^2}{c_s(c+c_s)}$ *with* $c_s = 0.5$, $\alpha = 0.3$, $\zeta = 0.2$, $\beta = 1.5$, $\delta = 0.141372$ *and* $\xi_{\text{nucl}} = 1.75$. *The time interval of study is* $[0, 50]$.

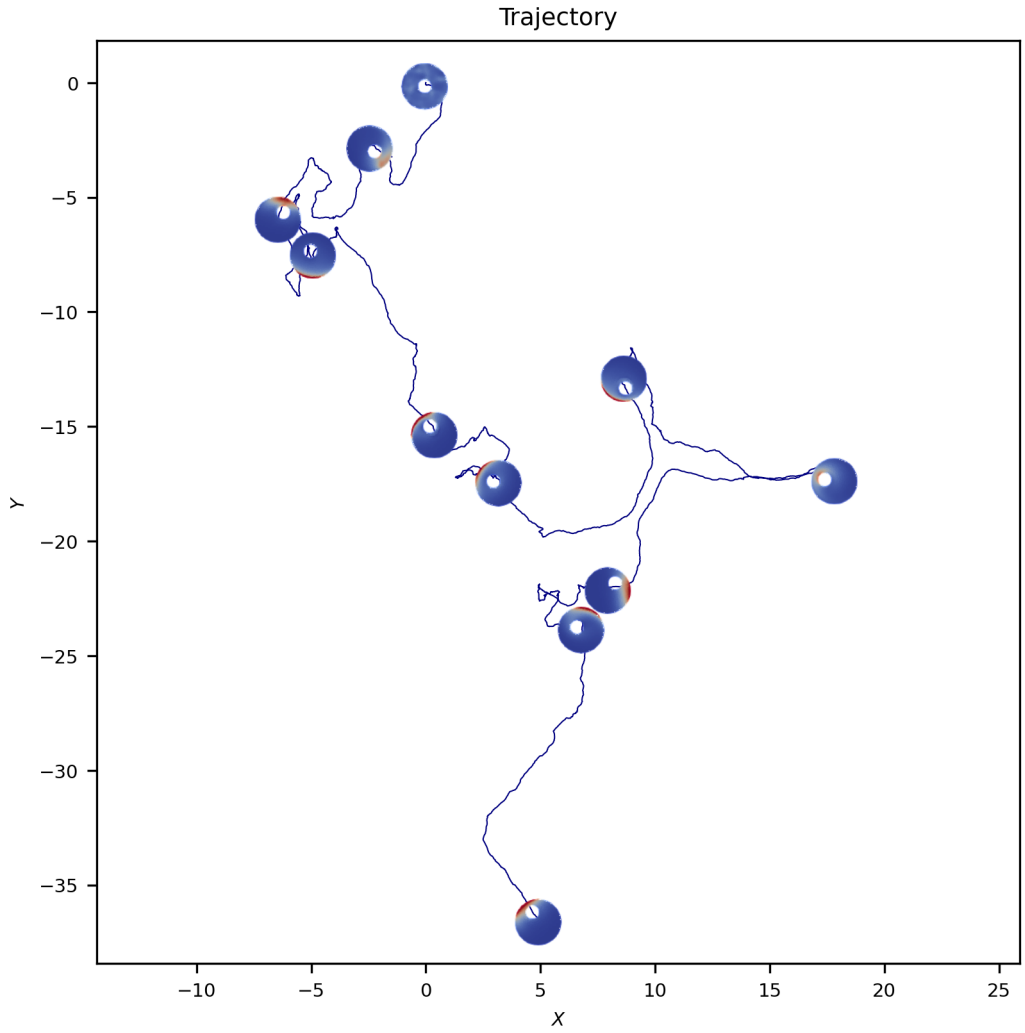

Figure 6.22: **Representation of the trajectory of cell with snapshots of the cell evolution.** *Snapshots of the cell evolution of the cell whose ttrajectory is represented in fig. 6.21 are added to the trajectory. Snapshots of the cell are shown at time* $t \in \{0, 5, 10, 15, \dots, 45, 50\}$. *The red area on the cell represents the area with high markers concentration whereas the dark blue area represents the area with low markers concentration. We can observe that the nucleus position inside the cell evolves with time. Moreover, once the cell is polarised, the nucleus position is at the rear part of the cell.*
The results presented here are obtained with the parameters $\Delta t = 0.005$, $R_0 = 1$, $R_{\text{nucl}} = 0.3$, $\mathbf{x}_{\text{nucl}}^{\text{in}} = (0; 0)$, $M = \pi$, $a = 1$, $c^{\text{in}} = \dfrac{M}{|\Omega \setminus N|}$, $\chi_c = \chi_c^* + 0.5$ *with* χ_c^* *given by* (6.8), $f_{\text{act}}(c) = \frac{c(1+c_s)^2}{c_s(c+c_s)}$ *with* $c_s = 0.5$, $\alpha = 0.3$, $\zeta = 0.2$, $\beta = 1.5$, $\delta = 0.141372$ *and* $\xi_{\text{nucl}} = 1.75$. *The time interval of study is* $[0, 50]$.

6.4.4 . Validation of the heuristic approach

In this section, we aim to study numerically the heuristic approach proposed in section section 1.3.9 for modelling the forces induced by the cell boundary on the nucleus and by the nucleus on the cell boundary. We therefore assume that $\mathbf{f}_{\mathrm{BN}}$ is defined by eq. (6.5) which we recall here:

$$\mathbf{f}_{\mathrm{BN}}(t) = -k\left(\mathbf{x}_{\mathrm{nucl}}(t) - \mathbf{x}_{\mathrm{cm}}(t)\right).$$

First, we check that this expression for $\mathbf{f}_{\mathrm{BN}}$ does indeed act on the nucleus to bring it back to the centre of the cell. Next, we check that the stationary state is indeed recovered with the numerical scheme and that we numerically recover the criterion on its stability. Finally, we study the trajectories obtained for different values of χ_c and compare the results obtained with those of section 6.4.3.1.

6.4.4.1 . Numerical verifications

In this subsection, we illustrate, numerically, the effect of the restoring force on the nucleus when we consider the heuristic approach. We aim to check that with this choice of force, the nucleus effectively returns to the centre of the cell. To verify this, we remove the coupling between marker concentration and fluid dynamics by assuming that $\chi_c = 0$ and study the evolution of the nucleus position in the cell reference frame.

To ensure this, for different values of R_0 and R_{nucl}, and k, we initially place the nucleus outside its equilibrium position and plot the evolution over time of the position of the nucleus in the cell reference frame. Whatever the initial position of the nucleus $\mathbf{x}^{\mathrm{in}}_{\mathrm{nucl}}$, whatever R_0 and R_{nucl} such that $B\left(\mathbf{x}^{\mathrm{in}}_{\mathrm{nucl}}, R_{\mathrm{nucl}}\right) \subset B\left(0, R_0\right)$, we observe that as long as $\beta > 1$ and $\delta > 0$, the nucleus returns to its equilibrium position (see fig. 6.23). This confirms that the heuristic approach is in accordance with the biological context.

In fig. 6.23, we have choose k in order to compare it with the result of fig. 6.4. R_0 and R_{nucl} are equals in both cases and k is such that $-k = \dfrac{\delta\pi R_0\left(R_0\left(1-\beta\right) - R_{\mathrm{nucl}}\right)}{\left(R_0 - R_{\mathrm{nucl}}\right)^{\beta+1}}$. The nucleus returns slower to the centre of the cell with the heuristic approach.

Secondly, we check that, with the heuristic choice of the force, the numerical scheme proposed in algorithm 6.1 is consistent with the mathematical study of the model. We therefore check that if $\alpha = 0$ then we recover the stationary state (6.7) as well as the result on the stability of the latter stated in theorem 6.2.2.

We observe that with this choice for the boundary force on the nucleus, the scheme still captures the stationary state well. Indeed, as illustrated in fig. 6.24 if the initial condition is the stationnary state, then the velocity of the cell remains zero over time and the position of the nucleus at the centre of the cell is maintained. We also observe that the distribution of markers is weel conserved over time. Moreover, we can observe that the quantity of markers is well conserved over time, which is in agreement with eq. (6.6) (see fig. 6.25).

We also check that, with this choice of force, the numerical scheme gives results in accordance with theorem 6.2.2. We therefore study the linear stability of the stationary state numerically. As previously, we choose a perturbation of the stationary state as the initial condition and observe, depending on the value of χ_c, whether the system returns to the stationary state. We choose the same perturbation of the initial condition defined by eq. (6.39).

As illustrated in fig. 6.26 for the case where $R_0 = 1$ and $R_{\mathrm{nucl}} = 0.3$, we correctly find the criterion on the linear stablity of the stationary state. Indeed, when $\chi_c < \chi_c^*$, we have that the norm of the velocity decreases very quickly towards 0 then is constant equal to 0. This

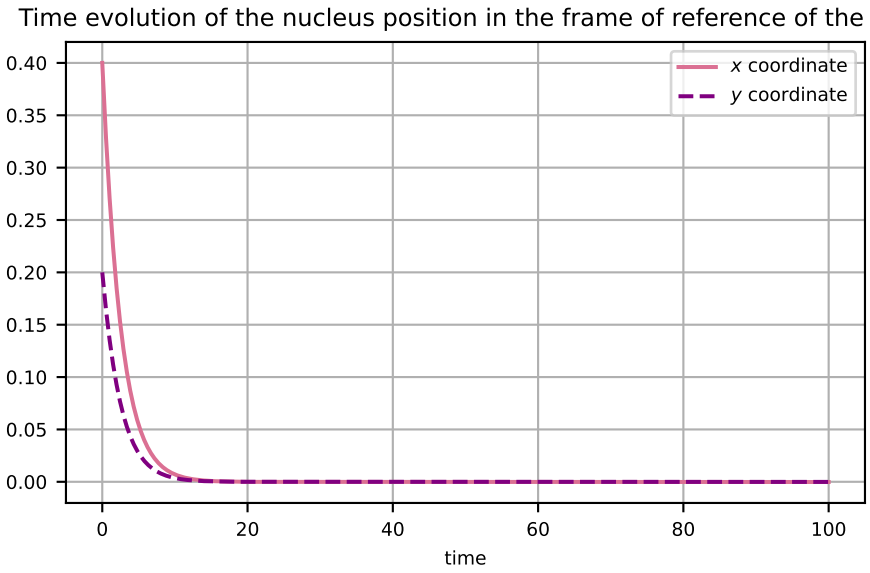

Figure 6.23: **Illustration of the nucleus dynamic without coupling with the markers concentration.** *The time evolution of the nucleus position in the cell frame of reference is represented. We can observe that the nucleus quickly returns to the centre of the cell, as desired.*
The results presented here are obtained with the parameters $\Delta t = 0.005$, $R_0 = 1$, $R_{\text{nucl}} = 0.3$, $\mathbf{x}_{\text{nucl}}^{\text{in}} = (0.4; 0.2)$, $\chi_c = 0$, $k = 0.866677$, *and* $\xi_{\text{nucl}} = 1$.

illustrates that when $\chi_c < \chi_c^*$ the stationary state is stable. Also, when $\chi_c > \chi_c^*$, we observe that the norm increases rapidly towards a strictly positive value and then becomes constant. This suggests that when $\chi_c > \chi_c^*$ there are stable travelling waves.

The choice of the parameters allows to compare the results obtained in fig. 6.26 with the result obtained in fig. 6.7. We can see that for the same choice of χ_c the cells simulated with $\mathbf{f}_{\text{BN}}$ defined by eq. (6.4) and those where $\mathbf{f}_{\text{BN}}$ is defined by eq. (6.5) go at the same velocity. It also seems that in both cases, the cells converge towards a travelling wave at the same velocity.

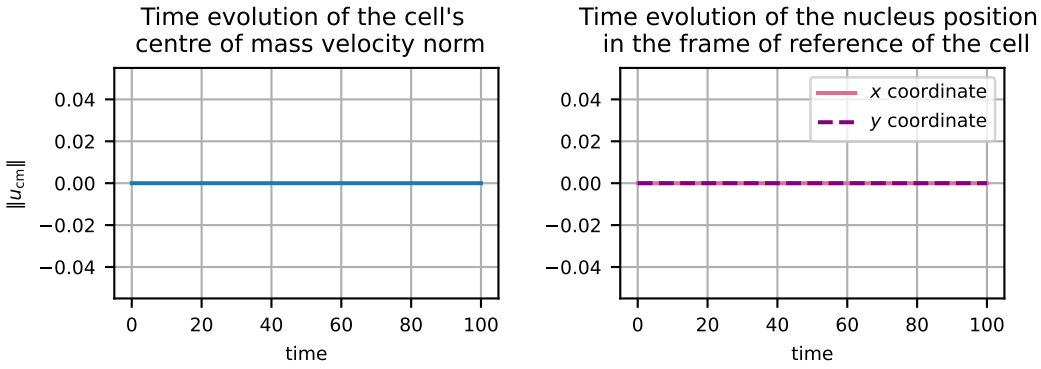

Figure 6.24: **Example of capturing the stationary state using the numerical scheme.** *The curve on the left represents the evolution of the velocity norm over time. We can observe that this remains zero throughout the study interval* $[0, 100]$*. The curves on the right represent the evolution over time of the coordinates of the nucleus position. We can see that the position of the nucleus is preserved over the study interval.*
The results presented here are obtained with the parameters $\Delta t = 0.005$, $R_0 = 1$, $R_{\text{nucl}} = 0.3$, $\mathbf{x}_{\text{nucl}}^{\text{in}} = (0; 0)$, $c^{\text{in}}(\mathbf{x}) = \frac{M}{\pi\left(R_0^2 - R_{\text{nucl}}^2\right)}$, $M = \pi$, $a = 1$, $\chi_c = 0.733956$, $f_{\text{act}}(c) = \frac{c(1+c_s)^2}{c_s(c+c_s)}$ *with* $c_s = 0.5$, $k = 0.866677$, *and* $\xi_{\text{nucl}} = 1$.

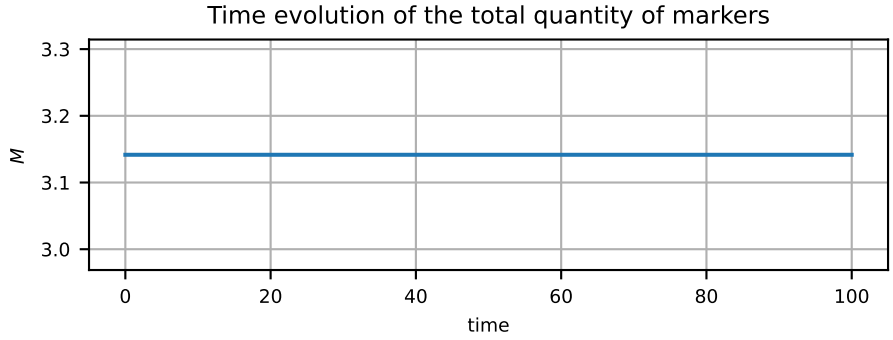

Figure 6.25: **Illustration of the conservation of the total quantity of markers.** *The curve represents the evolution of the total quantity of markers over time. We note that this remains constant throughout the study interval* $[0, 100]$.
The results presented here are obtained with the parameters $\Delta t = 0.005$, $R_0 = 1$, $R_{\text{nucl}} = 0.3$, $\mathbf{x}_{\text{nucl}}^{\text{in}} = (0; 0)$, $c^{\text{in}}(\mathbf{x}) = \frac{M}{\pi\left(R_0^2 - R_{\text{nucl}}^2\right)}$, $M = \pi$, $a = 1$, $\chi_c = 0.5$, $f_{\text{act}}(c) = \frac{c(1+c_s)^2}{c_s(c+c_s)}$ *with* $c_s = 0.5$, $k = 0.866677$, *and* $\xi_{\text{nucl}} = 1$.

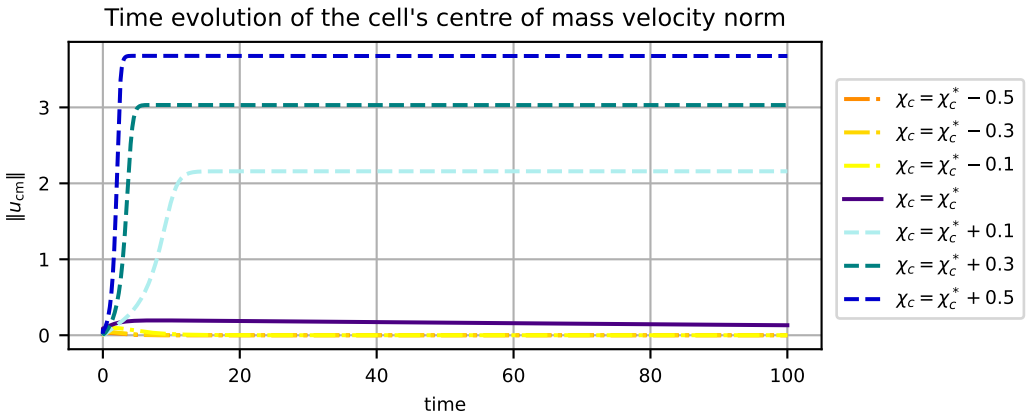

Figure 6.26: **Numerical illustration of theorem 6.2.2.** *Each curve represents the evolution of the cell's centre of mass velocity norm of a cell for different values of χ_c (see legend on the right). When $\chi_c < \chi_c^*$ the norm of the velocity decreases very rapidly towards 0 (dashdotted curves in overlapping shades of orange), whereas when $\chi_c > \chi_c^*$ it increases rapidly towards a non-zero value (dashed curves in shades of blue) . The critical case $\chi_c = \chi_c^*$ is also represented (dark curve), here the norm of the velocity is close to zero and decreases.*
The results presented here are obtained with the parameters $\Delta t = 0.005$, $R_0 = 1$, $R_{\text{nucl}} = 0.3$, $\mathbf{x}_{\text{nucl}}^{\text{in}} = (0.1; 0)$, $M = \pi$, $a = 1$, c^{in} given by eq. (6.39) and χ_c^* given by (6.8), $f_{\text{act}}(c) = \frac{c(1+c_s)^2}{c_s(c+c_s)}$ with $c_s = 0.5$, $k = 0.866677$ and $\xi_{\text{nucl}} = 1$.

6.4.4.2 . Impact of the nucleus on the trajectories

In this section, we want to illustrate the impact of the nucleus on trajectories. In order to be able to compare with the results of sections 4.4.2 and 5.4.2 obtained respectively in the case of the crown model and the model with a rigid particle, we follow the same procedure. We fix all the parameters and vary only χ_c. We thus set for the numerical results presented, $R_0 = 1$, $R_{\text{nucl}} = 0.3$, $M = \pi$ and $a = 1$. The initial position of the nucleus is set to $\mathbf{x}_{\text{nucl}}^{\text{in}} = (0; 0)$. As an initial condition c^{in} for the concentration of markers, we choose the function defined for all $\mathbf{x} \in \Omega \setminus N$ by $c^{\text{in}}(\mathbf{x}) = \dfrac{M}{|\Omega \setminus N|}$. The noise parameters are set to $\alpha = 0.3$ and $\zeta = 0.2$. The nucleus dynamic parameters are set to $\xi_{\text{nucl}} = 1$ and $k = 0.866677$. Finally, the numerical simulations are performed over the time interval $[0, 15]$ with $\Delta t = 0.005$.

Here are the results when $\chi_c = \chi_c^* - 0.3$, $\chi_c = \chi_c^*$ and $\chi_c = \chi_c^* + 0.5$ with χ_c^* defined in eq. (6.8).

Case where $\chi_c = \chi_c^* - 0.3$ In this paragraph, we present the results when $\chi_c = \chi_c^* - 0.3$. Visually, and like in the first case (see section 6.4.3), the trajectories do not seem Brownian. We can observe trajectories with parts that appear to be persistent. The trajectories look intermittent (see fig. 6.27). This is confirmed by the study of the EASD and MSD, which are between 1 and 2 (see fig. 6.29). The UCSP law is always satisfied by the trajectories (see fig. 6.28). We observe that the trajectories obtained are similar to those obtained in section 6.4.3, the EASD and the MSD are similars. The average velocity of the cells is similar (see figs. 6.12 and 6.30). A minor difference is that the persistence times are higher when we consider that $\mathbf{f}_{\text{BN}}$ is given by the heuristic approach (see figs. 6.10 and 6.28).

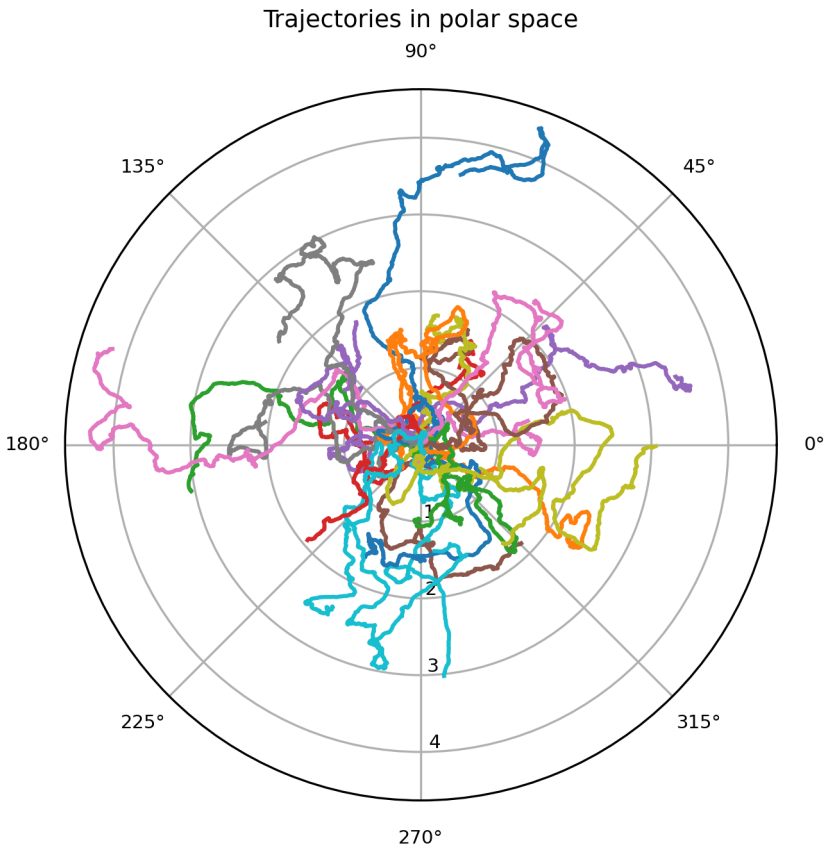

Figure 6.27: **Trajectories in polar coordinates in the case where $\chi_c < \chi_c^*$.** *Each curve represents, in polar coordinates, the trajectory of one cell simulated by algorithm 6.1 on the time interval $[0, 15]$. Visually, the trajectories seem to be intermittent. Thirty cells are represented.*
The results presented here are obtained with the parameters $\Delta t = 0.005$, $R_0 = 1$, $R_{\text{nucl}} = 0.3$, $\mathbf{x}_{\text{nucl}}^{\text{in}} = (0; 0)$, $M = \pi$, $a = 1$, $c^{\text{in}} = \dfrac{M}{|\Omega \setminus N|}$, $\chi_c = \chi_c^* - 0.3$ with χ_c^* given by (6.8), $f_{\text{act}}(c) = \frac{c(1+c_s)^2}{c_s(c+c_s)}$ with $c_s = 0.5$, $\alpha = 0.3$, $\zeta = 0.2$, $k = 0.866677$, and $\xi_{\text{nucl}} = 1$.

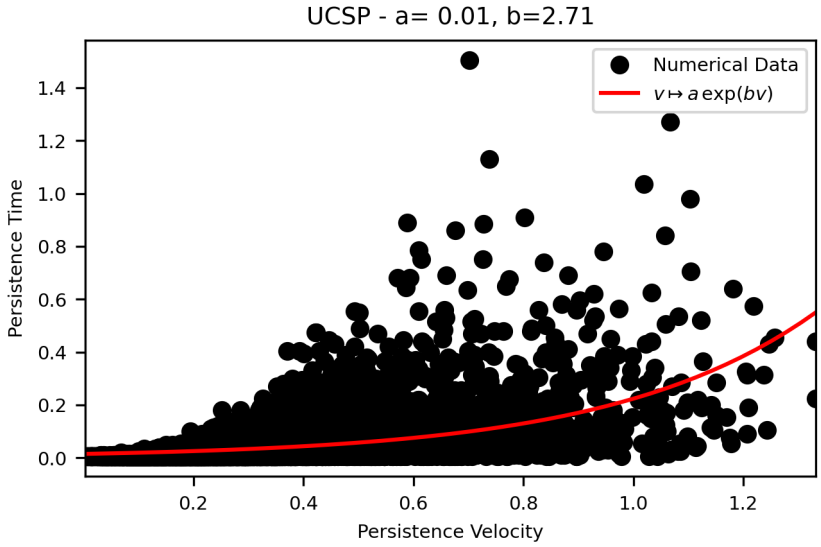

Figure 6.28: **Verification that the trajectories in fig. 6.27 satisfy the UCSP law (case when $\chi_c < \chi_c^*$).** *The persistence time of a locally persistent trajectory portion is plotted as a function of the persistence velocity. Each black dot corresponds to a datum. In red is plotted an interpolation of the points, of form $v \mapsto ae^{bv}$, which corresponds to the UCSP law. We can see that the data corresponds well to the interpolation and that the trajectories satisfy the UCSP law.*
The results presented here are obtained with the parameters $\Delta t = 0.005$, $R_0 = 1$, $R_{\text{nucl}} = 0.3$, $\mathbf{x}_{\text{nucl}}^{\text{in}} = (0;0)$, $M = \pi$, $a = 1$, $c^{\text{in}} = \dfrac{M}{|\Omega \setminus N|}$, $\chi_c = \chi_c^* - 0.3$ *with* χ_c^* *given by (6.8),* $f_{\text{act}}(c) = \frac{c(1+c_s)^2}{c_s(c+c_s)}$ *with* $c_s = 0.5$, $\alpha = 0.3$, $\zeta = 0.2$, $k = 0.866677$, *and* $\xi_{\text{nucl}} = 1$.

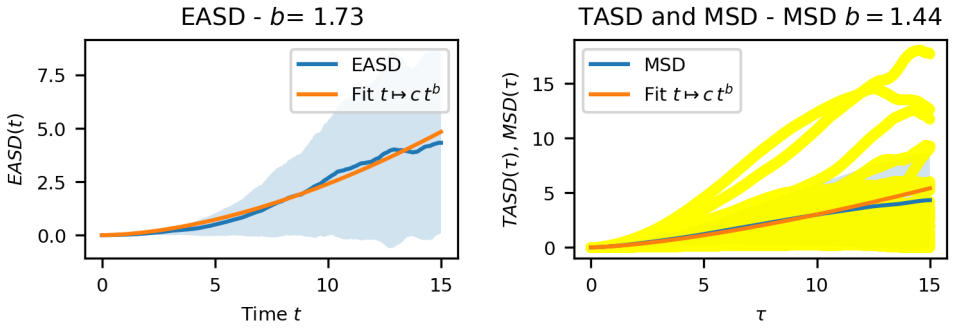

Figure 6.29: **Verification that the trajectories in fig. 6.27 are Brownian (case when $\chi_c < \chi_c^*$).** *On the left is shown in blue the EASD associated with the trajectories in fig. 6.27 and in orange the interpolation of the EASD, in the form $t \mapsto ct^b$. By the properties of the EASD, as b between 1 and 2, the trajectories in fig. 6.27 may be intermittent. This is confirmed by the study of the MSD, which is shown in blue on the right. Also shown on the right are the TASD of each cell in yellow and the interpolation of the MSD in form $t \mapsto ct^b$ in orange.*
The results presented here are obtained with the parameters $\Delta t = 0.005$, $R_0 = 1$, $R_{\text{nucl}} = 0.3$, $\mathbf{x}_{\text{nucl}}^{\text{in}} = (0;0)$, $M = \pi$, $a = 1$, $c^{\text{in}} = \dfrac{M}{|\Omega \setminus N|}$, $\chi_c = \chi_c^* - 0.3$ *with* χ_c^* *given by (6.8),* $f_{\text{act}}(c) = \frac{c(1+c_s)^2}{c_s(c+c_s)}$ *with* $c_s = 0.5$, $\alpha = 0.3$, $\zeta = 0.2$, $k = 0.866677$, *and* $\xi_{\text{nucl}} = 1$.

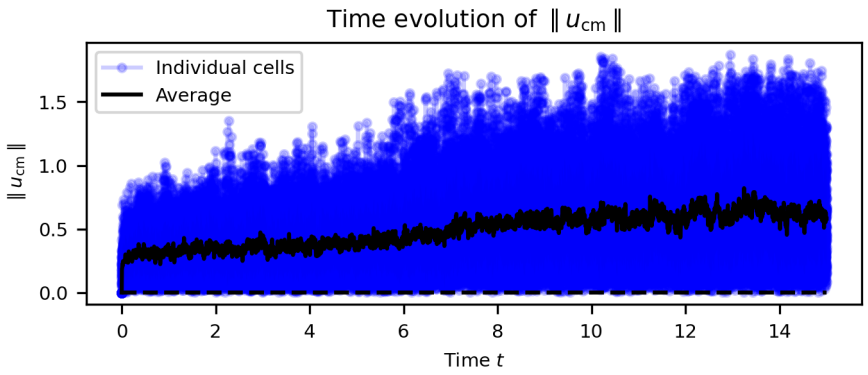

Figure 6.30: **Time evolution of the norm of the velocity of the cells whose trajectories are shown in fig. 6.27 (case when $\chi_c < \chi_c^*$).** *The blue lines show the evolution over time of the norm of the centre of mass velocity of each cell and the black line shows the evolution of the mean of the norms of the velocities of the cells.*
The results presented here are obtained with the parameters $\Delta t = 0.005$, $R_0 = 1$, $R_{\text{nucl}} = 0.3$, $\mathbf{x}_{\text{nucl}}^{\text{in}} = (0; 0)$, $M = \pi$, $a = 1$, $c^{\text{in}} = \dfrac{M}{|\Omega \setminus N|}$, $\chi_c = \chi_c^* - 0.3$ *with* χ_c^* *given by* (6.8), $f_{\text{act}}(c) = \frac{c(1+c_s)^2}{c_s(c+c_s)}$ *with* $c_s = 0.5$, $\alpha = 0.3$, $\zeta = 0.2$, $k = 0.866677$, *and* $\xi_{\text{nucl}} = 1$.

Case where $\chi_c = \chi_c^* + 0.5$ In this paragraph, we present the results when $\chi_c = \chi_c^* + 0.5$. As with the first modelisation of $\mathbf{f}_{\mathrm{BN}}$, visually, the trajectories seem intermittent (see fig. 6.31), which is in agreement with the EASD and MSD study, which is between 1 and 2 (see fig. 6.33). We can see that the trajectories satisfy the UCSP (see fig. 6.32). We observe that the trajectories obtained are similar to those obtained in section 6.4.3, the EASD and the MSD are similars. The average velocity of the cells is similar (see figs. 6.16 and 6.34). A minor difference is that the persistence times are higher when we consider that $\mathbf{f}_{\mathrm{BN}}$ is given by the heuristic approach (see figs. 6.14 and 6.32).

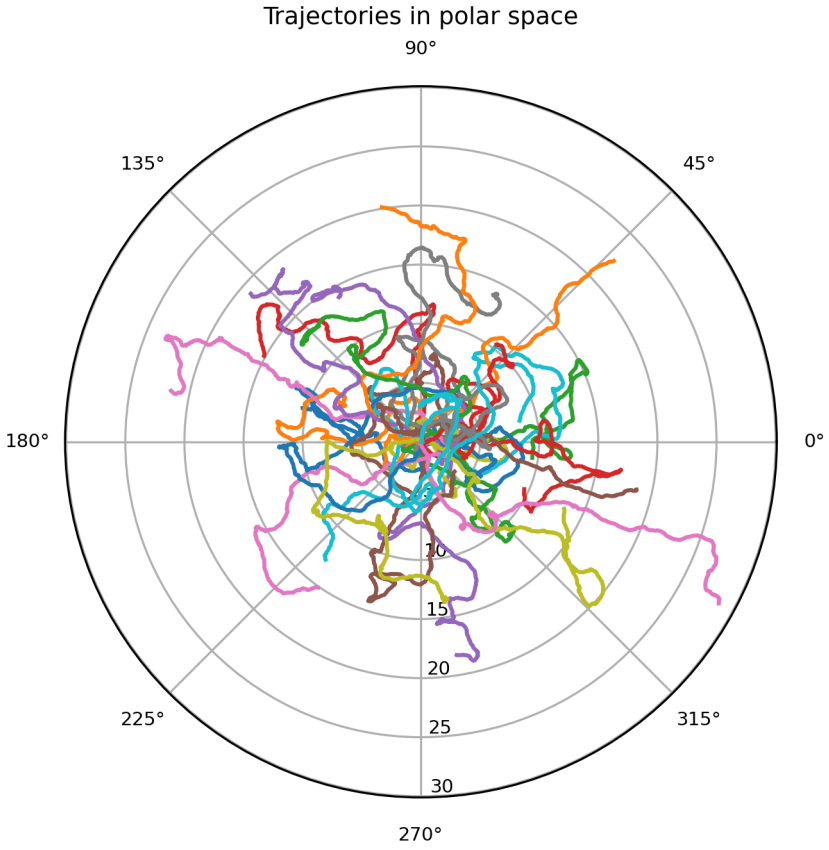

Figure 6.31: **Trajectories in polar coordinates in the case where $\chi_c > \chi_c^*$.** *Each curve represents, in polar coordinates, the trajectory of one cell simulated by algorithm 6.1 on the time interval $[0, 15]$. Visually, the trajectories seem to be intermittent. Thirty cells are represented.*
The results presented here are obtained with the parameters $\Delta t = 0.005$, $R_0 = 1$, $R_{\mathrm{nucl}} = 0.3$, $\mathbf{x}_{\mathrm{nucl}}^{\mathrm{in}} = (0; 0)$, $M = \pi$, $a = 1$, $c^{\mathrm{in}} = \dfrac{M}{|\Omega \setminus N|}$, $\chi_c = \chi_c^* + 0.5$ with χ_c^* given by (6.8), $f_{\mathrm{act}}(c) = \frac{c(1+c_s)^2}{c_s(c+c_s)}$ with $c_s = 0.5$, $\alpha = 0.3$, $\zeta = 0.2$, $k = 0.866677$, and $\xi_{\mathrm{nucl}} = 1$.

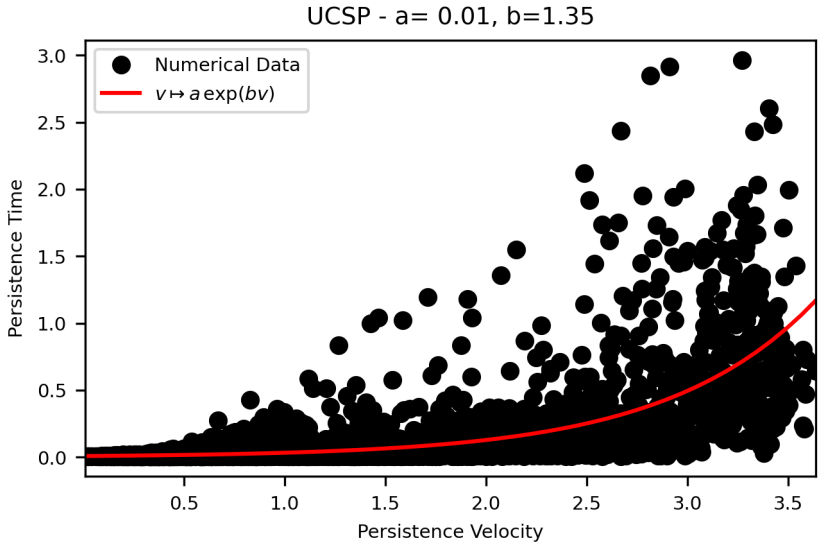

Figure 6.32: **Verification that the trajectories in fig. 6.31 satisfy the UCSP law (case when $\chi_c > \chi_c^*$).** *The persistence time of a locally persistent trajectory portion is plotted as a function of the persistence velocity. Each black dot corresponds to a datum. In red is plotted an interpolation of the points, of form $v \mapsto ae^{bv}$, which corresponds to the UCSP law. We can see that the data corresponds well to the interpolation and that the trajectories satisfy the UCSP law.*
The results presented here are obtained with the parameters $\Delta t = 0.005$, $R_0 = 1$, $R_{\text{nucl}} = 0.3$, $\mathbf{x}_{\text{nucl}}^{\text{in}} = (0;0)$, $M = \pi$, $a = 1$, $c^{\text{in}} = \dfrac{M}{|\Omega \setminus N|}$, $\chi_c = \chi_c^* + 0.5$ *with* χ_c^* *given by (6.8),* $f_{\text{act}}(c) = \frac{c(1+c_s)^2}{c_s(c+c_s)}$ *with* $c_s = 0.5$, $\alpha = 0.3$, $\zeta = 0.2$, $k = 0.866677$, *and* $\xi_{\text{nucl}} = 1$.

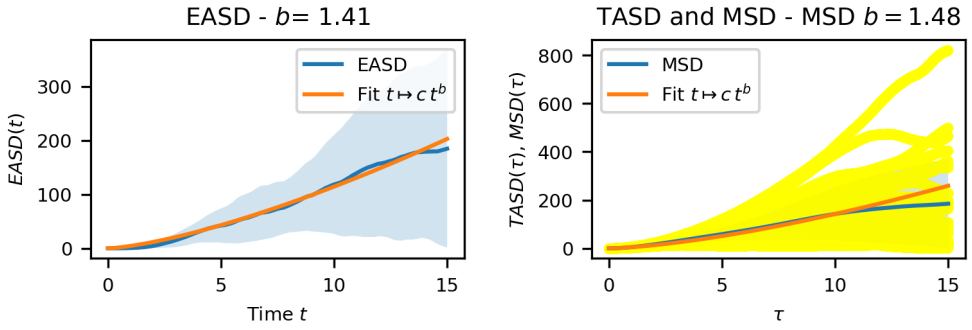

Figure 6.33: **Verification that the trajectories in fig. 6.31 are Brownian (case when $\chi_c > \chi_c^*$).** *On the left is shown in blue the EASD associated with the trajectories in fig. 6.31 and in orange the interpolation of the EASD, in the form $t \mapsto ct^b$. By the properties of the EASD, as b between 1 and 2, the trajectories in fig. 6.31 may be intermittent. This is confirmed by the study of the MSD, which is shown in blue on the right. Also shown on the right are the TASD of each cell in yellow and the interpolation of the MSD in form $t \mapsto ct^b$ in orange.*
The results presented here are obtained with the parameters $\Delta t = 0.005$, $R_0 = 1$, $R_{\text{nucl}} = 0.3$, $\mathbf{x}_{\text{nucl}}^{\text{in}} = (0;0)$, $M = \pi$, $a = 1$, $c^{\text{in}} = \dfrac{M}{|\Omega \setminus N|}$, $\chi_c = \chi_c^* + 0.5$ *with* χ_c^* *given by (6.8),* $f_{\text{act}}(c) = \frac{c(1+c_s)^2}{c_s(c+c_s)}$ *with* $c_s = 0.5$, $\alpha = 0.3$, $\zeta = 0.2$, $k = 0.866677$, *and* $\xi_{\text{nucl}} = 1$.

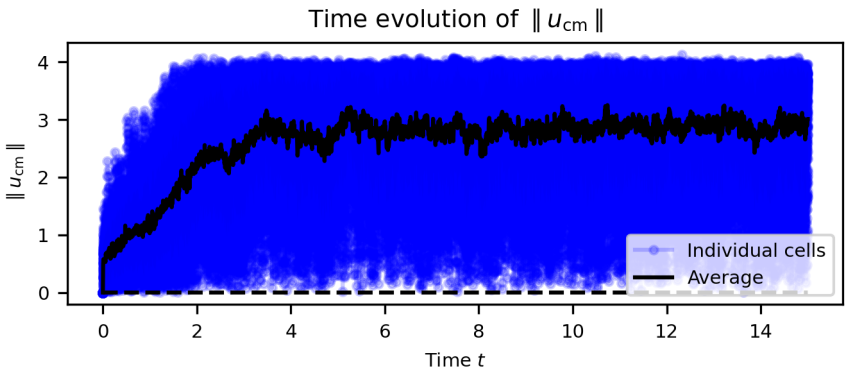

Figure 6.34: **Time evolution of the norm of the centre of mass velocity of the cells whose trajectories are shown in fig. 6.31 (case when $\chi_c > \chi_c^*$).** *The blue lines show the evolution over time of the norm of the velocity of each cell and the black line shows the evolution of the mean of the norms of the velocities of the cells.*
The results presented here are obtained with the parameters $\Delta t = 0.005$, $R_0 = 1$, $R_{\text{nucl}} = 0.3$, $\mathbf{x}_{\text{nucl}}^{\text{in}} = (0;0)$, $M = \pi$, $a = 1$, $c^{\text{in}} = \dfrac{M}{|\Omega \setminus N|}$, $\chi_c = \chi_c^* + 0.5$ *with* χ_c^* *given by* (6.8), $f_{\text{act}}(c) = \frac{c(1+c_s)^2}{c_s(c+c_s)}$ *with* $c_s = 0.5$, $\alpha = 0.3$, $\zeta = 0.2$, $k = 0.866677$, *and* $\xi_{\text{nucl}} = 1$.

Case where $\chi_c = \chi_c^*$ In this paragraph, we present the results when $\chi_c = \chi_c^*$. Visually, and like when we consider the first modelisation of $\mathbf{f}_{\mathrm{BN}}$, the trajectories seem intermittent (see fig. 6.35). This is confirmed by the study of the EASD and MSD, which are between 1 and 2 (see fig. 6.37). The UCSP law is always satisfied by the trajectories (see fig. 6.36). We observe that the trajectories obtained are similar to those obtained in section 6.4.3, the EASD and the MSD are similars. The average velocity of the cells is similar (see figs. 6.20 and 6.38).

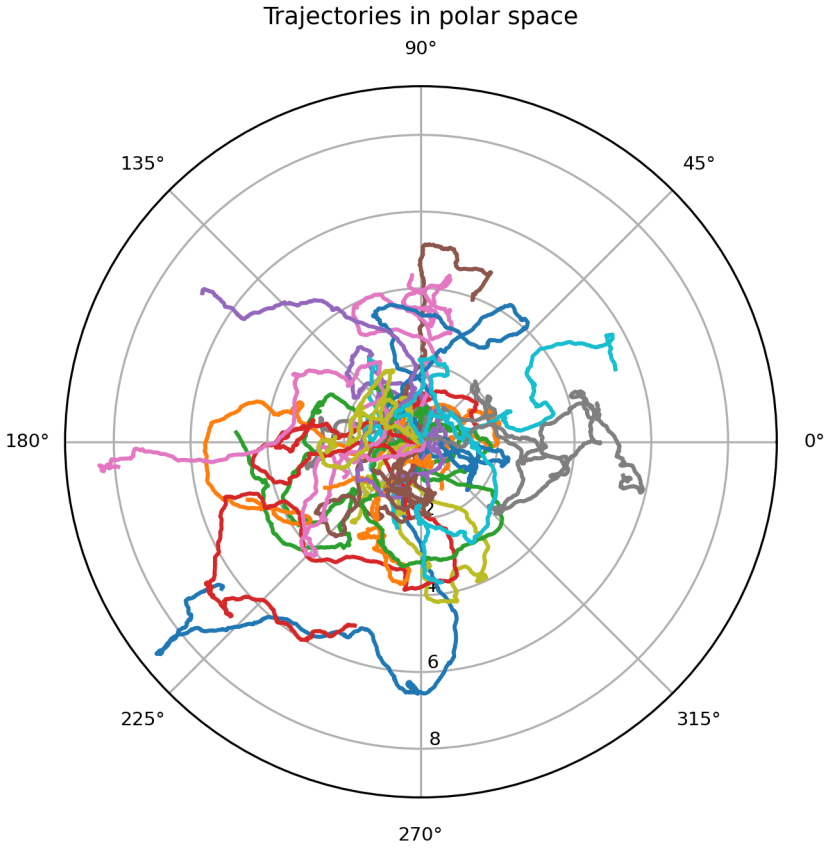

Figure 6.35: **Trajectories in polar coordinates in the case where $\chi_c = \chi_c^*$.** *Each curve represents, in polar coordinates, the trajectory of one cell simulated by algorithm 6.1 on the time interval $[0, 15]$. Visually, the trajectories seem to be intermittent. Thirty cells are represented.*
The results presented here are obtained with the parameters $\Delta t = 0.005$, $R_0 = 1$, $R_{\mathrm{nucl}} = 0.3$, $\mathbf{x}_{\mathrm{nucl}}^{\mathrm{in}} = (0; 0)$, $M = \pi$, $a = 1$, $c^{\mathrm{in}} = \dfrac{M}{|\Omega \setminus N|}$, $\chi_c = \chi_c^*$ with χ_c^* given by (6.8), $f_{\mathrm{act}}(c) = \frac{c(1+c_s)^2}{c_s(c+c_s)}$ with $c_s = 0.5$, $\alpha = 0.3$, $\zeta = 0.2$, $k = 0.866677$, and $\xi_{\mathrm{nucl}} = 1$.

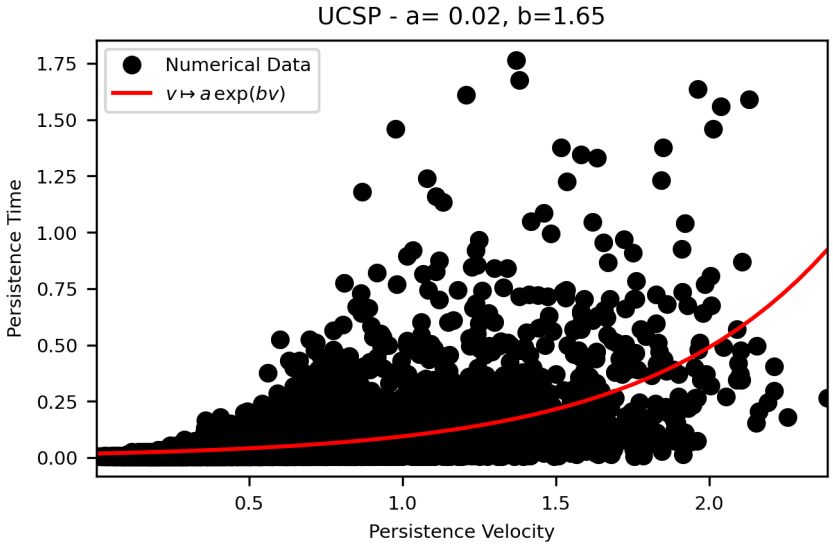

Figure 6.36: **Verification that the trajectories in fig. 6.35 satisfy the UCSP law (case when $\chi_c = \chi_c^*$).** *The persistence time of a locally persistent trajectory portion is plotted as a function of the persistence velocity. Each black dot corresponds to a datum. In red is plotted an interpolation of the points, of form $v \mapsto ae^{bv}$, which corresponds to the UCSP law. We can see that the data corresponds well to the interpolation and that the trajectories satisfy the UCSP law.*
The results presented here are obtained with the parameters $\Delta t = 0.005$, $R_0 = 1$, $R_{\text{nucl}} = 0.3$, $\mathbf{x}_{\text{nucl}}^{\text{in}} = (0;0)$, $M = \pi$, $a = 1$, $c^{\text{in}} = \dfrac{M}{|\Omega \setminus N|}$, $\chi_c = \chi_c^*$ with χ_c^* given by (6.8), $f_{\text{act}}(c) = \frac{c(1+c_s)^2}{c_s(c+c_s)}$ with $c_s = 0.5$, $\alpha = 0.3$, $\zeta = 0.2$, $k = 0.866677$, and $\xi_{\text{nucl}} = 1$.

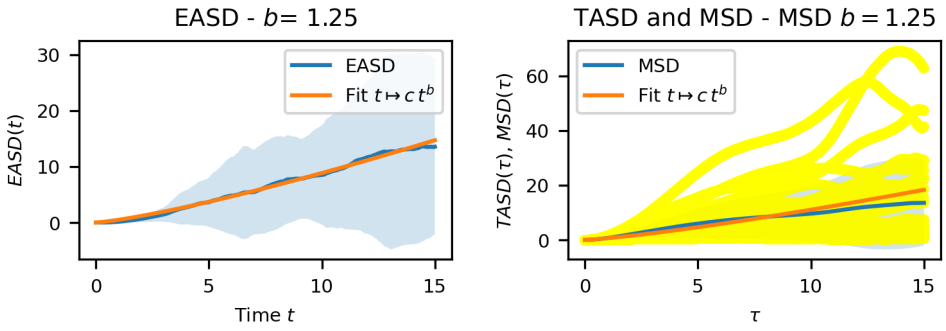

Figure 6.37: **Verification that the trajectories in fig. 6.35 are intermittent (case when $\chi_c = \chi_c^*$).** *On the left is shown in blue the EASD associated with the trajectories in fig. 6.35 and in orange the interpolation of the EASD, in the form $t \mapsto ct^b$. By the properties of the EASD, as b between 1 and 2, the trajectories in fig. 6.35 are neither Brownian neither persistent. This is confirmed by the study of the MSD, which is shown in blue on the right. Also shown on the right are the TASD of each cell in yellow and the interpolation of the MSD in form $t \mapsto ct^b$ in orange.*
The results presented here are obtained with the parameters $\Delta t = 0.005$, $R_0 = 1$, $R_{\text{nucl}} = 0.3$, $\mathbf{x}_{\text{nucl}}^{\text{in}} = (0;0)$, $M = \pi$, $a = 1$, $c^{\text{in}} = \dfrac{M}{|\Omega \setminus N|}$, $\chi_c = \chi_c^*$ with χ_c^* given by (6.8), $f_{\text{act}}(c) = \frac{c(1+c_s)^2}{c_s(c+c_s)}$ with $c_s = 0.5$, $\alpha = 0.3$, $\zeta = 0.2$, $k = 0.866677$, and $\xi_{\text{nucl}} = 1$.

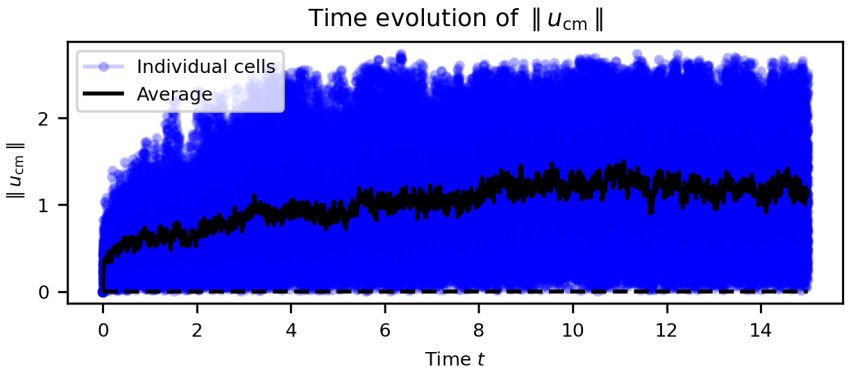

Figure 6.38: **Time evolution of the norm of the velocity of the cells whose trajectories are shown in fig. 6.17 (case when $\chi_c = \chi_c^*$).** *The blue lines show the evolution over time of the norm of the velocity of each cell and the black line shows the evolution of the mean of the norms of the velocities of the cells.*
The results presented here are obtained with the parameters $\Delta t = 0.005$, $R_0 = 1$, $R_{\text{nucl}} = 0.3$, $\mathbf{x}_{\text{nucl}}^{\text{in}} = (0; 0)$, $M = \pi$, $a = 1$, $c^{\text{in}} = \dfrac{M}{|\Omega \setminus N|}$, $\chi_c = \chi_c^*$ *with* χ_c^* *given by (6.8),* $f_{\text{act}}(c) = \frac{c(1+c_s)^2}{c_s(c+c_s)}$ *with* $c_s = 0.5$, $\alpha = 0.3$, $\zeta = 0.2$, $k = 0.866677$, *and* $\xi_{\text{nucl}} = 1$.

We therefore observe similar results with the two choices for the expression of forces induced by the nucleus on the cell boundary and by the cell boundary on the nucleus. This suggests that our heuristic approach can be seen as an approximation of the first modelling. We have therefore developed a model that allows the dynamics of the nucleus to be taken into account. Numerical simulations of the model highlight the role of the nucleus in cell polarisation and its impact on cell migration. The study of the model is continued in the next chapter with the study of the associated deformable model.

Conclusion and perspectives. The proposed model and the numerical simulations carried out highlight the role of the nucleus in cell motility and, in particular, in cell polarisation. The numerical simulations also validate the heuristic approach chosen to model the forces exerted between the cell boundary and the nucleus. We aim to continue investigating this heuristic in the context of both a deformable cell and a deformable nucleus. We also intend to continue studying this model by investigating the influence of the parameter ξ_{nucl} on the trajectories. In a future work, we aim to study the existence of travelling waves for the model as well as its long-time behaviour. We wish to prove the existence of stable travelling waves when $\chi_c > \chi_c^*$ and the convergence towards them. Finally, we hope to establish a bifurcation result from the stationary state to a travelling wave when χ_c becomes larger than χ_c^*.

Bibliography

Alazard, T., Magliocca, M., and Meunier, N. (2022). Traveling wave solution for a coupled incompressible Darcy's free boundary problem with surface tension. arXiv:2205.04365 [math]. 165

Boulakia, M., Genadot, A., and Thieullen, M. (2015). Simulation of SPDEs for Excitable Media Using Finite Elements. Journal of Scientific Computing, 65(1):171–195. 179

Hecht, F. (2012). New development in freefem++. J. Numer. Math., 20(3-4):251–265. 183

Lavi, I., Meunier, N., Voituriez, R., and Casademunt, J. (2020). Motility and morphodynamics of confined cells. Physical Review E, 101(2):022404. Publisher: American Physical Society. 165, 185

Lefebvre, A. (2007). Modélisation numérique d'écoulements fluide/particules. phdthesis, Université Paris Sud. 182

7 - Deformable cell model with a rigid nucleus

In this chapter, in collaboration with Nicolas Meunier and Raphaël Voituriez, we study the free-boundary model (1.1) in the case where the substrate is assumed to be homogeneous, the cell environment has no osbstacle or external signal, and we neglect the effects of undercooling and noise. After recalling the model of interest, we study its stationary states. We give a criterion for the stability of the radially symmetric stationary state. We then write a numerical scheme for the model. This scheme is obtained after semi-implicit discretisation in time and discretisation in space using a finite element method. The curvature is discretised implicitly. Two methods are proposed for handling potential contacts between the cell boundary and the nucleus. Finally, we present numerical results to highlight that the model gives qualitative results in line with the biological context. The simulations allow us to observe the different phases of polarisation followed by cell migration.

7.1 . Presentation of the model

In this section, we recall the general model (1.1) in the case where the substrate is homogeneous ($\xi_{\mathrm{M}} = 1$) and the environment outside the cell presents neither an external obstacle nor an external signal. We also neglect the effect of undercooling and noise. Under these assumptions, keeping the notations of chapter 1, the model studied is then given by:

$$
\begin{cases}
\mathbf{u} + \nabla P = 0 & \text{in } \Omega(t) \setminus N(t), & \text{(7.1a)}\\
\operatorname{div}(\mathbf{u}) = 0 & \text{in } \Omega(t) \setminus N(t), & \text{(7.1b)}\\
V_n = \mathbf{u} \cdot \mathbf{n} & \text{on } \partial\Omega(t), & \text{(7.1c)}\\
P = \gamma\kappa + \chi_c f_{\mathrm{act}}(c) - f_{\mathrm{NB}} & \text{on } \partial\Omega(t), & \text{(7.1d)}\\
\mathbf{u}_{\mathrm{nucl}}(t) = \dfrac{1}{\xi_{\mathrm{nucl}}|N|}\left(\displaystyle\int_{\partial N(t)} P(t,\mathbf{x})\mathbf{n}\,\mathrm{d}\sigma + \mathbf{f}_{\mathrm{BN}}\right) & & \text{(7.1e)}\\
\mathbf{u}\cdot\mathbf{n} = \mathbf{u}_{\mathrm{nucl}}\cdot\mathbf{n} & \text{on } \partial N(t), & \text{(7.1f)}\\
\partial_t c = \operatorname{div}(\nabla c - (1-a)\,\mathbf{u}c) & \text{in } \Omega(t) \setminus N(t), & \text{(7.1g)}\\
(\nabla c + a\mathbf{u}c)\cdot\mathbf{n} = 0 & \text{on } \partial(\Omega(t) \setminus N(t)), & \text{(7.1h)}\\
c(0,\mathbf{x}) = c^{\mathrm{in}}(\mathbf{x}) & \text{in } \Omega(0) \setminus N(0). & \text{(7.1i)}
\end{cases}
$$

We recall the expressions for $\mathbf{f}_{\mathrm{BN}}$ and f_{NB} defined by eqs. (1.22) and (1.23). For all $t \geq 0$ and $\mathbf{x} \in \partial\Omega(t)$, we have:

$$
\mathbf{f}_{\mathrm{BN}}(t) = \delta \int_{\partial\Omega(t)} \frac{\mathbf{v}_{\mathrm{BN}}\cdot\mathbf{n}}{\left(\|\mathbf{v}_{\mathrm{BN}}\| - R_{\mathrm{nucl}}\right)^{\beta}}\mathbf{n}\,\mathrm{d}\sigma, \tag{7.2}
$$

and

$$
f_{\mathrm{NB}}(t,\mathbf{x}) = -\delta\frac{\mathbf{v}_{\mathrm{BN}}\cdot\mathbf{n}}{\left(\|\mathbf{v}_{\mathrm{BN}}\| - R_{\mathrm{nucl}}\right)^{\beta}}, \tag{7.3}
$$

with $\beta > 1$, $\delta > 0$ and $\mathbf{v}_{\mathrm{BN}} = \mathbf{x}_{\mathrm{nucl}} - \mathbf{x}_B$ where $\mathbf{x}_B \in \partial\Omega(t)$.

We also recall that $\mathbf{f}_{\mathrm{BN}}$ and f_{NB} can also be defined by eqs. (1.24) and (1.25) and we recall that in this case, for all $t \geq 0$ and $\mathbf{x} \in \partial\Omega(t)$, we have:

$$\mathbf{f}_{\mathrm{BN}}(t) = -k\left(\mathbf{x}_{\mathrm{nucl}}(t) - \mathbf{x}_{\mathrm{cm}}(t)\right), \tag{7.4}$$

and

$$f_{\mathrm{NB}}(t, \mathbf{x}) = \frac{-k\left(\mathbf{x}_{\mathrm{cm}}(t) - \mathbf{x}_{\mathrm{nucl}}(t)\right) \cdot \mathbf{x}}{A_\Omega} \tag{7.5}$$

with $k > 0$ and $\mathbf{x}_{\mathrm{cm}}$ the centre of the cell.

We recall that the model is such that the total quantity of markers M is conserved over time and we have:

$$M = \int_{\Omega(t)\setminus N(t)} c(t, \mathbf{x})\, \mathrm{d}\mathbf{x}. \tag{7.6}$$

We also recall that the volume of the cell A_Ω is constant over time and we have:

$$A_\Omega = |\Omega(t)|. \tag{7.7}$$

7.2 . Study of the radial stationary state

In this section, by defining a stationary state, we prove the existence of stationary states and study the stability of the radially symmetric stationary state. In all this section, we consider that $\mathbf{f}_{\mathrm{BN}}$ and f_{NB} are defined by the expressions (7.2) and (7.3).

The results presented here holds true when we consider $\mathbf{f}_{\mathrm{BN}}$ and f_{NB} defined by the expressions (7.4) and (7.5), details are given in remarks 7.2.3 and 7.2.9.

7.2.1 . Definition of the stationary state

The following proposition defines and demonstrates the existence of stationary states.

Proposition 7.2.1. *A stationary state of the model defined by eq. (7.1) is characterised by:*

$$\begin{cases} \mathbf{u}(\mathbf{x}) = 0 & \mathbf{x} \in \Omega^0 \setminus N^0, \quad (7.8a) \\ P(\mathbf{x}) = P^0 \in \mathbb{R} & \mathbf{x} \in \Omega^0 \setminus N^0, \quad (7.8b) \\ \mathbf{u}_{\mathrm{nucl}} = 0, & (7.8c) \\ c(\mathbf{x}) = \dfrac{M}{A_\Omega - |N|} & \mathbf{x} \in \Omega^0 \setminus N^0, \quad (7.8d) \end{cases}$$

with $N^0 = B(0, R_{\mathrm{nucl}})$ and Ω^0 a convex such that for all $\mathbf{x} \in \partial\Omega^0$ it holds:

$$\gamma\kappa(\mathbf{x}) = f_{\mathrm{NB}}(\mathbf{x}) - \chi_c f_{\mathrm{act}}(c) + P^0. \tag{7.9}$$

Proof. The stationary problem asssociated with the model (7.1) is given as follows:

$$\begin{cases} \mathbf{u} + \nabla P = 0 & \text{in } \Omega \setminus N, \\ \operatorname{div}(\mathbf{u}) = 0 & \text{in } \Omega \setminus N, \\ P = \gamma\kappa + \chi_c f_{\mathrm{act}}(c) - f_{\mathrm{NB}} & \text{on } \partial\Omega, \\ \mathbf{u} \cdot \mathbf{n} = 0 & \text{on } \partial\Omega \cup \partial N, \\ \Delta c - (1-a)\,\mathbf{u} \cdot \nabla c = 0 & \text{in } \Omega \setminus N, \\ (\nabla c + a\mathbf{u}c) \cdot \mathbf{n} = 0 & \text{on } \partial\Omega \cup \partial N, \end{cases}$$

with Ω and N given. Without loss of generality we can assume that $N = B(0, R_{\text{nucl}})$.

Thus the problem on P reads:

$$\begin{cases} -\Delta P = 0 & \text{in } \Omega \setminus N, \\ -\nabla P \cdot \mathbf{n} = 0 & \text{on } \partial\Omega \cup \partial N, \\ P = \gamma\kappa + \chi_c f_{\text{act}}(c) - f_{\text{NB}} & \text{on } \partial\Omega. \end{cases}$$

The two first lines leads to the fact that P is such that $\nabla P = 0$ over $\Omega \setminus N$ and thus P is constant over $\Omega \setminus N$. We then have $\mathbf{u} = 0$

Substituting the value of $\mathbf{u}$ into the dynamics of concentration c, we obtain:

$$\begin{cases} -\Delta c = 0 & \text{in } \Omega \setminus N, \\ -\nabla c \cdot \mathbf{n} = 0 & \text{on } \partial\Omega \cup \partial N, \end{cases}$$

and c is constant over $\Omega \setminus N$. Using the constraint on the total quantity of markers (7.6), we deduce that for all $\mathbf{x} \in \Omega \setminus N$, $c(\mathbf{x}) = \dfrac{M}{|\Omega \setminus N|}$.

Finally, we deduce that Ω and N are such that for all $\mathbf{x} \in \partial\Omega$, we have:

$$P = \gamma\kappa(\mathbf{x}) + \chi_c f_{\text{act}}(c) - f_{\text{NB}}(\mathbf{x}).$$

We recognize the condition eq. (7.9). We prove by contradiction, that it implies that Ω is convex.

By contradiction, assume that there exists $\Omega \neq B(0, R_0)$ satisfying eq. (7.9). By assumptions on f_{NB}, the closer $\mathbf{x} \in \partial\Omega$ is to the nucleus, the greater $f_{\text{NB}}(\mathbf{x})$ is and for all $\mathbf{x} \in \partial\Omega$ we have $f_{\text{NB}}(\mathbf{x}) > 0$. Then, necessarily, Ω is convex.

Indeed, assume by contradiction there exists a point $\mathbf{x}_{\text{neg}} \in \partial\Omega$ such that $\kappa(\mathbf{x}_{\text{neg}}) < 0$. We assume that $\mathbf{x}_{\text{neg}}$ minimises the distance between the cell boundary and the nucleus among the points of negative curvature. As we assume the curvature to be positive for a circle and $\partial\Omega$ defined a close curve around N, there exists $\mathbf{x}_{\text{pos}} \in \partial\Omega$ such that $\kappa(\mathbf{x}_{\text{pos}}) > 0$ and such that the distance between $\mathbf{x}_{\text{pos}}$ and the nucleus is greater than the one between $\mathbf{x}_{\text{neg}}$ and the nucleus. Then in particular we have:

$$\gamma(\kappa(\mathbf{x}_{\text{pos}}) - \kappa(\mathbf{x}_{\text{neg}})) = f_{\text{NB}}(\mathbf{x}_{\text{pos}}) - f_{\text{NB}}(\mathbf{x}_{\text{neg}}),$$

with $\kappa(\mathbf{x}_{\text{pos}}) - \kappa(\mathbf{x}_{\text{neg}}) > 0$ and $f_{\text{NB}}(\mathbf{x}_{\text{pos}}) - f_{\text{NB}}(\mathbf{x}_{\text{neg}}) < 0$ which is absurd. □

The following proposition immediatly follows.

Proposition 7.2.2. *The model eq. (7.1) admits an unique radially symmetric stationary state given by:*

$$\begin{cases} \mathbf{u}^0(\mathbf{x}) = 0, & \text{(7.10a)} \\ P^0(\mathbf{x}) = \dfrac{\gamma}{R_0} + \chi_c f_{\text{act}}(c^0) - \dfrac{\delta R_0}{(R_0 - R_{\text{nucl}})^\beta}, & \text{(7.10b)} \\ \mathbf{u}^0_{\text{nucl}} = 0, & \text{(7.10c)} \\ c^0(\mathbf{x}) = \dfrac{M}{|\Omega^0 \setminus N^0|}, & \text{(7.10d)} \\ \Omega^0 = B(0, R_0) \text{ and } N^0 = B(0, R_{\text{nucl}}), & \text{(7.10e)} \end{cases}$$

with $R_0 = \sqrt{\frac{A_\Omega}{\pi}}$.

Remark 7.2.3. *We can note that if* $\mathbf{f}_{\mathrm{BN}}$ *and* f_{NB} *are defined by the expressions* (7.4) *and* (7.5)*, then eq.* (7.10) *is a radially symmetric stationary state of the model.*

In the sequel we denote:

$$\chi_c^* = \frac{1}{ac^0 f'_{\mathrm{act}}\left(c^0\right)}. \tag{7.11}$$

Theorem 7.2.4. *In the case where* $\xi_{\mathrm{nucl}} = 1$*, if* $\chi_c < \chi_c^*$*, then the stationary state* (7.10) *is linearly stable. On the opposite, if* $\chi_c > \chi_c^*$*, then the stationary state is linearly unstable.*

7.2.2 . Proof of theorem 7.2.4

The theorem is proved in five steps. The first consists of computing the linearised problem of problem (7.1) around the stationary state (7.10) and deducing an eigenvalue problem. The stationary state will then be stable if all the eigenvalues of the eigenvalue problem have a negative real part. The second step consists in establishing that the study of the spectrum of the eigenvalue problem can be decomposed into the study of the spectrum of simpler (P_m) problems indexed by $m \in \mathbb{N}$. This step is based on the radially symmetric nature of the problem and Fourier analysis. The third step consists in proving that for $m = 0$, the eigenvalues of (P_0) have all negative real parts. The fourth consists in showing that for $m \geq 2$, if $\chi_c < \chi_c^*$ then the eigenvalues of (P_m) are all negative real parts. The fifth consists in studying the case $m = 1$. We can then exhibit a positive real part eigenvalue of (P_1) when $\chi_c > \chi_c^*$. Also, using a graphical argument, it consists in illustrating that if $\chi_c < \chi_c^*$ then the eigenvalues of (P_1) have a negative real part. The arguments used are inspired by those of Lavi et al. (2020); Alazard et al. (2022) and are similar to those of sections 4.2.1.2, 5.2.2 and 6.2.2.

Step 1. The following lemma gives the expression for the linearised problem around the stationary state (7.10).

Lemma 7.2.5. *The linearised problem associated to eq.* (7.1) *around the stationary state* (7.10) *is given by:*

$$\begin{cases} -\Delta\tilde{P} = 0 & \text{in } \Omega^0 \setminus N^0, \quad (7.12a) \\ \partial_t \rho\left(t,\theta\right) = -\partial_r \tilde{P}\left(t, R_0, \theta\right) & \text{with } \theta \in (-\pi, \pi], \quad (7.12b) \\ \tilde{P} = \dfrac{-\gamma}{R_0^2}\left(\partial_{\theta\theta}^2 \rho + \rho\right) + \chi_c f'_{\mathrm{act}}\left(c^0\right)\tilde{c} & \\ \qquad + \dfrac{\delta\left(R_0\left(1-\beta\right) - R_{\mathrm{nucl}}\right)}{\left(R_0 - R_{\mathrm{nucl}}\right)^{\beta+1}}\left(\tilde{\mathbf{x}}_{\mathrm{nucl}} \cdot \mathbf{n} - \rho\right) & \text{on } \partial\Omega^0, \quad (7.12c) \\ \nabla\tilde{P} \cdot \mathbf{n} = -\tilde{\mathbf{u}}_{\mathrm{nucl}} \cdot \mathbf{n} & \text{on } \partial N^0, \quad (7.12d) \\ \partial_t \tilde{c} = \Delta\tilde{c} & \text{in } \Omega^0 \setminus N^0, \quad (7.12e) \\ \left(\nabla\tilde{c} - a\nabla\tilde{P}c^0\right) \cdot \mathbf{n} = 0 & \text{on } \partial\Omega^0 \cup \partial N^0, \quad (7.12f) \end{cases}$$

with

$$\tilde{\mathbf{u}}_{\mathrm{nucl}}\left(t\right) = \frac{1}{|N|}\left(\int_{\partial N^0} \tilde{P}\left(t,\mathbf{x}\right)\mathbf{n}\,\mathrm{d}\sigma + \frac{\delta R_0\left(R_0\left(1-\beta\right) - R_{\mathrm{nucl}}\right)}{\left(R_0 - R_{\mathrm{nucl}}\right)^{\beta+1}}\left(\pi\tilde{\mathbf{x}}_{\mathrm{nucl}}\left(t\right) - \int_0^{2\pi} \rho\left(t,\theta\right)\begin{pmatrix}\cos\theta \\ \sin\theta\end{pmatrix}\mathrm{d}\theta\right)\right), \tag{7.13}$$

and $\tilde{\mathbf{x}}_{\mathrm{nucl}} = (\tilde{x}_{\mathrm{nucl}}, \tilde{y}_{\mathrm{nucl}})$ *such that for all* $t \geq 0$*:*

$$\frac{\mathrm{d}}{\mathrm{d}t}\tilde{\mathbf{x}}_{\mathrm{nucl}}(t) = \tilde{\mathbf{u}}_{\mathrm{nucl}}.$$

Proof. We perform a formal expansion of the solutions of model (7.1) around the stationary state (7.10). Let $\varepsilon > 0$ small. For all $t \geq 0$, we set:

$$\Omega(t) = \{(r\cos\theta, r\sin\theta) \text{ s.t. } 0 \leq r < R_0 + \varepsilon\rho(t,\theta) \text{ and } \theta \in (-\pi, \pi]\}.$$

We also set:

$$N(t) = B(\mathbf{x}_{\mathrm{nucl}}(t), R_{\mathrm{nucl}}),$$

with

$$\mathbf{x}_{\mathrm{nucl}}(t) = \varepsilon\tilde{\mathbf{x}}_{\mathrm{nucl}}(t) + \mathcal{O}(\varepsilon^2)$$

and thus we set for all $t \geq 0$:

$$\mathbf{u}_{\mathrm{nucl}}(t) = \mathbf{u}^0_{\mathrm{nucl}} + \varepsilon\tilde{\mathbf{u}}_{\mathrm{nucl}}(t) + \mathcal{O}(\varepsilon^2).$$

Moreover, for all $t \geq 0$ and $\mathbf{x} \in \Omega^0 \setminus N^0$, we set:

$$P(t,\mathbf{x}) = P^0 + \varepsilon\tilde{P}(t,\mathbf{x}) + \mathcal{O}(\varepsilon^2),$$

and

$$c(t,\mathbf{x}) = c^0 + \varepsilon\tilde{c}(t,\mathbf{x}) + \mathcal{O}(\varepsilon^2).$$

As P_0 satisfies eq. (7.10b) and P satisfies eqs. (7.1a) and (7.1b), we have that in $\Omega^0 \setminus N^0$:

$$-\Delta\tilde{P} = 0.$$

In addition, using the parametrization of Ω boundary, we have that for all $t \geq 0$ and $\theta \in (-\pi, \pi]$, the expansion of f_{NB}, the outward normal vector $\mathbf{n}$ to Ω and the κ curvature are given by:

$$f_{\mathrm{NB}}(t,\theta) = \frac{\delta R_0}{(R_0 - R_{\mathrm{nucl}})^{\beta}} - \varepsilon\frac{\delta\left(R_0(1-\beta) - R_{\mathrm{nucl}}\right)}{(R_0 - R_{\mathrm{nucl}})^{\beta+1}}\left(\tilde{\mathbf{x}}_{\mathrm{nucl}}(t)\cdot\begin{pmatrix}\cos\theta\\ \sin\theta\end{pmatrix} - \rho(t,\theta)\right) + \mathcal{O}(\varepsilon^2),$$

$$\mathbf{n}(t,\theta) = \begin{pmatrix}\cos\theta\\ \sin\theta\end{pmatrix} - \varepsilon\frac{\partial_\theta\rho(t,\theta)}{R_0}\begin{pmatrix}-\sin\theta\\ \cos\theta\end{pmatrix} + \mathcal{O}(\varepsilon^2)$$

and

$$\kappa(t,\theta) = \frac{1}{R_0} - \varepsilon\frac{\partial^2_{\theta\theta}\rho(t,\theta) + \rho(t,\theta)}{R_0^2} + \mathcal{O}(\varepsilon^2).$$

Since, we also have:

$$f_{\mathrm{act}}(c) = f_{\mathrm{act}}(c^0) + \varepsilon\tilde{c}f'_{\mathrm{act}}(c^0) + \mathcal{O}(\varepsilon^2),$$

thus as P satisfies eq. (7.1d), it leads to the following boundary condition for $\tilde{P}$ on $\partial\Omega^0$:

$$\tilde{P} = \frac{-\gamma}{R_0^2}\left(\partial^2_{\theta\theta}\rho + \rho\right) + \chi_c f'_{\mathrm{act}}(c^0)\,\tilde{c}\frac{\delta\pi R^2_{\mathrm{nucl}}\left(R_0(1-\beta) - R_{\mathrm{nucl}}\right)}{(R_0 - R_{\mathrm{nucl}})^{\beta+1}}\left(\tilde{\mathbf{x}}_{\mathrm{nucl}}\cdot\mathbf{n} - \rho\right),$$

where in this case $\mathbf{n}$ denotes the outward normal vector to Ω^0.

Also, we have that the expansion of the normal velocity of the boundary is given for all $t \geq 0$ and $\theta \in (-\pi, \pi]$ by:

$$V_n = \varepsilon \partial_t \rho\left(t, \theta\right) + \mathcal{O}\left(\varepsilon^2\right).$$

As P satisfies eq. (7.1c), we have that $\tilde{P}$ satifies for all $t \geq 0$ and $\theta \in (-\pi, \pi]$:

$$\partial_t \rho\left(t, \theta\right) = -\partial_r \tilde{P}\left(t, R_0, \theta\right).$$

In addition, as P satisfies eq. (7.1f), we have that $\tilde{P}$ satisfies on ∂N^0:

$$-\nabla \tilde{P} \cdot \mathbf{n} = \tilde{\mathbf{u}}_{\mathrm{nucl}} \cdot \mathbf{n}.$$

Furthermore, we deduce from the expansion of f_{NB} the one of $\mathbf{f}_{\mathrm{BN}}$ and for all $t \geq 0$ we have:

$$\mathbf{f}_{\mathrm{BN}}\left(t\right) = \varepsilon \frac{\delta R_0 \left(R_0 \left(1-\beta\right) - R_{\mathrm{nucl}}\right)}{\left(R_0 - R_{\mathrm{nucl}}\right)^{\beta+1}} \left[\pi \tilde{\mathbf{x}}_{\mathrm{nucl}}\left(t\right) - \int_0^{2\pi} \rho\left(t, \theta\right) \begin{pmatrix} \cos\theta \\ \sin\theta \end{pmatrix} \mathrm{d}\theta\right] + \mathcal{O}\left(\varepsilon^2\right).$$

Thus we have:

$$\begin{aligned} \tilde{\mathbf{u}}_{\mathrm{nucl}}\left(t\right) = \frac{1}{\pi R_{\mathrm{nucl}}^2} \Bigg(& \int_{\partial N^0} \tilde{P}\left(t, \mathbf{x}\right) \mathbf{n} \, \mathrm{d}\sigma \\ & + \frac{\delta R_0 \left(R_0 \left(1-\beta\right) - R_{\mathrm{nucl}}\right)}{\left(R_0 - R_{\mathrm{nucl}}\right)^{\beta+1}} \left[\pi \tilde{\mathbf{x}}_{\mathrm{nucl}}\left(t\right) - \int_0^{2\pi} \rho\left(t, \theta\right) \begin{pmatrix} \cos\theta \\ \sin\theta \end{pmatrix} \mathrm{d}\theta\right] \Bigg). \end{aligned}$$

Using the fact that c^0 satisfies eq. (7.10d) and c satisfies eq. (7.1g), we deduce that in $\Omega^0 \setminus N^0$:

$$\partial_t \tilde{c} = \Delta \tilde{c}.$$

We also have on $\partial\Omega^0$ that:

$$\begin{aligned} \left(\nabla c + a \mathbf{u}_{\mathrm{cm}} c\right) \cdot \mathbf{n} &= \left(\nabla c^0 + \varepsilon \nabla \tilde{c} + a \mathbf{u}_{\mathrm{cm}}^0 c^0 + \varepsilon a \mathbf{u}_{\mathrm{cm}}^0 \tilde{c} + \varepsilon a \tilde{\mathbf{u}}_{\mathrm{cm}} c^0\right) \cdot \mathbf{n} + \mathcal{O}\left(\varepsilon^2\right) \\ &= \varepsilon \left(\nabla \tilde{c} + a \tilde{\mathbf{u}}_{\mathrm{cm}} c^0\right) \cdot \mathbf{n} + \mathcal{O}\left(\varepsilon^2\right), \end{aligned}$$

which leads to the boundary condition:

$$\left(\nabla \tilde{c} + a \tilde{\mathbf{u}}_{\mathrm{cm}} c^0\right) \cdot \mathbf{n} = 0 \qquad \text{on } \partial\Omega^0.$$

Similarly, we obtain the boundary condition on N^0:

$$\left(\nabla \tilde{c} + a \tilde{\mathbf{u}}_{\mathrm{nucl}} c^0\right) \cdot \mathbf{n} = 0.$$

□

The eigenvalue problem associated with eqs. (7.12) and (7.13) is given by:

$$\begin{cases} -\Delta \tilde{P} = 0 & \text{in } \Omega^0 \setminus N^0, \quad (7.14a) \\ \lambda \rho\left(\theta\right) = -\partial_r \tilde{P}\left(R_0, \theta\right) & \text{with } \theta \in (-\pi, \pi], \quad (7.14b) \\ \tilde{P} = \dfrac{-\gamma}{R_0^2}\left(\partial_{\theta\theta}^2 \rho + \rho\right) + \chi_c f_{\mathrm{act}}'\left(c^0\right) \tilde{c} & \\ \qquad + \dfrac{\delta \left(R_0 \left(1-\beta\right) - R_{\mathrm{nucl}}\right)}{\left(R_0 - R_{\mathrm{nucl}}\right)^{\beta+1}} \left(\tilde{\mathbf{x}}_{\mathrm{nucl}} \cdot \mathbf{n} - \rho\right) & \text{on } \partial\Omega^0, \quad (7.14c) \\ \nabla \tilde{P} \cdot \mathbf{n} = -\tilde{\mathbf{u}}_{\mathrm{nucl}} \cdot \mathbf{n} & \text{on } \partial N^0, \quad (7.14d) \\ \lambda \tilde{c} = \tilde{\mathbf{u}}_{\mathrm{nucl}} = \Delta \tilde{c} & \text{in } \Omega^0 \setminus N^0, \quad (7.14e) \\ \left(\nabla \tilde{c} - a \nabla \tilde{P} c^0\right) \cdot \mathbf{n} = 0 & \text{on } \partial\Omega^0 \cup \partial N^0, \quad (7.14f) \end{cases}$$

with

$$\lambda\tilde{\mathbf{x}}_{\mathrm{nucl}} = \frac{1}{|N|}\left(\int_{\partial N^0} \tilde{P}\left(\mathbf{x}\right)\mathbf{n}\,\mathrm{d}\sigma \right.$$
$$\left. + \frac{\delta R_0\left(R_0\left(1-\beta\right)-R_{\mathrm{nucl}}\right)}{\left(R_0-R_{\mathrm{nucl}}\right)^{\beta+1}}\left(\pi\tilde{\mathbf{x}}_{\mathrm{nucl}} - \int_0^{2\pi}\rho\left(\theta\right)\right)\begin{pmatrix}\cos\theta\\ \sin\theta\end{pmatrix}\mathrm{d}\theta\right), \quad (7.15)$$

where $\lambda \in \mathbb{C}$.

Step 2. Since problem (7.14) and (7.15) is radially symmetrical, we can use Fourier analysis to study its spectra. Let $\lambda \in \mathbb{C}$ and let $\left(\tilde{P}, \tilde{c}, \tilde{\rho}, \tilde{\mathbf{x}}_{\mathrm{nucl}}\right)$ be an eigenfunction associated with λ. In polar coordinates, for all $r \in \left(R_{\mathrm{nucl}}, R_0\right)$ and $\theta \in (-\pi, \pi]$, the Fourier decomposition of $\tilde{P}$ is given by:

$$\tilde{P}\left(r,\theta\right) = \sum_{m\in\mathbb{N}} P_{cm}\left(r\right)\cos\left(m\theta\right) + \sum_{m\in\mathbb{N}} P_{sm}\left(r\right)\sin\left(m\theta\right),$$

the one of $\tilde{c}$ by:

$$\tilde{c}\left(r,\theta\right) = \sum_{m\in\mathbb{N}} c_{cm}\left(r\right)\cos\left(m\theta\right) + \sum_{m\in\mathbb{N}} c_{sm}\left(r\right)\sin\left(m\theta\right),$$

and the one of $\tilde{\rho}$ by:

$$\tilde{\rho}\left(\theta\right) = \sum_{m\in\mathbb{N}} \rho_{cm}\cos\left(m\theta\right) + \sum_{m\in\mathbb{N}} \rho_{sm}\sin\left(m\theta\right),$$

with $P_{s0} = 0$, $c_{s0} = 0$ and $\rho_{s0} = 0$.

Thus we have:

$$\int_{\partial N^0} \tilde{P}\mathbf{n}\,\mathrm{d}\sigma = -\pi R_{\mathrm{nucl}}\begin{pmatrix}P_{c1}\left(R_{\mathrm{nucl}}\right)\\ P_{s1}\left(R_{\mathrm{nucl}}\right)\end{pmatrix},$$

and also:

$$\int_0^{2\pi}\tilde{\rho}\left(\theta\right)\begin{pmatrix}\cos\theta\\ \sin\theta\end{pmatrix}\mathrm{d}\theta = \pi\begin{pmatrix}\rho_{c1}\\ \rho_{s1}\end{pmatrix}.$$

It leads to:

$$\lambda\tilde{\mathbf{x}}_{\mathrm{nucl}} = -R_{\mathrm{nucl}}^{-1}\begin{pmatrix}P_{c1}\left(R_{\mathrm{nucl}}\right)\\ P_{s1}\left(R_{\mathrm{nucl}}\right)\end{pmatrix} + \frac{\delta R_0\left(R_0\left(1-\beta\right)-R_{\mathrm{nucl}}\right)}{R_{\mathrm{nucl}}^2\left(R_0-R_{\mathrm{nucl}}\right)^{\beta+1}}\left(\tilde{\mathbf{x}}_{\mathrm{nucl}} - \begin{pmatrix}\rho_{c1}\\ \rho_{s1}\end{pmatrix}\right).$$

Using the independence between the cosine and sine modes and due to the the linearity of the problem (7.14), we have that studying the spectrum of problem (7.14) is equivalent to studying, for all $m \neq 1$, the spectrum of the problem associated to each cosine and sine mode. By symmetry, we note that, without loss of generality, we can study only the cosine modes.

As $\tilde{P}$ satisfies the laplacian equation (7.14a), we have that for all $m \in \mathbb{N}$, there exists A_m, B_m, C_m and $D_m \in \mathbb{R}$ such that for all $r \in \left(R_{\mathrm{nucl}}, R_0\right)$:

$$\begin{cases} P_{cm}\left(r\right) = A_m r^m + C_m r^{-m}, \\ P_{sm}\left(r\right) = B_m r^m + D_m r^{-m}, \end{cases}$$

with $B_0 = C_0 = D_0 = 0$.

Thus by linearity of the problem (7.14) and the independence of the cosine and sine modes, we obtain that A_0 is such that:

$$A_0 = -\left(\frac{\gamma}{R_0^2} + \frac{\delta\left(R_0\left(1-\beta\right)-R_{\mathrm{nucl}}\right)}{\left(R_0-R_{\mathrm{nucl}}\right)^{\beta+1}}\right)\rho_{c0} + \chi_c f'_{\mathrm{act}}\left(c^0\right)c_{c0}\left(R_0\right).$$

Thus the mode $m = 0$ satisfies:

$$\left\{\begin{array}{ll} \lambda\rho_{c0} = 0, & \\ \lambda c_{c0}\left(r\right) = \left(\partial_{rr}^2 + \dfrac{1}{r}\partial_r\right) c_{c0}\left(r\right) & r \in \left(R_{\mathrm{nucl}}, R_0\right), \\ \partial_r c_{c0}\left(r\right) = 0 & r \in \left\{R_{\mathrm{nucl}}, R_0\right\}. \end{array}\right. \tag{P_0}$$

As $\tilde{P}$ satisfies the boundary conditions eqs. (7.14b) to (7.14d), we deduce that A_1, C_1 and ρ_{c1} satisfy:

$$\left\{\begin{array}{l} \lambda\rho_{c1} = -\left(A_1 - C_1 R_0^{-2}\right), \\ A_1 R_0 + C_1 R_0^{-1} = \chi_c f'_{\mathrm{act}}\left(c^0\right) c_{c1}\left(R_0\right) + \dfrac{\delta\left(R_0\left(1-\beta\right) - R_{\mathrm{nucl}}\right)}{\left(R_0 - R_{\mathrm{nucl}}\right)^{\beta+1}}\left(\tilde{x}_{\mathrm{nucl}} - \rho_{c1}\right), \\ -C_1 R_{\mathrm{nucl}}^{-2} = C_1 R_{\mathrm{nucl}}^{-2} - \dfrac{\delta R_0\left(R_0\left(1-\beta\right) - R_{\mathrm{nucl}}\right)}{R_{\mathrm{nucl}}^2\left(R_0 - R_{\mathrm{nucl}}\right)^{\beta+1}}\left(\tilde{x}_{\mathrm{nucl}} - \rho_{c1}\right). \end{array}\right.$$

Thus we deduce that:

$$\left\{\begin{array}{l} A_1 = \dfrac{\chi_c f'_{\mathrm{act}}\left(c^0\right) c_{c1}\left(R_0\right)}{R_0} + \dfrac{\delta\left(R_0\left(1-\beta\right) - R_{\mathrm{nucl}}\right)}{2R_0\left(R_0 - R_{\mathrm{nucl}}\right)^{\beta+1}}\left(\tilde{x}_{\mathrm{nucl}} - \rho_{c1}\right), \\ C_1 = \dfrac{\delta R_0\left(R_0\left(1-\beta\right) - R_{\mathrm{nucl}}\right)}{2\left(R_0 - R_{\mathrm{nucl}}\right)^{\beta+1}}\left(\tilde{x}_{\mathrm{nucl}} - \rho_{c1}\right), \\ \lambda\rho_{c1} = -\dfrac{\chi_c f'_{\mathrm{act}}\left(c^0\right) c_{c1}\left(R_0\right)}{R_0}. \end{array}\right.$$

It follows that:

$$\lambda\tilde{x}_{\mathrm{nucl}} = -\frac{\chi_c f'_{\mathrm{act}}\left(c^0\right) c\left(R_0\right)}{R_0} + \frac{\delta\pi\left(R_0^2 - R_{\mathrm{nucl}}^2\right)\left(R_0\left(1-\beta\right) - R_{\mathrm{nucl}}\right)}{2R_0 R_{\mathrm{nucl}}^2\left(R_0 - R_{\mathrm{nucl}}\right)^{\beta+1}}\left(\tilde{x}_{\mathrm{nucl}} - \rho_{c1}\right).$$

For the remaining part of the demonstration, we introduce the following notation:

$$K = \frac{\delta\left(R_0^2 - R_{\mathrm{nucl}}^2\right)\left(R_0\left(1-\beta\right) - R_{\mathrm{nucl}}\right)}{2R_0 R_{\mathrm{nucl}}^2\left(R_0 - R_{\mathrm{nucl}}\right)^{\beta+1}}. \tag{7.16}$$

We note that $K < 0$.

Thus the mode $m = 1$ satisfies:

$$\left\{\begin{array}{ll} \lambda\rho_{c1} = -\dfrac{\chi_c f'_{\mathrm{act}}\left(c^0\right) c_{c1}\left(R_0\right)}{R_0}, & \\ \lambda c_{c1} = \left(\partial_{rr}^2 + \dfrac{1}{r}\partial_r - \dfrac{1}{r^2}\right) c_{c1} & r \in \left(R_{\mathrm{nucl}}, R_0\right), \\ \partial_r c_{c1}\left(R_0\right) - ac^0\partial_r P_{c1}\left(R_0\right) = 0, & \\ \partial_r c_{c1}\left(R_{\mathrm{nucl}}\right) - ac^0\partial_r P_{c1}\left(R_{\mathrm{nucl}}\right) = 0, & \\ \lambda\tilde{x}_{\mathrm{nucl}} = -\dfrac{\chi_c f'_{\mathrm{act}}\left(c^0\right) c\left(R_0\right)}{R_0} + K\left(\tilde{x}_{\mathrm{nucl}} - \rho_{c1}\right), & \end{array}\right. \tag{P_1}$$

with P_{c1} defined for all $r \in \left(R_{\mathrm{nucl}}, R_0\right)$ by:

$$\begin{aligned} P_{c1}\left(r\right) = &\left[\frac{\chi_c f'_{\mathrm{act}}\left(c^0\right) c\left(R_0\right)}{R_0} + \frac{\delta\left(R_0\left(1-\beta\right) - R_{\mathrm{nucl}}\right)}{2R_0\left(R_0 - R_{\mathrm{nucl}}\right)^{\beta+1}}\left(\tilde{x}_{\mathrm{nucl}} - \rho\right)\right] r \\ &+ \frac{\delta R_0\left(R_0\left(1-\beta\right) - R_{\mathrm{nucl}}\right)}{2\left(R_0 - R_{\mathrm{nucl}}\right)^{\beta+1}}\left(\tilde{x}_{\mathrm{nucl}} - \rho\right)\frac{1}{r}. \end{aligned} \tag{7.17}$$

Finally, when $m \geq 2$, without using the expression of P_{cm} we have that the mode m satisfies:

$$\begin{cases} \left(\partial_{rr}^2 + \frac{1}{r}\partial_r - \frac{m^2}{r^2}\right) P_{cm} = 0 & r \in (R_{\text{nucl}}, R_0), \\ \lambda \rho_{cm} = -\partial_r P_{cm}(R_0), \\ P_{cm}(R_0) = \left(\frac{\gamma(m^2-1)}{R_0^2} - \frac{\delta(R_0(1-\beta) - R_{\text{nucl}})}{(R_0 - R_{\text{nucl}})^{\beta+1}}\right) \rho_{cm} \\ \qquad\qquad + \chi_c f'_{\text{act}}(c^0)\, c_{cm}(R_0), \\ \partial_r P_{cm}(R_{\text{nucl}}) = 0, \\ \lambda c_{cm} = \left(\partial_{rr}^2 + \frac{1}{r}\partial_r - \frac{m^2}{r^2}\right) c_{cm} & r \in (R_{\text{nucl}}, R_0), \\ \partial_r c_{cm}(R_0) - a c^0 \partial_r P_{cm}(R_0) = 0, \\ \partial_r c_{cm}(R_{\text{nucl}}) = 0. \end{cases} \tag{$\mathsf{P_m}$}$$

Step 3. Here we study the eigenvalues associated to ($\mathsf{P_o}$). Let $\lambda \in \mathbb{C}$ be an eigenvalue of ($\mathsf{P_o}$). There exists $(\rho_\lambda, c_\lambda)$ eigenfunctions satisfying ($\mathsf{P_o}$). If $\lambda \neq 0$ thus $\rho_\lambda = 0$ and setting for all $r \in (R_{\text{nucl}}, R_0)$ and $\theta \in (-\pi, \pi,]$, $c(r,\theta) = c_\lambda(r)$ we have that c satisfies:

$$\begin{cases} \lambda c = \Delta c & \text{in } \Omega^0 \setminus N^0, \\ \nabla c \cdot \mathbf{n} = 0 & \text{on } \partial\Omega^0 \cup \partial N^0. \end{cases}$$

We thus have:

$$\lambda \int_{\Omega^0 \setminus N^0} |c|^2 \, \mathrm{d}\mathbf{x} = \int_{\Omega^0 \setminus N^0} \Delta c \bar{c} \, \mathrm{d}\mathbf{x} = -\int_{\Omega^0 \setminus N^0} |\nabla c|^2 \, \mathrm{d}\mathbf{x}$$

and then necessary the real part of λ is negative.

Step 4. Let $m \geq 2$. We demonstrate that when $\chi_c < \chi_c^*$ then all the eigenvalues of ($\mathsf{P_m}$) have negative real part. Let $\lambda \in \mathbb{C}$ be an eigenvalue of ($\mathsf{P_m}$). There exists $(P_\lambda, \rho_\lambda, c_\lambda)$ eigenfunctions satisfying ($\mathsf{P_m}$). For all $r \in (R_{\text{nucl}}, R_0)$ and $\theta \in (-\pi, \pi,]$, we define the function P_m by $P_m(r,\theta) = P_\lambda(r)\cos(m\theta)$, the function ρ_m by $\rho_m(r,\theta) = \rho_\lambda \cos(m\theta)$ and the function c_m by $c_m(r,\theta) = c_\lambda(r)\cos(m\theta)$. As $(P_\lambda, \rho_\lambda, c_\lambda)$ satisfies ($\mathsf{P_m}$), we have (P_m, ρ_m, c_m) satisfies the following one:

$$\begin{cases} \Delta P_m = 0 & \text{in } \Omega^0 \setminus N^0, \\ \lambda \rho_m = -\nabla P_m \cdot \mathbf{n} & \text{on } \partial\Omega^0, \\ P_m = \left(\frac{\gamma(m^2-1)}{R_0^2} - \frac{\delta(R_0(1-\beta) - R_{\text{nucl}})}{(R_0 - R_{\text{nucl}})^{\beta+1}}\right) \rho_m + \chi_c f'_{\text{act}}(c^0)\, c_m & \text{on } \partial\Omega^0, \\ \nabla P_m \cdot \mathbf{n} = 0 & \text{on } \partial N^0, \\ \lambda c_m = \Delta c_m & \text{in } \Omega^0 \setminus N^0, \\ \left(\nabla c_m - a c^0 \nabla P_m\right) \cdot \mathbf{n} = 0 & \text{on } \partial\Omega^0, \\ \nabla c_m \cdot \mathbf{n} = 0 & \text{on } \partial N^0. \end{cases}$$

The function Q_m defined by $Q_m = c_m - ac^0 P_m$ satisfies the following problem:

$$\begin{cases} \Delta Q_m = \lambda c_m & \text{in } \Omega^0 \setminus N^0, \\ \nabla Q_m \cdot \mathbf{n} = 0 & \text{on } \partial\Omega^0, \\ \nabla Q_m \cdot \mathbf{n} = 0 & \text{on } \partial N^0, \\ \left(1 - \dfrac{\chi_c}{\chi_c^*}\right) P_m = \chi_c f'_{\text{act}}\left(c^0\right) Q_m & \\ \qquad + \left(\dfrac{\gamma\left(m^2-1\right)}{R_0^2} - \dfrac{\delta\left(R_0\left(1-\beta\right) - R_{\text{nucl}}\right)}{\left(R_0 - R_{\text{nucl}}\right)^{\beta+1}}\right) \rho_m & \text{on } \partial\Omega^0. \end{cases}$$

Thus we have:

$$\begin{aligned} \lambda \int_{\Omega^0 \setminus N^0} |c_m|^2 \, \mathrm{d}\mathbf{x} &= \int_{\Omega^0 \setminus N^0} \overline{c_m} \Delta Q_m \, \mathrm{d}\mathbf{x} = \int_{\Omega^0 \setminus N^0} \left(\overline{Q_m} + ac^0 \overline{P_m}\right) \Delta Q_m \, \mathrm{d}\mathbf{x} \\ &= -\int_{\Omega^0 \setminus N^0} |\nabla Q_m|^2 \, \mathrm{d}\mathbf{x} - ac^0 \int_{\Omega^0 \setminus N^0} \nabla \overline{P_m} \cdot \nabla Q_m \, \mathrm{d}\mathbf{x} \\ &= -\int_{\Omega^0 \setminus N^0} |\nabla Q_m|^2 \, \mathrm{d}\mathbf{x} - ac^0 \int_{\partial\Omega^0} Q_m \nabla \overline{P_m} \cdot \mathbf{n} \, \mathrm{d}\sigma. \end{aligned}$$

Since:

$$\begin{aligned} &\int_{\partial\Omega^0} Q_m \nabla \overline{P_m} \cdot \mathbf{n} \, \mathrm{d}\sigma \\ &= \frac{1}{\chi_c f'_{\text{act}}\left(c^0\right)} \left[\left(1 - \frac{\chi_c}{\chi_c^*}\right) \int_{\partial\Omega^0} P_m \nabla \overline{P_m} \cdot \mathbf{n} \, \mathrm{d}\sigma \right. \\ &\qquad \left. - \left(\frac{\gamma\left(m^2-1\right)}{R_0^2} - \frac{\delta\left(R_0\left(1-\beta\right) - R_{\text{nucl}}\right)}{\left(R_0 - R_{\text{nucl}}\right)^{\beta+1}}\right) \int_{\partial\Omega^0} \rho_m \nabla \overline{P_m} \cdot \mathbf{n} \, \mathrm{d}\sigma \right] \\ &= \frac{1}{\chi_c f'_{\text{act}}\left(c^0\right)} \left[\left(1 - \frac{\chi_c}{\chi_c^*}\right) \int_{\partial\Omega^0} \overline{P_m} \nabla P_m \cdot \mathbf{n} \, \mathrm{d}\sigma \right. \\ &\qquad \left. + \bar{\lambda} \left(\frac{\gamma\left(m^2-1\right)}{R_0^2} - \frac{\delta\left(R_0\left(1-\beta\right) - R_{\text{nucl}}\right)}{\left(R_0 - R_{\text{nucl}}\right)^{\beta+1}}\right) \int_{\partial\Omega^0} |\rho_m|^2 \, \mathrm{d}\sigma \right], \end{aligned}$$

we have:

$$\begin{aligned} &\lambda \int_{\Omega^0 \setminus N^0} |c_m|^2 \, \mathrm{d}\mathbf{x} + \bar{\lambda} ac^0 \left(\frac{\gamma\left(m^2-1\right)}{R_0^2} - \frac{\delta\left(R_0\left(1-\beta\right) - R_{\text{nucl}}\right)}{\left(R_0 - R_{\text{nucl}}\right)^{\beta+1}}\right) \int_{\partial\Omega^0} |\rho_m|^2 \, \mathrm{d}\sigma \\ &\qquad = -\int_{\Omega^0 \setminus N^0} |\nabla Q_m|^2 \, \mathrm{d}\mathbf{x} - \frac{ac^0}{\chi_c f'_{\text{act}}\left(c^0\right)} \left(1 - \frac{\chi_c}{\chi_c^*}\right) \int_{\partial\Omega^0} \overline{P_m} \nabla P_m \cdot \mathbf{n} \, \mathrm{d}\sigma. \end{aligned}$$

As $\beta > 1$, then $-\dfrac{\delta\left(R_0\left(1-\beta\right) - R_{\text{nucl}}\right)}{\left(R_0 - R_{\text{nucl}}\right)^{\beta+1}} > 0$ and it follows that when $m \geq 2$ and $\chi_c < \chi_c^*$ then λ has a negative real part.

Step 5. Lastly, we study the eigenvalues associated with the (P_1) problem. When $\chi_c > \chi_c^*$, we want to exhibit an eigenvalue of (P_1) with a positive real part. Conversely, when $\chi_c < \chi_c^*$, we want to show that all the eigenvalues of (P_1) have negative real parts. To do this, we first characterise the eigenfunctions associated with the eigenvalue λ (see lemma 7.2.6). Secondly,

we derive an explicit condition on the eigenvalues of (P_1) (see lemma 7.2.7), which allows us to exhibit a positive real part eigenvalue when $\chi_c > \chi_c^*$ (see lemma 7.2.8) and to give a graphical argument on the fact that all the eigenvalues of (P_1) are negative real part when $\chi_c < \chi_c^*$.

Lemma 7.2.6. *Let $\lambda \in \mathbb{C}$. The eigenfunctions of eq. (P_1) associated with the eigenvalue $\lambda \in \mathbb{C}$ are given by:*

$$\begin{pmatrix} c(r) \\ \rho \\ x_{\mathrm{nucl}} \end{pmatrix} = \begin{pmatrix} \beta_\lambda J_1\left(-\mathrm{i}\lambda^{\frac{1}{2}} r\right) + \gamma_\lambda Y_1\left(-\mathrm{i}\lambda^{\frac{1}{2}} r\right) \\ \hat{\rho}_\lambda \\ \hat{x}_{\mathrm{nucl},\lambda} \end{pmatrix}, \tag{7.18}$$

where $r \in (R_{\mathrm{nucl}}, R_0)$, J_1 and Y_1 denote respectively the Bessel function of the first kind of order 1 and that of the second kind of order 1 and $(\beta_\lambda, \gamma_\lambda, \hat{\rho}_\lambda, \hat{x}_{\mathrm{nucl},\lambda}) \in \mathbb{C}^4$ solution of:

$$\begin{aligned} &-\mathrm{i}\lambda^{\frac{1}{2}}\left(\beta_\lambda J_1'\left(-\mathrm{i}\lambda^{\frac{1}{2}} R_0\right) + \gamma_\lambda Y_1'\left(-\mathrm{i}\lambda^{\frac{1}{2}} R_0\right)\right) \\ &\qquad = \frac{a\chi_c c^0 f_{\mathrm{act}}'\left(c^0\right)}{R_0}\left(\beta_\lambda J_1\left(-\mathrm{i}\lambda^{\frac{1}{2}} R_0\right) + \gamma_\lambda Y_1\left(-\mathrm{i}\lambda^{\frac{1}{2}} R_0\right)\right), \end{aligned} \tag{7.19}$$

$$\begin{aligned} &-\mathrm{i}\lambda^{\frac{1}{2}}\left(\beta_\lambda J_1'\left(-\mathrm{i}\lambda^{\frac{1}{2}} R_{\mathrm{nucl}}\right) + \gamma_\lambda Y_1'\left(-\mathrm{i}\lambda^{\frac{1}{2}} R_{\mathrm{nucl}}\right)\right) \\ &\qquad = \frac{a\chi_c c^0 f_{\mathrm{act}}'\left(c^0\right)}{R_0}\left(\beta_\lambda J_1\left(-\mathrm{i}\lambda^{\frac{1}{2}} R_0\right) + \gamma_\lambda Y_1\left(-\mathrm{i}\lambda^{\frac{1}{2}} R_0\right)\right) \\ &\qquad\qquad - ac^0 \frac{\delta\left(R_0^2 - R_{\mathrm{nucl}}^2\right)\pi\left(R_0(1-\beta) - R_{\mathrm{nucl}}\right)}{2R_0\left(R_0 - R_{\mathrm{nucl}}\right)^{\beta+1}}\left(\hat{x}_{\mathrm{nucl},\lambda} - \hat{\rho}_\lambda\right) \end{aligned} \tag{7.20}$$

and

$$\lambda\left(\hat{x}_{\mathrm{nucl},\lambda} - \hat{\rho}_\lambda\right) = K\left(\hat{x}_{\mathrm{nucl},\lambda} - \hat{\rho}_\lambda\right), \tag{7.21}$$

where K is defined by eq. (7.16).

Proof. From the first line and the last line of eq. (P_1), we deduce that:

$$\rho = \hat{\rho}_\lambda \in \mathbb{C} \quad \text{and} \quad x_{\mathrm{nucl}} = \hat{x}_{\mathrm{nucl},\lambda} \in \mathbb{C}$$

satisfy

$$\lambda\left(x_{\mathrm{nucl},\lambda} - \rho_\lambda\right) = K\left(x_{\mathrm{nucl},\lambda} - \rho_\lambda\right).$$

From the definition of the Bessel functions, there exists β_λ and $\gamma_\lambda \in \mathbb{C}$ such that the solutions c of eq. (P_1) are given, for all $r \in (R_{\mathrm{nucl}}, R_0)$, by:

$$c(r) = \beta_\lambda J_1\left(-\mathrm{i}\lambda^{\frac{1}{2}} r\right) + \gamma_\lambda Y_1\left(-\mathrm{i}\lambda^{\frac{1}{2}} r\right).$$

Since

$$\partial_r c(r) = -\mathrm{i}\lambda^{\frac{1}{2}}\left(\beta_\lambda J_1'\left(-\mathrm{i}\lambda^{\frac{1}{2}} r\right) + \gamma_\lambda Y_1'\left(-\mathrm{i}\lambda^{\frac{1}{2}} r\right)\right),$$

the boundary conditions read eq. (7.19) and eq. (7.20). □

Lemma 7.2.7. *Let $\lambda \in \mathbb{C}$ be an eigenvalue of eq. (P_1). Then either*

$$\lambda = K$$

or λ is such that $G_1(\lambda) = 0$ with G_1 defined for all $z \in \mathbb{C}$ by:

$$\begin{aligned} G_1(z) = z &\left(J_1'\left(-\mathrm{i}z^{\frac{1}{2}}R_0\right)Y_1'\left(-\mathrm{i}z^{\frac{1}{2}}R_{\mathrm{nucl}}\right) - J_1'\left(-\mathrm{i}z^{\frac{1}{2}}R_{\mathrm{nucl}}\right)Y_1'\left(-\mathrm{i}z^{\frac{1}{2}}R_0\right)\right) \\ &+ \frac{\mathrm{i}z^{\frac{1}{2}}a\chi_c c^0 f'_{\mathrm{act}}(c^0)}{R_0}\left[J_1\left(-\mathrm{i}z^{\frac{1}{2}}R_0\right)Y_1'\left(-\mathrm{i}z^{\frac{1}{2}}R_0\right) - J_1'\left(-\mathrm{i}z^{\frac{1}{2}}R_0\right)Y_1\left(-\mathrm{i}z^{\frac{1}{2}}R_0\right)\right. \\ &\left. + J_1'\left(-\mathrm{i}z^{\frac{1}{2}}R_{\mathrm{nucl}}\right)Y_1\left(-\mathrm{i}z^{\frac{1}{2}}R_0\right) - J_1\left(-\mathrm{i}z^{\frac{1}{2}}R_0\right)Y_1'\left(-\mathrm{i}z^{\frac{1}{2}}R_{\mathrm{nucl}}\right)\right]. \end{aligned}$$

Proof. Let $\lambda \in \mathbb{C}$ be an eigenvalue of eq. (P_1). Then by lemma 7.2.6, λ is associate with an eigenfunction $(c, \rho, x_{\mathrm{nucl}})$ of the form (7.18). In particular it satisfies eq. (7.21). Then either we have

$$x_{\mathrm{nucl}} - \rho \neq 0 \quad \text{and} \quad \lambda = K,$$

or

$$x_{\mathrm{nucl}} - \rho = 0 \quad \text{and } \lambda \neq 0$$

with λ such that

$$\begin{aligned} &-\mathrm{i}\lambda^{\frac{1}{2}}\left(\beta_\lambda J_1'\left(-\mathrm{i}\lambda^{\frac{1}{2}}R_0\right) + \gamma_\lambda Y_1'\left(-\mathrm{i}\lambda^{\frac{1}{2}}R_0\right)\right) \\ &\qquad = \frac{a\chi_c c^0 f'_{\mathrm{act}}(c^0)}{R_0}\left(\beta_\lambda J_1\left(-\mathrm{i}\lambda^{\frac{1}{2}}R_0\right) + \gamma_\lambda Y_1\left(-\mathrm{i}\lambda^{\frac{1}{2}}R_0\right)\right), \end{aligned}$$

$$\begin{aligned} &-\mathrm{i}\lambda^{\frac{1}{2}}\left(\beta_\lambda J_1'\left(-\mathrm{i}\lambda^{\frac{1}{2}}R_{\mathrm{nucl}}\right) + \gamma_\lambda Y_1'\left(-\mathrm{i}\lambda^{\frac{1}{2}}R_{\mathrm{nucl}}\right)\right) \\ &\qquad = \frac{a\chi_c c^0 f'_{\mathrm{act}}(c^0)}{R_0}\left(\beta_\lambda J_1\left(-\mathrm{i}\lambda^{\frac{1}{2}}R_0\right) + \gamma_\lambda Y_1\left(-\mathrm{i}\lambda^{\frac{1}{2}}R_0\right)\right). \end{aligned}$$

Combining these two conditions leads to the condition $G_1(\lambda) = 0$. □

Lemma 7.2.8. *If $\chi_c > \chi_c^*$, then the eigenvalue problem defined by eq. (P_1) admits an eigenvalue with a positive real part.*

Proof. Let $\lambda \in \mathbb{C}$ be an eigenvalue of the problem defined by eq. (P_1). From lemma 7.2.7, we have that either $\lambda = K$ or λ is such that $G_1(\lambda) = 0$. Since $K < 0$ and we are looking to exhibit an eigenvalue with a positive real part, we assume $\lambda \neq K$ and thus λ such that $G_1(\lambda) = 0$. We perform the expansion of G_1 around 0. Using the properties of the Bessel functions, for λ close to zero, we have:

$$\begin{aligned} J_1\left(-\mathrm{i}\lambda^{\frac{1}{2}}R_0\right) &= \frac{-\mathrm{i}\lambda^{\frac{1}{2}}R_0}{2} + o(\lambda), \\ J_1'\left(-\mathrm{i}\lambda^{\frac{1}{2}}R_0\right) &= \frac{1}{2} + \frac{3R_0^2\lambda}{16} + o(\lambda), \\ Y_1\left(-\mathrm{i}\lambda^{\frac{1}{2}}R_0\right) &= \frac{-2\mathrm{i}}{\pi\lambda^{\frac{1}{2}}R_0} + \frac{\mathrm{i}(1-2\gamma)\lambda^{\frac{1}{2}}R_0}{2\pi} + \frac{2}{\pi}J_1\left(-\mathrm{i}\lambda^{\frac{1}{2}}R_0\right)\log\left(\frac{-\mathrm{i}\lambda^{\frac{1}{2}}R_0}{2}\right) + o(\lambda), \\ Y_1'\left(-\mathrm{i}\lambda^{\frac{1}{2}}R_0\right) &= \frac{-2}{\lambda R_0^2\pi} + \frac{1+2\gamma}{2\pi} - \frac{\lambda R_0^2(11-12\gamma)}{32\pi} + \frac{2}{\pi}J_1'\left(-\mathrm{i}\lambda^{\frac{1}{2}}R_0\right)\log\left(\frac{-\mathrm{i}\lambda^{\frac{1}{2}}R_0}{2}\right) + o(\lambda), \end{aligned}$$

where γ denotes the Euler's constant. Thus for λ close to zero, we have:

$$\begin{aligned} G_1(\lambda) &= \left(1 - a\chi_c c^0 f'_{\text{act}}\left(c^0\right)\right)\left(\frac{1}{R_0^2\pi} - \frac{1}{R_{\text{nucl}}^2\pi}\right) \\ &\quad + \frac{3\left(R_{\text{nucl}}^4 - R_0^4\right)}{8\pi R_0^2 R_{\text{nucl}}^2}\lambda - a\chi_c c^0 f'_{\text{act}}\left(c^0\right)\frac{3\left(R_0^2 - R_{\text{nucl}}^2\right)}{8\pi R_0^2}\lambda \\ &\quad + \frac{a\chi_c c^0 f'_{\text{act}}\left(c^0\right) - 1}{2\pi}\ln\left(\frac{R_0}{R_{\text{nucl}}}\right)\lambda + o(\lambda), \\ &= g(\lambda) + o(\lambda). \end{aligned}$$

The function g admits $\lambda_1 \in \mathbb{R}$ as root with λ_1 defined by:

$$\lambda_1 = -\frac{\left(1 - a\chi_c c^0 f'_{\text{act}}\left(c^0\right)\right)\left(\frac{1}{R_0^2\pi} - \frac{1}{R_{\text{nucl}}^2\pi}\right)}{\frac{3\left(R_{\text{nucl}}^4 - R_0^4\right)}{8\pi R_0^2 R_{\text{nucl}}^2} - a\chi_c c^0 f'_{\text{act}}\left(c^0\right)\frac{3\left(R_0^2 - R_{\text{nucl}}^2\right)}{8\pi R_0^2} + \frac{a\chi_c c^0 f'_{\text{act}}\left(c^0\right) - 1}{2\pi}\ln\left(\frac{R_0}{R_{\text{nucl}}}\right)}.$$

With the definition of χ_c^* given by eq. (7.11), we have:

$$\left(1 - a\chi_c c^0 f'_{\text{act}}\left(c^0\right)\right)\left(\frac{1}{R_0^2\pi} - \frac{1}{R_{\text{nucl}}^2\pi}\right) > 0 \iff \chi_c > \chi_c^*.$$

We also have:

$$\begin{aligned} &\frac{3\left(R_{\text{nucl}}^4 - R_0^4\right)}{8\pi R_0^2 R_{\text{nucl}}^2} - a\chi_c c^0 f'_{\text{act}}\left(c^0\right)\frac{3\left(R_0^2 - R_{\text{nucl}}^2\right)}{8\pi R_0^2} + \frac{a\chi_c c^0 f'_{\text{act}}\left(c^0\right) - 1}{2\pi}\ln\left(\frac{R_0}{R_{\text{nucl}}}\right) < 0 \\ \iff &\left[a\chi_c c^0 f'_{\text{act}}\left(c^0\right) < \frac{3\left(R_0^4 - R_{\text{nucl}}^4\right) + 4R_0^2 R_{\text{nucl}}^2 \ln\left(\frac{R_0}{R_{\text{nucl}}}\right)}{R_{\text{nucl}}^2\left(3\left(R_{\text{nucl}}^2 - R_0^2\right) + 4R_0^2\ln\left(\frac{R_0}{R_{\text{nucl}}}\right)\right)}\right. \\ &\qquad \left.\text{and } 3\left(R_{\text{nucl}}^2 - R_0^2\right) + 4R_0^2\ln\left(\frac{R_0}{R_{\text{nucl}}}\right) > 0\right] \text{ or } 3\left(R_{\text{nucl}}^2 - R_0^2\right) + 4R_0^2\ln\left(\frac{R_0}{R_{\text{nucl}}}\right) < 0. \end{aligned}$$

Moreover, if $3\left(R_{\text{nucl}}^2 - R_0^2\right) + 4R_0^2\ln\left(\frac{R_0}{R_{\text{nucl}}}\right) > 0$, then $\frac{3\left(R_0^4 - R_{\text{nucl}}^4\right) + 4R_0^2 R_{\text{nucl}}^2\ln\left(\frac{R_0}{R_{\text{nucl}}}\right)}{R_{\text{nucl}}^2\left(3\left(R_{\text{nucl}}^2 - R_0^2\right) + 4R_0^2\ln\left(\frac{R_0}{R_{\text{nucl}}}\right)\right)} > 1$. Thus λ_1 changes sign from negative to positive as χ_c exceeds χ_c^*. We can note that when χ_c close to χ_c^* then λ_1 approximates well a root of G_1 and that we have:

$$\lambda_1 = \left(a\chi_c c^0 f'_{\text{act}}\left(c^0\right) - 1\right)\frac{8\left(R_0^2 - R_{\text{nucl}}^2\right)}{3a\chi_c c^0 f'_{\text{act}}\left(c^0\right)\left(R_0^4 + R_0^2 R_{\text{nucl}}^2 - 2R_{\text{nucl}}^4\right)} + o\left(\left|a\chi_c c^0 f'_{\text{act}}\left(c^0\right) - 1\right|\right).$$

This eigenvalue is associated with the non-trivial eigenfunction:

$$\begin{pmatrix} c(r) \\ \rho \\ x_{\text{nucl}} \end{pmatrix} = \begin{pmatrix} \beta_{\lambda_1} J_1\left(-\mathrm{i}\lambda_1^{\frac{1}{2}} r\right) + \gamma_{\lambda_1} Y_1\left(-\mathrm{i}\lambda_1^{\frac{1}{2}} r\right) \\ 0 \\ 0 \end{pmatrix},$$

with

$$\begin{aligned} \beta_{\lambda_1} &= \left(\mathrm{i}\lambda_1^{\frac{1}{2}} Y_1'\left(-\mathrm{i}\lambda_1^{\frac{1}{2}} R_0\right) + \frac{a\chi_c c^0 f'_{\text{act}}\left(c^0\right)}{R_0} Y_1\left(-\mathrm{i}\lambda_1^{\frac{1}{2}} R_0\right)\right), \\ \gamma_{\lambda_1} &= -\left(\mathrm{i}\lambda_1^{\frac{1}{2}} J_1'\left(-\mathrm{i}\lambda_1^{\frac{1}{2}} R_0\right) + \frac{a\chi_c c^0 f'_{\text{act}}\left(c^0\right)}{R_0} J_1\left(-\mathrm{i}\lambda_1^{\frac{1}{2}} R_0\right)\right). \end{aligned}$$

□

To conclude the proof of the theorem, we need to show that when $\chi_c < \chi_c^*$ all the eigenvalues associated to (P_1) have negative real part. We give only a graphical illustration here. For several values of R_0, R_{nucl} and $\frac{\chi_c}{\chi_c^*}$, we represent the function G_1 by representing its real part, its imaginary part and its modulus (see fig. 7.1 for an example). We then observe that the root of G_1 with the largest real part seems to be a real root of G_1, which is confirmed by studying the imaginary part of G_1. Indeed, we notice that if $\lambda \in \mathbb{R}$ then $G_1(\lambda) \in \mathbb{R}$.

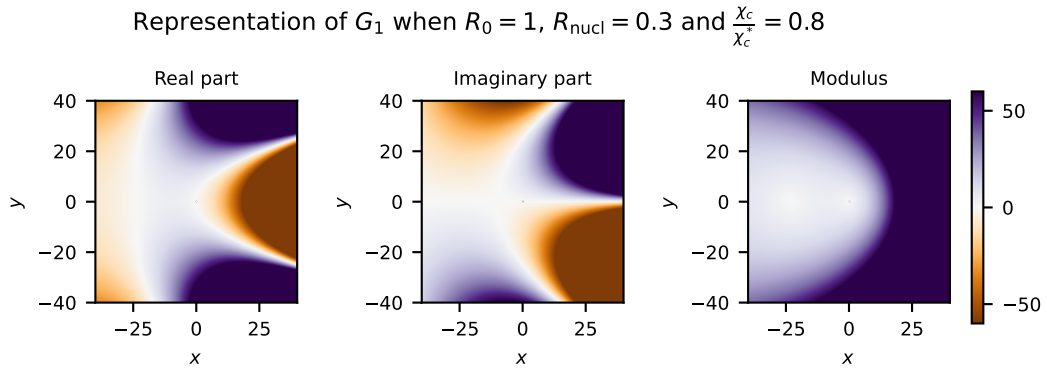

Figure 7.1: **Representation of G_1 in the complex framework for $R_0 = 1$, $R_{\text{nucl}} = 0.3$ and $\frac{\chi_c}{\chi_c^*} = 0.8$.** *Plots of the real part (left), the imaginary part (middle) and the modulus (right) of the function G_1 for $\lambda = x + \mathrm{i}y \in \mathbb{C}$ with $x, y \in [-40, 40]$. We observe that the root of G_1 with the greatest real part is a real root.*

We can therefore restrict the graphical study of G_1 to the graphical study of G_1 when $\lambda \in \mathbb{R}$. For R_0 and R_{nucl} fixed and for different values of $\frac{\chi_c}{\chi_c^*}$, we plot G_1 as a function of $\lambda \in \mathbb{R}$ (see fig. 7.2). This allows us to observe the largest real root of G_1 and we notice that when $\chi_c < \chi_c^*$ then this one is negative.

Remark 7.2.9. *If for the forces $\mathbf{f}_{\text{BN}}$ and f_{NB} we choose expressions eqs. (7.4) and (7.5), the result of the theorem 7.2.4 is still valid. Indeed, the proof is the same with $-k = \dfrac{\delta\pi R_0 (R_0(1-\beta) - R_{\text{nucl}})}{(R_0 - R_{\text{nucl}})^{\beta+1}}$. It suffices to note that the centre of mass of the perturbed domain is given for all $t \geq 0$ by:*

$$\tilde{\mathbf{x}}_{\text{cm}}(t) = \frac{1}{\pi} \int_{-\pi}^{\pi} \rho(t, \theta) \begin{pmatrix} \cos\theta \\ \sin\theta \end{pmatrix} \mathrm{d}\theta.$$

Using the Fourier decomposition of ρ, we then have:

$$\tilde{\mathbf{x}}_{\text{cm}}(t) = \begin{pmatrix} \rho_{c1}(t) \\ \rho_{s1}(t) \end{pmatrix}.$$

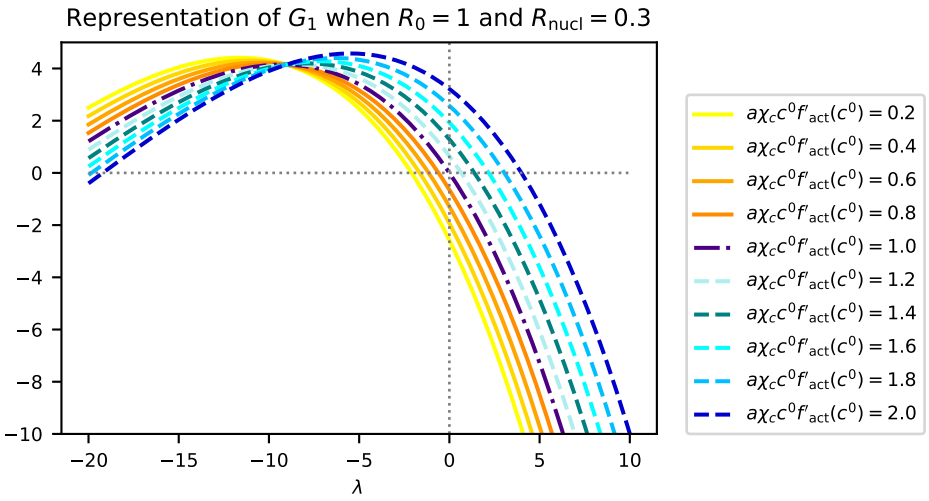

Figure 7.2: **Graphs of $\lambda \mapsto G_1(\lambda)$ for $\lambda \in \mathbb{R}$ when $R_0 = 1$ and $R_{\text{nucl}} = 0.3$ for different values of $\frac{\chi_c}{\chi_c^*} = a\chi_c c^0 f'\left(c^0\right)$.** *Each curve corresponds to a different value of χ_c. The solid yellow-orange curves correspond to the case where $\chi_c < \chi_c^*$, the dashed blue curves correspond to the case where $\chi_c > \chi_c^*$ and the dark dashdotted curve corresponds to the case where $\chi_c = 1\chi_c^*$. The grey dotted lines are the lines of equation $\lambda = 0$ and $y = 0$. In the case where $\chi_c < \chi_c^*$ we notice that G_1 seems to admit no positive root.*

7.3 . Finite element scheme

In this section, we write a finite element scheme of the model eq. (7.1) in order to be able to run some simulations of our model. This scheme will be implement in FreeFem ++ (Hecht, 2012). First, using a semi-implicit Euler scheme, the prolem eq. (7.1) is discretized in time. The curvature is discretised implicitly (Lavi et al., 2023). Secondly, the discrete problem on the fluid velocity and pressure is decomposed in three problem in order to separate the boundary conditions. Third we write the variational formulation of the discrete problem. Finally, using a Uzawa algorithm (Lefebvre, 2007) or a force the velocities are corrected to avoid potential contacts between the nucleus and the cell boundary.

7.3.1 . Time discretization

We discretize in time our model eq. (7.1). Let Δt be the time step. For $i \in \{0, \ldots, N_f\}$ with $N_f \in \mathbb{N}$, we denote $t^i = i\Delta t$, $\mathbf{u}^i = \mathbf{u}\left(t^i, \cdot\right)$, $P^i = P\left(t^i, \cdot\right)$ and $c^i = c\left(t^i, \cdot\right)$. We also denote $\Omega^i = \Omega\left(t^i\right)$ and $N^i = N\left(t^i\right)$, f^i_{NB} and $\mathbf{f}^i_{\text{BN}}$ the discrete forces between the nucleus and the cell boundary. We will use an implicit treatment of the curvature (Lavi, 2019). Let $\tilde{H}^{i+1}$ be an approximation of the vector curvature of $\partial\Omega^{i+1}$ expressed back in $\partial\Omega^i$.

The implicit-curvature discretization of eq. (7.1) is given by:

$$\begin{cases} \mathbf{u}^{i+1} + \nabla P^{i+1} = 0 & \text{in } \Omega^i \backslash N^i, \quad (7.22a) \\ \operatorname{div}\left(\mathbf{u}^{i+1}\right) = 0 & \text{in } \Omega^i \backslash N^i, \quad (7.22b) \\ P^{i+1}\mathbf{n} = \gamma \tilde{H}^{i+1} + \chi_c f_{\text{act}}\left(c^i\right)\mathbf{n} - f^i_{\text{NB}}\,\mathbf{n} & \text{on } \partial\Omega^i, \quad (7.22c) \\ \mathbf{u}^{i+1}\cdot\mathbf{n} = \mathbf{u}^{i+1}_{\text{nucl}}\cdot\mathbf{n} & \text{on } \partial N^i, \quad (7.22d) \\ \mathbf{u}^{i+1}_{\text{nucl}} = \dfrac{1}{\xi_{\text{nucl}}\,|N^i|}\left(\displaystyle\int_{\partial N^i} P^{i+1}\mathbf{n}\,\mathrm{d}\sigma + \mathbf{f}^i_{\text{BN}}\right), & \quad (7.22e) \end{cases}$$

and

$$\begin{cases} \dfrac{c^{i+1}-c^i}{\Delta t} = \operatorname{div}\left(\nabla c^{i+1} - (1-a)\,\mathbf{u}^{i+1}c^{i+1}\right) & \text{in } \Omega^i \backslash N^i, \quad (7.23a) \\ \left(\nabla c^{i+1} + a\mathbf{u}^{i+1}c^{i+1}\right)\cdot\mathbf{n} = 0 & \text{on } \partial\Omega^i \cup \partial N^i, \quad (7.23b) \end{cases}$$

with

$$\begin{cases} \Omega^{i+1} = \left(\mathrm{Id} + \Delta t\,\mathbf{u}^{i+1}\right)\left(\Omega^i\right), & (7.24a) \\ N^{i+1} = \left(\mathrm{Id} + \Delta t\,\mathbf{u}^{i+1}\right)\left(N^i\right). & (7.24b) \end{cases}$$

Let $\varphi^{i+1} = \mathrm{Id} + \Delta t\,\mathbf{u}^{i+1}$. We denote $\mathbf{t}^i$ and $\mathbf{t}^{i+1}$ the tangent vectors of respectively $\partial\Omega^i$ and $\partial\Omega^{i+1}$. Let $\mathbf{T}^{i+1}$ be the tangent vector of $\partial\Omega^{i+1}$ pulled back on $\partial\Omega^i$. We have:

$$\mathbf{T}^{i+1} = \mathbf{t}^{i+1}\circ\varphi^{i+1} = \frac{\left(I + \Delta t \nabla \mathbf{u}^{i+1}\right)\mathbf{t}^i}{\left|\left(I + \Delta t \nabla \mathbf{u}^{i+1}\right)\mathbf{t}^i\right|}. \quad (7.25)$$

Let $\mathbf{N}^{i+1}$ be the normal vector of $\partial\Omega^{i+1}$ pulled back on $\partial\Omega^i$ then we have $\mathbf{N}^{i+1} = \left(\mathbf{T}^{i+1}\right)^{\perp}$ and we have (Lavi et al., 2023):

$$\tilde{H}^{i+1} = -\left(\mathbf{t}^i\cdot\nabla\right)\mathbf{T}^{i+1}. \quad (7.26)$$

Note that the discretization chosen separates the resolution of the fluid velocity and pressure at the current time from the marker concentration at the current time.

7.3.2 . Decomposition of the fluid problem

We focus on the fluid velocity and pressure problem defined by eq. (7.22). We decompose it in three independent problems to separate the boundary conditions on $\partial\Omega^i$ and ∂N^i. We define as follows the three problems:

$$\begin{cases} \mathbf{u}_1 + \nabla P_1 = 0 & \text{in } \Omega^i \backslash N^i, \quad (7.27a) \\ \operatorname{div}\left(\mathbf{u}_1\right) = 0 & \text{in } \Omega^i \backslash N^i, \quad (7.27b) \\ P_1\mathbf{n} = \gamma \tilde{H}^{i+1} + \chi_c f_{\text{act}}\left(c^i\right) - f^i_{\text{NB}} & \text{on } \partial\Omega^i, \quad (7.27c) \\ \mathbf{u}_1 = 0 & \text{on } \partial N^i, \quad (7.27d) \end{cases}$$

$$\begin{cases} -\Delta P_2 = 0 & \text{in } \Omega^i \backslash N^i, \quad (7.28a) \\ P_2 = 0 & \text{on } \partial\Omega^i, \quad (7.28b) \\ \nabla P_2 = \mathbf{e_x} & \text{on } \partial N^i, \quad (7.28c) \end{cases}$$

$$\begin{cases} -\Delta P_3 = 0 & \text{in } \Omega^i \backslash N^i, \quad (7.29a) \\ P_3 = 0 & \text{on } \partial\Omega^i, \quad (7.29b) \\ \nabla P_3 = \mathbf{e_y} & \text{on } \partial N^i, \quad (7.29c) \end{cases}$$

where $\mathbf{e_x} = (1,0)$ and $\mathbf{e_y} = (0,1)$. We set $\mathbf{u}_2 = -\nabla P_2$ and $\mathbf{u}_3 = -\nabla P_3$.

Lemma 7.3.1. *If $(\mathbf{u}_1, P_1)$, P_2 and P_3 are respectively solutions of eqs. (7.27) to (7.29) then there exists $(\mu_1, \mu_2, \mu_3) \in \mathbb{R}^3$ such that $P = \mu_1 P_1 + \mu_2 P_2 + \mu_3 P_3$ and $\mathbf{u} = \mu_1 \mathbf{u}_1 + \mu_2 \mathbf{u}_2 + \mu_3 \mathbf{u}_3$ are solution of eq. (7.22).*

Proof. Let $P_j^x = \int_{\partial N^i} P_j n_x \, \mathrm{d}\sigma$ and $P_j^y = \int_{\partial N^i} P_j n_y \, \mathrm{d}\sigma$ for $j \in \{1,2,3\}$. Finding μ_1, μ_2 ans μ_3 satisfying the lemma is equivalent to solve a linear problem. A solution is given by:

$$\begin{cases} \mu_1 = 1, & (7.30a) \\ \mu_2 = \dfrac{\xi_{\text{nucl}} \left|N^i\right| (P_1^x + f_{\text{BN}}^x) + ((P_1^x + f_{\text{BN}}^x) P_3^y - P_3^x (P_1^y + f_{\text{BN}}^y))}{-\xi_{\text{nucl}}^2 \left|N^i\right|^2 - \xi_{\text{nucl}} \left|N^i\right| (P_2^x + P_3^y) + (P_3^x P_2^y - P_2^x P_3^y)}, & (7.30b) \\ \mu_3 = \dfrac{\xi_{\text{nucl}} \left|N^i\right| (P_1^y + f_{\text{BN}}^y) + (P_2^x (P_1^y + f_{\text{BN}}^y) - (P_1^x + f_{\text{BN}}^x) P_2^y)}{-\xi_{\text{nucl}}^2 \left|N^i\right|^2 - \xi_{\text{nucl}} \left|N^i\right| (P_2^x + P_3^y) + (P_3^x P_2^y - P_2^x P_3^y)}. & (7.30c) \end{cases}$$

□

7.3.3 . Spatial discretization

We discretize in space our time-discrete model eqs. (7.22) to (7.24). We use a finite element discretization. Let $\mathcal{T}$ be a triangulation of $\Omega^i \backslash N^i$. For all triangle $K \in \mathcal{T}$ we note $\left(\lambda_1^K, \lambda_2^K, \lambda_3^K\right)$ the barycentric coordinate functions of K. First we define the functional spaces needed. Let $\mathbb{P}_k$ be the set of polynomials of $\mathbb{R}^2$ of degrees less or equal k. Let $\mathcal{H}_{\mathbf{u}}$ be the functional space define by:

$$\mathcal{H}_{\mathbf{u}} = \left\{ v \in H^1\left(\Omega^i \backslash N^i\right) \mid \forall K \in \mathcal{T}, v_{|K} \in \mathbb{P}_1 \oplus \text{Span}\left\{\lambda_1^K, \lambda_2^K, \lambda_3^K\right\} \right\}$$

and let $\mathcal{H}_{\mathbf{u},0}$ be the functional space define by:

$$\mathcal{H}_{\mathbf{u},0} = \left\{ v \in \mathcal{H}_{\mathbf{u}} \middle| \, v = 0 \text{ on } \partial N^i \text{ a.e.} \right\}.$$

Let $\mathcal{H}_P$ be the functional space define by:

$$\mathcal{H}_P = \left\{ Q \in H^1\left(\Omega^i \backslash N^i\right) \mid \forall K \in \mathcal{T}, Q_{|K} \in \mathbb{P}_1 \right\}$$

and let $\mathcal{H}_{P,0}$ be the functional space define by:

$$\mathcal{H}_{P,0} = \left\{ Q \in \mathcal{H}_P \middle| \, Q = 0 \text{ on } \partial\Omega^i \text{ a.e.} \right\}.$$

7.3.3.1 . Variational formulation of the fluid problem

Instead of writing the variational formulation of eq. (7.22), we use the decomposition result and write the variational formulation of the three independent problems eq. (7.27)-eq. (7.28)-eq. (7.29).

The variational formulation of eq. (7.27) is given by:

$$\left\{\begin{array}{l}\text{Find } (\mathbf{u}_1, P_1) \in \mathcal{H}^2_{\mathbf{u},0} \times \mathcal{H}_P \text{ such that for all } \mathbf{v} \in \mathcal{H}^2_{\mathbf{u},0} \text{ and } Q \in \mathcal{H}_P, \text{ we have :} \\ \displaystyle\int_{\Omega^i \backslash N^i} \mathbf{u}_1 \cdot \mathbf{v} \, \mathrm{d}\mathbf{x} - \int_{\Omega^i \backslash N^i} P_1 \operatorname{div}(\mathbf{v}) \, \mathrm{d}\mathbf{x} + \int_{\partial\Omega^i} \gamma \tilde{H}^{i+1} \cdot \mathbf{v} \, \mathrm{d}\sigma \\ \qquad + \displaystyle\int_{\partial\Omega^i} \chi_c f_{\text{act}}\left(c^i\right) \mathbf{v} \cdot \mathbf{n} \, \mathrm{d}\sigma - \int_{\partial\Omega^i} f^i_{\text{NB}} \, \mathbf{v} \cdot \mathbf{n} \, \mathrm{d}\sigma = 0, \\ \displaystyle\int_{\Omega^i \backslash N^i} Q \operatorname{div}(\mathbf{u}_1) \, \mathrm{d}\mathbf{x} = 0.\end{array}\right. \tag{7.31}$$

The variational formulation of eq. (7.28) is given by:

$$\left\{\begin{array}{l}\text{Find } P_2 \in \mathcal{H}_{P,0} \text{ such that for all } Q \in \mathcal{H}_{P,0}, \text{ we have:} \\ \displaystyle\int_{\Omega^i \backslash N^i} \nabla P_2 \cdot \nabla Q \, \mathrm{d}\mathbf{x} - \int_{\partial N^i} Q n_x \, \mathrm{d}\sigma = 0.\end{array}\right. \tag{7.32}$$

The variational formulation of eq. (7.29) is given by:

$$\left\{\begin{array}{l}\text{Find } P_3 \in \mathcal{H}_{P,0} \text{ such that for all } Q \in \mathcal{H}_{P,0}, \text{ we have:} \\ \displaystyle\int_{\Omega^i \backslash N^i} \nabla P_3 \cdot \nabla Q \, \mathrm{d}\mathbf{x} - \int_{\partial N^i} Q n_y \, \mathrm{d}\sigma = 0.\end{array}\right. \tag{7.33}$$

7.3.3.2 . Implicit treatment of the curvature

The challenging point to solve the problem defined by eq. (7.31) is to compute $\tilde{H}^{i+1}$. We note $\mathbf{u}^{i+1} = \mathbf{u}_1 + \mu_2 \mathbf{u}_2 + \mu_3 \mathbf{u}_3$ where $\mathbf{u}_1$ is solution of eq. (7.31), $\mathbf{u}_2$ of eq. (7.32), $\mathbf{u}_3$ of eq. (7.33) and μ_2 and μ_3 given by eq. (7.30). Denoting F the perimeter of the domain in the deformed configuration, we have:

$$F\left(\mathbf{u}^{i+1}\right) = \mathcal{P}\left(\varphi^{i+1}(\Omega^i)\right) = \int_{\partial\Omega^i} \left|\left(I + \Delta t \nabla \mathbf{u}^{i+1}\right) \mathbf{t}^i\right| \mathrm{d}\sigma.$$

Assuming $\mathbf{u}_2$ and $\mathbf{u}_3$ given, we see F as a function of $\mathbf{u}_1$. We note it G and we have:

$$G(\mathbf{u}_1) = \int_{\partial\Omega^i} \left|\left(I + \Delta t \nabla\left(\mathbf{u}_1 + \mu_2 \mathbf{u}_2 + \mu_3 \mathbf{u}_3\right)\right) \mathbf{t}^i\right| \mathrm{d}\sigma = F\left(\mathbf{u}^{i+1}\right).$$

Using a Taylor expansion to the order 2, we have that for all $\mathbf{v} \in H^1\left(\Omega^i \backslash B^i\right)^2$:

$$G'(\mathbf{u}_1)(\mathbf{v}) = \Delta t \int_{\partial\Omega^i} \nabla \mathbf{v} \, \mathbf{t}^i \cdot \mathbf{T}^{i+1} \mathrm{d}\sigma = \Delta t \int_{\partial\Omega^i} \tilde{H}^{i+1} \cdot \mathbf{v} \, \mathrm{d}\sigma$$

and we also have that for all $\mathbf{v}, \mathbf{w} \in H^1\left(\Omega^i \backslash B^i\right)^2$:

$$G''(\mathbf{u}_1)(\mathbf{v}, \mathbf{w}) = \Delta t^2 \int_{\partial\Omega^i} \frac{\left(\nabla \mathbf{v} \, \mathbf{t}^i \cdot \mathbf{N}^{i+1}\right) \cdot \left(\nabla \mathbf{w} \, \mathbf{t}^i \cdot \mathbf{N}^{i+1}\right)}{\left|\left(I + \Delta t \nabla\left(\mathbf{u}_1 + \mu_2 \mathbf{u}_2 + \mu_3 \mathbf{u}_3\right)\right) \mathbf{t}^i\right|} \mathrm{d}\sigma.$$

We also remark that:

$$G(\mathbf{u}_1) \leq G(\mathbf{u}_1) + \Delta t \int_{\partial\Omega^i} \nabla \mathbf{v} \, \mathbf{t}^i \cdot \mathbf{T}^{i+1} \, \mathrm{d}\sigma + \frac{\Delta t^2}{2} \int_{\partial\Omega^i} \frac{\left(\nabla \mathbf{v} \, \mathbf{t}^i\right) \cdot \left(\nabla \mathbf{v} \, \mathbf{t}^i\right)}{\left|\left(I + \Delta t \nabla\left(\mathbf{u}_1 + \mu_2 \mathbf{u}_2 + \mu_3 \mathbf{u}_3\right)\right) \mathbf{t}^i\right|} \mathrm{d}\sigma$$

and we denote $\widetilde{G}(\mathbf{u})(\mathbf{v}, \mathbf{w}) = \Delta t^2 \displaystyle\int_{\partial\Omega^i} \frac{\left(\nabla \mathbf{v} \, \mathbf{t}^i\right) \cdot \left(\nabla \mathbf{w} \, \mathbf{t}^i\right)}{\left|\left(I + \Delta t \nabla\left(\mathbf{u} + \mu_2 \mathbf{u}_2 + \mu_3 \mathbf{u}_3\right)\right) \mathbf{t}^i\right|} \mathrm{d}\sigma.$

Thus, we use a Newton like method to approximate the solutions of eq. (7.31). We want to construct a sequence of functions $\left(\mathbf{u}_1^k, P_1^k\right)_k$ such that this sequence converges to $(\mathbf{u}_1, P_1)$. This sequence of functions is constructed as follows:

1. Let $\mathbf{u}_1^0 = 0$ and $P_1^0 = 0$.
2. While $\left|\mathbf{u}_1^{k+1} - \mathbf{u}_1^k\right| > \eta$ with $\eta > 0$ a small threshold, do:
   (a) Compute μ_2 and μ_3 associate to P_1^k, P_2 and P_3 using the expression of eq. (7.30).
   (b) Solve the following variational problem:

$$\begin{cases} \text{Find } (\mathbf{u}_1^{k+1}, P_1^{k+1}) \in \mathcal{H}^2_{\mathbf{u},0} \times \mathcal{H}_P \text{ s.t. for all } \mathbf{v} \in \mathcal{H}^2_{\mathbf{u},0} \text{ and } Q \in \mathcal{H}_P : \\ \displaystyle\int_{\Omega^i \backslash N^i} \mathbf{u}_1^{k+1} \cdot \mathbf{v} \, \mathrm{d}\mathbf{x} - \int_{\Omega^i \backslash N^i} P_1^{k+1} \operatorname{div}(\mathbf{v}) \, \mathrm{d}\mathbf{x} + \int_{\Omega^i \backslash N^i} Q \operatorname{div}\left(\mathbf{u}_1^{k+1}\right) \mathrm{d}\mathbf{x} \\ \qquad + \dfrac{\gamma}{\Delta t} G'\left(\mathbf{u}_1^k\right)(\mathbf{v}) + \dfrac{\gamma}{\Delta t} \widetilde{G}\left(\mathbf{u}_1^k\right)\left(\mathbf{u}_1^{k+1} - \mathbf{u}_1^k, \mathbf{v}\right) \\ \qquad + \displaystyle\int_{\partial\Omega^i} \chi_c f_{\mathrm{act}}\left(c^i\right) \mathbf{v} \cdot \mathbf{n} \, \mathrm{d}\sigma - \int_{\partial\Omega^i} f^i_{\mathrm{NB}} \mathbf{v} \cdot \mathbf{n} \, \mathrm{d}\sigma = 0. \end{cases} \tag{7.34}$$

3. Set $(\mathbf{u}_1, P_1) = \left(\mathbf{u}_1^{k+1}, P_1^{k+1}\right)$.

We assume our method to converge.

We can remark that in a certain sense the variational problem defined by eq. (7.31) is equivalent to the following minimization problem:

$$J(\mathbf{u}_1) = \min_{\mathbf{v} \in V(\Omega^i \backslash N^i)} J(\mathbf{v})$$

where

$$J(\mathbf{v}) = \frac{1}{2} \int_{\Omega^i \backslash N^i} |\mathbf{v}|^2 \, \mathrm{d}\mathbf{x} + \frac{\gamma}{\Delta t} G(\mathbf{v}) + \chi_c \int_{\partial\Omega^i} f_{\mathrm{act}}\left(c^i\right) \mathbf{v} \cdot \mathbf{n} \, \mathrm{d}\sigma - \int_{\partial\Omega^i} f^i_{\mathrm{NB}} \mathbf{v} \cdot \mathbf{n} \, \mathrm{d}\sigma$$

and

$$V\left(\Omega^i \backslash N^i\right) = \left\{ \mathbf{v} \in H^1\left(\Omega^i \backslash N^i\right)^2 \text{ such that } \operatorname{div}(\mathbf{v}) = 0 \text{ and } \nabla \times \mathbf{u} = 0 \text{ in } \Omega^i \backslash N^i \text{ a.e.} \right\}.$$

7.3.3.3 . Discretization of the concentration problem

At each step of the numerical simulations, the mesh is propagating with the velocity $\mathbf{u}_{\mathrm{mesh}}$ which satisfies:

$$\begin{cases} \Delta \mathbf{u}_{\mathrm{mesh}} = 0 & \text{in } \Omega^i \backslash N^i, \quad (7.35a) \\ \mathbf{u}_{\mathrm{mesh}} = \mathbf{u}^{i+1} & \text{on } \partial\Omega^i, \quad (7.35b) \\ \mathbf{u}_{\mathrm{mesh}} = \mathbf{u}^{i+1}_{\mathrm{nucl}} & \text{on } \partial N^i. \quad (7.35c) \end{cases}$$

Thus the mesh propagation induces advection at velocity $\mathbf{u}_{\mathrm{mesh}}$ of the markers concentration. Taking it into account leads to modify the discrete concentration problem eq. (7.23) as follows:

$$\begin{cases} \dfrac{c^{i+1} - c^i}{\Delta t} + (1-a)\, \mathbf{u}^{i+1} \cdot \nabla c^{i+1} - \mathbf{u}_{\mathrm{mesh}} \cdot \nabla c^{i+1} - \Delta c^{i+1} = 0 & \text{in } \Omega^i \backslash N^i, \quad (7.36a) \\ \left(\nabla c^{i+1} + a c^{i+1} \mathbf{u}^{i+1}\right) \cdot \mathbf{n} = 0 & \text{on } \partial\Omega^i \cup \partial N^i. \quad (7.36b) \end{cases}$$

The variational formulation of eq. (7.36) is given by:

$$\begin{cases} \text{Find } c^{i+1} \in \mathcal{H}_c \text{ such that for all } \psi \in \mathcal{H}_c, \text{ we have:} \\ \displaystyle\int_{\Omega^i \backslash N^i} \left(\frac{c^{i+1} - c^i}{\Delta t} \right) \psi \, \mathrm{d}\mathbf{x} + \int_{\Omega^i \backslash N^i} \operatorname{div}(\mathbf{u}_{\mathrm{mesh}})\, c^{i+1} \psi \, \mathrm{d}\mathbf{x} \\ \qquad - \displaystyle\int_{\Omega^i \backslash N^i} \left((1-a)\, \mathbf{u}^{i+1} c^{i+1} - \mathbf{u}_{\mathrm{mesh}} c^{i+1} - \nabla c^{i+1} \right) \cdot \nabla \psi \, \mathrm{d}\mathbf{x} = 0, \end{cases} \tag{7.37}$$

where $\mathcal{H}_c = \left\{ \psi \in H^1\left(\Omega^i \backslash N^i\right) \mid \forall K \in \mathcal{T}, \psi|_K \in \mathbb{P}_1 \oplus \operatorname{Span}\left\{\lambda_1^K, \lambda_2^K, \lambda_3^K\right\} \right\}$.

7.3.3.4 . Numerical scheme without taking care of the potential contacts between cell boundary and nucleus

The numerical scheme to solve the problem eq. (7.1) without taking care of the potential contacts between cell boundary and nucleus is given by the following algorithm:

Algorithm 7.1 : Time iteration of the numerical scheme obtained after time discretization and space discretization with a finite element method and an implicit curvature treatment.

1. Compute $\mathbf{u}^{i+1}$ and P^{i+1} using c^i and the decomposition method:

   (a) Solve the following variational formulation to compute P_2 and deduce from it $\mathbf{u}_2 = -\nabla P_2$:

$$\left\{ \begin{array}{l} \text{Find } P_2 \in \mathcal{H}_{P,0} \text{ such that for all } Q \in \mathcal{H}_{P,0}, \text{ we have:} \\ \displaystyle\int_{\Omega^i \setminus N^i} \nabla P_2 \cdot \nabla Q \, \mathrm{d}\mathbf{x} - \int_{\partial N^i} Q n_x \, \mathrm{d}\sigma = 0. \end{array} \right.$$

   (b) Solve the following variational formulation to compute P_3 and deduce from it $\mathbf{u}_3 = -\nabla P_3$:

$$\left\{ \begin{array}{l} \text{Find } P_3 \in \mathcal{H}_{P,0} \text{ such that for all } Q \in \mathcal{H}_{P,0}, \text{ we have:} \\ \displaystyle\int_{\Omega^i \setminus N^i} \nabla P_3 \cdot \nabla Q \, \mathrm{d}\mathbf{x} - \int_{\partial N^i} Q n_y \, \mathrm{d}\sigma = 0. \end{array} \right.$$

   (c) Using the Newton like method, compute $\mathbf{u}_1$ and P_1.

      i. Set $\mathbf{u}_1^0 = 0$ and $P_1^0 = 0$.

      ii. While $\left|\mathbf{u}_1^{k+1} - \mathbf{u}_1^k\right| > \eta$, compute μ_2 and μ_3 associate to P_1^k, P_2 and P_3 using the expression of eq. (7.30) and solve the following variational problem:

$$\left\{ \begin{array}{l} \text{Find } \left(\mathbf{u}_1^{k+1}, P_1^{k+1}\right) \in \mathcal{H}^2_{\mathbf{u},0} \times \mathcal{H}_P \text{ s.t. for all } \mathbf{v} \in \mathcal{H}^2_{\mathbf{u},0} \text{ and } Q \in \mathcal{H}_P : \\ \displaystyle\int_{\Omega^i \setminus N^i} \mathbf{u}_1^{k+1} \cdot \mathbf{v} \, \mathrm{d}\mathbf{x} - \int_{\Omega^i \setminus N^i} P_1^{k+1} \operatorname{div}(\mathbf{v}) \, \mathrm{d}\mathbf{x} + \int_{\Omega^i \setminus N^i} Q \operatorname{div}\left(\mathbf{u}_1^{k+1}\right) \mathrm{d}\mathbf{x} \\ \qquad + \dfrac{\gamma}{\Delta t} G'\left(\mathbf{u}_1^k\right)(\mathbf{v}) + \dfrac{\gamma}{\Delta t} \widetilde{G}\left(\mathbf{u}_1^k\right)\left(\mathbf{u}_1^{k+1} - \mathbf{u}_1^k, \mathbf{v}\right) \\ \qquad + \displaystyle\int_{\partial\Omega^i} \chi_c f_{\mathrm{act}}\left(c^i\right) \mathbf{v} \cdot \mathbf{n} \, \mathrm{d}\sigma - \int_{\partial\Omega^i} f^i_{\mathrm{NB}} \, \mathbf{v} \cdot \mathbf{n} \, \mathrm{d}\sigma = 0. \end{array} \right.$$

      iii. Set $(\mathbf{u}_1, P_1) = \left(\mathbf{u}_1^{k+1}, P_1^{k+1}\right)$.

   (d) Compute μ_2 and μ_3 associate to P_1, P_2 and P_3 using the expression of eq. (7.30) and deduce $\mathbf{u}^{i+1} = \mathbf{u}_1 + \mu_2 \mathbf{u}_2 + \mu_3 \mathbf{u}_3$ and $P^{i+1} = P_1 + \mu_2 P_2 + \mu_3 P_3$.

2. Computation of the nucleus velocity: $\mathbf{u}^{i+1}_{\mathrm{nucl}} = \dfrac{1}{\xi_{\mathrm{nucl}} \left|N^i\right|} \left(\displaystyle\int_{\partial N^i} P^{i+1} \mathbf{n} \, \mathrm{d}\sigma + \mathbf{f}^i_{\mathrm{BN}} \right)$.

3. Computation of the mesh velocity $\mathbf{u}_{\mathrm{mesh}}$.

4. Computation of the markers concentration c^{i+1} using $\mathbf{u}^{i+1}$ and $\mathbf{u}_{\mathrm{mesh}}$ by solving the following variational formulation:

$$\left\{ \begin{array}{l} \text{Find } c^{i+1} \in \mathcal{H}_c \text{ such that for all } \psi \in \mathcal{H}_c, \text{ we have:} \\ \displaystyle\int_{\Omega^i \setminus N^i} \left(\frac{c^{i+1} - c^i}{\Delta t} \right) \psi \, \mathrm{d}\mathbf{x} + \int_{\Omega^i \setminus N^i} \operatorname{div}\left(\mathbf{u}_{\mathrm{mesh}}\right) c^{i+1} \psi \, \mathrm{d}\mathbf{x} \\ \qquad - \displaystyle\int_{\Omega^i \setminus N^i} \left((1-a) \, \mathbf{u}^{i+1} c^{i+1} - \mathbf{u}_{\mathrm{mesh}} c^{i+1} - \nabla c^{i+1} \right) \cdot \nabla \psi \, \mathrm{d}\mathbf{x} = 0. \end{array} \right.$$

5. Update of the domain:

$$\begin{aligned} \Omega^{i+1} &= \left(\mathrm{Id} + \Delta t \, \mathbf{u}_{\mathrm{mesh}}\right)\left(\Omega^i\right), \\ N^{i+1} &= \left(\mathrm{Id} + \Delta t \, \mathbf{u}_{\mathrm{mesh}}\right)\left(N^i\right) \end{aligned}$$

7.3.4 . Contact between cell boundary and nucleus: utilization of a Uzawa algorithm

Numerically, there may be contact between the nucleus and the cell boundary. To avoid them, we use a contact algorithm based on a Uzawa algorithm. By projecting the fluid velocity and the nucleus velocity on an well suited space, the velocities are corrected (Lefebvre, 2007).

7.3.4.1 . Notations

In this subsection, we introduce the notations needed for the Uzawa algorithm. We fix the time and we assume to be at time t^i with $i \in \{0, \dots, N_f\}$. We recall that we assume the nucleus to be circular and we denote by $\mathbf{x}_{\text{nucl}} \in \Omega^i$ the position of the nucleus center and $R_{\text{nucl}} > 0$ the nucleus radius such that $N^i = B\left(\mathbf{x}_{\text{nucl}}, R_{\text{nucl}}\right) \subset \Omega^i$.

We cover $\partial\Omega^i$ with $N_p \in \mathbb{N}$ circular particles. We call them β_j where $j \in \{1, \dots, N\}$. For all $j \in \{1, \dots, N\}$, we assume there exists $\mathbf{x}_j \in \partial\Omega^i$ and $r_j > 0$ such that when we denote $\beta_j = B(\mathbf{x}_j, r_j)$ we have $\partial\Omega^i \subset \bigcup_{j=1}^{N_p} \beta_j$. We note $\mathbf{X} = \left(\mathbf{x}_{\text{nucl}}, \mathbf{x}_1, \dots, \mathbf{x}_{N_p}\right)$ the vector with all the particles' positions.

The distance between the nucleus and the boundary particle j is defined by:

$$D_j(\mathbf{X}) = |\mathbf{x}_{\text{nucl}} - \mathbf{x}_j| - R_{\text{nucl}} - r_j.$$

The gradient G_j of this distance D_j is defined as follow:

$$G_j(\mathbf{X}) = (\mathbf{e}_j(\mathbf{X}), 0, \dots, 0, -\mathbf{e}_j(\mathbf{X}), 0, \dots, 0)$$

where $\mathbf{e}_j(\mathbf{X}) = \dfrac{\mathbf{x}_{\text{nucl}} - \mathbf{x}_j}{|\mathbf{x}_{\text{nucl}} - \mathbf{x}_j|}$.

These notations are summerized in Figure 7.3.

For all $j \in \{1, \dots, N_p\}$, let $\mathbf{v}_j = \dfrac{1}{\pi r_j^2} \displaystyle\int_{\beta_j \cap \Omega^i} \mathbf{u}^{i+1} \, \mathrm{d}\mathbf{x}$ be the velocity of the boundary particle j. Let $\mathbf{V}$ be the vector with all the particle velocities:

$$\mathbf{V} = \left(\mathbf{u}_{\text{nucl}}^{i+1}, \mathbf{v}_1, \mathbf{v}_2, \dots, \mathbf{v}_{N_p}\right).$$

We remark that $\mathbf{V}$ depends only of $\mathbf{u}_{\text{nucl}}^{i+1}$ and $\mathbf{u}^{i+1}$. Let g be the function:

$$\begin{array}{rccl} g : & \mathbb{R}^2 \times H^1\left(\Omega^i \backslash N^i\right)^2 & \longrightarrow & \mathbb{R}^{2(N_p+1)} \\ & (\boldsymbol{v}, \mathbf{u}) & \longmapsto & \left(\boldsymbol{v}, \dfrac{1}{\pi r_1^2} \displaystyle\int_{\beta_1 \cap \Omega^i} \mathbf{u} \, \mathrm{d}\mathbf{x}, \ \dots, \dfrac{1}{\pi r_{N_p}^2} \displaystyle\int_{\beta_{N_p} \cap \Omega^i} \mathbf{u} \, \mathrm{d}\mathbf{x}\right) \end{array}$$

such that $\mathbf{V} = g\left(\mathbf{u}_{\text{nucl}}^{i+1}, \mathbf{u}^{i+1}\right)$.

7.3.4.2 . Uzawa algorithm

We want to find an admissible velocity space for the nucleus velocity and the fluid velocity. This space will be the space of the velocities ensuring that the nucleus is inside the cell and not in contact with the cell boundary. Thus for all $j \in \{1, \dots, N_p\}$, we want to have:

$$D_j(\mathbf{X} + \Delta t \mathbf{V}) \geq 0.$$

This condition means that at the next time the nucleus is always inside the cell at least at a distance $\min\limits_{j \in \{1, \dots, N_p\}} r_j$ from the cell boundary.

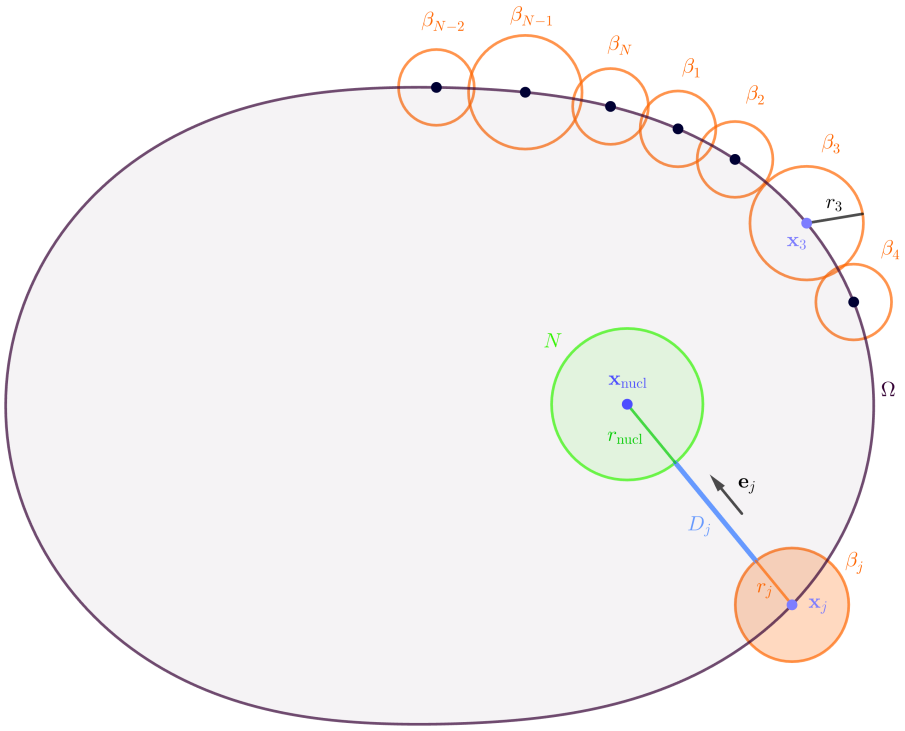

Figure 7.3: Notations for the Uzawa algorithm.

By linearizing this condition, we have:

$$D_j(\mathbf{X}) + \Delta t\, G_j(\mathbf{X}) \cdot \mathbf{V} \geq 0$$

and thus we deduce that an admissible velocity space is given by:

$$\mathcal{K}(\mathbf{X}) = \left\{ \begin{array}{c} (\boldsymbol{v}, \mathbf{u}) \in \mathbb{R}^2 \times H^1\left(\Omega^i \backslash N^i\right)^2 \text{ such that} \\ \forall j \in \{1, \ldots, N_p\},\ D_j(\mathbf{X}) + \Delta t\, G_j(\mathbf{X}) \cdot g\,(\boldsymbol{v}, \mathbf{u}) \geq 0 \end{array} \right\}.$$

We want ensure that $\left(\mathbf{u}_{\text{nucl}}^{i+1}, \mathbf{u}^{i+1}\right) \in \mathcal{K}(\mathbf{X})$. To do it, we project the *a priori* velocities (computed without taking care of the potential contact) in the admissible velocity space $\mathcal{K}(\mathbf{X})$. We deduce the corrected velocities.

Let $\left(\mathbf{u}_{\text{nucl}}^{i+\frac{1}{2}}, \mathbf{u}^{i+\frac{1}{2}}\right)$ be the *a priori* velocities of the nucleus and the fluid. Thus we search $\left(\mathbf{u}_{\text{nucl}}^{i+1}, \mathbf{u}^{i+1}\right)$ such that:

$$\left|\left(\mathbf{u}_{\text{nucl}}^{i+1}, \mathbf{u}^{i+1}\right) - \left(\mathbf{u}_{\text{nucl}}^{i+\frac{1}{2}}, \mathbf{u}^{i+\frac{1}{2}}\right)\right|^2 = \min_{(\boldsymbol{v}, \mathbf{v}) \in \mathcal{K}(\mathbf{X})} \left|(\boldsymbol{v}, \mathbf{v}) - \left(\mathbf{u}_{\text{nucl}}^{i+\frac{1}{2}}, \mathbf{u}^{i+\frac{1}{2}}\right)\right|^2. \tag{7.38}$$

From the appendix A of Lefebvre (2007), we know that if $\left(\mathbf{u}_{\text{nucl}}^{i+1}, \mathbf{u}^{i+1}, \lambda\right) \in \mathbb{R}^2 \times H^1\left(\Omega^i \backslash N^i\right)^2 \times \mathbb{R}^{N_p}$ is solution of the following problem (7.39) then $\left(\mathbf{u}_{\text{nucl}}^{i+1}, \mathbf{u}^{i+1}\right)$ is a solution of the minimization problem (7.38).

$$
\begin{cases}
\left(\mathbf{u}_{\text{nucl}}^{i+1}, \mathbf{u}^{i+1}\right) + \dfrac{1}{2}\Delta t \displaystyle\sum_{j=1}^{N_p} \left(-\lambda_j \mathbf{e}_j(\mathbf{X}), \lambda_j \frac{\mathbf{1}_{\{\mathbf{x}\in\beta_j\}}}{\pi r_j^2} \mathbf{e}_j(\mathbf{X}) \right) = \left(\mathbf{u}_{\text{nucl}}^{i+\frac{1}{2}}, \mathbf{u}^{i+\frac{1}{2}}\right), & \text{(7.39a)} \\
-\Delta t \left(\mathbf{e}_j(\mathbf{X}) \cdot \mathbf{u}_{\text{nucl}}^{i+1} - \mathbf{e}_j(\mathbf{X}) \cdot \displaystyle\int_{\beta_j \cap \Omega^i} \frac{\mathbf{u}^{i+1}}{\pi r_j^2} \, \mathrm{d}\mathbf{x} \right) \leq D_j\left(\mathbf{X}\right), & \text{(7.39b)} \\
\lambda_j \cdot \left(-\Delta t \mathbf{e}_j(\mathbf{X}) \cdot \mathbf{u}_{\text{nucl}}^{i+1} + \Delta t \mathbf{e}_j(\mathbf{X}) \cdot \displaystyle\int_{\beta_j \cap \Omega^i} \frac{\mathbf{u}^{i+1}}{\pi r_j^2} \, \mathrm{d}\mathbf{x} + D_j(\mathbf{X}) \right) = 0, & \text{(7.39c)}
\end{cases}
$$

for all $j \in \{1, \ldots, N_p\}$.

To solve eq. (7.39) and find the corrected velocities $\mathbf{u}_{\text{nucl}}^{i+1}$ and $\mathbf{u}^{i+1}$, we use the following Uzawa algorithm:

Algorithm 7.2 : Uzawa algorithm to correct the nucleus velocity and the fluid velocity in order to avoid contact between cell boundary and nucleus.

Assume $\mathbf{u}_{\text{nucl}}^{i+\frac{1}{2}}$ and $\mathbf{u}^{i+\frac{1}{2}}$ given.

1. Let $\boldsymbol{v}^0 \in \mathbb{R}^2$ and $\mathbf{v}^0 \in H^1\left(\Omega^i \backslash N^i\right)^2$.
   Let $\lambda^0 \in \mathbb{R}^{N_p}$.
   Let $\eta > 0$ small and $\rho > 0$ a projection step.
2. While $\left|\left(\boldsymbol{v}^{k+1}, \mathbf{v}^{k+1}\right) - \left(\boldsymbol{v}^k, \mathbf{v}^k\right)\right| > \eta$ or $\left|\lambda^{k+1} - \lambda^k\right| > \eta$ do:

   (a) $\boldsymbol{v}^{k+1} = \mathbf{u}_{\text{nucl}}^{i+\frac{1}{2}} + \dfrac{1}{2}\Delta t \displaystyle\sum_{j=1}^{N_p} \lambda_j^k \mathbf{e}_j(\mathbf{X})$.

   (b) $\mathbf{v}^{k+1} = \mathbf{u}^{i+\frac{1}{2}} - \dfrac{1}{2}\Delta t \displaystyle\sum_{j=1}^{N_p} \lambda_j^k \mathbf{e}_j(\mathbf{X}) \frac{\mathbf{1}_{\{\mathbf{x}\in\beta_j\}}}{\pi r_j^2}$.

   (c) $\lambda_j^{k+1} =$
   $\prod_{\mathbb{R}_+} \left[\lambda_j^k + \rho \left(-\Delta t \, \mathbf{e}_j(\mathbf{X}) \cdot \boldsymbol{v}^{k+1} + \Delta t \, \mathbf{e}_j(\mathbf{X}) \cdot \displaystyle\int_{\beta_j \cap \Omega^i} \frac{\mathbf{u}^{k+1}}{\pi r_j^2} \, \mathrm{d}\mathbf{x} - D_j(\mathbf{X}) \right) \right]$.

3. Update of nucleus and fluid velocities:

$$\mathbf{u}_{\text{nucl}}^{i+1} = \boldsymbol{v}^{k+1}$$

and

$$\mathbf{u}^{i+1} = \mathbf{v}^{k+1}.$$

7.3.5 . Numerical scheme

Finally, a time iteration of the numerical scheme to run simulations of the model eq. (7.1) is given by:

Algorithm 7.3 : Time iteration of the numerical scheme obtained after time discretization and space discretization with a finite element method and an implicit curvature treatment, with an Uzawa algorithm to manage potential contacts between the cell boundary and the nucleus.

1. Compute the *a priori* velocity $\mathbf{u}^{i+\frac{1}{2}}$ and the pressure P^{i+1} using the decomposition method:
   (a) Compute P_2 and $\mathbf{u}_2$ by solving a variational formulation.
   (b) Compute P_3 and $\mathbf{u}_3$ by solving a variational formulation.
   (c) Compute P_1 and $\mathbf{u}_1$ using the Newton like method and solving variational formulations.
   (d) Compute μ_2 and μ_3 associate to P_1, P_2 and P_3 using the expression of Equation eq. (7.30) and deduce $\mathbf{u}^{i+\frac{1}{2}} = \mathbf{u}_1 + \mu_2\mathbf{u}_2 + \mu_3\mathbf{u}_3$ and $P^{i+1} = P_1 + \mu_2 P_2 + \mu_3 P_3$.

   (See Algorithm 7.1 for more details)
2. Computation of the *a priori* nucleus velocity: $\mathbf{u}_{\text{nucl}}^{i+\frac{1}{2}} = \dfrac{1}{\xi_{\text{nucl}}\,|N^i|}\left(\displaystyle\int_{\partial N^i} P^{i+1}\mathbf{n}\,\mathrm{d}\sigma + \mathbf{f}_{\text{BN}}^i\right)$.
3. If the distance between the cell boundary and the nucleus is small then projection of the *a priori* velocities $\mathbf{u}_{\text{nucl}}^{i+\frac{1}{2}}$ and $\mathbf{u}^{i+\frac{1}{2}}$ in an admissible space via a Uzawa algorithm to compute the corrected velocities $\mathbf{u}_{\text{nucl}}^{i+1}$ and $\mathbf{u}^{i+1}$ (see Algorithm 7.2 for more details), else $\mathbf{u}_{\text{nucl}}^{i+1} = \mathbf{u}_{\text{nucl}}^{i+\frac{1}{2}}$ and $\mathbf{u}^{i+1} = \mathbf{u}^{i+\frac{1}{2}}$.
4. Computation of the mesh velocity $\mathbf{u}_{\text{mesh}}$.
5. Computation of the markers concentration c^{i+1} by solving a variational formulation (see Algorithm 7.1 for more details).
6. Update of the domain: computation of Ω^{i+1} and N^{i+1}.

One drawback of this numerical scheme 7.3, which uses an Uzawa algorithm to manage potential contacts between the cell boundary and the nucleus, is that it does not preserve the symmetry of the problem (7.1). If the initial data is symmetrical about an axis, then this symmetry is preserved over time. For this property to be preserved numerically, at each time iteration the mesh must be symmetrical with respect to this axis and also the balls covering the boundary of the cell used for the Uzawa algorithm must be arranged symmetrically. This is restrictive and we choose another approach to manage potential contacts between the cell boundary and the nucleus using a repulsion force.

7.3.6 . Contact between cell boundary and nucleus: utilization of a repulsion force

Based on a repulsive force, we present another way of avoiding potential contact between the cell boundary and the nucleus. We assume that the interaction between the cell boundary and the nucleus when they are close induces a force on both the nucleus and the cell boundary.

Let $f_{\text{cont}}^b(\mathbf{x}_B)$ and $f_{\text{cont}}^n(\mathbf{x}_N)$ be the force induced by the interaction between the cell boundary and the nucleus at the point $\mathbf{x}_B \in \partial\Omega$ and the point $\mathbf{x}_N \in \partial N$, respectively. We

have:

$$f^b_{\text{cont}}\left(\mathbf{x}_B\right) = \left(\int_{\partial N} \lambda \mathbb{1}_{d(\mathbf{x}_B,\tilde{\mathbf{x}})<r_0} \left(e^{-\frac{d(\mathbf{x}_B,\tilde{\mathbf{x}})}{r_1}} - e^{-\frac{r_0}{r_1}}\right) \mathbf{n}\, \mathrm{d}\sigma\right) \cdot \mathbf{n},$$

and

$$f^n_{\text{cont}}\left(\mathbf{x}_N\right) = \left(\int_{\partial \Omega} \lambda \mathbb{1}_{d(\mathbf{x}_N,\tilde{\mathbf{x}})<r_0} \left(e^{-\frac{d(\mathbf{x}_N,\tilde{\mathbf{x}})}{r_1}} - e^{-\frac{r_0}{r_1}}\right) \mathbf{n}\, \mathrm{d}\sigma\right) \cdot \mathbf{n},$$

with $\lambda > 0$, $r_0 > 0$, $r_1 > 0$, and for all $\mathbf{x}, \tilde{\mathbf{x}} \in \mathbb{R}^2$, $d\left(\mathbf{x}, \tilde{\mathbf{x}}\right)$ the euclidean distance between $\mathbf{x}$ and $\tilde{\mathbf{x}}$. We could say that the cell boundary perceives the nucleus as an obstacle and the nucleus perceives the cell boundary as an obstacle (see section 1.3.5.4).

This modifies the model by changing the boundary condition on the pressure (7.1d) and velocity of the nucleus (7.1e) as follows:

$$P = \gamma\kappa + \chi_c f_{\text{act}}\left(c\right) - f_{\text{NB}} - f^b_{\text{cont}} \qquad \text{on } \partial\Omega\left(t\right),$$

and

$$\mathbf{u}_{\text{nucl}}\left(t\right) = \frac{1}{\xi_{\text{nucl}}\left|N\right|}\left(\int_{\partial N(t)} P(t,\mathbf{x})\mathbf{n}\, \mathrm{d}\sigma + \mathbf{f}_{\text{BN}} + \mathbf{f}^n_{\text{cont}}\right),$$

with $\mathbf{f}^n_{\text{cont}} = \int_{\partial N} f^n_{\text{cont}}\left(\mathbf{x}\right)\mathbf{n}\, \mathrm{d}\sigma$.

Let $f^{b,i}_{\text{cont}}$ and $\mathbf{f}^{n,i}_{\text{cont}}$ be an approximation of the forces f^b_{cont} and $\mathbf{f}^n_{\text{cont}}$ at time t^i. The discrete boundary condition (7.22c) is then given by:

$$P^{i+1}\mathbf{n} = \gamma\tilde{H}^{i+1} + \chi_c f_{\text{act}}\left(c^i\right)\mathbf{n} - f^i_{\text{NB}}\,\mathbf{n} - f^{b,i}_{\text{cont}}\,\mathbf{n} \qquad \text{on } \partial\Omega^i.$$

The discrete nucleus velocity (7.22e) is given by:

$$\mathbf{u}^{i+1}_{\text{nucl}} = \frac{1}{\xi_{\text{nucl}}\left|N^i\right|}\left(\int_{\partial N^i} P^{i+1}\mathbf{n}\, \mathrm{d}\sigma + \mathbf{f}^i_{\text{BN}} + \mathbf{f}^{n,i}_{\text{cont}}\right).$$

Following exactly the same procedure as the one described in sections 7.3.2 and 7.3.3, we obtain that with this repulsive force to take care of the potential contact between the cell boundary and the nucleus, the numerical scheme to solve the problem eq. (7.1) is given by the following algorithm:

Algorithm 7.4 : Time iteration of the numerical scheme obtained after time discretization and space discretization with a finite element method and an implicit curvature treatment with a repulsive force to prevent potential contact between the cell boundary and the nucleus.

1. Compute $\mathbf{u}^{i+1}$ and P^{i+1} using c^i and the decomposition method:

   (a) Solve the following variational formulation to compute P_2 and deduce from it $\mathbf{u}_2 = -\nabla P_2$:

   $$\begin{cases} \text{Find } P_2 \in \mathcal{H}_{P,0} \text{ such that for all } Q \in \mathcal{H}_{P,0}, \text{ we have:} \\ \displaystyle\int_{\Omega^i \setminus N^i} \nabla P_2 \cdot \nabla Q \, \mathrm{d}\mathbf{x} - \int_{\partial N^i} Q n_x \, \mathrm{d}\sigma = 0. \end{cases}$$

   (b) Solve the following variational formulation to compute P_3 and deduce from it $\mathbf{u}_3 = -\nabla P_3$:

   $$\begin{cases} \text{Find } P_3 \in \mathcal{H}_{P,0} \text{ such that for all } Q \in \mathcal{H}_{P,0}, \text{ we have:} \\ \displaystyle\int_{\Omega^i \setminus N^i} \nabla P_3 \cdot \nabla Q \, \mathrm{d}\mathbf{x} - \int_{\partial N^i} Q n_y \, \mathrm{d}\sigma = 0. \end{cases}$$

   (c) Using the Newton like method, compute $\mathbf{u}_1$ and P_1.

   i. Set $\mathbf{u}_1^0 = 0$ and $P_1^0 = 0$.

   ii. While $\left|\mathbf{u}_1^{k+1} - \mathbf{u}_1^k\right| > \eta$, compute μ_2 and μ_3 associate to P_1^k, P_2 and P_3 using the expression of eq. (7.30) and solve the following variational problem:

   $$\begin{cases} \text{Find } (\mathbf{u}_1^{k+1}, P_1^{k+1}) \in \mathcal{H}^2_{\mathbf{u},0} \times \mathcal{H}_P \text{ s.t. for all } \mathbf{v} \in \mathcal{H}^2_{\mathbf{u},0} \text{ and } Q \in \mathcal{H}_P : \\ \displaystyle\int_{\Omega^i \setminus N^i} \mathbf{u}_1^{k+1} \cdot \mathbf{v} \, \mathrm{d}\mathbf{x} - \int_{\Omega^i \setminus N^i} P_1^{k+1} \operatorname{div}(\mathbf{v}) \, \mathrm{d}\mathbf{x} + \int_{\Omega^i \setminus N^i} Q \operatorname{div}\left(\mathbf{u}_1^{k+1}\right) \mathrm{d}\mathbf{x} \\ \qquad + \dfrac{\gamma}{\Delta t} G'\left(\mathbf{u}_1^k\right)(\mathbf{v}) + \dfrac{\gamma}{\Delta t} \widetilde{G}\left(\mathbf{u}_1^k\right)\left(\mathbf{u}_1^{k+1} - \mathbf{u}_1^k, \mathbf{v}\right) \\ \qquad + \displaystyle\int_{\partial\Omega^i} \chi_c f_{\mathrm{act}}\left(c^i\right) \mathbf{v} \cdot \mathbf{n} \, \mathrm{d}\sigma - \int_{\partial\Omega^i} f^i_{\mathrm{NB}} \, \mathbf{v} \cdot \mathbf{n} \, \mathrm{d}\sigma \\ \qquad - \int_{\partial\Omega^i} f^{b,i}_{\mathrm{cont}} \, \mathbf{v} \cdot \mathbf{n} \, \mathrm{d}\sigma = 0. \end{cases}$$

   iii. Set $(\mathbf{u}_1, P_1) = \left(\mathbf{u}_1^{k+1}, P_1^{k+1}\right)$.

   (d) Compute μ_2 and μ_3 associate to P_1, P_2 and P_3 using the expression of eq. (7.30) and deduce $\mathbf{u}^{i+1} = \mathbf{u}_1 + \mu_2 \mathbf{u}_2 + \mu_3 \mathbf{u}_3$ and $P^{i+1} = P_1 + \mu_2 P_2 + \mu_3 P_3$.

2. Computation of the nucleus velocity: $\mathbf{u}^{i+1}_{\mathrm{nucl}} = \dfrac{1}{\xi_{\mathrm{nucl}} \left|N^i\right|} \left(\displaystyle\int_{\partial N^i} P^{i+1} \mathbf{n} \, \mathrm{d}\sigma + \mathbf{f}^i_{\mathrm{BN}} + \mathbf{f}^{n,i}_{\mathrm{cont}} \right)$.

3. Computation of the mesh velocity $\mathbf{u}_{\mathrm{mesh}}$.

4. Computation of the markers concentration c^{i+1} using $\mathbf{u}^{i+1}$ and $\mathbf{u}_{\mathrm{mesh}}$ by solving the following variational formulation:

   $$\begin{cases} \text{Find } c^{i+1} \in \mathcal{H}_c \text{ such that for all } \psi \in \mathcal{H}_c, \text{ we have:} \\ \displaystyle\int_{\Omega^i \setminus N^i} \left(\frac{c^{i+1} - c^i}{\Delta t} \right) \psi \, \mathrm{d}\mathbf{x} + \int_{\Omega^i \setminus N^i} \operatorname{div}\left(\mathbf{u}_{\mathrm{mesh}}\right) c^{i+1} \psi \, \mathrm{d}\mathbf{x} \\ \qquad - \displaystyle\int_{\Omega^i \setminus N^i} \left((1-a) \, \mathbf{u}^{i+1} c^{i+1} - \mathbf{u}_{\mathrm{mesh}} c^{i+1} - \nabla c^{i+1} \right) \cdot \nabla \psi \, \mathrm{d}\mathbf{x} = 0. \end{cases}$$

5. Update of the domain:

   $$\Omega^{i+1} = \left(\mathrm{Id} + \Delta t \, \mathbf{u}_{\mathrm{mesh}}\right)\left(\Omega^i\right) \quad \text{and} \quad N^{i+1} = \left(\mathrm{Id} + \Delta t \, \mathbf{u}_{\mathrm{mesh}}\right)\left(N^i\right)$$

7.4 . Numerical results

7.4.1 . Illustration of the action of the restoring force on the nucleus

In this section, we illustrate the action of the forces induced by the nucleus on the cell boundary and the cell boundary on the nucleus. We aim to illustrate that the force induced by the boundary on the nucleus brings the nucleus back towards the centre of the cell. To do this, we consider the model without coupling with the markers concentration, i.e. with $\chi_c = 0$.

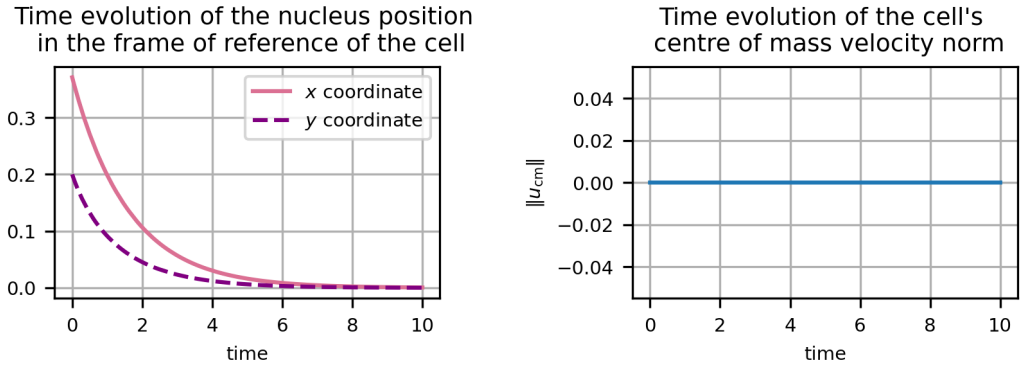

Figure 7.4: **Illustration of the nucleus dynamic without coupling with the markers concentration and surface tension.** *On the left is the time evolution of the nucleus position in the cell frame of reference. The cell frame of reference is centered on the cell centre of mass. We then observe that after a certain time, the position of the nucleus coincides with that of the cell's centre of mass. On the right is the time evolution of the cell's centre of mass velocity norm. We observe that is constant and equal to zero.*
The results presented here are obtained with the parameters $\Delta t = 0.00005$, $R_{\text{nucl}} = 0.3$, $\mathbf{x}^{\text{in}}_{\text{nucl}} = (0.4; 0.2)$, $\beta = 1.5$, $\delta = 0.141372$ *and* $\xi_{\text{nucl}} = 1$. *See fig. 7.5 for the initial cell domain.*

We then observe that the nucleus indeed returns to the centre of the cell. We also observe the action of the force induced by the cell boundary, which deforms the initial shape of the cell domain into a disk. We can note that the surface tension has also this effect on the cell domain.

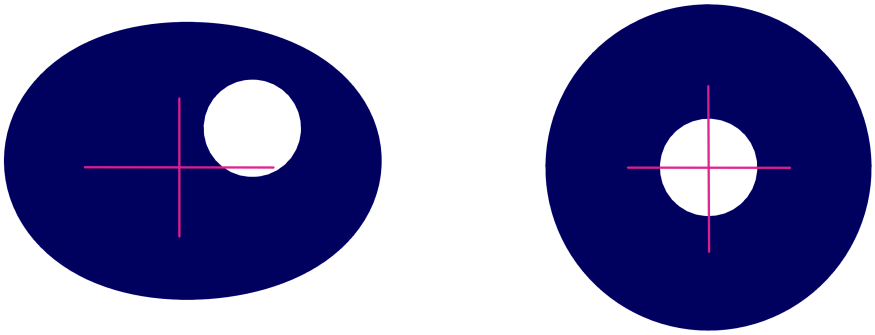

Figure 7.5: **Illustration of the time evolution of the domain without coupling with the markers concentration and surface tension.** *On the left is the initial cell domain. On the right is cell domain at time $t = 10$. We observe that at the final time the cell domain is a disk. The pink lines indicate the axes and the point $(0, 0)$.*
The results presented here are obtained with the parameters $\Delta t = 0.00005$, $R_{\text{nucl}} = 0.3$, $\mathbf{x}_{\text{nucl}}^{\text{in}} = (0.4; 0.2)$, $\beta = 1.5$, $\delta = 0.141372$ and $\xi_{\text{nucl}} = 1$.

7.4.2 . Illustration of the theorem 7.2.4

In this section, we check that the numerical scheme proposed in algorithm 7.4 is consistent with the mathematical study of the model. We therefore check that we recover the stationary state (7.10) as well as the result on the stability of the latter stated in theorem 7.2.4.

First, we check that the model captures the stationary state. To this aim, we choose as initial condition the stationary state. The initial geometry of the cell is given by $\Omega^{\text{in}} = B(0, R_0)$ and $N^{\text{in}} = B(0, R_{\text{nucl}})$ with $R_0 > R_{\text{nucl}} > 0$ and the initial marker concentration is given by $c^{\text{in}}(\mathbf{x}) = \dfrac{M}{|\Omega^{\text{in}} \setminus N^{\text{in}}|}$. As illustrated in fig. 7.6, the numerical scheme captures well the stationary state. The velocity remains zero over time, and the position of the nucleus and the geometry of the cell remain unchanged over time.

We check that the numerical scheme gives results in accordance with theorem 6.2.2. We therefore study the linear stability of the stationary state numerically. To do this, we choose a perturbation of the stationary state as the initial condition and observe, depending on the value of χ_c, whether the system returns to the stationary state.

The chosen stationary state perturbation is given by:

$$c^{\text{in}}(\mathbf{x}) = K(1 + X(\mathbf{x}))\mathbb{1}_{1+X(\mathbf{x})>0} \tag{7.40}$$

where for all $\mathbf{x} \in \Omega \setminus N$ we have $X(\mathbf{x}) \sim \mathcal{N}(0, 1)$ and K such that $\int_{\Omega\setminus N} c^{\text{in}}(\mathbf{x})\, d\mathbf{x} = M$.

As illustrated in fig. 7.7 for the case where $R_0 = 1$ and $R_{\text{nucl}} = 0.4$, we correctly find the criterion on the linear stablity of the stationary state. Indeed, when $\chi_c < \chi_c^*$, we have that the norm of the velocity decreases very quickly towards 0 then is constant equal to 0. This illustrates that when $\chi_c < \chi_c^*$ the stationary state is stable. Also, when $\chi_c > \chi_c^*$, we observe that the norm increases rapidly towards a strictly positive value and then becomes constant. This suggests that when $\chi_c > \chi_c^*$ there are stable travelling waves.

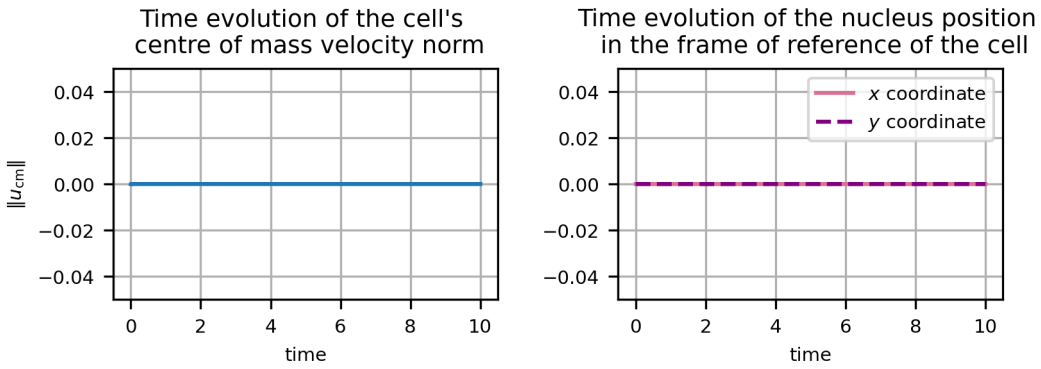

Figure 7.6: **Example of capturing the stationary state using the numerical scheme.** *The curve on the left represents the evolution of the velocity norm of the cell's centre of mass over time. We observe that this remains zero throughout the study interval* $[0, 10]$*. The curves on the right represent the evolution of the coordinates of the nucleus position over time. The nucleus position is preserved over the study interval.*
The results presented here are obtained with the parameters $\Delta t = 0.00005$, $R_0 = 1$, $R_{\text{nucl}} = 0.4$, $\mathbf{x}^{\text{in}}_{\text{nucl}} = (0; 0)$, $M = \pi$, $a = 1$, $c^{\text{in}} = \dfrac{M}{|\Omega \setminus N|}$, $\gamma = 1$, $\chi_c = 0.5$, $f_{\text{act}}(c) = \frac{c(1+c_s)^2}{c_s(c+c_s)}$ *with* $c_s = 0.5$,$\beta = 1.5$, $\delta = 0.141372$ *and* $\xi_{\text{nucl}} = 1$.

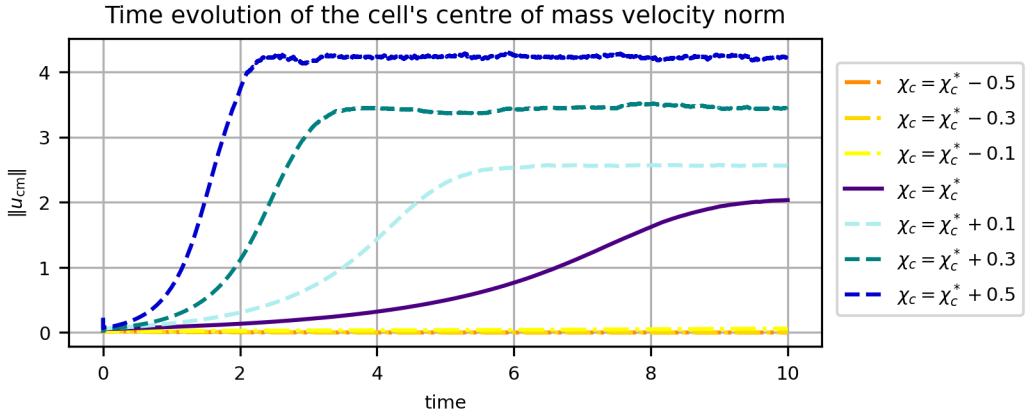

Figure 7.7: **Numerical illustration of theorem 7.2.4.** *Each curve represents the evolution of the cell's centre of mass velocity norm of a cell for different values of* χ_c *(see legend on the right). When* $\chi_c < \chi_c^*$ *the norm of the velocity decreases very rapidly towards* 0 *(dashdotted curves in overlapping shades of orange), whereas when* $\chi_c > \chi_c^*$ *it increases rapidly towards a non-zero value (dashed curves in shades of blue) . The critical case* $\chi_c = \chi_c^*$ *is also represented (dark curve), here the norm of the velocity is close to zero and decreases.*
The results presented here are obtained with the parameters $\Delta t = 0.00005$, $R_0 = 1$, $R_{\text{nucl}} = 0.4$, $\mathbf{x}^{\text{in}}_{\text{nucl}} = (0; 0)$, $M = \pi$, $a = 1$, $\gamma = 1$, c^{in} *given by eq. (7.40) and* χ_c^* *given by (7.11),* $f_{\text{act}}(c) = \frac{c(1+c_s)^2}{c_s(c+c_s)}$ *with* $c_s = 0.5$, $\beta = 1.5$, $\delta = 0.141372$ *and* $\xi_{\text{nucl}} = 1$.

7.4.3 . Capture of travelling waves

The numerical illustration of theorem 7.2.4 on the stability of the stationary state suggests that when $\chi_c > \chi_c^*$, the model admits progressive waves which are captured by the numerical scheme. We verify and illustrate this in this section.

As a remainder, a travelling wave is characterised by the cell moving at a given velocity. The geometry of the cell and the distribution of the marker concentration in the cell reference frame are conserved over time.

First, we plot the trajectories associated with the $\chi_c = \chi_c^* + 0.1$, $\chi_c = \chi_c^* + 0.3$ and $\chi_c = \chi_c^* + 0.5$ cases in the fig. 7.7. Each cell maintains its orientation over time, which, coupled with the fact that the norm of the velocity is constant, leads to a travelling wave (see fig. 7.8).

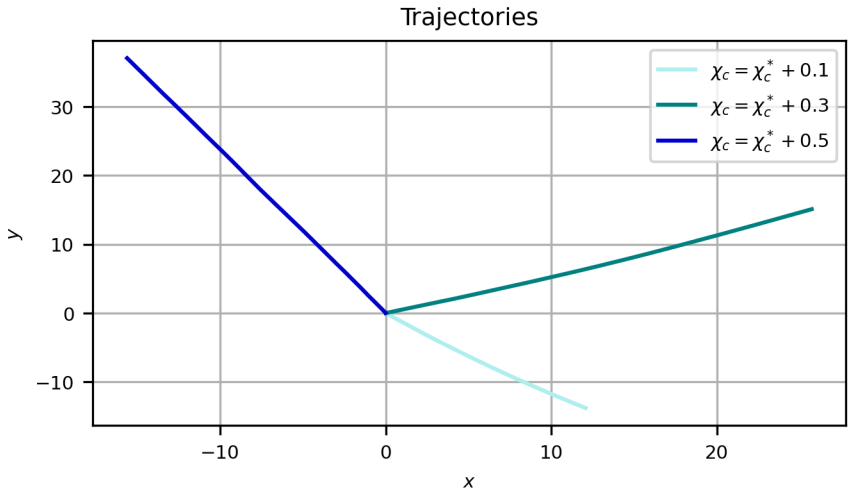

Figure 7.8: **Trajectories associated with the cells in fig. 6.7 in the case where $\chi_c > \chi_c^*$.** *Each curve represents the trajectory of one of the cells studied in figure 3. Only those where $\chi_c > \chi_c^*$ are represented, keeping the same colour coding (see legend on the right). We can therefore see that here the cells do not change orientation over time.*
The results presented here are obtained with the parameters $\Delta t = 0.00005$, $R_0 = 1$, $R_{\text{nucl}} = 0.4$, $\mathbf{x}_{\text{nucl}}^{\text{in}} = (0; 0)$, $M = \pi$, $a = 1$, $\gamma = 1$, c^{in} given by eq. (7.40), χ_c^* given by (7.11), $f_{\text{act}}(c) = \frac{c(1+c_s)^2}{c_s(c+c_s)}$ with $c_s = 0.5$, $\beta = 1.5$, $\delta = 0.141372$ and $\xi_{\text{nucl}} = 1$.

It remains to be verified that, when the velocity of the travelling wave is reached, the shape of the cell and the distribution of the markers within the cell are unchanged. To this end, we represent the cell at different times. We can see that initially the cell polarises, the nucleus moves to the area that will be the rear and the concentration of markers increases in this area. Then, once polarised, the cell maintains its shape and the distribution of the concentration of markers inside (see figs. 7.9 to 7.11). What we see is a travelling wave. We can see that, depending on the parameters, the shape of the cell, although similar, is different.

These observations are very interesting because they are in accordance with biological observations. They clearly show that the model allows us to reproduce in a qualitative way the polarisation and cell migration phenomena. Indeed, the numerical results in the figs. 7.9 to 7.11 highlight that, for a range of parameters, a perturbation in the stationary distribution of markers leads to cell polarisation and movement in a travelling wave regime.

The initial condition models a reorganization in the cytoskeleton. The cell geometry is symmetric, and the homogeneous distribution of markers is perturbed, leading to cell polarisation. Initially, the cell geometry is few altered, and the quantity of markers in the area that will become the rear of the cell increases, this can correspond to the slow rear retraction phase. Then, the geometry changes, defining the front and rear of the cell. It is challenging to assert that the model captures the fast rear retraction phase. Nevertheless, the nucleus and the rear edge of the cell move in the same direction, which will be the direction of the cell, and the rear edge of the cell moves faster than the nucleus. This results in the nucleus being positioned at the rear of the cell when it becomes polarised. Until the cell starts moving at a constant speed, the quantity of markers continues to increase at the cell rear. There are few markers at the cell leading edge. Since the markers are rear markers, they can model an inhibitor of actin polymerisation. The absence of markers in an area thus models a zone where actin is polymerised. This indicates that we indeed observe actin polymerisation at the front and the creation of the lamellipodium, which corresponds to the maturation phase. Thus the model reproduces well the polarisation phenomenon.

By considering that the four steps of the cell migration cycle occur simultaneously, obtaining a travelling wave indicates that the model accurately reproduces the phenomenon of cell migration.

Conclusion and perspectives. The proposed model and the numerical simulations performed allow us to qualitatively reproduce the phenomenon of polarisation and cell migration. In future work, we aim to define the travelling waves solutions of the model and study their existence. By continuing this study, we aim to characterise the long-term behaviour of the model. Finally, we hope to establish a bifurcation result from the stationary state to a traveling wave when χ_c becomes greater than χ_c^*.

Another perspective is to pursue the numerical study of the model to highlight the influence of each parameter on the model and the trajectory obtained. We also yearn to numerically study the heuristic approach concerning the forces acting between the nucleus and the edge of the cell and compare the results obtained via this heuristic with those presented here.

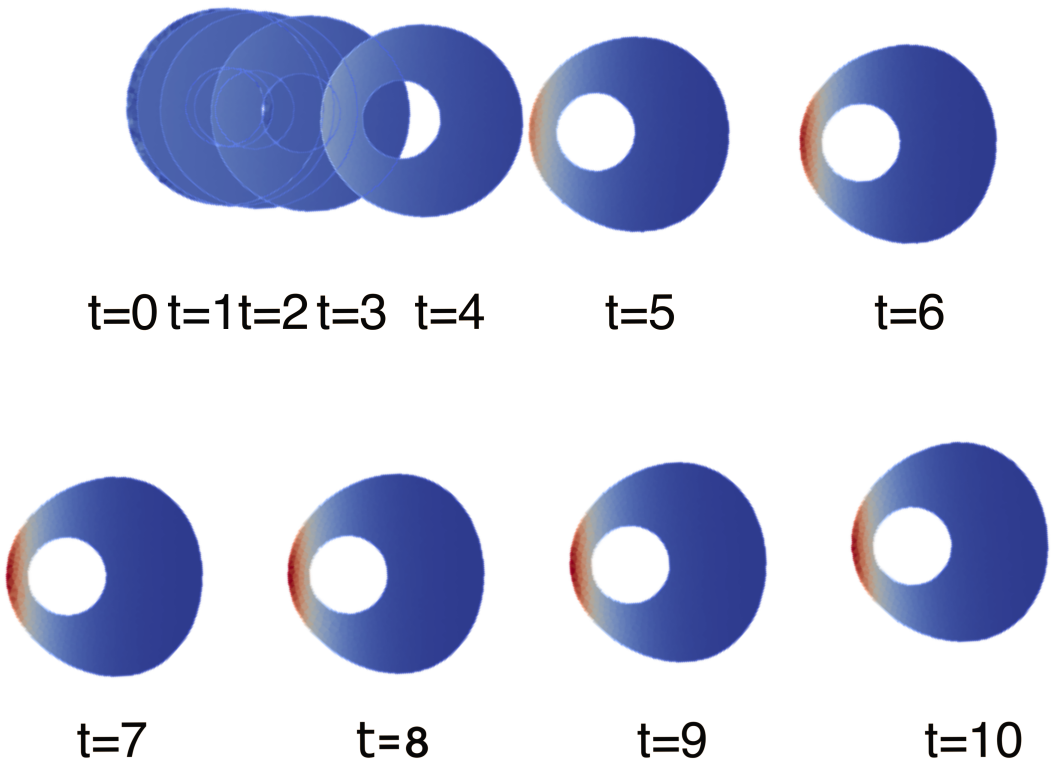

Figure 7.9: **Illustration of the convergence to a travelling wave when $\chi = \chi_c^* + 0.1$.** *Snapshots of the cell are shown at time $t \in \{0, 1, 2, \ldots, 9, 10\}$. We can see that for $t < 6$, the cell polarises: the nucleus is placed at the rear of the cell and the concentration of markers increases in this zone. Then, when $t \geq 6$, the travelling wave velocity is reached (see fig. 7.7) and we observe that the shape of the cell no longer changes, the position of the nucleus in the cell reference frame is fixed as is the distribution of the marker concentration. The cell retains its polarisation.*
The snapshots corresponds to the case $\chi_c = \chi_c^* + 0.1$ of the fig. 7.7. The red area represents the area with high markers concentration whereas the dark blue area represents the area with low markers concentration. For ease of reading, the travelling wave is represented along the axis defined by its direction. The two lines are normally aligned.

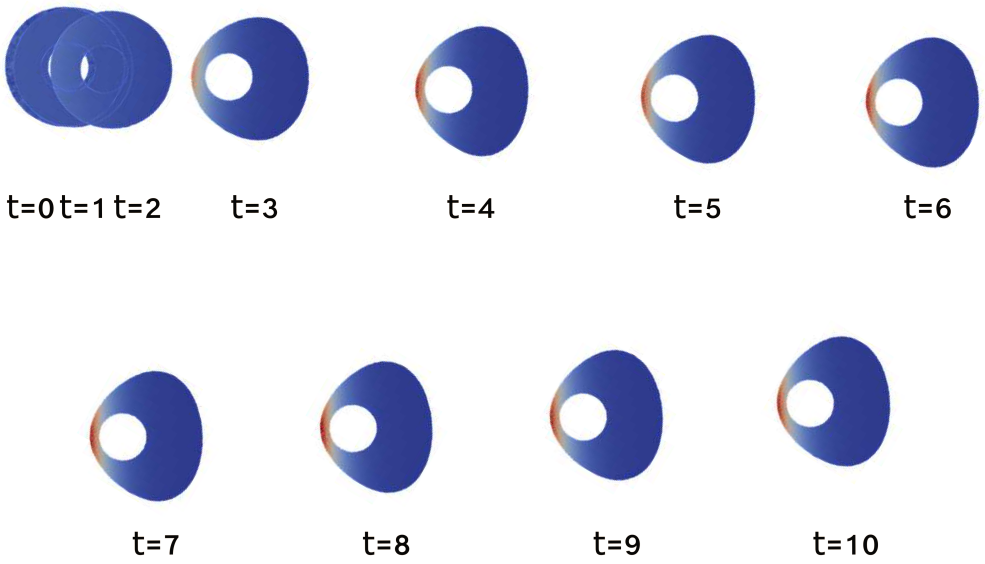

Figure 7.10: **Illustration of the convergence to a travelling wave when $\chi = \chi_c^* + 0.3$.** *Snapshots of the cell are shown at time $t \in \{0, 1, 2, \ldots, 9, 10\}$. We can see that for $t < 4$, the cell polarises: the nucleus is placed at the rear of the cell and the concentration of markers increases in this zone. Then, when $t \geq 4$, the travelling wave velocity is reached (see fig. 7.7) and we observe that the shape of the cell no longer changes, the position of the nucleus in the cell reference frame is fixed as is the distribution of the marker concentration. The cell retains its polarisation.*
The snapshots corresponds to the case $\chi_c = \chi_c^* + 0.3$ of the fig. 7.7. The red area represents the area with high markers concentration whereas the dark blue area represents the area with low markers concentration. For ease of reading, the travelling wave is represented along the axis defined by its direction. The two lines are normally aligned.

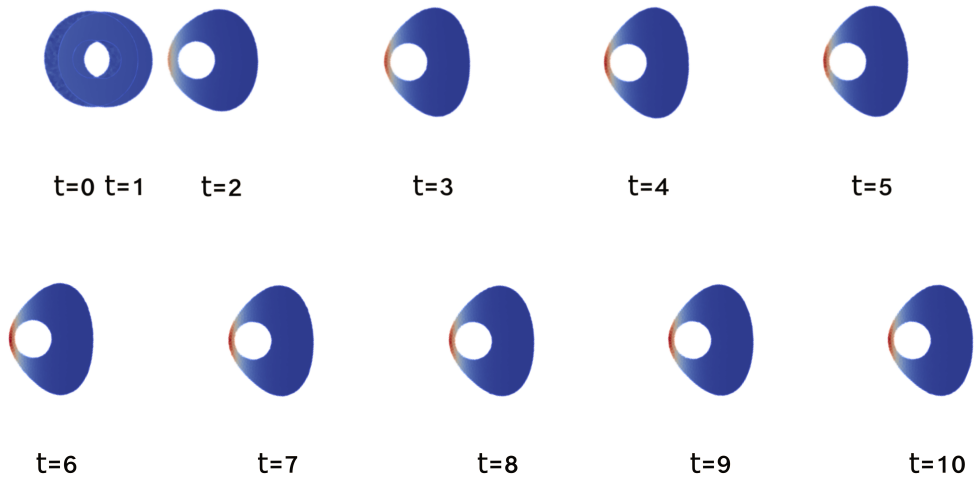

Figure 7.11: **Illustration of the convergence to a travelling wave when $\chi = \chi_c^* + 0.5$.** *Snapshots of the cell are shown at time $t \in \{0, 1, 2, \ldots, 9, 10\}$. We can see that for $t \leq 2$, the cell polarises: the nucleus is placed at the rear of the cell and the concentration of markers increases in this zone. Then, when $t \geq 3$, the travelling wave velocity is reached (see fig. 7.7) and we observe that the shape of the cell no longer changes, the position of the nucleus in the cell reference frame is fixed as is the distribution of the marker concentration. The cell retains its polarisation.*
The snapshots corresponds to the case $\chi_c = \chi_c^* + 0.5$ of the fig. 7.7. The red area represents the area with high markers concentration whereas the dark blue area represents the area with low markers concentration. For ease of reading, the travelling wave is represented along the axis defined by its direction. The two lines are normally aligned.

Bibliography

Alazard, T., Magliocca, M., and Meunier, N. (2022). Traveling wave solution for a coupled incompressible Darcy's free boundary problem with surface tension. arXiv:2205.04365 [math]. 220

Hecht, F. (2012). New development in freefem++. J. Numer. Math., 20(3-4):251–265. 231

Lavi, I. (2019). Physical modeling of cell motility and morphodynamics. phdthesis, Sorbonne Université. 231

Lavi, I., Meunier, N., and Pantz, O. (2023). Implicit like time discretization for the one-phase Hele-Shaw problem with surface tension. arXiv:2305.06180 [cs, math]. 231, 232

Lavi, I., Meunier, N., Voituriez, R., and Casademunt, J. (2020). Motility and morphodynamics of confined cells. Physical Review E, 101(2):022404. Publisher: American Physical Society. 220

Lefebvre, A. (2007). Modélisation numérique d'écoulements fluide/particules. phdthesis, Université Paris Sud. 231, 238, 239

8 - A 1 dimensional model of cell motility taking into account the nucleus

In this chapter, in collaboration with Thomas Lepoutre and Nicolas Meunier, we present a heuristic model of cell motility that includes the nucleus. The modelling of this model is inspired by the approach taken in chapter 1. The aim of this model is to highlight the properties of the nucleus and its impact on cell motility. We derive a one-dimensional model from the two-dimensional modelling. We study this one-dimensional model and proof that it is well-posed. The one-dimensional model considered is a non-local, non-linear Fokker-Planck equation. We then examine its stationary states. Finally, we write a finite volume numerical scheme for the model, which, once implemented in Python, allows for a numerical study of the model. The model reproduces behaviours consistent with the biological context. We emphasize that the model captures intermittent trajectories.

8.1 . Modelling

In this section, we aim to develop a model of cell motility that includes the nucleus in dimension 1. This model is derived from a two-dimensional model obtained through a heuristic approach. We simplify the nucleus to a point and model its influence on the cell and its boundary by acting on the markers attached to the boundary. Although different, the ideas of modelling are similar to the modelling approach taken in chapter 1.

8.1.1 . Model in dimension 2

Let $\Omega(t)$ be a subset of $\mathbb{R}^2$ which models the cell. We assume the cell to be filled by a fluid with velocity $\mathbf{u}$ and pressure P that models the cytoskeleton. Let $\mathbf{X}_N(t) \in \Omega(t)$ be the position of the nucleus at time $t \geq 0$.

We assume that the cell contains some markers of concentration c. These markers are polarity markers. We assume them to be rear markers. This means that the rear part of the cell is defines as the part with the most markers. We assume the markers to be transported by the fluid and to diffuse inside the cell. Thus for $t > 0$ and $\mathbf{x} \in \Omega(t)$, we have:

$$\partial_t c(t,\mathbf{x}) = \Delta c(t,\mathbf{x}) - (1-a)\operatorname{div}\left[\mathbf{u}(t,\mathbf{x})\, c(t,\mathbf{x})\right] \tag{8.1}$$

with $0 \leq a \leq 1$.

We also assume these markers can attach and detach to the membrane. Let $\mu(t,\mathbf{x})$ be the concentration of markers at the point $\mathbf{x} \in \partial\Omega(t)$ at time $t > 0$. The rate of attachment to the membrane at the point $\mathbf{x} \in \partial\Omega(t)$ depends on the position of the nucleus. We denote $\alpha(\mathbf{X}_N, \mathbf{x})$ this rate. We assume that the closer $\mathbf{x}$ and $\mathbf{X}_N$ are the smaller $\alpha(\mathbf{X}_N, \mathbf{x})$ is. We also assume that there exists $A > \varepsilon > 0$ such that for all $\mathbf{x} \in \partial\Omega(t)$ and $\mathbf{X}_N \in \Omega(t)$, $\varepsilon \leq \alpha(\mathbf{X}_N, \mathbf{x}) \leq A$. We do this assumption in order to model the fact that the nucleus acts on the cell boundary. The rate of detachment of the membrane is constant over $\partial\Omega(t)$ and we denote it β. Thus for $t > 0$ and $\mathbf{x} \in \partial\Omega(t)$, the dynamic of the markers concentration at the membrane is given by:

$$\partial_t \mu(t,\mathbf{x}) = \alpha(\mathbf{X}_N(t), \mathbf{x})\, c(t,\mathbf{x}) - \beta\mu(t,\mathbf{x}). \tag{8.2}$$

We also assume the total quantity of markers to be constant in time. Thus we impose:

$$\int_{\Omega(t)} c\left(t,\mathbf{x}\right)\,\mathrm{d}\mathbf{x}+\int_{\partial\Omega(t)}\mu\left(t,\mathbf{x}\right)\,\mathrm{d}\sigma=M$$

with M independent of the time. The following border condition ensures it:

$$\left[\nabla c\left(t,\mathbf{x}\right)+a\mathbf{u}\left(t,\mathbf{x}\right)c\left(t,\mathbf{x}\right)\right]\cdot\mathbf{n}=-\partial_t\mu\left(t,\mathbf{x}\right),\quad \mathbf{x}\in\partial\Omega\left(t\right),t>0. \tag{8.3}$$

We want to write the problem for the fluid velocity and pressure. As in Lavi et al. (2020), we assume there is a coupling between the fluid and the marker concentration and the markers to be rear markers. Thus we have:

$$\begin{cases}\mathbf{u}+\nabla P=0 & \text{in }\Omega\left(t\right), & \text{(8.4a)}\\ \mathrm{div}\left(\mathbf{u}\right)=0 & \text{in }\Omega\left(t\right), & \text{(8.4b)}\\ P=\gamma\kappa+\chi_c f_{\mathrm{act}}\left(\mu\right) & \text{on }\partial\Omega\left(t\right), & \text{(8.4c)}\\ V_n=\mathbf{u}\cdot\mathbf{n} & \text{on }\partial\Omega\left(t\right). & \text{(8.4d)}\end{cases}$$

To ensure the assumption of rear markers we assume that f_{act} is such that $f'_{\mathrm{act}}\left(\mu_0\right)=1$ with μ_0 the markers concentration at the membrane associated to the mean planar concentration steady state.

Finally, we write the dynamics on $\mathbf{X}_N$. We assume the nucleus to rubs against the substrate, that the fluid acts on it and that the cytoskeleton imposes a restoring force to its equilibrium position $\mathbf{X}_{\mathrm{eq}}$. We assume to have $\mathbf{X}_{\mathrm{eq}}=\mathbf{X}_{\mathrm{cm}}$ the position of the center of mass. Thus with the force balance, we have for all $t>0$:

$$\frac{\mathrm{d}}{\mathrm{d}t}\mathbf{X}_N\left(t\right)=-k_r\left(\mathbf{X}_N\left(t\right)-\mathbf{X}_{\mathrm{eq}}\left(t\right)\right)-k_f\mathbf{u}\left(t,\mathbf{X}_N\left(t\right)\right) \tag{8.5}$$

with $k_r>0$ and $k_f>0$.

Thus, combining eqs. (8.1) to (8.5), the model in dimension 2 is given by:

$$\begin{cases}\mathbf{u}+\nabla P=0 & \text{in }\Omega\left(t\right), & \text{(8.6a)}\\ \mathrm{div}\left(\mathbf{u}\right)=0 & \text{in }\Omega\left(t\right), & \text{(8.6b)}\\ P=\gamma\kappa+\chi_c f_{\mathrm{act}}\left(\mu\right) & \text{on }\partial\Omega\left(t\right), & \text{(8.6c)}\\ V_n=\mathbf{u}\cdot\mathbf{n} & \text{on }\partial\Omega\left(t\right), & \text{(8.6d)}\\ \partial_t c\left(t,\mathbf{x}\right)=\Delta c\left(t,\mathbf{x}\right)-\left(1-a\right)\mathrm{div}\left[\mathbf{u}\left(t,\mathbf{x}\right)c\left(t,\mathbf{x}\right)\right] & \text{in }\Omega\left(t\right), & \text{(8.6e)}\\ \left[\nabla c\left(t,\mathbf{x}\right)+a\mathbf{u}\left(t,\mathbf{x}\right)c\left(t,\mathbf{x}\right)\right]\cdot\mathbf{n}=-\partial_t\mu\left(t,\mathbf{x}\right) & \text{on }\partial\Omega\left(t\right), & \text{(8.6f)}\\ \partial_t\mu\left(t,\mathbf{x}\right)=\alpha\left(\mathbf{X}_N\left(t\right),\mathbf{x}\right)c\left(t,\mathbf{x}\right)-\beta\mu\left(t,\mathbf{x}\right) & \text{on }\partial\Omega\left(t\right), & \text{(8.6g)}\\ \frac{\mathrm{d}}{\mathrm{d}t}\mathbf{X}_N\left(t\right)=-k_r\left(\mathbf{X}_N\left(t\right)-\mathbf{X}_{\mathrm{eq}}\left(t\right)\right)-k_f\mathbf{u}\left(t,\mathbf{X}_N\left(t\right)\right), & & \text{(8.6h)}\\ c\left(0,\mathbf{x}\right)=c^0\left(\mathbf{x}\right),\ \mu_\pm\left(0,\mathbf{x}\right)=\mu_\pm^0\left(\mathbf{x}\right),\ \mathbf{X}_N\left(0\right)=\mathbf{X}_N^0, & \mathbf{x}\in\partial\Omega\left(0\right), & \text{(8.6i)}\end{cases}$$

with c^0, $\mu_\pm^0$ and X_N^0 given.

8.1.2 . Model in dimension 1

We want to write an analogous problem in dimension 1 to the model (8.6). We keep the notations of the previous section. The cell is modeled by a segment $\left[b_-\left(t\right),b_+\left(t\right)\right]$. The incompressibility constraint impose that the length of the cell domain $b_+\left(t\right)-b_-\left(t\right)$ is constant in time. We assume to have $\left[b_-\left(0\right),b_+\left(0\right)\right]=\left[-1,1\right]$. Thus for all $t>0$, we have $b_+\left(t\right)-b_-\left(t\right)=2$.

We set $\mu_-(t) = \mu(b_-(t))$, $\mu_+(t) = \mu(b_+(t))$ and $\delta\mu(t) = \mu_-(t) - \mu_+(t)$. We also denote $\alpha_+(X_N(t)) = \alpha(X_N(t), b_+(t))$ and $\alpha_-(X_N(t)) = \alpha(X_N(t), b_-(t))$.

Moreover, we assume there exists $0 < d < 1$ such that α_+ is a continuous non increasing function such that for $x < b_+(t) - d$, $\alpha_+(x) = A$ and for $x > b_+(t)$, $\alpha_+(x) = \varepsilon$. On the contrary, we assume α_- to be a continuous non decreasing function such that for $x < b_-(t)$, $\alpha_-(x) = \varepsilon$ and for $x > b_-(t) + d$, $\alpha_-(x) = A$. We also assume that the dynamic at the two cell border is the same, then for all $x \in [b_-(t), b_+(t)]$ $\alpha_-(x) = \alpha_+(b_+(t) + b_-(t) - x)$. We assume α_+ and α_- to be Lipschitz functions. An example of such functions is given in fig. 8.1.

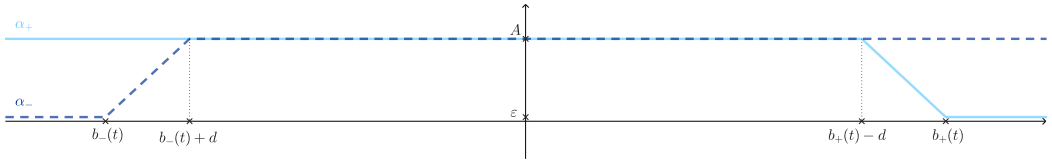

Figure 8.1: **Examples of the functions α_+ and α_-.**

In dimension 1, the problem on the fluid writes as:

$$\begin{cases} u + \partial_x P = 0 & \text{in }]b_-(t), b_+(t)[, \quad (8.7a) \\ \partial_x u = 0 & \text{in }]b_-(t), b_+(t)[, \quad (8.7b) \\ P = \chi_c f_{\text{act}}(\mu) & \text{on } \{b_-(t), b_+(t)\}, \quad (8.7c) \\ \dfrac{\mathrm{d}b_-}{\mathrm{d}t} = \dfrac{\mathrm{d}b_+}{\mathrm{d}t} = u. & \quad (8.7d) \end{cases}$$

From eq. (8.7b), there exists a function K_1 depending only of the time such that for all $x \in [b_-(t), b_+(t)]$ and $t > 0$:

$$u(t,x) = K_1(t).$$

Thus from it and eq. (8.7c), there exists a function K_2 depending only of the time such that for all $x \in [b_-(t), b_+(t)]$ and $t > 0$:

$$P(t,x) = -K_1(t)\, x + K_2(t).$$

Thus we deduce from eq. (8.7c), that for all $t > 0$ and $x \in [b_-(t), b_+(t)]$:

$$u(t,x) = \frac{\chi_c f_{\text{act}}(\mu_-(t)) - \chi_c f_{\text{act}}(\mu_+(t))}{b_+(t) - b_-(t)}.$$

Assuming that $f_{\text{act}}(\mu) = \mu$, we have for all $t > 0$ and $x \in [b_-(t), b_+(t)]$:

$$u(t,x) = \frac{\chi_c}{2}\delta\mu(t).$$

Then in dimension 1, the problem on the concentration of markers is given by:

$$\begin{aligned} &\partial_t c(t,x) = \partial^2_{xx} c(t,x) - (1-a)\,\partial_x\left[\frac{\chi_c}{2}\delta\mu(t)\, c(t,x)\right] && x \in]b_-(t), b_+(t)[, \\ &\partial_x c(t, b_+(t)) + \frac{a\chi_c}{2}\delta\mu(t)\, c(t, b_+(t)) = -\frac{\mathrm{d}}{\mathrm{d}t}\mu_+(t), \\ &\partial_x c(t, b_-(t)) + \frac{a\chi_c}{2}\delta\mu(t)\, c(t, b_-(t)) = \frac{\mathrm{d}}{\mathrm{d}t}\mu_-(t), \\ &\frac{\mathrm{d}}{\mathrm{d}t}\mu_\pm(t) = \alpha_\pm(X_N(t))\, c(t,x) - \beta\mu_\pm(t) && x \in \{b_-(t), b_+(t)\}. \end{aligned}$$

Thus, by setting $\eta = \dfrac{a\chi_c}{2}$, we have in the frame of reference of the cell:

$$\begin{aligned}
&\partial_t c(t,x) = \partial^2_{xx} c(t,x) + \partial_x \left[\eta\, \delta\mu(t)\, c(t,x)\right] && x \in]-1,1[\,,\\
&\partial_x c(t,\pm 1) + \eta\, \delta\mu(t)\, c(t,\pm 1) = \mp \frac{\mathrm{d}}{\mathrm{d}t}\mu_\pm(t)\,,\\
&\frac{\mathrm{d}}{\mathrm{d}t}\mu_\pm(t) = \alpha_\pm\left(X_N(t)\right) c(t,\pm 1) - \beta \mu_\pm(t)\,.
\end{aligned}$$

Finally, in the frame of reference of the substrate, the dynamic on the nucleus position writes:

$$\frac{\mathrm{d}}{\mathrm{d}t} X_N(t) = -k_1 \left(X_N(t) - \frac{b_+(t) - b_-(t)}{2} \right) - k_2 \delta\mu(t)\,,$$

with $k_1 = k_r$ and $k_2 = \dfrac{\chi_c}{2} k_f$. Then, in the frame of reference of the cell, the dynamic on the nucleus writes:

$$\frac{\mathrm{d}}{\mathrm{d}t} X_N(t) = -k_1 X_N(t) - k_2 \delta\mu(t)\,.$$

We can solve it explicitly and we have:

$$X_N(t) = X_N(0)\, e^{-k_1 t} - k_2 \int_0^t \delta\mu(s)\, e^{k_1(s-t)}\, \mathrm{d}s.$$

Finally the model studied in dimension 1 is the following:

$$\begin{cases}
\partial_t c(t,x) = \partial^2_{xx} c(t,x) + \partial_x \left[\eta\, \delta\mu(t)\, c(t,x)\right], & x \in]-1,1[\,, & \text{(8.8a)}\\
\partial_x c(t,\pm 1) + \eta\, \delta\mu(t)\, c(t,\pm 1) = \mp \dfrac{\mathrm{d}}{\mathrm{d}t}\mu_\pm(t)\,, & & \text{(8.8b)}\\
\dfrac{\mathrm{d}}{\mathrm{d}t}\mu_\pm(t) = \alpha_\pm\left(X_N(t)\right) c(t,\pm 1) - \beta\mu_\pm(t)\,, & & \text{(8.8c)}\\
X_N(t) = X_N^0 e^{-k_1 t} - k_2 \displaystyle\int_0^t \delta\mu(s)\, e^{k_1(s-t)}\, \mathrm{d}s, & & \text{(8.8d)}\\
c(0,x) = c^0(x)\,,\ \mu_\pm(0) = \mu_\pm^0,\ X_N(0) = X_N^0, & x \in]-1,1[\,, & \text{(8.8e)}
\end{cases}$$

with c^0, $\mu_\pm^0$ and X_N^0 given.

8.2 . Well-posedness of the model

In this section we prove the following result.

Proposition 8.2.1. *Assume that c^0 is such that $\int_{-1}^1 c^0(x) \log c^0(x)\, \mathrm{d}x < +\infty$. Assume moreover that $\mu_+^0, \mu_-^0 \in [0, M]$ are such that $\int_{-1}^1 c^0(x)\, \mathrm{d}x + \mu_+^0 + \mu_-^0 = M$. Assume also that $X_N^0 \in [-1,1]$. Then there exists a unique solution (c, μ_+, μ_-, X_N) to the problem (8.8) for all time.*

To prove proposition 8.2.1, as in Lepoutre and Meunier (2022), we will first study an uncoupled model associate to (8.8) and then use a fixed point argument. We use ideas similar to those in chapter 2.

8.2.1 . An uncoupled PDE

First, we study the following uncoupled PDE system where μ_+, μ_- and v are given and for all $t > 0$, $\alpha_\pm(t) = \alpha_\pm(X_N(t))$ with X_N given:

$$\begin{cases} \partial_t c(t,x) = \partial^2_{xx} c(t,x) + \partial_x [v(t)\, c(t,x)] & x \in [-1,1] \quad (8.9a) \\ \partial_x c(t,1) + v(t)\, c(t,1) = -(\alpha_+(t)\, c(t,1) - \beta\mu_+(t)) & \quad (8.9b) \\ \partial_x c(t,-1) + v(t)\, c(t,-1) = \alpha_-(t)\, c(t,-1) - \beta\mu_-(t) & \quad (8.9c) \\ c(0,x) = c^0(x) & x \in [-1,1] \quad (8.9d) \\ \mu_\pm(0) = \mu^0_\pm. & \quad (8.9e) \end{cases}$$

We assume c^0, μ^0_+ and μ^0_- to be such that:

$$\int_{-1}^{1} c^0(x)\, \mathrm{d}x + \mu^0_- + \mu^0_+ = M.$$

We want to prove that this problem admits a global solution.

For smooth μ_+, μ_-, α_+, α_-, v and c^0, (8.9) is a parabolic problem and then there exists a local solution c defined over $[0,T]$.

Lemma 8.2.2. *Assume $c^0 \geq 0$ and for all $t \geq 0$, $\mu_\pm(t) \geq 0$, $\alpha_\pm(t) \geq 0$. Let c be a solution of (8.9) define on $[0,T] \times [-1,1]$. Then c is nonnegative.*

Proof. Let c be a solution of (8.9). We denote $c_- = \min(c, 0)$. We want to prove that $c_- = 0$. Using the Stampacchia argument, we have :

$$\begin{aligned} \frac{1}{2}\frac{\mathrm{d}}{\mathrm{d}t}\|c_-(t)\|^2_{L^2} &= \int_{-1}^{1} \partial_t c(t,x) \cdot c_-(t,x)\, \mathrm{d}x \\ &= -[\alpha_+(t)\, c(t,1) - \beta\mu_+(t)]\, c_-(t,1) - [\alpha_-(t)\, c(t,-1) - \beta\mu_-(t)]\, c_-(t,-1) \\ &\quad - \int_{-1}^{1} (\partial_x c_-(t,x))^2 + v(t)\, c(t,x)\, \partial_x c_-(t,x)\, \mathrm{d}x \\ &= -\alpha_+(t)\, (c_-(t,1))^2 - \alpha_-(t)\, (c_-(t,-1))^2 + \beta\mu_+(t)\, c_-(t,1) \\ &\quad + \beta\mu_-(t)\, c_-(t,-1) - \|\partial_x c_-(t)\|^2_{L^2} - \int_{-1}^{1} v(t)\, c_-(t,x)\, \partial_x c_-(t,x)\, \mathrm{d}x \\ &\leq -\|\partial_x c_-(t)\|^2_{L^2} - \int_{-1}^{1} v(t)\, c_-(t,x)\, \partial_x c_-(t,x)\, \mathrm{d}x \\ &\leq \frac{1}{4}|v(t)|^2 \|c_-(t)\|^2_{L^2}. \end{aligned}$$

We also have $\|c_-(0)\|^2_{L^2} = 0$. Using Gronwall's lemma, we have that for all $t \in [0,T]$, $\|c_-(t)\|^2_{L^2} = 0$. Thus for all $t \in [0,T]$ and $x \in [-1,1]$, we have $c(t,x) \geq 0$. □

Lemma 8.2.3. *Assume that $c^0 \in L^1(-1,1)$ is a positive function such that $\int_{-1}^{1} c^0(x) \log c^0(x)\, \mathrm{d}x < +\infty$. Assume also that $\mu_\pm \in C^0(\mathbb{R}_+)$ satisfy for all $t > 0$, $0 < \mu^0_\pm e^{-\beta t} \leq \mu_\pm(t) \leq M$. Assume moreover that $v \in C^0(\mathbb{R}_+) \cap L^\infty(\mathbb{R}_+)$. Then the solution of the uncoupled system (8.9) exists globally in $L^\infty_{loc}(\mathbb{R}_+, L\log L(-1,1)) \cap L^1_{loc}(\mathbb{R}_+, W^{1,1}(-1,1))$.*

Proof. First, for all $t \geq 0$, we have:

$$\begin{aligned}\frac{\mathrm{d}}{\mathrm{d}t}\int_{-1}^{1} c(t,x)\ \mathrm{d}x &= \int_{-1}^{1} \partial_t c(t,x)\ \mathrm{d}x \\ &= -\left(\alpha_+(t)\, c(t,1) - \beta\mu_+(t)\right) - \left(\alpha_-(t)\, c(t,-1) - \beta\mu_-(t)\right) \\ &\leq \beta\left(\mu_+(t) + \mu_-(t)\right) \\ &\leq 2\beta M.\end{aligned}$$

Thus, for all $t \geq 0$, we have:

$$\int_{-1}^{1} c(t,x)\ \mathrm{d}x \leq \int_{-1}^{1} c^0(x)\ \mathrm{d}x + 2\beta M t.$$

Using the convexity of the function $x \mapsto (\alpha_\pm(t)\, x - \beta\mu_\pm(t)) \log x$, we have that for all $t \geq 0$ and $x \in [-1,1]$:

$$\left(\alpha_\pm(t)\, c(t,x) - \beta\mu_\pm(t)\right)\log c(t,x) - \left(\alpha_\pm(t) - \beta\mu_\pm(t)\right)\log\left(\frac{\beta}{\alpha_\pm(t)}\mu_\pm(t)\right) \geq 0.$$

We also have:

$$\begin{aligned}&\frac{\mathrm{d}}{\mathrm{d}t}\int_{-1}^{1} c(t,x)\log c(t,x) - c(t,x)\ \mathrm{d}x \\ &= \int_{-1}^{1} \partial_t c(t,x)\log c(t,x)\ \mathrm{d}x \\ &= -\left(\alpha_+(t)\, c(t,1) - \beta\mu_+(t)\right)\log c(t,1) - \left(\alpha_-(t)\, c(t,-1) - \beta\mu_-(t)\right)\log c(t,-1) \\ &\quad - \int_{-1}^{1} \left(c(t,x)\,\partial_x \log c(t,x) + v(t)\, c(t,x)\right)\partial_x \log c(t,x)\ \mathrm{d}x \\ &\leq -\left(\alpha_+(t) - \beta\mu_+(t)\right)\log\left(\frac{\beta}{\alpha_+(t)}\mu_+(t)\right) - \left(\alpha_-(t) - \beta\mu_-(t)\right)\log\left(\frac{\beta}{\alpha_-(t)}\mu_-(t)\right) \\ &\quad - \int_{-1}^{1} c(t,x)\left|\partial_x \log c(t,x)\right|^2\ \mathrm{d}x - \int_{-1}^{1} c(t,x)\, v(t)\,\partial_x \log c(t,x)\ \mathrm{d}x \\ &\leq C_1 + 2A\beta t - \frac{1}{2}\int_{-1}^{1} c(t,x)\left|\partial_x \log c(t,x)\right|^2\ \mathrm{d}x + \frac{1}{2}\left|v(t)\right|^2 \int_{-1}^{1} c(t,x)\ \mathrm{d}x \\ &\leq C_1 + 2A\beta t - \frac{1}{2}\int_{-1}^{1} c(t,x)\left|\partial_x \log c(t,x)\right|^2\ \mathrm{d}x \\ &\quad + \frac{1}{2}\|v\|_{L^\infty}^2\left(\int_{-1}^{1} c^0(x)\ \mathrm{d}x + 2M\beta t\right),\end{aligned} \tag{8.10}$$

with $C_1 > 0$.

Then, integrating the previous inequality, we have:

$$\begin{aligned}\int_{-1}^{1} c(t,x)\log c(t,x)\ \mathrm{d}x &\leq \int_{-1}^{1} c^0(x)\log c^0(x)\ \mathrm{d}x + C_1 t + A\beta t^2 \\ &\quad + \frac{1}{2}\|v\|_{L^\infty}^2\left(t\int_{-1}^{1} c^0(x)\ \mathrm{d}x + M\beta t^2\right) \\ &\leq C_2\left(1 + t^2\right),\end{aligned}$$

with $C_2 > 0$.

We can apply lemma 2.2.2 and we have:

$$\int_{-1}^{1} c\left(t,x\right)\left|\log c\left(t,x\right)\right| \,\mathrm{d}x \leq C_3\left(1+t^2\right),$$

with $C_3 > 0$.

Then, integrating eq. (8.10), we also have:

$$\begin{aligned}\int_0^t \int_{-1}^{1} c\left(s,x\right)\left|\partial_x \log c\left(s,x\right)\right|^2 \,\mathrm{d}x\,\mathrm{d}s &\leq C_4\left(1+t^2\right) - \int_{-1}^{1} c\left(t,x\right)\log c\left(t,x\right)\,\mathrm{d}x \\ &\leq C_4\left(1+t^2\right) + \int_{-1}^{1} c\left(t,x\right)\left|\log c\left(t,x\right)\right|\,\mathrm{d}x \\ &\leq C_5\left(1+t^2\right),\end{aligned}$$

with $C_4 > 0$ and $C_5 > 0$.

Thus, finally, we have:

$$\begin{aligned}\int_0^t \int_{-1}^{1} \left|\partial_x c\left(s,x\right)\right| \,\mathrm{d}x\,\mathrm{d}s &= \int_0^t \int_{-1}^{1} c\left(s,x\right)\left|\partial_x \log c\left(s,x\right)\right| \,\mathrm{d}x\,\mathrm{d}s \\ &\leq \left(\int_0^t \int_{-1}^{1} c\left(s,x\right)\,\mathrm{d}x\,\mathrm{d}s\right)^{\frac{1}{2}} \left(\int_0^t \int_{-1}^{1} c\left(s,x\right)\left|\partial_x \log c\left(s,x\right)\right|^2 \,\mathrm{d}x\,\mathrm{d}s\right)^{\frac{1}{2}} \\ &\leq C_6\left(1+t^2\right),\end{aligned}$$

with $C_6 > 0$ and this leads to the global existence of c. □

Remark 8.2.4. *This prooff generalizes the one made in section 2.2.2 to attachment rate that depend on time.*

8.2.2 . Fixed point mapping

8.2.2.1 . Useful results

Let c_1 and c_2 be two solutions of (8.9) with two different inputs $\left(\mu_{\pm}^1, X_N^1, v^1\right)$ and $\left(\mu_{\pm}^2, X_N^2, v^2\right)$. We denote $\alpha_{\pm}^1 = \alpha_{\pm} \circ X_N^1$ and $\alpha_{\pm}^2 = \alpha_{\pm} \circ X_N^2$. As in Lepoutre and Meunier (2022) or in section 2.2.3 to compare these two solutions, we introduce the Gajewski metric:

$$d_G\left(c_1,c_2\right) = \int_{-1}^{1} h\left(c_1\right) + h\left(c_2\right) - 2h\left(\frac{c_1+c_2}{2}\right)\,\mathrm{d}x$$

where h is the following function:

$$h\left(a\right) = a\log a - a + 1.$$

We define the function Δ_h by:

$$\Delta_h\left(c_1,c_2\right) = h\left(c_1\right) + h\left(c_2\right) - 2h\left(\frac{c_1+c_2}{2}\right).$$

We recall the following lemma from Lepoutre and Meunier (2022).

Lemma 8.2.5. *For all $a, b > 0$ and c_1, c_2 positive functions, the following inequalities hold*

$$0 \leq \frac{1}{4}\frac{\left(b-a\right)^2}{a+b} \leq \frac{1}{4}\frac{\left(b-a\right)^2}{\max\left(a,b\right)} \leq \Delta_h\left(a,b\right) \leq \frac{1}{4}\frac{\left(b-a\right)^2}{\min\left(a,b\right)}$$

and

$$d_G(c_1, c_2) \geq \frac{1}{4} \frac{\left(\int_{-1}^{1} c_1 \, \mathrm{d}x - \int_{-1}^{1} c_2 \, \mathrm{d}x\right)^2}{\int_{-1}^{1} c_1 \, \mathrm{d}x + \int_{-1}^{1} c_2 \, \mathrm{d}x}.$$

We introduce the following notations $c_m = \dfrac{c_1 + c_2}{2}$, $q_1 = \dfrac{c_1}{c_m}$ and $q_2 = \dfrac{c_2}{c_m}$.

Lemma 8.2.6. *For all a_1, a_2 such that $0 < \varepsilon \leq a_1, a_2 \leq A$ and c_1, c_2 positive functions, there exists a constant $C(\varepsilon, A) > 0$ such that:*

$$-\left[a_1 c_1 \log q_1 + a_2 c_2 \log q_2\right] \leq -\Delta_h\left(a_1 c_1, a_2 c_2\right) + C(A, \varepsilon)\left(a_1 c_1 + a_2 c_2\right)\left|a_2 - a_1\right|^2.$$

Proof. We introduce the following notations for $i \in \{1, 2\}$:

$$q_i^a = \frac{2 a_i c_i}{a_1 c_1 + a_2 c_2},$$

$$p_i = \frac{a_i c_i}{a_1 c_1 + a_2 c_2}$$

and thus for $j \neq i$ we have:

$$\frac{q_i}{q_i^a} = \frac{a_1 c_1 + a_2 c_2}{a_i (c_1 + c_2)} = \frac{a_j}{a_2 p_1 + a_1 p_2},$$

where we recall that $q_i = \frac{2 c_i}{c_1 + c_2}$. We can also notice that $p_1 + p_2 = 1$.

We have:

$$\begin{aligned} a_1 c_1 \log q_1 + a_2 c_2 \log q_2 &= a_1 c_1 \left(\log q_1^a + \log \frac{q_1}{q_1^a}\right) + a_2 c_2 \left(\log q_2^a + \log \frac{q_2}{q_2^a}\right), \\ &= \Delta_h(a_1 c_1, a_2 c_2) + \left(a_1 c_1 + a_2 c_2\right)\left(p_1 \log a_2 + p_2 \log a_1 - \log(a_2 p_1 + a_1 p_2)\right). \end{aligned}$$

Denoting $\lambda = \log a_2 - \log a_1$, we have:

$$\log(a_2 p_1 + a_1 p_2) - p_1 \log a_2 - p_2 \log a_1 = \log(e^{\lambda} p_1 + p_2) - p_1 \lambda.$$

By studying the derivative the function $x \mapsto \log(e^{\lambda} x + 1 - x) - x\lambda$ we found that this function admits a maximum in $x = \frac{1}{\lambda} - \frac{1}{e^{\lambda} - 1} \in [0, 1]$. Thus we have:

$$\log(a_2 p_1 + a_1 p_2) - p_1 \log a_2 - p_2 \log a_1 \leq \log\left(\frac{e^{\lambda} - 1}{\lambda}\right) - 1 + \frac{\lambda}{e^{\lambda} - 1}.$$

Using a Taylor-Lagrange inequality, it follows that:

$$\log(a_2 p_1 + a_1 p_2) - p_1 \log a_2 - p_2 \log a_1 \leq C(A, \varepsilon)\left|a_2 - a_1\right|^2.$$

Hence the result. □

Lemma 8.2.7. *There exists $C(A,\varepsilon)>0$ such that for all $t>0$ the following inequality hold:*

$$\begin{aligned}\frac{\mathrm{d}}{\mathrm{d}t}d_G(c_1,c_2)(t) \leq\ & \beta\left(\Delta_h\left(\mu_+^1(t),\mu_+^2(t)\right)+\Delta_h\left(\mu_-^1(t),\mu_-^2(t)\right)\right)\\ &-\Delta_h\left(\alpha_+^1(t)c_1(t,1),\alpha_+^2(t)c_2(t,1)\right)\\ &-\Delta_h\left(\alpha_-^1(t)c_1(t,-1),\alpha_-^2(t)c_2(t,-1)\right)\\ &+C(A,\varepsilon)\left(\alpha_+^1(t)c_1(t,1)+\alpha_+^2(t)c_2(t,1)\right)\left|\alpha_+^2(t)-\alpha_+^1(t)\right|^2\\ &+C(A,\varepsilon)\left(\alpha_-^1(t)c_1(t,-1)+\alpha_-^2(t)c_2(t,-1)\right)\left|\alpha_-^2(t)-\alpha_-^1(t)\right|^2\\ &-\frac{3}{4}\int_{-1}^1 c_1(t,x)\left|\partial_x\log q_1(t,x)\right|^2+c_2(t,x)\left|\partial_x\log q_2(t,x)\right|^2\,\mathrm{d}x\\ &+\frac{1}{2}\left(v^1(t)-v^2(t)\right)^2\int_{-1}^1 c_m(t,x)\,\mathrm{d}x.\end{aligned}$$

Proof. We have

$$\begin{aligned}\frac{\mathrm{d}}{\mathrm{d}t}d_G(c_1,c_2)(t) &= \int_{-1}^1 \partial_t c_1(t,x)\log q_1(t,x)+\partial_t c_2(t,x)\log q_2(t,x)\,\mathrm{d}x\\ &=\sum_{i=1}^2 \beta\left[\mu_+^i(t)\log q_i(t,1)+\mu_-^i\log q_i(t,-1)\right]\\ &\quad-\left[c_1(t,1)\alpha_+^1(t)\log q_1(t,1)+c_2(t,1)\alpha_+^2(t)\log q_2(t,1)\right]\\ &\quad-\left[c_1(t,-1)\alpha_-^1(t)\log q_1(t,-1)+c_2(t,-1)\alpha_-^2(t)\log q_2(t,-1)\right]\\ &\quad-\sum_{i=1}^2\int_{-1}^1 c_m(t,x)\left(\partial_x\log c_i(t,x)+v^i(t)\right)\partial_x q_i(t,x)\,\mathrm{d}x.\end{aligned}$$

We notice that the function $q\mapsto \mu_+\log q+\mu_-\log(2-q)$ reaches its maximum for the value $q^*=\dfrac{2\mu_+}{\mu_++\mu_-}$. Then we have:

$$\sum_{i=1}^2\beta\ \left[\mu_+^i(t)\log q_i(t,1)+\mu_-^i\log q_i(t,-1)\right]\leq\beta\left(\Delta_h\left(\mu_+^1(t),\mu_+^2(t)\right)+\Delta_h\left(\mu_-^1(t),\mu_-^2(t)\right)\right).$$

We also have

$$\begin{aligned}&-\int_{-1}^1 c_m(t,x)\left(v^1(t)-v^2(t)\right)\partial_x q_1(t,x)\,\mathrm{d}x\\ &=-\frac{1}{2}\int_{-1}^1 c_1(t,x)\left(v^1(t)-v^2(t)\right)\partial_x\log q_1(t,x)\,\mathrm{d}x\\ &\quad+\frac{1}{2}\int_{-1}^1 c_2(t,x)\left(v^1(t)-v^2(t)\right)\partial_x\log q_2(t,x)\,\mathrm{d}x\\ &\leq\frac{1}{4}\int_{-1}^1 c_1(t,x)\left(v^1(t)-v^2(t)\right)^2\mathrm{d}x+\frac{1}{4}c_1(t,x)\left(\partial_x\log q_1(t,x)\right)^2\mathrm{d}x\\ &\quad+\frac{1}{4}\int_{-1}^1 c_2(t,x)\left(v^1(t)-v^2(t)\right)^2\mathrm{d}x+\frac{1}{4}c_2(t,x)\left(\partial_x\log q_2(t,x)\right)^2\mathrm{d}x\\ &\leq\frac{1}{2}\left(v^1(t)-v^2(t)\right)^2\int_{-1}^1 c_m(t,x)\,\mathrm{d}x\\ &\quad+\frac{1}{4}\int_{-1}^1 c_1(t,x)\left|\partial_x\log q_1(t,x)\right|^2+c_2(t,x)\left|\partial_x\log q_2(t,x)\right|^2\mathrm{d}x\end{aligned}$$

and

$$\frac{c_1+c_2}{q_1\left(2-q_1\right)}\left|\partial_x q_1\right|^2=c_1\left|\partial_x \log q_1\right|^2+c_2\left|\partial_x \log q_2\right|^2.$$

Finally, using the result of lemma 8.2.6, we have the following upper bound:

$$\begin{aligned}
&-\left[c_1(t,1)\,\alpha_+^1(t)\log q_1(t,1)+c_2(t,1)\,\alpha_+^2(t)\log q_2(t,1)\right]\\
&-\left[c_1(t,-1)\,\alpha_-^1(t)\log q_1(t,-1)+c_2(t,-1)\,\alpha_-^2(t)\log q_2(t,-1)\right]\\
&\quad\leq-\Delta_h\left(\alpha_+^1(t)\,c_1(t,1),\alpha_+^2(t)\,c_2(t,1)\right)-\Delta_h\left(\alpha_-^1(t)\,c_1(t,-1),\alpha_-^2(t)\,c_2(t,-1)\right)\\
&\qquad+C(A,\varepsilon)\left(\alpha_+^1(t)\,c_1(t,1)+\alpha_+^2(t)\,c_2(t,1)\right)\left|\alpha_+^2(t)-\alpha_+^1(t)\right|^2\\
&\qquad+C(A,\varepsilon)\left(\alpha_-^1(t)\,c_1(t,-1)+\alpha_-^2(t)\,c_2(t,-1)\right)\left|\alpha_-^2(t)-\alpha_-^1(t)\right|^2.
\end{aligned}$$

By combining all this, the desired result is obtained. □

8.2.2.2 . The fixed point mapping

For a fixed $T>0$, we define the following space $\mathcal{X}$

$$\mathcal{X}=\left\{\begin{array}{l}(\mu_+,\mu_-,X_N)\in C(0,T),\forall t\in(0,T)\\ 0<\mu_\pm^0e^{-\beta t}\leq\mu_\pm(t)\leq M \text{ and } -1\leq X_N(t)\leq 1\end{array}\right\}.$$

We want to study (8.9) with $v(t)=\eta\left(\mu_-(t)-\mu_+(t)\right)$. From the previous section, we know that, with this choice of velocity, (8.9) admits a global solution.

We also define:

$$\nu_\pm(t)=\mu_\pm^0e^{-\beta t}+\int_0^t\alpha_\pm\left(X_N(s)\right)e^{\beta(s-t)}c(s,\pm1)\,\mathrm{d}s$$

and the truncation function χ_μ such that for all $x\in\mathbb{R}$:

$$\chi_\mu(x)=\left\{\begin{array}{ll}0 & \text{if } x<0,\\ x & \text{if } 0\leq x\leq M,\\ 1 & \text{if } x>M.\end{array}\right.$$

We define the truncation function χ_{x} such that for all $x\in\mathbb{R}$:

$$\chi_{\mathrm{x}}(x)=\left\{\begin{array}{ll}-1 & \text{if } x<-1,\\ x & \text{if } -1\leq x\leq 1,\\ 1 & \text{if } x>1.\end{array}\right.$$

Finally we define the mapping F by:

$$\begin{array}{rccc}F: & \mathcal{X} & \longrightarrow & \mathcal{X}\\ & (\mu_+,\mu_-,X_N) & \longmapsto & \left(\chi_\mu(\nu_+),\chi_\mu(\nu_-),\chi_{\mathrm{x}}(X_N)\right).\end{array}$$

We denote by F^n the function composed n times with itself, that is $F^n=F\circ F\circ\cdots\circ F$. We assume that the two solutions c_1 and c_2 obtained with different inputs $\left(\mu_\pm^1,X_N^1,v^1\right)$ and $\left(\mu_\pm^2,X_N^2,v^2\right)$ are obtained with the same initial conditions c^0, μ_+^0, μ_-^0 and $X_N(0)$.

Proposition 8.2.8. *For all $\left(\mu_+^1,\mu_-^1,X_N^1\right),\left(\mu_+^2,\mu_-^2,X_N^2\right)\in X$, there exists $C(T)$ such that:*

$$\left\|F^n\left(\mu_+^1,\mu_-^1,X_N^1\right)-F^n\left(\mu_+^2,\mu_-^2,X_N^2\right)\right\|_{\mathcal{X}}\leq\frac{\left(C(T)\,T\right)^n}{n!}\left\|\left(\mu_+^1,\mu_-^1,X_N^1\right)-\left(\mu_+^2,\mu_-^2,X_N^2\right)\right\|_{\mathcal{X}}.$$

Proof. Let $\left(\mu_+^1, \mu_-^1, X_N^1\right)$, $\left(\mu_+^2, \mu_-^2, X_N^2\right)$ be two elements of $\mathcal{X}$. For all $t > 0$ and $i \in \{1, 2\}$, we denote $\alpha_\pm^i(t) = \alpha_\pm\left(X_N^i(t)\right)$. We have:

$$\begin{aligned}
&\left\|F\left(\mu_+^1, \mu_-^1, X_N^1\right) - F\left(\mu_+^2, \mu_-^2, X_N^2\right)\right\|_{\mathcal{X}}^2 \\
&\qquad = \int_0^T \left(\chi_\mu\left(\nu_+^1(t)\right) - \chi_\mu\left(\nu_+^2(t)\right)\right)^2 + \left(\chi_\mu\left(\nu_-^1(t)\right) - \chi_\mu\left(\nu_-^2(t)\right)\right)^2 \\
&\qquad\qquad + \left(\chi_{\mathsf{x}}\left(X_N^1(t)\right) - \chi_{\mathsf{x}}\left(X_N^2(t)\right)\right)^2 \mathrm{d}t
\end{aligned}$$

Integrating the inequality of lemma 8.2.7, we have:

$$\begin{aligned}
&d_G(c_1, c_2)(t) - d_G(c_1, c_2)(0) \\
&\leq \int_0^t \beta\left(\Delta_h\left(\mu_+^1(s), \mu_+^2(s)\right) + \Delta_h\left(\mu_-^1(s), \mu_-^2(s)\right)\right) \mathrm{d}s \\
&\quad - \int_0^t \Delta_h\left(\alpha_+^1(s) c_1(s, 1), \alpha_+^2(s) c_2(s, 1)\right) - \Delta_h\left(\alpha_-^1(s) c_1(s, -1), \alpha_-^2(s) c_2(s, -1)\right) \mathrm{d}s \\
&\quad + \int_0^t C(A, \varepsilon)\left(\alpha_+^1(s) c_1(s, 1) + \alpha_+^2(s) c_2(s, 1)\right)\left|\alpha_+^2(s) - \alpha_+^1(s)\right|^2 \mathrm{d}s \\
&\quad + \int_0^t C(A, \varepsilon)\left(\alpha_-^1(s) c_1(s, -1) + \alpha_-^2(s) c_2(s, -1)\right)\left|\alpha_-^2(s) - \alpha_-^1(s)\right|^2 \mathrm{d}s \\
&\quad - \frac{3}{4}\int_0^t \int_{-1}^1 c_1(s, x)\left|\partial_x \log q_1(s, x)\right|^2 + c_2(s, x)\left|\partial_x \log q_2(s, x)\right|^2 \mathrm{d}x\,\mathrm{d}s \\
&\quad + \frac{1}{2}\int_0^t \left(v^1(s) - v^2(s)\right)^2 \int_{-1}^1 c_m(s, x) \mathrm{d}x\,\mathrm{d}s.
\end{aligned}$$

Since the initial conditions are the same, we have $d_G(c_1, c_2)(t) \geq 0$ and $d_G(c_1, c_2)(0) = 0$. It leads to:

$$\begin{aligned}
&\int_0^t \Delta_h\left(\alpha_+^1(s) c_1(s, 1), \alpha_+^2(s) c_2(s, 1)\right) + \Delta_h\left(\alpha_-^1(s) c_1(s, -1), \alpha_-^2(s) c_2(s, -1)\right) \mathrm{d}s \\
&\quad \leq \int_0^t \beta\left(\Delta_h\left(\mu_+^1(s), \mu_+^2(s)\right) + \Delta_h\left(\mu_-^1(s), \mu_-^2(s)\right)\right) \mathrm{d}s \\
&\qquad + \int_0^t C(A, \varepsilon)\left(\alpha_+^1(s) c_1(s, 1) + \alpha_+^2(s) c_2(s, 1)\right)\left|\alpha_+^2(s) - \alpha_+^1(s)\right|^2 \mathrm{d}s \\
&\qquad + \int_0^t C(A, \varepsilon)\left(\alpha_-^1(s) c_1(s, -1) + \alpha_-^2(s) c_2(s, -1)\right)\left|\alpha_-^2(s) - \alpha_-^1(s)\right|^2 \mathrm{d}s \\
&\qquad + \frac{1}{2}\int_0^t \left(v^1(s) - v^2(s)\right)^2 \int_{-1}^1 c_m(s, x) \mathrm{d}x\,\mathrm{d}s.
\end{aligned}$$

Using the result of lemma 8.2.5, we have:

$$\Delta_h\left(\mu_\pm^1(s), \mu_\pm^2(s)\right) \leq \frac{e^{\beta s}}{4\mu_\pm^0}\left(\mu_\pm^1(s) - \mu_\pm^2(s)\right)^2.$$

Using the border condition (8.8c), we have:

$$\begin{aligned}
\frac{\mathrm{d}}{\mathrm{d}t}\int_{-1}^1 c_1(s, x) + c_2(s, x) \mathrm{d}x &\leq \beta\left(\mu_+^1(s) - \mu_-^1(s) + \mu_+^2(s) - \mu_-^2(s)\right) \\
&\leq 4\beta M.
\end{aligned}$$

This leads to:

$$\begin{aligned}
&\left\|\alpha_{\pm}^{1}(\cdot)\, c_1(\cdot,\pm 1)+\alpha_{\pm}^{2}(\cdot)\, c_2(\cdot,\pm 1)\right\|_{L^{\infty}([0,t])}\\
&\quad\leq \sup_{s\in[0,t]}\left|\beta\left(\mu_{+}^{1}(s)-\mu_{-}^{1}(s)+\mu_{+}^{2}(s)-\mu_{-}^{2}(s)\right)-\frac{\mathrm{d}}{\mathrm{d}t}\int_{-1}^{1} c_1(s,x)+c_2(s,x)\,\mathrm{d}x\right|\\
&\quad\leq \sup_{s\in[0,t]}\left[\left|\beta\left(\mu_{+}^{1}(s)-\mu_{-}^{1}(s)+\mu_{+}^{2}(s)-\mu_{-}^{2}(s)\right)\right|+\left|\frac{\mathrm{d}}{\mathrm{d}t}\int_{-1}^{1} c_1(s,x)+c_2(s,x)\,\mathrm{d}x\right|\right]\\
&\quad\leq 8\beta M.
\end{aligned}$$

Thus using Hölder inequality, we have:

$$\begin{aligned}
&\int_0^t\left(\alpha_{\pm}^{1}(s)\, c_1(s,\pm 1)+\alpha_{\pm}^{2}(s)\, c_2(s,\pm 1)\right)\left|\alpha_{\pm}^{2}(s)-\alpha_{\pm}^{1}(s)\right|^2\,\mathrm{d}s\\
&\quad\leq 8\beta M\int_0^t\left|\alpha_{\pm}^{1}(s)-\alpha_{\pm}^{2}(s)\right|^2\,\mathrm{d}s.
\end{aligned}$$

Hence:

$$\begin{aligned}
&\int_0^t \Delta_h\left(\alpha_{+}^{1}(s)\, c_1(s,1),\alpha_{+}^{2}(s)\, c_2(s,1)\right)+\Delta_h\left(\alpha_{-}^{1}(s)\, c_1(s,-1),\alpha_{-}^{2}(s)\, c_2(s,-1)\right)\,\mathrm{d}s\\
&\quad\leq C_1(t)\int_0^t\left(\mu_{+}^{1}(s)-\mu_{+}^{2}(s)\right)^2+\left(\mu_{-}^{1}(s)-\mu_{-}^{2}(s)\right)^2\,\mathrm{d}s\\
&\qquad+8\beta MC(A,\varepsilon)\int_0^t\left(\alpha_{+}^{1}(s)-\alpha_{+}^{2}(s)\right)^2+\left(\alpha_{-}^{1}(s)-\alpha_{-}^{2}(s)\right)^2\,\mathrm{d}s,
\end{aligned}\tag{8.11}$$

with $C_1(t)=\max\left(\frac{e^{\beta t}}{4\mu_{+}^{0}},\frac{e^{\beta t}}{4\mu_{-}^{0}},\eta^2\int_{-1}^{1}c^0(x)\,\mathrm{d}x+2\eta^2\beta Mt\right)$.

Then using a Cauchy-Schwarz inequality, we have:

$$\begin{aligned}
&\left(\int_0^t\left(\alpha_{\pm}^{1}(s)\, c_1(s,\pm 1)-\alpha_{\pm}^{2}(s)\, c_2(s,\pm 1)\right)e^{\beta(s-t)}\,\mathrm{d}s\right)^2\\
&\leq\int_0^t\frac{\left(\alpha_{\pm}^{1}(s)\, c_1(s,\pm 1)-\alpha_{\pm}^{2}(s)\, c_2(s,\pm 1)\right)^2}{\alpha_{\pm}^{1}(s)\, c_1(s,\pm 1)+\alpha_{\pm}^{2}(s)\, c_2(s,\pm 1)}\,\mathrm{d}s\cdot\int_0^t\left(\alpha_{\pm}^{1}(s)\, c_1(s,\pm 1)+\alpha_{\pm}^{2}(s)\, c_2(s,\pm 1)\right)e^{2\beta(s-t)}\,\mathrm{d}s\\
&\leq\int_0^t\frac{\left(\alpha_{\pm}^{1}(s)\, c_1(s,\pm 1)-\alpha_{\pm}^{2}(s)\, c_2(s,\pm 1)\right)^2}{\alpha_{\pm}^{1}(s)\, c_1(s,\pm 1)+\alpha_{\pm}^{2}(s)\, c_2(s,\pm 1)}\,\mathrm{d}s\cdot\int_0^t\alpha_{\pm}^{1}(s)\, c_1(s,\pm 1)+\alpha_{\pm}^{2}(s)\, c_2(s,\pm 1)\,\mathrm{d}s\\
&\leq 4\beta Mt\int_0^t\Delta_h\left(\alpha_{\pm}^{1}(s)\, c_1(s,\pm 1),\alpha_{\pm}^{2}(s)\, c_2(s,\pm 1)\right)\,\mathrm{d}s.
\end{aligned}$$

Which combined with eq. (8.11) leads to:

$$\begin{aligned}
&\left(\int_0^t\left(\alpha_{+}^{1}(s)\, c_1(s,1)-\alpha_{+}^{2}(s)\, c_2(s,1)\right)e^{\beta(t-s)}\,\mathrm{d}s\right)^2+\left(\int_0^t\left(\alpha_{-}^{1}(s)\, c_1(s,-1)-\alpha_{-}^{2}(s)\, c_2(s,-1)\right)e^{\beta(t-s)}\,\mathrm{d}s\right)^2\\
&\quad\leq C_2(t)\int_0^t\left(\mu_{+}^{1}(s)-\mu_{+}^{2}(s)\right)^2+\left(\mu_{-}^{1}(s)-\mu_{-}^{2}(s)\right)^2\,\mathrm{d}s\\
&\qquad+C_3(t)\int_0^t\left(\alpha_{+}^{1}(s)-\alpha_{+}^{2}(s)\right)^2+\left(\alpha_{-}^{1}(s)-\alpha_{-}^{2}(s)\right)^2\,\mathrm{d}s,
\end{aligned}$$

where $C_2(t)=C_1(t)\cdot 4\beta Mt$ and $C_3(t)=8\beta MC(A,\varepsilon)$.

Then we have:

$$\begin{aligned}
&\left(\chi_\mu\left(\nu_+^1(t)\right)-\chi_\mu\left(\nu_+^2(t)\right)\right)^2+\left(\chi_\mu\left(\nu_-^1(t)\right)-\chi_\mu\left(\nu_-^2(t)\right)\right)^2\\
&\leq\left(\nu_+^1(t)-\nu_+^2(t)\right)^2+\left(\nu_-^1(t)-\nu_-^2(t)\right)^2\\
&\leq\left(\int_0^t\left(\alpha_+^1(s)\,c_1(s,1)-\alpha_+^2(s)\,c_2(s,1)\right)e^{\beta(s-t)}\,\mathrm{d}s\right)^2\\
&\quad+\left(\int_0^t\left(\alpha_-^1(s)\,c_1(s,-1)-\alpha_-^2(s)\,c_2(s,-1)\right)e^{\beta(s-t)}\,\mathrm{d}s\right)^2\\
&\leq C_2(t)\int_0^t\left(\mu_+^1(s)-\mu_+^2(s)\right)^2+\left(\mu_-^1(s)-\mu_-^2(s)\right)^2\,\mathrm{d}s\\
&\quad+C_3(t)\int_0^t\left(\alpha_+^1(s)-\alpha_+^2(s)\right)^2+\left(\alpha_-^1(s)-\alpha_-^2(s)\right)^2\,\mathrm{d}s.
\end{aligned}$$

Using the fact that $\alpha_\pm$ are K-Lipschitz functions, we have:

$$\begin{aligned}
&\left(\chi_\mu\left(\nu_+^1(t)\right)-\chi_\mu\left(\nu_+^2(t)\right)\right)^2+\left(\chi_\mu\left(\nu_-^1(t)\right)-\chi_\mu\left(\nu_-^2(t)\right)\right)^2\\
&\leq C_2(t)\int_0^t\left(\mu_+^1(s)-\mu_+^2(s)\right)^2+\left(\mu_-^1(s)-\mu_-^2(s)\right)^2\,\mathrm{d}s\\
&\quad+2KC_3(t)\int_0^t\left(X_N^1(s)-X_N^2(s)\right)^2\,\mathrm{d}s.
\end{aligned}$$

Thus we have:

$$\begin{aligned}
&\left\|F\left(\mu_+^1,\mu_-^1,X_N^1\right)-F\left(\mu_+^2,\mu_-^2,X_N^2\right)\right\|_X\\
&\quad\leq K(T)\int_0^T\int_0^t\left(\mu_+^1(s)-\mu_+^2(s)\right)^2+\left(\mu_-^1(s)-\mu_-^2(s)\right)^2+\left(X_N^1(s)-X_N^2(s)\right)^2\,\mathrm{d}s\,\mathrm{d}t,
\end{aligned}$$

which leads to the result. □

8.3 . Stationary solutions

In this section, we compute the stationary states of the model (8.8). To do this, we set the time derivative to zero and solve the associated spatial ODE. We obtain that there exists one stationary state that is not in motion. Moreover, there exists $m_1, m_2 \in \mathbb{R}$ such that when $M \in]m_1, m_2]$ there exists two stationary solutions that are in steady motion.

For the remainder of this chapter, we introduce the following function Q defined for all $x \in \left[-\frac{k_1}{k_2}, \frac{k_1}{k_2}\right]$ by:

$$Q(x)=\begin{cases}\dfrac{\beta\left(1-e^{-2\eta x}\right)+\eta x\left(\alpha_-\left(-\frac{k_2}{k_1}x\right)+\alpha_+\left(-\frac{k_2}{k_1}x\right)e^{-2\eta x}\right)}{\eta\left(\alpha_-\left(-\frac{k_2}{k_1}x\right)-\alpha_+\left(-\frac{k_2}{k_1}x\right)e^{-2\eta x}\right)} & \text{if } x\neq 0,\\ \dfrac{\beta}{A\eta}+\dfrac{1}{\eta} & \text{if } x=0.\end{cases}$$

Proposition 8.3.1. *The model (8.8) admits a non-polarised stationary state given by:*

$$\begin{cases} c^s(x) = \dfrac{M\beta}{2(A+\beta)}, & \text{(8.12a)} \\ \mu_+^s = \mu_-^s = \dfrac{MA}{2(A+\beta)}, & \text{(8.12b)} \\ X_N^s = 0. & \text{(8.12c)} \end{cases}$$

In addition, if $M \in \left]\frac{\beta}{A\eta} + \frac{1}{\eta}, Q\left(\frac{k_1}{k_2}\right)\right]$*, then there exists* $\nu^s \in \left]0, \frac{k_1}{k_2}\right]$ *such that* $Q(\nu^s) = M$ *and the model (8.8) admits two steady motion solutions given by:*

$$\begin{cases} c^\nu(x) = \dfrac{\beta\nu e^{-\eta\nu(x+1)}}{\alpha_-(X_N^\nu) - \alpha_+(X_N^\nu)e^{-2\eta\nu}}, & \text{(8.13a)} \\ \mu_+^\nu = \dfrac{\alpha_+(X_N^\nu)\nu e^{-2\eta\nu}}{\alpha_-(X_N^\nu) - \alpha_+(X_N^\nu)e^{-2\eta\nu}}, & \text{(8.13b)} \\ \mu_-^\nu = \dfrac{\alpha_-(X_N^\nu)\nu}{\alpha_-(X_N^\nu) - \alpha_+(X_N^\nu)e^{-2\eta\nu}}, & \text{(8.13c)} \\ X_N^\nu = -\dfrac{k_2}{k_1}\nu, & \text{(8.13d)} \end{cases}$$

with $\nu \in \{\nu^s, -\nu^s\}$.

Proof. If it exists, a stationary state of the model (8.8) is solution of the following problem:

$$\begin{cases} c''(x) + \eta\,\delta\mu\,c'(x) = 0, & x \in]-1,1[, & \text{(8.14a)} \\ c'(\pm 1) + \eta\,\delta\mu\,c(\pm 1) = 0, & & \text{(8.14b)} \\ \alpha_\pm(X_N)\,c(\pm 1) - \beta\mu_\pm = 0, & & \text{(8.14c)} \\ X_N = -\dfrac{k_2}{k_1}\delta\mu, & & \text{(8.14d)} \\ M = \displaystyle\int_{-1}^{1} c(x)\,\mathrm{d}x + \mu_- + \mu_+. & & \text{(8.14e)} \end{cases}$$

If $\delta\mu = 0$, then $X_N = 0$ and $\alpha_\pm(X_N) = A$. We deduce from eqs. (8.14a) and (8.14b) that for all $x \in [-1,1]$ we have:

$$c(x) = c(-1).$$

Thus, using eq. (8.14c) it leads to:

$$\mu_\pm = \frac{Ac(-1)}{\beta}$$

From the mass constraint (8.14e), we deduce that

$$c(-1) = \frac{M\beta}{2(\beta+A)},$$

and then

$$\mu_\pm = \frac{MA}{2(\beta+A)}$$

If $\delta\mu \neq 0$, if it exists, a solution of eq. (8.14) should be of the form:

$$\begin{cases} c(x) = \dfrac{\beta\,\delta\mu\, e^{-\eta\,\delta\mu(x+1)}}{\alpha_-(X_N) - \alpha_+(X_N)\, e^{-2\eta\,\delta\mu}}, \\ \mu_+ = \dfrac{\alpha_+(X_N)\;\delta\mu\, e^{-2\eta\,\delta\mu}}{\alpha_-(X_N) - \alpha_+(X_N)\, e^{-2\eta\,\delta\mu}}, \\ \mu_- = \dfrac{\alpha_-(X_N)\;\delta\mu}{\alpha_-(X_N) - \alpha_+(X_N)\, e^{-2\eta\,\delta\mu}}, \\ M = \displaystyle\int_{-1}^{1} c(x)\;\mathrm{d}x + \mu_- + \mu_+, \\ X_N = -\dfrac{k_1}{k_2}\delta\mu \in [-1,1] \end{cases}$$

We remark that:

$$\int_{-1}^{1} c(x)\;\mathrm{d}x + \mu_- + \mu_+ = Q(\delta\mu)\,.$$

We also remark that Q is an even function and, graphically, we have:

x	$-\frac{k_1}{k_2}$	0	$+\frac{k_1}{k_2}$
Q	$Q\left(\frac{k_1}{k_2}\right)$ ↘	$\frac{\beta}{\eta\alpha} + \frac{1}{\eta}$	↗ $Q\left(\frac{k_1}{k_2}\right)$

and the equation $Q(\delta\mu) = M$ admits exactly two solutions if $M \in \left]\frac{\beta}{\eta\alpha} + \frac{1}{\eta}, Q\left(\frac{k_1}{k_2}\right)\right[$. □

8.4 . Numerical study

8.4.1 . Numerical scheme

In this section, we detail the numerical scheme used to simulate the model (8.8). This numerical scheme is obtained after a semi-implicit discretisation in time and a finite volume approximation in space. The numerical scheme is analogous to the one obtained in section 2.4.

Grids definition We want to simulate eq. (8.8) over the time interval $[0,T]$, where $T > 0$. Let $\Delta t > 0$ be the time step. We discretize $[0,T]$ by the set of points $\{t^n = n\,\Delta t,\ n \in \{0,\dots,N\}\}$, where $N = \lfloor \frac{T}{\Delta t} \rfloor$.

Let $J \in \mathbb{N}$. We discretize the space interval $[-1,1]$ into $J+1$ intervals of the same length Δx. We denote by $\left(x_{j-\frac{1}{2}}\right)_{j\in\{0,\dots,J+1\}}$ a regular mesh of $[-1,1]$ and we set:

$$\begin{aligned} & x_{-\frac{1}{2}} = -1, \\ & \Delta x = x_{\frac{1}{2}} - x_{-\frac{1}{2}}, \\ & x_j = \frac{x_{j-\frac{1}{2}} + x_{j+\frac{1}{2}}}{2} = -1 + \left(j + \frac{1}{2}\right)\Delta x \quad j \in \{0,\dots,J\}\,. \end{aligned}$$

Finite volume approximation For all $n \in \{0, \dots, N\}$ and $j \in \{0, \dots, J\}$, we denote c_j^n an approximation of the function c at the time t^n and at position x_j. We set:

$$c_j^n = \frac{1}{\Delta x} \int_{\Lambda_j} c\left(t^n, x\right) \mathrm{d}x.$$

Similarly, we denote by μ_+^n an approximation of $\mu_+\left(t^n\right)$, μ_-^n an approximation of $\mu_-\left(t^n\right)$ and X_N^n an approximation of $X_N\left(t^n\right)$. We also denote $\delta\mu^n = \mu_-^n - \mu_+^n$.

First, we write the semi-implicit Euler scheme in time associate to eq. (8.8). For all $n \in \{0, \dots, N-1\}$, we have:

$$\begin{cases} \dfrac{c\left(t^{n+1}, x\right) - c\left(t^n, x\right)}{\Delta t} = \partial_x \left[\partial_x c\left(t^{n+1}, x\right) + \eta\, \delta\mu^n c\left(t^n, x\right)\right] \qquad x \in [-1, 1], & \text{(8.15a)} \\ \partial_x c\left(t^{n+1}, \pm 1\right) + \eta\, \delta\mu^n c\left(t^{n+1}, \pm 1\right) = \mp \dfrac{\mu_\pm^{n+1} - \mu_\pm^n}{\Delta t}, & \text{(8.15b)} \\ \dfrac{\mu_\pm^{n+1} - \mu_\pm^n}{\Delta t} = \alpha_\pm\left(X_N^n\right) c\left(t^n, \pm 1\right) - \beta \mu_\pm^{n+1}, & \text{(8.15c)} \\ \dfrac{X_N^{n+1} - X_N^n}{\Delta t} = -k_1 X_N^{n+1} - k_2\, \delta\mu^{n+1}. & \text{(8.15d)} \end{cases}$$

Then integrating eq. (8.15) over Λ_j for $j \in \{1, \dots, J-1\}$ and using an upwind approximation for the transport term we get:

$$c_j^{n+1} = c_j^n + \frac{\Delta t}{\Delta x^2}\left[c_{j+1}^{n+1} - 2c_j^{n+1} + c_{j-1}^{n+1}\right] + \eta \frac{\Delta t}{\Delta x}\left[A^{\mathrm{up}}\left(\delta\mu^n, c_j^n, c_{j+1}^n\right) - A^{\mathrm{up}}\left(\delta\mu^n, c_{j-1}^n, c_j^n\right)\right],$$

where

$$A^{\mathrm{up}}\left(v, x_+, x_-\right) = \begin{cases} v x_+ & \text{if } v \geq 0, \\ v x_- & \text{if } v < 0. \end{cases}$$

For $j = 0$ and $j = J$, we also integrate eq. (8.15a) and we use the boundaries condition (8.15b) to obtain:

$$\begin{aligned} c_0^{n+1} &= c_0^n + \frac{\Delta t}{\Delta x^2}\left[c_1^{n+1} - c_0^{n+1}\right] + \eta \frac{\Delta t}{\Delta x} A^{\mathrm{up}}\left(\delta\mu^n, c_0^n, c_1^n\right) - \frac{1}{\Delta x}\left(\mu_-^{n+1} - \mu_-^n\right), \\ c_J^{n+1} &= c_J^n - \frac{\Delta t}{\Delta x^2}\left[c_J^{n+1} - c_{J-1}^{n+1}\right] - \eta \frac{\Delta t}{\Delta x} A^{\mathrm{up}}\left(\delta\mu^n, c_{J-1}^n, c_J^n\right) - \frac{1}{\Delta x}\left(\mu_+^{n+1} - \mu_+^n\right). \end{aligned}$$

Moreover we have:

$$\begin{cases} \mu_-^{n+1} = \dfrac{1}{1 + \Delta t\, \beta}\left(\mu_-^n + \Delta t\, \alpha_-\left(X_N^n\right) c_0^n\right), & \text{(8.16a)} \\ \mu_+^{n+1} = \dfrac{1}{1 + \Delta t\, \beta}\left(\mu_+^n + \Delta t\, \alpha_+\left(X_N^n\right) c_J^n\right), & \text{(8.16b)} \\ X_N^{n+1} = \dfrac{1}{1 + \Delta t\, k_1}\left(X_N^n - k_2 \Delta t\, \delta\mu^{n+1}\right). & \text{(8.16c)} \end{cases}$$

Towards a matrix formulation We store the approximate value of c on $[-1, 1]$ at time t^n in a vector C^n, with $n \in \{0, \dots, N\}$. We have

$$C^n = \begin{bmatrix} c_0^n \\ \vdots \\ c_J^n \end{bmatrix}.$$

We introduce the following notations. Let D be the following diffusion matrix:

$$D = \frac{\Delta t}{\Delta x^2} \begin{bmatrix} -1 & 1 & 0 & \cdots & \cdots & 0 \\ 1 & -2 & 1 & \ddots & & \vdots \\ 0 & \ddots & \ddots & \ddots & \ddots & \vdots \\ \vdots & \ddots & \ddots & \ddots & \ddots & 0 \\ \vdots & & \ddots & \ddots & -2 & 1 \\ 0 & \cdots & \cdots & 0 & 1 & -1 \end{bmatrix}.$$

For all $n \in \{0, \dots, N-1\}$, let A^n be the following transport matrix:

$$A^n = \eta \frac{\Delta t}{\Delta x} \max\left(\delta\mu^n, 0\right) \begin{bmatrix} 1 & 0 & \cdots & \cdots & 0 \\ -1 & 1 & 0 & \cdots & 0 \\ 0 & \ddots & \ddots & \ddots & \vdots \\ \vdots & \ddots & \ddots & 1 & 0 \\ 0 & \cdots & 0 & -1 & 0 \end{bmatrix}$$
$$+ \eta \frac{\Delta t}{\Delta x} \min\left(\delta\mu^n, 0\right) \begin{bmatrix} 0 & 1 & 0 & \cdots & 0 \\ 0 & -1 & \ddots & \ddots & \vdots \\ \vdots & \ddots & \ddots & \ddots & 0 \\ 0 & \cdots & 0 & -1 & 1 \\ 0 & \cdots & \cdots & 0 & -1 \end{bmatrix}.$$

For all $n \in \{0, \dots, N-1\}$, let B^n be the following vector:

$$B^n = \frac{1}{\Delta x} \begin{bmatrix} \mu_-^{n+1} - \mu_-^n \\ 0 \\ \vdots \\ 0 \\ \mu_+^{n+1} - \mu_+^n \end{bmatrix}.$$

Then, in the matrix formulation, eqs. (8.15) and (8.16) rewrites:

$$C^{n+1} = C^n + D \cdot C^{n+1} + A^n \cdot C^n - B^n,$$

which leads to:

$$C^{n+1} = (Id - D)^{-1} \left(C^n + A^n \cdot C^n - B^n\right). \tag{8.17}$$

Numerical scheme The numerical scheme to simulate eq. (8.8) is given by the following algorithm:

Algorithm 8.1 : Numerical scheme to simulate eq. (8.8) using a semi-implicit Euler approximation in time and a finite volume approximation in space.

1. Initialisation.
   - $c_j^0 = \dfrac{1}{\Delta x}\displaystyle\int_{\Lambda_j} c^0(x)\,\mathrm{d}x$,
   - $\mu_\pm^0 = \mu_\pm(0)$,
   - $X_N^0 = X_N(0)$.
2. Time iteration. For $n \in \{0,\dots,N-1\}$, do:
   (a) Computation of μ_-^{n+1} using eq. (8.16a):
   $$\mu_-^{n+1} = \frac{1}{1+\Delta t\,\beta}\left(\mu_-^n + \Delta t\,\alpha_-\left(X_N^n\right)c_0^n\right).$$
   (b) Computation of μ_+^{n+1} using eq. (8.16b):
   $$\mu_+^{n+1} = \frac{1}{1+\Delta t\,\beta}\left(\mu_+^n + \Delta t\,\alpha_+\left(X_N^n\right)c_J^n\right).$$
   (c) Computation of X_N^{n+1} using eq. (8.16c):
   $$X_N^{n+1} = \frac{1}{1+\Delta t\,k_1}\left(X_N^n - k_2\Delta t\,\delta\mu^{n+1}\right).$$
   (d) Computation of the matrix A^n and the vector B^n in order to compute C^{n+1} using eq. (8.17):
   $$C^{n+1} = (Id - D)^{-1}\left(C^n + A^n\cdot C^n - B^n\right).$$

Remark 8.4.1. *We can remark that this scheme preserves the conservation of the mass. Indeed, for all $n \in \{0,\dots,N\}$, we have*

$$\sum_{j=0}^{J} c_j^n + \mu_-^n + \mu_-^n = \sum_{j=0}^{J} c_j^0 + \mu_-^0 + \mu_-^0.$$

8.4.2 . Numerical results

Using numerical simulations, we aim to show that this dimension 1 model illustrates the role of the nucleus in cell motility. First, we check that the discretisation and its implementation allow us to find the stationary states described in the proposition 8.3.1. Next, we investigate the role of the nucleus.

For all the numerical illustrations in this section, the functions α_+ and α_- are defined for all $x \in \mathbb{R}$ by:

$$\alpha_+(x) = A\mathbb{1}_{x<d} + \left[\frac{(A-\varepsilon)(x-1)}{d-1} + \varepsilon\right]\mathbb{1}_{d\le x\le 1} + \varepsilon\mathbb{1}_{x>1}, \tag{8.18}$$

$$\alpha_-(x) = \varepsilon\mathbb{1}_{x<-1} + \left[\frac{(A-\varepsilon)(x+1)}{1-d} + \varepsilon\right]\mathbb{1}_{-1\le x\le -d} + A\mathbb{1}_{x>-d}. \tag{8.19}$$

To begin, we verify that the numerical scheme captures the unpolarised stationary state (8.12). To do this, we fix the discretisation by fixing the time step Δt and the space step Δx

and take the following initial condition:

$$\begin{cases} c_j^0 = \dfrac{M\beta}{2\left(A+\beta\right)} & j \in \{0,\dots,J\}, \quad \text{(8.20a)} \\ \mu_+^0 = \mu_-^0 = \dfrac{MA}{2\left(A+\beta\right)}, & \text{(8.20b)} \\ X_N^0 = 0, & \text{(8.20c)} \end{cases}$$

which corresponds to the discretisation of the stationary state (8.12).

Whatever the value of the other parameters, we observe that (8.20) is a stationary state of the numerical scheme (see fig. 8.2 for an example). We observe that the velocity of the cell remains constant over time and is equal to zero. The position of the nucleus remains stable and stays at the center of the cell. The initial quantity of markers on the membrane is also maintained over time.

Next, we check that the numerical scheme accurately captures the steady motion solutions (8.13). To do this, first we set the discretization by fixing Δt and Δx and choose parameters. Then we use a dichotomy algorithm to find ν such that $Q\left(\nu\right) = M$ with $\nu \in \left]0, \frac{k_1}{k_2}\right]$. We then choose as initial condition for the numerical scheme the following one:

$$\begin{cases} X_N^0 = -\dfrac{k_2}{k_1}\nu, & \text{(8.21a)} \\ c_j^0 = \dfrac{1}{\Delta x}\displaystyle\int_{\Lambda_j} \frac{\beta\nu e^{-\eta\nu(x+1)}}{\alpha_-\left(X_N^0\right) - \alpha_+\left(X_N^0\right)e^{-2\eta\nu}}\,\mathrm{d}x \qquad j \in \{0,\dots,J\}, & \text{(8.21b)} \\ \mu_+^0 = \dfrac{\alpha_+\left(X_N^0\right)\nu e^{-2\eta\nu}}{\alpha_-\left(X_N^0\right) - \alpha_+\left(X_N^0\right)e^{-2\eta\nu}}, & \text{(8.21c)} \\ \mu_-^0 = \dfrac{\alpha_-\left(X_N^0\right)\nu}{\alpha_-\left(X_N^0\right) - \alpha_+\left(X_N^0\right)e^{-2\eta\nu}}. & \text{(8.21d)} \end{cases}$$

We observe that as soon as there exists ν such that $Q\left(\nu\right) = M$ with $\nu \in \left]0, \frac{k_1}{k_2}\right]$, then (8.21) is a steady motion solution of the numerical scheme (see fig. 8.3 for an example). We observe that the cell's velocity remains constant over time and is equal to its initial value. The nucleus's position is maintained over time. Additionally, the initial quantity of markers on the membrane is preserved, the cell remains polarised. Moreover the scheme also capture the second steady motion solution associate to $-\nu$. We can also note that the nucleus is place at the rear of the cell.

Thus, the numerical scheme algorithm 8.1 proposed to simulate the model (8.8) correctly reproduces the results of the equation. We now aim to illustrate the role of the nucleus in cell motility. To this end, we find a range of parameters for which the cell exhibits intermittent behaviour, meaning that it has phases where it is polarised and phases where it is not. We can discern two different types of behaviour.

The first corresponds to a cell that polarises and moves in one direction, then stops, polarises again to move in the same direction, stops and so on. It seems that after a certain time, the cell becomes polarised and maintains its polarisation. The fig. 8.4 illustrates this. Indeed, we observe that, initially, the cell polarises, in absolute value the velocity increases and the nucleus moves backwards. As soon as the nucleus reaches the boundary of the cell, the cell depolarises, the nucleus returns towards the centre of the cell and the velocity becomes

(a) Evolution of the cell velocity.

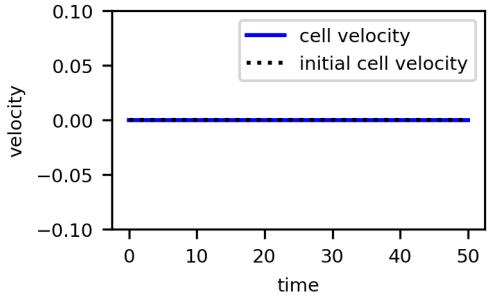

(b) Evolution of the nucleus position in the cell frame of reference.

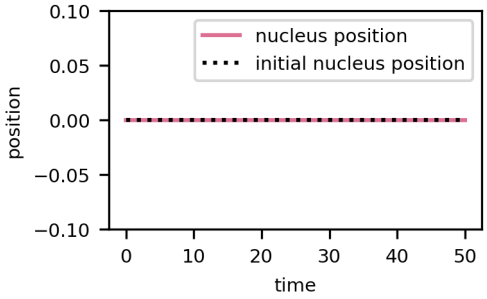

(c) Evolution of the markers quantity at the membrane.

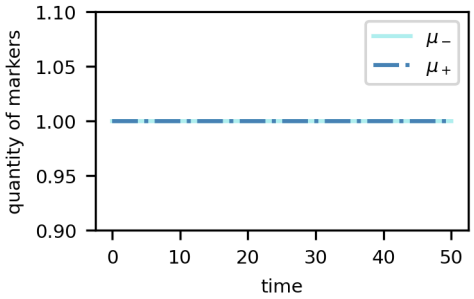

(d) Evolution of the total quantity of markers.

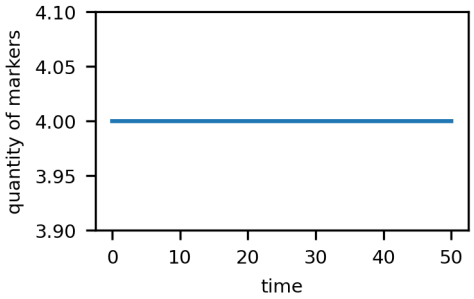

Figure 8.2: **Example of capturing the unpolarised stationary state with the numerical scheme.** *The graph on top left (figure* (a)*) represents the time evolution of the cell velocity. The velocity is constant and equal to zero. The graph on the top right (figure* (b)*) represents the time evolution of the nucleus position in the cell frame of reference. The nucleus remains at the centre of the cell. The graph on the bottom left (figure* (c)*) represents the time evolution of the markers quantity at the membrane. We can see that at both ends of the cell the quantity of markers is constant over time and equal. The cell therefore remains unpolarised. The graph on the bottom right (figure* (d)*) represents the time evolution of the total quantity of markers which remains conserved over time.*
The results presented here are obtained with the parameters $\Delta t = 0.0001$, $\Delta x = 0.004$, *the initial condition given by* (8.20), $M = 4$, $a = 1$, $\chi_c = 1$, $\beta = 1$, $A = 1$, $\varepsilon = 0.001$, $d = 0.9$, α_+ *and* α_- *given by eqs.* (8.18) *and* (8.19), $k_1 = 0.2$ *and* $k_2 = 0.7$.

(a) Evolution of the cell velocity.

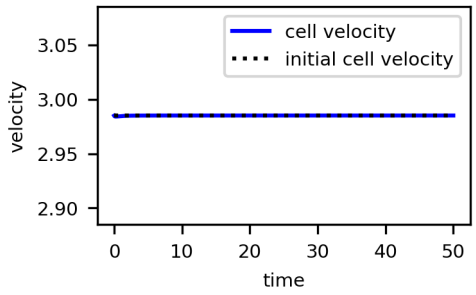

(b) Evolution of the nucleus position in the cell frame of reference.

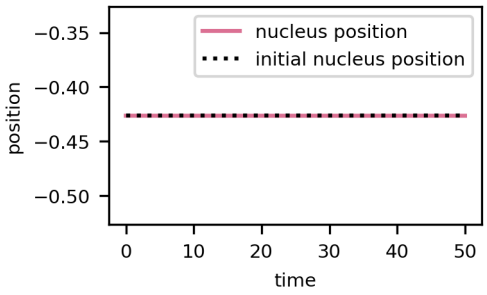

(c) Evolution of the markers quantity at the membrane.

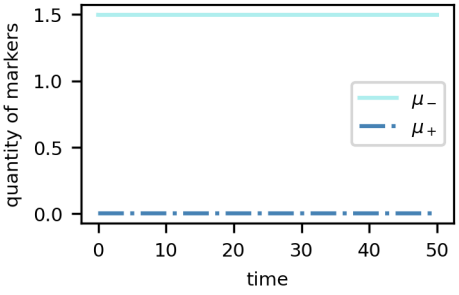

(d) Evolution of the total quantity of markers.

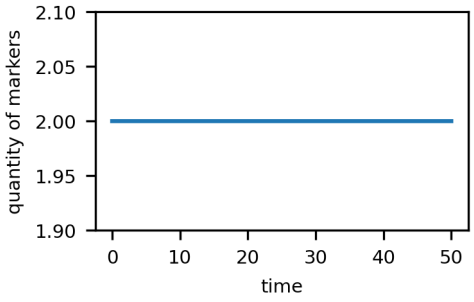

Figure 8.3: **Example of capturing the polarised steady motion solutions with the numerical scheme.** *The graph on top left (figure* (a)*) represents the time evolution of the cell velocity. The velocity is constant and equal to its initial value. The graph on the top right (figure* (b)*) represents the time evolution of the nucleus position in the cell frame of reference. The nucleus remains at its initial position. The graph on the bottom left (figure* (c)*) represents the time evolution of the markers quantity at the membrane. We can see that at both ends of the cell the quantity of markers is constant over time. The cell therefore remains polarised. The graph on the bottom right (figure* (d)*) represents the time evolution of the total quantity of markers which remains conserved over time. The results presented here are obtained with the parameters* $\Delta t = 0.0001$, $\Delta x = 0.004$, *the initial condition given by* (8.21) *with* $\nu = 1.4925228058$, $M = 2$, $a = 1$, $\chi_c = 1$, $\beta = 1$, $A = 1$, $\varepsilon = 0.001$, $d = 0.9$, α_+ *and* α_- *given by eqs.* (8.18) *and* (8.19), $k_1 = 0.2$ *and* $k_2 = 0.7$.

zero. Since the velocity is zero, the cell stops. The cell then polarises again and starts moving again. Once the nucleus reaches the boundary of the cell, the cell depolarises once again. This highlights a stop-and-go phenomenon.

The second corresponds to an oscillating cell. The cell polarises, stops very briefly and then polarises again in the opposite direction. The fig. 8.5 illustrates this. Initially, the cell becomes polarised, the velocity increases in absolute terms and the nucleus moves backwards. As soon as the nucleus reaches the boundary of the cell, the cell depolarises, the nucleus moves back towards the centre of the cell and the velocity decreases. The cell then immediately polarises in the other direction. We can note that the nucleus is located at the rear of the cell.

These numerical simulations highlight a particular limitation of this model: the nucleus can exit the cell. However, this is not necessarily a defect. In fact, in the reference frame of the cell, $X_N = 1$ and $X_N \geq 1$ convey the same information and result in the same dynamics. This is because we assume that for all $x \geq 1$ and $x \leq -1$, the functions α_+ and α_- are constant, and that $\delta\mu$ depends on the position of the nucleus through the functions α_+ and α_-. Moreover, the position of the nucleus is determined solely by its initial position and $\delta\mu$.

Conclusion. The numerical study of the model highlights that the proposed heuristics for the dynamics of the nucleus give results that are consistent with the biological context. We spontaneously observe the polarisation of the cell with the nucleus at the rear of the cell. The attachment dynamics modified by the presence of the nucleus seem to allow the depolarisation of the cell and the observation of intermittent behaviour.

(a) Evolution of the cell velocity.

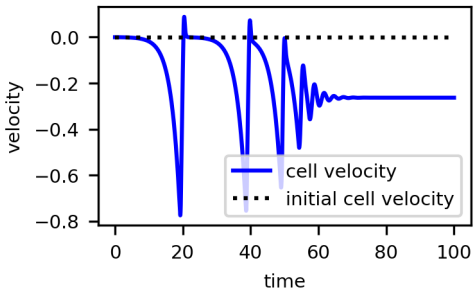

(b) Evolution of the nucleus position in the cell frame of reference.

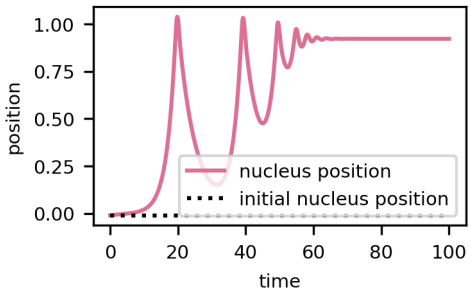

(c) Evolution of the markers quantity at the membrane.

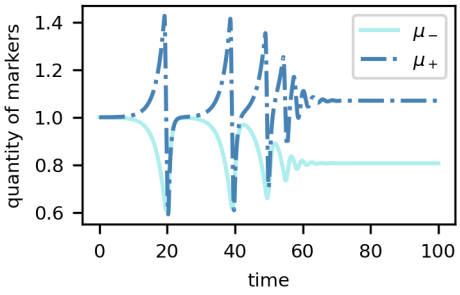

(d) Evolution of the total quantity of markers.

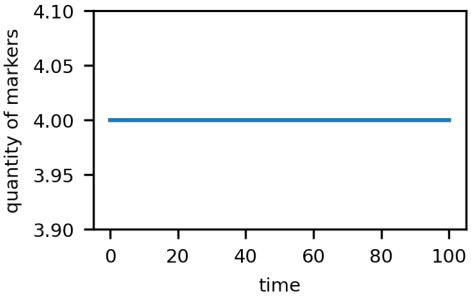

Figure 8.4: **Example of capturing an intermittent behaviour.** *The graph on top left (figure* (a)*) represents the time evolution of the cell velocity. We observe the velocity suddenly decreases and then increases to zero, a pattern that repeats multiple times before stabilising at a constant value. The graph on the top right (figure* (b)*) represents the time evolution of the nucleus position in the cell frame of reference. Before stabilising to a position at the rear of the cell, the position of the nucleus oscillate. The graph on the bottom left (figure* (c)*) represents the time evolution of the markers quantity at the membrane. We can observe the polarisation and depolarisation. The graph on the bottom right (figure* (d)*) represents the time evolution of the total quantity of markers which remains conserved over time.*
The results presented here are obtained with the parameters $\Delta t = 0.0001$, $\Delta x = 0.004$, *the initial condition given by* $c_j^0 = \left(\frac{M\beta}{2(A+\beta)} + X_j\right) \mathbb{1}_{\frac{M\beta}{2(A+\beta)}+X_j \geq 0} + \frac{M\beta}{2(A+\beta)} \mathbb{1}_{\frac{M\beta}{2(A+\beta)}+X_j<0}$ *with* X_j *a realisation of the random variable* $Y \sim \mathcal{N}(0, 0.01)$, $X_N^0 = X \mathbb{1}_{X\in[-1,1]}$ *with* X *a realisation of the random variable* Y *and* $\mu_\pm^0 = \left(\frac{MA}{2(A+\beta)} + X_\pm\right) \mathbb{1}_{\frac{MA}{2(A+\beta)}+X_\pm \geq 0} + \frac{MA}{2(A+\beta)} \mathbb{1}_{\frac{MA}{2(A+\beta)}+X_\pm<0}$ *with* $X_\pm$ *a realisation of the random variable* $Z \sim \mathcal{N}(0, 0.001)$, $M = 4$, $a = 1$, $\chi_c = 2$, $\beta = 1$, $A = 1$, $\varepsilon = 0.001$, $d = 0.9$, α_+ *and* α_- *given by eqs.* (8.18) *and* (8.19), $k_1 = 0.2$ *and* $k_2 = 0.7$.

(a) Evolution of the cell velocity.

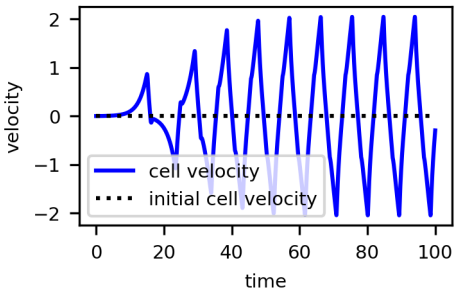

(b) Evolution of the nucleus position in the cell frame of reference.

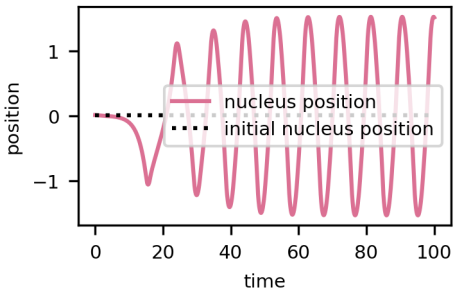

(c) Evolution of the markers quantity at the membrane.

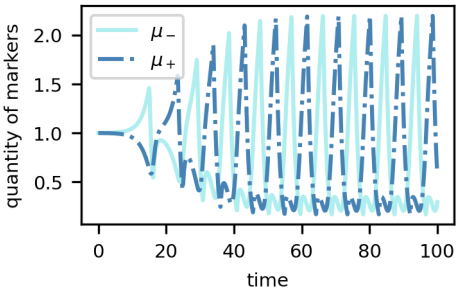

(d) Evolution of the total quantity of markers.

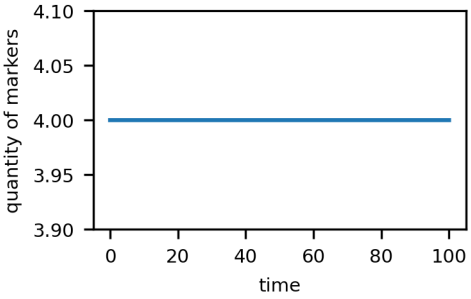

Figure 8.5: **Example of capturing an intermittent behaviour.** *The graph on top left (figure* (a)*) represents the time evolution of the cell velocity. We notice that the velocity alternately decreases and increases, exhibiting an oscillatory pattern. The graph on the top right (figure* (b)*) represents the time evolution of the nucleus position in the cell frame of reference. The nucleus position oscillate. The graph on the bottom left (figure* (c)*) represents the time evolution of the markers quantity at the membrane. We can observe the alternance of polarisation in one direction and in the other. The graph on the bottom right (figure* (d)*) represents the time evolution of the total quantity of markers which remains conserved over time.*
The results presented here are obtained with the parameters $\Delta t = 0.0001$, $\Delta x = 0.004$, *the initial condition given by* $c_j^0 = \left(\frac{M\beta}{2(A+\beta)} + X_j\right) \mathbb{1}_{\frac{M\beta}{2(A+\beta)}+X_j \geq 0} + \frac{M\beta}{2(A+\beta)} \mathbb{1}_{\frac{M\beta}{2(A+\beta)}+X_j<0}$ *with* X_j *a realisation of the random variable* $Y \sim \mathcal{N}(0, 0.01)$, $X_N^0 = X \mathbb{1}_{X \in [-1,1]}$ *with* X *a realisation of the random variable* Y *and* $\mu_\pm^0 = \left(\frac{MA}{2(A+\beta)} + X_\pm\right) \mathbb{1}_{\frac{MA}{2(A+\beta)}+X_\pm \geq 0} + \frac{MA}{2(A+\beta)} \mathbb{1}_{\frac{MA}{2(A+\beta)}+X_\pm<0}$ *with* $X_\pm$ *a realisation of the random variable* $Z \sim \mathcal{N}(0, 0.001)$, $M = 4$, $a = 1$, $\chi_c = 2.5$, $\beta = 1$, $A = 1$, $\varepsilon = 0.001$, $d = 0.9$, α_+ *and* α_- *given by eqs.* (8.18) *and* (8.19), $k_1 = 0.2$ *and* $k_2 = 0.7$.

Bibliography

Lavi, I., Meunier, N., Voituriez, R., and Casademunt, J. (2020). Motility and morphodynamics of confined cells. Physical Review E, 101(2):022404. Publisher: American Physical Society. 254

Lepoutre, T. and Meunier, N. (2022). Analysis of a model of cell crawling migration. Communications in Mathematical Sciences, 20(6):1589–1611. 256, 259

9 - Deformable cell with undercooling effect

In this chapter, we present and study a deformable model to investigate the effect of undercooling on cell motility. This model is a specific case of the general model (1.1), where we do not consider the dynamics of the nucleus, we assume the substrate is homogeneous without obstacles or external signals and, we neglect the effect of the noise. We first present the model under study. Then, we study the stationary states of the model and their stability. This analysis highlights the stabilizing effect of undercooling. We prove the existence of non-trivial traveling waves using a bifurcation argument. Finally, we present a numerical scheme in order to simulate the model.

9.1 . Modelling

In this section, based on the general model eq. (1.1), we derive a model of cell motility when we neglect the effects of the nucleus but take into account the friction of the cell boundary. We assume that the substrate is homogeneous and that the cell's environment has no external signals or obstacles. Keeping the notations of chapter 1, the model is given by:

$$\begin{cases} \mathbf{u} + \nabla P = 0 & \text{in } \Omega(t), & \text{(9.1a)} \\ \operatorname{div}(\mathbf{u}) = 0 & \text{in } \Omega(t), & \text{(9.1b)} \\ V_n = \mathbf{u} \cdot \mathbf{n} & \text{on } \partial\Omega(t), & \text{(9.1c)} \\ P = \gamma\kappa + \chi_c f_{\text{act}}(c) + \chi_u f_{\text{und}}(V_n) & \text{on } \partial\Omega(t), & \text{(9.1d)} \\ \partial_t c = \operatorname{div}(\nabla c - (1-a)\mathbf{u}c) & \text{in } \Omega(t), & \text{(9.1e)} \\ (\nabla c + a\mathbf{u}c) \cdot \mathbf{n} = 0 & \text{on } \partial\Omega(t), & \text{(9.1f)} \\ c(0,\mathbf{x}) = c^{\text{in}}(\mathbf{x}) & \text{in } \Omega(0). & \text{(9.1g)} \end{cases}$$

We recall that f_{und} satisfies assumptions 1.13, i.e.

$$\begin{aligned} & f_{\text{und}} \in C^1\left(\mathbb{R}^+\right), & \text{(9.2a)} \\ & f_{\text{und}} \text{ is an odd and increasing function,} & \text{(9.2b)} \\ & f'_{\text{und}}(0) > 0. & \text{(9.2c)} \end{aligned}$$

Let $\mathbf{u}_{\text{cm}}$ be the velocity of the centre of mass. For all $t \geq 0$, we have:

$$\mathbf{u}_{\text{cm}}(t) = -\frac{1}{A_\Omega} \int_{\partial\Omega(t)} \left(\chi_c f_{\text{act}}(c) + \chi_u f_{\text{und}}(V_n)\right) \mathbf{n} \, \mathrm{d}\sigma. \tag{9.3}$$

The model under study can be seen as an enhancement of the model of Lavi et al. (2020): the model of Lavi et al. (2020) is recovered when $\chi_u = 0$. In Alazard et al. (2022), it is shown that the model admits a unique stable radial stationary state if $\chi_c < \chi^* = \frac{1}{ac^0 f'_{\text{act}}(c^0)}$, where c^0 is the stationary concentration, and is unstable otherwise. The existence of traveling waves when $\chi_c > \chi^*$ is also demonstrated.

9.2 . Study of the stationary state

In this section, we study the radially symmetric stationary state of the model. First, we establish the existence of a stationary state and give its expression, then study its linear stability.

9.2.1 . Stationary state and linear stability

Proposition 9.2.1. *The model (9.1) admits an unique stationary state given by:*

$$\begin{cases} c^0(\mathbf{x}) = \dfrac{M}{|\Omega|} & \mathbf{x} \in \Omega^0, \quad (9.4a) \\ P^0(\mathbf{x}) = \dfrac{\gamma}{R_0} + \chi_c f_{\text{act}}\left(c^0(\mathbf{x})\right) & \mathbf{x} \in \Omega^0, \quad (9.4b) \\ \mathbf{u}^0(\mathbf{x}) = 0 & \mathbf{x} \in \Omega^0, \quad (9.4c) \\ \Omega^0 = B(0, R_0), & (9.4d) \end{cases}$$

where $R_0 = \sqrt{\dfrac{A_\Omega}{\pi}}$. *This stationary state is radially symmetric.*

Proof. The stationary problem associated with the model (9.1) is given by:

$$\begin{cases} \mathbf{u} + \nabla P = 0 & \text{in } \Omega, \quad (9.5a) \\ \operatorname{div}(\mathbf{u}) = 0 & \text{in } \Omega, \quad (9.5b) \\ \mathbf{u} \cdot \mathbf{n} = 0 & \text{on } \partial\Omega, \quad (9.5c) \\ P = \gamma\kappa + \chi_c f_{\text{act}}(c) & \text{on } \partial\Omega, \quad (9.5d) \\ \operatorname{div}(\nabla c - (1-a)\,\mathbf{u}c) = 0 & \text{in } \Omega, \quad (9.5e) \\ (\nabla c + a\mathbf{u}c) \cdot \mathbf{n} = 0 & \text{on } \partial\Omega, \quad (9.5f) \end{cases}$$

From eqs. (9.5a) to (9.5c) P satisfies:

$$\begin{cases} -\Delta P = 0 & \text{in } \Omega, \\ \nabla P \cdot \mathbf{n} = 0 & \text{on } \partial\Omega. \end{cases}$$

Then we have that P is constant over Ω and therefore $\mathbf{u} = 0$.

It follows that c satisfies:

$$\begin{cases} \Delta c = 0 & \text{in } \Omega, \\ \nabla c \cdot \mathbf{n} = 0 & \text{on } \partial\Omega. \end{cases}$$

So c is constant over Ω and usign the constraint on the total quantity of markers, we have that:

$$c(\mathbf{x}) = \frac{M}{|\Omega|}, \qquad \mathbf{x} \in \Omega$$

Thus, using eq. (9.5d), we deduce that necessarily the mean curvature must be constant on $\partial\Omega$ and therefore $\Omega = B(0, R_0)$, where R_0 is the radius preserving the area of the cell domain. We then have:

$$P(\mathbf{x}) = \frac{\gamma}{R_0} + \chi_c f_{\text{act}}(c(\mathbf{x})), \qquad \mathbf{x} \in \Omega.$$

□

Let χ_c^* be defined by:

$$\chi_c^* = \frac{R_0 + \chi_u f'_{\text{und}}(0)}{R_0 a c^0 f'_{\text{act}}(c^0)}. \tag{9.6}$$

Theorem 9.2.2. *If* $\dfrac{\chi_c}{\chi_c^*} < 1$ *then the stationary state (9.4) is linearly stable. On the opposite, if* $\dfrac{\chi_c}{\chi_c^*} > 1$, *then the stationary state (9.4) is linearly unstable.*

9.2.2 . Proof of theorem 9.2.2

To prove the theorem 9.2.2, inspired by Alazard et al. (2022), we first linearise the problem (9.1) around the stationary state (9.4) (see lemma 9.2.3). We derive an eigenvalue problem from this linearised problem and study its spectrum. To this end, we prove that, using Fourier analysis, we can decompose the study of the spectrum into the study of the spectrum of simpler problems (see lemma 9.2.4). Next, we demonstrate that when $\frac{\chi_c}{\chi_c^*} < 1$ then the eigenvalues are all negative real parts (see lemma 9.2.6 and remark 9.2.7). Finally, from the decomposition of the spectrum study, we derive an explicit condition on the eigenvalues (see lemma 9.2.9). Thus, when $\frac{\chi_c}{\chi_c^*} > 1$, we can exhibit a positive real part eigenvalue. This shows the theorem 9.2.2.

Lemma 9.2.3. *The linearised problem associated to eq.* (9.1) *around the stationary state* (9.4) *is given by:*

$$\begin{cases} -\Delta\tilde{P} = 0 & \text{in } \Omega^0, \quad (9.7a) \\ \partial_t\rho\left(t,\theta\right) = -\partial_r\tilde{P}\left(t,R_0,\theta\right) & \theta\in(-\pi,\pi], \quad (9.7b) \\ \tilde{P} = -\frac{\gamma}{R_0^2}\left(\partial_{\theta\theta}^2\rho+\rho\right)+\chi_c\tilde{c}f'_{\text{act}}\left(c^0\right)-\chi_u\partial_r\tilde{P}f'_{\text{und}}\left(0\right) & \text{on } \partial\Omega^0, \quad (9.7c) \\ \partial_t\tilde{c} = \Delta\tilde{c} & \text{in } \Omega^0, \quad (9.7d) \\ \left(\nabla\tilde{c}-a\nabla\tilde{P}\,c^0\right)\cdot\mathbf{n} = 0 & \text{on } \partial\Omega^0. \quad (9.7e) \end{cases}$$

Proof. We perform a formal expansion of the solution $(c,\mathbf{u})$ near the stationary state $\left(c^0,\mathbf{u}^0\right)$. Let $\varepsilon>0$ small. For all $t\geq 0$ we set:

$$\Omega\left(t\right) = \left\{(x,y) = (r\cos\theta, r\sin\theta) \text{ s.t. } 0\leq r < R_0+\varepsilon\rho\left(t,\theta\right) \text{ and } \theta\in(-\pi,\pi]\right\}, \quad (9.8)$$

and for all $\mathbf{x}\in\Omega\left(t\right)$:

$$\begin{aligned} c\left(t,\mathbf{x}\right) &= c^0+\varepsilon\tilde{c}\left(t,\mathbf{x}\right)+\mathcal{O}\left(\varepsilon^2\right), \\ P\left(t,\mathbf{x}\right) &= P^0+\varepsilon\tilde{P}\left(t,\mathbf{x}\right)+\mathcal{O}\left(\varepsilon^2\right), \end{aligned}$$

Using the fact that P^0 satisfies eq. (9.4b) and P satisfies eqs. (9.1a) and (9.1b), we deduce that:

$$-\Delta\tilde{P} = 0, \qquad \text{in } \Omega^0.$$

From eq. (9.8), we can parameterise the boundary of the domain Ω and thus we obtain that, for all $\theta\in(-\pi,\pi]$ and $r\in\mathbb{R}_+$ such that $(r\cos\theta, r\sin\theta)\in\partial\Omega\left(t\right)$, the outward normal vector is expressed as:

$$\mathbf{n}\left(t,r,\theta\right) = \frac{\nabla\left(r-\left(R_0+\varepsilon\rho\left(t,\theta\right)\right)\right)}{\left|\nabla\left(r-\left(R_0+\varepsilon\rho\left(t,\theta\right)\right)\right)\right|} = \frac{1}{\left|\nabla\left(r-\left(R_0+\varepsilon\rho\left(t,\theta\right)\right)\right)\right|}\begin{pmatrix}\cos\theta+\varepsilon\dfrac{\partial_\theta\rho\left(t,\theta\right)}{r}\sin\theta \\ \sin\theta-\varepsilon\dfrac{\partial_\theta\rho\left(t,\theta\right)}{r}\cos\theta\end{pmatrix},$$

which leads to the fact for all $\theta\in(-\pi,\pi]$ we have:

$$\mathbf{n}\left(t,\theta\right) = \begin{pmatrix}\cos\theta\\ \sin\theta\end{pmatrix}-\varepsilon\frac{\partial_\theta\rho\left(t,\theta\right)}{R_0}\begin{pmatrix}-\sin\theta\\ \cos\theta\end{pmatrix}+\mathcal{O}\left(\varepsilon^2\right).$$

Thus, on $\partial\Omega(t)$, we have:

$$\nabla P \cdot \mathbf{n} = \nabla P^0 \cdot \mathbf{n} - \varepsilon \partial_r \tilde{P} + \mathcal{O}\left(\varepsilon^2\right)$$

and also:

$$V_n = \varepsilon \partial_t \rho(t,\theta) + \mathcal{O}\left(\varepsilon^2\right).$$

Using eq. (9.1c), we can therefore deduce that, for all $\theta \in (-\pi,\pi]$ and $t \geq 0$, we have:

$$\partial_t \rho(t,\theta) = -\partial_r \tilde{P}(t, R_0, \theta)$$

The linearisation of the curvature is given for all $\theta \in (-\pi,\pi]$ and $t \geq 0$ by:

$$\kappa(t,\theta) = \frac{1}{R_0} - \frac{\varepsilon}{R_0^2}\left(\partial^2_{\theta\theta}\rho(t,\theta) + \rho(t,\theta)\right) + \mathcal{O}\left(\varepsilon^2\right).$$

Since

$$f_{\text{act}}(c) = f_{\text{act}}\left(c^0\right) + \varepsilon \tilde{c} f'_{\text{act}}\left(c^0\right) + \mathcal{O}\left(\varepsilon^2\right)$$

and

$$f_{\text{und}}(V_n) = \varepsilon \partial_t \rho(t,\theta) f'_{\text{und}}(0) + \mathcal{O}\left(\varepsilon^2\right),$$

we have that eq. (9.1d) leads to that on $\partial\Omega^0$ we have:

$$\tilde{P} = -\frac{\gamma}{R_0^2}\left(\partial^2_{\theta\theta}\rho + \rho\right) + \chi_c \tilde{c} f'_{\text{act}}\left(c^0\right) + \chi_u \partial_t \rho f'_{\text{und}}(0).$$

Moreover, using the fact that c^0 satisfies eq. (9.4a) and c satisfies eqs. (9.1e) and (9.1f), we deduce that in Ω^0:

$$\partial_t \tilde{c} = \Delta \tilde{c}.$$

We also have on $\partial\Omega^0$ that:

$$(\nabla c - a \nabla P\, c) \cdot \mathbf{n} = \varepsilon\left(\nabla \tilde{c} - a \nabla \tilde{P}\, c^0\right) \cdot \mathbf{n} + \mathcal{O}\left(\varepsilon^2\right),$$

which leads to:

$$\left(\nabla \tilde{c} - a \nabla \tilde{P}\, c^0\right) \cdot \mathbf{n} = 0 \qquad \text{on } \partial\Omega^0.$$

□

As the problem (9.7) is radially symmetric, the spectral analysis can be performed using Fourier analysis.

The eigenvalue problem associated with the linearized problem (9.7) is given by:

$$\begin{cases} -\Delta \tilde{P} = 0 & \text{in } \Omega^0, \quad (9.9a) \\ \lambda \rho(\theta) = -\partial_r \tilde{P}(R_0, \theta) & \theta \in (-\pi,\pi], \quad (9.9b) \\ \tilde{P} = -\frac{\gamma}{R_0^2}\left(\partial^2_{\theta\theta}\rho + \rho\right) + \chi_c \tilde{c} f'_{\text{act}}\left(c^0\right) - \chi_u \partial_r \tilde{P} f'_{\text{und}}(0) & \text{on } \partial\Omega^0, \quad (9.9c) \\ \lambda \tilde{c} = \Delta \tilde{c} & \text{in } \Omega^0, \quad (9.9d) \\ \left(\nabla \tilde{c} - a \nabla \tilde{P}\, c^0\right) \cdot \mathbf{n} = 0 & \text{on } \partial\Omega^0, \quad (9.9e) \end{cases}$$

where $\lambda \in \mathbb{C}$.

Lemma 9.2.4. *Let $\lambda \in \mathbb{C}$. The eigenfunctions, satisfying eq. (9.9) associated with the eigenvalue λ are of the form:*

$$\begin{aligned}
\rho(\theta) &= \sum_{m\in\mathbb{N}} \rho_{cm} \cos(m\theta) + \sum_{m\in\mathbb{N}} \rho_{sm} \sin(m\theta), \\
c(r,\theta) &= \sum_{m\in\mathbb{N}} c_{cm}(r) \cos(m\theta) + \sum_{m\in\mathbb{N}} c_{sm}(r) \sin(m\theta), \\
P(r,\theta) &= \sum_{m\in\mathbb{N}} P_{cm}(r) \cos(m\theta) + \sum_{m\in\mathbb{N}} P_{sm}(r) \sin(m\theta),
\end{aligned}$$

with for all $m \in \mathbb{N}$, $(\rho_{cm}, c_{cm}, P_{cm})$ (resp. $(\rho_{sm}, c_{sm}, P_{sm})$) satisfying:

$$\begin{cases}
-\left(\partial_{rr}^2 + \frac{1}{r}\partial_r - \frac{m^2}{r^2}\right) P_{cm} = 0 & r \in (0, R_0), \quad \text{(9.10a)} \\
\lambda \rho_{cm} = -\partial_r P_{cm}(R_0), & \text{(9.10b)} \\
P_{cm}(R_0) = \frac{\gamma}{R_0^2}\left(m^2-1\right)\rho_{cm} + \chi_c c_{cm}(R_0) f'_{\text{act}}\left(c^0\right) & \text{(9.10c)} \\
\qquad\qquad - \chi_u \partial_r P_{cm}(R_0) f'_{\text{und}}(0), & \\
\lambda c_{cm} = \left(\partial_{rr}^2 + \frac{1}{r}\partial_r - \frac{m^2}{r^2}\right) c_{cm} & r \in (0, R_0), \quad \text{(9.10d)} \\
\partial_r c_{cm}(R_0) - a \partial_r P_{cm}(R_0)\, c^0 = 0. & \text{(9.10e)}
\end{cases}$$

Proof. The result follows from the linearity of eq. (9.9), the independence of the cosine and sine modes and the fact that for all $m \in \mathbb{N}$:

$$\partial_{\theta\theta}^2 \rho_{m\lambda} = -m^2 \rho_{m\lambda}.$$

□

Remark 9.2.5. *We deduce from lemma 9.2.4 and the independence of the cosine and sine perturbations that studying the eigenvalues of eq. (9.9) is equivalent to the study, for all $m \in \mathbb{N}$, of those of eq. (9.10). Indeed, if $\lambda \in \mathbb{C}$ is an eigenvalue of eq. (9.10) associated with the eigenfunctions $(\rho_\lambda, c_\lambda, P_\lambda)$ then λ is an eigenvalue of eq. (9.9) associated with the eigenfunctions:*

$$\begin{aligned}
\rho(\theta) &= \rho_\lambda \cos(m\theta), \\
c(r,\theta) &= c_\lambda(r) \cos(m\theta), \\
P(r,\theta) &= P_\lambda(r) \cos(m\theta).
\end{aligned}$$

Lemma 9.2.6. *If $m \geq 1$ and $0 \leq \chi_c \leq \frac{1}{ac^0 f'_{\text{act}}(c^0)}$, then all the eigenvalues of eq. (9.10) have non-positive real parts.*

Proof. Let $m \geq 1$. Let $\lambda \in \mathbb{C}$ be a eigenvalue of eq. (9.10). Let ρ_m, c_m and P_m satisfy eq. (9.10). For all $r \in (0, R_0)$ and $\theta \in (-\pi, \pi]$, we set:

$$\begin{aligned}
\rho(\theta) &= \rho_m \cos(m\theta), \\
c(r,\theta) &= c_m(r) \cos(m\theta), \\
P(r,\theta) &= P_m(r) \cos(m\theta).
\end{aligned}$$

We also set $Q = c - ac^0 P$. Thus Q follows the following problem:

$$\begin{cases}
-\Delta Q = \Delta c & \text{in } \Omega^0, \quad \text{(9.11a)} \\
\left(1 - a\chi_c c^0 f'_{\text{act}}\left(c^0\right)\right) P = \frac{\gamma}{R_0^2}\left(m^2-1\right)\rho + \chi_c f'_{\text{act}}\left(c^0\right) Q + \lambda \chi_u f'_{\text{und}}(0)\,\rho & \text{on } \partial\Omega^0, \quad \text{(9.11b)} \\
\nabla Q \cdot \mathbf{n} = 0 & \text{on } \partial\Omega^0. \quad \text{(9.11c)}
\end{cases}$$

Thus using eqs. (9.10) and (9.11) we compute:

$$\begin{aligned}\lambda\int_{\Omega^0}|c|^2\,\mathrm{d}\mathbf{x}&=\int_{\Omega^0}\bar{c}\Delta c\,\mathrm{d}\mathbf{x}=\int_{\Omega^0}\left(\bar{Q}+ac^0\bar{P}\right)\Delta Q\,\mathrm{d}\mathbf{x}\\&=-\int_{\Omega^0}|\nabla Q|^2\,\mathrm{d}\mathbf{x}-ac^0\int_{\Omega^0}\nabla\bar{P}\cdot\nabla Q\,\mathrm{d}\mathbf{x}\\&=-\int_{\Omega^0}|\nabla Q|^2\,\mathrm{d}\mathbf{x}-ac^0\int_{\partial\Omega^0}Q\nabla\bar{P}\cdot\mathbf{n}\,\mathrm{d}\sigma.\end{aligned}$$

Since

$$\begin{aligned}\int_{\partial\Omega^0}Q\nabla\bar{P}\cdot\mathbf{n}\,\mathrm{d}\sigma&=\frac{1}{\chi_c f'_{\mathrm{act}}\left(c^0\right)}\left[\int_{\partial\Omega^0}\left(1-ac^0\chi_c f'_{\mathrm{act}}\left(c^0\right)\right)P\nabla\bar{P}\cdot\mathbf{n}\,\mathrm{d}\sigma\right.\\&\qquad\left.-\left(\frac{\gamma}{R_0^2}\left(m^2-1\right)+\lambda\chi_u f'_{\mathrm{und}}\left(0\right)\right)\int_{\partial\Omega^0}\rho\nabla\bar{P}\cdot\mathbf{n}\,\mathrm{d}\sigma\right]\\&=\frac{1}{\chi_c f'_{\mathrm{act}}\left(c^0\right)}\left[\left(1-ac^0\chi_c f'_{\mathrm{act}}\left(c^0\right)\right)\int_{\Omega^0}|\nabla P|^2\,\mathrm{d}\mathbf{x}\right.\\&\qquad+\bar{\lambda}\frac{\gamma}{R_0^2}\left(m^2-1\right)\int_{\partial\Omega^0}|\rho|^2\,\mathrm{d}\sigma\\&\qquad\left.+\chi_u f'_{\mathrm{und}}\left(0\right)\int_{\partial\Omega^0}|\nabla P\cdot\mathbf{n}|^2\,\mathrm{d}\sigma\right].\end{aligned}$$

We deduce that for all $\lambda\in\mathbb{C}$ eigenvalue of $\mathcal{A}_m$ we have:

$$\begin{aligned}&\lambda\int_{\Omega^0}|c|^2\,\mathrm{d}\mathbf{x}+\frac{\bar{\lambda}}{\chi_c f'_{\mathrm{act}}\left(\tilde{c}\right)}\frac{\gamma}{R_0^2}\left(m^2-1\right)\int_{\partial\Omega^0}|\rho|^2\,\mathrm{d}\sigma\\&=-\int_{\Omega^0}|\nabla Q|^2\,\mathrm{d}\mathbf{x}-a\tilde{c}\frac{1-ac^0\chi_c f'_{\mathrm{act}}\left(c^0\right)}{\chi_c f'_{\mathrm{act}}\left(c^0\right)}\int_{\Omega^0}|\nabla P|^2\,\mathrm{d}\mathbf{x}-\frac{\chi_u f'_{\mathrm{und}}\left(0\right)}{\chi_c f'_{\mathrm{act}}\left(c^0\right)}\int_{\partial\Omega^0}|\nabla P\cdot\mathbf{n}|^2\,\mathrm{d}\sigma.\end{aligned}$$

The result follows from this equality. □

Remark 9.2.7. *It seems that the result holds for all $\chi_c>0$ as long as $\frac{\chi_c}{\chi_c^*}\leq 1$. We do not prove this here. However, the study of travelling waves in section 9.3 and the bifurcation result of theorem 9.3.3 suggest that the result may indeed extend to all χ_c such that $\frac{\chi_c}{\chi_c^*}\leq 1$.*

Lemma 9.2.8. *Let $m\in\mathbb{N}$. The eigenfunctions of eq. (9.10) associated with the eigenvalue $\lambda\in\mathbb{C}$ are given by:*

$$\begin{pmatrix}\rho\\c\left(r\right)\\P\left(r\right)\end{pmatrix}=\begin{pmatrix}\hat{\rho}_{m\lambda}\\\hat{c}_{m\lambda}I_m\left(-r\lambda^{\frac{1}{2}}\right)\\\hat{P}_{m\lambda}r^m\end{pmatrix},$$

where $0\leq r<R_0$ and $\left(\hat{\rho}_{m\lambda},\hat{c}_{m\lambda},\hat{P}_{m\lambda}\right)\in\mathbb{C}^3$ solution of:

$$\begin{cases}\lambda\hat{\rho}_{m\lambda}=-mR_0^{m-1}\hat{P}_{m\lambda},&\text{(9.12a)}\\R_0^m\hat{P}_{m\lambda}=\left(\frac{\gamma}{R_0^2}\left(m^2-1\right)+\lambda\chi_u f'_{\mathrm{und}}\left(0\right)\right)\hat{\rho}_{m\lambda}+\chi_c f'_{\mathrm{act}}\left(c^0\right)I_m\left(-R_0\lambda^{\frac{1}{2}}\right)\hat{c}_{m\lambda},&\text{(9.12b)}\\\frac{\lambda^{\frac{1}{2}}}{2}\left(I_{m-1}\left(-R_0\lambda^{\frac{1}{2}}\right)+I_{m+1}\left(-R_0\lambda^{\frac{1}{2}}\right)\right)\hat{c}_{m\lambda}=\lambda ac^0\hat{\rho}_{m\lambda}.&\text{(9.12c)}\end{cases}$$

Proof. From lemma 9.2.4, we deduce that for all $0 \leq r < R_0$ that:

$$\rho = \hat{\rho}_{m\lambda} \in \mathbb{C}$$

and since P satisfies eq. (9.10a), the laplace equation:

$$P(r) = \hat{P}_{m\lambda} r^m,$$

with $\hat{P}_{m\lambda} \in \mathbb{C}$. Moreover, as c satisfies eq. (9.10d) and thus, by the definition of Bessel functions, we have:

$$c(r) = \hat{c}_{m\lambda} I_m\left(-r\lambda^{\frac{1}{2}}\right),$$

where $0 \leq r < R_0$, $\hat{c}_{m\lambda} \in \mathbb{C}$ and I_m is the modified Bessel function of the first kind of order m.

As ρ and P satisfy eq. (9.10b), it follows that:

$$\lambda\hat{\rho}_{m\lambda} = -m\hat{P}_{m\lambda} R_0^{m-1}.$$

Likewise, since ρ, c and P satisfy eq. (9.10c), we have that:

$$\hat{P}_{m\lambda} R_0^m = \frac{\gamma}{R_0^2}\left(m^2-1\right)\hat{\rho}_{m\lambda} + \chi_c f'_{\text{act}}\left(c^0\right)\hat{c}_{m\lambda} I_m\left(-R_0\lambda^{\frac{1}{2}}\right) - m\chi_u f'_{\text{und}}(0)\, R_0^{m-1}\hat{P}_{m\lambda}.$$

Combining this with the previous equality, we obtain that:

$$R_0^m\hat{P}_{m\lambda} = \left(\frac{\gamma}{R_0^2}\left(m^2-1\right) + \lambda\chi_u f'_{\text{und}}(0)\right)\hat{\rho}_{m\lambda} + \chi_c f'_{\text{act}}\left(c^0\right) I_m\left(-R_0\lambda^{\frac{1}{2}}\right)\hat{c}_{m\lambda}.$$

Finally as ρ, c and P satisfy eqs. (9.10b) and (9.10e), we have:

$$-\lambda^{\frac{1}{2}} I'_m\left(-R_0\lambda^{\frac{1}{2}}\right)\hat{c}_{m\lambda} + \lambda a c^0\hat{\rho}_{m\lambda} = 0.$$

Using the properties of Bessel functions, we deduce that:

$$\frac{\lambda^{\frac{1}{2}}}{2}\left(I_{m-1}\left(-R_0\lambda^{\frac{1}{2}}\right) + I_{m+1}\left(-R_0\lambda^{\frac{1}{2}}\right)\right)\hat{c}_{m\lambda} = \lambda a c^0\hat{\rho}_{m\lambda}.$$

□

From the previous lemma, we derive the following result on the eigenvalues of eq. (9.10).

Lemma 9.2.9. *Let $m \in \mathbb{N}$. Let $\lambda \in \mathbb{C}$ be an eigenvalue of eq. (9.10), then λ is such that*

$$H_m(\lambda) = 0,$$

with H_m defined for all $z \in \mathbb{C}$ by:

$$H_m(z) = \frac{z^{\frac{1}{2}}}{2}\left[z\left(1 + \frac{m}{R_0}\chi_u f'_{\text{und}}(0)\right) + \frac{\gamma}{R_0^3} m\left(m^2-1\right)\right]\left[I_{m-1}\left(-R_0 z^{\frac{1}{2}}\right) + I_{m+1}\left(-R_0 z^{\frac{1}{2}}\right)\right] + zm\frac{a\chi_c c^0 f'_{\text{act}}}{R_0} I_m\left(-R_0 z^{\frac{1}{2}}\right).$$

Proposition 9.2.10. *1. If $0 \leq \dfrac{\chi_c}{\chi_c^*} < 1$, then eq. (9.9) admits $\lambda = 0$ as an eigenvalue of multiplicity three and all its other eigenvalues have a negative real part.*

2. *If* $\frac{\chi_c}{\chi_c^*} > 1$*, then eq.* (9.9) *admits a positive eigenvalue.*

Proof. When $m = 0$, for all $z \in \mathbb{C}$, we have:

$$H_0(z) = z^{\frac{3}{2}} I_1\left(-R_0 z^{\frac{1}{2}}\right).$$

$z = 0$ is a solution of $H_0(z) = 0$. This eigenvalue is associated with the eigenfunctions defined for all $r \in [0, R_0)$ by:

$$\begin{pmatrix} \hat{\rho}_{00}^1 \\ \hat{c}_{00}^1(r) \\ \hat{P}_{00}^1(r) \end{pmatrix} = \begin{pmatrix} 1 \\ 0 \\ -\frac{\gamma}{R_0^2} \end{pmatrix} \quad \text{and} \quad \begin{pmatrix} \hat{\rho}_{00}^2 \\ \hat{c}_{00}^2(r) \\ \hat{P}_{00}^2(r) \end{pmatrix} = \begin{pmatrix} 0 \\ 1 \\ \chi_c f'_{\text{act}}(c^0) \end{pmatrix}.$$

The other roots of H_0 are given by $\lambda_{0k} = -\frac{x_{1k}^2}{R_0^2}$ where $x_{1k} \in \mathbb{R}$ is the k^{th} root of J_1, the Bessel function of the first kind of order 1. We have that the eigenvalue $\lambda_{0k} < 0$ is associated with the eigenfunction defined for all $r \in [0, R_0)$ by:

$$\begin{pmatrix} \hat{\rho}_{0k} \\ \hat{c}_{0k}(r) \\ \hat{P}_{0k}(r) \end{pmatrix} = \begin{pmatrix} 0 \\ J_0\left(\frac{x_{1k}}{R_0} r\right) \\ \chi_c f'_{\text{act}}(c^0) J_0(x_{1k}) \end{pmatrix}.$$

When $m = 1$, for all $z \in \mathbb{C}$ we have:

$$H_1(z) = \frac{z^{\frac{3}{2}}}{2}\left(1 + \frac{1}{R_0}\chi_u f'_{\text{und}}(0)\right)\left[I_0\left(-R_0 z^{\frac{1}{2}}\right) + I_2\left(-R_0 z^{\frac{1}{2}}\right)\right] + z\frac{a\chi_c c^0 f'_{\text{act}}}{R_0} I_1\left(-R_0 z^{\frac{1}{2}}\right)$$

Thus $z = 0$ is a solution of $H_1(z) = 0$. This eigenvalue is associated with the eigenfunction defined for all $r \in [0, R_0)$ by:

$$\begin{pmatrix} \hat{\rho}_{10} \\ \hat{c}_{10}(r) \\ \hat{P}_{10}(r) \end{pmatrix} = \begin{pmatrix} 1 \\ 0 \\ 0 \end{pmatrix}.$$

If $m \geq 2$ then $z = 0$ is solution of $H_m(z) = 0$. Nevertheless, since $\gamma > 0$, from eq. (9.12) and $I_m(0) = 0$, we deduce that $\lambda = 0$ is associate to the zero eigenfunction defined for all $r \in [0, R_0)$ by:

$$\begin{pmatrix} \hat{\rho}_{m0} \\ \hat{c}_{m0}(r) \\ \hat{P}_{m0}(r) \end{pmatrix} = \begin{pmatrix} 0 \\ 0 \\ 0 \end{pmatrix}$$

and $\lambda = 0$ is not an eigenvalue of eq. (9.10) when $m \geq 2$. We can therefore conclude about item 1 using remark 9.2.7.

In order to exhibit a positive eigenvalue, we expand H_1 around 0. For all z close to 0, we have:

$$H_1(z) = \frac{z^{\frac{3}{2}}}{2}\left(1 + \frac{\chi_u f'_{\text{und}}(0)}{R_0} - ac^0\chi_c f'_{\text{act}}(c^0) + \frac{R_0^2 z}{8}\left(3 + \frac{3\chi_u f'_{\text{und}}(0)}{R_0} - ac^0\chi_c f'_{\text{act}}(c^0)\right)\right) + \mathcal{O}\left(|z|^{\frac{7}{2}}\right)$$

The function $z \mapsto 1 + \frac{\chi_u f'_{\text{und}}(0)}{R_0} - ac^0 \chi_c f'_{\text{act}}\left(c^0\right) + \frac{R_0^2 z}{8}\left(3 + \frac{3\chi_u f'_{\text{und}}(0)}{R_0} - ac^0 \chi_c f'_{\text{act}}\left(c^0\right)\right)$ admits z_1 as root, with z_1 defined by:

$$z_1 = \frac{8\left(ac^0 \chi_c f'_{\text{act}}\left(c^0\right) - 1 - \frac{\chi_u f'_{\text{und}}(0)}{R_0}\right)}{R_0^2\left(3\left(1 + \frac{\chi_u f'_{\text{und}}(0)}{R_0}\right) - ac^0 \chi_c f'_{\text{act}}\left(c^0\right)\right)}.$$

$z_1 \in \mathbb{R}$ changes sign and becomes positive when χ_c exceeds $\dfrac{R_0 + \chi_u f'_{\text{und}}(0)}{R_0 ac^0 f'_{\text{act}}\left(c^0\right)} = \chi_c^*$. Furthermore, z_1 approaches a true root λ_1 of H_1. Indeed, when $ac^0 \chi_c f'_{\text{act}}\left(c^0\right)$ close to $1 + \frac{\chi_u f'_{\text{und}}(0)}{R_0}$, we have:

$$\lambda_1 = \frac{4}{R_0^2}\left(ac^0 \chi_c f'_{\text{act}}\left(c^0\right) - 1 + \frac{\chi_u f'_{\text{und}}(0)}{R_0}\right) + o\left(\left|ac^0 \chi_c f'_{\text{act}}\left(c^0\right) - 1 + \frac{\chi_u f'_{\text{und}}(0)}{R_0}\right|\right)$$

associated with the eigenfunction defined for all $r \in [0, R_0)$ by:

$$\begin{pmatrix} \hat{\rho}_{1\lambda_1} \\ \hat{c}_{1\lambda_1}(r) \\ \hat{P}_{1\lambda_1}(r) \end{pmatrix} = \begin{pmatrix} \dfrac{-\chi_c f'_{\text{act}} I_1\left(-R_0 \lambda_1^{\frac{1}{2}}\right)}{R_0 + \chi_u f'_{\text{und}}(0)} \\ \lambda_1 I_1\left(-r\lambda_1^{\frac{1}{2}}\right) \\ \dfrac{\chi_c f'_{\text{act}} I_1\left(-R_0 \lambda_1^{\frac{1}{2}}\right)\lambda_1}{R_0 + \chi_u f'_{\text{und}}(0)} r \end{pmatrix}.$$

Thus when $\chi_c > \chi_c^*$, eq. (9.9) admits λ_1 as positive eigenvalue. □

9.3 . Existence of travelling wave

In this section, we define and characterise the travelling wave solutions of the model. Using a bifurcation argument, we prove that such solutions exist.

9.3.1 . Definition and characterisation of the travelling waves

A travelling wave is characterised by a domain with a fixed shape $\tilde{\Omega}$ moving at a constant velocity $V \in \mathbb{R}$ in a fixed direction $\mathbf{w} \in \mathbb{R}^2$. We then have:

$$\Omega(t) = \tilde{\Omega} + tV\mathbf{w}.$$

Without loss of generality, assume that $V > 0$ and $\mathbf{w} = (1, 0)$. In this case, the normal velocity at the boundary of the cell satisfies $V_n = Vn_x$.

Using the travelling wave ansatz:

$$c = c(x - Vt, y), \qquad P = P(x - Vt, y), \qquad \Omega(t) = \tilde{\Omega} + (Vt, 0),$$

we obtain that a solution of model (9.1), which is a travelling wave for this model, is defined as follows in definition 9.3.1.

Definition 9.3.1. *A travelling wave of the model (9.1) is given by a domain $\tilde{\Omega} \subset \mathbb{R}^2$, $V > 0$ a real velocity and two functions P and c satisfying:*

$$\begin{cases} -\Delta P = 0 & \text{in } \tilde{\Omega}, & \text{(9.13a)} \\ P = \gamma\kappa + \chi_c f_{\text{act}}(c) + \chi_u f_{\text{und}}(V n_x) & \text{on } \partial\tilde{\Omega}, & \text{(9.13b)} \\ -\nabla P \cdot \mathbf{n} = V n_x & \text{on } \partial\tilde{\Omega}, & \text{(9.13c)} \\ \operatorname{div}((V,0)\, c + \nabla c + (1-a)\nabla P c) = 0 & \text{in } \tilde{\Omega}, & \text{(9.13d)} \\ (\nabla c + a(V,0)\, c) \cdot \mathbf{n} = 0 & \text{on } \partial\tilde{\Omega}. & \text{(9.13e)} \end{cases}$$

Proposition 9.3.2. *Let $V > 0$ be given. If c and P are solutions of eq. (9.13) associated with V then c and P are of the form:*

$$\begin{aligned} P(x,y) &= p_1 - Vx && \text{with } p_1 \in \mathbb{R}, \\ c(x,y) &= \frac{M}{\int_{\tilde{\Omega}} e^{-aVx'} \,\mathrm{d}x' \,\mathrm{d}y'} e^{-aVx}, \end{aligned}$$

where $(x,y) \in \tilde{\Omega}$ and we recall that $M \geq 0$ is the total quantity of markers.

Furthermore, $\partial\tilde{\Omega}$ is characterised by the curvature equation:

$$\gamma\kappa(x,y) = p_1 - Vx - \chi_c f_{\text{act}}\left(\frac{M e^{-aVx}}{\int_{\tilde{\Omega}} e^{-aVx'} \,\mathrm{d}x' \,\mathrm{d}y'}\right) - \chi_u f_{\text{und}}(V n_x), \quad (x,y) \in \partial\tilde{\Omega}. \tag{9.14}$$

Proof. We set $\tilde{\mathbf{u}} = -\nabla P - \mathbf{u}_{\text{cm}}$ where $\mathbf{u}_{\text{cm}}$ is defined by eq. (9.3). The travelling wave assumption implies that $\mathbf{u}_{\text{cm}} = (V,0)$. Thus, setting $\phi = -P - Vx$ we have:

$$\tilde{\mathbf{u}} = \nabla\phi.$$

Moreover, from eq. (9.13a), we deduce that ϕ satisfies $-\Delta\phi = 0$ in $\tilde{\Omega}$ and from (9.13c) we deduce that ϕ also satisfies $\nabla\phi \cdot \mathbf{n} = 0$ on $\partial\tilde{\Omega}$. On the one hand, we have that:

$$\int_{\tilde{\Omega}} |\nabla\phi|^2 \,\mathrm{d}\mathbf{x} = -\int_{\tilde{\Omega}} \phi\Delta\phi \,\mathrm{d}\mathbf{x} + \int_{\partial\tilde{\Omega}} \phi\nabla\phi \cdot \mathbf{n} \,\mathrm{d}\sigma = 0.$$

On the another hand, we have that:

$$\int_{\tilde{\Omega}} |\nabla\phi|^2 \,\mathrm{d}\mathbf{x} = \int_{\tilde{\Omega}} |\tilde{\mathbf{u}}|^2 \,\mathrm{d}\mathbf{x}.$$

Thus we have that $\tilde{\mathbf{u}} = 0$ on $\tilde{\Omega}$. It follows that for all $(x,y) \in \tilde{\Omega}$:

$$P(x,y) = p_1 - Vx,$$

with $p_1 \in \mathbb{R}$.

By substituting $\nabla P = -(V,0)$ in eqs. (9.13d) and (9.13e), the concentration of markers satisfies the following problem:

$$\begin{cases} \operatorname{div}(\nabla c + a(V,0)\, c) = 0 & \text{in } \tilde{\Omega}, & \text{(9.15a)} \\ (\nabla c + a(V,0)\, c) \cdot \mathbf{n} = 0 & \text{on } \partial\tilde{\Omega}. & \text{(9.15b)} \end{cases}$$

The non-negative solutions of eq. (9.15) are given by:

$$c(x,y) = c_1 e^{-aVx}, \tag{9.16}$$

with $c_1 > 0$ and $(x,y) \in \tilde{\Omega}$. Indeed, we can see that functions of the form (9.16) are solutions of eq. (9.15). If we assume that $c(x,y) = c_1(x,y)\, e^{-aVx}$ is a solution of eq. (9.15), then we have that:

$$\begin{aligned} 0 &= \int_{\tilde{\Omega}} c_1(x,y) \operatorname{div}\left(\nabla c(x,y) + a(V,0)\, c(x,y)\right) \mathrm{d}x\, \mathrm{d}y \\ &= \int_{\tilde{\Omega}} \nabla c_1(x,y) \cdot \left(\nabla c(x,y) + a(V,0)\, c(x,y)\right) \mathrm{d}x\, \mathrm{d}y \\ &= \int_{\tilde{\Omega}} \left|\nabla c_1(x,y)\right|^2 e^{-aVx}\, \mathrm{d}x\, \mathrm{d}y, \end{aligned}$$

from which we deduce that $|\nabla c_1| = 0$ on $\tilde{\Omega}$. Finally, remember that the total number of markers M is constant, so c_1 must be such that $\int_{\tilde{\Omega}} c_1 e^{-aVx}\, \mathrm{d}x\, \mathrm{d}y = M$. This leads to

$$c_1 = \frac{M}{\int_{\tilde{\Omega}} c_1 e^{-aVx'}\, \mathrm{d}x'\, \mathrm{d}y'}.$$

To find the curvature equation (9.14), we inject the expressions found for P and c into equation (9.13b). □

Theorem 9.3.3. *Assume that f_{act} satisfies assumptions (1.12). For all $a \in (0,1]$, $\gamma > 0$, $R_0 > 0$ and $\chi_u > 0$ there exists a one parameter family of travelling wave solutions $\left(\tilde{\Omega}_\chi, V_\chi\right)$ of eq. (9.1), parametrized by $\chi \in (\chi_c^*, +\infty)$ such that $\left|\tilde{\Omega}_\chi\right| = \pi R_0^2$.*

9.3.2 . Proof of theorem 9.3.3

Since the disc of radius R_0 with $V = 0$ is a solution of (9.13), we seek other solutions of eq. (9.13) such that the domain $\tilde{\Omega}$ is a perturbation of the disc. We therefore look for $\tilde{\Omega}$ such that:

$$\tilde{\Omega} = \{(r\cos(\theta), r\sin(\theta)) \text{ s.t. } 0 \le r \le R_0 + \rho(\theta) \text{ and } \theta \in (-\pi, \pi]\}$$

with $\rho : \mathbb{R} \to (-R_0, +\infty)$ a 2π-periodic function satifying:

$$\int_{-\pi}^{\pi} \left(R_0 + \rho(\theta)\right)^2 - R_0^2\, \mathrm{d}\theta = 0.$$

This latter condition ensures that $\left|\tilde{\Omega}\right| = \pi R_0^2$. The boundary of domain $\tilde{\Omega}$ is parametrized by:

$$\{(R_0 + \rho(\theta))\cos\theta, (R_0 + \rho(\theta))\sin\theta\} \quad \text{for } \theta \in (-\pi, \pi].$$

For all $\theta \in (-\pi, \pi]$, the outward normal vector to $\partial\tilde{\Omega}$ is given by:

$$\mathbf{n}(\theta) = \begin{pmatrix} n_1(\theta) \\ n_2(\theta) \end{pmatrix} = \frac{1}{\left(\left(R_0 + \rho(\theta)\right)^2 + \rho'(\theta)^2\right)^{\frac{1}{2}}} \begin{pmatrix} \left(R_0 + \rho(\theta)\right)\cos\theta + \rho'(\theta)\sin\theta \\ \left(R_0 + \rho(\theta)\right)\sin\theta - \rho'(\theta)\cos\theta \end{pmatrix}$$

and the mean curvature by:

$$\kappa(\theta) = \frac{\left(R_0 + \rho(\theta)\right)^2 + 2\rho'(\theta)^2 - \left(R_0 + \rho(\theta)\right)\rho''(\theta)}{\left(\left(R_0 + \rho(\theta)\right)^2 + \rho'(\theta)^2\right)^{\frac{3}{2}}}. \tag{9.17}$$

The condition on the boundary domain eq. (9.14) can be expressed as:

$$\gamma\kappa(\theta) + V(R_0 + \rho(\theta))\cos\theta + \chi_c f_{\text{act}}\left(c_1(V,\rho)\, e^{-aV(R_0+\rho(\theta))\cos\theta}\right) + \chi_u f_{\text{und}}(Vn_1(\theta)) = p_1, \tag{9.18}$$

where $\theta \in (-\pi, \pi]$ and $c_1(V,\rho) = \dfrac{M}{\int_{-\pi}^{\pi}\int_0^{R_0+\rho(\theta)} e^{-aVr\cos\theta} r \,\mathrm{d}r\,\mathrm{d}\theta}$.

As we are looking for travelling waves in the x-direction, we restrict ourselves to domains $\tilde{\Omega}$ symmetrical about the x-axis. We then introduce the functional spaces:

$$X = \left\{\rho \in \mathcal{C}^{2,\alpha}_{\text{per}}(-\pi,\pi) : \rho(\theta) = \rho(-\theta), \forall\theta \in (-\pi,\pi)\right\},$$
$$Y = \left\{\rho \in \mathcal{C}^{0,\alpha}_{\text{per}}(-\pi,\pi) : \rho(\theta) = \rho(-\theta), \forall\theta \in (-\pi,\pi)\right\}.$$

Therefore, the existence of a boundary $\partial\tilde{\Omega}$ solving eq. (9.14) is equivalent to the existence of a function $\rho \in X$ solving eq. (9.18).

Let $\mathcal{F} : \mathbb{R}\times X\times\mathbb{R}\times\mathbb{R} \to Y\times\mathbb{R}\times\mathbb{R}$ the functional defined for all $(\chi_c,\rho,V,p_1) \in \mathbb{R}\times X\times\mathbb{R}\times\mathbb{R}$ by:

$$\begin{aligned}\mathcal{F}(\chi_c,\rho,V,p_1) = \Big(&\gamma\kappa(\theta) + \chi_c f_{\text{act}}\left(c_1(V,\rho)\, e^{-aV(R_0+\rho(\theta))\cos\theta}\right) + \chi_u f_{\text{und}}(Vn_1(\theta)) \\ &+ V(R_0+\rho(\theta))\cos\theta - p_1 - \frac{\gamma}{R_0}; \\ &\int_{-\pi}^{\pi}(R_0+\rho(\theta))^2 - R_0^2\,\mathrm{d}\theta; \int_{-\pi}^{\pi}\rho(\theta)\cos\theta\,\mathrm{d}\theta\Big).\end{aligned} \tag{9.19}$$

Lemma 9.3.4. *The functional $\mathcal{F}$ defined by (9.19) satisfies the following properties:*

1. $\mathcal{F}(\chi_c,0,0,0) = 0$ *for all* $\chi_c \in \mathbb{R}$.
2. $\operatorname{Ker}\partial_{(\rho,V,p_1)}\mathcal{F}(\chi_c^*,0,0,0)$ *is a one dimensional subspace of* $X\times\mathbb{R}\times\mathbb{R}$ *spanned by* $(0,1,0)$.
3. $\operatorname{Range}\partial_{(\rho,V,p_1)}\mathcal{F}(\chi_c^*,0,0,0)$ *is a closed subspace of* $Y\times\mathbb{R}\times\mathbb{R}$ *of codimension* 1.
4. $\partial_{\chi_c}\partial_{(\rho,V,p_1)}\mathcal{F}(\chi_c^*,0,0,0)[0,1,0] \notin \operatorname{Range}\partial_{(\rho,V,p_1)}\mathcal{F}(\chi_c^*,0,0,0)$.

Proof. *Item 1.* When $\rho = 0$, using the expression of the mean curvature (9.17), we have for all $\theta \in (-\pi,\pi]$, $\kappa(\theta) = \frac{1}{R_0}$. Thus for all $\chi_c \in \mathbb{R}$, we have $\mathcal{F}(\chi_c,0,0,0) = 0$.

Item 2. Let $\chi_c \in \mathbb{R}$. Let $\mathcal{L}_{\chi_c}$ be the linear operator defined by:

$$\begin{array}{rccl}\mathcal{L}_{\chi_c} & : & X\times\mathbb{R}\times\mathbb{R} & \to & Y\times\mathbb{R}\times\mathbb{R} \\ & & (\rho,V,p_1) & \mapsto & \mathcal{F}_\rho(\chi_c,0,0,0)[\rho] + \mathcal{F}_V(\chi_c,0,0,0)[V] + \mathcal{F}_{p_1}(\chi_c,0,0,0)[p_1].\end{array}$$

For all $(\rho,V,p_1) \in X\times\mathbb{R}\times\mathbb{R}$ we have:

$$\begin{aligned}\mathcal{L}_{\chi_c}(\rho,V,p_1) = \Big(&-\gamma\frac{\rho+\rho''}{R_0^2} - \frac{\chi_c c^0 f'_{\text{act}}(c^0)}{R_0}\int_{-\pi}^{\pi}\rho(\theta)\,\mathrm{d}\theta - ac^0\chi_c f'_{\text{act}}(c^0)R_0V\cos\theta \\ &+ R_0V\cos\theta - p_1 + \chi_u f'_{\text{und}}(0)V\cos\theta; \\ &2R_0\int_{-\pi}^{\pi}\rho(\theta)\,\mathrm{d}\theta; \int_{-\pi}^{\pi}\rho(\theta)\cos\theta\,\mathrm{d}\theta\Big)\end{aligned}$$

and thus in particular for $\chi_c = \chi_c^*$ we have:

$$\begin{aligned}\mathcal{L}_{\chi_c^*}(\rho,V,p_1) = \Big(&-\gamma\frac{\rho+\rho''}{R_0^2} - \frac{R_0+\chi_u f'_{\text{und}}(0)}{aR_0^2}\int_{-\pi}^{\pi}\rho(\theta)\,\mathrm{d}\theta - p_1; \\ &2R_0\int_{-\pi}^{\pi}\rho(\theta)\,\mathrm{d}\theta; \int_{-\pi}^{\pi}\rho(\theta)\cos\theta\,\mathrm{d}\theta\Big).\end{aligned}$$

The elements (ρ, V, p_1) of $\operatorname{Ker} \partial_{(\rho,V,p_1)} \mathcal{F}(\chi_c^*, 0, 0, 0)$ are therefore such that

$$\rho'' + \rho = -\frac{R_0^2}{\gamma} p_1, \tag{9.20}$$

with the conditions

$$\begin{cases} \displaystyle\int_{-\pi}^{\pi} \rho(\theta)\, \mathrm{d}\theta = 0, \\ \displaystyle\int_{-\pi}^{\pi} \rho(\theta) \cos\theta \, \mathrm{d}\theta = 0, \\ \rho \text{ even function.} \end{cases}$$

As ρ even, necessarily the condition $\int_{-\pi}^{\pi} \rho(\theta) \sin\theta \, \mathrm{d}\theta = 0$ holds. The solutions to the differential equation (9.20) are given, for all $\theta \in (-\pi, \pi]$, by

$$\rho(\theta) = A \cos\theta + B \sin\theta - \frac{R_0^2}{\gamma} p_1$$

where $A, B \in \mathbb{R}$.

We have:

$$\int_{-\pi}^{\pi} \rho(\theta)\, \mathrm{d}\theta = -2\pi \frac{R_0^2}{\gamma} p_1$$

and thus necessarily $p_1 = 0$. This leads to:

$$\int_{-\pi}^{\pi} \rho(\theta) \cos\theta \, \mathrm{d}\theta = A\pi,$$
$$\int_{-\pi}^{\pi} \rho(\theta) \sin\theta \, \mathrm{d}\theta = B\pi$$

which implies $A = 0$ and $B = 0$. We then have $\rho = 0$ and

$$\operatorname{Ker} \partial_{(\rho,V,p_1)} \mathcal{F}(\chi_c^*, 0, 0, 0) = \operatorname{Span}\{(0, 1, 0)\}.$$

Item 3. To prove this property, we demonstrate that:

$$\operatorname{Range} \partial_{(\rho,V,p_1)} \mathcal{F}(\chi_c^*, 0, 0, 0) = \left\{ (h, C_1, C_2) \in Y \times \mathbb{R} \times \mathbb{R} \text{ s.t. } \int_{-\pi}^{\pi} h(\theta) \cos\theta \, \mathrm{d}\theta = 0 \right\}.$$

Let $(h, C_1, C_2) \in \operatorname{Range} \partial_{(\rho,V,p_1)} \mathcal{F}(\chi_c^*, 0, 0, 0)$. Thus there exists $\rho \in X$ and $p_1 \in \mathbb{R}$ such that:

$$-\gamma \frac{\rho + \rho''}{R_0^2} - \frac{R_0 + \chi_u f'_{\mathrm{und}}(0)}{a R_0^2} \int_{-\pi}^{\pi} \rho(\theta)\, \mathrm{d}\theta - p_1 = h. \tag{9.21}$$

By multiplying it by $\cos\theta$ and integrating it over $[-\pi, \pi]$ we obtain that necessarily h is such that:

$$\int_{-\pi}^{\pi} h(\theta) \cos\theta \, \mathrm{d}\theta = 0.$$

Reciprocally, let $h \in \mathcal{C}^{0,\alpha}_{\mathrm{per}}(-\pi, \pi)$ and $p_1 \in \mathbb{R}$. The eq. (9.21) admits a soution in $\mathcal{C}^{2,\alpha}_{\mathrm{per}}(-\pi, \pi)$ if and only if $\int_{-\pi}^{\pi} h(\theta) \cos\theta \, \mathrm{d}\theta = \int_{-\pi}^{\pi} h(\theta) \sin\theta \, \mathrm{d}\theta = 0$. The general solutions are of the form:

$$\rho(\theta) = \overline{\rho}(\theta) + k_1 \cos(\theta) + k_2 \sin(\theta),$$

where $\overline{\rho}$ is an even particular solution.

Let $(h, C_1, C_2) \in \operatorname{Range} \partial_{(\rho,V,p_1)} \mathcal{F}(\chi_c^*, 0, 0, 0)$. As $h \in Y$, necessarily $\int_{-\pi}^{\pi} h(\theta) \sin\theta \, \mathrm{d}\theta = 0$. Assume that $\int_{-\pi}^{\pi} h(\theta) \cos\theta \, \mathrm{d}\theta = 0$. There exists $\rho \in X$ solution of eq. (9.21). Taking the even part of the general solutions, we have that:

$$\rho(\theta) = \frac{1}{2}\left[\overline{\rho}(\theta) + \overline{\rho}(-\theta)\right] + k_1 \cos(\theta).$$

We choose k_1 such that $\int_{-\pi}^{\pi} \rho(\theta) \cos\theta \, \mathrm{d}\theta = C_2$.

Integrating eq. (9.21) with respect to θ yields to:

$$\left(-\frac{\gamma}{R_0^2} - \frac{2\pi\left(R_0 + \chi_u f'_{\mathrm{und}}(0)\right)}{aR_0^2}\right)\int_{-\pi}^{\pi} \rho(\theta) \, \mathrm{d}\theta - 2\pi p_1 = \int_{-\pi}^{\pi} h(\theta) \, \mathrm{d}\theta.$$

We thus choose p_1 such that $\int_{-\pi}^{\pi} \rho(\theta) \, \mathrm{d}\theta = C_1$.

Item 4. For all $(\chi_c, \rho, V, p_1) \in \mathbb{R} \times X \times \mathbb{R} \times \mathbb{R}$ we have:

$$\partial_{\chi_c} \mathcal{L}_{\chi_c}(\rho, V, p_1) = \left(-\frac{c^0 f'_{\mathrm{act}}\left(c^0\right)}{R_0}\int_{-\pi}^{\pi} \rho(\theta) \, \mathrm{d}\theta - ac^0 f'_{\mathrm{act}}\left(c^0\right) R_0 V \cos\theta \, ; 0 \, ; 0 \, ; 0\right).$$

In particular, we have for $\chi_c = \chi_c^*$ and $(\rho, V, p_1) = (0, 1, 0)$:

$$\partial_{\chi_c} \mathcal{L}_{\chi_c^*}(0, 1, 0) = \left(-ac^0 f'_{\mathrm{act}}\left(c^0\right) R_0 \cos\theta \, ; 0 \, ; 0 \, ; 0\right).$$

By contradiction, assume that $\partial_{\chi_c} \partial_{(\rho,V,p_1)} \mathcal{F}(\chi_c^*, 0, 0, 0)[0, 1, 0] \in \operatorname{Range} \partial_{(\rho,V,p_1)} \mathcal{F}(\chi_c^*, 0, 0, 0)$. Then there exists $(\rho, V, p_1) \in X \times \mathbb{R} \times \mathbb{R}$ such that:

$$\begin{cases} \gamma\dfrac{\rho + \rho''}{R_0^2} + \dfrac{R_0 + \chi_u f'_{\mathrm{und}}(0)}{aR_0^2}\displaystyle\int_{-\pi}^{\pi} \rho(\theta) \, \mathrm{d}\theta + p_1 = ac^0 f'_{\mathrm{act}}\left(c^0\right) R_0 \cos\theta \\ \displaystyle\int_{-\pi}^{\pi} \rho(\theta) \, \mathrm{d}\theta = \int_{-\pi}^{\pi} \rho(\theta) \cos\theta \, \mathrm{d}\theta = \int_{-\pi}^{\pi} \rho(\theta) \sin\theta \, \mathrm{d}\theta = 0. \end{cases}$$

By multiplying by $\cos(\theta)$ and integrating the first line over $[-\pi, \pi]$, we obtain:

$$\begin{aligned} &\gamma\int_{-\pi}^{\pi} \rho(\theta) \cos\theta \, \mathrm{d}\theta + \gamma\int_{-\pi}^{\pi} \rho''(\theta) \cos\theta \, \mathrm{d}\theta \\ &\quad + \left(\frac{R_0 + \chi_u f'_{\mathrm{und}}(0)}{a}\int_{-\pi}^{\pi} \rho(\theta) \, \mathrm{d}\theta + p_1\right)\int_{-\pi}^{\pi} \cos\theta \, \mathrm{d}\theta = ac^0 f'_{\mathrm{act}}\left(c^0\right) R_0^3 \int_{-\pi}^{\pi} \cos^2\theta \, \mathrm{d}\theta. \end{aligned}$$

Since $\rho \in X$, ρ is 2π-periodic and thus $\int_{-\pi}^{\pi} \rho''(\theta) \cos\theta \, \mathrm{d}\theta = \int_{-\pi}^{\pi} \rho(\theta) \cos\theta \, \mathrm{d}\theta$. Then we have:

$$ac^0 f'_{\mathrm{act}}\left(c^0\right) R_0^3 \pi = 0,$$

which is a contradiction as $a > 0$, $f'_{\mathrm{act}}\left(c^0\right) > 0$, $c^0 > 0$ and $R_0 > 0$. □

We can therefore apply the Crandall-Rabinowitz bifurcation theorem (Crandall and Rabinowitz, 1971) to the functional $\mathcal{F}$ around the bifurcation point $(\chi_c^*, 0, 0, 0)$. Then for any complement $Z = Z_1 \times Z_2 \times Z_3$ of $\operatorname{Ker} \mathcal{F}(\chi_c^*, 0, 0, 0)$ in $X \times \mathbb{R} \times \mathbb{R}$, there exists a neighborhood N of $(\chi_c^*, 0, 0, 0)$ in $\mathbb{R} \times X \times \mathbb{R} \times \mathbb{R}$, an interval $I = (-\varepsilon, \varepsilon)$ for some $\varepsilon > 0$ and four continuous functions $\varphi : I \to \mathbb{R}$, $\psi_1 : I \to Z_1$, $\psi_2 : I \to Z_2$ and $\psi_3 : I \to Z_3$ such that for all $s \in I$:

$$\mathcal{F}\left(\varphi(s), \psi_1(s), \psi_2(s), \psi_3(s)\right) = (0, 0, 0, 0)$$

and

$$\varphi(0) = \chi_c^*, \quad \psi_1(0) = 0, \quad \psi_2(0) = 0, \quad \psi_3(0) = 0.$$

We can note that for all $s \in (-\varepsilon, \varepsilon)$, $\psi_1(s)$ denotes a function.
In particular, the Crandall-Rabinowitz bifurcation theorem implies that the solutions (χ_c, ρ, V, p_1) of the equation $\mathcal{F}(\chi_c, \rho, V, p_1) = (0,0,0,0)$ are of the form:

$$\begin{cases} \chi_c(s) = \varphi(s), & (9.22) \\ \rho(s,\theta) = s\psi_1(s)(\theta), & (9.23) \\ V(s) = s + s\psi_2(s), & (9.24) \\ p_1(s) = s\psi_3(s), & (9.25) \end{cases}$$

where $s \in I$ and $\theta \in (-\pi, \pi]$. In addition, they satisfy for all $\theta \in (-\pi, \pi]$:

$$\begin{aligned} &\chi_c(0) = \chi_c^*, \\ &\rho(0,\theta) = 0 \quad \text{and} \quad \partial_s \rho(0,\theta) = 0, \\ &V(0) = 0 \quad \text{and} \quad V'(0) = 1, \\ &p_1(0) = 0 \quad \text{and} \quad p_1'(0) = 0. \end{aligned}$$

Thus we have for all $s \in I$:

$$V(s) = s + o(s).$$

As (χ_c, ρ, V, p_1) is solution of the equation $\mathcal{F}(\chi_c, \rho, V, p_1) = (0,0,0,0)$, we have for all $s \in I$:

$$\int_{-\pi}^{\pi} \rho(s,\theta)\cos\theta \,\mathrm{d}\theta = 0 \quad \text{and} \quad \int_{-\pi}^{\pi} (R_0 + \rho(s,\theta))^2 - R_0^2 \,\mathrm{d}\theta = 0.$$

Thus we deduce that for all $n \in \mathbb{N}$ we have:

$$\int_{-\pi}^{\pi} \partial_s^n \rho(0,\theta)\cos\theta \,\mathrm{d}\theta = 0,$$

and

$$\int_{-\pi}^{\pi} \partial_s^2 \rho(0,\theta) \,\mathrm{d}\theta = 0.$$

Lemma 9.3.5. *Assume*

$$\partial_\theta^n \rho(0,\theta) = \partial_\theta^n \partial_s \rho(0,\theta) = 0, \quad \forall n \in \mathbb{N}, \forall \theta \in (-\pi, \pi].$$

Then, we have $\chi_c'(0) = 0$.

Proof. For all $s \in I$ and $\theta \in (-\pi, \pi]$, we set

$$z(s,\theta) = c_1(V(s), \rho(s,\theta)) e^{-aV(s)(R_0+\rho(s,\theta))\cos\theta}.$$

We thus have:

$$z(0,\theta) = c_1(V(0), \rho(0,\theta)) e^{-aV(0)(R_0+\rho(0,\theta))\cos\theta} = c^0.$$

We differenciate with respect to s the first component of $\mathcal{F}$ and we have for all $s \in I$ and $\theta \in (-\pi, \pi]$:

$$\begin{aligned} 0 = \gamma \partial_s \kappa(s,\theta) + \chi_c'(s) f_{\mathrm{act}}(z(s,\theta)) + \chi_c(s) f_{\mathrm{act}}'(z(s,\theta)) \partial_s z(s,\theta) \\ + \chi_u f_{\mathrm{und}}'(V(s) n_1(s,\theta)) (V'(s) n_1(s,\theta) + V(s) \partial_s n_1(s,\theta)) \\ + V'(s)(R_0 + \rho(s,\theta))\cos\theta + V(s)\partial_s \rho(s,\theta)\cos\theta - p_1'(s). \quad (9.26) \end{aligned}$$

Evaluating it at $s = 0$, it leads to:

$$0 = \gamma \partial_s \kappa (0, \theta) + \chi_c' (0) f_{\text{act}} \left(c^0\right) + \chi_c^* f_{\text{act}}' \left(c^0\right) \partial_s z (0, \theta) + \chi_u f_{\text{und}}' (0) n_1 (0, \theta) + R_0 \cos\theta.$$

As $\partial_\theta \rho (s, \theta) = s \partial_\theta \psi_1 (s, \theta)$, we have $\partial_\theta \rho (0, \theta) = 0$. We then have:

$$n_1 (0, \theta) = \frac{1}{R_0} \left(R_0 \cos\theta + \partial_\theta \rho (0, \theta) \sin\theta\right) = \cos\theta.$$

Moreover, as for all $s \in I$ and $\theta \in (-\pi, \pi]$ we have:

$$\begin{aligned} \partial_s z (s, \theta) = & \left(\partial_1 c_1 \left(V (s), \rho (s, \theta)\right) V' (s) + \partial_2 c_1 \left(V (s), \rho (s, \theta)\right) \partial_s \rho (s, \theta)\right) e^{-aV(s)(R_0 + \rho(s,\theta))\cos\theta} \\ & - a \left(V' (s) \left(R_0 + \rho (s, \theta)\right) + V (s) \partial_s \rho (s, \theta)\right) \cos\theta c_1 \left(V (s), \rho (s, \theta)\right) e^{-aV(s)(R_0 + \rho(s,\theta))\cos\theta}. \end{aligned}$$

As $\partial_1 c_1 (0, 0) = 0$, it follows that:

$$\partial_s z (0, \theta) = -aR_0 \cos\theta c^0.$$

Finally, using the definition of χ_c^* (cf eq. (9.6)), we have for all $\theta \in (-\pi, \pi]$:

$$\begin{aligned} 0 &= \gamma \partial_s \kappa (0, \theta) + \chi_c' (0) f_{\text{act}} \left(c^0\right) + \left(\chi_u f_{\text{und}}' (0) + R_0 - \chi_c^* a R_0 c^0 f_{\text{act}}' \left(c^0\right)\right) \cos\theta \\ &= \gamma \partial_s \kappa (0, \theta) + \chi_c' (0) f_{\text{act}} \left(c^0\right). \end{aligned}$$

As for all $\theta \in (-\pi, \pi]$ we have $\partial_s \kappa (0, \theta) = 0$, it follows that necessarily $\chi_c' (0) = 0$. □

Lemma 9.3.6. *Assume*

$$\partial_\theta^n \rho (0, \theta) = \partial_\theta^n \partial_s \rho (0, \theta) = \partial_\theta^n \partial_s^2 \rho (0, \theta) = 0, \quad \forall n \in \mathbb{N}, \forall \theta \in (-\pi, \pi].$$

Then, we have

$$\chi_c'' (0) = -\frac{\left(R_0 + \chi_u f_{\text{und}}' (0)\right) a R_0}{2 \left(f_{\text{act}}' \left(c^0\right)\right)^2} \left(f_{\text{act}}'' \left(c^0\right) + \frac{M}{2\pi R_0^2} f_{\text{act}}''' \left(c^0\right)\right) + \frac{\chi_u f_{\text{und}}''' (0)}{3ac^0 R_0 f_{\text{act}}' \left(c^0\right)}.$$

Proof. We differenciate twice with respect to s eq. (9.26). We thus have for all $s \in I$ and $\theta \in (-\pi, \pi]$:

$$\begin{aligned} 0 = & \gamma \partial_{sss}^3 \kappa (s, \theta) + \chi_c''' (s) f_{\text{act}} (z (s, \theta)) + 3\chi_c'' (s) f_{\text{act}}' (z (s, \theta)) \partial_s z (s, \theta) \\ & + 3\chi_c' (s) f_{\text{act}}' (z (s, \theta)) \partial_{ss}^2 z (s, \theta) + 3\chi_c' (s) f_{\text{act}}'' (z (s, \theta)) \left(\partial_s z (s, \theta)\right)^2 \\ & + 3\chi_c (s) f_{\text{act}}'' (z (s, \theta)) \partial_s z (s, \theta) \partial_{ss}^2 z (s, \theta) + \chi_c (s) f_{\text{act}}''' (z (s, \theta)) \left(\partial_s z (s, \theta)\right)^3 \\ & + \chi_c (s) f_{\text{act}}' (z (s, \theta)) \partial_{sss}^3 z (s, \theta) \\ & + \chi_u f_{\text{und}}''' \left(V (s) n_1 (s, \theta)\right) \left(V' (s) n_1 (s, \theta) + V (s) \partial_s n_1 (s, \theta)\right)^3 \\ & + 3\chi_u f_{\text{und}}'' \left(V (s) n_1 (s, \theta)\right) \left(V' (s) n_1 (s, \theta) + V (s) \partial_s n_1 (s, \theta)\right) V'' (s) n_1 (s, \theta) \\ & + 3\chi_u f_{\text{und}}'' \left(V (s) n_1 (s, \theta)\right) \left(V' (s) n_1 (s, \theta) + V (s) \partial_s n_1 (s, \theta)\right) 2V' (s) \partial_s n_1 (s, \theta) \\ & + 3\chi_u f_{\text{und}}'' \left(V (s) n_1 (s, \theta)\right) \left(V' (s) n_1 (s, \theta) + V (s) \partial_s n_1 (s, \theta)\right) V (s) \partial_{ss}^2 n_1 (s, \theta) \\ & + \chi_u f_{\text{und}}' \left(V (s) n_1 (s, \theta)\right) \left(V''' (s) n_1 (s, \theta) + 3V'' (s) \partial_s n_1 (s, \theta)\right) \\ & + \chi_u f_{\text{und}}' \left(V (s) n_1 (s, \theta)\right) \left(3V' (s) \partial_{ss}^2 n_1 (s, \theta) + V (s) \partial_{sss}^3 n_1 (s, \theta)\right) \\ & + V''' (s) \left(R_0 + \rho (s, \theta)\right) \cos\theta + 3V'' (s) \partial_s \rho (s, \theta) \cos\theta + 3V' (s) \partial_{ss}^2 \rho (s, \theta) \cos\theta \\ & + V (s) \partial_{sss}^3 \rho (s, \theta) \cos\theta - p_1''' (s). \end{aligned}$$

Using the fact that for all $\theta \in (-\pi, \pi]$ we have $\partial_s z(0,\theta) = -ac^0 R_0 \cos\theta$ and the result of the previous lemma, it follows that:

$$\begin{aligned}
0 =& \gamma \partial^3_{sss}\kappa(0,\theta) + \chi_c'''(0) f_{\text{act}}\left(c^0\right) - 3ac^0 R_0 \chi_c''(0) f'_{\text{act}}\left(c^0\right)\cos\theta \\
&- 3\chi_c^* ac^0 R_0 \cos\theta \partial^2_{ss} z(0,\theta) f''_{\text{act}}\left(c^0\right) \\
&- \chi_c^* f'''_{\text{act}}\left(c^0\right)\left(ac^0 R_0\cos\theta\right)^3 + \chi_c^* f'_{\text{act}}\left(c^0\right)\partial^3_{sss} z(0,\theta) + \chi_u f'''_{\text{und}}(0)\cos^3\theta \\
&+ 3\chi_u f''_{\text{und}}(0)\cos^2\theta V''(0) + \chi_u f'_{\text{und}}(0)\left(V'''(0)\cos\theta + 3\partial^2_{ss} n_1(0,\theta)\right) \\
&+ V'''(0) R_0\cos\theta + 3\partial^2_{ss}\rho(0,\theta)\cos\theta - p_1'''(0).
\end{aligned}$$

We multiply the previous equality by $\cos\theta$ and integrate in θ over $(-\pi,\pi)$, we thus have:

$$\begin{aligned}
0 =& \gamma \int_{-\pi}^{\pi} \partial^3_{sss}\kappa(0,\theta)\cos\theta\,\mathrm{d}\theta - 3\pi ac^0 R_0 \chi_c''(0) f'_{\text{act}}\left(c^0\right) \\
&- 3\chi_c^* ac^0 R_0 f''_{\text{act}}\left(c^0\right)\int_{-\pi}^{\pi} \partial^2_{ss} z(0,\theta)\cos^2\theta\,\mathrm{d}\theta \\
&- \frac{3}{4}\chi_c^* f'''_{\text{act}}\left(c^0\right)\pi\left(ac^0 R_0\right)^3 + \chi_c^* f'_{\text{act}}\left(c^0\right)\int_{-\pi}^{\pi}\partial^3_{sss} z(0,\theta)\cos\theta\,\mathrm{d}\theta \\
&+ \frac{3}{4}\chi_u f'''_{\text{und}}(0)\pi + \chi_u f'_{\text{und}}(0) V'''(0)\pi + V'''(0) R_0\pi.
\end{aligned}$$

From Alazard et al. (2022) (appendix C), we have for all $\theta \in (-\pi,\pi]$:

$$\int_{-\pi}^{\pi} \partial^2_{ss} z(0,\theta)\cos^2\theta\,\mathrm{d}\theta = \frac{a^2 M}{2},$$

$$\int_{-\pi}^{\pi} \partial^3_{sss} z(0,\theta)\cos\theta\,\mathrm{d}\theta = -\frac{aM}{R_0} V'''(0) - \frac{2M}{\pi R_0^3}\int_{-\pi}^{\pi}\partial^3_{sss}\rho(0,\theta)\cos\theta\,\mathrm{d}\theta,$$

and

$$\int_{-\pi}^{\pi} \partial^3_{sss}\kappa(0,\theta)\cos\theta\,\mathrm{d}\theta = 0.$$

It follows that:

$$\begin{aligned}
0 &= -3\pi ac^0 R_0 \chi_c''(0) f'_{\text{act}}\left(c^0\right) - \frac{3}{2}\chi_c^* a^3 c^0 R_0 f''_{\text{act}}\left(c^0\right) M \\
&\quad - \frac{1}{R_0} aM\chi_c^* f'_{\text{act}}\left(c^0\right) V'''(0) - \frac{3}{4}\pi\chi_c^* f'''_{\text{act}}\left(c^0\right)\left(ac^0 R_0\right)^3 \\
&\quad + \chi_u f'''_{\text{und}}(0)\pi + \chi_u f'_{\text{und}}(0) V'''(0)\pi + V'''(0) R_0\pi, \\
&= -3\pi ac^0 R_0 f'_{\text{act}}\left(c^0\right)\chi_c''(0) - \frac{3\chi_c^* a^3 M^2}{2\pi R_0}\left(f''_{\text{act}}\left(c^0\right) + \frac{M}{2\pi R_0^2} f'''_{\text{act}}\left(c^0\right)\right) + \frac{3}{4}\pi\chi_u f'''_{\text{und}}(0).
\end{aligned}$$

It leads to:

$$\chi_c''(0) = \frac{-\chi_c^* a^2 M}{2\pi f'_{\text{act}}\left(c^0\right)}\left(f''_{\text{act}}\left(c^0\right) + \frac{M}{2\pi R_0^2} f'''_{\text{act}}\left(c^0\right)\right) + \frac{\chi_u f'''_{\text{und}}(0)}{4ac^0 R_0 f'_{\text{act}}\left(c^0\right)}.$$

We conclude using the expressions of χ_c^* and of c^0. □

Conclusion and perspectives. By studying the model with the undercooling effect, we have proved that this effect stabilises the model. Indeed, we can compare the threshold at which the bifurcation towards a travelling wave occurs with and without this effect (see Alazard et al. (2022) for the case without the undercooling effect). We have shown that this threshold is higher when the undercooling effect is taken into account.

In a work in progress, in collaboration with Nicolas Meunier and Olivier Pantz, we are studying different approaches for discretising the model with an implicit time discretisation of the curvature and the undercooling effect. Finite element methods are used for the spatial discretisations. The term added by the undercooling effect requires precautions to be taken regarding the functional spaces chosen to discretise the model. The velocity trace on the domain boundary must always be well defined. This work is an extension of Lavi et al. (2023).

Bibliography

Alazard, T., Magliocca, M., and Meunier, N. (2022). Traveling wave solution for a coupled incompressible Darcy's free boundary problem with surface tension. arXiv:2205.04365 [math]. 279, 281, 295, 296

Crandall, M. G. and Rabinowitz, P. H. (1971). Bifurcation from simple eigenvalues. Journal of Functional Analysis, 8(2):321–340. 292

Lavi, I., Meunier, N., and Pantz, O. (2023). Implicit like time discretization for the one-phase Hele-Shaw problem with surface tension. arXiv:2305.06180 [cs, math]. 296

Lavi, I., Meunier, N., Voituriez, R., and Casademunt, J. (2020). Motility and morphodynamics of confined cells. Physical Review E, 101(2):022404. Publisher: American Physical Society. 279

10 - Model in dimension 2 with an external signal

In this chapter, in the first section we introduce a model of cell motility in presence of an external signal. This model is deduce from the general model (1.1) in the case where we assume the substrate to be homogeneous (ξ_M is independent of the space), there is no obstacles and we neglect the nucleus. We define the stationary states of the model and prove their existence. We then study their stability. Secondly, we study the associated rigid model. We study its stationary states and their stability. We then write a numerical scheme to simulate the rigid model and show using numerical simulations that there is a trade-off between the force induced at the cell boundary by the polarity markers present in the cell and the force induced at the cell boundary by the external signal.

10.1 . Modelling

In this section, we introduce the model under study. This model is a special case of the general model (1.1). We assume that the substrate is homogeneous, i.e. that ξ_{M} is independent of space and we set for all $\mathbf{x} \in \mathbb{R}^2$, $\xi_{\mathrm{M}}(\mathbf{x}) = 1$. We neglect the effect of undercooling. We also assume that there are no obstacles in the cell's environment. Next, we neglect the dynamics of the nucleus. We then assume that the fluid domain coincides with that of the cell. The effects of noise are initially neglected. The model studied is given by:

$$\begin{cases} \mathbf{u} + \nabla P = 0 & \text{in } \Omega(t), & \text{(10.1a)} \\ \operatorname{div}(\mathbf{u}) = 0 & \text{in } \Omega(t), & \text{(10.1b)} \\ P = \gamma\kappa + \chi_c f_{\mathrm{act}}(c) + \chi_s g(\nabla s \cdot \mathbf{n}) & \text{on } \partial\Omega(t), & \text{(10.1c)} \\ V_n = \mathbf{u} \cdot \mathbf{n} & \text{on } \partial\Omega(t), & \text{(10.1d)} \\ \partial_t c = \operatorname{div}(\nabla c - (1-a)\,\mathbf{u}c) & \text{in } \Omega(t), & \text{(10.1e)} \\ (\nabla c + a\mathbf{u}c) \cdot \mathbf{n} = 0 & \text{on } \partial\Omega(t), & \text{(10.1f)} \\ c(0,\mathbf{x}) = c^{\mathrm{in}}(\mathbf{x}) & \text{in } \Omega(0). & \text{(10.1g)} \end{cases}$$

We recall that f_{act} statisfies the following assumptions eq. (1.12):

$$\begin{aligned} &f_{\mathrm{act}} \in C^1(\mathbb{R}^+), \\ &f_{\mathrm{act}} \text{ is an increasing function}, \\ &f_{\mathrm{act}}(0) = 0, \\ &\lim_{x \to +\infty} f_{\mathrm{act}}(x) = L_c < +\infty, \end{aligned}$$

and g satisfies the following one eq. (1.14):

$$\begin{aligned} &g \in C^1(\mathbb{R}), \\ &g \text{ is an odd function and a increasing function}, \\ &\lim_{x \to +\infty} g(x) = L_s < +\infty. \end{aligned}$$

We can observe that we retain the properties of preservation over time of the area of cell A_Ω and the total quantity of markers M. We thus have for all $t \geq 0$:

$$A_\Omega = \int_{\Omega(t)} 1 \, \mathrm{d}\mathbf{x},$$

and

$$M = \int_{\Omega(t)} c\,(t, \mathbf{x})\ \mathrm{d}\mathbf{x}. \tag{10.2}$$

Let $\mathbf{x}_{\mathrm{cm}}\,(t)$ be the centre of mass of $\Omega\,(t)$ at time $t \geq 0$. We have:

$$\mathbf{x}_{\mathrm{cm}}\,(t) = \frac{1}{A_\Omega} \int_{\Omega(t)} (x, y)\ \mathrm{d}x\,\mathrm{d}y.$$

We also define the velocity of the centre of mass $\mathbf{u}_{\mathrm{cm}}$. For all $t \geq 0$, we have:

$$\mathbf{u}_{\mathrm{cm}}\,(t) = \frac{\mathrm{d}}{\mathrm{d}t}\mathbf{x}_{\mathrm{cm}}\,(t)\,.$$

For all ≥ 0, we have:

$$\begin{aligned}
\frac{\mathrm{d}}{\mathrm{d}t}\int_{\Omega(t)} x\,\mathrm{d}x\,\mathrm{d}y &= \int_{\partial\Omega(t)} xV_n\,\mathrm{d}\sigma = \int_{\partial\Omega(t)} x\mathbf{u}\cdot\mathbf{n}\,\mathrm{d}\sigma = \int_{\Omega(t)} \mathrm{div}\,(x\mathbf{u})\ \mathrm{d}x\,\mathrm{d}y \\
&= \int_{\Omega(t)} \nabla x\cdot\mathbf{u}\,\mathrm{d}x\,\mathrm{d}y = -\int_{\Omega(t)} \nabla x\cdot\nabla P\,\mathrm{d}x\,\mathrm{d}y = -\int_{\Omega(t)} \mathrm{div}\,(P\nabla x)\ \mathrm{d}x\,\mathrm{d}y \\
&= -\int_{\partial\Omega(t)} P\nabla x\cdot\mathbf{n}\,\mathrm{d}\sigma = -\int_{\partial\Omega(t)} \left(\gamma\kappa + \chi_c f_{\mathrm{act}}\,(c) + \chi_s g\,(\nabla s\cdot\mathbf{n})\right)\mathbf{n}_x\,\mathrm{d}\sigma,
\end{aligned}$$

where we used the incompresisbility constraint (10.1b), the darcy law (10.1a) and the boundary condition (10.1c). Analogously, we have:

$$\frac{\mathrm{d}}{\mathrm{d}t}\int_{\Omega(t)} y\,\mathrm{d}x\,\mathrm{d}y = -\int_{\partial\Omega(t)} \left(\gamma\kappa + \chi_c f_{\mathrm{act}}\,(c) + \chi_s g\,(\nabla s\cdot\mathbf{n})\right)\mathbf{n}_y\,\mathrm{d}\sigma.$$

Since $\int_{\partial\Omega(t)} \kappa\mathbf{n}\,\mathrm{d}\sigma = 0$, it follows:

$$\mathbf{u}_{\mathrm{cm}}\,(t) = -\frac{1}{A_\Omega}\int_{\partial\Omega(t)} \left(\chi_c f_{\mathrm{act}}\,(c) + \chi_s g\,(\nabla s\cdot\mathbf{n})\right)\mathbf{n}\,\mathrm{d}\sigma. \tag{10.3}$$

10.2 . Stationary state

This section is devoted to the search of the stationary radially symmetric states of the model (10.1). We restrict our study to the case where the external signal is radially symmetrical. Thus, we assume that there exists a function $\psi_s : \mathbb{R}^+ \longrightarrow \mathbb{R}$ such that for all $\mathbf{x} \in \mathbb{R}^2$, the external signal is given by:

$$s\,(\mathbf{x}) = \psi_s\,(\|\mathbf{x}\|)\,. \tag{10.4}$$

In the sequel, for all $\mathbf{x} \in \mathbb{R}^2$, $s\,(\mathbf{x})$ is denoted simply by $s\,(r)$ where $r = \|\mathbf{x}\|$. We also assume that s is differentiable.

Proposition 10.2.1. *Under the assumption (10.4), the model (10.1) admits an unique stationary radially symmetric solution. This solution is given by:*

$$\begin{cases}
\mathbf{u}^0 = 0 & \text{in } \Omega^0, \quad (10.5a)\\
P^0 = \dfrac{\gamma}{R_0} + \chi_c f_{\mathrm{act}}\left(c^0\right) + \chi_s g\left(s'\left(R_0\right)\right) & \text{in } \Omega^0, \quad (10.5b)\\
c^0 = \dfrac{M}{\pi R_0^2} & \text{in } \Omega^0, \quad (10.5c)\\
\Omega^0 = B\,(0, R_0)\,, & (10.5d)
\end{cases}$$

where $R_0 = \sqrt{\frac{A_\Omega}{\pi}}$.

Proof. We are looking for radially symmetric solutions. Thus, necessarily, for all $t \geq 0$, $\Omega(t) = B(0, R_0) = \Omega^0$. Moreover, stationary radially symmetric solutions of the model (10.1) are characterized by:

$$\begin{cases} \mathbf{u} + \nabla P = 0 & \text{in } \Omega^0, \quad (10.6a) \\ \operatorname{div}(\mathbf{u}) = 0 & \text{in } \Omega^0, \quad (10.6b) \\ P = \dfrac{\gamma}{R_0} + \chi_c f_{\text{act}}(c) + \chi_s g(s'(R_0)) & \text{in } \Omega^0, \quad (10.6c) \\ V_n = \mathbf{u} \cdot \mathbf{n} = 0 & \text{on } \partial\Omega^0, \quad (10.6d) \\ 0 = \operatorname{div}(\nabla c - (1-a)\mathbf{u}c) & \text{in } \Omega^0, \quad (10.6e) \\ (\nabla c + a\mathbf{u}c) \cdot \mathbf{n} = 0 & \text{on } \partial\Omega^0. \quad (10.6f) \end{cases}$$

From eqs. (10.6a), (10.6b) and (10.6d) we deduce that:

$$\begin{cases} -\Delta P = 0 & \text{in } \Omega^0, \\ -\nabla P \cdot \mathbf{n} = 0 & \text{on } \partial\Omega^0. \end{cases}$$

Thus, we have:

$$\nabla P = 0 \quad \text{in } \Omega^0,$$

it follows that $\mathbf{u} = 0$ in Ω^0 and P is constant over Ω^0.

Using this, eqs. (10.6e) and (10.6f) can be rewritten as follows:

$$\begin{cases} \Delta c = 0 & \text{in } \Omega^0, \\ \nabla c \cdot \mathbf{n} = 0 & \text{on } \partial\Omega^0. \end{cases}$$

This leads to c being constant over Ω^0. Using the constraint on the total quantity of markers eq. (10.2), we have:

$$c = \frac{M}{\pi R_0^2}.$$

From the assumption (10.4), we have that $g(s)$ is constant over $\partial\Omega^0$. Then we deduce from eq. (10.6c) the value of P. □

10.3 . Linear stability analysis

In this section, to characterise the stationary state $(\mathbf{u}^0, P^0, c^0, \Omega^0)$ given by (10.5), we perform a linear stability analysis. We restrict our analysis to the case of monotonic external signal. We assume that there exists a function $\psi_s : \mathbb{R}^+ \longrightarrow \mathbb{R}^+$ and $\eta \in \mathbb{R}$ such that for all $\mathbf{x} \in \mathbb{R}^2$ we have:

$$s(\mathbf{x}) = \eta\, \psi_s(\|\mathbf{x}\|).$$

Moreover ψ_s is assumed to be an non-decreasing function. Thus if $\eta > 0$, the signal is said to be attractive in 0 whereas if $\eta < 0$, the signal is said to be repulsive in 0. Therefore, in the case of an attractive signal in 0 for all $r \geq 0$ we have $s'(r) \geq 0$ and in the case of a repulsive signal in 0 for all $r \geq 0$ we have $s'(r) \leq 0$. Moreover, we assume that s is two-times differentiable.

In the remainder of this section, we prove the following theorem concerning the stability of the stationary state when the signal is attractive.

Theorem 10.3.1. *Assume that $K_s > 0$. We then have:*

1. *If $0 < \dfrac{\chi_c}{\chi_c^*} \leq 1$ then $\mathcal{A}$ admits $\lambda = 0$ as eigenvalue with multiplicity two and all the others eigenvalues have non-positive real parts.*
2. *If $\dfrac{\chi_c}{\chi_c^*} > 1 + \frac{3}{8} K_s R_0$ then $\mathcal{A}$ admits at least a positive eigenvalue $\lambda > 0$.*

Where K_s is defined by:

$$K_s = \chi_s g' \left(s' \left(R_0 \right) \right) s'' \left(R_0 \right), \tag{10.7}$$

and χ_c^* by:

$$\chi_c^* = \frac{1}{a c^0 f'_{\text{act}} \left(c^0 \right)}. \tag{10.8}$$

The proof follows the ideas of Alazard et al. (2022); Lavi et al. (2020).

10.3.1 . The linearized problem

Proposition 10.3.2. *The problem linearised around the stationary radially symmetric state (10.5) associated with model (10.1) is given by:*

$$\frac{\mathrm{d}}{\mathrm{d}t} \begin{pmatrix} \rho \\ c \end{pmatrix} = \mathcal{A} \begin{pmatrix} \rho \\ c \end{pmatrix}, \tag{10.9}$$

where $\mathcal{A}$ is the operator defined on $H^3 \left(\partial \Omega^0 \right) \times H^2 \left(\Omega^0 \right)$ by

$$\mathcal{A} : \begin{pmatrix} \rho \\ c \end{pmatrix} \mapsto \begin{pmatrix} \mathcal{I} \left[\dfrac{\gamma}{R_0^2} \left(\partial_{\theta\theta}^2 \rho + \rho \right) - \chi_c f'_{\text{act}}(c^0) c - \rho K_s \right] \\ \Delta c \end{pmatrix}$$

with the boundary condition

$$\partial_r c = -a c^0 \mathcal{I} \left[\frac{\gamma}{R_0^2} \left(\partial_{\theta\theta}^2 \rho + \rho \right) - \chi_c f'_{\text{act}}(c^0) c - \rho K_s \right] \quad \text{on } \partial \Omega^0. \tag{10.10}$$

In proposition 10.3.2, $\mathcal{I}$ denotes the Dirichlet-to-Neumann operator. We recall from Evans (2010) that this operator is defined as follows:

Definition 10.3.3. *For $\psi \in H^1(\partial \Omega^0)$, the Dirichlet-to-Neumann operator $\mathcal{I}$ is defined by:*

$$\mathcal{I}[\psi] = \nabla q \cdot \boldsymbol{n},$$

where q denotes the harmonic extension of ψ to the disk Ω^0, that is

$$-\Delta q = 0 \quad \text{in } \Omega^0, \qquad q = \psi \quad \text{on } \partial \Omega^0.$$

Proof. Let $\varepsilon > 0$. We consider the following perturbation of the free boundary stationary domain (10.5d):

$$\Omega \left(t \right) = \left\{ (x, y) = (r \cos\theta, r \sin\theta) \text{ s.t. } 0 \leq r < R_0 + \varepsilon \rho \left(t, \theta \right) \text{ and } \theta \in (-\pi, \pi] \right\}. \tag{10.11}$$

We formally develop the solution (P, c) of the model (10.1) close to the radially symmetrical solution $\left(P^0, c^0 \right)$ given by (10.5):

$$\begin{aligned} P \left(t, r, \theta \right) &= P^0 + \varepsilon \tilde{P} \left(t, r, \theta \right) + \mathcal{O} \left(\varepsilon^2 \right) && \text{in } Omega \left(t \right), \\ c \left(t, r, \theta \right) &= c^0 + \varepsilon \tilde{c} \left(t, r, \theta \right) + \mathcal{O} \left(\varepsilon^2 \right) && \text{in } \Omega \left(t \right). \end{aligned}$$

From eqs. (10.1a) and (10.1b) we deduce that for all $t \geq 0$, we have:

$$\Delta \tilde{P} = 0 \quad \text{in } \Omega^0. \tag{10.12}$$

From eq. (10.11), we deduce that for all $t \geq 0$, the perturbed domain boundary $\partial\Omega(t)$ can be parametrized by:

$$\begin{array}{rccl} \varphi: & (-\pi, \pi] & \longrightarrow & \partial\Omega(t) \\ & \theta & \longmapsto & ((R_0 + \varepsilon\rho(t,\theta))\cos\theta, (R_0 + \varepsilon\rho(t,\theta))\sin\theta). \end{array}$$

Therefore, for all $t \geq 0$, the outward normal vector to $\partial\Omega(t)$ at the point $\mathbf{x} = \varphi(\theta)$ with $\theta \in (-\pi, \pi]$, is given by:

$$\begin{aligned} \mathbf{n}(\theta) &= \begin{pmatrix} \dfrac{(R_0 + \varepsilon\rho(t,\theta))\cos\theta + \varepsilon\partial_\theta\rho(t,\theta)\sin\theta}{\left((R_0 + \varepsilon\rho(t,\theta))^2 + (\varepsilon\partial_\theta\rho(t,\theta))^2\right)^{\frac{1}{2}}} \\ \dfrac{(R_0 + \varepsilon\rho(t,\theta))\sin\theta - \varepsilon\partial_\theta\rho(t,\theta)\cos\theta}{\left((R_0 + \varepsilon\rho(t,\theta))^2 + (\varepsilon\partial_\theta\rho(t,\theta))^2\right)^{\frac{1}{2}}} \end{pmatrix} \\ &= \begin{pmatrix} \cos\theta + \varepsilon\frac{1}{R_0}\partial_\theta\rho(t,\theta)\sin\theta \\ \sin\theta - \varepsilon\frac{1}{R_0}\partial_\theta\rho(t,\theta)\cos\theta \end{pmatrix} + \mathcal{O}(\varepsilon^2). \end{aligned} \tag{10.13}$$

For all $t \geq 0$, $\theta \in (-\pi, \pi]$ and $r \in [0, R_0 + \varepsilon\rho(t,\theta)]$, we have:

$$\nabla P(t,r,\theta) = \partial_r P(t,r,\theta)\,\mathbf{e}_r + \frac{1}{r}\partial_\theta P(t,r,\theta)\,\mathbf{e}_\theta, \tag{10.14}$$

with $\mathbf{e}_r = \begin{pmatrix}\cos\theta \\ \sin\theta\end{pmatrix}$ and $\mathbf{e}_\theta = \begin{pmatrix}\sin\theta \\ -\cos\theta\end{pmatrix}$. Then, combining eqs. (10.13) and (10.14), we obtain that on $\partial\Omega(t)$:

$$\begin{aligned} \nabla P \cdot \mathbf{n} = &\frac{1}{R_0 + \varepsilon\rho(t,\theta)}\partial_\theta P(t, R_0 + \varepsilon\rho(t,\theta), \theta)\,\frac{\varepsilon}{R_0}\partial_\theta\rho(t,\theta) \\ &+ \partial_r P(t, R_0 + \varepsilon\rho(t,\theta), \theta) + \mathcal{O}(\varepsilon^2). \end{aligned}$$

Using

$$\frac{1}{R_0 + \varepsilon\rho(t,\theta)} = \frac{1}{R_0} - \varepsilon\frac{\rho(t,\theta)}{R_0^2} + \mathcal{O}(\varepsilon^2),$$

we derive that:

$$\nabla P \cdot \mathbf{n} = \partial_r P(t, R_0, \theta) + \varepsilon\rho(t,\theta)\,\partial^2_{rr} P(t, R_0, \theta) + \frac{\varepsilon}{R_0^2}\partial_\theta P(t, R_0, \theta)\,\partial_\theta\rho(t,\theta) + \mathcal{O}(\varepsilon^2)$$

which leads to

$$\nabla P \cdot \mathbf{n} = \varepsilon\partial_r\tilde{P}(t, R_0, \theta) + \mathcal{O}(\varepsilon^2). \tag{10.15}$$

We denote $\mathcal{V}$ the boundary velocity. We have:

$$\mathcal{V} = \frac{\mathrm{d}}{\mathrm{d}t}\begin{pmatrix}(R_0 + \varepsilon\rho(t,\theta))\cos\theta \\ (R_0 + \varepsilon\rho(t,\theta))\sin\theta\end{pmatrix} = \begin{pmatrix}\varepsilon\partial_t\rho(t,\theta)\cos\theta \\ \varepsilon\partial_t\rho(t,\theta)\sin\theta\end{pmatrix}.$$

Then, using eq. (10.13), we have:

$$V_n = \mathcal{V} \cdot \mathbf{n} = \varepsilon\partial_t\rho(t,\theta) + \mathcal{O}(\varepsilon^2). \tag{10.16}$$

Combining eqs. (10.1a), (10.1d), (10.15) and (10.16) yields for all $t \geq 0$ and $\theta \in (-\pi, \pi]$:

$$\partial_t \rho(t,\theta) = -\partial_r \tilde{P}(t, R_0, \theta). \tag{10.17}$$

Using again the fact that $\partial\Omega(t)$ can be parametrized by φ, we have that for all $t \geq 0$ and $\theta \in (-\pi, \pi]$, the curvature at the point $\mathbf{x} = \varphi(\theta)$ is given by:

$$\kappa(\theta) = \frac{(R_0 + \varepsilon\rho(t,\theta))^2 - \varepsilon\partial^2_{\theta\theta}\rho(t,\theta)(R_0 + \varepsilon\rho(t,\theta)) + 2\varepsilon^2(\partial_\theta\rho(t,\theta))^2}{\left((R_0 + \varepsilon\rho(t,\theta))^2 + (\varepsilon\partial_\theta\rho(t,\theta))^2\right)^{\frac{3}{2}}}.$$

Thus we have:

$$\kappa(\theta) = \frac{1}{R_0} - \frac{\varepsilon}{R_0^2}\left(\partial^2_{\theta\theta}\rho(t,\theta) + \rho(t,\theta)\right) + \mathcal{O}(\varepsilon^2).$$

Since

$$f_{\text{act}}(c) = f_{\text{act}}\left(c^0 + \varepsilon\tilde{c} + \mathcal{O}(\varepsilon^2)\right) = f_{\text{act}}(c^0) + \varepsilon\tilde{c} f'_{\text{act}}(c^0) + \mathcal{O}(\varepsilon^2)$$

and

$$g(s'(R_0 + \varepsilon\rho(t,\theta))) = g(s'(R_0)) + \varepsilon\rho(t,\theta)\, s''(R_0)\, g'(s(R_0)) + \mathcal{O}(\varepsilon^2),$$

it follows from eq. (10.1c) that for all $t \geq 0$ and $\theta \in (-\pi, \pi]$ we have:

$$\tilde{P}(t, R_0, \theta) = -\frac{\gamma}{R_0^2}\left(\partial^2_{\theta\theta}\rho(t,\theta) + \rho(t,\theta)\right) + \chi_c\tilde{c}(t, R_0, \theta) f'_{\text{act}}(c^0) + \rho K_s. \tag{10.18}$$

We have:

$$\partial_t c(t,r,\theta) = \partial_t c^0(t,r,\theta) + \varepsilon\partial_t\tilde{c}(t,r,\theta) + \mathcal{O}(\varepsilon^2) = \varepsilon\partial_t\tilde{c}(t,r,\theta) + \mathcal{O}(\varepsilon^2)$$

and

$$\begin{aligned}\operatorname{div}(\nabla c - (1-a)\mathbf{u}c) &= \operatorname{div}(\nabla c + (1-a)\nabla P c) \\ &= \operatorname{div}\left(\nabla c^0 + (1-a)\nabla P^0 c^0\right) + \varepsilon\Delta\tilde{c} + \mathcal{O}(\varepsilon^2).\end{aligned}$$

Thus, using eq. (10.1e), it follows that:

$$\partial_t\tilde{c} = \Delta\tilde{c} \quad \text{in } \Omega^0. \tag{10.19}$$

We also have:

$$(\nabla c + a\mathbf{u}c)\cdot\mathbf{n} = (\nabla c - a\nabla P c)\cdot\mathbf{n} = \left(\nabla c^0 - a\nabla P^0 c^0\right)\cdot\mathbf{n} + \varepsilon\left(\nabla\tilde{c} - a\nabla\tilde{P}c^0\right)\cdot\mathbf{n} + \mathcal{O}(\varepsilon^2).$$

Using eq. (10.1f) we deduce that:

$$\left(\nabla\tilde{c} - a\nabla\tilde{P}c^0\right)\cdot\mathbf{n} = 0 \quad \text{on } \partial\Omega^0. \tag{10.20}$$

The linearised problem of model (10.1) around stationary state (10.5) is therefore given by eqs. (10.12) and (10.17) to (10.20). Using the definition of the Dirichlet-to-Neumann operator, we deduce that the linearised problem can be rewritten in the form eq. (10.9) with the boundary condition eq. (10.10). □

10.3.2 . The eigenvalue problem for $\mathcal{A}$

In this section we study the eigenvalue problem for $\mathcal{A}$. To do this, as the problem is radially symmetric, we can use Fourier analysis.

The eigenvalue problem for $\mathcal{A}$ is given by the search of $\lambda \in \mathbb{C}$ such that:

$$\mathcal{A}\begin{pmatrix}\rho\\ c\end{pmatrix} = \lambda\begin{pmatrix}\rho\\ c\end{pmatrix}.$$

Lemma 10.3.4. *Given* $\begin{pmatrix}\rho\\ c\end{pmatrix}$ *with Fourier series, then eqs.* (10.9) *and* (10.10) *describes a closed dynamical system for the cosine (resp. sine) perturbations.*

Proof. Let

$$\begin{pmatrix}\rho(\theta)\\ c(r,\theta)\end{pmatrix} = \sum_{m\in\mathbb{N}}\begin{pmatrix}\hat{\rho}_{cm}\\ \hat{c}_{cm}(r)\end{pmatrix}\cos(m\theta) + \sum_{m\in\mathbb{N}}\begin{pmatrix}\hat{\rho}_{sm}\\ \hat{c}_{sm}(r)\end{pmatrix}\sin(m\theta)$$

be the Fourier mode decomposition of $\begin{pmatrix}\rho\\ c\end{pmatrix}$. By linearity of the operator $\mathcal{A}$ we have:

$$\mathcal{A}\begin{pmatrix}\rho\\ c\end{pmatrix} = \sum_{m\in\mathbb{N}}\mathcal{A}_m\begin{pmatrix}\hat{\rho}_{cm}\\ \hat{c}_{cm}(r)\end{pmatrix}\cos(m\theta) + \sum_{m\in\mathbb{N}}\mathcal{A}_m\begin{pmatrix}\hat{\rho}_{sm}\\ \hat{c}_{sm}(r)\end{pmatrix}\sin(m\theta),$$

with $\mathcal{A}_m$ defined by

$$\mathcal{A}_m\begin{pmatrix}\hat{\rho}\\ \hat{c}(r)\end{pmatrix} = \begin{pmatrix}\mathcal{I}\left[-\frac{\gamma}{R_0^2}(m^2-1)\hat{\rho} - \chi_c f'_{\mathrm{act}}(c^0)\hat{c} - \hat{\rho}\,K_s\right]\\ \left(\partial_{rr}^2 + r^{-1}\partial_r - r^{-2}m^2\right)\hat{c}(r)\end{pmatrix}. \tag{10.21}$$

Furthermore, the boundary condition (10.10) on $\partial\Omega^0$ is

$$\partial_r\hat{c}(R_0) = -ac^0\,\mathcal{I}\left[-\frac{\gamma}{R_0^2}(m^2-1)\hat{\rho} - \chi_c f'_{\mathrm{act}}(c^0)\hat{c} - \hat{\rho}\,K_s\right].$$

□

Remark 10.3.5. *Without loss of generality, by symmetry of the problem around the x-axis, we can deduce from lemma 10.3.4 that if λ is an eigenvalue of $\mathcal{A}$, then the eigenfunctions associated with λ are of the form*

$$\begin{pmatrix}\rho(\theta)\\ c(r,\theta)\end{pmatrix} = \sum_{m\in\mathbb{N}}\begin{pmatrix}\hat{\rho}_{m\lambda}\\ \hat{c}_{m\lambda}(r)\end{pmatrix}\cos(m\theta),$$

such that for all $m\in\mathbb{N}$, $\begin{pmatrix}\hat{\rho}_{m\lambda}\\ \hat{c}_{m\lambda}\end{pmatrix}$ satisfy

$$\mathcal{A}_m\begin{pmatrix}\hat{\rho}_{m\lambda}\\ \hat{c}_{m\lambda}\end{pmatrix} = \lambda\begin{pmatrix}\hat{\rho}_{m\lambda}\\ \hat{c}_{m\lambda}\end{pmatrix}$$

and

$$\partial_r\hat{c}_{m\lambda}(R_0) = -ac^0\,\mathcal{I}\left[-\frac{\gamma}{R_0^2}(m^2-1)\hat{\rho}_{m\lambda} - \chi_c f'_{\mathrm{act}}(c^0)\hat{c}_{m\lambda} - \hat{\rho}_{m\lambda}\,K_s\right],$$

with $\mathcal{A}_m$ defined by eq. (10.21)*.*

Using the definition of the Dirichlet-to-Neumann operator, we deduce the following usefull lemma.

Lemma 10.3.6. *Let $m \in \mathbb{N}$. The eigenvalue problem on $\mathcal{A}_m$:*

$$\mathcal{A}_m \begin{pmatrix} \hat{\rho} \\ \hat{c} \end{pmatrix} = \lambda \begin{pmatrix} \hat{\rho} \\ \hat{c} \end{pmatrix}$$

and

$$\partial_r \hat{c}(R_0) = -ac^0 \mathcal{I}\left[-\frac{\gamma}{R_0^2}(m^2-1)\hat{\rho} - \chi_c f'_{\text{act}}(c^0)\hat{c} - \hat{\rho}\, K_s \right],$$

is equivalent to the following problem:

$$\begin{cases} \lambda\rho = -\partial_r P & \text{on } \partial\Omega^0, & \text{(10.22a)} \\ -\Delta P = 0 & \text{in } \Omega^0, & \text{(10.22b)} \\ P = \dfrac{\gamma}{R_0^2}\left(m^2-1\right)\rho + \chi_c f'_{\text{act}}\left(c^0\right) c + \rho\, K_s & \text{on } \partial\Omega^0, & \text{(10.22c)} \\ \lambda c = \Delta c & \text{in } \Omega^0, & \text{(10.22d)} \\ \partial_r c = ac^0 \partial_r P & \text{on } \partial\Omega^0. & \text{(10.22e)} \end{cases}$$

10.3.3 . Spectrum of $\mathcal{A}$

In this section, we study the spectrum of the operator $\mathcal{A}$. Thanks to remark 10.3.5, this study can be reduced to the study of the spectrum of $\mathcal{A}_m$ for all $m \in \mathbb{N}$.

Proposition 10.3.7. *Assume*

- $K_s \geq 0$,
- $0 \leq \dfrac{\chi_c}{\chi_c^*} \leq 1$ *where χ_c^* definded by eq. (10.8),*
- $\chi_c > 0$,
- $\chi_s > 0$,

then, for all $m \geq 1$, all the eigenvalues of $\mathcal{A}_m$ have non-positive real parts.

Proof. Let $m \geq 1$. Let $\lambda \in \mathbb{C}$ be a eigenvalue of $\mathcal{A}_m$.

We set $Q = c - ac^0 P$ where P and c satisfy eq. (10.22). Thus Q follows the following problem:

$$\begin{cases} -\Delta Q = \Delta c & \text{in } \Omega^0, & \text{(10.23a)} \\ \left(1 - \dfrac{\chi_c}{\chi_c^*}\right) P = \dfrac{\gamma}{R_0^2}\left(m^2-1\right)\rho + \chi_c f'_{\text{act}}\left(c^0\right) Q + \rho\, K_s & \text{on } \partial\Omega^0, & \text{(10.23b)} \\ \nabla Q \cdot \mathbf{n} = 0 & \text{on } \partial\Omega^0, & \text{(10.23c)} \end{cases}$$

where P, c and ρ satisfy eq. (10.22).

Thus using eqs. (10.22) and (10.23) we compute:

$$\begin{aligned} \lambda \int_{\Omega^0} |c|^2 \,\mathrm{d}\mathbf{x} = \int_{\Omega^0} \bar{c}\Delta c \,\mathrm{d}\mathbf{x} &= \int_{\Omega^0} \left(\bar{Q} + ac^0\bar{P}\right)\Delta Q \,\mathrm{d}\mathbf{x} \\ &= -\int_{\Omega^0} |\nabla Q|^2 \,\mathrm{d}\mathbf{x} - ac^0 \int_{\Omega^0} \nabla\bar{P}\cdot\nabla Q \,\mathrm{d}\mathbf{x}. \end{aligned}$$

Since

$$\begin{aligned}\int_{\Omega^0} \nabla \bar{P} \cdot \nabla Q \, \mathrm{d}\mathbf{x} &= \int_{\partial\Omega^0} Q \nabla \bar{P} \cdot \mathbf{n} \, \mathrm{d}\sigma \\ &= \frac{1}{\chi_c f'_{\mathrm{act}}(c^0)} \int_{\partial\Omega^0} \left(1 - \frac{\chi_c}{\chi_c^*}\right) P \nabla \bar{P} \cdot \mathbf{n} \, \mathrm{d}\sigma \\ &\quad + \frac{1}{\chi_c f'_{\mathrm{act}}(c^0)} \int_{\partial\Omega^0} \left(\frac{\gamma}{R_0^2}\left(m^2-1\right)\rho + \rho K_s\right) \bar{\lambda}\bar{\rho} \, \mathrm{d}\sigma \\ &= \frac{1 - \frac{\chi_c}{\chi_c^*}}{\chi_c f'_{\mathrm{act}}(c^0)} \int_{\Omega^0} |\nabla P|^2 \, \mathrm{d}\mathbf{x} \\ &\quad + \frac{\bar{\lambda}}{\chi_c f'_{\mathrm{act}}(c^0)} \left(\frac{\gamma}{R_0^2}\left(m^2-1\right) + K_s\right) \int_{\partial\Omega^0} |\rho|^2 \, \mathrm{d}\sigma.\end{aligned}$$

We deduce that for all $\lambda \in \mathbb{C}$ eigenvalue of $\mathcal{A}_m$ we have:

$$\begin{aligned}\lambda \int_{\Omega^0} |c|^2 \, \mathrm{d}\mathbf{x} + \frac{\bar{\lambda}}{\chi_c f'_{\mathrm{act}}(c^0)} \left(\frac{\gamma}{R_0^2}\left(m^2-1\right) + K_s\right) \int_{\partial\Omega^0} |\rho|^2 \, \mathrm{d}\sigma \\ = -\int_{\Omega^0} |\nabla Q|^2 \, \mathrm{d}\mathbf{x} - ac^0 \frac{1 - \frac{\chi_c}{\chi_c^*}}{\chi_c f'_{\mathrm{act}}(c^0)} \int_{\Omega^0} |\nabla P|^2 \, \mathrm{d}\mathbf{x}.\end{aligned}$$

The result follows from this equality. □

Lemma 10.3.8. *For $m \in \mathbb{N}$, the eigenfunctions of $\mathcal{A}_m$ associated with the eigenvalue $\lambda \in \mathbb{C}$ are*

$$\begin{pmatrix} \rho(\theta) \\ c(r,\theta) \end{pmatrix} = \begin{pmatrix} \hat{\rho}_{m\lambda} \\ \hat{c}_{m\lambda} I_m\left(-r\lambda^{1/2}\right) \end{pmatrix} \cos(m\theta),$$

with $0 < r < R_0$, $\theta \in (-\pi, \pi]$ and $(\hat{c}_{m\lambda}, \hat{\rho}_{m\lambda}) \in \mathbb{C}^2$ solutions of

$$\begin{cases} \left(\lambda + \dfrac{\gamma}{R_0^3} m\left(m^2-1\right) + \dfrac{m}{R_0} K_s\right) \hat{\rho}_{m\lambda} = -\dfrac{m\chi_c}{R_0} f'_{\mathrm{act}}(c^0) \, I_m\left(-R_0\lambda^{1/2}\right) \hat{c}_{m\lambda}, \\ \dfrac{\sqrt{\lambda}}{2}\left(I_{m-1}\left(-R_0\lambda^{1/2}\right) + I_{m+1}\left(-R_0\lambda^{1/2}\right)\right) \hat{c}_{m\lambda} = \lambda a c^0 \, \hat{\rho}_{m\lambda}. \end{cases}$$

Proof. In what follows, we consider only the smooth solutions at $r = 0$. Let $\lambda \in \mathbb{C}$ be an eigenvalue of $\mathcal{A}_m$ and let $\begin{pmatrix} \rho(\theta) \\ c(r,\theta) \end{pmatrix}$ be the eigenfunctions associated. Thanks to the lemma 10.3.6, we can use the representation (10.22) of the eigenvalue problem. P therefore satisfies Laplace's equation. There exists $A_{m\lambda} \in \mathbb{C}$ such that for all $0 < r < R_0$ and $\theta \in (-\pi, \pi]$ we have:

$$P(r,\theta) = A_{m\lambda} r^m \cos(m\theta).$$

For all $\theta \in (-\pi, \pi]$, we set $\rho(\theta) = \hat{\rho}_{m\lambda} \cos(m\theta)$. Using eq. (10.22a), we get that:

$$\lambda \hat{\rho}_{m\lambda} = -m R_0^{m-1} A_{m\lambda}.$$

We also set for all $r \in [0, R_0)$ and $\theta \in (-\pi, \pi]$, $c(r,\theta) = \hat{c}_{m\lambda}(r)\cos(m\theta)$. From eq. (10.22c), we deduce that:

$$A_{m\lambda} R_0^m = \frac{\gamma}{R_0^2}\left(m^2-1\right)\hat{\rho}_{m\lambda} + \chi_c f'_{\mathrm{act}}\left(c^0\right)\hat{c}_{m\lambda}(R_0) + \hat{\rho}_{m\lambda} K_s,$$

which leads to

$$\left(\lambda + \frac{\gamma}{R_0^3} m\left(m^2-1\right) + \frac{m}{R_0} K_s\right)\hat{\rho}_{m\lambda} = -\frac{m\chi_c}{R_0} f'_{\mathrm{act}}\left(c^0\right)\hat{c}_{m\lambda}(R_0).$$

Since c satisfies equation (10.22d), we deduce that $\hat{c}_{m\lambda}$ satisfies the following equation for $r \in [0, R_0)$:

$$\left(\partial_{rr}^2 + \frac{1}{r}\partial_r - \frac{m^2}{r^2}\right)\hat{c}_{m\lambda}(r) = \lambda \hat{c}_{m\lambda}(r).$$

The solutions of this equation are known and depend of the modified Bessel function of the first kind of order m, denoted by I_m. Thus we have for $r \in [0, R_0)$:

$$\hat{c}_{m\lambda}(r) = \hat{c}_{m\lambda} I_m\left(-r\sqrt{\lambda}\right),$$

where $\hat{c}_{m\lambda} \in \mathbb{C}$.

Using the boundary condition eq. (10.22e), we get that:

$$\partial_r \hat{c}_{m\lambda}(R_0) = -\lambda a c^0 \hat{\rho}_{m\lambda}.$$

Thus, thanks to the property of the Bessel function, we deduce that:

$$\frac{\sqrt{\lambda}}{2}\left(I_{m-1}\left(-R_0\lambda^{1/2}\right) + I_{m+1}\left(-R_0\lambda^{1/2}\right)\right)\hat{c}_{m\lambda} = \lambda a c^0 \hat{\rho}_{m\lambda}.$$

□

For $m \in \mathbb{N}$, let H_m be the function defined by:

$$\begin{aligned} H_m(z) = \frac{\sqrt{z}}{2}\left(z + \frac{\gamma}{R_0^3} m\left(m^2-1\right) + \frac{m}{R_0}K_s\right)\left(I_{m-1}\left(-R_0 z^{1/2}\right) + I_{m+1}\left(-R_0 z^{1/2}\right)\right) \\ + z a c^0 \frac{m\chi_c}{R_0} f'_{\text{act}}\left(c^0\right) I_m\left(-R_0 z^{1/2}\right), \end{aligned} \tag{10.24}$$

for $z \in \mathbb{C}$.

We deduce from the previous lemma 10.3.8 that the eigenvalue equation is given by

$$H_m(z) = 0.$$

Hence we have the following result on the spectrum of $\mathcal{A}_m$.

Lemma 10.3.9. *The spectrum of $\mathcal{A}_m$ is*

$$\text{sp}(\mathcal{A}_m) = \{\lambda \in \mathbb{C} \text{ s.t. } H_m(\lambda) = 0\}.$$

Finally, we prove Theorem 10.3.1, which we recall here:

Theorem 10.3.10. *Assume that $K_s > 0$. We then have:*

1. *If $0 < \dfrac{\chi_c}{\chi_c^*} \leq 1$ then $\mathcal{A}$ admits $\lambda = 0$ as eigenvalue with multiplicity two and all the others eigenvalues have non-positive real parts.*
2. *If $\dfrac{\chi_c}{\chi_c^*} > 1 + \frac{3}{8}K_s R_0$ then $\mathcal{A}$ admits at least a positive eigenvalue $\lambda > 0$.*

Proof. From remark 10.3.5, we recall that to study the spectrum of $\mathcal{A}$ it is sufficient to study the spectrum of $\mathcal{A}_m$ for all $m \in \mathbb{N}$. We also recall that the eigenfunction of $\mathcal{A}_m$ associated with the eigenvalue λ is given by:

$$v_{m\lambda}(r,\theta) = \begin{pmatrix} \hat{\rho}_{m\lambda} \\ \hat{c}_{m\lambda} I_m\left(-r\sqrt{\lambda}\right) \end{pmatrix} \cos(m\theta). \tag{10.25}$$

Proof of 1.
First we study the case $m = 0$. In this case we have:

$$H_0(\lambda) = \lambda^{\frac{3}{2}} I_1\left(-R_0\sqrt{\lambda}\right).$$

We have that $\lambda = 0$ is solution of the eigenvalue equation $H_0(\lambda) = 0$. Using the result of lemma 10.3.8 we deduce that $\lambda = 0$ is associated with the two followings eigenfunctions:

$$v_{00}^1(r,\theta) = \begin{pmatrix} 1 \\ 0 \end{pmatrix} \quad \text{and} \quad v_{00}^2(r,\theta) = \begin{pmatrix} 0 \\ 1 \end{pmatrix}.$$

The other roots of H_0 are given by $\lambda_{0k} = -\frac{x_{1k}^2}{R_0^2}$ where x_{1k} is the k-th root of J_1 the Bessel function of the first kind of order 1. Thus, since $x_{1k} > 0$ for all k, we have $\lambda_{0k} < 0$ and λ_{0k} is associated to the following eigenfunction:

$$v_{0k}(r,\theta) = \begin{pmatrix} 0 \\ J_0(x_{1k} r) \end{pmatrix}.$$

Secondly we study the case $m \geq 1$. We observe that $\lambda = 0$ is solution of $H_m(\lambda) = 0$. The eigenfunction associated to $\lambda = 0$ is the zero function:

$$v_{m0}(r,\theta) = \begin{pmatrix} 0 \\ 0 \end{pmatrix} \cos(m\theta).$$

Indeed, from the result of lemma 10.3.8, we deduce that $\hat{\rho}_{m0} = 0$. Moreover we have $I_m(0) = 0$. Thus $\lambda = 0$ is not an eigenvalue of $\mathcal{A}_m$ for $m \geq 1$.

Since $K_s > 0$ and $0 < \frac{\chi_c}{\chi_c^*} \leq 1$, we deduce from the proposition 10.3.7 that all the other eigenvalues of $\mathcal{A}_m$ have non-positive real parts.

Proof of 2.
We want to find a strictly positive eigenvalue of $\mathcal{A}$. To do this, we expand H_1 around $\lambda = 0$. Using the properties of Bessel functions, we have:

$$H_1(\lambda) = \frac{\sqrt{\lambda}}{2}\left(\frac{K_s}{R_0} + \left(1 + \frac{3}{8}K_s R_0 - ac^0\chi_c f'_{\text{act}}(c^0)\right)\lambda\right) + \mathcal{O}\left(|\lambda|^{\frac{5}{2}}\right).$$

The function $\lambda \mapsto \frac{K_s}{R_0} + \left(1 + \frac{3}{8}K_s R_0 - ac^0\chi_c f'_{\text{act}}(c^0)\right)\lambda$ admits

$$\lambda_1 = -\frac{K_s}{R_0 + \frac{3}{8}K_s R_0^2 - \frac{\chi_c}{\chi_c^*}R_0}$$

as its root. Under the assumption $K_s > 0$, we have:

$$\lambda_1 > 0 \iff \frac{\chi_c}{\chi_c^*} > 1 + \frac{3}{8}K_s R_0.$$

when $\frac{\chi_c}{\chi_c^*}$ is close to $1 + \frac{3}{8}K_s R_0$, we can note that λ_1 tends to not be close to 0. We use a graphical argument to conclude. For a value of K_s, we plot the function H_1 for different values of $\frac{\chi_c}{\chi_c^*}$ (see figs. 10.1 to 10.3). We plot its real part, its imaginary part and its modulus. We see that when $\frac{\chi_c}{\chi_c^*} > 1 + \frac{3}{8}K_s R_0$ then there is a root of H_1 with a positive real part. The fig. 10.2 suggests that $\frac{\chi_c}{\chi_c^*} > 1 + \frac{3}{8}K_s R_0$ is indeed the criterion from which we can exhibit a positive real part eigenvalue. Thus, when $\frac{\chi_c}{\chi_c^*} > 1 + \frac{3}{8}K_s R_0$ the stationary state is unstable.

□

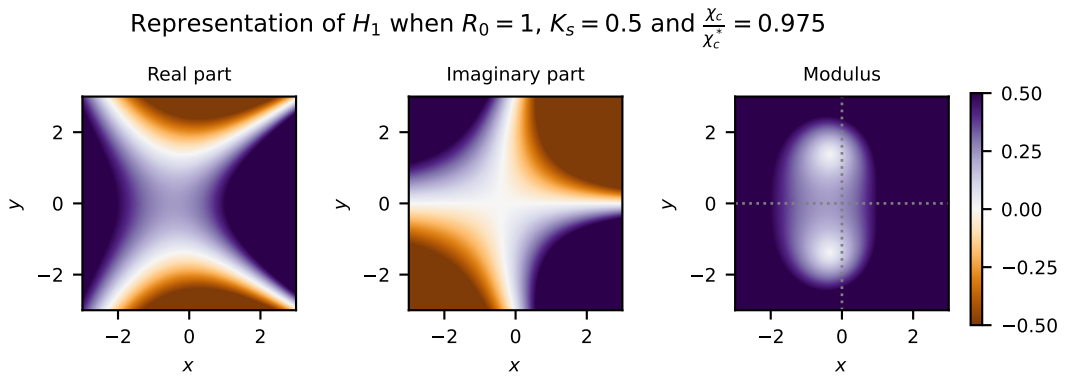

Figure 10.1: **Representation of H_1 in the complex framework for $R_0 = 1$, $K_s = 0.5$ and $\frac{\chi_c}{\chi_c^*} = 0.975$.** *Plots of the real part (left), the imaginary part (middle) and the modulus (right) of the function H_1 for $\lambda = x + \mathrm{i}y \in \mathbb{C}$ with $x, y \in [-3, 3]$. We are in the case where $\frac{\chi_c}{\chi_c^*} < 1 + \frac{3}{8} K_s R_0$, we observe that the root of H_1 with the greatest real part have negative real part.*

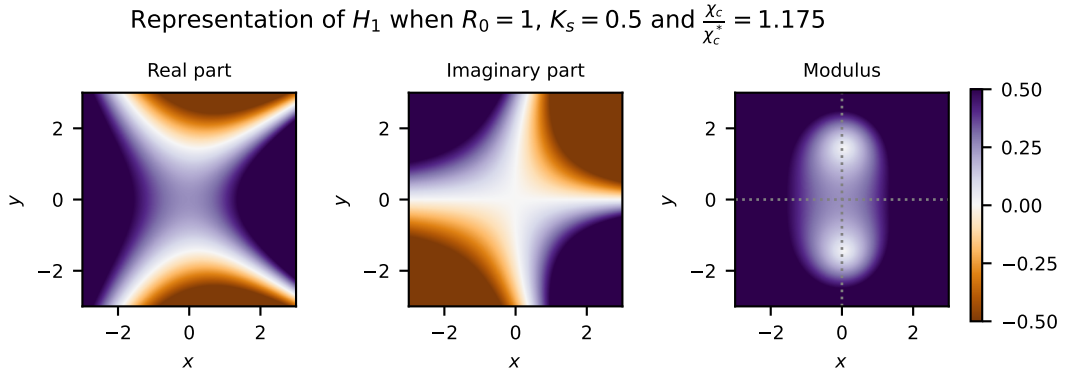

Figure 10.2: **Representation of H_1 in the complex framework for $R_0 = 1$, $K_s = 0.5$ and $\frac{\chi_c}{\chi_c^*} = 1.175$.** *Plots of the real part (left), the imaginary part (middle) and the modulus (right) of the function H_1 for $\lambda = x + \mathrm{i}y \in \mathbb{C}$ with $x, y \in [-3, 3]$. We are in the case where $\frac{\chi_c}{\chi_c^*} = 1 + \frac{3}{8} K_s R_0$, we observe that the root of H_1 with the greatest real part seems to have zero as real part.*

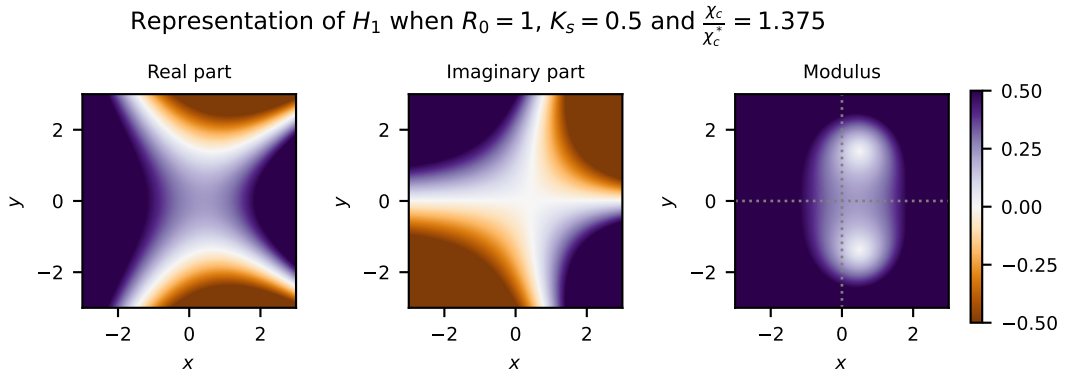

Figure 10.3: **Representation of H_1 in the complex framework for $R_0 = 1$, $K_s = 0.5$ and $\frac{\chi_c}{\chi_c^*} = 1.375$.** *Plots of the real part (left), the imaginary part (middle) and the modulus (right) of the function H_1 for $\lambda = x + \mathrm{i}y \in \mathbb{C}$ with $x, y \in [-3, 3]$. We are in the case where $\frac{\chi_c}{\chi_c^*} > 1 + \frac{3}{8} K_s R_0$, we observe that the root of H_1 with the greatest real part seems to have positive real part.*

10.4 . Study of the associated rigid model

In this scetion we study the rigid model associated with model (10.1). Informally, this is obtained when the surface tension tends towards infinity. We assume the cell to be rigid and to have a circular shape: $\Omega(t)$ is a disk of radius $R_0 > 0$. We assume that the the velocity of the centre of mass in the rigid case is the same as in the deformable one. Thus the cell boundary moves at the velocity of the centre of mass. The rigid model associated with the deformable model (10.1) is then given by:

$$\begin{cases} \partial_t c = \operatorname{div}\left(\nabla c - (1-a)\,\mathbf{u}c\right) & \text{in } \Omega(t), \quad (10.26a) \\ \left(\nabla c + a\mathbf{u}c\right)\cdot \mathbf{n} = 0 & \text{on } \partial\Omega(t), \quad (10.26b) \\ \mathbf{u}(t) = -\dfrac{1}{A_\Omega}\displaystyle\int_{\partial\Omega(t)} \left(\chi_c f_{\text{act}}(c) + \chi_s g\left(\nabla s\cdot\mathbf{n}\right)\right)\mathbf{n}\,\mathrm{d}\sigma, & (10.26c) \\ \Omega(t) = B(0,R_0) + \displaystyle\int_0^t \mathbf{u}(s)\,\mathrm{d}s. & (10.26d) \end{cases}$$

The eq. (10.2) remains true in the rigid case.

Under the assumption of radially symmetric signal eq. (10.4), we prove that the model eq. (10.26) admits a unique stationary state and study its stability.

10.4.1 . Stationary state

Proposition 10.4.1. *Under the assumption eq. (10.4), the model (10.26) admits an unique stationary radially symmetric solution. This solution is given by:*

$$\begin{cases} c^0 = \dfrac{M}{\pi R_0^2} & \text{in } \Omega^0, \quad (10.27a) \\ \mathbf{u}^0 = 0 & \text{in } \Omega^0, \quad (10.27b) \\ \Omega^0 = B(0,R_0). & (10.27c) \end{cases}$$

Proof. The stationary problem associated with the model (10.26) is given as follows:

$$\begin{cases} \Delta c = 0 & \text{in } \Omega^0, \\ \nabla c\cdot\mathbf{n} = 0 & \text{on } \partial\Omega^0, \\ \mathbf{u}^0 = 0 & \text{in } \Omega^0, \\ \Omega^0 = B(0,R_0). \end{cases}$$

Necessarily c is constant over Ω^0. Using the constraint on the total quantity of markers eq. (10.2), we deduce that for $\mathbf{x}\in\Omega^0$, $c(\mathbf{x}) = \dfrac{M}{\pi R_0^2}$. □

We study the stability of the stationary state when the signal is attractive ($K_s > 0$).

Theorem 10.4.2. *In the case where K_s defined by eq. (10.7) is positive, if $\frac{\chi_c}{\chi_c^*} < 1 + \frac{3}{8}K_s R_0$ the stationary state (10.27) is linearly stable. On the opposite, if $\frac{\chi_c}{\chi_c^*} > 1 + \frac{3}{8}K_s R_0$ the stationary state (10.27) is linearly unstable.*

10.4.2 . Proof of theorem 10.4.2

To study the linear stability of the stationary state (10.27) and proof theorem 10.4.2, we proceed in three steps. First, we linearise the problem (10.26) around this stationary state. From the linearisation of the problem, we derive an eigenvalue problem. Secondly, we study this eigenvalue problem. We study the sign of the real part of the eigenvalues: when there is an eigenvalue with a positive real part, the stationary state is linearly unstable, whereas when all the eigenvalues have a negative real part, the stationary state is linearly stable. To do this, we use Fourier analysis to decompose the eigenvalue problem into simpler problems. Finally, we derive an explicit condition on the eigenvalues. We conclude with a graphical argument. The arguments used are inspired by those of Lavi et al. (2020); Alazard et al. (2022) and are similar to those of sections 4.2.1.2, 5.2.2 and 6.2.2.

Step 1. The linearised problem associated with the model (10.26) around the stationary state (10.27) in the following lemma. Then we deduce an eigenvalue problem associated to this linearised problem.

Lemma 10.4.3. *The linearised problem associated to eq.* (10.26) *around the stationary state* (10.27) *is given by:*

$$\begin{cases} \partial_t \tilde{c} = \Delta \tilde{c} & \text{in } \Omega^0, \quad (10.28a) \\ \left(\nabla \tilde{c} + a \tilde{\mathbf{u}} c^0\right) \cdot \mathbf{n} = 0 & \text{on } \partial\Omega^0, \quad (10.28b) \\ \tilde{\mathbf{u}}\left(t\right) = \dfrac{-\chi_c f'_{\text{act}}\left(c^0\right)}{A_\Omega} \displaystyle\int_{\partial\Omega^0} \tilde{c}\left(t, \mathbf{x}\right) \mathbf{n} \, \mathrm{d}\sigma - \dfrac{K_s}{R_0} \tilde{\mathbf{x}}_{\text{cell}}\left(t\right), & (10.28c) \end{cases}$$

where $\tilde{\mathbf{x}}_{\text{cell}} = \left(\tilde{x}_{\text{cell}}, \tilde{y}_{\text{cell}}\right)$ *such that for all* $t \geq 0$*:*

$$\frac{\mathrm{d}}{\mathrm{d}t} \tilde{\mathbf{x}}_{\text{cell}}\left(t\right) = \tilde{\mathbf{u}}\left(t\right).$$

K_s *is defined by eq.* (10.7)*.*

Proof. We perform a formal expansion of the solutions of model (10.26) around the stationary state (10.27). Let $\varepsilon > 0$ small. For all $t \geq 0$, we set:

$$\Omega\left(t\right) = B\left(\mathbf{x}_{\text{cell}}\left(t\right), R_0\right),$$

with

$$\mathbf{x}_{\text{cell}}\left(t\right) = \varepsilon \tilde{\mathbf{x}}_{\text{cell}}\left(t\right) + \mathcal{O}\left(\varepsilon^2\right).$$

Thus we can set for all $t \geq 0$:

$$\mathbf{u}\left(t\right) = \mathbf{u}^0 + \varepsilon \tilde{\mathbf{u}}\left(t\right) + \mathcal{O}\left(\varepsilon^2\right).$$

Moreover, for all $t \geq 0$ and $\mathbf{x} \in \Omega^0$, we set:

$$c\left(t, \mathbf{x}\right) = c^0 + \varepsilon \tilde{c}\left(t, \mathbf{x}\right) + \mathcal{O}\left(\varepsilon^2\right).$$

Using the fact that c^0 satisfies eq. (10.27a) and c satisfies (10.26a), we deduce that in Ω^0:

$$\partial_t \tilde{c} = \Delta \tilde{c}.$$

We also have on $\partial\Omega^0$ that:

$$\begin{aligned}(\nabla c + a\mathbf{u}c)\cdot\mathbf{n} &= \left(\nabla c^0 + \varepsilon\nabla\tilde{c} + a\mathbf{u}^0c^0 + \varepsilon a\mathbf{u}^0\tilde{c} + \varepsilon a\tilde{\mathbf{u}}c^0\right)\cdot\mathbf{n} + \mathcal{O}\left(\varepsilon^2\right)\\ &= \varepsilon\left(\nabla\tilde{c} + a\tilde{\mathbf{u}}c^0\right)\cdot\mathbf{n} + \mathcal{O}\left(\varepsilon^2\right),\end{aligned}$$

which leads to the boundary condition:

$$\left(\nabla\tilde{c} + a\tilde{\mathbf{u}}c^0\right)\cdot\mathbf{n} = 0 \qquad \text{on } \partial\Omega^0.$$

Moreover, we have:

$$\begin{aligned}\int_{\partial\Omega(t)} f_{\text{act}}(c)\,\mathbf{n}\,\mathrm{d}\sigma &= \int_{\partial\Omega(t)} f_{\text{act}}\left(c^0\right) + \varepsilon\tilde{c}f'_{\text{act}}\left(c^0\right)\mathbf{n}\,\mathrm{d}\sigma + \mathcal{O}\left(\varepsilon^2\right)\\ &= \varepsilon f'_{\text{act}}\left(c^0\right)\int_{\partial\Omega(t)}\tilde{c}\mathbf{n}\,\mathrm{d}\sigma + \mathcal{O}\left(\varepsilon^2\right)\\ &= \varepsilon f'_{\text{act}}\left(c^0\right)\int_{\partial\Omega^0}\tilde{c}\mathbf{n}\,\mathrm{d}\sigma + \mathcal{O}\left(\varepsilon^2\right).\end{aligned}$$

We also have:

$$\begin{aligned}&\int_{\partial\Omega(t)} g\left(\nabla s(\mathbf{x})\cdot\mathbf{n}\right)\mathbf{n}\,\mathrm{d}\sigma\\ &= \int_0^{2\pi} g\left(\nabla s\begin{pmatrix}R_0\cos\theta\\ R_0\sin\theta\end{pmatrix}\cdot\begin{pmatrix}\cos\theta\\ \sin\theta\end{pmatrix}\right)\begin{pmatrix}\cos\theta\\ \sin\theta\end{pmatrix}\mathrm{d}\theta\\ &\quad + \varepsilon\int_0^{2\pi} g'\left(\nabla s\begin{pmatrix}R_0\cos\theta\\ R_0\sin\theta\end{pmatrix}\cdot\begin{pmatrix}\cos\theta\\ \sin\theta\end{pmatrix}\right)H(s)\begin{pmatrix}R_0\cos\theta\\ R_0\sin\theta\end{pmatrix}\tilde{\mathbf{x}}_{\text{cell}}\cdot\begin{pmatrix}\cos\theta\\ \sin\theta\end{pmatrix}\mathrm{d}\theta + \mathcal{O}\left(\varepsilon^2\right)\\ &= \varepsilon g'\left(s'(R_0)\right)s''(R_0)\,\pi\tilde{\mathbf{x}}_{\text{cell}} + \mathcal{O}\left(\varepsilon^2\right)\end{aligned}$$

Thus we deduce that

$$\tilde{\mathbf{u}} = \frac{-\chi_c f'_{\text{act}}\left(c^0\right)}{A_\Omega}\int_{\partial\Omega^0}\tilde{c}\mathbf{n}\,\mathrm{d}\sigma - \frac{K_s R_0\pi}{A_\Omega}\tilde{\mathbf{x}}_{\text{cell}}.$$

□

The eigenvalue problem associated with eq. (10.28) is given by:

$$\begin{cases}\lambda\tilde{c} = \Delta\tilde{c} & \text{in } \Omega^0, \quad (10.29a)\\ \left(\nabla\tilde{c} + a\tilde{\mathbf{u}}c^0\right)\cdot\mathbf{n} = 0 & \text{on } \partial\Omega^0, \quad (10.29b)\\ \tilde{\mathbf{u}} = \lambda\tilde{\mathbf{x}}_{\text{cell}} = \dfrac{-\chi_c f'_{\text{act}}\left(c^0\right)}{A_\Omega}\displaystyle\int_{\partial\Omega^0}\tilde{c}(\mathbf{x})\,\mathbf{n}\,\mathrm{d}\sigma - \frac{K_s}{R_0}\tilde{\mathbf{x}}_{\text{cell}}. & (10.29c)\end{cases}$$

where $\lambda\in\mathbb{C}$.

Step 2. Using Fourier analysis and the radially symmetric nature of the problem (10.29), we show the following lemma, which reduces the spectral study of eq. (10.29) to a simpler problem.

Lemma 10.4.4. *The problem (10.29) admits an eigenvalue with a positive real part if and only if the following problem eqs. (10.30) and (10.31) admits one.*

$$\begin{cases} \lambda c = \left(\partial_{rr}^2 + \dfrac{1}{r}\partial_r - \dfrac{1}{r^2}\right) c & r \in (0, R_0)\,, \quad (10.30a) \\ \partial_r c\,(R_0) + a\tilde{u}c^0 = 0, & (10.30b) \\ \lambda \tilde{x}_{\text{cell}} = \tilde{u}, & (10.30c) \end{cases}$$

with

$$\tilde{u} = \frac{-\chi_c f'_{\text{act}}\left(c^0\right)}{R_0} c\,(R_0) - \frac{K_s}{R_0}\pi\tilde{x}_{\text{cell}}. \quad (10.31)$$

Proof. Since problem (10.29) is radially symmetrical, we can use Fourier analysis to study its spectra. Let $\lambda \in \mathbb{C}$ and let $(\tilde{c}, \tilde{\mathbf{u}})$ be an eigenfunction associated with λ. In polar coordinates, for all $r \in (0, R_0)$ and $\theta \in (-\pi, \pi]$, the Fourier decomposition of $\tilde{c}$ is given by:

$$\tilde{c}\,(r, \theta) = \sum_{m\in\mathbb{N}} c_{cm}\,(r)\cos(m\theta) + \sum_{m\in\mathbb{N}} c_{sm}\,(r)\sin(m\theta)\,.$$

Thus, we have:

$$\int_{\partial\Omega} \tilde{c}\mathbf{n}\,\mathrm{d}\sigma = \pi R_0 \begin{pmatrix} c_{c1}\,(R_0) \\ c_{s1}\,(R_0) \end{pmatrix}.$$

It follows that:

$$\tilde{\mathbf{u}} = \frac{-\chi_c f'_{\text{act}}\left(c^0\right)}{R_0} \begin{pmatrix} c_{c1}\,(R_0) \\ c_{s1}\,(R_0) \end{pmatrix} - \frac{K_s}{R_0}\tilde{\mathbf{x}}_{\text{cell}}.$$

By linearity of eq. (10.29) and independence of the cosine and sine modes, we deduce that for all $m \neq 1$, c_{cm} and c_{sm} satisfy:

$$\begin{cases} \lambda c_m = \left(\partial_{rr}^2 + \dfrac{1}{r}\partial_r - \dfrac{m^2}{r^2}\right) c_m & r \in (0, R_0)\,, \quad (10.32a) \\ \partial_r c_m = 0 & r = R_0. \quad (10.32b) \end{cases}$$

Moreover, in the case where $m = 1$, we have that c_{c1} satisfies:

$$\begin{cases} \lambda c_{c1} = \left(\partial_{rr}^2 + \dfrac{1}{r}\partial_r - \dfrac{m^2}{r^2}\right) c_{c1} & r \in (0, R_0)\,, \quad (10.33a) \\ \partial_r c_{c1}\,(R_0) + a\tilde{\mathbf{u}}_x c^0 = 0, & (10.33b) \end{cases}$$

and similarly, c_{s1} satisfies:

$$\begin{cases} \lambda c_{s1} = \left(\partial_{rr}^2 + \dfrac{1}{r}\partial_r - \dfrac{m^2}{r^2}\right) c_{s1} & r \in (0, R_0)\,, \quad (10.34a) \\ \partial_r c_{s1}\,(R_0) + a\tilde{\mathbf{u}}_y c^0 = 0, & (10.34b) \end{cases}$$

where $\tilde{\mathbf{u}}_x$ and $\tilde{\mathbf{u}}_y$ denotes the two coordinates of $\tilde{\mathbf{u}}$. We can note that $\tilde{\mathbf{u}}$ depends only on the mode $m = 1$ which allows us to use the independence of the cosine and sine modes.

We then have that studying the spectrum of problem (10.29) is equivalent to studying, for all $m \neq 1$, the spectrum of problem (10.32) and those of problems (10.33) and (10.34). We note that for all $m \neq 1$, the eigenvalues of problem (10.32), which corresponds to the heat equation, have negative real parts. Thus, if problem (10.29) has a positive real part eigenvalue, then problem (10.33) or problem (10.34) has a positive real part eigenvalue. By symmetry, we see that problems (10.33) and (10.34) are analogous. We therefore restrict our spectral study of problem (10.29) to the spectral study of the problem (10.33). □

Step 3. We study the spectral problem (10.30) and show with a graphical argument that when $\chi_c < \chi_c^*$ then all the eigenvalues of eq. (10.30) are of negative real part and that if $\chi_c > \chi_c^*$ then there exists an eigenvalue of eq. (10.30) of positive real part.

Lemma 10.4.5. *Let $\lambda \in \mathbb{C}$. The eigenfunctions of eqs. (10.30) and (10.31) associated with the eigenvalue $\lambda \in \mathbb{C}$ are given by:*

$$\begin{pmatrix} c(r) \\ x_{\text{cell}} \end{pmatrix} = \begin{pmatrix} \beta_\lambda I_1\left(-\lambda^{\frac{1}{2}} r\right) \\ \hat{x}_{\text{cell},\lambda} \end{pmatrix}, \tag{10.35}$$

where $r \in (0, R_0)$, H_1 denotes the modified Bessel function of the first kind of order 1 and $(\beta_\lambda, \hat{x}_{\text{cell},\lambda}) \in \mathbb{C}^2$ solution of:

$$-\lambda^{\frac{1}{2}} \beta_\lambda I_1'\left(-\lambda^{\frac{1}{2}} R_0\right) = \lambda a c^0 \hat{x}_{\text{cell},\lambda}, \tag{10.36}$$

and

$$\left(\lambda + \frac{K_s}{R_0}\right) \hat{x}_{\text{cell},\lambda} = \frac{-\chi_c f'_{\text{act}}\left(c^0\right)}{R_0} \beta_\lambda I_1\left(-\lambda^{\frac{1}{2}} R_0\right). \tag{10.37}$$

Proof. From eq. (10.30c), we deduce that:

$$x_{\text{cell}} = \hat{x}_{\text{cell},\lambda} \in \mathbb{C}$$

satisfy

$$\lambda x_{\text{cell}} = \tilde{u}.$$

Combining it with the expression of $\tilde{u}$, we deduce that:

$$\lambda x_{\text{cell}} = \frac{-\chi_c f'_{\text{act}}\left(c^0\right)}{R_0} \beta_\lambda I_1\left(-\lambda^{\frac{1}{2}} r\right) - \frac{K_s}{R_0} \pi x_{\text{cell}}. \tag{10.38}$$

From the definition of the Bessel functions, there exists $\beta_\lambda \in \mathbb{C}$ such that the solutions c of eq. (10.30a) are given, for all $r \in (0, R_0)$, by:

$$c(r) = \beta_\lambda I_1\left(-\lambda^{\frac{1}{2}} r\right).$$

Then, using eq. (10.38), the the boundary condition eq. (10.30b) reads eq. (10.36). □

The following lemma follows:

Lemma 10.4.6. *Let $\lambda \in \mathbb{C}$ be an eigenvalue of eqs. (10.30) and (10.31). Then λ is such that $H_1(\lambda) = 0$ with H_1 defined for all $z \in \mathbb{C}$ by:*

$$H_1(z) = \frac{\sqrt{z}}{2}\left(z + \frac{1}{R_0} K_s\right)\left(I_0\left(-R_0 z^{1/2}\right) + I_2\left(-R_0 z^{1/2}\right)\right) + z a c^0 \frac{\chi_c}{R_0} f'_{\text{act}}\left(c^0\right) I_1\left(-R_0 z^{1/2}\right).$$

We find the same function H_1 as in the deformable case (see eq. (10.24)). By carrying out the same graphical study as in the deformable case (see figs. 10.1 to 10.3), we observe that the roots if $\frac{\chi_c}{\chi_c^*} < 1 + \frac{3}{8} K_s R_0$ the roots of H_1 have negative real parts whereas when $\frac{\chi_c}{\chi_c^*} > 1 + \frac{3}{8} K_s R_0$, there exists a root of H_1 with a positive real part.

10.5 . Numerical study of the rigid model

In this section, we first design a finite element numerical scheme to perform numerical simulations of the rigid model. Secondly, using numerical simulations, we illustrate that there is a trade-off between the cell that listens to its polarity and the cell that is attracted by an attractive signal source. We also show that there is a range of parameters for which the cell is able to follow a moving attractive signal source.

10.5.1 . Numerical scheme

In this section we write a finite element scheme to run simulations of the rigid model eq. (10.26). This scheme is obtained after an implicit time discretization and a finite element discretization in space.

10.5.1.1 . Time discretization

We discretize in time our model eq. (10.26). Let Δt be the time step. For $i \in \{0, \dots, N_f\}$ with $N_f \in \mathbb{N}$, we denote $t^i = i\Delta t$, $\mathbf{u}^i = \mathbf{u}\left(t^i\right)$, $c^i = c\left(t^i, \cdot\right)$, and $\Omega^i \Omega\left(t^i\right)$. We also denote by s^i the external signal at time t^i.

The implicit discretization of the problem is given by:

$$\begin{cases} \dfrac{c^{i+1} - c^i}{\Delta t} = \operatorname{div}\left(\nabla c^{i+1} + a\mathbf{u}^{i+1} c^{i+1}\right) & \text{in } \Omega^i, \quad (10.39a) \\ \left(\nabla c^{i+1} + a\mathbf{u}^{i+1} c^{i+1}\right) \cdot \mathbf{n} = 0 & \text{on } \partial\Omega^i, \quad (10.39b) \\ \mathbf{u}^i = \dfrac{-1}{A_\Omega} \displaystyle\int_{\partial\Omega^i} \chi_c f_{\text{act}}\left(c^i\right) \mathbf{n} + \chi_s g\left(\nabla s^i \cdot \mathbf{n}\right) \mathbf{n} \, \mathrm{d}\sigma, & (10.39c) \\ \Omega^{i+1} = \left(\mathrm{Id} + \Delta t \, \mathbf{u}^{i+1}\right)\left(\Omega^i\right). & (10.39d) \end{cases}$$

10.5.1.2 . Spatial discretization

We discretize in space our time-discrete model eq. (10.39). We use a finite element discretization. Let $\mathcal{T}$ be a triangulation of Ω^i. For all triangle $K \in \mathcal{T}$ we note $\left(\lambda_1^K, \lambda_2^K, \lambda_3^K\right)$ the barycentric coordinate functions of K. Let $\mathbb{P}_k$ be the set of polynomials of $\mathbb{R}^2$ of degrees less or equal k. Let $\mathcal{H}_c$ be the functional space define by:

$$\mathcal{H}_c = \left\{\psi \in H^1\left(\Omega^i\right) \mid \forall K \in \mathcal{T}, \psi|_K \in \mathbb{P}_1 \oplus \operatorname{Span}\left\{\lambda_1^K, \lambda_2^K, \lambda_3^K\right\}\right\}.$$

10.5.1.3 . Variational formulation of the discrete problem on the concentration

The variational formulation of eq. (10.39) is given by:

$$\begin{cases} \text{Find } c^{i+1} \in \mathcal{H}_c \text{ such that for all } \psi \in \mathcal{H}_c, \text{ we have:} \\ \displaystyle\int_{\Omega^i} \left(\frac{c^{i+1} - c^i}{\Delta t}\right) \psi \, \mathrm{d}\mathbf{x} \\ \qquad + \displaystyle\int_{\Omega^i} \left(a\mathbf{u}^{i+1} c^{i+1} + \nabla c^{i+1}\right) \cdot \nabla\psi \, \mathrm{d}\mathbf{x} = 0. \end{cases} \quad (10.40)$$

10.5.1.4 . Numerical scheme

After initialization with c^{in} given, a time iteration of the numerical scheme to simulate the problem (10.26) is given by the following algorithm:

Algorithm 10.1 : Numerical scheme to simulate the model eq. (10.26) obtained after time discretization and space discretization with a finite element method.

1. Initialisation: $c^0 = c^{\text{in}}$ the given initial condition and definition of the mesh.
2. Time iteration:
   (a) Compute $\mathbf{u}^{i+1} = \dfrac{-1}{A_\Omega} \int_{\partial\Omega^i} \chi_c f_{\text{act}}\left(c^i\right)\mathbf{n} + \chi_s g\left(\nabla s^i \cdot \mathbf{n}\right)\mathbf{n}\,\mathrm{d}\sigma$.
   (b) Computation of the markers concentration c^{i+1} using $\mathbf{u}^{i+1}$ by solving the variational formulation eq. (10.40).
   (c) Update of the domain:

$$\Omega^{i+1} = \left(\mathrm{Id} + \Delta t\, \mathbf{u}^{i+1}\right)\left(\Omega^i\right).$$

10.5.2 . Numerical results

We implement the numerical scheme using FreeFEM++ (Hecht, 2012). Using numerical simulations, we want to highlight that despite the presence of an attractive signal source, the cell does not always find the signal source. To illustrate this, we assume that the cell is initially located at $(0, 0)$ and that a signal source is located at $(4, 0)$. The cell is initially unpolarised. We simulate trajectories for different values of χ_c and χ_s.

We observe that for small values of χ_c, whatever the value of χ_s, the cell finds the signal source. These are the values for which the stationary state is stable. Once the signal source is found, the cell stops (see figs. 10.4 and 10.5).

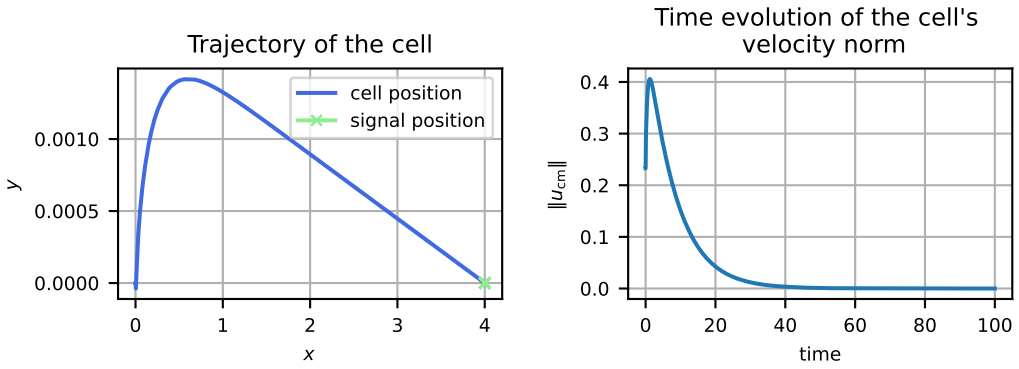

Figure 10.4: **Trajectory and cell velocity evolution in presence of an attractive signal source in the case where $\chi_c = 0.5$ and $\chi_s = 0.5$.** *On the left is represented the trajectory of the cell and position of the signal source. On the right is represented the time evolution of the cell's velocity norm. We observe that the cell rapidly finds the signal source. Once this is found, the cell stops.*
The results presented here are obtained with the parameters $\Delta t = 0.005$, $R_0 = 1$, $M = \pi$, $a = 1$, $c^{\text{in}} = \dfrac{M}{|\Omega \setminus N|}$, $\chi_c = 0.5$, $f_{\text{act}}(c) = \frac{c(1+c_s)^2}{c_s(c+c_s)}$ *with* $c_s = 0.5$, $\chi_s = 0.5$, $s(\mathbf{x}) = 0.25\,|\mathbf{x} - \mathbf{x}_{\text{signal}}|^2$, *with* $\mathbf{x}_{\text{signal}} = (0, 4)$, $g(x) = \tanh(\varsigma_s x)$ *with* $\varsigma_s = 0.25$.

When χ_c is large, we see that the cell is initially attracted towards the signal source. How-

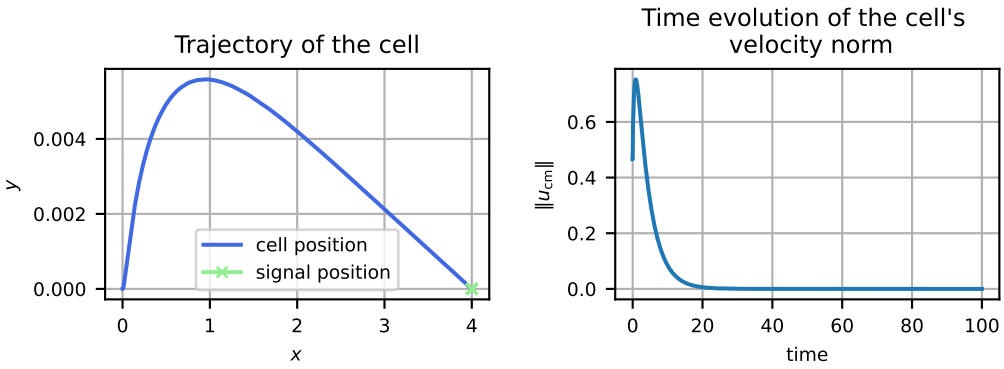

Figure 10.5: **Trajectory and cell velocity evolution in presence of an attractive signal source in the case where $\chi_c = 0.5$ and $\chi_s = 1$.** *On the left is represented the trajectory of the cell and position of the signal source. On the right is represented the time evolution of the cell's velocity norm. We observe that the cell rapidly finds the signal source. Once this is found, the cell stops.*
The results presented here are obtained with the parameters $\Delta t = 0.005$, $R_0 = 1$, $M = \pi$, $a = 1$, $c^{\text{in}} = \dfrac{M}{|\Omega \setminus N|}$, $\chi_c = 0.5$, $f_{\text{act}}(c) = \frac{c(1+c_s)^2}{c_s(c+c_s)}$ *with* $c_s = 0.5$, $\chi_s = 1$, $s(\mathbf{x}) = 0.25\,|\mathbf{x} - \mathbf{x}_{\text{signal}}|^2$, *with* $\mathbf{x}_{\text{signal}} = (0, 4)$, $g(x) = \tanh(\varsigma_s x)$ *with* $\varsigma_s = 0.25$.

ever, it does not stop and continues on its way. While remaining polarised and listening to its own polarisation, the cell remains attracted by the signal. We observe a trade-off between the two forces, that induced by the cell's polarisation and that induced by the external signal. The cell rotates around the signal source at a constant velocity. We can see that the larger χ_s is, the closer the cell is to the signal source (see figs. 10.6 and 10.7).

These observations highlight the existing trade-off between the force induced by the external signal and the force induced by the markers. It also highlights the fact that the chosen modelling implies that the signal source has an influence on the cell whatever the position of the cell. In order not to have this second effect, one possibility is to restrict the action of the signal source to a certain area.

Conclusion and perspectives. We have thus presented a model that takes external signals into account. We aim to continue the observations made on this model. Initially, we wish to study the impact of the external signal when its action is restricted to a certain area. We also aim to perform numerical simulations in the deformable case to characterise the influence of the external signal on the shape of the cell.

Additionally, we aim to pursue an ongoing work when the cell is in the presence of an obstacle and a source of an attractive signal. We aim to characterise the cases where the cell finds the signal source. Numerically, we obtain situations where the cell finds the signal source (see fig. 10.8), others where the cell stays behind the obstacle, and finally situations where the cell bypasses the obstacle but does not find the signal source.

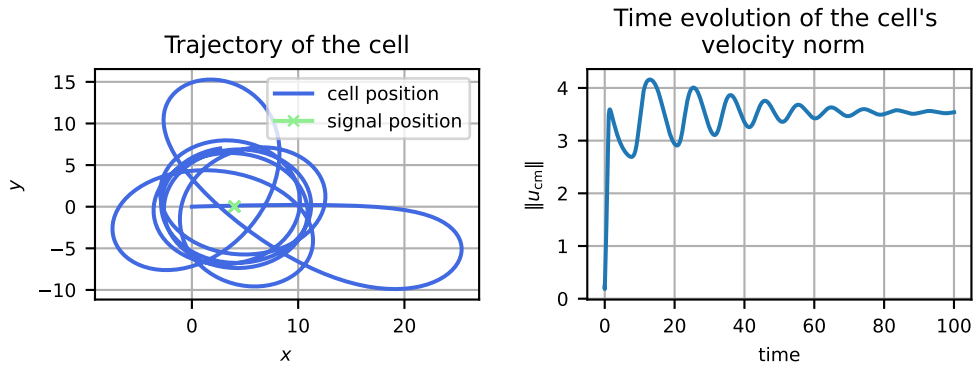

Figure 10.6: **Trajectory and cell velocity evolution in presence of an attractive signal source in the case where $\chi_c = 1.5$ and $\chi_s = 0.5$.** *On the left is represented the trajectory of the cell and position of the signal source. On the right is represented the time evolution of the cell's velocity norm. We can see that the cell is first attracted in the direction of the signal source. The cell does not stop once it has reached the source of the signal. We observe a balance between the forces induced by the external signal and the polarity markers on the boundary of the cell. The cell has a circular movement around the signal source. We can see that the cell is farest to the signal source in the case illustrated here than in the case illustrated in fig. 10.7.*
The results presented here are obtained with the parameters $\Delta t = 0.005$, $R_0 = 1$, $M = \pi$, $a = 1$, $c^{\text{in}} = \dfrac{M}{|\Omega \setminus N|}$, $\chi_c = 1.5$, $f_{\text{act}}(c) = \frac{c(1+c_s)^2}{c_s(c+c_s)}$ *with* $c_s = 0.5$, $\chi_s = 0.5$, $s(\mathbf{x}) = 0.25\,|\mathbf{x} - \mathbf{x}_{\text{signal}}|^2$, *with* $\mathbf{x}_{\text{signal}} = (0, 4)$, $g(x) = \tanh(\varsigma_s x)$ *with* $\varsigma_s = 0.25$.

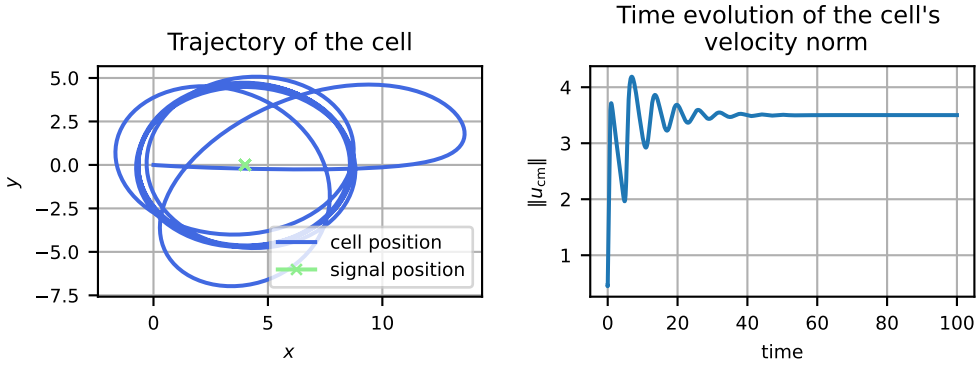

Figure 10.7: **Trajectory and cell velocity evolution in presence of an attractive signal source in the case where $\chi_c = 1.5$ and $\chi_s = 1$.** *On the left is represented the trajectory of the cell and position of the signal source. On the right is represented the time evolution of the cell's velocity norm. We can see that the cell is first attracted in the direction of the signal source. The cell does not stop once it has reached the source of the signal. We observe a balance between the forces induced by the external signal and the polarity markers on the boundary of the cell. The cell has a circular movement around the signal source. We can see that the cell is closest to the signal source in the case illustrated here than in the case illustrated in fig. 10.6.*
The results presented here are obtained with the parameters $\Delta t = 0.005$, $R_0 = 1$, $M = \pi$, $a = 1$, $c^{\text{in}} = \dfrac{M}{|\Omega \setminus N|}$, $\chi_c = 1.5$, $f_{\text{act}}(c) = \frac{c(1+c_s)^2}{c_s(c+c_s)}$ *with* $c_s = 0.5$, $\chi_s = 1$, $s(\mathbf{x}) = 0.25\,|\mathbf{x} - \mathbf{x}_{\text{signal}}|^2$, *with* $\mathbf{x}_{\text{signal}} = (0, 4)$, $g(x) = \tanh(\varsigma_s x)$ *with* $\varsigma_s = 0.25$.

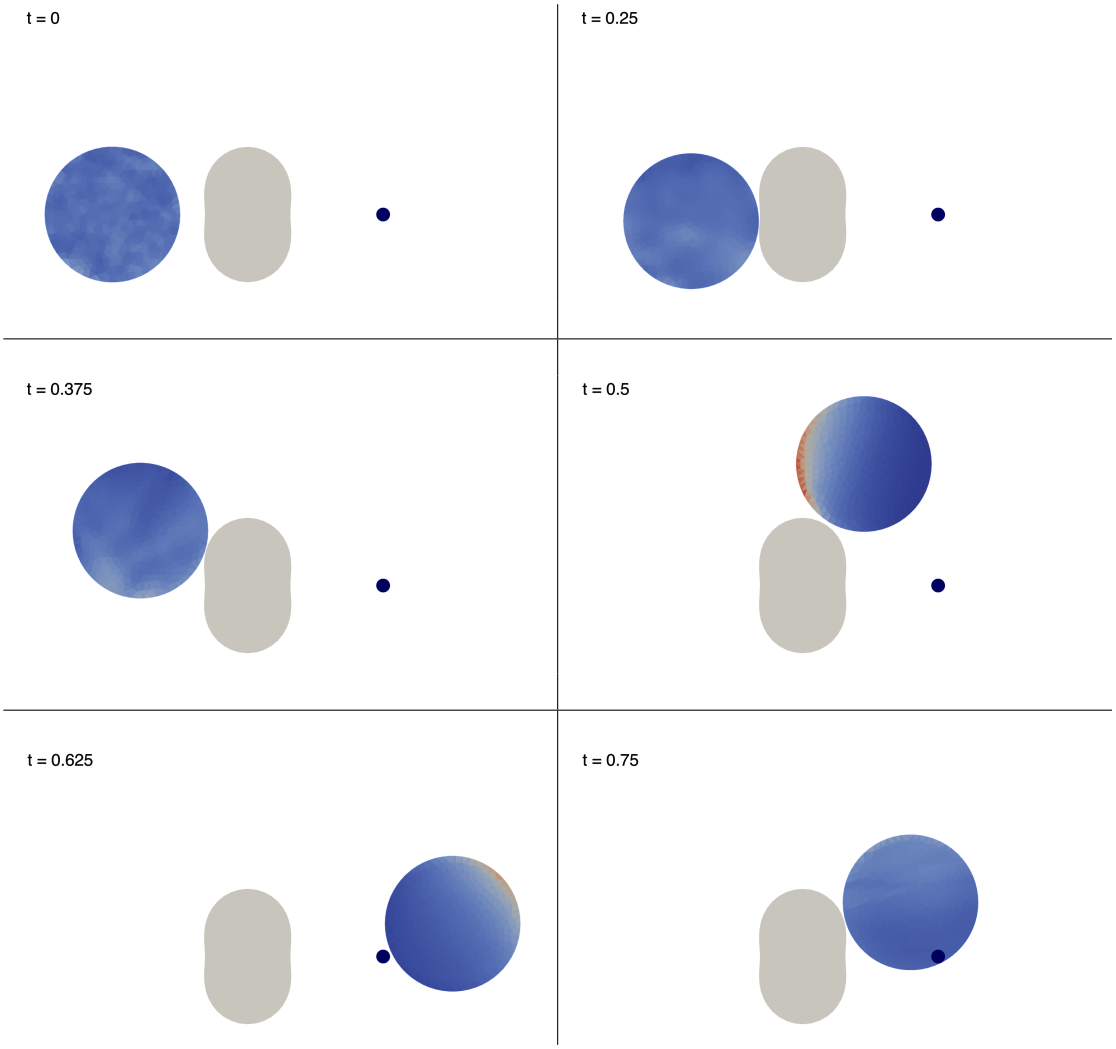

Figure 10.8: **Snapshots of the evolution of the cell position in presence of an external obstacle and external attractive signal.** *Snapshots at time $t = 0$, $t = 0.25$, $t = 0.375$, $t = 0.5$, $t = 0.625$, and $t = 0.75$ of the cell organisation in presence of an external obstacle and an external signal. The red area of cell represents the area with high markers concentration and the area in dark blue the one with low markers concentration. The gray shape represents the obstacle and the dark dot represent the position of the attractive signal. We can observe that the cell bypasses the obstacles and finds the signal source. The contact between the cell and the obstacle is managed by a Uzawa algorithm.*
The results presented here are obtained with the parameters $\Delta t = 0.005$, $R_0 = 1$, $M = \pi$, $a = 1$, $c^{\text{in}}(\mathbf{x}) = K(1 + X(\mathbf{x}))\mathbb{1}_{1+X(\mathbf{x})>0}$ where for all $\mathbf{x} \in \Omega$ we have $X(\mathbf{x}) \sim \mathcal{N}(0,1)$ and K such that $\int_\Omega c^{\text{in}}(\mathbf{x})\,\mathrm{d}\mathbf{x} = M$, $\chi_c = 1$, $f_{\text{act}}(c) = \frac{c(1+c_s)^2}{c_s(c+c_s)}$ with $c_s = 0.5$, $\chi_s = 1$, and $s(\mathbf{x}) = 0.25\,|\mathbf{x} - \mathbf{x}_{\text{signal}}|^2$, with $\mathbf{x}_{\text{signal}} = (0,4)$, $g(x) = \tanh(\varsigma_s x)$ with $\varsigma_s = 0.5$.

Bibliography

Alazard, T., Magliocca, M., and Meunier, N. (2022). Traveling wave solution for a coupled incompressible Darcy's free boundary problem with surface tension. arXiv:2205.04365 [math]. 300, 311

Evans, L. C. (2010). Partial Differential Equations: Second Edition, volume 19 of Graduate Studies in Mathematics. American mathematical society edition. 300

Hecht, F. (2012). New development in freefem++. J. Numer. Math., 20(3-4):251–265. 316

Lavi, I., Meunier, N., Voituriez, R., and Casademunt, J. (2020). Motility and morphodynamics of confined cells. Physical Review E, 101(2):022404. Publisher: American Physical Society. 300, 311

11 - Modeling Compartmentalization within Intracellular Signaling Pathway

In this chapter, we present a work done during the summer school CEMRACS 2022 on Transport in Physic, Biology and Urban traffic. This work was done in collaboration with Juan Calvo, Erwan Hingant, Saoussen Latrach, Nathan Quiblier and Romain Yvinec. This work is submitted and accepted.

In this work, we present a novel approach to modeling receptor-activated signaling pathways that take into account the compartmentalization of receptors and their effectors, both on the cell surface and in dynamic intracellular vesicles called endosomes. The first building block of the model concerns compartment dynamics. It takes into account creation of de novo endosomes, i.e. endocytosis, and further recycling of endosomes to the cell surface or degradation, as well as fusion of endosomes via coagulation dynamics. The second building block concerns biochemical reactions on the cell surface and within intra-cellular compartments. Both building blocks are coupled by the transfer of molecules that occurs at each event that modifies the compartments.

The model is formulated as a integro-partial differential equation, with transport and coagulation operators, and source terms, coupled to an integro-differential equation. In this work, we prove sufficient conditions to obtain exponential ergodicity for the size distribution of intracellular compartments. We further design a finite volume scheme to simulate our model. Finally, we show two application cases that show qualitative agreement with recently published data, proving that our model can help capture the spatio-temporal complexity of receptor-activated signaling pathway.

11.1 . Introduction

G Protein Coupled Receptors (GPCR) are a large class of transmembrane receptors: they are proteins located at the cell surface (plasma membrane) that are specialized in receiving (binding to) extracellular molecules, called ligand. The ligand-bound receptor will subsequently affect biochemical changes through the plasma membrane towards intracellular molecules. GPCR thus play a key role in the signal transduction, which allows long range cell communications mediated by ligand (*e.g.* hormones, cytokines, growth factors *etc*) and leads to major changes in the metabolism and activity of a cell (Lefkowitz, 2013; Roth et al., 2015). In addition, GPCR form an important class of targeted pharmaceutical agents in many different physiological contexts.

A receptor-activated signalling pathway, or biochemical cascade, is a chain of biochemical events activated by a receptor upon ligand binding. A series of signal transducers, or effector molecules, are activated within a reaction network (with typically many feedbacks and/or feedforward loops) and ultimately leads to a cell response, *e.g.* changes in gene expression, cell growth, metabolism (Kholodenko, 2006). Recently, it has been shown that GPCR are pleiotropic: they are able to selectively activate different signalling pathways. Distinct biochemical events can indeed be modulated by the nature of the ligand (either native physiological ligand or pharmaceutical agent) and the specific 3D conformational structured adopted

by the ligand-bound receptor. This pleiotropy sheds light into important cell regulation mechanisms that need to be taken into account to design efficient therapeutic strategies (Kenakin, 2019).

GPCR do not permanently stay at the plasma membrane. Rather, an important desensitization mechanism of signaling pathways is receptor endocytosis. Receptor endocytosis is the internalization inside the cell of a vesicle surrounded by an area of cell membrane which contains receptor (and other) molecules. Endocytosis is an active form of transport of molecules. The vesicles, called endosomes, and their molecular content, can further be degraded by cell machinery through hydrolytic enzymes, or be partly recycled back to the plasma membrane. These spatial movements induce, upon ligand binding, an heterogeneous population of receptors spread out between plasma membrane and a dynamic population of endosomes with distinct micro-environment. Within the context of receptor-activated signalling pathways, the processes of endocytosis, degradation and/or recycling are commonly referred to receptor trafficking, and provide further cell regulation mechanisms of signaling pathways (Birtwistle and Kholodenko, 2009). Key evidence have indeed shown that the intra-cellular traffic of internalized receptors has a major impact in cell response to a given stimuli (Jean-Alphonse and Hanyaloglu, 2011; Vilardaga et al., 2014).

In this work, we will focus our applications on a specific class of receptors that share in common the activation of the same effector molecule, the cyclic adenosine monophosphate (cAMP). For a number of GPCR among this class, including the Beta-2 Adrenergic Receptors (β2AR) (Kim et al., 2021), the parathyroid hormone receptor (PTHR) (Jean-Alphonse et al., 2014), the luteinizing hormone receptor (LHR) (Lyga et al., 2016), or the follicle-stimulating hormone receptor (FSHR) (Sayers and Hanyaloglu, 2018), after ligand binding, the production of cAMP occurs first at the plasma membrane and later on from a highly dynamic pool of endosomes following internalization of the receptor by endocytosis. This spatio-temporal dimension of signaling has been found to have a significant impact on physiological functions, such as the control of serum calcium by PTHR signaling (White et al., 2021), or the resumption of meiosis by LHCGR signaling (Lyga et al., 2016).

Thus, to faithfully represent the complexity of signalling pathways, we need to take into account the dynamic of the transient pool of specialised endosomes (Sorkin and von Zastrow, 2009; Birtwistle and Kholodenko, 2009; Villaseñor et al., 2016) following receptor stimulation, and its role on the reaction networks involved in the signalling pathways. The current biological hypothesis is that the endosomal compartments provide a dynamic and heterogeneous compartmentalised structure that allows specialised effector molecules to be separated from the bulk cytoplasm (physically separated through a lipid bilayer) in order to have a proper function of the cell response.

Classical ways to model the dynamic behaviour of signalling pathways use Chemical Reaction Networks (Ingalls, 2013), either in a deterministic formalism using ordinary differential equations (Feinberg, 2019), or in a stochastic formalism (typically when few molecules are present) using continuous-time Markov chains (Anderson and Kurtz, 2015). Both approaches typically assume the law of mass action and an idealised homogeneous environment. When spatial dynamics is important to take into account, one may use reaction-diffusion models to represent for instance spatial gradients (Kholodenko, 2006), or compartmental models, to physically represent segregation between static compartments (Weddell and Imoukhuede, 2017). Note that in most applied literature, like in the field of epidemiology (*e.g.* SIR model),

compartmental models refers to finite-dimensional dynamical systems where one variable is associated to each compartment, and the model described fluxes between compartments.

Up to our knowledge, relatively few works have addressed the issue of representing explicitly the segregation of molecules in a dynamic environment. The peculiarity of receptor trafficking at play within signalling pathways is that the endosomal compartments are created upon receptor activation, and their number, their size and their molecular content evolved dynamically, within a similar time scale than that of the signalling pathways activation. A first attempt of defining such models, within the context of signalling pathways, dates back to Foret et al. (2012) and uses a deterministic population dynamics formalism to follow a population of compartments, structured by their size and molecular content, and which undergo coagulation-fragmentation like dynamics, representing endocytosis, fusion, fission, recycling and degradation. Recently, a stochastic counterpart has been proposed by Duso and Zechner (2020); Pietzsch et al. (2021); Anderson and Howells (2023). To the best of our knowledge, a model that represents the chemical reactions that take place both at plasma membrane and within a dynamic population of endosomal compartment has never been considered and represents a novelty of our current work.

In this work, we define and study the long-time behavior and numerical schemes of minimal deterministic models that can represent compartmentalised signalling pathways, taking inspiration from Foret et al. (2012). Furthermore, we provide two simple examples of our model that show that this model is able to represent qualitatively main experimental observations on cAMP signaling from Jean-Alphonse et al. (2014); White et al. (2021).

In section 11.2, we describe two minimal models, structured with respectively one or two variables, that can represent the size-distribution of the endosomal compartment population and their molecular content. In section 11.3, we study the long time behavior of the model structured with a single variable. In section 11.4, we present a numerical scheme for the more general model, structured with two variables. In section 11.5, we present some numerical simulations that provide qualitative comparisons with experimental observations.

11.2 . Modelling compartmentalised signalling pathways

The first objective is to be able to define a model to simulate the endosomal compartment dynamics from their size structure perspective only. We adopt a deterministic population dynamic approach, where individuals are structured by a single positive variable (their size). From biological observations, the main processes that shape the size distribution of the endosomal population include:

- Endocytosis: creation of a de-novo compartment from the cell membrane;
- Removal of compartment: either recycling back to the cell membrane, or degradation through lysosomal pathways;
- Fusion: binary coagulation of compartments.

Let $g = g(t, r)$ be the population density of endosomal compartments at time $t \in \mathbb{R}^+$ and size (volume) $r \in \mathbb{R}^+$. The evolution equation for g, that takes into account the three mechanisms above is given by, for all $t > 0$ and $r > 0$:

$$\frac{\partial g(t,r)}{\partial t} = \underbrace{Q(g,g)(t,r)}_{\text{coagulation}} + \underbrace{\alpha(r)}_{\text{endocytosis}} - \underbrace{\gamma(r)g(t,r)}_{\text{removal}}, \tag{M1}$$

where

$$Q(g,g)(t,r) = \frac{1}{2}\int_0^r \kappa(r-r',r')g(t,r-r')g(t,r')\mathrm{d}r' - \int_0^\infty \kappa(r,r')g(t,r)g(t,r')\mathrm{d}r' . \tag{11.1}$$

In the sequel, we denote $g(0,r) = g_0(r)$ the initial condition of Eq. (M1). A similar equation may be found in Foret et al. (2012); Alexandrov et al. (2022). The coagulation operator is quadratic: two compartments of respective size r, r' fuse in one compartment of size $r + r'$ at rate $\kappa(r,r')$. One obtains Eq. (11.1) by considering all compartments that reach size r and all that leave size r. The kernel $\kappa \geq 0$ is symmetric ($\kappa(r,r') = \kappa(r',r)$), such that the coagulation operator Eq. (11.1) preserves mass ($\int rQ(g,g)(r)dr = 0$). In particular, we have (at least formally),

$$\frac{\mathrm{d}}{\mathrm{d}t}\int_0^\infty rg(t,r)dr = \int_0^\infty r\alpha(r)\mathrm{d}r - \int_0^\infty \gamma(r)rg(t,r)\mathrm{d}r . \tag{11.2}$$

Endocytosis is a zero-order process at rate α (source term), compartment removal is a first-order process and occurs at a rate γ. In the sequel, model (M1) will be referred as our 1D model.

The second modelling step is to include molecular content into Eq. (M1). One may first think as an additional one dimensional structure variable[1]. The first example we have in mind is the quantity of (active) receptor within each compartment, which is of primary interest to represent receptor trafficking within cells (see application in subsection 11.5.1). The second example we have in mind is the production of cAMP effector molecules, both at the plasma membrane and within each endosomes (see application in subsection 11.5.2). Thanks to this second structuring variable, besides compartment dynamics, we aim to represent:

- Biochemical reactions inside each compartment. Reaction rates are dependent on local abundances of molecular species, as well as the size (and more generally other physical variable like pH) of the compartment.
- Biochemical reactions that occur at the plasma membrane.
- Molecular conservation laws that may hold at each event that modifies the compartments, in particular between membrane and compartments. Hence we will now distinguish between compartment degradation and compartment recycling.

Let $f = f(t,r,a)$ be the population density of compartments at time $t \in \mathbb{R}^+$, size (volume) $r \in \mathbb{R}^+$ and molecular content $a \in \mathbb{R}^+$. Let also $M = M(t) \in \mathbb{R}^+$ be the molecular quantity at the plasma membrane. The joint evolution equation for f, M is , for all $t > 0$, $r > 0$ and $a > 0$,

[1] In future work, this additional structure variable could be an arbitrary finite dimensional variable to represent other molecular actors of signalling pathways that are either physically located at the plasma membrane, in the endosomal compartments or at the vicinity of those.

$$\frac{\partial f(t,r,a)}{\partial t} + \underbrace{\frac{\partial \left(V(r,a) f(t,r,a)\right)}{\partial a}}_{\text{reactions}} = \underbrace{\tilde{Q}(f,f)(t,r,a)}_{\text{coagulation}} + \underbrace{\alpha(r,a,M(t))}_{\text{endocytosis}} - \underbrace{\gamma(r,a) f(t,r,a)}_{\text{degradation}} - \underbrace{\lambda(r,a) f(t,r,a)}_{\text{recycling}}, \quad \text{(M2a)}$$

$$\frac{\mathrm{d}M(t)}{\mathrm{d}t} = \underbrace{J_M(M(t))}_{\text{reactions}} - \underbrace{\int_0^\infty \int_0^\infty a\alpha(r,a,M(t))\mathrm{d}a\mathrm{d}r}_{\text{endocytosis}} + \underbrace{\int_0^\infty \int_0^\infty a\lambda(r,a) f(t,r,a)\mathrm{d}a\mathrm{d}r}_{\text{recycling}}, \quad \text{(M2b)}$$

where

$$\tilde{Q}(f,f)(t,r,a) = \frac{1}{2}\int_0^r \int_0^a \kappa(r-r',r') f(t,r-r',a-a') f(t,r',a')\mathrm{d}a'\mathrm{d}r' - \int_0^\infty \int_0^\infty \kappa(r,r') f(t,r,a) f(t,r',a')\mathrm{d}a'\mathrm{d}r' . \quad (11.3)$$

In the sequel, we denote $f(0,r,a) = f_0(r,a)$ and $M(0) = M_0$ the initial conditions of Eqs. (M2a)-(M2b).

In Eq. (M2a), the extension of the coagulation and endocytosis processes to include the second structuring variable a is clear. Note that we chose the coagulation kernel to be dependent on the size of the compartments (not their molecular content), for the sake of simplicity. The removal terms are now splitted in two: the degradation occurs at rate γ, and the recycling occur at rate λ. The transport term represents the biochemical reactions that modify the molecular content within each compartment, and which occur at rate $V(r,a)$. Also, the endocytosis rate α is necessarily dependent on the molecular content of the plasma membrane M, to avoid negative values for M, e.g. $\alpha(r,a,0) = 0$. In Eq. (M2b), J_M represent biochemical reactions that occur at the plasma membrane, and the two integral terms represent the molecules that are lost or gained at the plasma membrane through respectively the endocytosis or recycling processes. The Eq. (M2b) on the scalar variable M was not present in Foret et al. (2012) and, to the best of our knowledge, it is a novelty of our model. Still interpreting the molecular content as a quantity of receptors, it allows to represent conservation laws of receptors between plasma membrane and endosomal compartments, giving a satisfactory representation of the biological concept of receptor *trafficking*: receptors (together with other molecules) undergo directed movement back-and-forth between plasma membrane and intra-cellular endosomal compartments. In particular, we have (at least formally),

$$\frac{\mathrm{d}}{\mathrm{d}t}\left(\int_0^\infty \int_0^\infty r f(t,r,a)\mathrm{d}r\mathrm{d}a\right) = \int_0^\infty \int_0^\infty r\alpha(r,a,M(t))\mathrm{d}r\mathrm{d}a - \int_0^\infty \int_0^\infty \gamma(r,a) r f(t,r,a)\mathrm{d}r\mathrm{d}a - \int_0^\infty \int_0^\infty \lambda(r,a) r f(t,r,a)\mathrm{d}r\mathrm{d}a , \quad (11.4)$$

and

$$\frac{\mathrm{d}}{\mathrm{d}t}\left(\int_0^\infty \int_0^\infty a f(t,r,a)\mathrm{d}r\mathrm{d}a + M(t)\right) = J_M(M(t)) + \int_0^\infty \int_0^\infty V(r,a) f(t,r,a)\mathrm{d}r\mathrm{d}a - \int_0^\infty \int_0^\infty \gamma(r,a) a f(t,r)\mathrm{d}r\mathrm{d}a . \quad (11.5)$$

The choice of the rate functions α, γ, λ and κ mainly governs the compartment size dynamics. In Foret et al. (2012); Alexandrov et al. (2022), the authors consider a one-dimensional model (M1) with constant coagulation kernel, constant first-order rate γ, and exponentially decaying source rate $\alpha(r) = Ce^{-r/a_0}$. The choice of the rate functions V and J_M will mainly impact the molecular content at the plasma membrane and within compartments. Its choice may be guided by the underlying chemical reactions that take place at the plasma membrane and within compartments. Linear or polynomial functions may thus be suitable to represent mass action kinetic law.

In the sequel, the model given by Eqs. (M2a)-(M2b) will be referred as our 2D model.

In the remaining, in Eq. (M1), Eqs. (M2a)-(M2b), all rate functions and initial conditions are nonnegative. Further, we do not address in this paper the well-posedness of solutions of either Eq. (M1) or Eqs. (M2a)-(M2b) and rather take for granted that a unique sufficiently smooth nonnegative solution is given.

11.3 . Long time behavior of the 1D model (M1)

In this section we provide sufficient conditions so that Eq. (M1) exhibits a unique globally stable steady state. The large-time behaviour of this equation -also known as *coagulation equation with source and efflux* (Chae and Dubovskii, 1995), has been studied first in Gajewski (1983) with drift, in Dubovskii (1994); Laurençot (2020) without efflux, in Vásquez (2015) with a bounded coagulation kernel and in Ghosh et al. (2023) with a singular coagulation kernel. Here, we limit ourselves to give a self-contained proof of exponential stability of the steady state in L^1 with bounded coagulation kernel. We mainly use a contraction argument, taking inspiration from Collet and Goudon (1999).

Theorem 11.3.1. *Let g_0, α, κ, γ nonnegative. Assume α is integrable, κ and γ are bounded and morevover $\inf \gamma = \gamma_0 > 0$. If*

$$3\|\kappa\|_{L^\infty}\|\alpha\|_{L^1} < \gamma_0^2\,, \tag{11.6}$$

then there exists a unique nonnegative stationary solution in $L^1(\mathbb{R}_+)$ of Eq. (M1), denoted by g_∞. Moreover,

$$\|g_\infty\|_{L^1} \leq \tfrac{\|\alpha\|_{L^1}}{\gamma_0}\,,$$

and for every solution $g \in C(\mathbb{R}_+, L^1(\mathbb{R}_+))$ we have

$$\lim_{t\to+\infty} \|g(t) - g_\infty\|_{L^1} = 0\,.$$

The convergence is at least exponential with rate $\frac{\gamma_0^2 - 3\|\kappa\|_{L^\infty}\|\alpha\|_{L^1}}{\gamma_0} > 0$.

We do not expect condition (11.6) to be optimal. See the discussion in Section 11.4.2. We assume here that well-posedness of a unique nonegative solution $g \in C(\mathbb{R}_+, L^1(\mathbb{R}_+))$ of Eq. (M1) is given. We note that this implicitly imposes conditions on the rate functions and the initial condition, which will at least need to be nonnegative and integrable. See Canizo (2006) for more details.

Proof. First we prove existence and uniqueness of a stationary solution g_∞ thanks to a Banach fixed point argument. Let us define

$$X = \left\{ g \in L^1(\mathbb{R}_+) \,:\, g \geq 0,\ \|g\|_{L^1} \leq \frac{\|\alpha\|_{L^1}}{\gamma_0} \right\}.$$

Consider a constant $K \geq \|\gamma\|_{L^\infty} + \|\kappa\|_{L^\infty} \frac{\|\alpha\|_{L^1}}{\gamma_0}$. For $g \in X$ we define

$$T_K g = \frac{1}{K} \left(\alpha - \gamma g + Q(g,g) + Kg \right).$$

The operator T_K is well-defined since $Q(g,g)$ is also well-defined for any integrable g provided that κ is bounded (Collet and Goudon, 1999, Lemma 3). We aim to apply Banach's fixed point theorem for T_K on X -which is a closed subset of the Banach space $L^1(\mathbb{R}_+)$; this will give a stationary solution of Eq. (M1). Let $g \in X$, we have that

$$T_K g \geq \frac{1}{K} \left(K - \|\gamma\|_{L^\infty} - \|\kappa\|_{L^\infty} \|g\|_{L^1} \right) g \,. \tag{11.7}$$

Indeed, g and α are positive and κ is bounded, thus

$$Q(g,g) \geq -g(r) \int_0^\infty \kappa(r,r') g(r') \mathrm{d}r' \geq -\|\kappa\|_{L^\infty} \|g\|_{L^1} g(r) \,,$$

which leads to Eq. (11.7) thanks to the boundedness of γ. The fact that $\|g\|_{L^1} \leq \frac{\|\alpha\|_{L^1}}{\gamma_0}$ and the condition on K entail the positivity of $T_K f$. Then, because

$$\int_0^\infty Q(g,g) \, \mathrm{d}r = -\frac{1}{2} \int_0^\infty \int_0^\infty \kappa(r',r) g(r') g(r) \mathrm{d}r' \mathrm{d}r \leq 0 \,,$$

we deduce that

$$\|T_K g\|_{L^1} = \int_0^\infty \frac{1}{K} \left(\alpha(r) - \gamma g(r) + Q(g,g)(r) + Kg(r) \right) \mathrm{d}r \leq \frac{\|\alpha\|_{L^1}}{K} + \frac{K - \gamma_0}{K} \|g\| \,.$$

But $K \geq \|\gamma\|_{L^\infty} \geq \gamma_0$, thus, for $g \in X$,

$$K \|T_K g\|_{L^1} \leq \|\alpha\|_{L^1} + (K - \gamma_0) \frac{\|\alpha\|_{L^1}}{\gamma_0} \leq K \frac{\|\alpha\|_{L^1}}{\gamma_0} \,,$$

and we conclude that $T_K g$ belongs to X. We now show that T_K is a contraction on X. Let g and h in X. It is straightforward to check that

$$\|T_K g - T_K h\|_{L^1} \leq (1 - \frac{\gamma_0}{K}) \|g - h\|_{L^1} + \frac{1}{K} \|Q(g,g) - Q(h,h)\|_{L^1} \,.$$

By a simple computation (see e.g. Collet and Goudon (1999, Lemma 3) or Vásquez (2015); Canizo (2006)),

$$\begin{aligned} \|Q(g,g) - Q(h,h)\|_{L^1} &\leq \frac{3}{2} \|\kappa\|_{L^\infty} (\|g\|_{L^1} + \|h\|_{L^1}) \|g - h\|_{L^1} \\ &\leq 3 \|\kappa\|_{L^\infty} \frac{\|\alpha\|_{L^1}}{\gamma_0} \|g - h\|_{L^1} \,. \end{aligned} \tag{11.8}$$

Thus, we have

$$\|T_K g - T_K h\|_{L^1} \leq \left(1 + \frac{1}{K} (3 \|\kappa\|_{L^\infty} \frac{\|\alpha\|_{L^1}}{\gamma_0} - \gamma_0) \right) \|g - h\|_{L^1} \,.$$

Then the hypothesis Eq. (11.6) allows us to conclude that there exists a unique fixed point to T_K in X. Moreover, this is the unique stationary solution which is positive and belongs to

L^1. Indeed, assume we have a positive stationary solution $g \notin X$ i.e. in L^1 satisfying $\gamma_0 \int g > \|\alpha\|_{L^1}$. Then

$$0 = \int_0^\infty (\alpha(r) - \gamma(r)g(r) + Q(g,g)(r))\, \mathrm{d}r \leq \|\alpha\|_{L^1} - \gamma_0 \int_0^\infty g(r)\, \mathrm{d}r < 0\,,$$

which is a contradiction.

We now turn to the proof of asymptotic stability. Let $g \in C(\mathbb{R}_+, L^1(\mathbb{R}_+))$ be a nonnegative solution to Eq. (M1) in the sense of distributions and let $g_\infty \in L^1(\mathbb{R}_+)$ be the stationary solution. We first provide a bound on g. We have

$$\frac{d}{dt}\int_0^\infty g(t,r)\mathrm{d}r = \|\alpha\|_{L^1} - \gamma_0 \int_0^\infty g(t,r)\mathrm{d}r + \int_0^\infty Q(g,g)(t,r)\mathrm{d}r \leq \|\alpha\|_{L^1} - \gamma_0 \int_0^\infty g(t,r)\mathrm{d}r\,.$$

Thus,

$$\|g(t,\cdot)\|_{L^1} \leq \|g(0,\cdot)\|_{L^1} e^{-\gamma_0 t} + \frac{\|\alpha\|_{L^1}}{\gamma_0}\,.$$

It is a classical computation that

$$\frac{\partial}{\partial_t}|g - g_\infty| = -\gamma(r)|g - g_\infty| + (Q(g,g) - Q(g_\infty, g_\infty))\, sign(g - g_\infty).$$

Thus, using Eq. (11.8),

$$\begin{aligned}\frac{\mathrm{d}}{\mathrm{d}t}\|g(t,\cdot) - g_\infty\|_{L^1} &\leq \left[-\gamma_0 + \frac{3}{2}\|\kappa\|_{L^\infty}\left(\|g(0,\cdot)\|_{L^1}e^{-\gamma_0 t} + \frac{\|\alpha\|_{L^1}}{\gamma_0} + \|g_\infty\|_{L^1}\right)\right] \\ &\qquad \times \|g(t,\cdot) - g_\infty\|_{L^1} \\ &\leq \left(3\|\kappa\|_{L^\infty}\frac{\|\alpha\|_{L^1}}{\gamma_0} - \gamma_0 + \frac{3}{2}\|\kappa\|_{L^\infty}\|g(0,\cdot)\|_{L^1}e^{-\gamma_0 t}\right)\|g(t,\cdot) - g_\infty\|_{L^1}.\end{aligned}$$

We conclude that

$$\|g(t,\cdot) - g_\infty\|_{L^1} \leq \|g(0,\cdot) - g_\infty\|_{L^1} e^{\frac{3\|\kappa\|_{L^\infty}}{2\gamma_0}\|g(0,\cdot)\|_{L^1} - \frac{\gamma_0^2 - 3\|\kappa\|_{L^\infty}\|\alpha\|_{L^1}}{\gamma_0}t}\,,$$

which ends the proof. □

11.4 . Numerical scheme for 1D and 2D models

In this section, we detail our Finite Volume numerical scheme used to simulate our models, and numerically illustrate their properties. In order to tackle the complexity of the model, we decided to construct a conservative scheme that preserves moments of the solution. To that, we use of the finite volume scheme framework, after reformulating the coagulation operator in a divergence form in the spirit of Bourgade and Filbet (2007); Hingant and Sepúlveda (2015). The transport term is treated by an up-wind scheme. Remaining terms are approximated in a standard way. Time is treated by a first order Euler explicit approximation.

11.4.1 . Finite volume scheme

We want to write a numerical scheme of the 2D model, Eqs. (M2a)-(M2b) using a finite volume method.

First we can remark that, for $r > 0$ and $a > 0$, we can rewrite our Eq. (M2a) in the following conservative form Bourgade and Filbet (2007)

$$\begin{aligned}\partial_t f(t,r,a) =& \frac{1}{ra}\partial_r\partial_a \mathcal{C}(f)(t,r,a) - \partial_a\left(V(r,a) f(t,r,a)\right) \\ &+ \alpha(r,a,M(t)) - \lambda(r,a) f(t,r,a) - \gamma(r,a) f(t,r,a),\end{aligned} \tag{11.9}$$

where

$$\mathcal{C}(f)(t,r,a) = \int_0^r \int_0^a r'a' \tilde{Q}(f,f)(t,r',a') \mathrm{d}a' \mathrm{d}r'.$$

From Eq. (11.9), we will first detail the truncation we use (step (i)) and the discretization (step (ii)). Then, we detail the finite volume approximation of the coagulation and first-order transport operator in the right-hand side of Eq. (11.9) (step (iii)). We finally sum-up the numerical scheme in the last step (step (iv)).

(i) Truncation As in Hingant and Sepúlveda (2015); Bourgade and Filbet (2007), to study our equation, we will truncate the size variable to a maximal value $R > 0$ and the quantity of reactants variable to a maximal value $A > 0$ and we will choose a truncation of the functional $\mathcal{C}$. We chose the following truncation, given by, for any $r \leq R$ and $a \leq A$,

$$\begin{aligned}\mathcal{C}_{\mathsf{c}}^{RA}(f)(t,r,a) =& \frac{1}{2}\int_0^r \int_0^a r'a' \int_0^{r'} \int_0^{a'} \kappa(r'-r'',r'') \dots \\ &\dots f(t,r'-r'',a'-a'') f(t,r'',a'') \mathrm{d}a'' \mathrm{d}r'' \mathrm{d}a' \mathrm{d}r' \\ &- \int_0^r \int_0^a r'a' f(t,r',a') \int_0^{R-r'} \int_0^{A-a'} \kappa(r',r'') f(t,r'',a'') \mathrm{d}a'' \mathrm{d}r'' \mathrm{d}a' \mathrm{d}r'.\end{aligned} \tag{11.10}$$

The truncation in Eq. (11.10) ensures that no cluster of size larger than R and molecular content larger than A arise. It can be obtained from Eq. (11.3) using the truncated kernel $\kappa(r,r')\mathbf{1}_{r+r'<R}\mathbf{1}_{a+a'<A}$ instead of $\kappa(r,r')$. The equation we will numerically approximate is a truncated version of Eq. (11.9) on the time interval $[0,T]$, where $T > 0$. We then look at the equation, for any $0 < t < T$, $0 < r \leq R$ and $0 < a \leq A$,

$$\begin{aligned}\partial_t f^{RA}(t,r,a) =& \frac{1}{ra}\partial_r\partial_a \mathcal{C}_{\mathsf{c}}^{RA}\left(f^{RA}\right)(t,r,a) - \partial_a\left(V(r,a) f^{RA}(t,r,a)\right) \\ &+ \alpha(r,a,M(t)) - \lambda(r,a) f^{RA}(t,r,a) - \gamma(r,a) f^{RA}(t,r,a).\end{aligned} \tag{11.11}$$

Heuristically, we expect f^{RA} to be close to f as long as the mass of f outside $[0,R/2]\times[0,A/2]$ is small (so that coagulation that leads to compartment of size larger than R and molecular content larger than A are unlikely). We call Eq. (11.11) a conservative truncation of Eq. (11.9) because the choice of the truncation of the coagulation operator does not lead to a loss of mass in the first moments. In particular, f^{RA} satisfies, at least formally, (compare to Eqs. (11.4)-

(11.5)),

$$\begin{aligned}\frac{\mathrm{d}}{\mathrm{d}t}\left(\int_0^\infty\int_0^\infty rf^{RA}(t,r,a)\mathrm{d}r\mathrm{d}a\right) =& \int_0^\infty\int_0^\infty r\alpha(r,a,M)\mathrm{d}r\mathrm{d}a \\ &- \int_0^\infty\int_0^\infty \gamma(r,a)rf^{RA}(t,r,a)\mathrm{d}r\mathrm{d}a \\ &- \int_0^\infty\int_0^\infty \lambda(r,a)rf^{RA}(t,r,a)\mathrm{d}r\mathrm{d}a\,,\end{aligned} \tag{11.12}$$

and

$$\begin{aligned}\frac{\mathrm{d}}{\mathrm{d}t}\left(\int_0^\infty\int_0^\infty af^{RA}(t,r,a)\mathrm{d}r\mathrm{d}a + M(t)\right) =& J_M(M(t)) \\ &+ \int_0^\infty\int_0^\infty V(r,a)f^{RA}(t,r,a)\mathrm{d}r\mathrm{d}a \\ &- \int_0^\infty\int_0^\infty \gamma(r,a)af^{RA}(t,r)\mathrm{d}r\mathrm{d}a\,.\end{aligned} \tag{11.13}$$

We choose to use a conservative truncation for our scheme in order to construct a scheme that preserves the conservation properties (11.12)-(11.13), as we will verify it in the case of pure coagulation.

(ii) Grids definition Let $I^r \in \mathbb{N}$. We discretize the size interval $[0,R]$ into I^r intervals. We denote by $\left(r_{i-\frac{1}{2}}\right)_{i\in\{1,\dots,I^r+1\}}$ a regular mesh of $[0,R]$ with size step Δr and we set

$$r_i = \frac{r_{i-\frac{1}{2}} + r_{i+\frac{1}{2}}}{2} = \left(i-\frac{1}{2}\right)\Delta r, \quad i\in\{1,\dots,I^r\}\,.$$

Let $I^a \in \mathbb{N}$. We discretize the size interval $[0,A]$ into I^a intervals. We denote by $\left(a_{j-\frac{1}{2}}\right)_{j\in\{1,\dots,I^a+1\}}$ a regular mesh of $[0,A]$ with step Δa and we set

$$a_j = \frac{a_{j-\frac{1}{2}} + a_{j+\frac{1}{2}}}{2} = \left(j-\frac{1}{2}\right)\Delta a, \quad j\in\{1,\dots,I^a\}\,.$$

For all $i\in\{1,\dots,I^r\}$ and $j\in\{1,\dots,I^a\}$, we set

$$\Lambda_{ij} = \left[r_{i-\frac{1}{2}}, r_{i+\frac{1}{2}}\right] \times \left[a_{j-\frac{1}{2}}, a_{j+\frac{1}{2}}\right].$$

Let $\Delta t > 0$ be the time step. We discretize $[0,T]$ by the set of points $\{t^n = n\,\Delta t,\ n\in\{0,\dots,N\}\}$, where $N = \lfloor \frac{T}{\Delta t}\rfloor$.

(iii) Finite volume approximation For all $n\in\{0,\dots,N\}$, $i\in\{1,\dots,I^r\}$ and $j\in\{1,\dots,I^a\}$, we denote $f^n_{i,j}$ an approximation of the function f^{RA} at the point (t^n, r_i, a_j). We will recursively calculate $f^n_{i,j}$ such that

$$f^n_{i,j} \approx \frac{1}{\Delta r\Delta a}\int_{\Lambda_{ij}} f^{RA}\left(t^n, r, a\right)\mathrm{d}a\mathrm{d}r.$$

Similarly, we denote by M^n an approximation of $M(t^n)$. First, we write the explicit forward Euler scheme in time associated to the Eq. (11.11). For all $n \in \{0, \dots, N-1\}$, we have

$$\begin{aligned}\frac{f^{RA}\left(t^{n+1}, r, a\right) - f^{RA}\left(t^n, r, a\right)}{\Delta t} =& \frac{1}{ra}\partial_r \partial_a \mathcal{C}_{\mathsf{c}}^{RA}\left(f^{RA}\right)\left(t^n, r, a\right) \\ & - \partial_a\left(V(r,a) f^{RA}\left(t^n, r, a\right)\right) + \alpha\left(r, a, M^n\right) \\ & - \lambda(r,a) f^{RA}\left(t^n, r, a\right) - \gamma(r,a) f^{RA}\left(t^n, r, a\right) \\ & + O(\Delta t).\end{aligned} \tag{11.14}$$

For each $i \in \{1, \dots, I^r\}$ and $j \in \{1, \dots, I^a\}$, we will integrate Eq. (11.14) over Λ_{ij}. We first deal with the coagulation operator. Approximating ra by the constant $r_{i-\frac{1}{2}} a_{j-\frac{1}{2}}$ on Λ_{ij}, and integrating, we obtain

$$\begin{aligned}&\int_{\Lambda_{ij}} \frac{1}{ra}\partial_r \partial_a \mathcal{C}_{\mathsf{c}}^{RA}\left(f^{RA}\right)\left(t^n, r, a\right) \mathrm{d}a\mathrm{d}r \\ &\quad \approx \frac{1}{r_{i-\frac{1}{2}} a_{j-\frac{1}{2}}}\Bigg(\mathcal{C}_{\mathsf{c}}^{RA}\left(f^{RA}\right)\left(t^n, r_{i+\frac{1}{2}}, a_{j+\frac{1}{2}}\right) - \mathcal{C}_{\mathsf{c}}^{RA}\left(f^{RA}\right)\left(t^n, r_{i-\frac{1}{2}}, a_{j+\frac{1}{2}}\right) \\ &\qquad\qquad - \mathcal{C}_{\mathsf{c}}^{RA}\left(f^{RA}\right)\left(t^n, r_{i+\frac{1}{2}}, a_{j-\frac{1}{2}}\right) + \mathcal{C}_{\mathsf{c}}^{RA}\left(f^{RA}\right)\left(t^n, r_{i-\frac{1}{2}}, a_{j-\frac{1}{2}}\right)\Bigg).\end{aligned} \tag{11.15}$$

Using a change of variable $r' - r'' \to r'$ in Eq. (11.10), and decomposing the first two integrals in telescopic sums we have,

$$\begin{aligned}&\mathcal{C}_{\mathsf{c}}^{RA}\left(f^{RA}\right)\left(t^n, r_{i+\frac{1}{2}}, a_{j+\frac{1}{2}}\right) = \\ &\quad \frac{1}{2}\sum_{k=1}^{i}\sum_{m=1}^{j}\int_{r_{k-\frac{1}{2}}}^{r_{k+\frac{1}{2}}}\int_{a_{m-\frac{1}{2}}}^{a_{m+\frac{1}{2}}}\int_0^{r_{i+\frac{1}{2}}-r'}\int_0^{a_{j+\frac{1}{2}}-a'}(a'+a'')(r'+r'')\kappa(r', r'')\dots \\ &\qquad\qquad \dots f^{RA}\left(t^n, r', a'\right) f^{RA}\left(t^n, r'', a''\right)\mathrm{d}a''\mathrm{d}r''\mathrm{d}a'\mathrm{d}r' \\ &\quad - \sum_{k=1}^{i}\sum_{m=1}^{j}\int_{r_{k-\frac{1}{2}}}^{r_{k+\frac{1}{2}}}\int_{a_{m-\frac{1}{2}}}^{a_{m+\frac{1}{2}}} r'a' f^{RA}\left(t^n, r', a'\right)\dots \\ &\qquad\qquad \dots \int_0^{R-r'}\int_0^{A-a'}\kappa(r', r'') f^{RA}\left(t^n, r'', a''\right)\mathrm{d}a''\mathrm{d}r''\mathrm{d}a'\mathrm{d}r'.\end{aligned}$$

Further, setting $\kappa_{k,k'} = \frac{1}{\Delta r^2}\int_{r_{k-\frac{1}{2}}}^{r_{k+\frac{1}{2}}}\int_{r_{k'-\frac{1}{2}}}^{r_{k'+\frac{1}{2}}}\kappa(r, r')\,\mathrm{d}r'\mathrm{d}r$, and approximating again product terms ra by their left value on Λ_{ij}, we approximate $\mathcal{C}_{\mathsf{c}}^{RA}$ by:

$$\begin{aligned}&\mathcal{C}_{\mathsf{c}}^{RA}\left(f^{RA}\right)\left(t^n, r_{i+\frac{1}{2}}, a_{j+\frac{1}{2}}\right) \\ &\approx \frac{1}{2}(\Delta r \Delta a)^2 \sum_{k=1}^{i}\sum_{m=1}^{j}\sum_{k'=1}^{i-k+1}\sum_{m'=1}^{j-m+1}\left(a_{m-\frac{1}{2}} + a_{m'-\frac{1}{2}}\right)\left(r_{k-\frac{1}{2}} + r_{k'-\frac{1}{2}}\right)\kappa_{k,k'} f^n_{k,m} f^n_{k',m'} \\ &\quad - (\Delta r \Delta a)^2 \sum_{k=1}^{i}\sum_{m=1}^{j}\sum_{k'=1}^{I^r-k+1}\sum_{m'=1}^{I^a-m+1} a_{m-\frac{1}{2}} r_{k-\frac{1}{2}} \kappa_{k,k'} f^n_{k,m} f^n_{k',m'},\end{aligned} \tag{11.16}$$

Plugging this latter approximation (11.16) into Eq. (11.15), we finally define the approximation of the coagulation operator, as

$$Q_{i,j}^n(f,f) = (\Delta r \Delta a)^2 \left(\frac{1}{2} \sum_{k=1}^{i} \sum_{m=1}^{j} \kappa_{k,i-k+1} f_{k,m}^n f_{i-k+1,j-m+1}^n - f_{i,j}^n \sum_{k=1}^{I^r-i+1} \sum_{m=1}^{I^a-j+1} \kappa_{i,k} f_{k,m}^n \right). \quad (11.17)$$

Note that the approximation $Q_{i,j}^n$ of $\tilde{Q}\left(f^{RA}, f^{RA}\right)$ is conservative (in the sense that it preserves the first moments in r and a), as we will show in the next section. Then, we use an upwind approximation for the transport term, together with an integration of transport velocity over r using the midpoint rule:

$$\begin{aligned}
&\int_{\Lambda_{ij}} \partial_a \left(V(r,a) f^{RA}(t,r,a) \right) da dr \\
&\qquad = \int_{r_{i-\frac{1}{2}}}^{r_{i+\frac{1}{2}}} \left(V\left(r, a_{j+\frac{1}{2}}\right) f^{RA}\left(t, r, a_{j+\frac{1}{2}}\right) \right) \mathrm{d}r \\
&\qquad - \int_{r_{i-\frac{1}{2}}}^{r_{i+\frac{1}{2}}} \left(V\left(r, a_{j-\frac{1}{2}}\right) f^{RA}\left(t, r, a_{j-\frac{1}{2}}\right) \right) \mathrm{d}r \\
&\quad \approx W_{i,j+\frac{1}{2}} f^{RA}\left(t, r_i, a_{j+\frac{1}{2}}\right) \Delta r - W_{i,j-\frac{1}{2}} f^{RA}\left(t, r_i, a_{j-\frac{1}{2}}\right) \Delta r \\
&\qquad \approx \Delta r \cdot \left[A^{\mathsf{up}}\left(W_{i,j+\frac{1}{2}}, f_{i,j}^n, f_{i,j+1}^n \right) - A^{\mathsf{up}}\left(W_{i,j-\frac{1}{2}}, f_{i,j-1}^n, f_{i,j}^n \right) \right], \quad (11.18)
\end{aligned}$$

where $W_{i,j-\frac{1}{2}} = \frac{1}{2}\left(V\left(r_{i+\frac{1}{2}}, a_{j-\frac{1}{2}}\right) + V\left(r_{i-\frac{1}{2}}, a_{j-\frac{1}{2}}\right) \right)$, $f_{i,0}^n = f_{i,I^r+1}^n = 0$, and the operator A^{up} is

$$A^{\mathsf{up}}(u, f_+, f_-) = \begin{cases} u f_+ & \text{if } u \geq 0, \\ u f_- & \text{if } u < 0. \end{cases}$$

(iv) Finite volume scheme Finally, the scheme of the model (M2a)-(M2b) is given by:

- Initialization for $i \in \{1, \ldots, I^r\}$ and $j \in \{1, \ldots, I^a\}$ we set

$$f_{i,j}^0 = \frac{1}{\Delta r \Delta a} \int_{\Lambda_{ij}} f(0, r, a) \, da dr.$$

- Time iteration: for all $n \in \{1, \ldots, N\}$, $i \in \{1, \ldots, I^r\}$ and $j \in \{1, \ldots, I^a\}$, using Eqs. (11.17)-

(11.18), and using an explicit forward Euler scheme in time for M, we set:

$$\begin{aligned} f_{i,j}^{n+1} =& f_{i,j}^n + \frac{\Delta t}{\Delta r \Delta a} Q_{i,j}^n (f,f) \\ & - \frac{\Delta t}{\Delta a}\left[A^{\text{up}}\left(W_{i,j+\frac{1}{2}}, f_{i,j}^n, f_{i,j+1}^n\right) - A^{\text{up}}\left(W_{i,j-\frac{1}{2}}, f_{i,j-1}^n, f_{i,j}^n\right)\right] \\ & + \frac{\Delta t}{\Delta r \Delta a}\left[\int_{\Lambda_{ij}} \alpha(r,a,M^n)\,\mathrm{d}a\mathrm{d}r - f_{i,j}^n \int_{\Lambda_{ij}} \lambda(r,a)\,\mathrm{d}a\mathrm{d}r \right. \\ & \qquad \left. - f_{i,j}^n \int_{\Lambda_{ij}} \gamma(r,a)\,\mathrm{d}a\mathrm{d}r\right]. \end{aligned} \tag{11.19}$$

$$\begin{aligned} M^{n+1} =& M^n + \Delta t\, J_M(M^n) - \Delta t \int_0^R \int_0^A a'\alpha(r',a',M^n)\,\mathrm{d}a'\mathrm{d}r' \\ & + \Delta t \sum_{i=1}^{I^r}\sum_{j=1}^{I^a} f_{i,j}^n \int_{\Lambda_{ij}} a\lambda(r,a)\,\mathrm{d}a\mathrm{d}r. \end{aligned}$$

The remaining integrals in Eq. (11.19) are calculated using an automatic adaptive numerical integration method, detailed in Genz and Malik (1980) and implemented in the Julia package HCubature[2].

Remark 11.4.1. *With the same tools, we can write a scheme in dimension 1 for model (M1), noticing that if we set $h(t,r) = rg(t,r)$ we have*

$$\partial_t h(t,r) = -\partial_r J(g)(t,r) + r\alpha(r, M(t)) - \gamma(r)\, h(t,r),$$

where $J(g)$ is defined as follows

$$J(g)(t,r) = \int_0^r \int_{r-r'}^{\infty} r'\kappa(r',r'')\, g(t,r')\, g(t,r'')\,\mathrm{d}r''\mathrm{d}r'.$$

A conservative truncation is then given by the following:

$$J_c^R(g)(t,r) = \int_0^r \int_{r-r'}^{R-r'} r'\kappa(r',r'')\, g(t,r')\, g(t,r'')\,\mathrm{d}r''\,\mathrm{d}r'.$$

11.4.2 . Numerical tests

In this section, we will investigate the behavior of the numerical scheme given by Eq. (11.19) in some particular cases. We aim to verify the conservation laws satisfied by the numerical scheme, the consistency and convergence properties of the numerical scheme, as well as to illustrate the long-time behavior we proved in Theorem 11.3.1.

Conservation laws and consistency. First, we will evaluate the numerical scheme in the case of a pure coagulation model ($\alpha = \gamma = \lambda = V = J_M = 0$). We consider the pure coagulation equation:

$$\partial_t f(t,r,a) = \tilde{Q}(f(t), f(t))(r,a), \quad \text{with } t>0, r>0 \text{ and } a>0. \tag{11.20}$$

[2] https://github.com/JuliaMath/HCubature.jl

The discrete equation associated to Eq. (11.20) is given by, as a special case of Eq. (11.19) when $\alpha = \gamma = \lambda = V = J_M = 0$,

$$f_{i,j}^{n+1} = f_{i,j}^{n} + \frac{\Delta t}{\Delta r \Delta a} Q_{i,j}^{n}\left(f, f\right), \; n \in \{1, \ldots, N\}, i \in \{1, \ldots, I^r\} \text{ and } j \in \{1, \ldots, I^a\}, \quad (11.21)$$

and where $Q_{i,j}^{n}$ is defined in Eq. (11.17). We remark that we keep the same properties on the moments dynamics for the two Eqs. (11.20) and (11.21). For some test function φ, we define $H\left(\varphi, t\right)$ the moment of f associated with the function φ at time $t > 0$,

$$H\left(\varphi, t\right) := \int_0^\infty \int_0^\infty \varphi\left(r, a\right) f\left(t, r, a\right) \mathrm{d}a\mathrm{d}r,$$

and $H^n\left(\varphi\right)$ its discrete analogue moment, associated with the function φ at time t^n with $n \in \{1, \ldots, N\}$,

$$H^n\left(\varphi\right) := \Delta r \Delta a \sum_{i=1}^{I^r} \sum_{j=1}^{I^a} \varphi\left(r_{i-\frac{1}{2}}, a_{j-\frac{1}{2}}\right) f_{i,j}^{n}. \quad (11.22)$$

Then

$$\begin{aligned}
\frac{\mathrm{d}}{\mathrm{d}t} H\left(\varphi, t\right) &= \frac{\mathrm{d}}{\mathrm{d}t}\left[\int_0^\infty \int_0^\infty \varphi\left(r, a\right) f\left(t, r, a\right) \mathrm{d}a\mathrm{d}r\right] \\
&= \int_0^\infty \int_0^\infty \varphi\left(r, a\right) \tilde{Q}\left(f\left(t\right), f\left(t\right)\right)\left(r, a\right) \mathrm{d}a\mathrm{d}r \\
&= \frac{1}{2} \int_0^\infty \int_0^\infty \int_0^\infty \int_0^\infty \left[\varphi\left(r + r', a + a'\right) - \varphi\left(r, a\right) - \varphi\left(r', a'\right)\right] \\
&\qquad \kappa\left(r, r'\right) f\left(t, r, a\right) f\left(t, r', a'\right) \mathrm{d}a'\mathrm{d}r'\mathrm{d}a\mathrm{d}r,
\end{aligned}$$

and similarly

$$\begin{aligned}
\frac{H^{n+1}\left(\varphi\right) - H^n\left(\varphi\right)}{\Delta t} = \frac{\left(\Delta r \Delta a\right)^2}{2} \sum_{i=1}^{I^r} \sum_{j=1}^{I^a} \sum_{k=1}^{I^r - i + 1} \sum_{m=1}^{I^a - j + 1} &\left[\varphi\left(r_{i+k-1-\frac{1}{2}}, a_{j+m-1-\frac{1}{2}}\right)\right. \\
&\left. - \varphi\left(r_{i-\frac{1}{2}}, a_{j-\frac{1}{2}}\right) - \varphi\left(r_{k-\frac{1}{2}}, a_{m-\frac{1}{2}}\right)\right] \kappa_{i,k} f_{i,j}^{n} f_{k,m}^{n}.
\end{aligned}$$

Thus choosing $\varphi\left(r, a\right) = r$ or $\varphi\left(r, a\right) = a$, we have that the first-order moments are constant in time both at the discrete and continuous levels, consistently with Eqs. (11.4)-(11.5) and Eqs. (11.12)-(11.13) for the pure coagulation case. We also have that the zeroth-order moments are non-increasing functions of time in both cases.

For the pure coagulation model given by Eq. (11.20), choosing an affine kernel $\kappa\left(r, r'\right) = K_0 + K_1\left(r + r'\right)$ leads to a closed moment equation in the form of an ODE system. Indeed, in such case, it is easy to see that we have the following ODE system for the moments of order 0 and 1:

$$\begin{cases}
\dfrac{\mathrm{d}}{\mathrm{d}t} H\left(1, t\right) = -\dfrac{1}{2} K_0 \left(H\left(1, t\right)\right)^2 - K_1 H\left(1, t\right) H\left(r, t\right), \\
\dfrac{\mathrm{d}}{\mathrm{d}t} H\left(r, t\right) = 0, \\
\dfrac{\mathrm{d}}{\mathrm{d}t} H\left(a, t\right) = 0.
\end{cases} \quad (11.23)$$

Eq. (11.23) is of the form of a Bernoulli differential equation, and its analytical solution can be computed. The pure coagulation case with an affine kernel is thus an appropriate

setting to compare analytical solutions with moments associated to our numerical scheme (11.21) calculated by Eq. (11.22). For this purpose, we introduce the following notation, for $x > 0$:

$$\mathcal{N}_x(\mu, \sigma) = \frac{1}{\sqrt{2\pi}\sigma} e^{-\frac{1}{2}\left(\frac{x-\mu}{\sigma}\right)^2} \mathbf{1}_{x>0} \,. \tag{11.24}$$

We approximate the pure coagulation Eq. (11.20) using the scheme Eq. (11.21) with the following numerical parameters:

$$T = 1 \,, \Delta t = 10^{-4} \,, \quad R = A = 10 \,, \Delta r = \Delta a = 0.25 \,. \tag{11.25}$$

We study two cases. The first one is the case of a constant kernel with the following model parameters:

$$\begin{aligned} f_0(r,a) &= 0.5 \cdot \left[\mathcal{N}_r(1.5, 0.15) \times \mathcal{N}_a(0.5, 0.3) + \mathcal{N}_r(0.5, 0.3) \times \mathcal{N}_a(1.5, 0.15)\right] \,, \\ \kappa(r, r') &= 0.5 \,. \end{aligned} \tag{11.26}$$

The second one is the case of an affine kernel with the following model parameters:

$$\begin{aligned} f_0(r,a) &= 0.5 \cdot \left[\mathcal{N}_r(1.5, 0.15) \times \mathcal{N}_a(0.5, 0.3) + \mathcal{N}_r(0.5, 0.3) \times \mathcal{N}_a(1.5, 0.15)\right] \,, \\ \kappa(r, r') &= 0.5 + 0.1\,(r + r') \,. \end{aligned} \tag{11.27}$$

As expected, we recover from our numerical scheme (11.21) that the moment of order 0 is a nonincreasing function and the moments of order 1 are constant (Figure 11.1). Moreover, we also observed that these numerical results are very close to the analytical solutions directly computed from Eq. (11.23) (Figures 11.2 and 11.3). Relative error of moments of order 0 are increasing through time, as expected from the fact that the size-truncation of the numerical scheme (11.21) implies more and more error as compartments gets bigger in pure-coagulation dynamics.

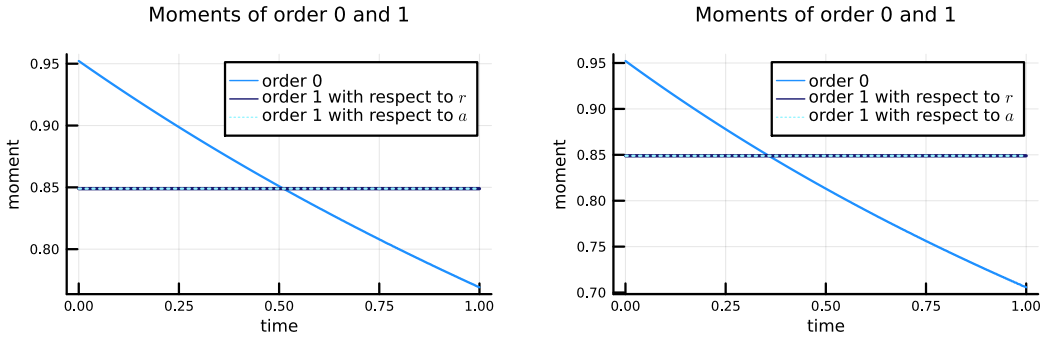

Figure 11.1: *Time evolution of the moments of order 0 and 1 (see inserted legend) computed from our pure coagulation numerical scheme (11.21), with the constant kernel and the model parameters (11.26) for the left picture and with the constant kernel and the model parameters (11.27) for the right one. The results are obtained with the numerical parameters (11.25). In both cases, the moment of order 0 is a nonincreasing function and the moments of order 1 are constant. With the choice of our initial condition, both moments of order 1 in r and a superimposed.*

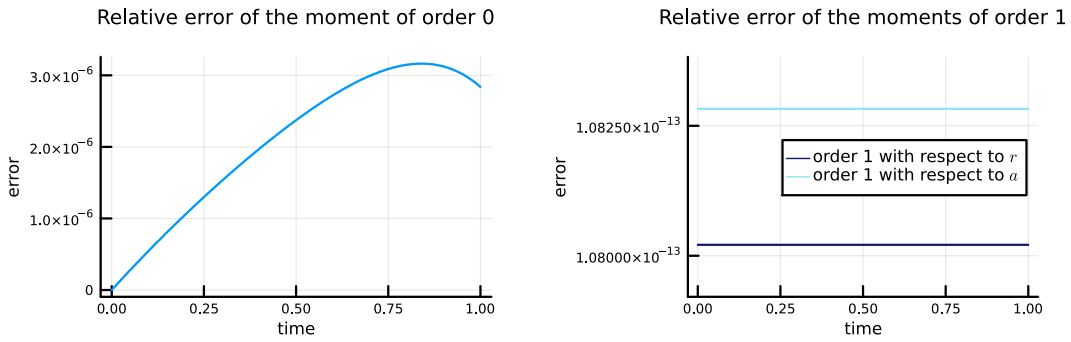

Figure 11.2: *Relative error of the moments of order 0 (left panel) and 1 (right panel) between moments computed from our pure coagulation numerical scheme* (11.21) *and from the analytical solution of the ODE system Eq.* (11.23)*, in the case of a constant kernel* (11.26) *with the same parameters as in the left panel of Figure 11.1.*

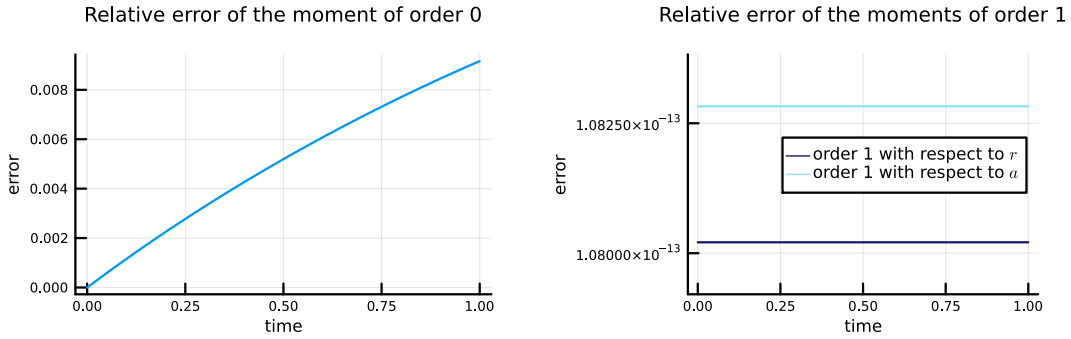

Figure 11.3: *Relative error of the moments of order 0 (left panel) and 1 (right panel) between moments computed from our pure coagulation numerical scheme* (11.21) *and from the analytical solution of the ODE system Eq.* (11.23)*, in the case of an affine kernel* (11.27) *with the same parameters as in the right panel of Figure 11.1.*

Convergence. We now investigate the convergence property of our numerical scheme given by Eq. (11.19) in a more general setting. We want to illustrate the convergence of the numerical scheme as the size steps Δr and Δa decreases to 0. Regarding stability, we expect the numerical scheme to be conditionally stable for small enough $\frac{\Delta t}{\Delta r \Delta a}$ as our scheme is a first-order finite volume scheme, but the proof of stability is out of the scope of this paper. See for instance Bourgade and Filbet (2007) for stability results on the coagulation part. We thus fix a small enough time step Δt and choose $\Delta r = \Delta a = h$ with linearly decreasing h in a $log2$ scale, namely $h_m = \frac{h_0}{2^m}$ for integers m from 0 to 11 and $h_0 = \frac{1}{2}$. The finite volume size is then decreasing from h_0^2 to $\left(\frac{h_0}{2^{11}}\right)^2$. We choose the finest solution as reference solution and compare the solutions defined on the coarser grids to this reference solution with the following different norms, defined for a function f and $k, l \in \mathbb{N}$ as follows:

$$\|f\|_{k,l} = \int_0^R \int_0^A r^k a^l \left|f\left(r,a\right)\right| \mathrm{d}a\mathrm{d}r.$$

Those moment-based norms are natural within the context of coagulation equations, see e.g. Eqs. (11.12)-(11.13). The fact that the grids are nested allows to compute the following errors, for $m \in \{0, ...10\}$,

$$\|E(h_m, t^n)\|_{k,l} = h_{11}^2 \sum_{i=1}^{R/h_{11}} \sum_{j=1}^{A/h_{11}} r_{i-\frac{1}{2}}^k a_{j-\frac{1}{2}}^l \mid f_{i,j}^{n,h_m} - f_{i,j}^{n,h_{11}} \mid , \tag{11.28}$$

where the value of $f_{i,j}^{n,h_m}$ are extended from the coarser grid to the finer grid by taking its value constant over the subdomains defined by the finer grid. We compute the errors defined in Eq. (11.28) up to second order moments ($0 \leq k + l \leq 2$) in two different cases as we detail now. For that aim, we introduce the notation, for $x > 0$,

$$\mathcal{P}_x(\bar{x}, \epsilon) = \left(\frac{\bar{x} + \epsilon - x}{\bar{x} + \epsilon} \right)^{\frac{1}{3}} \left(\frac{x}{\bar{x}} \right)^{\frac{2}{3}} . \tag{11.29}$$

(i) Case 1 We approximate the pure coagulation case Eq. (11.20) (Figure 11.4) with the numerical parameters

$$\Delta t = 0.0005 , \quad R = A = 3 , \Delta r = \Delta a = h_m , \tag{11.30}$$

and the model parameters

$$\begin{aligned} f_0(r, a) &= 0.5 \cdot [\mathcal{N}_r(1.5, 0.15) \times \mathcal{N}_a(0.5, 0.3) + \mathcal{N}_r(0.5, 0.3) \times \mathcal{N}_a(1.5, 0.15)] , \\ \kappa(r, r') &= 0.5 . \end{aligned} \tag{11.31}$$

(ii) Case 2 We approximate the general case Eqs. (M2a)-(M2b) (Figure 11.5), with the model parameters

$$\begin{aligned} f_0(r, a) &= 0.5 \cdot [\mathcal{N}_r(1.5, 0.15) \times \mathcal{N}_a(0.5, 0.3) + \mathcal{N}_r(0.5, 0.3) \times \mathcal{N}_a(1.5, 0.15)] , \\ M_0 &= 20 , \\ \kappa(r, r') &= 0.5 , \\ \alpha(r, a, M) &= 0.1 \cdot M \cdot [\mathcal{N}_r(0.6, 0.01) \times \mathcal{N}_a(0.3, 0.05) + \mathcal{N}_r(0.3, 0.05) \times \mathcal{N}_a(0.6, 0.01)] , \\ \gamma(r, a) &= 20 (r - 5)^4 \mathbf{1}_{r>5} + 10^{-5} , \\ \lambda(r, a) &= 10^{-2} \cdot \mathcal{P}_r(10, 0) , \\ V(r, a) &= 0 , \\ J_M(M) &= 0 , \end{aligned} \tag{11.32}$$

and the same numerical parameters as in Eq. (11.30). In both cases, we observe that the error decreases linearly (in log-log scale) when the size of the discretization step h does. For both cases, the order of the scheme appears to be 1.

Long-time behavior. Finally, we we illustrate the long-time behavior of the numerical solutions and test the optimality of the conditions from the long time behavior given in Theorem 11.3.1 for the one dimensional model (M1), with the numerical parameters

$$\Delta t = 0.05 , \quad R = 5 , I^r = 301 , \tag{11.33}$$

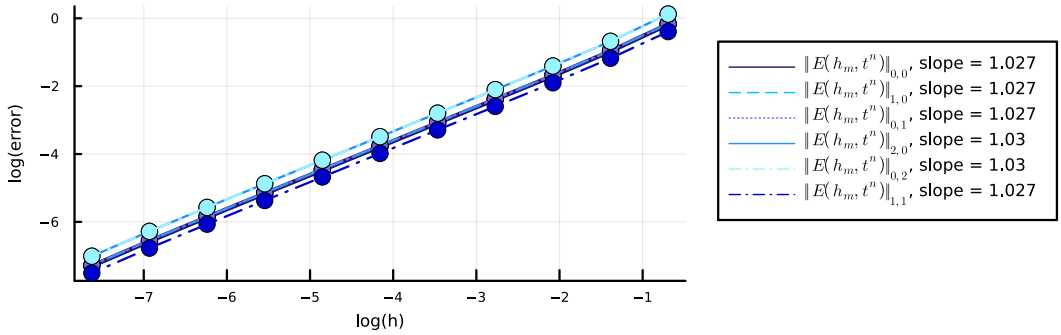

Figure 11.4: *Illustration of the convergence of the numerical scheme* (11.21) *in the case of the pure coagulation (case 1, numerical and model parameters given by Eqs.* (11.30)-(11.31)*) . We plot the error as a function of the grid size h, in log-log scale, using the six different norms $\|E(h_m,t^n)\|_{k,l}$ defined in Eq.* (11.28) *for $0 \leq k+l \leq 2$ (see inserted legend).*

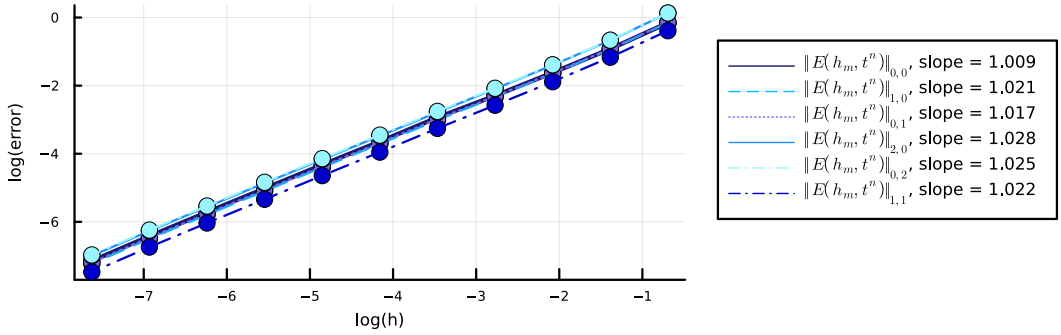

Figure 11.5: *Illustration of the convergence of the numerical scheme* (11.19) *in case 2 (numerical and model parameters given by Eqs.* (11.30)-(11.32)*). See legend of Figure 11.4.*

and the model parameters

$$\begin{aligned} f_0(r,a) &= 0.5 \cdot \mathcal{N}_r(0.2, 0.15)\,, \\ \kappa(r,r') &= 1\,, \\ \alpha(r,M) &= M \cdot \mathcal{N}_r(0.6, 0.1)\,. \end{aligned} \tag{11.34}$$

We show in Figure 11.6 two cases. In the first one (left hand-side), we use $\gamma(r) = \sqrt{3.1}$ together with Eq. (11.34), for which the condition Eq. (11.6) of Theorem 11.3.1 is satisfied. In the second one (right hand-side), we use $\gamma(r) = 0.7$ together with Eq. (11.34), for which the condition Eq. (11.6) is not satisfied. In both cases, the curves for $t = 10$ and $t = 50$ are superimposed, and we observe that the solution seems to converge to a stationary state. Numerically, while we verify the conclusion of Theorem 11.3.1 holds true, it seems that the condition Eq. (11.6) is too restrictive since the scheme stays stable in a wider range of parameters such that the condition Eq. (11.6) is not satisfied.

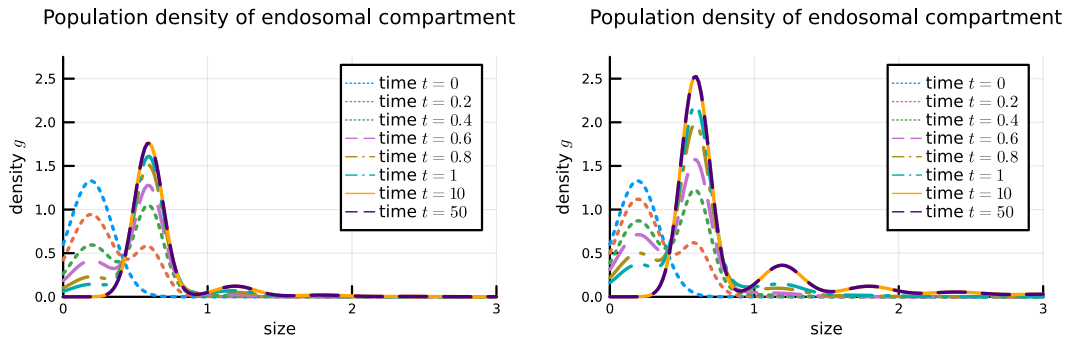

Figure 11.6: *Size-distribution of the population density g of endosomal compartement for model (M1) at different times (see inserted legend) and parameters given by Eqs. (11.33)-(11.34). On the left hand-side the condition Eq. (11.6) is satisfied ($\gamma(r) = \sqrt{3.1}$) whereas on the right hand-side the condition Eq. (11.6) is not satisfied ($\gamma(r) = 0.7$). In both cases, the curves for $t = 10$ and $t = 50$ are superimposed.*

11.5 . Applications

In this section we provide two applications of our 2D model given by Eqs. (M2a)-(M2b), that show good qualitative agreement with published experimental data on receptor-activated signaling pathways. Our simulations also provide additional insight, which calls for new experiments.

11.5.1 . Receptor trafficking

The 2D model given by Eqs. (M2a)-(M2b) is ideally suited to model receptor trafficking from plasma membrane to endocytic comparments. As detailed in the introduction, the GPCR are typically located at the surface of the cells, on the plasma membrane. Upon ligand binding, the GPCR activate several signalling pathways as well as their own internalization through endocytosis. The vesicles still carry the internalised receptors on their surface. Endosomes are then sorted thanks to complex processes which are not yet fully understood, but that depends both on the nature of the receptor and the ligand. Internalized receptors can indeed commit to several endosomal compartments of different kinds, and be recycled at the cell surface, which could impact on the kinetic profile of the receptor and its signalling pathways. Consequently, endocytosis regulate receptor cell surface density and signaling profile, and endosomal targeting of receptors may produce specificity in the signaling pathways. In particular, it has been shown (Jean-Alphonse et al., 2014) that the LHR and the B2AR are two GPCR that undergo divergent trafficking to distinct endosomal compartments. B2AR traffics mostly to early endosomes (EEs) and LHR to pre-early endosomes (pre-EEs). In short, the authors in Jean-Alphonse et al. (2014) demonstrate that LHR endosome sizes increased over time quickly before reaching a plateau, producing a small endosome population (400-500 nm of diameter). The mean B2AR endosome sizes are bigger (1200-1400 nm of diameter). They also see that B2AR was more internalized than LHR in percentage but both receptors are equally recycled. The objective of this section is to provide numerical simulations of our model (M2a)-(M2b) that can reproduce these two distinct scenarios.

In order to compare qualitatively our model with the experimental results presented in

Jean-Alphonse et al. (2014), we choose the following parametrization (we recall definitions in Eqs. (11.24)-(11.29)):

$$\begin{aligned} f_0(r,a) &= 0\,, \\ M_0 &= 7.2\times 10^{-4}\,, \\ \kappa(r,r') &= K_0\,, \\ \alpha(r,a,M) &= \overline{\alpha}\mathcal{N}_r(200,10)\times\mathcal{N}_a(r,0.5)\times M\,, \\ \gamma(r,a) &= 10^{-5}+2\times 10^{1}\times\left(\frac{r-1950}{50}\right)^4\mathbf{1}_{\{r>1950\}}\,, \\ \lambda(r,a) &= 10^{-2}\times\mathcal{P}_r(2000,0)\,, \\ V(r,a) &= 0\,, \\ J_M(M) &= 0\,, \end{aligned} \tag{11.35}$$

which we interpret as follows. Endosomes fuse at a constant coagulation kernel κ, whose rate will depend on the receptor. Endosomes are created with a size following a Gaussian law and with a quantity of reactant proportional to their size, and the rate $\overline{\alpha} > 0$ will depend on the receptor. Small endosomes are degraded at constant (low) rate, and degradation rates quickly increases for endosomes large enough. Endosomes recycling increase with the surface of endosomes and decreases with their volume ($\lambda \propto r^{\frac{2}{3}} - r$). We don't consider reactions, e.g. V and J_M are taken as null functions.

For the numerical scheme, we take

$$T = 30, \Delta t = 10^{-1}, \quad I^r = I^a = 30, R = A = 2000. \tag{11.36}$$

To explain the qualitative differences between LHR and B2AR trafficking observed in Jean-Alphonse et al. (2014), we tested two hypotheses here.

- (H1) In the first hypothesis (Figure 11.7), we modify only the internalization rate $\overline{\alpha} > 0$ between LHR and B2AR, with a higher internalization rate for the B2AR, keeping all the remaining parameters the same. This hypothesis is in line with Jean-Alphonse et al. (2014). LHR and B2AR affect only the endocytosis rate as follows (refer to Eq. (11.35)):

Parameters	K_0	$\overline{\alpha}$
LHR	5×10^{-1}	8×10^{-5}
B2AR	5×10^{-1}	3×10^{-4}

(11.37)

- (H2) In the second hypothesis (Figure 11.8), both the internalization rate and the coagulation rate are higher for the B2AR compared to the LHR (H2). LHR and B2AR affect the internalization and the coagulation rate as follows:

Parameters	K_0	$\overline{\alpha}$
LHR	5×10^{-3}	8×10^{-5}
B2AR	5×10^{-1}	3×10^{-4}

(11.38)

In Jean-Alphonse et al. (2014), mean and variance of the size of the endosomal populations are measured at different time after ligand stimulation, as well as the internalization ratio, which corresponds to the fraction of internalised receptors among the total number of receptors

initially present at the plasma membrane. Consistently, we define in the model the internalization ratio as $\frac{\|f\|_{0,1}(t)}{M_0}$. In both hypotheses the internalization ratio is well reproduced by the model, compared to Jean-Alphonse et al. (2014). The major discrepancy of the first hypothesis with the experiments is the variance in size of the endosomal population, which seems too high compared to experimentation. Furthermore the production of large endosomes with LHR seems too high and similar to the ones of B2AR (Figure 11.7). In the second hypothesis, however, these two discrepancies are not present anymore (Figure 11.8). These results indicate that the differences in endosome dynamics between LHR and B2AR signaling pathways seem not only due to a difference in internalization rate, but probably also to the coagulation dynamics inside cells. Difference in coagulation dynamics may be explained by differences in endosomes sorting and/or differences in molecular composition of endosomes, which are believed to be of different nature between LHR and B2AR vesicles (Jean-Alphonse et al., 2014).

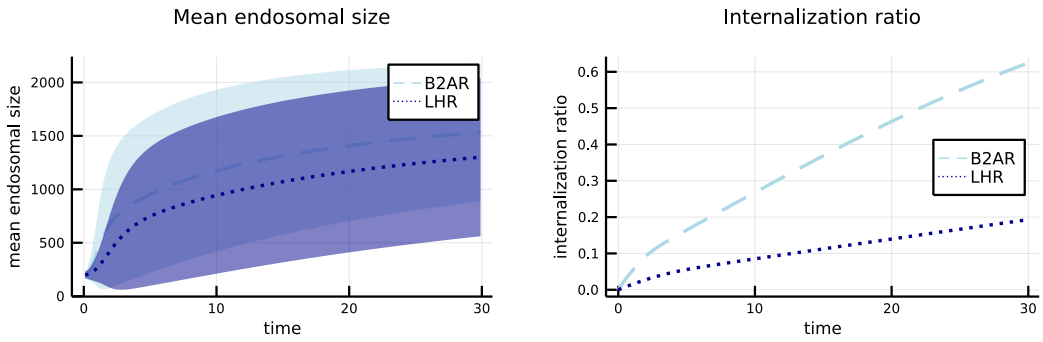

Figure 11.7: *Time evolution of the endosomal size (left panel) and internalization ratio (right panel). We numerically simulate the 2D model given by Eqs.* (M2a)-(M2b) *with parameters given by.* (11.35)-(11.36)-(11.37) *(LHR and B2AR affect only the internalization rate). On the left panel, the dashed blue (resp. dotted purple) line represents the mean endosomal size for B2AR (resp. LHR), that corresponds to* $\|f\|_{1,0}(t)/\|f\|_{0,0}(t)$*, and the shaded light area represents its standard deviation. On the right panel, the dashed blue (resp. dotted purple) line represents the internalization ratio for B2AR (resp. LHR), that corresponds to* $\frac{\|f\|_{0,1}(t)}{M_0}$.

11.5.2 . Second effector signaling

The second application of our model we present here concerns the efficacy of second messenger molecules production as a function of the localization of the active receptor. We focus on the production of cAMP induced by the activation of the PTHR. Recent discoveries find that the PTHR may engage cAMP signaling not only at the cell's plasma membrane but also in early endosomes after receptor internalization through endocytosis (Vilardaga et al., 2014). Furthermore, the full-length parathyroid hormone (LA-PTH) induces through the activation of PTHR an augmentation of production of cAMP in the endosomes, whereas the ligand PTH 7D (PTHR peptide ligand through amino acid epimerization at position 7 of PTH^{1-34}) induces the production of cAMP at the plasma membrane. In White et al. (2021), the authors show that even if the production place is different, the total amount of cAMP stays the same after some time, a phenomenon that could be named location-biased, and that can have implications for the cellular response. The objective of this section is to provide numerical simulations of our

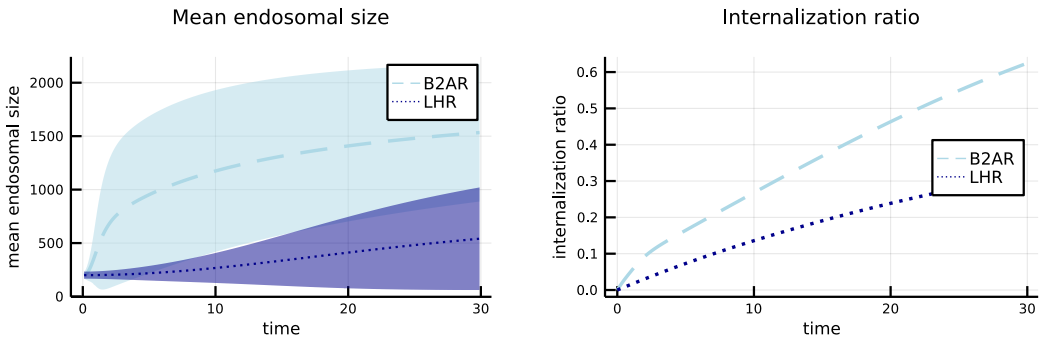

Figure 11.8: *Time evolution of the endosomal size (left panel) and internalization ratio (right panel). We numerically simulate the 2D model given by Eqs.* (M2a)-(M2b) *with parameters given by.* (11.35)-(11.36)-(11.38) *(LHR and B2AR affect the internalization and the coagulation rate). See legend of Figure 11.7 for details.*

model (M2a)-(M2b) that can reproduce these two distinct scenarios.

We could reproduce qualitatively these observations with our model following this parametrization:

$$\begin{aligned}
f_0(r,a) &= 0\,,\\
M_0 &= 0\,,\\
\kappa(r,r') &= 2\times 10^{-1}\,,\\
\alpha(r,a,M) &= \mathcal{N}_r(200,10)\times\mathcal{N}_a(0,0.1))\times M\,,\\
\gamma(r,a) &= \mathcal{P}_r(2000,100)\mathbf{1}_{\{r\le 1950\}} + 2\times 10^2\times\left(\frac{r-1950}{50}\right)^4\mathbf{1}_{\{r>1950\}}\,,\\
\lambda(r,a) &= 10^{-2}\times\mathcal{P}_r(2000,100)\,,\\
V(r,a) &= \left(v_s\mathbf{1}_{\{\epsilon\le r\le\bar r\}} + v_l\mathbf{1}_{\{\bar r<r\}}\right)\times\left(1-\frac{a}{pr}\right)\,,\quad \epsilon = 10/3, \bar r = 500\,,\\
J_M(M) &= v_M\times\left(\frac{\bar M - M}{\bar M}\right)\,,
\end{aligned} \tag{11.39}$$

which we interpret as follows. Endosomes fuse via a constant coagulation kernel, and are created with a size following a Gaussian law and with a quantity of reactant, independently of the size, taken as a positive fraction of the quantity M present at the plasma membrane. Endosomes recycling and degradation increase with the surface of endosomes and decrease with their volume (λ and $\gamma \propto r^{\frac{2}{3}} - r$). cAMP is produced at the plasma membrane at constant rate and linearly degraded, where both the saturation $\bar M$, and the production rate v_M may depend on the ligand. cAMP is produced in endosomes at two different rates, v_s, for the endosomes smaller than $\bar r$ and v_l, for larger endosomes. Also the amount of saturation depends linearly on the size of the endosomes (caracterized by a portion p of r). Here v_s, v_l and p may depend on the ligand.

For the numerical scheme, we take

$$\Delta t = 3^{-2},\quad I^r = I^a = 30, R = 2000, A = 30\,. \tag{11.40}$$

We have two different hypotheses to explain the different qualitative behaviour of the two ligand LA-PTH and PTH 7D described above:

- (H1) Suppose LA-PTH and PTH 7D differs in cAMP production kinetics only in terms of rate (Figure 11.9), with a higher rate for LA-PTH at the plasma membrane ($v_M^{PTH7D} < v_M^{LA-PTH}$), and a higher rate for PTH 7D in the endosomes ($v_s^{LA-PTH} < v_s^{PTH7D}$ and $v_l^{LA-PTH} < v_l^{PTH7D}$).

Parameters	v_s	v_l	p	v_M	$\bar{M}$
LA-PTH	0.05	0.02	$1/20$	3.5	10
PTH 7D	5	2	$1/20$	0.035	10

(11.41)

- (H2) Suppose LA-PTH and PTH 7D differs in cAMP production kinetics not only in terms of rate but also in terms of saturation (Figure 11.10) with $\bar{M}^{LA-PTH} > \bar{M}^{PTH^{7D}}$ and $p^{PTH^{7D}} > p^{LA-PTH}$.

Parameters	v_s	v_l	p	v_M	$\bar{M}$
LA-PTH	0.5	0.2	$1/200$	3.5	10
PTH 7D	5	2	$1/20$	0.35	1

(11.42)

With both hypotheses, we observe a much more efficient cAMP production at the plasma membrane with LA-PTH and a much more efficient cAMP production in the endosomes with PTH 7D (Figures 11.9 and 11.10). Consistently with the observation in White et al. (2021), both total responses have similar magnitude for the time period of the numerical simulation.

However, from the numerical simulation presented in figures 11.9 and 11.10, the cAMP production has already reached a "stable" state at $T = 20$ for LA-PTH, while it keeps increaseasing for PTH 7D. Therefore, a longer time measurement could discriminate between both ligands.

Also we could notice a fine kinetic difference between the responses induces by LA-PTH and PTH 7D with the two hypotheses. Indeed, PTH 7D leads to a convex kinetic production of cAMP during the early dynamics, which switches to a concave kinetic at later time. Whereas with LA-PTH the production stays concave all time long. Of course this behaviour may be quite complicated to observe experimentally due to the accuracy of the measures.

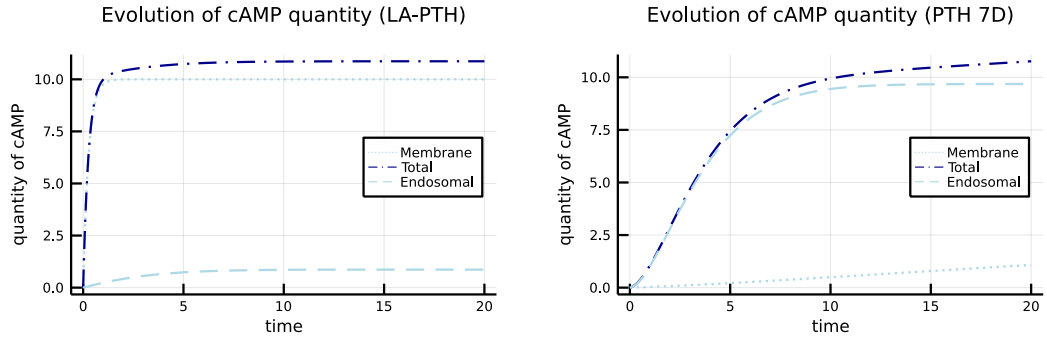

Figure 11.9: *Time evolution of the cAMP production for the LA-PTH ligand (left panel) and the PTH-7D ligand (right panel). We numerically simulate the 2D model given by Eqs.* (M2a)-(M2b) *with parameters given by.* (11.39)-(11.40)-(11.41) *(cAMP kinetic parameters differ between PTH 7D and LA-PTH only by the production rate). In both panels, the dotted blue line shows the endosomal quantity of cAMP, given by* $\|f\|_{0,1}(t)$*, the dashed blue line shows the cAMP quantity at the plasma membrane, given by* $M(t)$*, and the dashed-dotted purple line shows the total cAMP quantity (*$\|f\|_{0,1}(t) + M(t)$*).*

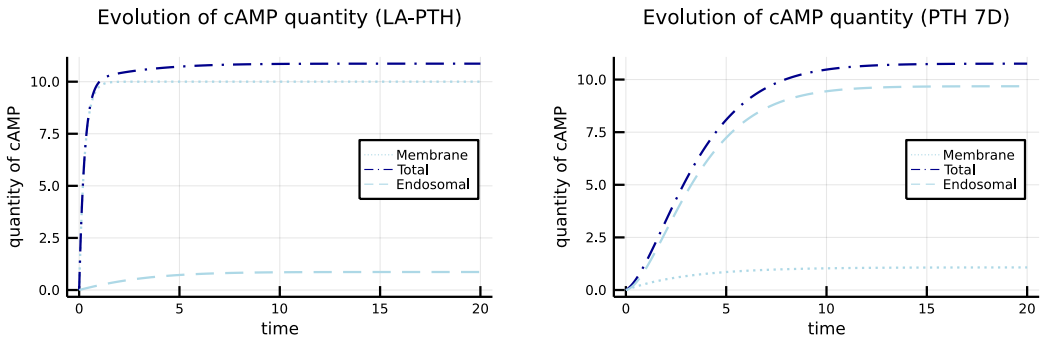

Figure 11.10: *Time evolution of the cAMP production for the LA-PTH ligand (left panel) and the PTH-7D ligand (right panel). We numerically simulate the 2D model given by Eqs.* (M2a)-(M2b) *with parameters given by.* (11.39)-(11.40)-(11.42) *(cAMP kinetic parameters differ between PTH 7D and LA-PTH both by the production rate and capacity of production.). See legend of Figure 11.9 for details.*

Bibliography

Alexandrov, D. V., Korabel, N., Currell, F., and Fedotov, S. (2022). Dynamics of intracellular clusters of nanoparticles. Cancer Nanotechnology, 13(1):15. 324, 326

Anderson, D. F. and Howells, A. S. (2023). Stochastic Reaction Networks Within Interacting Compartments. Bulletin of Mathematical Biology, 85(10):87. 323

Anderson, D. F. and Kurtz, T. G. (2015). Stochastic Analysis of Biochemical Systems. Number 1.2 in Mathematical Biosciences Institute Lecture Series. Springer international publishing edition. 322

Birtwistle, M. R. and Kholodenko, B. N. (2009). Endocytosis and signalling: A meeting with mathematics. Mol Oncol, 3(4):308–320. 322

Bourgade, J.-P. and Filbet, F. (2007). Convergence of a finite volume scheme for coagulation-fragmentation equations. Mathematics of Computation, 77(262):851–883. 328, 329, 336

Canizo, J. A. (2006). Some problems related to the study of interaction kernels: coagulation, fragmentation and diffusion in kinetic and quantum equations. PhD thesis, Universidad de Granada. 326, 327

Chae, D. and Dubovskii, P. B. (1995). Existence and uniqueness for spatially inhomogeneous coagulation equation with sources and effluxes. 46(4):580–594. 326

Collet, J.-F. and Goudon, T. (1999). Lifshitz-slyozov equations: The model with encounters. 28(6):545–573. 326, 327

Dubovskii, P. B. (1994). Mathematical theory of coagulation. 326

Duso, L. and Zechner, C. (2020). Stochastic reaction networks in dynamic compartment populations. Proceedings of the National Academy of Sciences, 117(37):22674–22683. 323

Feinberg, M. (2019). Foundations of Chemical Reaction Network Theory. Applied Mathematical Sciences. Springer International Publishing. 322

Foret, L., Dawson, J. E., Villaseñor, R., Collinet, C., Deutsch, A., Brusch, L., Zerial, M., Kalaidzidis, Y., and Jülicher, F. (2012). A general theoretical framework to infer endosomal network dynamics from quantitative image analysis. Curr Biol, 22(15):1381–1390. 323, 324, 325, 326

Gajewski, H. (1983). On a first order partial differential equation with nonlocal nonlinearity. 111(1):289–300. 326

Genz, A. C. and Malik, A. A. (1980). Remarks on algorithm 006: An adaptive algorithm for numerical integration over an N-dimensional rectangular region. Journal of Computational and Applied Mathematics, 6(4):295–302. 333

Ghosh, D., Paul, J., and Kumar, J. (2023). On equilibrium solution to a singular coagulation equation with source and efflux. 422:114909. 326

Hingant, E. and Sepúlveda, M. (2015). Derivation and mathematical study of a sorption-coagulation equation. Nonlinearity, 28(10):3623–3661. 328, 329

Ingalls, B. (2013). Mathematical Modeling in Systems Biology. Mit press edition. tex.ids= ingallsMathematicalModellingSystems2012. 322

Jean-Alphonse, F., Bowersox, S., Chen, S., Beard, G., Puthenveedu, M. A., and Hanyaloglu, A. C. (2014). Spatially Restricted G Protein-coupled Receptor Activity via Divergent Endocytic Compartments. J Biol Chem, 289(7):3960–3977. 322, 323, 339, 340, 341

Jean-Alphonse, F. and Hanyaloglu, A. C. (2011). Regulation of GPCR signal networks via membrane trafficking. Molecular and Cellular Endocrinology, 331(2):205–214. 322

Kenakin, T. (2019). Biased Receptor Signaling in Drug Discovery. Pharmacological Reviews, 71(2):267–315. 322

Kholodenko, B. N. (2006). Cell-signalling dynamics in time and space. Nature Reviews Molecular Cell Biology, 7(3):165–176. 321, 322

Kim, H., Lee, H. N., Choi, J., and Seong, J. (2021). Spatiotemporal Characterization of GPCR Activity and Function during Endosomal Trafficking Pathway. Anal. Chem., page acs.analchem.0c03323. 322

Laurençot, P. (2020). Stationary solutions to smoluchowski's coagulation equation with source. 6:137. 326

Lefkowitz, R. J. (2013). A brief history of G-protein coupled receptors (Nobel Lecture). Angewandte Chemie (International Ed. in English), 52(25):6366–6378. 321

Lyga, S., Volpe, S., Werthmann, R. C., Götz, K., Sungkaworn, T., Lohse, M. J., and Calebiro, D. (2016). Persistent cAMP Signaling by Internalized LH Receptors in Ovarian Follicles. Endocrinology, 157(4):1613–1621. 322

Pietzsch, T., Duso, L., and Zechner, C. (2021). Compartor: a toolbox for the automatic generation of moment equations for dynamic compartment populations. Bioinformatics, 37(17):2782–2784. 323

Roth, S., Kholodenko, B. N., Smit, M. J., and Bruggeman, F. J. (2015). G Protein-Coupled Receptor Signalling Networks from a Systems Perspective. Molecular Pharmacology. Publisher: American Society for Pharmacology and Experimental Therapeutics Section: Minireview. 321

Sayers, N. and Hanyaloglu, A. C. (2018). Intracellular Follicle-Stimulating Hormone Receptor Trafficking and Signaling. Frontiers in Endocrinology, 9. 322

Sorkin, A. and von Zastrow, M. (2009). Endocytosis and signalling: Intertwining molecular networks. Nat Rev Mol Cell Biol, 10(9):609–622. 322

Vásquez, M. O. (2015). Ecuaciones en derivadas parciales para el análisis de modelos biopoliméricos. PhD thesis, Universidad de Granada. 326, 327

Vilardaga, J.-P., Jean-Alphonse, F., and Gardella, T. J. (2014). Endosomal generation of cAMP in GPCR signaling. Nat Chem Biol, 10(9):700–706. 322, 341

Villaseñor, R., Kalaidzidis, Y., and Zerial, M. (2016). Signal processing by the endosomal system. Current Opinion in Cell Biology, 39:53–60. 322

Weddell, J. C. and Imoukhuede, P. I. (2017). Integrative meta-modeling identifies endocytic vesicles, late endosome and the nucleus as the cellular compartments primarily directing RTK signaling. Integrative Biology, 9(5):464–484. 322

White, A. D., Peña, K. A., Clark, L. J., Maria, C. S., Liu, S., Jean-Alphonse, F. G., Lee, J. Y., Lei, S., Cheng, Z., Tu, C.-L., Fang, F., Szeto, N., Gardella, T. J., Xiao, K., Gellman, S. H., Bahar, I., Sutkeviciute, I., Chang, W., and Vilardaga, J.-P. (2021). Spatial bias in cAMP generation determines biological responses to PTH type 1 receptor activation. Science Signaling, 14(703):eabc5944. 322, 323, 341, 343